POLYURETHANE-BASED SIMULTANEOUS INTERPENETRATING POLYMER NETWORKS OF CONTROLLED MICROPHASE MORPHOLOGY AND HIGH DAMPING CHARACTERISTICS.

by

Franz-Ulrich Schäfer,

Diplom-Ingenieur (FH) Chemie/Kunststoffe,
CChem., M.R.S.C.

A Doctoral thesis
submitted in partial fulfilment of the requirements
for the award of
Doctor of Philosophy
of
Loughborough University

Supervisor: Professor Douglas Hourston
Institute of Polymer Technology
and Materials Engineering
June 1996

POLYURETHANE-BASED SIMULTANEOUS INTERPENETRATING POLYMER NETWORKS OF CONTROLLED MICROPHASE MORPHOLOGY AND HIGH DAMPING CHARACTERISTICS.

by

Franz-Ulrich Schäfer,

Diplom-Ingenieur (FH) Chemie/Kunststoffe,

CChem., M.R.S.C.

A Doctoral thesis

submitted in partial fulfilment of the requirements

for the award of

Doctor of Philosophy

of

Loughborough University

Supervisor: Professor Douglas Hourston

Institute of Polymer Technology

and Materials Engineering

June 1996

To my parents, my brother and Carolina.

ACKNOWLEDGEMENTS.

Firstly, I would like to thank my supervisor, Professor Doug Hourston, for his friendship, enthusiasm and excellent supervision throughout this project. The latter would not have been as instructive and rewarding without his guidance and encouragement to publish and present results at international conferences.

Many thanks to John Bates for his invaluable help in preparing the scanning and transmission electron micrographs, which represent an important part of this investigation. I extend my thanks to Dr. David Ross for making the wide-angle X-ray diffraction measurements.

At Lancaster University, I would like to thank Mo Song for the modulated-temperature differential scanning calorimetry measurements and very fruitful subsequent discussions, Dr. Barry Hunt for help with vapour pressure osmometry and gel permeation chromatography measurements, Dr. Tom Huckerby and Dr. Colin Peacock for conducting the NMR studies and the Karl Fischer water content determinations, respectively.

I also would like to extend my thanks to Ray Owens and Trevor Atkinson and to my fellow students in the research group and Institute without whom this project would not have been so fruitful and enjoyable.

Finally, I want to thank the German Academic Exchange Service, DAAD, and IPTME for partially funding this project.

ABSTRACT.

A number of simultaneous interpenetrating polymer networks (IPNs) were investigated with regard to morphology and energy absorbing ability. The materials were all based on polyurethane (PUR) with the second polymer components being polystyrene (PS) or poly(ethyl methacrylate) (PEMA). Also, three-component IPNs were synthesised. This was achieved by incorporating functionalised PS latex particles into a PUR/poly(butyl methacrylate) (PBMA) IPN. The morphology of the IPNs was determined with dynamic mechanical thermal analysis (DMTA), transmission (TEM) and scanning (SEM) electron microscopy and modulated-temperature differential scanning calorimetry (M-TDSC). The mechanical properties were investigated using tensile testing and hardness measurements.

The PUR/PS IPNs were found to be grossly phase separated at every composition, even when crosslinked at very high levels. However, a structural modification of the materials was conducted by introducing inter-network grafting, compatibilisers and ionic interactions. All three structure modifications proved successful in achieving a finer morphology. By conducting a stirred synthesis, a very complicated morphology with a very high and broad transition was obtained. The PUR/PEMA IPNs were semi-miscible and the 70:30 composition exhibited a very broad, almost rectangular, transition as evidenced by DMTA data. Phase domains between 1 - 500 nm were found by TEM. The degree of mixing and, thus, the location and breadth of the transition could be adjusted by varying the composition and the crosslink densities in both networks. Also, variation of the chemical nature of the PUR soft and hard segments proved successful in obtaining a broad transition range.

Materials with a controlled microheterogeneous morphology which exhibited excellent energy absorbing characteristics were developed. PUR/PEMA IPNs generally exhibited better damping properties as indicated by the area under the linear loss modulus (LA) and loss factor (TA) curves. Some of these materials exhibited values for the loss factor of ≥ 0.3 spanning a temperature range of more than 170°C. The study of IPNs containing latex particles revealed promising results. Further concentrating on this approach might yield damping materials with even broader energy absorbing temperature/frequency ranges.

TABLE OF CONTENTS.

3. EXPERIMENTAL

3.1 Materials

3.2 Experimental Apparatus

3.3 Experimental Technique

3.4 Analysis of Products

4. THE POLYURETHANE NETWORK

5. POLYURETHANE / POLYSTYRENE IPNS

1. INTRODUCTION

1.1 Need for Multicomponent Polymers and High Damping Materials

Applications for high technology polymers are growing in such diverse fields as biomedical applications, electronics and in the automotive industry. Novel speciality polymers are replacing steel, wood or other polymers to result in improved products, and they are also needed in new applications. However, the development of new monomers to produce these speciality polymers is expensive, time-consuming and difficult[1]. Therefore, alternative ways of developing polymeric materials with new improved properties have to be investigated. Recently, new metallocene catalysts[2] were developed which allowed the production of a great number of olefin and aromatic polymers with a controlled molar mass, narrow polydispersity and extreme stereoregularity. This resulted in materials with new enhanced properties. Another way of engineering materials with improved properties is by blending different polymers[3]. Amongst the various types of polymer blends that exist are statistical, block and graft copolymers. A more recent type of polymer blend are interpenetrating polymer networks (IPNs)[4]. Interpenetrating polymer network technology was used in this study, since it allows a good control over the blend morphology. Controlling the IPN miscibility and morphology is of crucial importance for the development of good energy absorbing materials.

While this Century is primarily concerned with energy production, uncontrolled energy evolving as a by-product from the use of machinery is unwanted and has to be absorbed. Apart from heat, this uncontrolled energy can be experienced in form of vibrations and sound i.e. noise. Sound waves have a longitudinal character while pressure waves travelling through solids, vibrations, can have longitudinal and shear character[5].Vibrations and noise can be encountered everywhere[6,7], such as the workplace, in the household, in a ship or car, in the air or even in space. The detrimental effect of vibrations and noise is obvious. They can cause[6] fatigue in products which leads to failure, malfunction and lower performance levels. Furthermore, they can interfere with processes, decrease the product life cycle and increase maintenance costs. Vibrations also might produce noise. For an average young person, the range of vibrational disturbances perceivable as sound spans 3

decades from 20 Hz to 20 kHz[8]. Noise has been proven to be a considerable health hazard[9] and sensibility in this area is growing. Studies have revealed that exposure to noise may have severe consequences depending on level, length and type of noise exposure. Besides the evident effects like permanent and irreversible hearing loss, communication, task and sleep interference and annoyance, there are more subtle consequences. Noise may produce high blood pressure, contribute to heart and circulatory diseases and cause extreme emotions and behaviour[10].

It is thus evident that damping is extremely important and essential[11] for individuals as well as for industry and in some military applications. Recently, damping is becoming even more important[12] due to the trend towards energy conservation. This brings about lighter weight and higher speed products, sensibly increasing acoustic and vibrational disturbances. Damping is omnipresent in nature, and, therefore, all acoustic and vibrational energy is ultimately degraded into thermal energy[13]. This may occur[14] through losses at medium boundaries or frictional and heat conduction losses in the medium. For damping purposes, however, only energy dissipation that takes place in short times and over small distances is of interest.

In order to design a damping system, there are several steps to consider. Amongst others, these include[15] to define the environmental conditions and the damping system required to eliminate the problem. This is followed by the selection of the appropriate damping materials. Finally, the required damping design has to be developed. Acoustic damping can be achieved[16] in different ways. One method is to isolate the sound, i.e. through quarter-wave plates. The other principle is based on the destructive interference of the sound waves, which can be achieved with honeycomb structures and hollow cavities. A rather novel method of vibration damping using the destructive principle are piezoelectric ceramics[17]. They convert mechanical energy through changes in geometrical shape into electrical energy and subsequently into heat. Further damping devices are electromagnetic vibration dampers consisting of magnet-conductor configurations[18].

This research is concerned with the development of damping materials with a high intrinsic energy absorbing ability spanning a broad temperature range. The interesting method with respect to this research is damping with polymers, polymer blends and polymer composites. In viscoelastic polymers, the most important mechanism of

energy attenuation[13] is the conversion into heat by molecular relaxation processes. Damping with polymers is a particularly good way, because of the ease of their application by either trowel, brush or spray[19,20], their high efficiency combined with versatility, and, finally, the relatively low costs involved. In damping with polymers, two major applications of polymeric damping system can be encountered[7,8]; extensional and constrained layer systems. In extensional damping systems, one single polymer is applied on the carrier surface[21,22]. Constrained layer damping consists of a two-layer system[23] where the viscoelastic damping material is located between a substrate and a stiff constrained layer.

As already stated, this research is concerned with the development of polymeric damping materials with a high intrinsic damping ability. The IPN technology was used to combine two polymer networks resulting in materials with a controlled degree of phase separation. IPNs of a microphase morphology are capable of adding to the previously mentioned advantages of polymers a further crucial one, that is broad service temperature and frequency ranges. IPNs that have been investigated for this kind of application are surveyed in chapter 2. More work on the IPN morphology, and means of controlling the transition temperatures of polymer blends is necessary to gain a better understanding of how synthesis parameters influence the structure and properties of complex polymer systems. Generally applicable methods of increasing polymer miscibility resulting in a controlled morphology are needed. In using those principles for damping applications, multiphase polymers with a broad transition zone can be developed. Thus, a wider choice of high damping materials will become available. This will enable the damping engineer to choose the most appropriate viscoelastic damping material for any given application in any given environment.

1.2 Objectives of the Present Study

The purpose of this study was two-fold. First, the study was concerned with a detailed investigation of the morphology, phase continuity and mechanical properties of simultaneous IPNs. These IPNs were composed of an elastomeric polyurethane network containing the aliphatic tetramethylene xylenediisocyanate which had not been used previously in IPN preparations. Polystyrene and poly(ethyl methacrylate) were chosen as second polymers in order to investigate immiscible and semi-miscible

polymer pairs. The control of the degree of miscibility in an IPN is crucial for the development of a wide damping range. Therefore, it was attempted to gain a better understanding by which means and to what extent the IPN microstructure, the phase domain size and its distribution, and the phase continuity can be influenced. Besides different second polymer components, the factors studied comprised variations in the polyurethane network, such as the chemical nature and molar mass of the soft segment and the type of the hard segment. Further factors included (i) the IPN composition with regard to the two components, (ii) the crosslink densities in both polymer networks, and (iii) the introduction of chemical bonding and (iv) physical interactions between the polymer networks. Finally, the direct determination of the morphology via transmission and scanning electron microscopy was compared with indirect methods, principal among them dynamic mechanical thermal analysis and modulated-temperature differential scanning calorimetry.

Second, it was attempted to develop polymer-based damping materials with a high intrinsic damping ability using the IPN topology. Choosing two polymers with their transition regions far apart might result in IPNs capable of high damping over a broad temperature and frequency region. In order to further broaden the damping range three-component IPNs were developed by the incorporation of functional latex particles into an IPN. This research should have a very practical use in improving and widening the choice of possible damping materials available. Also, it was intended to develop materials for different temperature regions.

Thus, in brief, the principal objectives of the present study were the following.

1) To elucidate and compare the morphologies, i.e. the phase domain sizes and shape, of an immiscible polyurethane/polystyrene IPN and a semi-miscible polyurethane/poly(ethyl methacrylate) IPN.
2) To investigate the phase continuity of the latter as a function of IPN composition.
3) To develop IPNs of a controlled microheterogeneous morphology by variation of the crosslink denisty and the introduction of chemical and physical intermacromolecular interactions.
4) To develop high damping IPNs and characterise their damping characteristics using dynamic mechanical thermal analysis.

5) To develop three-component IPNs with glassy functionalised latex particles to extend the damping and useful operating ranges to higher temperatures.

1.3 Research Plan

1.3.1 Experimental Plan

A multitude of factors are important for the development and investigation of IPNs with high damping characteristics. The schematic overview in figure 1.1 shows important factors influencing the IPN morphology and, thus, the IPN damping properties and where this research tackled the task.

First, a number of polyurethane homonetworks with different crosslink denisties and hard and soft segments were prepared. The influence of the variation of the PUR network on the dynamic mechanical properties was studied. This was done with the aim of choosing one suitable PUR material for intense study in the IPNs. Furthermore, a basis for comparision was obtained for the variation of the PUR network in the IPNs. The knowledge of the behaviour of the PUR homonetwork was crucial in order to be able to explain the by far more complicated IPN behaviour. With the selected PUR network, the influence of the composition and the crosslink densities in both networks were investigated in an immiscible polyurethane (PUR)/polystyrene (PS) IPN and in a semi-miscible polyurethane/poly(ethyl methacrylate) (PEMA) IPN. Following the composition studies, mainly one composition was chosen for the subsequent studies such as, for example, the crosslinking study. This was the 60:40 composition for the PUR/PS IPNs and the 70:30 composition for the PUR/PEMA IPNs. Both these compositions exhibited very special properties. Furthermore, both polymers were present in sizeable quantities. From dynamic mechanical thermal analysis, contributions from both components were easily detectable allowing for a good observation of any possible transition shifting or broadening effect.

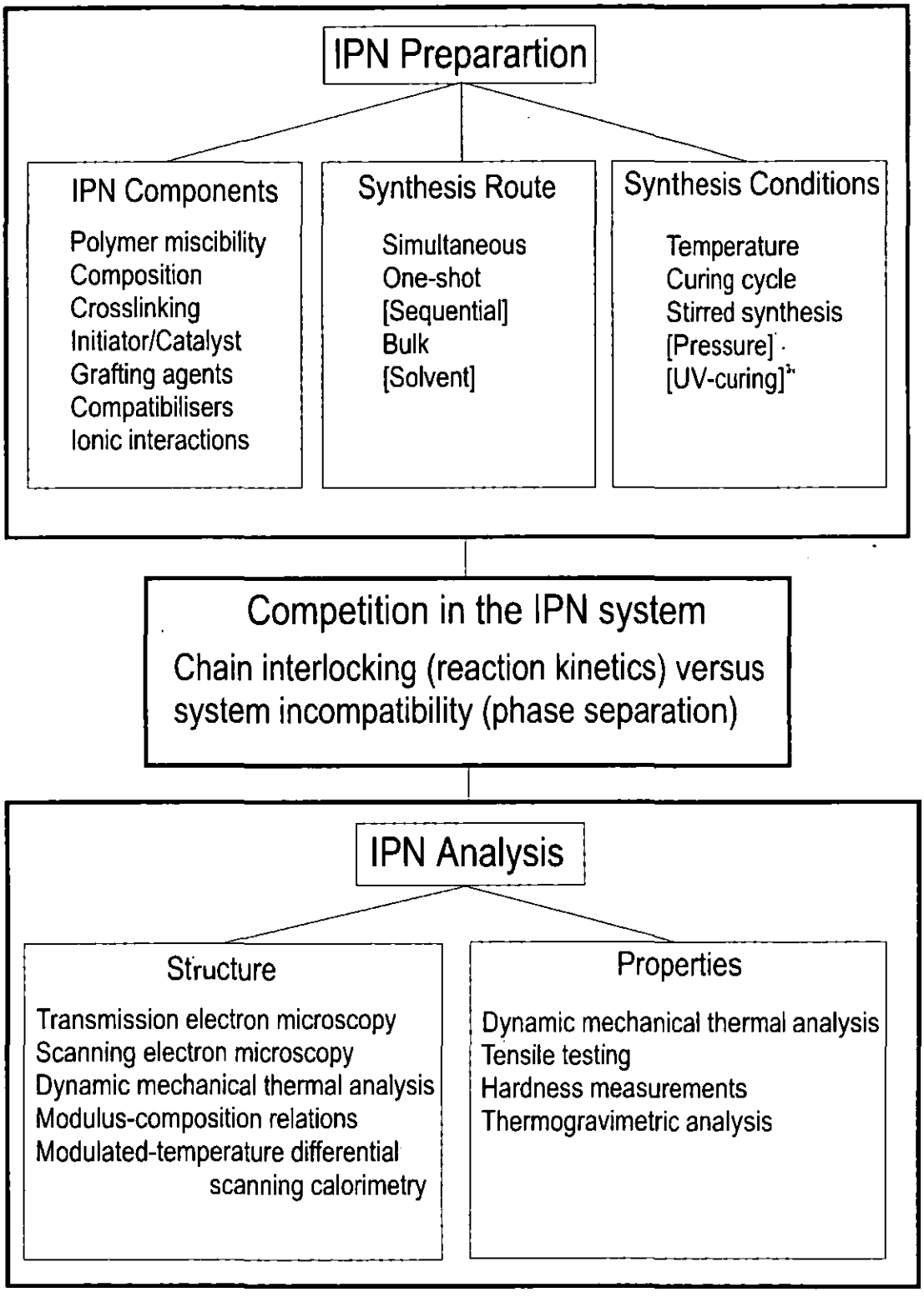

Figure 1.1 Development and investigation of IPNs for damping.

Modification of the immiscible PUR/PS IPN at the 60:40 composition was conducted to bring about increased component mixing. The techniques used were the introduction of chemical bonds between the two networks through the use various difunctional grafting agents, the incorporation of a number of urethane acrylate compatibilisers into the PS network and the introduction of ionic interactions via carboxylic acid- and tertiary amine group-containing monomers. The influence of the variation of the PUR soft and hard segment was studied in the 70:30 PUR/PEMA IPN.

To broaden further the damping range, functional PS latex particles were introduced into a 70:30 PUR/poly(butyl methacrylate) IPN. Generally, it has to be re-emphasised that because of the multitude of variables, the design of the experiments had to be chosen in a way to restrict the number of IPN materials to be synthesised. Therefore, only the best materials such as the 70:30 compositions for the PUR/PEMA IPN were taken to conduct further studies, rather than to investigate all possible combinations.

1.3.2 Documentation of the Research

Following this introduction, the theoretical background is divided up into 3 parts, (i) interpenetrating polymer networks, (ii) damping with polymers and (iii) polyurethane network. These topics are essential for the understanding of this investigation and, thus, briefly reviewed with special focus on this research. Reference is usually made to how far the background and literature information concerns the present study.

Characterisation results of raw materials are given in the experimental chapter. Although most raw materials were characterised, only few examples are given for reasons of limited space. Furthermore, the synthesis of the in-house prepared compatibilisers is dealt with in the same chapter. An exception to this was made for chapter 7 (IPNs containing latex particles), where the synthesis and characterisation was included in the results chapter. This was done since the preparation of the IPNs with latex particles differed considerably form that of the two-component IPNs. The principal analysis techniques together with the instruments used for the

characterisation of the IPN films are briefly introduced in the experimental chapter. Emphasis is placed on the dynamic mechanical thermal analysis (DMTA) since the latter was the principal technique used in the present study, giving information about the IPN morphology and damping characteristics.

Results and discussion are presented in the chapters 4 to 7. DMTA data of all materials synthesised are shown under the respective subdivisions together with results from tensile testing. In many cases the DMTA Tg behaviour was compared to that obtained by modulated-temperature differential scanning calorimetry (M-TDSC). In most cases the morphology was further elucidated by transmission and scanning electron microscopy. Further characterisation techniques that were less commonly used such as, thermogravimetry and modulus-composition studies were compiled under the respective sections of the IPNs investigted.

The report concludes (chapter 8) by summarising the findings of the various IPN multiphase morphologies and by delineating how control of the IPN morphology was achieved to produce high damping materials.

2. BACKGROUND AND LITERATURE SURVEY

2.1 Interpenetrating Polymer Networks (IPNs)

The properties of polymers and polymer blends are dependent upon the chemical structure of their constituent monomers, on their topology and their morphology. Research into different polymer topologies and the blending of polymers has reached paramount importance, since the development of new monomers is very difficult and expensive[1]. The use of different polymer topologies (figure 2.1) represents a means of combining various existing polymers resulting in special properties.

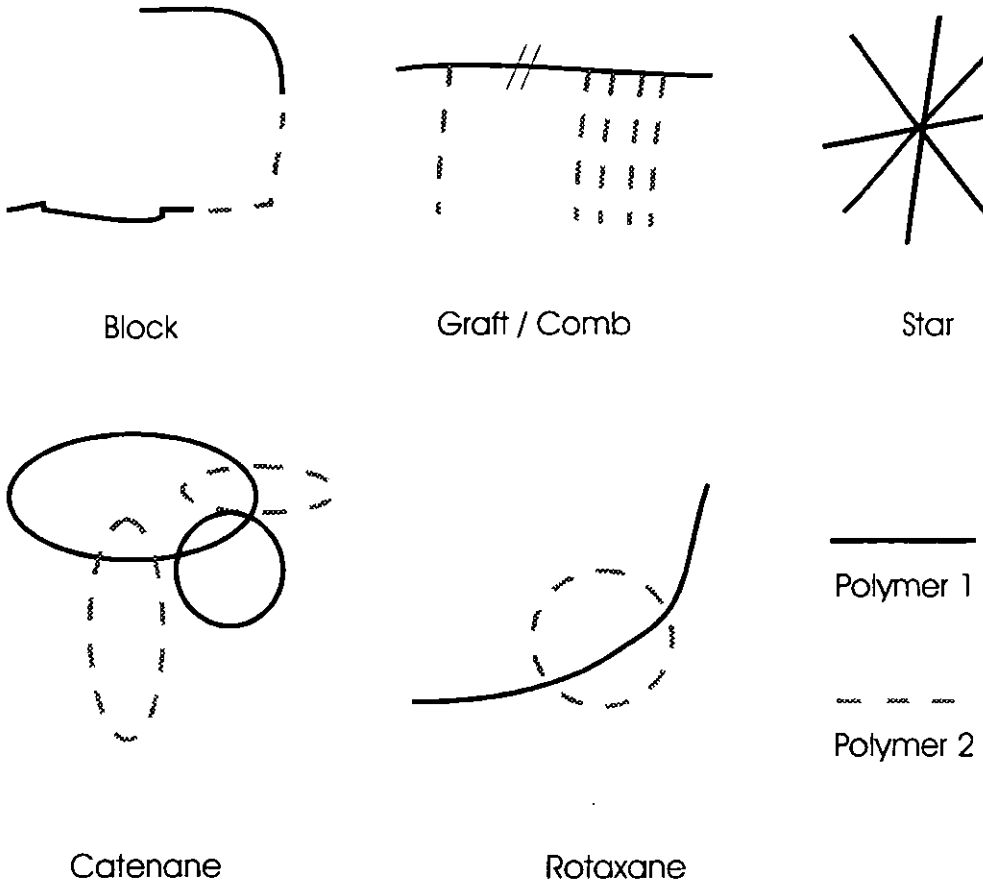

Figure 2.1 Polymer topologies and catenane structure.

Interpenetrating polymer networks (IPNs) play a very distinctive role with this respect. Due to their catenane structure (figure 2.1), a forced mixing on a segmental/molecular basis is possible. This in turn might create a very broad transition region spanning both polymer transitions[1]. The IPN topology was chosen for this

study, since for good energy absorbing materials high damping over a broad temperature and frequency range is desired. Some general terms and concepts concerning IPNs are reported below. Special attention is given to the IPN morphology, since this is the preponderant characteristic[4] of an IPN, influencing mechanical and physical properties such as its damping ability. The subject has been recently reviewed[4,24,25].

2.1.1 Definition, History, Synthesis and Applications of IPNs

Definition. An interpenetrating polymer network may be defined as an intimate combination of two or more network polymers, one of which is in network form, the other being synthesised in the presence of the first[4]. Ideally, only physical entanglements between the networks exist and no covalent bonds are present. A schematic representation of a full IPN, a semi-IPN and possible network defects is shown in figure 2.2.

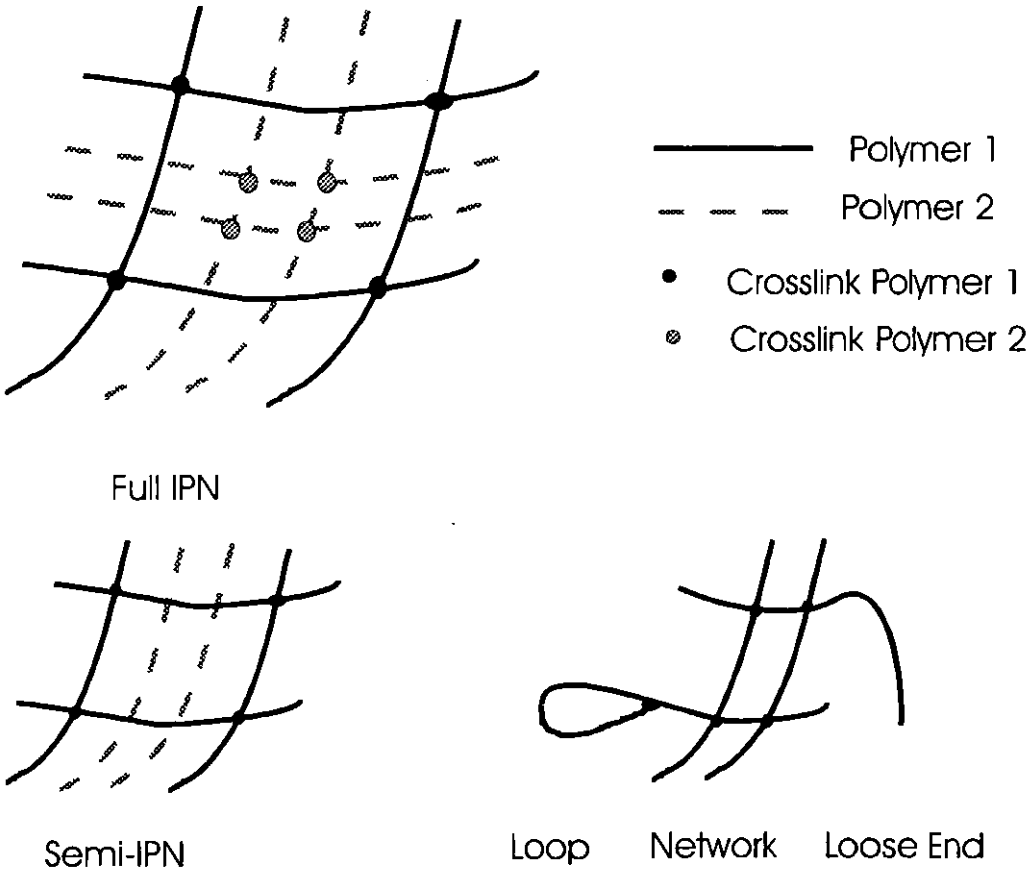

Figure 2.2 Interpenetrating polymer networks and network defaults.

IPNs can also be characterised by a high entropy of mixing, comparing the monomer - monomer mixing in simultaneous IPNs to polymer - polymer mixing in polymer blends. It is believed that the synergistic effects[24,25] in their properties spring from the catenane structure, i.e. interlocking rings with no chemical bonds between them. Also, possible grafting during the network formation could account for the special properties. Technically, IPNs are a kind of polymer blend, yet, they can be distinguished[25] from simple block and graft polymers by their characteristic properties. IPNs are thermosets, therefore, swell but do not dissolve in solvents and creep and flow are suppressed[4]. The latter statements do, however, not apply to thermoplastic IPNs[26]. A classification of the different IPN types is given[27] in table 2.1.

Table 2.1 Different types of interpenetrating polymer networks.

IPN Type	Characteristics
Homo IPN	Both networks consist of the same polymer.
Sequential IPN	Monomer 2 is swollen in network polymer 1 and polymerised in situ.
Simultaneous IPN	Monomers 1 and 2 and their cross-linking agents and initiators are introduced simultaneously and polymerised by non-interfering modes.
Semi-1 IPN	IPN in which polymer 1 is crosslinked (network) and polymer 2 is linear.
Semi-2 IPN	IPN in which polymer 2 is crosslinked (network) and polymer 1 is linear.
Pseudo IPN	IPN in which one polymer is linear (alternate notation to semi IPN).
Elastomeric IEN	Two latex emulsions containing elastomeric polymers are mixed and subsequently crosslinked.

Latex IPN	Sequential IPNs in which both networks are present in the individual single latex particles. A core shell structure can be built up by first polymerising monomer 1 (seed latex) and subsequent addition of monomer 2 (without new emulsifier).
Thermoplastic IPN	IPN of two linear polymers containing physical cross-links only.
Grafted IPN	Both networks are connected by chemical bonds (e.g. by addition of multifunctional monomers or through grafting sites in network 1).
Filled IPN	IPN containing inorganic (or organic) fillers.

History and nomenclature. Pioneers in the field of IPN research were Aylsworth[27] early in this century and Millar[28] in the beginning of the sixties. The latter created the name interpenetrating polymer network. The type of IPN he investigated were polystyrene/polystyrene homo IPNs which are still referred to as Millar IPNs. The strong interest in IPNs commenced in 1969, when two papers by Sperling[29] and Frisch[30] were published on IPNs prepared from dissimilar network polymers. Both research teams are still very active today (1996). They have greatly contributed to the interest in these materials, an interest which is mounting steadily as it is documented through several hundred literature citations[31]. Despite the intensive research into IPNs that has been going on for several years, no final decision about the nomenclature has been made. A nomenclature document has been published by the IUPAC Nomenclature Committee[32] and is now under consideration[33]. The proposal includes the use of cross-polyurethane-inter-cross polystyrene to describe an IPN that is composed of a polyurethane and a polystyrene network blend. In most publications, however, the shorter form, PUR/PS IPN, is used and, for reasons of simplicity, it will also be employed throughout this study.

Synthesis of IPNs. As already hinted through the multitude of IPN types (table 2.1), a great number of synthesis methods for IPNs exist[4,34,35]. The following represent the three major synthesis routes.

(a) **Sequential IPNs.** Monomer 1 is polymerised first. The resulting polymer network is then swollen with monomer 2, crosslinker and initiator and polymerised in situ[36]. One disadvantage of this preparation mode is that sufficient time has to be allowed for the monomer 2 mixture to be distributed homogeneously in polymer network 1. Also, because of its synthesis procedure, not all compositions can be prepared. The composition range is determined by the extent to which network 1 can be swollen with the monomer.

(b) **Latex IPNs.** A latex IPN is made by conventional emulsion polymerisation techniques. First, the monomer 1 network is synthesised in the micelle, then, monomer 2 is added without new soap[37-40]. The advantage of this method is that the resulting network does not extend macroscopically throughout the finished material. Thus, latex IPNs can be processed like thermoplastics. A slight drawback, however, is that interpenetration of the two networks is poor and predominantly core-shell morphologies have been obtained[4] with the more hydrophilic polymer network constituting the shell.

(c) **Simultaneous IPNs.** Both monomers or prepolymers are polymerised in the presence of each other by independent, non-interfering reaction routes[24,25,41]. Materials prepared by the simultaneous route have been found to exhibit particularly good properties. For this reason, and for the ease of preparation, this preparation mode was chosen in this study. It will be further elaborated in section 2.1.2.

Applications of IPNs. Applications of IPNs can be found[4,24,25] in very different areas. Very often they are not labelled as IPNs, and, consequently, not recognised as such. Applications include the use as sheet moulding compounds[42] and in reaction injection moulding applications[43], as ion exchange resins[44] , dialysis[45] and gas separation[46] membranes and in dental applications[47]. IPNs are employed to improve leather articles[48], and are seen in the fields of coatings[49] and adhesives[50]. A more recent application is as devices in controlled drug delivery systems[51]. Because of their ability to phase separate reversibly at high temperatures and, thereby, reflect impinging sunlight, IPNs have found use in solar panels[52] to regulate the temperature of the underlying materials. Their very special mechanical properties make them highly interesting for noise and vibration damping[13,53-55]. The latter application was investigated in the present study. All IPNs studied were simultaneous IPNs,

synthesised via the one-shot process. Due to the reaction conditions, the polyurethane network polymerised first in most cases. Besides the full IPN type, also grafted and to a very limited extent semi- IPNs and polyblends were investigated.

2.1.2 Simultaneous Interpenetrating Polymer Networks

As already described, this technique involves[4,24,25,56,57] the simultaneous mixing of two monomers or prepolymers together with the crosslinkers and initiators or catalysts followed by the synthesis of two polymer networks by independent reaction mechanisms. The most vital requirement is that the reactions proceed by two non-interfering pathways[4], since otherwise one single copolymer network would be obtained. In most cases, a condensation reaction is conducted together with a polyaddition reaction. The major advantage of the simultaneous preparation process, which is also called the one-shot technique, over the sequential preparation is its simplicity[24]. As opposed to the sequential method, the simultaneous method is a one-step preparation and does not require to allow the swollen polymer network time for an homogeneous distribution of the monomer and crosslinker 2 and the initiator. Also, simultaneous IPNs can be easily processed, for example[4], by prepolymerising the mix until just short of the gel point, followed by pumping it into a mould or die, with continued polymerisation. PUR/epoxy simultaneous IPNs[43] are, for example, used in reaction injection moulding (RIM) applications. As a consequence, the simultaneous preparation can be most readily employed in industrial applications which has led to a comprehensive study of these IPNs[4]. Besides the above mentioned ease of preparation, simultaneous IPNs allow for a wider range of properties to be engineered[58]. In sequential IPNs, the maximum incorporation of monomer 2 depends upon the equilibrium swelling of polymer 1. Therefore, a wider range of compositions can be produced in simultaneous IPNs, where any composition of monomers can be combined.

A number of comparisons[56-59] between simultaneous and sequential IPNs have been made. However, no clear conclusions have been reached in terms of the influence of the preparation mode on the IPN morphology. Akay and Rollins[58] compared simultaneous and sequential PUR/PMMA IPNs. Scanning electron micrographs indicated that the simultaneous IPNs were considerably more homogeneous than the corresponding sequential ones. Also, the simultaneous synthesis resulted in a greater

synergism with respect to impact strength, elongation at break and tensile strength. However, most researchers found that sequential IPNs exhibited a finer, more homogeneous morphology. Fox and co-workers[59] investigated sequential and simultaneous PUR/poly-(n-butyl acrylate-co-n-butyl methacrylate) IPNs. They found that the simultaneous IPN exhibited a lower and broader loss factor peak than the respective sequential IPN. As a consequence, also greater values for the half-peak width of the loss factor of the simultaneous IPN were found. Both are an indication of greater phase separation in the simultaneous IPN. Regarding the material properties, simultaneous IPNs were found[4] more often than sequential IPNs to exhibit properties better than the average of the two constituent polymers. A possible test of difference between simultaneous and sequential IPNs is whether one network is strained. Sperling[56,57] pointed out that in most sequential IPNs, network 1 is swollen and strained at points in the synthesis, whereas in most of the simultaneous IPNs both networks are relaxed throughout.

It has been found that one key factor determining the morphology of simultaneous IPNs and, hence, their mechanical properties are the relative rates of formation of the two networks[58-65]. Meyer and Widmaier[62-65] were particularly interested in investigating the influence of the kinetics of network formation on morphology and dynamic mechanical properties. They emphasised that even though the monomers are mixed and transferred simultaneously into a mould, the reactions of these monomers do not necessarily proceed at the same time or reaction rate. They, therefore, adapted the term "in situ sequential" IPNs[62] for materials where network 1 was formed before the onset of the reaction of network 2. In principle, three such cases of simultaneous IPNs can be distinguished[56]. Network 1 can be formed first, followed by the polymerisation of monomer and crosslinker 2. Conversely, network 2 can be formed first, followed by the formation of network 1. Also, both networks can be formed in a truly simultaneous way. Reacting one monomer first can be achieved through the appropriate choice of initiator and reaction conditions, since the type and amount of initiator or catalyst and the reaction temperature are crucial for most polymerisations. For example, photo-initiation or initiation via a redox system have be used[66,67] to conduct polymerisations at low temperatures. Recently, a study comparing the three cases of simultaneous IPNs was conducted. Using an acrylate/epoxy system, Suzuki and co-workers[68] found that the IPNs resulting from

the three synthesis variations exhibited markedly different properties. They greatly varied in density and revealed a different morphology. The acrylic monomer polymerised first resulted in a heterogeneous structure, while with the remaining two methods a much more homogeneous product was obtained[68]. Song[69] investigated castor oil-PUR/epoxy-episulfide IPN using small angle x-ray scattering (SAXS) measurements. He found that the phase domains became smaller with decreasing differences in time to gel of the two components. Different results were obtained by Parizel and co-workers[70]. Investigating the IPN morphology using N.M.R. lineshape studies, they found that a sequentially synthesised simultaneous PUR/PAc IPN exhibited a noticeably finer morphology than the corresponding truly simultaneous one. Tung and Hsu[71] investigated the influence of the relative rates of network formation on the dynamic mechanical properties of a simultaneous PUR/poly(methyl acrylate) IPN. Conducting the IPN reaction without PUR catalyst at 80°C resulted in two loss factor maxima. Under these reaction conditions, both reactions were believed to have proceeded simultaneously. By the addition of the PUR-catalyst, dibutyltin dilaurate, and conducting the reaction at 35°C the PUR network was completely formed before the onset of the poly(methyl acrylate) polymerisation. Under these conditions, improved phase mixing as shown as one broad loss factor maximum was achieved. In an early study, Sperling's research team[72] found that simultaneous gelation in an epoxy/poly-(n-butyl acrylate) IPN resulted in a fine phase domain structure, whereas non-simultaneous gelation produced materials with larger phase domains. The materials prepared under non-simultaneous gelation conditions were considerably stronger and had higher tensile strengths.

A great number of simultaneous IPNs with chemically different second polymers have been investigated. These include IPN pairs of PUR/acrylics[72], PUR/methacrylics[58], PUR/styrenics[64], PUR/siloxanes[73], PUR/epoxy[69] and epoxy/acrylic[68]. An entirely radical simultaneous IPN[74] was synthesised by the use of two distinct initiators, monomers of different reactivity (methyl methacrylate and diallyl carbonate of bisphenol A) and by conducting the synthesis in situ sequentially at two different temperatures.

With exception of the last two combinations, all others include polyurethane as one IPN component. The importance of polyurethane[57] in these IPNs is justified by the relatively easy synthesis, the high versatility of polyurethane chemistry and

outstanding mechanical properties of polyurethane elastomers. Two recent brief reviews by Sperling[75] and Hur et al.[76] on PUR/PMMA IPNs confirm the importance of PUR-based IPNs, especially with PMMA as second polymer. In early studies[77-81] by the Kim, Klempner and Frisch team the synthesis and morphology[77], the density and glass transition behaviour[78], the volume resistivity behaviour[79] and the viscoelastic[80] and engineering properties[81] of simultaneous PUR/PMMA IPNs were investigated. Recently, PUR/PMMA IPNs with PUR contents of less than 10% were studied to order to prepare transparent, high impact cast sheets of PMMA[82]. Akay and Rollins[58,83] undertook a full composition study to investigate transition broadening and WLF relationship[83] and morphology and modulus-composition relations[58] in PUR/PMMA IPNs. More studies on the morphology of simultaneous semi and full PUR/PMMA IPNs were undertaken using nuclear magnetic resonance relaxation times[70,84]. Most recently, fundamental studies on gelation and phase separation were conducted by Mishra and Sperling[85]. They developed metastable phase diagrams where the four components (both "monomers" and both polymers) of the model PUR/PMMA IPN system were positioned at the edges of a tetrahedron. This allowed visualisation of the IPN formation process and provided direction for controlling the specific order of three events. These were the gelation of polymer 1, the gelation of polymer 2 and phase separation of polymer 1 from polymer 2. Further, Mishra and co-workers[86] also investigating the partitioning of MMA monomer in late polymerisation stages of simultaneous PUR/PMMA IPNs.

Even though the PUR component allows for much variation, the PURs investigated in IPNs have consisted in most cases of diphenylmethane diisocyanate (MDI) or toluene diisocyanate (TDI) as diisocyanate, butanediol (BD) and trimethylol propane (TMP) as chain extender and crosslinker and poly(oxytetramethylene) glycol (PTHF) or poly(oxypropylene) glycol (PPG) as polyols. Recently, a new avenue has been followed by the use of renewable resource materials[87] as polyols. Castor oil[75] has been proven to be one of the more versatile renewable resource monomers, partly because of its relatively high purity. Patel and co-workers[88] and Sperling and Manson[89] have used castor oil and lesquerella oil as polyols. Both teams were able to prepare PUR/styrenic IPNs with good mechanical properties such as good impact resistance and tensile strength. Also, lignin[90] has been used as polyol to synthesise simultaneous PUR/PMMA IPNs with good mechanical properties. The properties

were found to vary in a predictable manner and could be controlled notably through the variation of the crosslink density.

In combining a rubbery and a glassy network, IPNs ranging from a filler-reinforced elastomeric material to a leathery material and to a rubber-reinforced plastic can be prepared[77]. The properties of an IPN depend on its morphology and in particular on which component becomes the continuous phase.

2.1.3 IPN Morphology and Factors Influencing Phase Separation

IPN morphology and phase separation. The morphology of an IPN is its predominant feature, differentiating it from other polymer blends. It controls the mechanical and physical properties making it an new class of polymeric material[4]. Various degrees of phase separation can be synthesised. In most IPNs, phase separation does occur similarly to other multicomponent polymer systems[56], yet not as extensively as in common polymer blends. The morphology in IPNs can vary from a microphase separation with phase domains of 2 - 50 nanometers in diameter to a macrophase morphology. Highly immiscible polymers may yield phase domains of a few micrometers. The former can only be detected using instrumentation, like transmission electron microscopy with magnifications up to 300,000 times. For the latter the naked eye might suffice. With two miscible polymers complete mixing occurs and a non-resolvable domain structure has been reported for a polystyrene/poly(phenylene oxide) IPN[91]. However, complete homogeneity is a phenomenon rarely achieved[92], not even with homo IPNs.

Two mechanisms of phase separation[93,94] are known in polymer blends, nucleation and growth[95] and spinodal decomposition[96]. For the nucleation and growth mechanism, an initial fragment, the so-called critical nuclei, and some activation energy are necessary conditions. Further characteristics are that the domains tend to be spherical in nature, that their size increases with time and that the diffusion into the immediate vicinity of the nucleus is downhill. In the spinodal decomposition mechanism, interconnected cylinders tend to form and the size of the phases remains constant but their composition changes with time. Further characteristics are[25] that an uphill diffusion from the low concentration region into the domain takes place and that the resulting phases exhibit a high level of interconnectivity. When both mechanisms are observed for the same system, the nucleation and growth mechanism

occurs first, and then switches over to spinodal composition as the system goes deeper into the phase separation region of the phase diagram[25]. Figure 2.3 depicts both mechanisms[94] of phase separation.

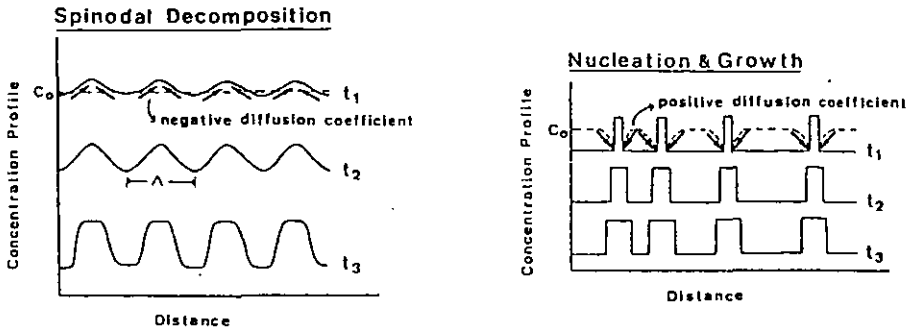

Figure 2.3 Mechanisms of phase separation after Sperling[94]

It is believed that phase separation via the spinodal decomposition mechanism often leads to two highly interconnected phases that extend throughout the entire material. This situation of two phases that are continuous in space is often encountered in IPNs, particularly in simultaneous IPNs that have gelled simultaneously[56]. An illustration of dual phase continuity[97] is given in figure 2.4.

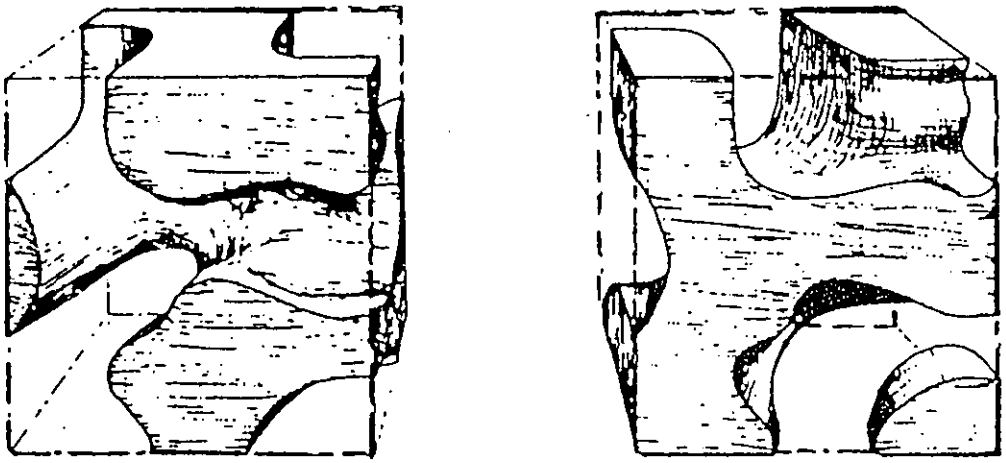

Figure 2.4 Dual phase continuity in IPNs after Gergen[97]

Amongst the factors determining the phase continuity[26,98] in polymer blends are the volume fractions and viscosities of each component. The relative rates of formation of the networks are particularly important in IPNs. The network that forms first[99] is likely to represent the continuous phase.

Materials possessing dual phase continuity exhibit very special properties[4]. Since mechanical and physical properties such as hardness, modulus and glass transition temperature can be related to the phase continuity and blend miscibility, the IPN morphology can be investigated by studying these properties.

Methods of studying the morphology and miscibility. The morphology, i.e. the phase domain size and shape, the phase continuity and the miscibility of polymer blends and IPNs can be investigated by different methods. Electron microscopy techniques such as scanning (SEM)[65] and transmission (TEM)[53,100] electron microscopy are very powerful tools in morphological investigations. A prerequisite for the use of TEM, however, is a sufficient difference in electron density of the two polymers. The electron contrast can be improved by preferentially staining[101] one polymer with osmium[102] or ruthenium tetroxides. If no stainable moieties such as double bonds or reactive groups are present, techniques other than TEM have to be applied. Recently, much research on IPN morphology has been conducted[103] using beam scattering techniques. The latter encompass small-angle light (SALS), X-ray (SAXS)[104,105] and neutron (SANS)[92,106] scattering techniques. The basic principle underlying these techniques is the same, with the wavelength used being the major difference. An incident beam is scattered by the sample and detected at some angle and intensity. The selection of the appropriate scattering technique[1] depends upon the contrast factor and the domain size range to be investigated. The contrast factor is related to the differences in refractive indices (SALS), electron densities (SAXS) and neutron-scattering cross-section (SANS).

The miscibility of a polymer blend can be characterised[1,107] studying optical, morphological, glass transition temperature and crystalline melting behaviour and molecular interactions and relaxation times. The Tg of a polymer blend is most commonly used to conduct miscibility and phase composition studies of polymer blends. This can be done using differential scanning calorimetry (DSC)[108], dielectric

relaxation methods (DETA)[109] and dynamic mechanical thermal analysis (DMTA)[58]. The dynamic moduli obtained from the DMTA can also be used in modulus-composition studies[110,111] to make predictions about phase continuity. Limitations to the use of the Tg for miscibility studies are encountered[1] for polymers with similar Tgs, and compositions with only a small quantity of one polymer being present. Furthermore, only domains down to the order of 10 nm can be resolved. Spectroscopy such as nuclear magnetic resonance spectroscopy (NMR)[70,84] and infra-red spectroscopy (IR) are by far more sensitive methods in assessing the polymer blend miscibility. The NMR method[107] measures the mobility of specific groups which is influenced by miscibility. The miscibility of certain polymer blends containing hydrogen bonds can be studied by IR spectroscopy. This is due to the fact that hydrogen bonds are very strong and affect the molecular vibrations of nearby groups.

One of the least sensitive technique to study blend miscibility is to evaluate the clarity or optical transparency of a film. The transparency is controlled by the size of the phase domains. Thus, clear material indicates very small or non-existent domains. However, the latter is only valid if the refractive indices of both polymers are different and the domain sizes are not much smaller than the wavelength of the light. Nevissas et al.[112] investigated PUR/PS IPNs with respect to transparency. They found that inter-network grafting is a more powerful means of affecting the IPN morphology than is increasing the crosslink density in either of the networks.

In this study, TEM, SEM and Tg methods i.e. DMTA and modulated-temperature DSC (M-TDSC) were extensively used to investigate IPN morphology and the factors influencing it. These techniques are further described in the experimental chapter.

The previously mentioned methods to study the polymer morphology have their specific limitations and cover different domains size ranges. Figure 2.5 indicates the methods that can be used for given domain size ranges[107].

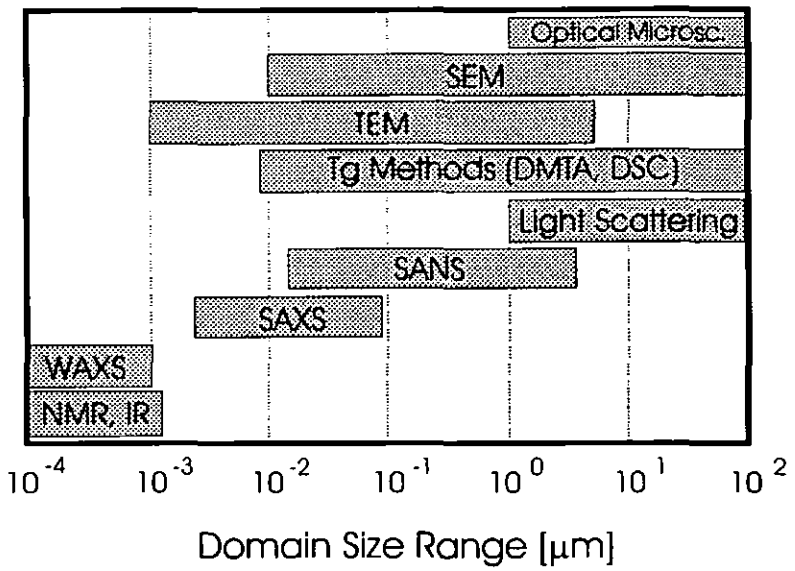

Figure 2.5 Size range covered by various techniques[107]

2.1.4 Factors Influencing IPN Morphology

The factors influencing IPN morphology are numerous[4,24] and are inter-related. No clear division between contributing thermodynamic and kinetic factors[113], chemical and physical characteristics and the preparation process[114] can be made. The underlying competition in the forming multiphase material is the chemical kinetics of crosslinking and network formation against the physical kinetics of phase separation. The following points are crucial in determining the morphology of simultaneous IPNs.

(a) Selection/miscibility of the polymer pair.

(b) Method and order of synthesis.

(c) Composition of the IPN.

(d) Crosslink density of the networks.

(e) Structure modification of one or both components (grafting, ionic interactions).

(f) Reaction rates and network formation rates.

(g) Synthesis conditions (temperature, pressure, solvent).

The above factors have been subject to intensive investigations. The most important ones have been proven to be the miscibility of the polymers, the method and order of synthesis, the IPN composition and the extent of crosslinking and inter-network grafting. The latter factors will be outlined in some more detail, since they concern this investigation.

Miscibility of constituent polymers. Phase separation in IPNs depends primarily on the miscibility of the constituent homopolymers[24]. Nearly all two-polymer compositions form immiscible phases, as in graft and block copolymers. The two-phase morphology is due to the well-known phenomenon of thermodynamic immiscibility[3,115]. However, some exceptions[116,117] exist. This phenomenon of thermodynamic immiscibility is explained by the Gibbs equation for the free energy of mixing. The Gibbs free energy of mixing ΔG_m is expressed as

$$\Delta G_m = \Delta H_m - T\Delta S_m, \qquad (2.1)$$

where ΔH_m is the enthalpy of mixing, T the absolute temperature in K and ΔS_m the entropy of mixing. For spontaneous mixing to occur ΔG_m must be negative. On mixing of two polymers, the entropy is always positive, with the entropic term increasing with temperature[118]. However, in polymers, contrary to small molecules, the gain of entropy on mixing long chain molecules is very low, thus, usually making the enthalpy the decisive factor. The enthalpic term is governed[93,118] by the solubility parameter which is the square root of the cohesive energy density. For most polymer pairs, the heat of mixing is positive. An exception are blends involving component specific interactions, such as hydrogen bonding. In general, miscibility of two polymers is likely if the difference in their solubility parameter δ is less than 0.3 $(J\ cm^{-3})^{1/2}$. Phase diagrams of two-component polymer blends considering composition and temperature have been constructed[3]. Polymer blends may either exhibit a lower critical solution temperature (LCST) or an upper critical solution temperature (UCST) (figure 2.6).

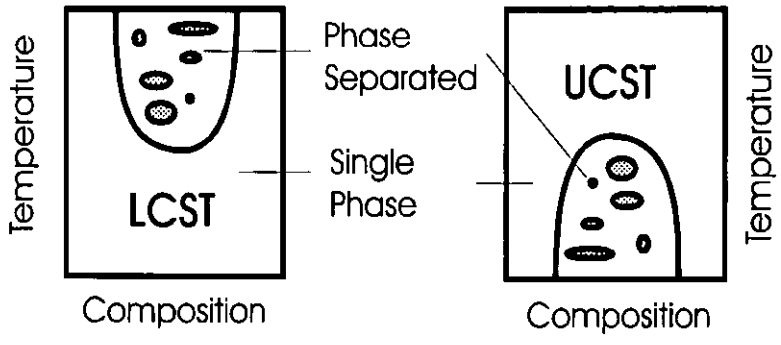

Figure 2.6 Schematic phase diagram showing LCST and UCST.

A lower critical solution temperature, with phase separation occurring as the temperature increases, is more commonly encountered. This is due to the disappearance of intermolecular attractive forces that tend to be overruled by the high internal energy of the molecules[57]. Usually positive heats of mixing result in overall positive ΔG_m, which is an indication of poor mixing and phase separation. For a free energy of mixing near zero, a microheterogeneous structure tending towards homogeneous morphology is present. The importance of this structure for damping is emphasised in section 2.2. So far, very few phase diagrams for IPNs have been developed[57, 85] and it is still unclear whether IPNs tend to exhibit an UCST or a LCST. The latter was observed[52] in a poly(propylene oxide)/styrene-hydroxyethyl methacrylate IPN that reversibly phase separated at high temperatures and was used to protect solar panels[52] from overheating.

Thus, phase separation occurs because as the molecular weight increases ΔG_m changes from negative to positive. In IPNs, however, complete miscibility of the polymers is not necessary to result in materials with little phase separation[4]. Permanent entanglements, once formed by interpenetration, restrict chain mobility and so prevent phase separation from taking place. Therefore, phase separation is kinetically controlled[119,120] by the rate of network formation as opposed to the rate of phase separation. If gelation happens before the onset of phase separation, then the phase domain size tends to be small. However, if the miscibility of the polymers is very poor, then, the thermodynamic forces are predominant and act before the kinetic ramification (gelation) can prevent phase separation. In particular, in simultaneous IPNs, the latter will result in large phase domain sizes[57].

Method and order of synthesis. As already mentioned in section 2.1.2, sequential IPNs tend to be less phase separated than their simultaneous counterparts. Furthermore, simultaneous IPNs do not exhibit the maximum in mechanical properties and the greatest amount of homogeneity if synthesised in a truly simultaneous way. Meyer et al.[121] recently found in a study on PUR/polystyrene (PS) IPNs that if the conversion curves of the PS formation were close (or crossing) to the PUR, only poor PUR yields and mechanical properties resulted. This confirmed his earlier results[122]

and similar findings were experienced by Touhsaent et al.[72] in an epoxy/polyethyl acrylate simultaneous IPN.

Generally valid, however, particularly for sequential IPNs, is the finding of the predominant effect of the first formed network[36,123]. Huelck and co-workers[36] studied sequential poly(ethyl acrylate)/PS IPNs varying the order of synthesis. By inverting the order of synthesis, they found that the first network formed executed the greatest control over the morphology. Donatelli et al.[100] made similar findings. Both attributed this to the fact that the first network constitutes the more continuous phase in the system. In general, the polymer with the higher concentration or the lower viscosity constitutes the continuous phase in a polymer blend[4]. Although, if both IPN polymers are crosslinked very often a dual phase morphology develops.

IPN composition. The weight fractions of each polymer in the IPN strongly determine the material properties. In combining an elastomeric and a plastic polymer, a reinforced rubber or a high impact plastic are obtained, depending upon which materials constitutes the continuous phase.

Recently, Akay and Rollins[58,83] investigated the composition range of simultaneous and sequential PUR/PMMA IPNs. They compared the elastic modulus to the modulus-composition models by Davies[124,125] and Budiansky[126]. The former predicts dual-phase continuity which is expressed by a higher modulus than the linear logarithmic rule of mixing. The Budiansky model predicts phase inversion at mid-range compositions. Plotting the elastic moduli versus IPN composition, Akay and Rollins[58,83] found the sequential IPN to comply with the dual-phase continuity model, whereas the simultaneous IPN followed the phase inversion model. Phase inversion took place around the 70:30 PUR/PMMA composition.

Several researchers have found[4] that phase inversion occurred at compositions between 20-40% of polymer 2. The Kim, Klempner and Frisch team investigated simultaneous PUR/PMMA[77,80] and PUR/PS IPNs[127] varying the composition. For both IPNs, they found phase inversion to take place between the 80/20 and the 70/30 composition as substantiated by dynamic mechanical analysis, hardness measurements and transmission electron microscopy.

Extent of crosslinking. The crosslink density is believed[25] to be an important factor influencing the network morphology. A tighter network restricts the size of the phase domains and, thus, results in a finer morphology. This is true for semi and full IPNs. In the latter a marked difference was observed between a high crosslink density in network 1 or network 2. Donatelli et al.[100] found that a high crosslink density in network 1 limits the domain size of network 2 in the IPN. Hourston et al.[50,128,129] investigated the relation between crosslink density, morphology and mechanical properties in PUR/PMMA semi-2 IPNs. In order to establish this relation, they determined the average molecular weight between the crosslinks, M_c, by equilibrium swelling and the Mooney-Rivilin technique. Varying the amount of divinylbenzene in network 2, they found[128] with decreasing M_c an increase in the degree of mixing. This was expressed through the shift and decrease in size of the PUR peak, and an increase in the loss factor peak width. The shift of the PMMA Tg peak to higher temperatures (and not inwards as would be expected because of increased mixing) was attributed to both the copolymer effect and the decrease in M_c. Similar results were obtained in another study on semi-2 IPNs by Hourston and McCluskey[50]. Their study[129] on semi-1 IPNs, however, revealed clearly that increasing the crosslink density in the first formed network produced a much more dramatic effect than experienced when increasing the crosslink density in the second network.

High degrees of phase mixing in polymer blends as obtained through increased crosslinking are highly desired for energy absorption applications where broad glass transitions ranges are needed. However, high levels of crosslinker decrease the values for the loss factor and bring about stiffening and brittleness of the material. As a consequence, limits of crosslinker incorporation do exist for damping materials. However, it was proven in some studies that relatively small percentages of crosslinking agent are sufficient to bring about greater phase mixing. Nevisass et al.[130] found an increase in transparency, i.e. phase homogeneity, with levels of 1-3 % crosslinking agent. A 5% level did not exhibit any improvement over 3 % in the PUR/PS IPN.

Thus, generally, an increase in crosslink level (especially in network 1) may have positive repercussions on the morphology, creating a finer cell structure. Sperling and Widmaier[131] pointed out that even though a polymer becomes more immiscible as the

molar mass is raised, phase mixing in an IPN increases as the crosslink level is raised, despite the increased molar mass.

However, these earlier studies were all conducted with immiscible or at best semi-miscible polymer pairs. Recently, studying miscible polymer pairs, a different trend for the miscible systems was observed[57]. Studying a sequential poly(vinyl methyl ether) (PVME)/PS IPN, Fay et al.[132] found the IPN to phase separate at the mid-range compositions, whereas the corresponding polymer blend exhibited one phase over the entire composition range as was substantiated by differential scanning calorimetry and dynamic mechanical analysis. Using SANS, Bauer et al.[132] also found a deuterated PS (PSD)/PVME semi-2 IPN to be less miscible than the corresponding polymer blend.

Inter-network grafting and ionic interactions. Inter-network grafting is reported to have a marked effect on the morphology of an IPN. The chemical crosslinks introduced between both polymer networks are known[134] to reduce phase separation, and, hence, create smaller phase domain sizes. The greater miscibility introduces an inward shift of the Tgs of the constituent polymers. Ideally for damping applications, it might result in one broad transition region. This phenomenon has been experienced by several researchers. Most recently Chou and Lee[135] investigated kinetical, rheological and morphological changes in 50:50 PUR/unsaturated polyester (UPE) IPNs. In their study, grafting was brought about through pendent functional groups of the unsaturated polyester. Three types of UPE were compared: an uncapped type with an acid value of about 35, a partially capped OH-free type (acid value of 26), and, finally, a capped UPE with no remaining reactive end-groups. TEM studies revealed clearly that grafting played an important role in reducing the extent of phase separation between the two networks. The grafted IPN showed domains of a tenth of a micrometer compared to a few micrometers for the ungrafted type. Also, the loss tangent transition of the fully grafted IPN exhibited an almost rectangular transition, whereas for the non-grafted IPN two separate peaks could be observed. The partially capped OH-free type was situated somewhat in-between. Bauer et al.[105,136,137] investigated the effect of grafting in PMMA-based semi-2 IPNs. PSD and poly(ethylene oxide) PEO were used as second components and grafting was brought about by functionalised PMMA macromonomers. Using SANS and SAXS, they found

in both cases complete miscibility for the grafted IPNs, whereas the ungrafted counterparts exhibited strong phase separation. In a study of grafted PUR/PMMA semi-1 IPNs, Hourston and Zia[138] incorporated an α,ω-poly(butadiene) diol into the PUR network. The unsaturation in the PUR network reacted with the propagating methyl methacrylate polymer. The observed Tg shift of the PUR component to higher temperatures (in contrast to the constant PMMA Tg) was explained by segmental restriction of the PUR network. The constant PMMA Tg was believed to stem from PMMA segments constituting a pure phase. With decreasing M_c, the level of grafting was found to increase. Further indications of the efficiency of inter-network grafting was given by Scarito and Sperling[139]. With an introduction of only 3% of glycidyl methacrylate into a epoxy/acrylic IPN, materials exhibiting only one transition temperature were obtained. With the same percentage of the difunctional monomer, 2-hydroxyethyl methacrylate (HEMA), in a PUR/PS IPN, Nevisass et al.[112] experienced a significant increase in the system's transparency.

Grafting is also known to occur accidentally. However, it is believed that the extent of it is very low[140,141]. Widmaier and Sperling[142] found a level of less than 5% in a study on poly-(n-butyl acrylate)/PS semi-2 IPNs. Moreover, it was observed[25] that if the amount of grafting is quite inferior to the amount of network crosslinking, then the former is practically negligible. No further effects on morphology and physical properties were then observed.

Besides the formation of chemical links between the two networks the introduction of physical interactions has also proven to be successful. Ionic bonding through the presence of charged groups, hydrogen bonding and strong polar interactions have proven successful in affecting the IPN morphology. Xiao et al.[143] introduced opposite charged groups into a PUR/PMMA IPNs. The interaction between the tertiary amine and carboxyl groups greatly improved the miscibility of these otherwise immiscible polymer pairs. With increased content of ionic groups, the phase domain sizes decreased from 300 nm to 7-10 nm. Hsieh et al.[144,145] conducted a similar study of PUR/PS IPNs, again using tertiary amine and carboxyl groups. Characterisation by DMTA analysis resulted in one transition peak. SEM micrographs confirmed a one phase morphology of this otherwise immiscible polymer pair. Xiao and Frisch[146] introduced additional hydrogen bonding into a simultaneous PUR/PMMA IPN. On adding methacrylic acid (MAA) to the reaction mixture, a P(MMA-MAA) copolymer

network was formed. Hydrogen bonding[146] between the carboxyl group of the MAA and the urethane groups of the PUR hard segment considerably improved the IPN miscibility.

The kinetic factors comprise the reaction rate of the polymer and polymer network formation. The degree of polymerisation at the time of gelation is important, since polymerisation is accompanied by simultaneous phase separation. The rate of phase separation is strongly dependent on the viscosity of the reaction medium. A high viscosity will result in a decreased mobility of the polymer chains, and, thereby, reduce the level of phase separation. Therefore, the synthesis conditions such as the synthesis temperature[66,67] and also the synthesis pressure[147,148] are further important factors influencing the IPN morphology.

Lee et al.[66,67] found in a study of photolytically initiated PUR/PS IPNs that a low synthesis temperature of 0°C resulted in a finer morphology. Compared to the synthesis at 50°C, the domain size decreased from 50-100 nm to 20-40 nm at 0°C. The higher mixture viscosity at low temperatures, which reduces the rate of phase separation, was believed to be responsible for the smaller domain sizes. A further effect might have stemmed from a decreased driving force to phase separate. Most polymer blends exhibit a lower critical solution temperature and phase separate with increasing temperature. The Lee and Kim team[147,148] also investigated the influence of the synthesis pressure on IPN morphology. They synthesised PUR/PMMA and PUR/PS IPNs at pressures up to 20,000 atm. The phase domain sizes decreased considerably with increasing pressure. Comparing full IPNs with semi-1 IPNs, semi-2 IPNs and polymer blends synthesised at high pressure, they found increased mixing in full IPNs whereas polymer blends exhibited a higher degree of phase separation. A further way to enhance phase mixing is to conduct the IPN synthesis in a common solvent[149] for both polymers. The PS domains in a PUR/PS IPN were more uniform and the domain size reduced compared with the corresponding IPNs synthesised in bulk. Kim and Kim[149] attributed this to the fact that the onset of phase separation took place at a later stage in the reaction.

2.2 Damping with Polymers and IPNs

2.2.1 Energy Absorption with Polymers

Polymers can absorb mechanical energy and convert this energy partly into heat through viscous deformation[150]. The most important mechanism of energy absorption in viscoelastic polymers is the conversion into heat by a gain in internal rotational and vibrational energy through molecular relaxation processes[16]. The principal molecular relaxation takes place[151] at the glass transition temperature, where the onset of large segmental movements begins. Further - though by far less important - absorption mechanisms in polymers include[93] the conversion of mechanical energy into potential energy through structural rearrangements in molecules such as for example[152] a molecular change from a chair to an energy richer boat conformation. Energy might also be consumed through association and dissociation between different ionic species and complexes as was observed[152] in an ionomer latex interpenetrating polymer network. Besides (i), the intrinsic energy absorption through conversion into heat, further energy attenuation mechanisms are reported[16,153] for inhomogeneous polymeric materials. These are (ii) scattering by inhomogeneities e.g. in filled polymers, (iii) redirection and (iv) mode conversion at boundaries in polymeric foams. Polymers can be applied directly to surfaces by towel, brush or spray[13] as an extensional damping system or sandwiched between two stiff layers, as in constrained layer damping[150,153] (figure 2.7).

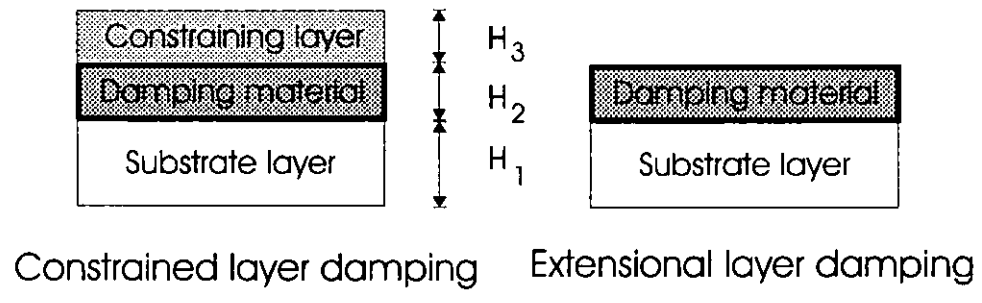

Figure 2.7 Damping configurations with polymers.

In extensional or free layer damping, the viscoelastic layer is deformed in extension and compression in parallel to the substrate surface[22]. The system's effectiveness increases with the layer thickness of the viscoelastic material, the storage modulus and the tan δ. The advantages of extensional layer damping are low cost and ease of application[13], whereas the constrained layer system offers a more efficient damping treatment[150] for a given weight. In constrained layer damping, the principal deformation of the viscoelastic layer occurs as shear. Here, maximisation of the loss factor, tan δ, is the target, and tan δ along with the stiffness and geometric parameters of the system determine the overall damping ability[22]. Equations approximately describing the performance of such a system were given[153] for extensional layer damping (equation 2.2) and for constrained layer damping (equation 2.3).

$$\tan \delta_{system} = k\,(E_2/E_1)(H_2/H_1)^2 \tan \delta_2 \qquad (2.2)$$

$$\tan \delta_{system} = k\,(E_3/E_1)(H_3/H_1)^2 \tan \delta_2 \qquad (2.3)$$

Here k is a constant, E and H are the Young's modulus and the layer thickness and the subscripts 1,2 and 3 refer to the substrate, the viscoelastic layer and the constraining layer, respectively. Therefore, damping is dependent on the damping material loss factor and loss modulus, the substrate modulus, and the constraining layer modulus.

2.2.2 Basic Damping Concepts

Damping is a dynamic mechanical term involving[93] the storage modulus E', the loss modulus E" and the loss tangent δ. The latter two terms express numerically the damping ability of polymeric systems and peak about the glass transition temperature region of the polymers. The macroscopic damping process in polymers can best be examined and visualised[154] using models borrowed from basic mechanics. Combining the elastic behaviour of a massless spring, following Hooke's law, and the viscous response of a Newtonian dashpot (figure 2.8), a damping model for viscoelastic polymers can be obtained[155].

(a) Spring (b) Dashpot

Figure 2.8 Model for elastic and viscous material responses.

In mathematical terms, the response of a perfectly elastic material, the Hookean spring, is given[155] by

$$\sigma = E\,\varepsilon, \qquad (2.4)$$

where σ represents the tensile stress, E is the constant of proportionality, Young's modulus and ε is the tensile strain. The ideal viscous liquid is represented[156] by the dashpot and follows

$$\sigma = \eta\, d\varepsilon/dt, \qquad (2.5)$$

where η stands for the coefficient of viscosity and t is the time. Viscoelastic polymers exhibit a response intermediate between these two extreme models[155]. In combining the elastic response of a spring and the viscous response of a dashpot, models (figure 2.9) exhibiting viscoelastic behaviour can be obtained[154].

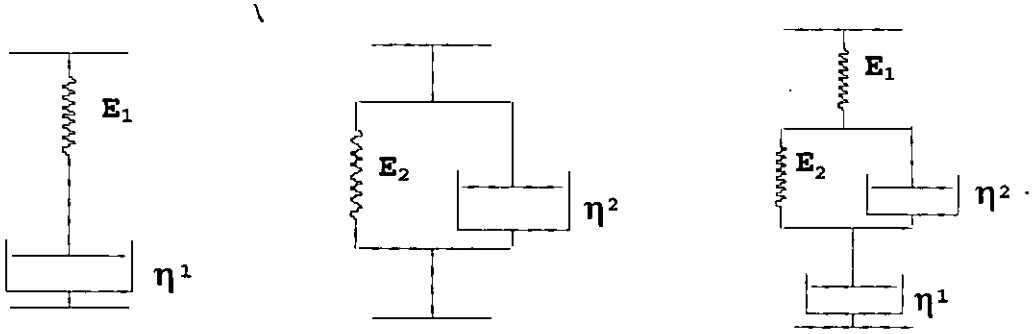

(a) Maxwell Element (b) Kelvin-Voigt Element (c) 4-Element Model

Figure 2.9 Models for analysing damping.

The Maxwell element represents an elastic element exhibiting an instantaneous response and a viscous element with a viscosity dependent response in series[154]. It describes liquid behaviour or may be used to estimate the stress relaxation characteristics of linear viscoelastic polymers[156]. The Voigt-Kelvin element describes

solid behaviour and creep to a first approximation[154]. An improvement, combining both former models, is the four-element model[93]. The former comprises an elastic element and a viscous element positioned in parallel and one further of each element integrated into the system in series (figure 2.9). It describes both, creep and stress relaxation and gives an approximate representation of the observed behaviour of polymers in the viscoelastic range[93]. The mathematical treatment of these models is given elsewhere[21,155].

In addition to creep and stress relaxation, the above mechanical elements can also model[93,155] loss and storage characteristics of polymers submitted to cyclic motions. When energy is applied to a viscoelastic polymeric material, part of it is stored as mechanical energy represented through the storage modulus E', while the rest of it is converted into heat through viscous deformation[13]. The latter part is the loss modulus E". Figure 2.10 (a) is a simple illustration of this behaviour[13].

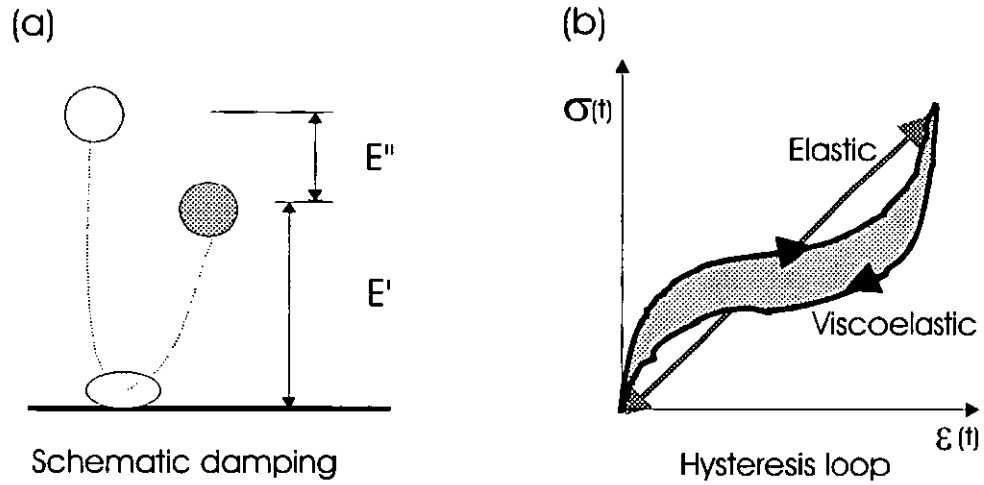

Figure 2.10 Illustration of viscoelastic damping and hysteresis curve.

As the ball bounces, part of the potential energy is stored and leads to the rebound. The difference in the potential energies equals the amount of energy lost in heat. If the energy applied to polymers is of periodic nature, then the polymers show hysteresis phenomena[152] (figure 2.10 (b)). By plotting the stress σ against the strain ε for a cycle of oscillation, a hysteresis loop is obtained. The area within the hysteresis curve in the stress-strain diagram represents the amount of mechanical energy lost as

heat per cycle. The amount of vibrational energy absorbed per cycle, which is equal to the amount of heat W emitted[157], is:

$$W = \pi E'' A^2, \qquad (2.6)$$

where A is the amplitude of strain and E" the loss modulus.

If a sinusoidal stress is applied to a viscoelastic polymer, the resulting strain response will be between that of an ideal elastic solid after Hooke's law and an ideal fluid following Newton's law[156]. The sinusoidally varying strain ε is described[155] by the following equation.

$$\varepsilon = \varepsilon_0 \sin \omega t, \qquad (2.7)$$

where ε_0 is the maximum strain, ω represents the angular frequency and t the time. The induced stress is then given[155] by

$$\sigma = \sigma_0 \sin (\omega t + \delta), \qquad (2.8)$$

where σ_0 is the maximum stress. Thus, the induced strain will lag behind the applied stress by the phase angle δ (figure 2.11).

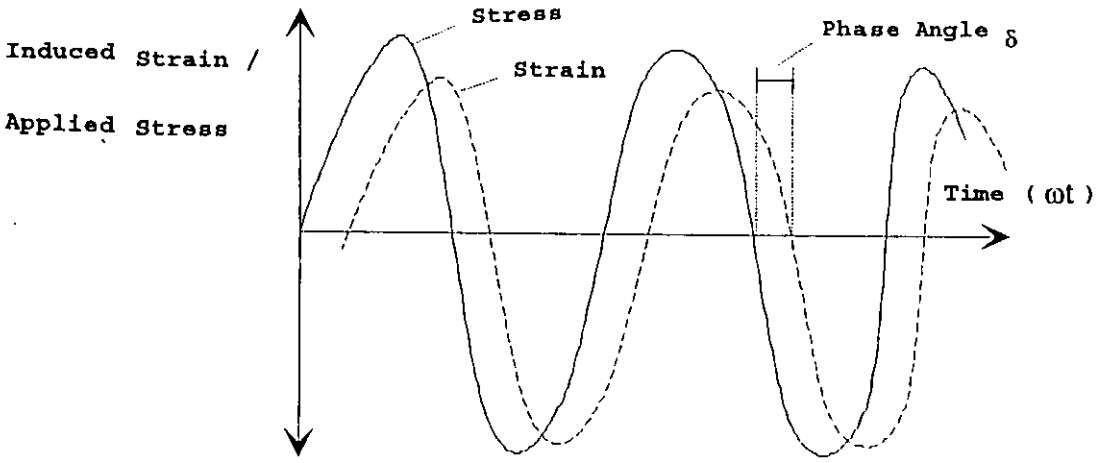

Figure 2.11 Applied stress and induced strain and phase angle δ.

Expanding equation 2.7 and subsequently substituting equation 2.8 with $\sigma_0 = (E'/\cos \delta)\varepsilon_0$ and $\sigma_0 = (E''/\sin \delta)\, \varepsilon_0$ gives:

$$\sigma = \sigma_0 \sin \omega t \cos \delta + \sigma_0 \cos \omega t \sin \delta \qquad (2.9)$$

$$\sigma = \varepsilon_0 E' \sin \omega t + \varepsilon_0 E'' \cos \omega t \qquad (2.10)$$

From equation 2.10, it can be seen that the stress can be considered to consist of two components. Thus, the resulting stress can be divided[155] into an elastic component that is in-phase with the applied strain ($\delta = 0°$) and governed by the storage modulus E', and a viscous component that leads the strain by the phase angle δ by 90° and is governed by the loss modulus E" (figure 2.12).

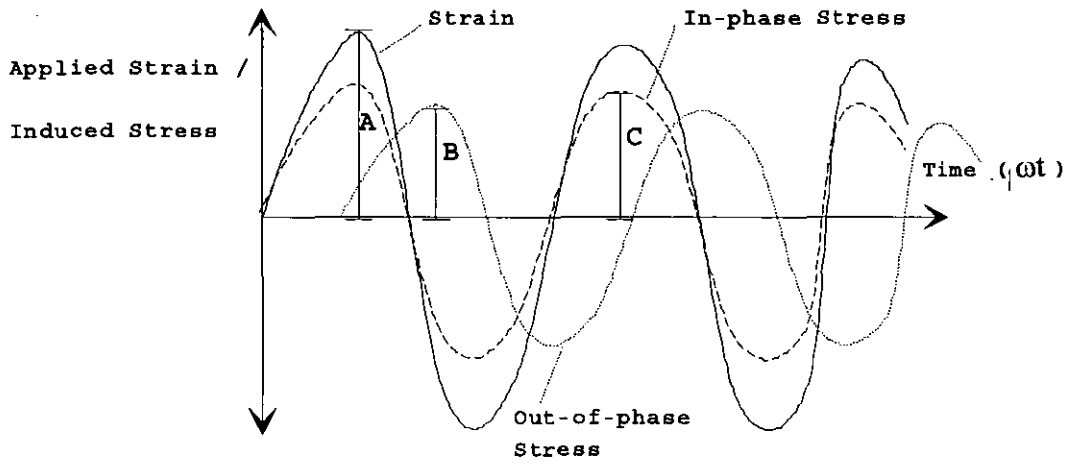

Figure 2.12 The stress components and definition of E' and E".

From figure 2.12, the storage modulus E' and loss modulus E" can be defined[158] using the strain amplitude A, the out-of-phase amplitude B and the in-phase amplitude C.

$$E' = C / A \qquad (2.11)$$

$$E'' = B / A \qquad (2.12)$$

The phasor diagram below (figure 2.13) shows[158] the relation between the dynamic moduli and the phase angle δ.

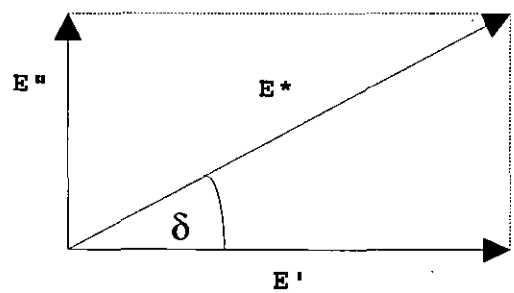

Figure 2.13 Phasor diagram for complex modulus E* and phase lag tan δ.

Considering the energy lost through absorption in the material, the equation for the complex modulus E* results:

$$E^* = E' + iE'', \qquad (2.13)$$

where E' is the storage modulus, E'' represents[118] the loss modulus and $i = (-1)^{1/2}$. E' is also referred[156] to as the real part of the complex modulus and E'' as the imaginary part. The tangent of the phase angle δ is referred to as the loss factor or loss tangent and is a measure[21] of the ratio of energy lost to energy stored in a cyclic deformation. From figure 2.13, it can be seen that

$$\tan \delta = E'' / E'. \qquad (2.14)$$

2.2.3 Measurement of Damping Ability and High Damping Materials.

Although it is the ultimate application that determines the sound and vibration damping performance of a given system, a ranking of materials of interest can be obtained through erstwhile mentioned dynamic mechanical analysis techniques. Hereby, the viscoelastic properties, i.e. the storage modulus E' (elastic response), the loss modulus E'' (viscous response) and the loss tangent, tan δ (E''/E'), are of particular interest.

Dynamic mechanical thermal analysis (DMTA) is in principle very similar to spectroscopy techniques like infra-red spectroscopy[159]. Consequently, the former is sometimes referred to as dynamic mechanical spectroscopy. In both techniques absorption takes place at the natural frequency of the chemical group i.e. polymer, and an absorption peak can be found[13]. However, in DMTA, unlike in infra-red spectroscopy, temperature usually is the parameter varied and the frequency is kept constant[93]. It is done this way since temperature effects are more distinct in polymers[13]. Dynamic mechanical spectroscopy is utilised[151,158] to investigate the molecular structure as well as to determine engineering properties i.e. the sound absorption properties of polymer systems. Different apparatus exist[13,156,160] for the determination of the complex dynamic modulus. Most experimental techniques determine moduli, like for example the torsion braid and torsional pendulum determining the shear modulus G, and the Rheovibron and Polymer Laboratories DMTA determining Young's modulus E. The three moduli, the shear modulus G, Young's modulus E and the bulk modulus B, are related in the following way[93]:

$$E = 2\,G\,(1 + \upsilon) = 3\,B\,(1 - 2\upsilon), \qquad (2.15)$$

where υ is Poisson's ratio. For elastomers $\upsilon \cong 0.5$[154] and, therefore, the Young's modulus $E \cong 3\ G$. In this study, the Polymer Laboratories Dynamic Mechanical Thermal Analyser was used for the determination of the storage and loss moduli and the loss factor tan δ. A description of this instrument, the test conditions and of the conclusions that can be drawn from DMTA data are given in the experimental chapter, section 3.4.1.

The loss modulus E" and the loss factor tan δ are the most commonly used terms to assess the damping ability of materials. However, there exist various related terms to express the efficiency of damping materials and damping systems. Amongst these are the logarithmic decrement Δ[13], the percent critical damping %C.D[4] and the Oberst damping factor K[161-163].

Most recently, a considerable amount of interest[164-169] has focused on the areas under the linear loss modulus (LA) and loss factor (TA) versus temperature curves. Chang et al.[164-166] assumed that the area under the linear loss modulus curve LA is a function of the glassy modulus, rubbery modulus, average activation energy of glass transition and the glass transition temperature. The basic theory for the group contribution analysis[165,168] is that the structural groups within the repeat unit contribute to the total loss area on additive weight fraction bases, W_i.

$$LA = \sum^{n}_{i=1}(LA)_i\ M_i/M = \sum^{n}_{i=1} W_i/M, \qquad (2.16)$$

where $(LA)_i$ is the loss area contributed by the ith group and n is the number of moieties in the mer. M_i is the molecular weight of the ith group of the mer, M is the molecular weight of the entire mer. The molar loss constants and contributions to the loss area have been reported[133] for a significant number of structural groups. Thus, application of the group contribution theory enables a predictive analysis of a polymeric material. Recently, however, limitations[153] to this theory were found. The group contribution was unable to predict the loss areas of filled polymers and composites[170] and of partially miscible polymer systems[171] i.e. IPNs. This state of forced miscibility and microheterogeneous morphology are believed[153] to be the foundation for the high damping ability of interpenetrating polymer networks.

It would be important to find a similar treatment for the area under the linear loss factor versus temperature curve TA, in particular in view of constrained layer

damping applications. However, no such predictive treatment has been found[167,168]. This is due to the fact that tan δ involves the quotient of E"/E'. The storage modulus E' decreases by three decades when the polymer goes through the glass transition and has defied[57,168] theoretical prediction of its exact shape. One drawback of using TA to express the damping ability is that its experimental determination is often difficult because the sample fails or becomes too soft to allow the instrument to record at elevated temperature[153]. In that case, extrapolation[168] of the tan δ curve can still be applied to obtain an approximate value for TA.

Defining a good damping material depends upon the type of application and the operating conditions. However, some general assessments with regard to the loss factor versus temperature curve can be made. In polymeric materials, values for the loss factor can be encountered[172] from the range of 0.01 to 2. The energy absorbing properties are a function of temperature and frequency, and the value of tan δ is undergoing a maximum in every polymer system[158]. A polymeric material possessing a tan δ value greater than 0.3 over a temperature range superior to 70 °C is deemed[172] to have good damping properties. However, there is always a trade-off[173,174] between the damping properties and the mechanical properties of a given polymer system. Increasing the loss factor tan δ to high values will result in improved damping. However, the physical and mechanical properties will suffer considerably. Damping does not increase[175] in a linear fashion with tan δ, and for values above 0.4 or 0.5 the gain in energy absorption ability is only very small. This was shown through mathematical modelling involving the transmissibility T, which is defined[176] as the ratio of the transmitted to the exciting displacement. The graphic representation of the transmissibility versus tan δ values shows the transmissibility approaching the x axis in form of an asymptote. Thus, important gains in energy absorbing ability are made by increasing tan δ from 0.1 to 0.2. However an increase from 0.4 to 0.5 does not greatly improve damping. For loss tangent values higher than 0.5 hardly any further decrease in the transmissibility is found. From these data it can be understood that a high damping plateau with tan δ values between 0.3 and 0.5 is desired in most applications. The temperature and frequency dependence of damping imposes the second requirement which is exhibiting this value over a broad temperature region[113]. Homopolymers exhibit a glass transition range[173] and, thus, high damping region of

around 20-30°C. In practical damping applications, this working region is not sufficient[113] due to variations in ambient temperature and frequency of sound and vibrations. For example, in order to cover the three decades of the audible frequency range, a high damping efficiency over at least 20°C is required at one constant temperature. Furthermore, great temperature variations of up to 60°C occur frequently in real damping applications such as, for example, in aeroplanes. Therefore, it is evident, that systems with high damping over broad Tg transitions of 80°C and more are desired to cover wide temperature and frequency ranges. However, the height and the width of the damping peak cannot be chosen arbitrarily[173,174]. It is generally observed that broad transitions have lower damping peaks than narrow ones. Thus, broadening of transitions is done at the expense of lowering the tan δ height.

The phenomenon of the glass transition and its temperature and frequency dependency determine the damping ability of polymeric materials and are, therefore, further introduced in the following section.

2.2.4 Glass Transition Temperature: Temperature and Frequency Dependency

Five viscoelastic regions of polymers. In polymers, there exist[93] 5 regions of viscoelastic behaviour (figure 2.14).

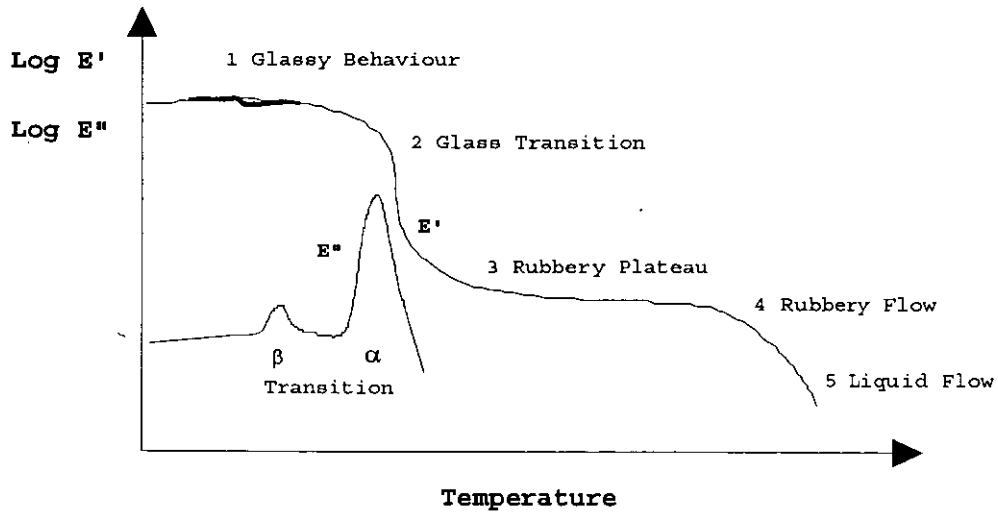

Figure 2.14 The five viscoelastic regions of polymers.

With increasing temperature, polymers undergo changes from the glassy state to the glass transition region, thereafter to the rubbery plateau and the rubbery flow region and finally attain liquid flow characteristics[93,177]. Depending on crystallinity, crosslinking, chain flexibility and molecular weight, the different regions are more or less pronounced[93]. Increasing the crystallinity reduces the magnitude of the glass transition and the drop in modulus is less pronounced. The glass transition may be shifted[151] to a higher temperature by increasing the crosslinking level, and, to a much lesser extent, by a higher molar mass of the polymer. Also, the rubbery plateau will be prolonged by both higher crosslinking and a higher molar mass.

The loss modulus E" and tan δ peaks appear[4] in the glass transition region, about Tg, and that is where the polymer exhibits the greatest energy absorbing capability, and, thus, damping efficiency (figure 2.14). It is, therefore, necessary to describe this phenomenon.

The glass transition temperature (Tg). At Tg, the polymer undergoes the change from a rigid, essentially elastic glass with a Young's modulus of about $3x10^9$ Pa to a flexible rubber. Thereby, the modulus typically decreases by a factor of 10^3 over a 20-30°C temperature range[21,93,154]. In the glassy state, the amorphous polymer chains are largely frozen into a rigid, disordered structure exhibiting a high modulus and a low loss factor[157]. Some less pronounced transitions that take place at temperatures lower than the glass transition impart limited (side) chain mobility. The Tg is a secondary transition and is conventionally labelled with α. With decreasing temperature, further transitions are assigned as β, γ and δ. The glass transition temperature can be determined[158] using dilatometry, thermal mechanical analysis (TMA), dynamic mechanical thermal analysis (DMTA) or differential scanning calorimetry (DSC) with the latter two being most commonly used. Three major theoretical interpretations exist[93,177] to describe the phenomena observed at the glass transition temperature. These include the classical free-volume theory[21,155] which introduces free volume in the form of voids as a requirement for the onset of co-ordinated molecular motion. Other approaches are made via kinetics and a thermodynamic theory[93]. Here, only a brief phenomenological treatment of the Tg can be given. As frozen segments obtain mechanical energy at Tg, the onset of molecular motion has begun. At the Tg, there is a dynamic equilibrium between

frozen chain segments and segments that are free to move[179]. Co-ordinated motions of the backbone and side branches take place. Backbone chains with some 10-50 atoms involved are believed[93] to reptate back and forth. The motion of flexible backbone and side branches of the molecule over stiffer neighbours is believed[4,56] to be important for the damping mechanism. These motions on segmental/molecular basis transform mechanical energy of vibrations and sound waves into thermal energy, heat, hence reducing transmitted noise and vibrations[166]. The β-transition involves motions of shorter chain segments such as iso-axial arrangements of 4-8 C-atoms. Recently, theories have come forth[13] that short chain motions like the β-transitions strongly contribute to the damping ability of some polymers, since it has been observed that the loss modulus - temperature curve was independent of the crosslinking up to very high levels of ca. 25%. With these high crosslinking levels, the conventionally assumed reptations of e.g. 50 backbone molecules are no longer possible.

The location of the glass transition temperature Tg depends upon a number of factors which have been subject to extensive investigations[180]. These include[181] steric effects, backbone flexibility, pendant groups, polarity, crystallinity and the extent of crosslinking. The glass transition temperature can be shifted[13,152] by incorporating plasticisers, fillers and a second polymer component. In the latter case, this might be achieved through random copolymerisation with a second monomer creating a statistical copolymer, or by polymer blending creating a miscible polymer blend. Then, the single glass transition temperature will be intermediate between those of the homopolymers. The Tg shift can be predicted[93,154] using the Pochan[182], Gordon-Taylor[183] or Fox[184] equation. The Fox equation which is characterised by a convex curve shape is most commonly used.

$$1/Tg = M_1/Tg_1 + M_2/Tg_2 \qquad (2.17)$$

The subscripts 1 and 2 refer to the two polymers, M is the weight fraction and Tg is in absolute temperature units.

Temperature and frequency dependency of damping. The glass transition temperature of polymers involves[164] both frequency i.e. time and temperature effects. Consequently, damping is also a function of both, the frequency of the vibrational energy applied and the ambient temperature. When dynamic mechanical

measurements are performed at various frequencies, then, the loss factor peak which represents the glass transition shifts to higher temperatures at higher frequencies. figure 2.15 illustrates the rule of thumb[185] that one decade of frequency approximately shifts the Tg temperature by 6-7°C.

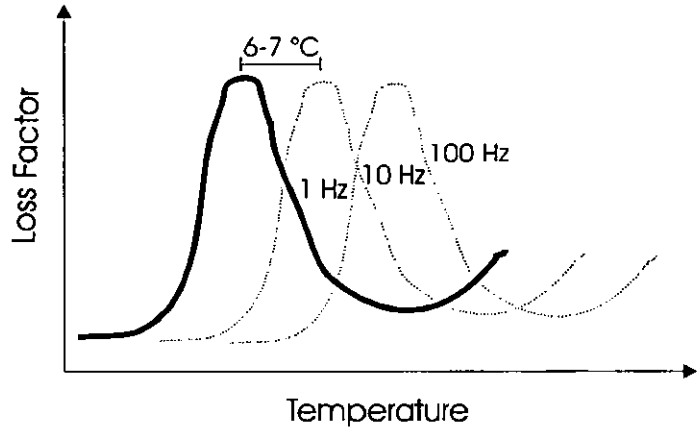

Figure 2.15 Frequency-dependent damping ability of homopolymers.

Time-temperature superposition principle. It was found[118] that a plot of the modulus against temperature at constant time (frequency) yields the same curve shape as a plot at constant temperature varying the frequency. This implies[177] an equivalence between temperature and time effects for viscoelastic materials. This principle has proven to be very helpful. In dynamic mechanical analysis, it would be very time consuming to measure long time spans and low frequencies, thus covering the whole temperature range[93,177]. However, applying the time-temperature superposition principle, master curves for a given material can be readily obtained[186]. This can be done through i.e. varying the temperature at one fixed frequency. The concept behind this approach is that data curves collected at different temperatures are only shifted horizontally along the log frequency or time axis, while the shape or nature of the curve (relaxation process) is not altered[177]. This technique enables predictions of mechanical polymer behaviour over broad frequency ranges or long periods of time. It is, therefore, commonly used[21] to obtain long-term properties of glassy polymers from relatively short-time tests.

Williams-Landel-Ferry (WLF) equation. The most important model to describe[21] the magnitude of shift at each temperature relates to the Williams-Landel-Ferry free

volume concept and the WLF equation. The shift factor a_T is given[187,188] by the following equation.

$$\log a_T = - C_1(T-T_0) / (C_2+T-T_0), \qquad (2.18)$$

where C_1 and C_2 are constants and T_0 a reference temperature. Thus, the shift factor a_T is a function of the temperature and the constants. Values of C_1 and C_2 for different polymers are summarised in the literature[21]. If the reference temperature is the Tg of the polymer, then C_1 = 17.44 and C_2 = 51.6 which are dependent on free volume are good approximations for amorphous polymers.

2.2.5 Damping with IPNs

IPNs represent very interesting damping materials, firstly, since they can be tailored to measure by choosing two polymer components with Tgs in the desired temperature range. Secondly, suitably chosen IPN components allow damping over a wide temperature range. This is due to their special microheterogeneous morphology.

Transition broadening: Polymer blends, fillers, plasticisers. Generally, homopolymers and statistical copolymers exhibit effective damping properties only over a temperature range of 20-30 °C[154], centred about the glass transition (section 2.2). Multicomponent polymer systems can be used[13] to produce systems with a controlled degree of mixing which is required for effective damping over a broad temperature range. However, limitations to mixing or blending of different polymers exist due to the incompatibility of most polymer blends.

Fillers and plasticisers are often added to polymers to alter[151] their mechanical properties. In damping applications, they can be used[13] to shift and broaden the glass transition of the polymer. Plasticisers are used to shift systematically the Tg transition to lower temperatures. A broadening effect of the transition is also observed[189]. Contrary to plasticisers, fillers tend to shift the glass transition to higher temperatures. However, two distinct cases have to be distinguished[13]. If the filler is inert and no interactions with the polymer are present, then the storage modulus E' is increased[151] both below and above the Tg. However, the location of the Tg is not altered. If the polymer adheres to the filler, then the free volume may be reduced[13] and a Tg shift to higher temperatures can be observed. Fillers can not only shift and broaden the

transition, but can also impart[153] additional damping mechanisms to the polymer. Fillers can (i) resonate by absorbing impinging energy, (ii) reflect sound waves back through the polymer and (iii) act as a miniature constrained layer system[153,166].

Microheterogeneous morphology. In damping applications, no complete miscibility of the polymer blend is required. Conversely, an intermediate structure with phase domains in the order of a few tens of nanometers is desired in order to result in materials with a broad transition region. Dynamic mechanical thermal analysis data of polymer blends of different degrees of phase mixing/miscibility are shown in figure 2.16. The DMTA data are related[190] to the respective transmission electron micrographs to illustrate the relation between morphology and properties, i.e. energy absorbing ability.

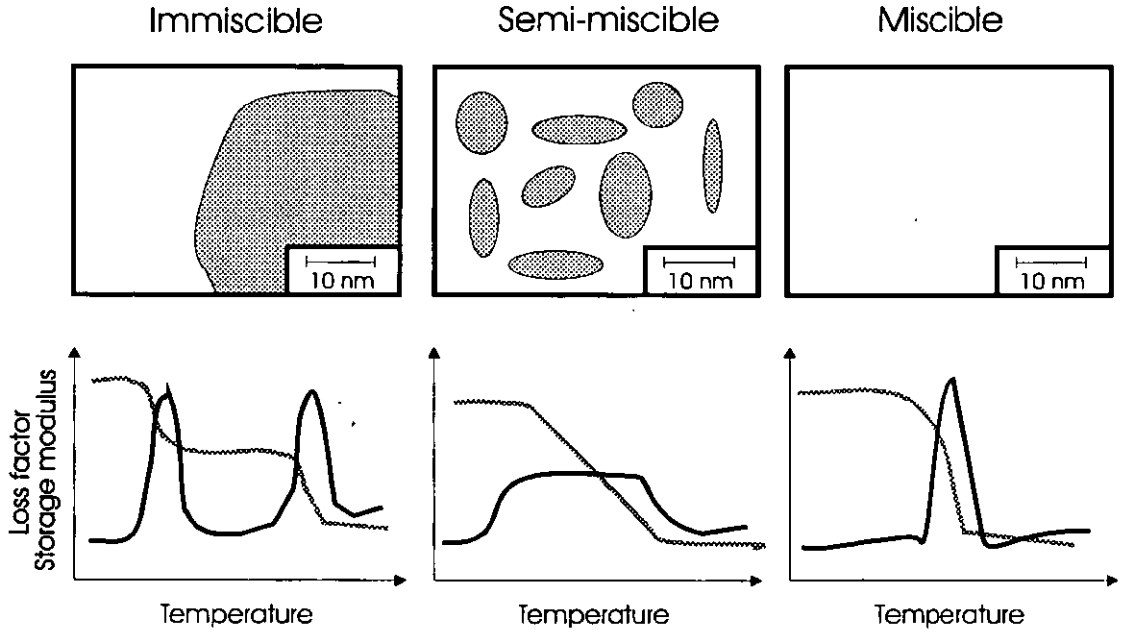

Figure 2.16 Schematic diagram of transmission electron micrographs and DMTA data.

Polymer blends with poor miscibility and, thus, poor phase mixing show two separate Tgs reflected in two tan δ peaks[4] (figure 2.16). The tan δ values in-between those peaks are very low and, thus, so is the damping ability. Electron micrographs of these materials show well-defined phases with phase domains ranging from a few hundred nanometers to several microns. Conversely, miscible polymer blends will exhibit a

high degree of phase mixing which results in one loss factor transition peak located somewhere in-between the two initial peaks of the homopolymers. Such systems do not have any significant advantage over homopolymers in damping applications[4]. Transmission electron micrographs of this material show no phase structure.

For semi-miscible polymers, a situation intermediate between these two extremes is obtained. With increasing miscibility of the two polymers, an inward shift of the transition peaks can be observed, accompanied by an increase of the inter-transition tan δ values. If both polymers are semi-miscible, a microheterogeneous morphology with phase domains[36] in the order of 10 - 20 nm can result. This implies that phase separation takes place[4] below the level of a single polymer chain. The microheterogeneous morphology results in a complex phase behaviour i.e. in a broad transition region. This broad transition is caused[36] by a distribution of sub-phases of varying composition. Almost every little unit is made[166] up of a different material composition. Hence, its glass transition appears at a different temperature.

Thus, a microheterogeneous morphology is highly desired in damping materials (section 2.2.1). It is more frequently encountered in IPNs than in conventional polymer blends because the former represent[153] one possibility of circumventing the thermodynamic immiscibility by support of kinetics (section 2.1.4). Permanent entanglements, mostly through covalent bonds, are brought about before phase separation starts to occur. Due to the forced mixing on a molecular or segmental level, a broadening and shifting of the transition temperatures is observed. Besides microheterogeneity in segmental mixing[191], further explanations of the broadening of the glass transition temperature in IPNs include smearing[21] of phase transitions, compound transitions caused by imposed physical restrictions through the rigid polymer on the segmental mobility of the elastomer component[192] and a fine dispersion of the component domains[77]. IPNs, therefore, represent a means of attaining[4] an intimate mixture of polymers that otherwise would exhibit a much coarser morphology. Microheterogeneous IPNs are capable of exhibiting a good energy absorption ability covering very broad temperature use ranges, with ranges of from 100-120°C being reported[193]. On the other hand, a broadening or shift in the transition temperature is a good indication for actual occurrence of interpenetration[77,129]. The transition behaviour can be influenced by the previously discussed factors (section 2.1.4) such as the crosslink density and the miscibility of

network components. This, in turn, has important repercussions[168] on the IPN damping effectiveness. Energy absorption with IPNs has been reviewed recently[13,152,153,166].

IPNs investigated. Because of the obvious advantageous properties of IPNs in damping applications, interest in this field is a truly universal one. Table 2.2 gives an overview of the major research teams in the area of sound and vibration damping with IPNs[114].

Table 2.2 Research teams in sound and vibration damping with IPNs[114].

Group	Institute	IPNs studied	Reference
Hourston	Loughborough University, UK	PUR/acrylic full and semi simultaneous IPNs PUR/polyester IPNs PUR/PS IPNs Acrylic latex IPNs	128,129 110,194 54 53 195
Sperling and Thomas	Lehigh University, USA	Full, semi and filled IPNs based on acrylic polymers	89,114 131,168
Klempner and Frisch	University of Detroit, USA	PUR/epoxy IPNs fillers, foams	153,196
Meyer and Widmeier	Institut Charles Sadron, France	PUR/PMMA semi and full simultaneous IPNs	119-122
Williams	University of Toronto, Canada	PUR/epoxy simultaneous IPNs	197
Fox	Naval Research Laboratory, Fl, USA	PUR/PBMA IPNs	59
Yao	Naval Academy Wuhan, China	PUR/acrylic IPNs PEEK/epoxy IPNs	172 113
Ting	Naval Research Laboratory, Orlando, USA	PUR/epoxy	198

A brief summary of high damping materials based on IPNs is given in the following. The first network formed determines the IPN properties to a great extent (section 2.1.4). Also, the chemical composition of the damping material greatly influences the loss area, LA (section 2.2.2). Consequently, a classification of the IPNs was made

into different polymer groups. Good damping materials should exhibit[72] tan δ > 0.3 over at least 70 °C (section 2.2.2).

Acrylic/methacrylic IPNs. Foster and Sperling[199] synthesised a series of acrylic/methacrylic sequential IPNs. Good damping materials were obtained with a 75/25 full PnBA/PnBMA IPN exhibiting tan δ values between 0.4-0.5 over nearly a 100°C temperature range. Similar good results were obtained[199] with a PnBMA/PnBA semi-2 IPN exhibiting tan δ of 0.4-0.85 over 100°C. A further improvement of 15-20 % of the tan δ values was achieved by filler (graphite) addition.

Poly(vinyl isobutylether)/PMMA IPNs. A poly(vinyl isobutylether)/PMMA sequential IPN exhibited[200] tan δ over 0.4 between 10 and 60°C. Hourston and McCluskey[200] observed from the E' and E" versus temperature plot a two-phase system.

PUR/PMMA IPNs. It has been observed[83,194] in various studies that a 70/30 PU/PMMA IPN yields very broad loss tangent transitions with an almost rectangular damping transition. Using a semi-1 IPN, Hourston and co-workers[128,129] investigated the effects of the isocyanate/hydroxyl ratio in the PU network on the linear PMMA component and the average molecular weight between crosslinks. The lowest Mc was found for a NCO:OH ratio of 1.1:1. Decreasing M_c resulted in a pronounced stiffening of the IPN. With respect to the PMMA ratio, plots of tan δ showed two glass transition peaks in all compositions investigated (20, 40, and 60 wt.% PUR). Increasing the PUR component shifted the peak slightly towards higher temperatures, also an increase in the peak height resulted. In opposition to that, the PMMA peak stayed in place, however, a broadening could be observed. The best result was yielded with the 60 wt.% PUR semi-1 IPN exhibiting good damping behaviour (tan δ > 0.3) from -30 to +60°C. In a PhD thesis[194] from Hourston's research group, grafted PUR/PMMA full IPNs were synthesised. Chughtai[194] found good damping values in this series. This was particularly true for a grafted 70/30 PUR/PMMA, with an inter-network grafting level of 10% grafting agent. A tan δ value > 0.3 over a temperature range as broad as 120°C was obtained.

PUR/unsaturated polyester (UPES). Hourston and Zia[54] studied a kind of semi-2 PUR/UPES IPN, crosslinked with styrene and methyl acrylate. Weight ratios ranging

from 30-70 % PUR content were investigated. The greatest half-peak width was experienced with the 70 % PUR composition, ranging over 132°C. It consisted in fact of one major transition and a small one at around -20°C, possessing a maximum tan δ height of 0.52. Micrographs of the semi-2 IPNs indicated that the materials could be regarded as rubber-modified glassy polymer systems. The study of Chou and Lee[135] on grafted and ungrafted 50:50 PUR/UPE IPNs resulted in an almost rectangular transition for the grafted IPN. Loss tangent values of greater than 0.2 were found over a temperature range of 60°C, ranging from 50-110°C.

PUR/epoxy IPNs. In a study on PUR/epoxy systems Klempner et al.[201] found that a reduced post-curing time yielded higher loss tangent peaks and a broader transition range. Higher levels of chain extenders were observed to introduce a broadening of the loss peak going together with a decrease in its magnitude. Also, a shift to slightly higher temperatures caused by an increased amount of hard blocks in the segmented polyurethane was observed[202]. PUR/epoxy semi IPNs were investigated by Wong and Williams[197]. A 70:30 wt. % composition resulted in a broad tan δ peak exhibiting tan δ values greater than 0.3 starting from 0°C to 100°C. The 70:30 composition revealed two distinct transition peaks. Only one major peak with a shoulder was found for 50:50 PUR/E composition. However, the tan δ transition was clearly smaller than for the former system.

2.3 Polyurethane (PUR) Network

The basic principles of PUR reactions with a focus on solid PUR elastomers are briefly summarised in the following section. This is done because PUR represents one of the basic components of the IPNs synthesised in the present study. It is present in all materials reported. Also, in most of the materials synthesised, it forms the first network, which is known[99] to have a marked influence on the properties of the entire composition. Due to the wide variety of its possible constituent components[203-205], it represents a means of readily influencing the properties of the IPNs. Also, further components with OH or NCO functionality can be easily incorporated. For this reason, considerations of the possible synthesis routes, catalysis of the reaction, possible side reactions and the reactivity of the raw materials, polyurethane morphology, as well as the segmented character and resulting properties are of great interest.

2.3.1 Chemical Nature, Types and Applications and Safety

Polyurethanes were developed[203] by Bayer (IG Farben) in 1938 as a response to the polyamide discovered earlier by Carrothers (DuPont). They have become a very important class of materials today due to their great versatility.

Chemical nature. The term PUR is used for a class of materials containing the urethane link in the main chain (figure 2.17).

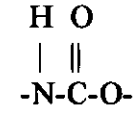

Figure 2.17 Urethane link.

PURs do not merely consist of the urethane links, but also contain segments of a different chemical nature. These can be[204] aliphatic or aromatic hydrocarbons, ether or ester groups. Hence, PURs can be visualised as a kind of block polymer with the repeating unit $(AB)_n$. The type and extent to which the other segments are present determine the technological properties. Association of the urethane links by hydrogen bonding introduces a kind of physical crosslinking into a thermoplastic PUR.

Chemical crosslinking as in PUR elastomers or thermosets is brought about[205] by either the use of a polyisocyanate or, more commonly, the use of a polyfunctional hydroxyl compound. More generally, the segmented character, that is to say the interactions within the urethane links in the matrix of aliphatic hydrocarbons guarantees the high wear resistance and elasticity as well as good solvent and oil resistance of PURs.

Types and applications. The possibility of wide variations in synthesis and choice of raw materials makes PURs very versatile polymers. Moreover, a wide variety of additives[204] such as catalysis, blowing agents, surfactants, dyes and pigments, fillers, flame retardants and smoke suppressants permit the production of a tailor-made product for special needs. Therefore, PURs can be found[177,206] in diverse forms from foams, fibres and elastomers to adhesives and coatings. They can be applied via reaction injection moulding (RIM) techniques as well as through extrusion or spraying. Typical applications for PUR products are in the automotive sector, in the construction industry, in insulation applications and, more recently, also in medical devices.

Safety. A number of chemicals, such as amine and tin catalysts, used in the polyurethane preparation represent a health hazard. However, due to the quantities involved, the main health hazard[204] is the isocyanates. Inhlation and absorption are the two main risks. Depending on the type and reactivity, the isocyanates may attack the respiratory system, the eyes or irritate the skin. Continued exposure to high levels of isocyanates may create sensitisation and chronic lung conditions. Isocyanate spills have to be covered with saw dust and neutralised with a decontamination liquid. A solution of 10% ammonia (or sodium carbonate) in water with 2% detergent suits[207] this purpose.

2.3.2 Synthesis, Catalysis, Raw Materials for Solid PURs and Further Isocyanate Reactions

Synthesis. Chemically, PURs are usually obtained by an addition reaction of a polyisocyanate with a polyfunctional reactant possessing active hydrogen atoms. Most commonly, polyethers or glycols with hydroxyl groups are used (equation 2.19).

$$n\ O{=}C{=}N\text{ - }R\text{ - }N{=}C{=}O \;+\; n\ HO\text{ - }R'\text{ - }OH$$

Diisocyanate Glycol

(2.19)

$$\text{----> } HO\text{-}R'(\text{-}OOCNH\text{-}R\text{-}NHCOO\text{-}R')_{n-1}\text{-}OOCNH\text{-}R\text{-}NCO$$

Polyurethane

From the technological point of view, PURs can be synthesised[205] via three main processes, distinguished through the preparation medium. A solvent-free polymerisation in bulk, a solution polymerisation and emulsion polymerisation in an aqueous system. Furthermore, a single-stage process, the one-shot technique, can be distinguished, where all raw materials are placed into the reaction vessel or mould and reacted simultaneously. The two-stage process involves first the preparation of a reactive polyisocyanate-terminated prepolymer, which is then followed by chain extension through short-chain diols, amines or water. The latter is therefore also referred to as the prepolymer process.

While solution polymerisation was used to synthesise the urethane acrylate compatibilisers in the present study, the polyurethanes in the interpenetrating polymer networks were reacted in bulk by reactive moulding. Because of the rapid build up of the viscosity, even at elevated temperatures, this synthesis route normally leads to relatively low molecular weights. This was of minor importance in this project since crosslinking circumvents this problem.

Further isocyanate reactions and urethane degradation. Since isocyanates react readily[204] with hydrogen-active compounds many more reactions are possible than with hydroxyl compounds (equation 2.19). The most important reactions are listed below, since they have to be considered as they might affect stoichiometry, and yield additional branching and crosslinking of the interpenetrating polymer networks. The reactions can be divided up into three main groups. Mechanisms of urethane degradation are listed under the point 4.

1) Primary reactions of isocyanates with hydrogen-active compounds.

Amongst these reactions, the one of isocyanate with water is of particular importance due to the omnipresence of humidity. It is detrimental to the production of solid

polyurethanes since it affects the PUR stoichiometry and in its course carbon dioxide is liberated which results in products with entrapped gas. Thus, great care has to be taken that all raw materials are water-free.

• With water

$$R\text{-}NCO + H_2O \text{ -----> } \underset{\text{Carbamic acid (unstable)}}{R\text{-}NHCOOH} \text{ -----> } \underset{\text{Amine}}{R\text{-}NH_2} + CO_2\uparrow \qquad (2.20)$$

The amine will react further with free isocyanate groups:

• With amines.

$$R\text{-}NCO + R'\text{-}NH_2 \text{ ----> } \underset{\text{Urea}}{R\text{-}NH\text{-}CO\text{-}NH\text{-}R'} \qquad (2.21)$$

• With carboxylic acids.

$$R\text{-}NCO + R'\text{-}COOH \text{ -----> } \underset{\text{Amide}}{R\text{-}CO\text{-}NH\text{-}R'} + CO_2\uparrow \qquad (2.22)$$

2) Secondary reactions of isocyanates with isocyanate adducts.

These reactions mainly occur only at temperatures above 100°C. Secondary reactions can be responsible[177] for the introduction of branching and crosslinking of the polyurethane. The introduced crosslinks, however, are much weaker than triol-based ones and start to dissociate at temperatures between 140 - 160 °C.

• With urethanes.

$$R\text{-}NCO + R'\text{-}NH\text{-}CO\text{-}O\text{-}R'' \text{ -----> } \underset{\text{Allophanate}}{R\text{-}NH\text{-}CO\text{-}N(R')\text{-}CO\text{-}O\text{-}R''} \qquad (2.23)$$

• With ureas.

$$R\text{-}NCO + R'\text{-}NH\text{-}CO\text{-}NH\text{-}R'' \text{ -----> } \underset{\text{Biuret}}{R\text{-}NH\text{-}CO\text{-}N(R')\text{-}CO\text{-}NH\text{-}R''} \qquad (2.24)$$

• With amides.

$$R\text{-}NCO + R'\text{-}NH\text{-}CO\text{-}R'' \text{ -----> } \underset{\text{Acyl Urea}}{R\text{-}NH\text{-}CO\text{-}N(R')\text{-}CO\text{-}R''} \qquad (2.25)$$

3) Auto-addition reactions of isocyanates.

This is a further type of reaction which can introduce branching and crosslinking. The formation of dimers (only aromatic ones) and trimers are favoured[208] by certain

catalysts such as phosphine compounds. Trimerisation is an important reaction since it can lead to branching in the production of polyurethanes.

• Dimerisation

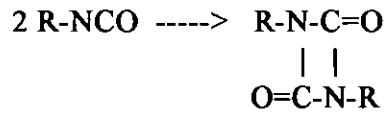

(2.26)

Uretdione

(2.27)

Carbodiimide

• Trimerisation

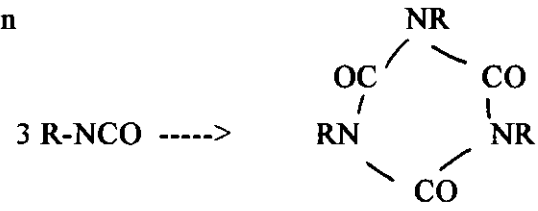

(2.28)

Isocyanurate

4) Thermal decomposition of urethanes.

At higher temperatures, thermal decomposition of polyurethanes can take place. Three main reactions are reported[206]. Dissociation into the isocyanate and the alcohol (equation 2.29) may start to take place at temperatures between 120-150°C. Formation of a primary amine, CO_2 and an olefin (equation 2.30) or of a secondary amine and CO_2 (equation 2.31) necessitate temperatures above 200°C.

(2.29)

(2.30)

(2.31)

Catalysis. The urethane reaction can be controlled to a certain degree by the choice of the reactants, i.e. the isocyanate and the hydrogen-active compound, and the reaction conditions such as temperature and reaction medium. An added catalyst, however, exerts a much more powerful effect on the reaction rate[208], and also on the type of reaction favoured. Generally, catalysis effects are very pronounced at low temperatures. Their efficiency is strongly influenced[204] by the respective nucleophilic or electrophilic strength and by steric hindrance between the reactants and catalyst.

The isocyanate group contains a high degree of unsaturation. For the electronic structure of isocyanates, the following three resonance structures are possible (four for aromatic isocyanates):

$$R\text{-}\overset{-}{N}\text{-}\overset{+}{C}\text{=}O \longleftrightarrow R\text{-}N\text{=}C\text{=}O \longleftrightarrow R\text{-}\overset{+}{N}\text{=}\overset{-}{C}\text{-}O \quad [\longleftrightarrow Ar\text{=}\overset{-}{N}\text{-}\overset{+}{C}\text{=}O] \qquad (2.32)$$

The reaction of isocyanates with hydrogen-active compounds involves a nucleophilic addition of the active hydrogen group to the positive carbonyl atom of the isocyanate group. In principle, the urethane formation with polyols, for example, is possible in the absence of catalysts, only autocatalysed by a second hydroxyl compound. The presence of tertiary amines or metal salts, however, yields a reaction rate of up to 1000 times higher[210] than the autocatalysed system. The urethane reaction can be catalysed[204, 208] in three ways. According to the way and the type of catalyst, different reactions are favoured.

Acid catalysis. Catalysis with acid compounds is possible[203], but is very efficient. By increasing the electron density on the oxygen atom, the carbon is somewhat more deshielded, and, therefore, susceptible to attack by a nucleophile.

Basic catalysis with tertiary amines. Basic catalysts (electron donors) such as tertiary amines are much stronger catalysts and generally favour[208] the amine and water reactions. Trimerisation is also encouraged by very strong bases. Tertiary amines form a complex with the carbon atom of the isocyanate group.

Catalysis with Lewis acids (metal salts). Lewis acids, such as organotin compounds (e.g. stannous octoate), are very strong urethane catalysts. This is particularly true[208] for the polyol - isocyanate reaction where they show a distinctive advantage over bases. Other organometals favour different reactions. Lead compounds, for example, are known[208] to encourage the reaction with urethanes to allophanates.

Raw materials for solid polyurethanes. Like most of the polyurethane types, solid polyurethane block copolymers usually are a combination of three basic components.

They comprise a diisocyanate, a polymeric (oligomeric) polyol and a short chained diol or diamine called a chain extender. In elastomeric polyurethanes, the latter is usually partly replaced by a trifunctional alcohol such as trimethylol propane.

Diisocyanates. The most common way of preparing isocyanates is by phosgenation of primary amines using HCl abstraction[204]. The structural formulae of important diisocyanates are presented in figure 2.18.

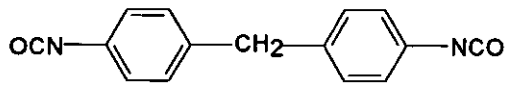

4,4'-Diphenylmethane diisocyanate (MDI)

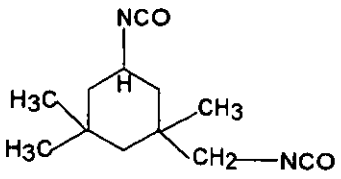

Isophorone diisocyanate (IPDI)

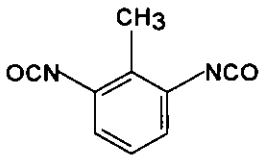

2,6-Toluene diisocyanate (TDI)

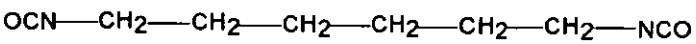

Hexamethylene diisocyanate (HDI)

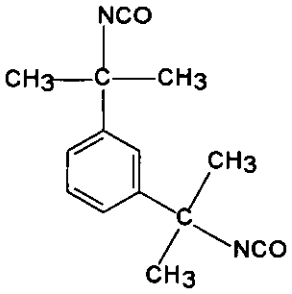

m-Tetramethylxylene diisocyanate (TMXDI)

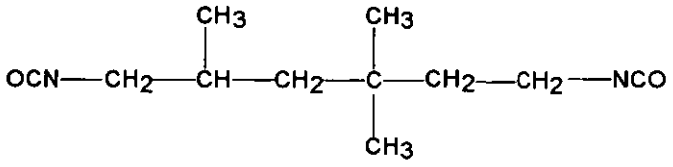

2,4,4-Trimethylhexamethylene diisocyanate (HDI)

Figure 2.18 Structural formulae of important diisocyanates.

The reactivity of isocyanate groups varies considerably. Generally, electron-withdrawing substituents increase the partial positive charge on the isocyanate carbon. Decreasing the electron density at the site of reaction, the carbon atom, favours the necessary attack by an electron donor[208]. Consequently, aromatic diisocyanates are far more reactive than aliphatic ones, since the conjugation with the phenyl ring leads

to an increase in the partial positive state of the NCO carbon (equation 2.32). In addition, tertiary isocyanate groups, such as those in TMXDI, are much less reactive than primary ones, with secondary ones being intermediate. This is due to the positive inductive effect of the alkyl groups. Furthermore, a strong steric hindrance through e.g. methyl groups contributes to a strongly decreased reactivity in some isocyanates (e.g. TMXDI). In a number of diisocyanates the NCO groups have a distinctly different reactivity[177]. In IPDI this is due to the different chemical environment, i.e. one NCO is of a primary nature, while the other is a secondary NCO group. In 2,4-TDI the NCO in the 2 position is 7-10 times less reactive that the other, mainly due to the steric hindrance of the methyl group.

The isocyanates used in this study were TMXDI, MDI, TDI, IPDI, HDI and HMDI. They have been chosen because of their very different reactivity rates and chemical structure.

Polymeric (oligomeric) polyols. The two major polyol classes used in the PUR synthesis are[204] polyester- and polyether-based (figure 2.19).

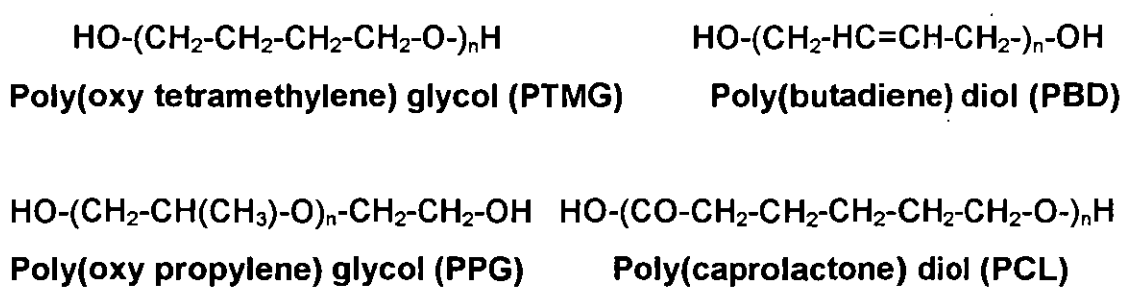

Figure 2.19 Representation of important polyols.

Polyether polyols represent 90 % of the polyol share and are formed through an anionic polyaddition mechanism. The reaction is usually initiated via an alcoholate ion, which reacts readily with monomeric epoxides. Termination by the addition of acids or water leads predominately to secondary hydroxyl groups in the polyol. The latter are less reactive[203] than primary ones by a factor of 10. Therefore, ethylene oxide is usually used to tip polyoxypropylene polyols.

Polyether and polyester polyols have a different property profile[204,211] and are, thus, employed according to the requirements of the application. Polyester glycols generally

impart better mechanical properties, UV stability and resistance to lipophile solvents. Polyether-based glycols show a greater resistance to hydrolysis, microbes and fungi[211] as well as an improved low temperature impact resistance. Polycaprolactone esters represent a means of imparting an increased hydrolysis resistance, while still offering the good mechanical properties of polyesters. They are also of lower viscosity and have a better cold flexing performance (lower glass transition temperatures) than the latter.

Further macroglycols used in polyurethane preparation include[204] natural products such as the trifunctional castor oil[203] and hydroxyl-terminated resins of polystyrene, poly(methyl methacrylate), polybutadiene[212] and polyisobutylene. More recently, a different class of polyether polyols have been developed. These are polymer-grafted polyether polyols[213] containing a stable vinyl polymer dispersion, mainly styrene and acrylonitrile[213]. Further modified polyether polyols include[207] polyharnstoff dispersion (PHD) polyols and polyols containing polyurethane dispersions.

In the present study, PPG, PTMG (PTHF) and PCL glycols of different molar masses represented the soft segment of the PUR. With the use of a polybutadiene diol in the grafting study, it was attempted to incorporate unsaturation into the polyurethane.

Chain extenders. These short-chain hydrogen-active components are mostly diols such as 1,4-dihydroxy butanediol diols (or triols like trimethylol propane) or diamines. The latter are predominately used if outstanding mechanical properties are desired. These are obtained due to the strong interactions between the forming urea links. It was found[214] that an even number of C-atoms in the main chain allows a more regular hard block structure, and thus a more segmented structure, to develop. Water is also sometimes used as a chain extender in foam compositions. The reactivity of the polyol and other hydrogen-active compounds varies strongly and is dependent[203] upon the basicity of the functional group. Consequently, primary hydroxyl groups are more reactive by far than secondary ones, with phenols still reacting much slower. Contrary to the isocyanate, an electron withdrawing substituent decreases the reactivity of the hydroxyl compound. Compared to other hydrogen-active compounds[203] which could represent competing reactions to the polyol-isocyanate reaction the latter one is rather found to be of medium reactivity (figure 2.20).

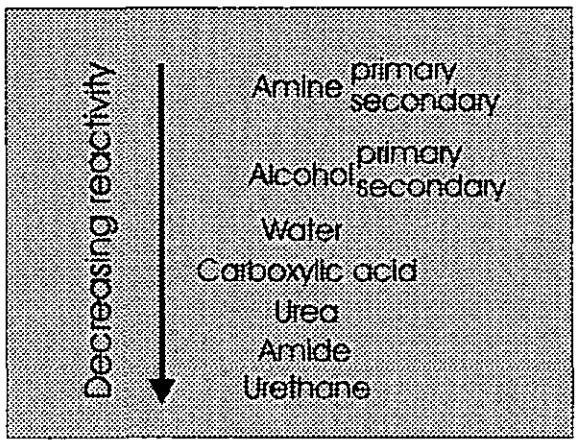

Figure 2.20 Reactivity of hydrogen-active compounds towards isocyanates.

By the choice of catalyst, a particular reaction can be favoured. In uncatalysed reactions, primary amines have the highest reactivity by far towards isocyanates. While the uncatalysed reaction with amines already proceeds at 0 °C, alcohols and water generally need slight heating (25 - 50 °C) and reactions with secondary isocyanate addition products (urea, amide, urethane) usually require temperatures above 100 °C[203]. In this study, butane diol was used in limited instances. Most materials were prepared with the trifunctional chain extender trimethylolpropane which at the same time acted as the PUR crosslinking agent.

2.3.3 PUR Elastomers: Morphology, Segmented Character and Damping

Polyurethane elastomers can be divided up into two groups. Thermoplastic polyurethane elastomers (TPURs) are crosslinked only by physical bonds of the urethane links in domains. Since these associations are mainly caused by hydrogen-bonding, they dissociate at higher temperatures (>150 °C) and TPURs can be readily processed using extrusion and injection moulding. The other group of elastomers contains covalent bonds forming a true loose network. This chemical crosslinking[205] can be brought about either by using trifunctional starting materials such as trimethylolpropane or a triisocyanate, or by a surplus of isocyante which may lead to the formation of allophanate (biuret) links (equations 2.23 and 2.24). Chemical crosslinking can disturb the segmental character and the non-covalent intermolecular attractive forces of a polyurethane. As a result, the mechanical properties of a chemically crosslinked material can be inferior to a physically crosslinked thermoplastic polyurethane elastomer. This was experienced in a study[205] where the

modulus and tensile strength went through a minimum with increasing crosslink density before increasing finally at very high crosslink levels. In opposition to that, increased crosslink density brought about the expected decrease in swelling. Generally, it is believed[205] that in polyurethanes with strong secondary interactions, i.e. polyester-based types, covalent crosslinking has a more detrimental effect on the mechanical properties than in materials with only weak attractive forces. An example for the latter type is a polyurethane, based on polyether with pendant methyl groups and chain extended by a diol. This type of material was used predominantly in the present study and here increasing crosslink density brings about improved physical properties.

Morphology. PURs have a block copolymer $(AB)_n$-type structure with urethane links alternating with the polyol chain. Consequently, the polyurethane morphology is dependent[207] upon its constituent raw material characteristics (chemical composition, oligomeric polyol chain length and flexibility, degree of crosslinking and branching), and, to an equal extent, upon the potential interchain forces. These interactions between the polymer chains are mainly occasioned by hydrogen bonds between the urethane links in the main chain. A PUR containing few urethane links (hard segments) compared to hydrocarbon units (soft segments) can behave like a thermoplastic elastomer. Increasing the amount of hard segments can transform a soft, malleable material into a hard and brittle solid. As previously indicated, most solid polyurethanes consist of three chemically different main building blocks, a diisocyanate, a chain extender and a polyol. As a consequence, they usually have a segmented character (figure 2.21).

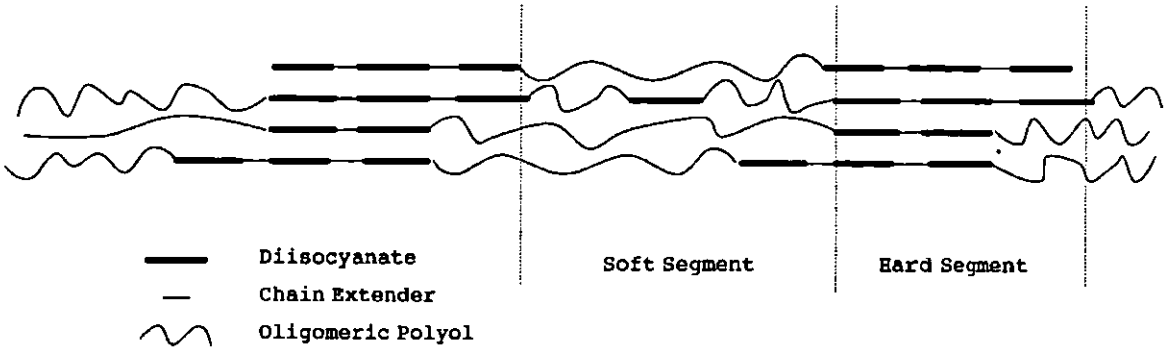

Figure 2.21 Segmented PUR with hard segment chain interaction.

The formation of hard and soft segments during the reaction is mainly related to the fact that the low molar mass glycol has a relatively high polarity[204] and, therefore, has only a limited miscibility, e.g. with a polyether glycol and a diisocyanate. As a consequence, covalently bond microphases of hard and soft segments are formed.

Hard segment. In segmented PURs, the hard segments[216] are located in cylindrical domains typically between 2.5 - 12.5 nm, embedded in the soft segment matrix. They mainly consist of urethane, urea, allophanate, biuret, and amid groups. These are very rigid groups held together[207] by hydrogen-bonding and π-electron interactions between the aromatic rings of the diisocyanates. The hard segments are a reinforcement on a molecular basis and can be seen either as a kind of crosslinking agent or a filler[217]. Thus, the melting point is strongly influenced by the hard segment. Depending on the primary structure of the hard segment (chemical nature, length of hard segment, degree of segregation), more or less ordered 3-dimensional proximity zones are formed[218]. Thus, the degree of order in the hard segments depends largely upon the symmetry of the diisocyanate and also on the number of C-atoms in the chain extender (an even number enhances hard segment stability). Chain conformation models of the hard domain showing the secondary structure with hydrogen-bonding have been established[219] by X-ray analysis. A more recent study[220] of the microphase structure was undertaken using SAXS. From investigating PURs based on symmetric MDI and asymmetric TDI diisocyanates, the effects of hard-segment sequence length were elucidated. It was concluded that folding of the longer hard segments back into the hard segment domain does occur. The hard segment domains are sometimes very irregular[221] due to their distribution width[222], and due to soft segments crossing the hard segment domains. The latter can represent up to 30% of the soft segment chains[223] and lead to incomplete segregation in the material. A more regular configuration of the hard segment can be achieved by annealing[204] slightly below the melting temperature. The hard segment imparts modulus, tear and tensile strength and determines the upper use temperatures[224], whereas the low temperature properties are only moderately influenced by the hard block.

Soft segment. The soft segment alternates with stiff oligourethane units and consists of mobile, flexible chains that are present in coiled conformation. It owes its name to its state at ambient temperatures, since the glass transition is usually clearly below 0 °C. Its predominant feature are long flexible alkyl, alkoxy or hydrocarbon chains. These are found in oligomeric polyols based on polyethers, polyesters (caprolactones) or other dihydroxy-terminated polymers such as poly(butadiene) diol with a typical molar mass of 400-8000 Daltons. Molar mass, functionality and chain structure determine the location of the glass transition temperature of the polyurethane. Furthermore, the chemical nature of the flexible chain determines the extent of segregation with the hard segment. If the soft segment is to some degree miscible with the hard segment, then the Tg transition is shifted to higher temperatures. This is caused by single hard segments dissolved in the soft segment matrix or by an incomplete segregation with the hard segment (soft segments trapped in the hard domains). The miscibility is influenced by the extent of the possible hard - soft segment interactions and the degree of order in the hard segment. A poly(butadiene) diol is not miscible with the hard segment, while the ether oxygen of poly(oxypropylene) glycols can interact with the acid H-atoms of the hard segments. Polyester-based polyols normally yield hardly segmented PURs due to the strong interaction of the ester link with the urethane links. The soft segment determines[216] the elastic nature and primarily the low temperature performance of the product. It also has an impact on hardness, tear strength and modulus.

Degree of segregation in the PUR. Phase segregation in PURs occurs due to the differences of the energies of cohesion of the constituent blocks. A compilation of some estimated cohesion energies[225] shows that the urethane and urea group have very high cohesion energies with the ester group having a lower one, and a methylene group having still a lower value. This difference of cohesion forces and lack of possible interactions between the blocks (e.g. urethane and ether) yields phase separated structures. At lower temperatures, the hard segment is immiscible with the soft segment. Therefore, upon cooling, a two-phase solid is observed[218]. Heating the material to higher temperatures can sometimes yield a single-phase melt.

The extent to which the polyurethane is phase separated is determined by a number of factors[204], including the chemical nature of the constituent raw materials, their interactions and the kinetic and thermal history of the reaction.

- Interactions between hard segments. Increasing the interactions (hydrogen-bonding and π electron interaction) between the hard segments yields a stronger phase separated product. Stronger interactions arise from the use of symmetric diisocyanates and by using chain extenders without bulky substituent. Amines yield urea links which are known[225] to exhibit stronger hydrogen-bonding. Also, an even number of carbons in the chain has been found to promote a more regular hard segment structure. Another way to obtain strong, hard segment interactions is to promote a regular hard segment length, i.e. to have a narrow hard segment length distribution.
- Affinity of the hard segment with the soft segment. The affinity between the hard and the soft segment is dependent upon the extent to which the polyol is capable of participating in hydrogen-bond formation with the urethane link. Thus, polyester polyols with the ester link have a far higher affinity with the urethane link than has the ether bond of polyether polyols, and so decrease segregation.
- Kinetics of the reaction and thermal history of the polyurethane. A fast reaction system does not allow the raw materials to phase separate before the polyaddition reaction takes place. Annealing the finished product for several hours slightly below the melting point of the hard segments leads to a more segregated structure.
- Type of synthesis route. The prepolymer route is known[204] to produce products of a more regular structure, which can therefore associate in a more ordered way. The one-shot route thus yields less segregated products.
- Miscibility of the starting materials. It has been commonly assumed that microphase separation starts from a homogeneous mixture of the monomers involved in the synthesis. Recently, however, workers have found[226] that in some systems the polymerisation starts from an already phase separated system. In a system composed of TDI, TDI end-capped hydroxyl-terminated polybutadiene and butadiene diol, separate phases were present right from the beginning of the reaction[226]. It was concluded that the dispersed butadiene diol droplets predetermined the phase separation with domains of several microns. It was proposed[226] that a similar reactant

incompatibility might also occur with other macroglycols (polyoxypropylene glycol), however, on a below micron scale.

Transitions in PURs. The transitions in polyurethanes can be very complicated due to the above mentioned influencing factors of the morphology (figure 2.22).

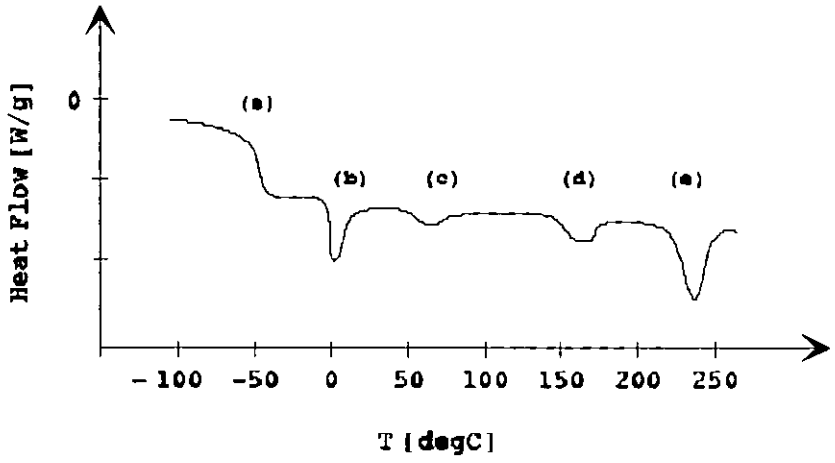

Figure 2.22 Possible transitions in PURs.

(a) Glass transition of pure polyol soft segment domains.
(b) Melting point of crystalline soft segment.
(c) Melting of hard segments of short range order or
breaking of hard-soft segment attractions.
(d) Melting of hard segments of long range order.
(e) Melting point of crystalline hard segments.

However, two transitions are always encountered. The one below room temperature is ascribed[207] to the glass transition temperature of the soft segment. The other, the dissociation of the hard segment, usually takes place well above 150 °C. Far more complicated situations can be obtained due to the presence of hard segments in the soft segment and vice versa. Also, crystallisation in either segment might introduce further endothermic losses. If the soft segment domains are mixed with some hard segments, then the glass transition of soft segment is smeared to higher temperatures. Differential scanning calorimetry has played an important role[227,228] in the elucidation

of the hard segment morphology. Usually, three hard segment endotherms can be observed, at 60-80 °C, 120-190 °C and above 200 °C. The former two are dependent[217] on the thermal history of the polyurethane. During ageing, they tend to shift towards higher temperatures. The location of the melting point of the crystalline hard segments is independent of annealing and quenching.

PURs for damping. As mentioned earlier, a good damping material is characterised by a high loss factor over a broad temperature range (section 2.2.3). The PUR transitions indicate that by decreasing the segregation between the hard and the soft segment in the polyurethane a broader soft segment glass transition temperature can result. However, one draw-back is that a less segregated material generally possesses poorer physical properties. The transition zone between the hard segment and soft segment phase is crucial for broadening the damping range. The amount and nature of it determine the damping behaviour of polyurethanes. The existence of this transition zone is due to a certain hard - soft segment miscibility. Consequently, the miscibility between the two phases has to be improved[113] in order to develop good damping materials. To do so the following has to be considered:

- The crystallinity in both hard and soft segment has to be reduced by using unsymmetrical raw materials.
- A decrease of hard - hard segment interactions has to be brought about by using unsymmetrical diisocyanates and diol chain extenders with bulky side groups and uneven C-atom number. Also, the introduction of free ends in the polyurethane can act as an internal compatibiliser and so weaken the interactions between two adjacent chains (oligourethane links).
- Increasing hard - soft segment interactions improves their compatibility. This can be done by choosing an unsymmetrical polyol that contains polar groups (polyester polyol) and has a broad molecular mass distribution. Also, the mixing of polyols of different molecular mass and polarity in the chains (e.g. PPG with PEA) can prove successful.
- The one-shot route usually yields broader distributions than the prepolymer route.
- By encouraging a fast reaction, kinetic control of phase separation can be achieved. The polyaddition takes place before the phase separation can develop.

2.3.4 Analysis of PUR, Raw Materials and Derivatives

Some important analytical methods for the characterisation of the PUR raw materials are briefly mentioned in the experimental part. This includes the determination of the NCO number of isocyanates and the hydroxyl number of polyols. Two further methods are infra-red and nuclear magnetic resonance spectroscopy. The latter was used to assure the purity of the isocyanates (section 3.1). Some characteristic IR-absorption bands of PURs and derivatives are given in the following.

Infra-red spectroscopy of PURs. Infra-red analysis plays an important role in understanding the bulk and surface properties of polyurethanes[229]. It is also very useful as a means to study the reaction rate of the polyurethane formation by monitoring the rate of disappearance of the NCO absorption band. In the present study, this was done to study the kinetics of the IPN formation. Furthermore, it is also possible to verify if a reaction has gone to completion since the NCO peak is easily discernible. The more important band spectra in urethane chemistry[229] are listed in table 2.3.

Table 2.3 IR bands of functional groups found in PURs.

Functional Group	Assignment/Type	Wave Length Absorption [nm]
N-H (amide)	ν (stretching)	3200-3500 3400 (H-bonded) 3300 (unbonded)
N=C=O (isocyanate)	ν (stretching)	2230
C=O (carbonyl)	ν (stretching)	1630-1780 1730 (unbonded) 1700 (H-bonded)
C=C (aromatic ring)	ν (stretching)	1590-1610
C-N + N-H (amide II)	ν (stretching)+ δ (in-plane bending)	1500-1540
C-N + N-H (amide III)	ν (stretching)+ δ (in-plane bending)	1230-1290
C-O-C (aliphatic ether)	ν (stretching)	1080-1120

3. EXPERIMENTAL

3.1 Materials

3.1.1 Compilation of Raw Materials

With exception of the compatibilisers which were synthesised in-house, all raw materials were obtained from commercial sources. All materials used are listed in table 3.1.

Table 3.1 Materials used in this study.

Name of Compound (Abbreviation)	Supplier	Function
Polyurethane network		
1,1,3,3-Tetramethylxylene diisocyanate (**TMXDI**)	CyTec	Diisocyanate
Isophorone diisocyanate (**IPDI**)	Hüls AG	Diisocyanate
Toluene diisocyanate (**TDI**)	Aldrich	Diisocyanate
4,4'-Methanediphenyl diisocyanate (**MDI**)	Kemira	Diisocyanate
2,2,4-Trimethylhexamethylene diisocyanate (**TMDI**)	Hüls AG	Diisocyanate
Poly(oxypropylene) glycol M.W. 425 (**PPG425**)	Aldrich	Polyol
Poly(oxypropylene) glycol M.W. 1025 (**PPG1025**)	BDH	Polyol
Poly(oxypropylene) glycol M.W. 2025 (**PPG2025**)	BDH	Polyol
Poly(oxypropylene) glycol M.W. 4000 (**PPG4000**)	Aldrich	Polyol
Poly(oxytetramethylene) glycol 1000 (**PTMG1000**)	Aldrich	Polyol
Poly(oxytetramethylene) glycol 2000 (**PTMG2000**)	Aldrich	Polyol
Poly(caprolactone) glycol M.W.1000 (**PCL1000**)	Interox Chem.	Polyol
Poly(caprolactone) glycol M.W.2000 (**PCL2000**)	Interox Chem.	Polyol
Poly(butadiene) diol M.W. 2500 (**PBD2500**)	Aldrich	Polyol
Trimethylol propane (**TMP**)	Aldrich	Crosslinker
Butane-1,4-diol (**BD**)	Aldrich	Chain extender
Stannous octoate (**SnOc**)	Sigma	Catalyst

Glassy network		
Methyl methacrylate (**MMA**)	Aldrich	Monomer
Ethyl methacrylate (**EMA**)	Aldrich	Monomer
Butyl methacrylate (**BMA**)	Aldrich	Monomer
Styrene (**S**)	Aldrich	Monomer
Tetraethyleneglycol dimethacrylate (**TEGDM**)	Aldrich	Crosslinker
Divinylbenzene (**DVB**)	Aldrich	Crosslinker
Azobiisobutyronitrile (**AIBN**)	BDH	Initiator

Grafting agents, compatibilisers and ionic groups		
Benzene-1-(1-isocyanato-1-methylethyl) -3-(1-methylethenyl) (**TMI**)	CyTec Grafting Agent	
2-Hydroxyethyl methacrylate (**HEMA**)	Aldrich	Grafting Agent
7-Octene-1,2-diol (**OD**)	Aldrich	Grafting Agent
2-Butene-1,4-diol (**BED**)	Aldrich	Grafting Agent
TMI-PPG-TMI (**PPG-TMI**)	in house	Compatibiliser
HEMA-TMXDI-HEMA (**TMXDI-HEMA**)	in house	Compatibiliser
HEMA-TMXDI-PPG1000-TMXDI-HEMA (**UA2**)	in house	Compatibiliser
N-Methyldiethanolamine (**MDEA**)	Aldrich	Ionic group
Methacrylic acid (**MAA**)	Aldrich	Ionic group

Emulsion polymerisation		
4,4'-Azobis (4-cyanovaleric acid) (**AVAC**)	Aldrich	Initiator
Dodecyl sulfate sodium salt (**DSS**)	Aldrich	Emulsifier

Structural formulae of the diisocyanates and the polyols used in this study were given in section 2.3.2. Further representations of important materials are given in figure 3.1.

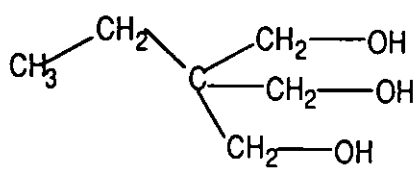

TMP

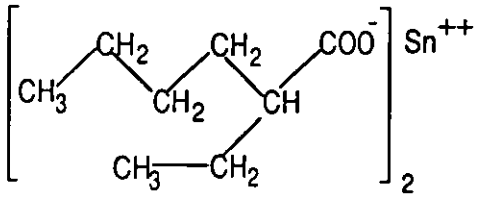

SnOc

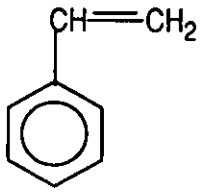

S

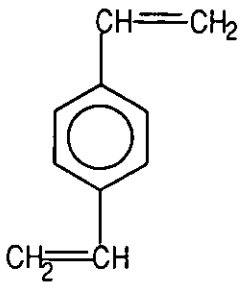

DVB

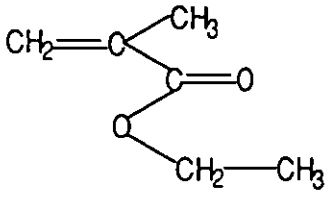

EMA

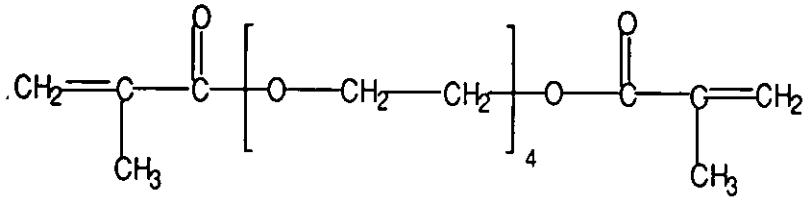

TEGDM

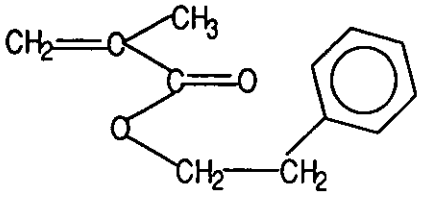

EPMA

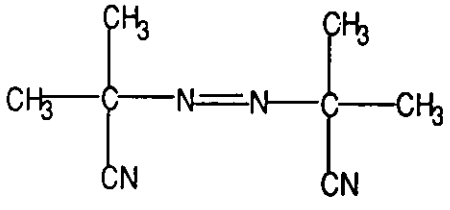

AIBN

Figure 3.1 Representation of important raw materials.

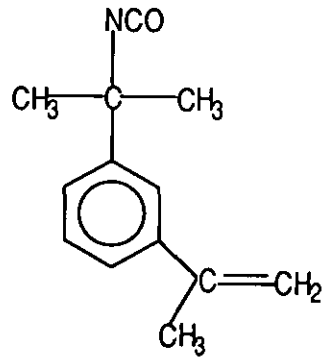

TMI

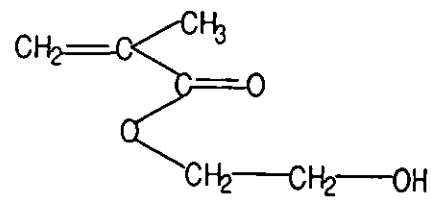

HEMA

Figure 3.1 continued (Representation of important raw materials.)

3.1.2 Synthesis of the Urethane Acrylate-type Compatibilisers

Following the principle of like dissolves like[3], chemically similar components are an obvious choice for a compatibiliser. Thus, the three different urethane acrylate type compatibilisers were prepared from the raw materials used in the polyurethane network.

a) A difunctional urethane acrylate involving PPG 1025, TMXDI and HEMA.

HEMA-TMXDI-(PPG 1025-TMXDI)$_n$-HEMA, with n=1

b) A simple HEMA-terminated TMXDI.

HEMA-TMXDI-HEMA

c) A simple TMI-terminated glycol.

TMI-PPG1025-TMI

Preparation. All addition reactions were conducted under nitrogen in toluene, which had previously been dried over molecular sieve. The reaction temperature was set at 40°C. For all preparations, the catalyst concentration was kept at 1 weight % stannous octoate. The syntheses of compatibiliser b) and c) were straightforward. First, the difunctional component and the catalyst were placed into a three-necked flask. Then, the stoichiometric amount of the end-capping agent was gradually added with stirring. A direct complete addition might have caused local overheating, which in turn could have initiated the polymerisation of the vinyl groups. For compatibiliser a), the

stoichiometric addition of the materials proceeded step-wise in order to assure the closest outcome to the products. 1 h stirring was allowed in-between the addition steps. Finally, HEMA was added to end-cap the compatibiliser. The toluene was distilled off using a rotary evaporator at 40°C. No further purification of the products was undertaken.

Products. Resin-type liquids with very different viscosities were obtained. The viscosity was dominated by the interactions (hydrogen-bonding) between the urethane links. Thus, it was not surprising that the urethane acrylate of the lowest molar mass, HEMA-TMXDI-HEMA, exhibited the highest viscosity at room temperature. It had the highest volume fraction of urethane links. At 60°C, the interactions were much weaker and a pourable liquid was obtained. All urethane acrylates were analysed by FTIR spectroscopy, to ascertain that the hydroxyl and isocyanate groups had reacted, and that the unsaturation was still present. The GPC data for the highest molar mass compatibiliser (a) indicated that a distribution of different species was present.

3.1.3 Purification by Degassing

All starting materials were degassed prior to use in order to avoid the formation of air bubbles in the curing film. This was done by applying a high vacuum at room temperature. Only highly volatile raw materials like the monomers were not submitted to this procedure. The hygroscopic polyols were degassed at 80°C. This is the generally applied[230] procedure to remove traces of water. The purified materials had a nitrogen blanket applied over them and were then stored in a desiccator over silica gel.

3.1.4 Characterisation of the Raw Materials

Generally, the raw materials were used as supplied. However, it was important to ascertain that the raw materials for the polyurethane reaction were pure. This was essential since in the case of the diisocyanate and the glycol stoichiometric quantities of both components had to be used. Accordingly, the latter were characterised with respect to purity and functionality. For the same reason, the molar mass of the polyol and potential grafting agent poly(butadiene) diol was also determined.

3.1.4.1 Isocyanate Number of Diisocyanates

The isocyanate content of all diisocyanates was determined using the dibutylamine back-titration method[205]. The reaction of diisocyanates with primary or secondary amines yields the corresponding urea. The excess amine was then back-titrated with hydrochloric acid using bromophenol blue as indicator. A colour change from blue to yellow that persists 15s indicated the end-point. The NCO content is given by the following equation.

% NCO = 4.2 N (ml sample - ml blank) 100/1000 W, (3.1)

where W represents the sample weight in grams and N the normality of the HCl solution. All isocyanates were found to be within the limits of the theoretical values, and, therefore, taken as 100 % pure.

3.1.4.2 Hydroxyl Number of Polyols

Various methods of hydroxyl number determination exist for the different kinds of hydroxyl-terminated materials. David and Staley[230] recommended the phthalation method for polyols. A small sample of the polyol is reacted for one hour at 115°C with an excess of phthalic anhydride using pyridine as solvent. Back-titration of the excess reagent using KOH and phenolphthalein as indicator allows the determination of the OH value (equation 3.2).

OH value = 56.1 N (ml blank- ml sample)/ sample weight, [illegible] (3.2)

where N is the normality of the NaOH solution. Three samples were run and the average compared to the blank. The hydroxyl numbers of the polyols used in this study were in good accordance with the numbers provided by the suppliers. Thus, the quoted molar masses were used in the calculation.

3.1.4.3 Melting point by DSC and Water Content of Polyols

The melting points of the at room temperature crystalline polyols were determined by differential scanning calorimetry (DSC). The instrument is described in section 3.4.4. Using a heating ramp of 10°C/min, the following values for the polyol melting points and the heats of fusion were obtained (table 3.1).

Table 3.1 Melting points and heats of fusion of crystalline polyols.

Polyol	Melting point, T_m [°C]	Heat of fusion [J/g]
PTMG1000	24	86
PTMG2000	33	107
PCL1000	36	52
PCL2000	53	72

The water content of the polyols had to be determined since isocyanates react with water to yield urea linkages (section 2.3.2). Furthermore, this reaction liberates CO_2 (equation 2.20) which would introduce unwanted bubbles into the IPN film. The water content determination after Karl Fischer is[231] the most important chemical method of this kind. In the course of the reaction of water with the Karl Fischer reagents (iodine, pyridine, sulphur dioxide and methanol), the reduction of I_2 to HI is monitored to determine the water content.

$$C_5H_5N\ I_2 + C_5H_5N\ SO_2 + C_5H_5N + H_2O \qquad (3.3)$$
$$\text{----> } 2\ C_5H_5N\ HI + C_5H_5N\ SO_3$$

The end point can be detected visually (colour change from yellow to brown) or by electrometric methods. In this study, the electrometric method was utilised using a Baird and Tatlock AF3 instrument. The water content of all the polyols used was found to be less than to 0.01%by wt.

3.1.4.4 Molar Mass Determination by GPC and VPO

Two methods were used to determine the molecular weight of the polyols in particular of the poly(butadiene) diol and of the urethane acrylate compatibilisers. The absolute determination of the number average molar mass (Mn) by vapour pressure osmometry (VPO) was necessary for the correct stoichiometry of the NCO:OH ratio. Gel permeation chromatography (GPC) yields only relative values for Mn if no standards of the sample polymer are available. However, GPC provides information about the molecular weight distribution, which is sometimes a very important quantity.

Gel permeation chromatography. The molar mass distribution[177] of a polymeric sample is an important characteristic. Gel permeation chromatography is based on a molecular size separation process. Small molecules more frequently penetrate the gel and are thus eluted later. The elution times are compared to a standard calibration series of known molar mass. This is most commonly polystyrene. The theory to this analysis technique is described elsewhere[177].

In this study, GPC was utilised to determine the molar mass distribution of the in-house synthesised urethane acrylate compatibiliser UA2. Also, the grafting agent poly(butadiene) diol was examined. Figure 3.2 shows the data of the in-house synthesised urethane acrylate compatibiliser type (a).

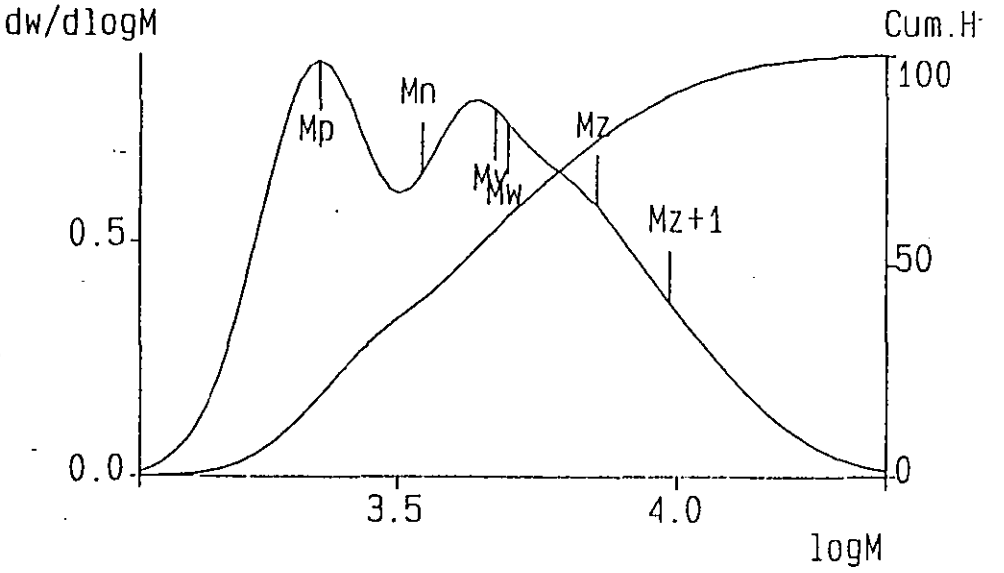

Figure 3.2 GPC data of the urethane acrylate compatibiliser (a).

From this GPC data of the urethane acrylate compatibiliser type (a) (UA2), it can be seen that besides the main product with one PPG 1025 unit, n = 1, also some material with n = 2 and of type (b) were present (section 3.1.2.1). Compared to the bimodal molar mass distribution of UA2, PBD2500 exhibited one peak only.

Vapour pressure osmometry. Vapour pressure osmometry was carried out in order to determine the absolute number average molar mass, M_n, of the polybutadiene diol grafting agent. After Raoult's law[232] for an ideal solution, the partial vapour pressure of each component is proportional to its mole fraction. For the VPO determination, two drops are suspended side by side in a thermostatted chamber saturated with solvent vapour. However, the difference in vapour pressure is not measured directly, but the temperature difference. Greater condensation (or lower evaporation) will provoke a higher temperature at the solution drop. The difference in temperature is proportional to the vapour pressure lowering. A plot of the resistance difference divided by the concentration, Δ R/c, against the concentration c yields a straight line with the intercept K/Mn.

$$\Delta R/c = K/Mn + a2c \qquad (3.4)$$

A calibration with a concentration series of a known solute (e.g. benzil in the range from 0.005 to 0.05 M) permits the determination of K, after which M_n of the unknown sample can be determined. Since in colligative methods all molecules contribute to the molecular weight, solvents and solutes must be extremely pure.

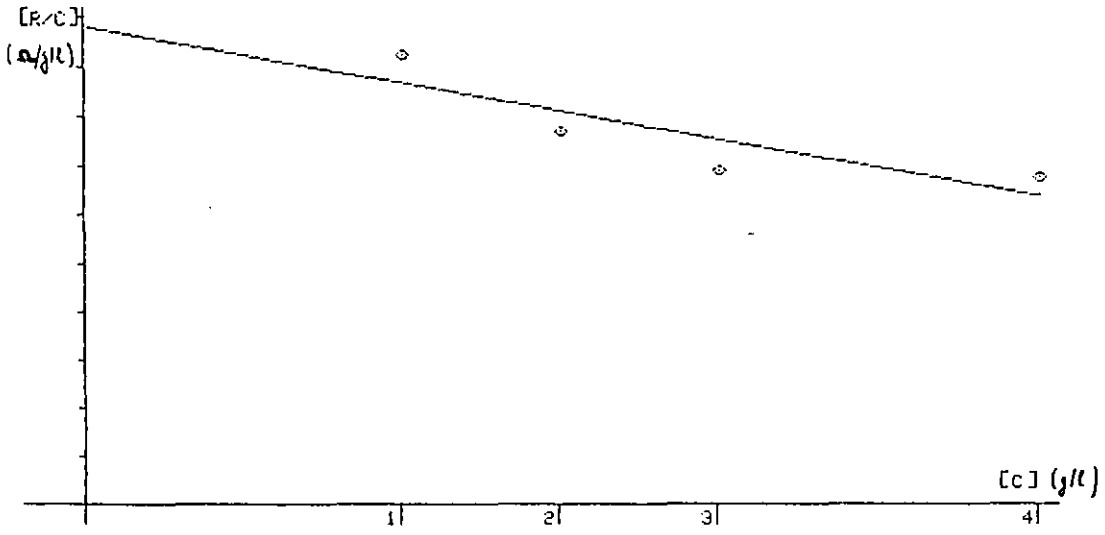

Figure 3.3 VPO data of the poly(butadiene) diol.

The M_n of the poly(butadiene) diol was found to be 2500 g/mol by VPO. This compared to a value of 3800 g/mol by GPC using polystyrene standards (section 3.1.2.2). The M_n determined by VPO was taken for the IPN calculations.

3.1.4.5 Spectroscopic Analyses: NMR and FTIR

In order to assure the purity of the raw materials, spectroscopic analyses were conducted. The diisocyanates and the diols were analysed by NMR and FTIR spectroscopy.

NMR Spectroscopy. The diisocyanates were analysed in $CDCl_3$ using a Bruker 400 MHz spectrometer. It was found that all the materials were of high purity. The ^{1}H and ^{13}C spectra of TMXDI are shown in figure 3.4.

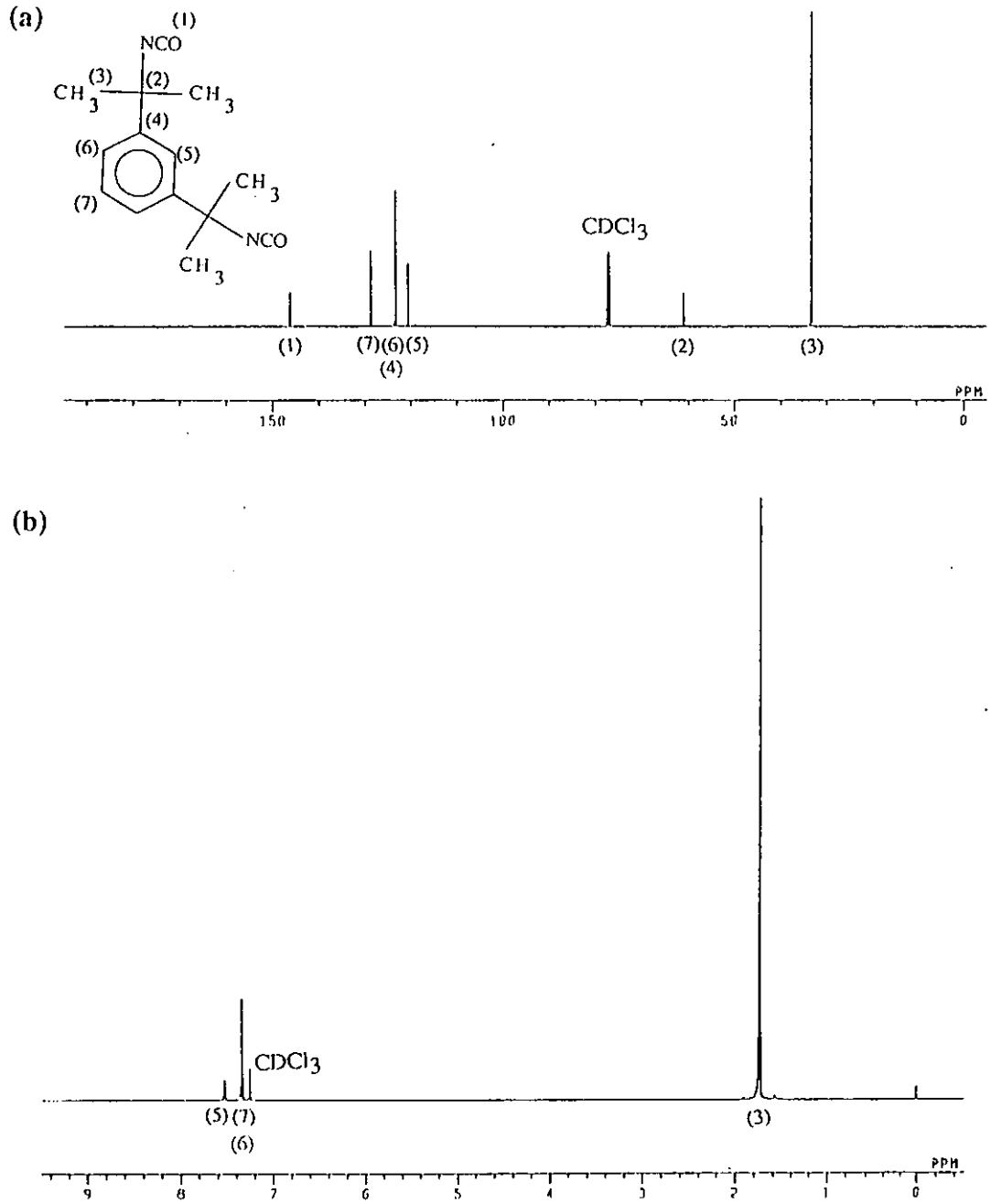

Figure 3.4 Carbon 13 (a) and proton (b) NMR of pure TMXDI.

FTIR spectroscopy. Besides the commercially obtained raw materials, the in-house synthesised materials were also subjected to FTIR analysis. This was of particular importance in the case of the urethane acrylate compatibilisers. It had to be confirmed that no functional moiety that could react with the forming polyurethane network was present. This way it could be ascertained that only physical interactions between the two networks took place, as opposed to the chemical links that were introduced in the grafted IPNs. FTIR data showing the disappearance of the NCO and OH moieties in the isocyanate and polyol, respectively, are show in figure 3.5.

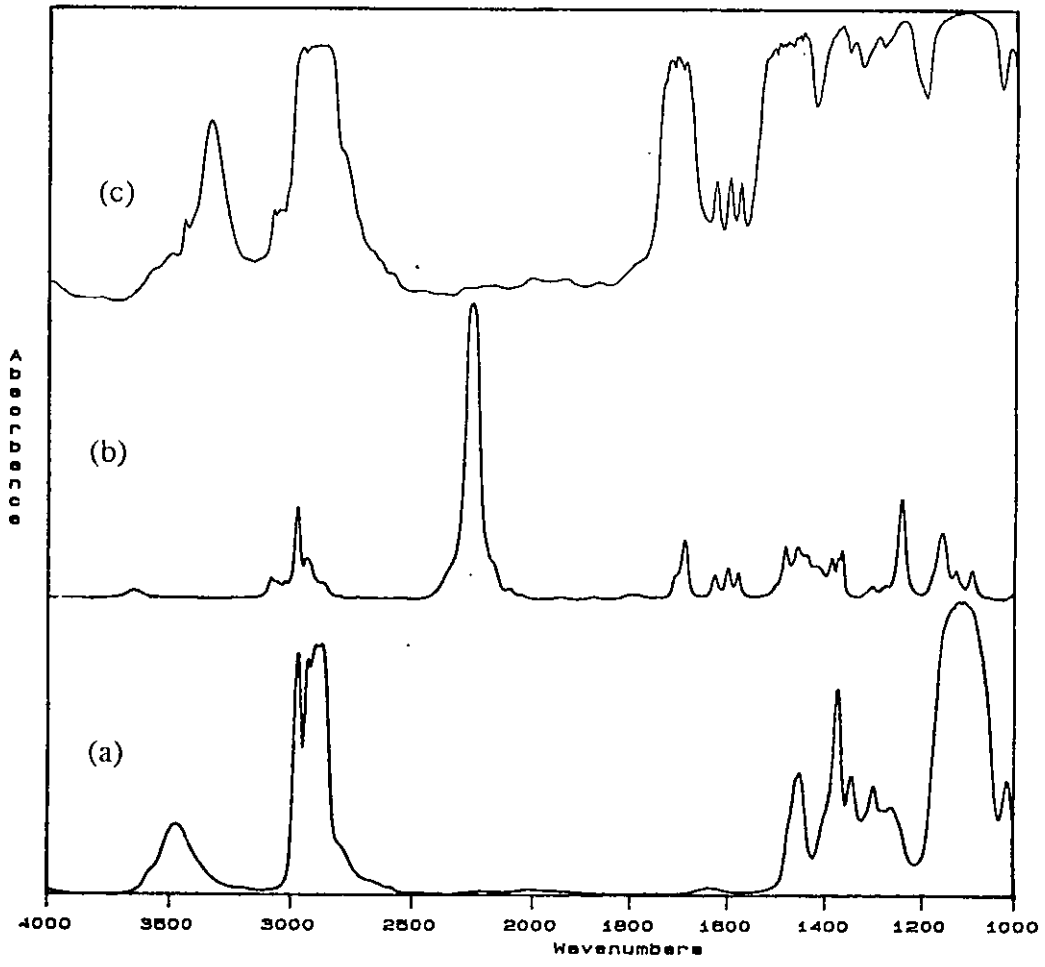

Figure 3.5 Staggered FTIR-specra of urethane acrylate compatibiliser (TMI-PPG1025) and its raw materials. (a) PPG1025, (b) TMI and (c) TMI-PPG1025.

The three staggered traces are (a) the poly(oxypropylene) diol PPG1025, (b) the grafting agent TMI and the resulting adduct (c) the TMI-PPG1025. It can be seen in spectrum (c) that both the NCO peak at 2230 cm^{-1} and the OH peak at 3500 cm^{-1} have disappeared, while the vinyl band at 1635 cm^{-1} is still present. Bands that have appeared which indicate urethane formation are the N-H stretching band between 3300 and 3500 cm^{-1}, the carbonyl band between 1700 - 1730 cm^{-1} and the combined C-N stretching and N-H in-plane bending around 1500-1540 cm^{-1}(section 2.3.4). All urethane acrylate compatibilisers were confirmed fully reacted prior to use.

3.2 Experimental Apparatus

The main experimental apparatus consisting of the mixing apparatus, the mould and the curing oven is described briefly in the following.

3.2.1 Mixing Apparatus

A high speed stirrer (type Heidolph RZR 1) from Heidolph was used for thoroughly mixing the components. Initially, a three-necked 250 ml reaction vessel was used for the mixing of the components (figure 3.6).

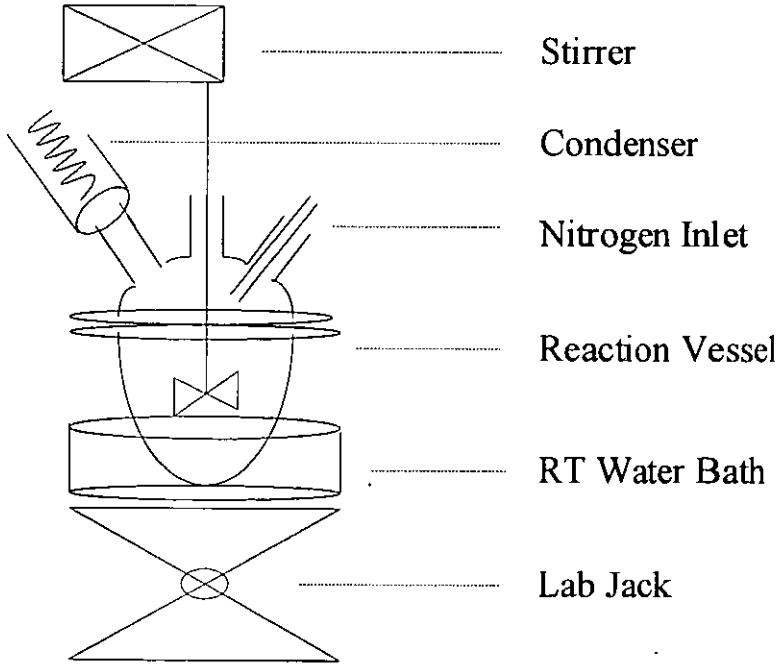

Figure 3.6 Schematic representation of mixing apparatus.

In the course of the study, it was observed that a disposable glass jar could be used as a substitute. With exception of the condenser that was omitted, the basic set-up was similar. The glass jar lid contained two openings, one fitting the stirrer shaft, the other served as a nitrogen inlet.

3.2.2 Moulds

4 O-ring-type steel moulds of 140 mm diameter were used in this study. A 6 mm diameter nitrile rubber gasket acted as a seal and spacer between the two metal plates. The system was hold together by 5 spring-loaded screws. The moulds were coated twice with release spray. The release agent used was Cil Release 1711~Plus from Compounding Ingredients Limited.

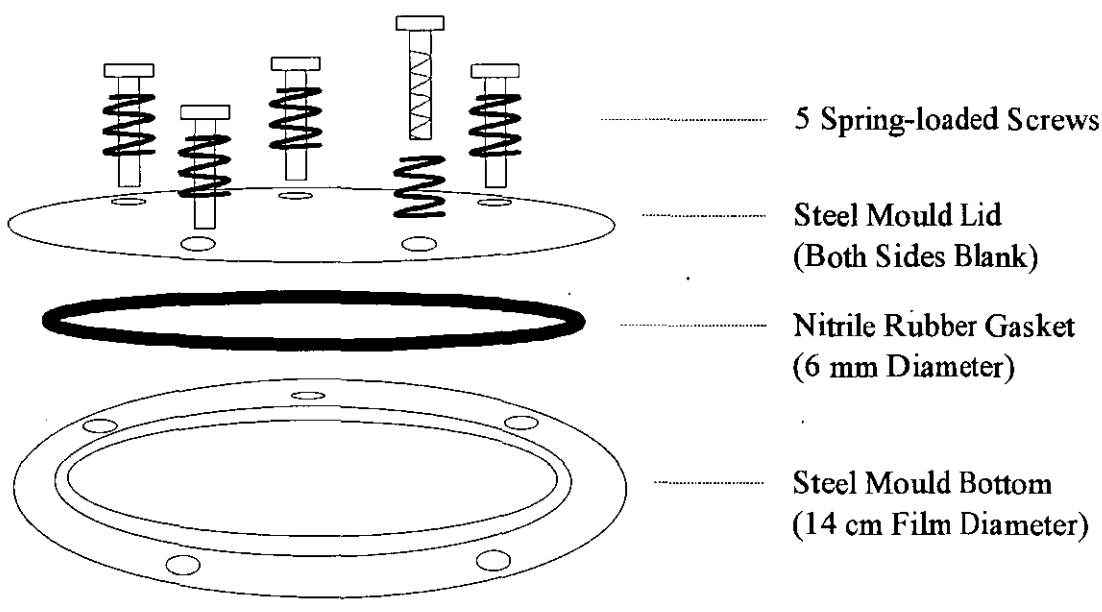

Figure 3.7 Schematic representation of the O-ring mould.

3.2.3 Open Air Oven

A Hearson open air oven was used for the curing of the samples. Four moulds could be contained simultaneously. Temperature readings of two degrees Celsius below and above the setting temperature were considered as permissible for a correct curing cycle.

3.3 Experimental Technique

3.3.1 Calculation Principles of IPN Formulations and Catalyst Concentrations

For the ease and security of manipulation, all calculations were carried out using a Microsoft Quattro Pro data spreadsheet. The parameters to vary were placed on the top of the sheet. These included the 8 points that are briefly outlined in the following text. The spreadsheet used with a full compilation of an exemplary calculation is depicted in figure 3.8.

- **Ratio polyurethane component/polymer component**. In order to calculate the ratio, the complete polyurethane component, including the diisocyanate, the polyol and the catalyst was related to the complete polymer component (monomer, crosslinker and initiator). Neither grafting agents nor compatibilisers were included in either of the former components.
- **Isocyanate/hydroxyl ratio**. Apart from one study (section 4.4.4), this ratio was kept constant throughout at NCO/OH = 1.1:1.0. Not only the polyurethane component was considered to calculate the ratio. The functional groups introduced by the grafting agents were also taken into account. TMI, for example, was considered in the NCO part, whereas the diols like 7-octene-1,2-diol were added to the OH part.
- **Diol/triol ratio**. The total moles of diol were referred to the moles of triol. The difunctional grafting agents were included in form of diols in this calculation.
- **Polyurethane catalyst**. The catalyst was calculated in weight % of the total PUR component. The amount of catalyst was varied according to the amount of PUR present.
- **Crosslinking agent**. The calculation was conducted in mole % with respect to the monomer used. The unsaturation of the grafting agent was not heeded in this calculation.
- **Initiator**. The initiator was calculated in mole % with respect to the unsaturated double bonds present in the system. The initiator - other than the catalyst - is consumed by the initiation reaction, and its amount influences the molar mass of the polymer. Thus, the mole % of the initiator were referred to the moles of monomer plus the moles of the di-functional crosslinking agent and the moles of the grafting agent.

29-Aug-94

EXPERIMENT NO.: IPN 143

Objective: Compatabiliser Study

Composition of IPN Formula

Parameters to Choose			
IPN ratio PU / Polymer:	60	:	40
Polyurethane components			
Isocyanate / hydroxyl ratio:	1.1	:	1
Diol / Triol:	3	:	1
PU catalyst [PUweight%]:			1.2%
Polymer components			
Cross-linking agent [mole%]:			5.0%
Initiator [mole%]:			1.0%
Compatabiliser			
TMI-PPG 425			5.0%
Total mould weight [g]:			35.0

Calculated Weights	Subst.	M.W.	Moles		Theor.	Actual
Diisocyanate	TMXDI	244.34	1.2375	302.37	5.40	
Diol	PPG	1025.00	0.7500	768.75	13.72	
Triol	TMP	134.18	0.2500	33.55	0.60	
Catalyst	SnOc	405.10	0.0331	13.42	0.24	
Total				1118.08	19.95	
Monomer	S	104.15	1.0000	104.15	12.32	
Crosslinker	DVB	130.19	0.0500	6.51	0.77	
Initiator	AIBN	164.21	0.0110	1.81	0.21	
Total				112.47	13.30	
TMI-PPG 425					1.75	
Total					35.00	

Comments	
Solubility:	PU comp.: PS comp.: Blend:
Mixing:	Stirrer setting at 3; mixing for 5 min.
Cloud point:	Minutes after blending:
Degassing:	1 times for 5 min in total.
Moulding:	Mixture viscosity: Visual appearence:
	Moulding into cold (RT) mould; demoulding at 120 degC.
Cure:	24 h at 60 C; 24 h at 80 C; 24 h at 90 C; 2 h at 120 C.
Product:	Air entrapped: Mould fill: Film surface:

Figure 3.8 Example of the calculation sheet.

• **Grafting agent and compatibiliser**. Both were incorporated in weight % of the total component weight, this is the polyurethane component and the polymer component plus the former components themselves.

• **Total component weight**. It consisted of the sum of the polyurethane, the polymer component and the grafting agent or compatibiliser.

No arithmetic considerations were given to the purity of the chemicals used. The basic polyurethane components, i.e. the polyols and the diisocyanates, were found to be pure (section 3.1). All other chemicals used were of a grade higher than 95%. The only exception was divinylbenzene. It contained isomers, and, thus, was only of 55% purity.

Catalyst concentration and mixture viscosity. In this study, the monomer initially served as a solvent for the forming polyurethane. Thus, depending upon the IPN composition - 10% monomer or 50%, for example - and the rate of formation of the polyurethane network, different reaction mixture viscosities were obtained.
However, good films could only be prepared with ease at a controlled viscosity of the mixture. It should not be to low, otherwise good mould filling was difficult to realise. A too high viscosity on the other hand made complete degassing and good moulding impossible. Consequently, the concentration of the stannous octoate had to be adapted to the composition and the amount of diisocyanate used. Therefore, gelation studies with different amounts of catalyst had to be conducted. It was noted that SnOc of a shelf life of 6 months was slightly less efficient than a new one, even though it had been stored in a desiccator under nitrogen. Furthermore, it had to be taken into account that the amount of catalyst to be used also varied considerably with a change in diisocyanate reactivity. In figure 3.9, the percentages used with the TMXDI series are given. For other diisocyantes, up to 50 % less had to be used in order to yield the same moulding viscosity.

For the preparation of the PUR homonetworks a fixed catalyst level of 0.2 weight % was employed.

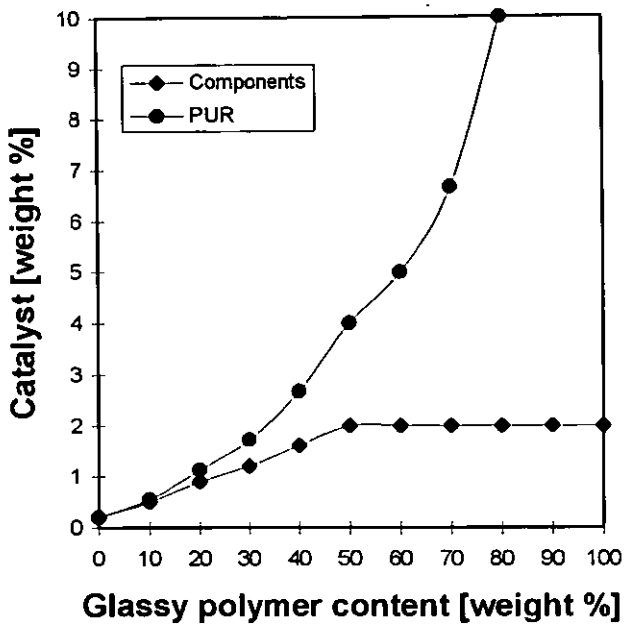

Figure 3.9 Catalyst concentration as a function of composition. Graph for TMXDI-based PUR:PS IPNs (diol/triol 3:1).

The two full data series show the amount of SnOc used with respect to the PUR weight and the total component weight. In order not to exceed a total of 2 weight % of stannous octoate in the system, the higher glassy polymer content mixtures (60-100%) were moulded at low viscosity. In addition to the PUR content, the crosslink density of the PUR also had an influence on the viscosity of the reaction mixture. An increase of the low molar mass TMP compared to PPG1025 resulted in a higher hard segment content. Since the formation of the urethane links is exothermic, a greater number of formed urethane links caused the temperature of the reaction mix to rise and increased further the PUR reaction rate. Thus, at higher PUR crosslinking levels, the catalyst concentration had to be cut back to compensate for the before mentioned phenomenon. The two data series in figure 3.9 are given for PPG1025/TMP ratios of 3:1.

3.3.2 Synthesis of IPNs

A schematic summary of the IPN sheet preparation is given in figure 3.10. The single stages are explained in more detail in the section below.

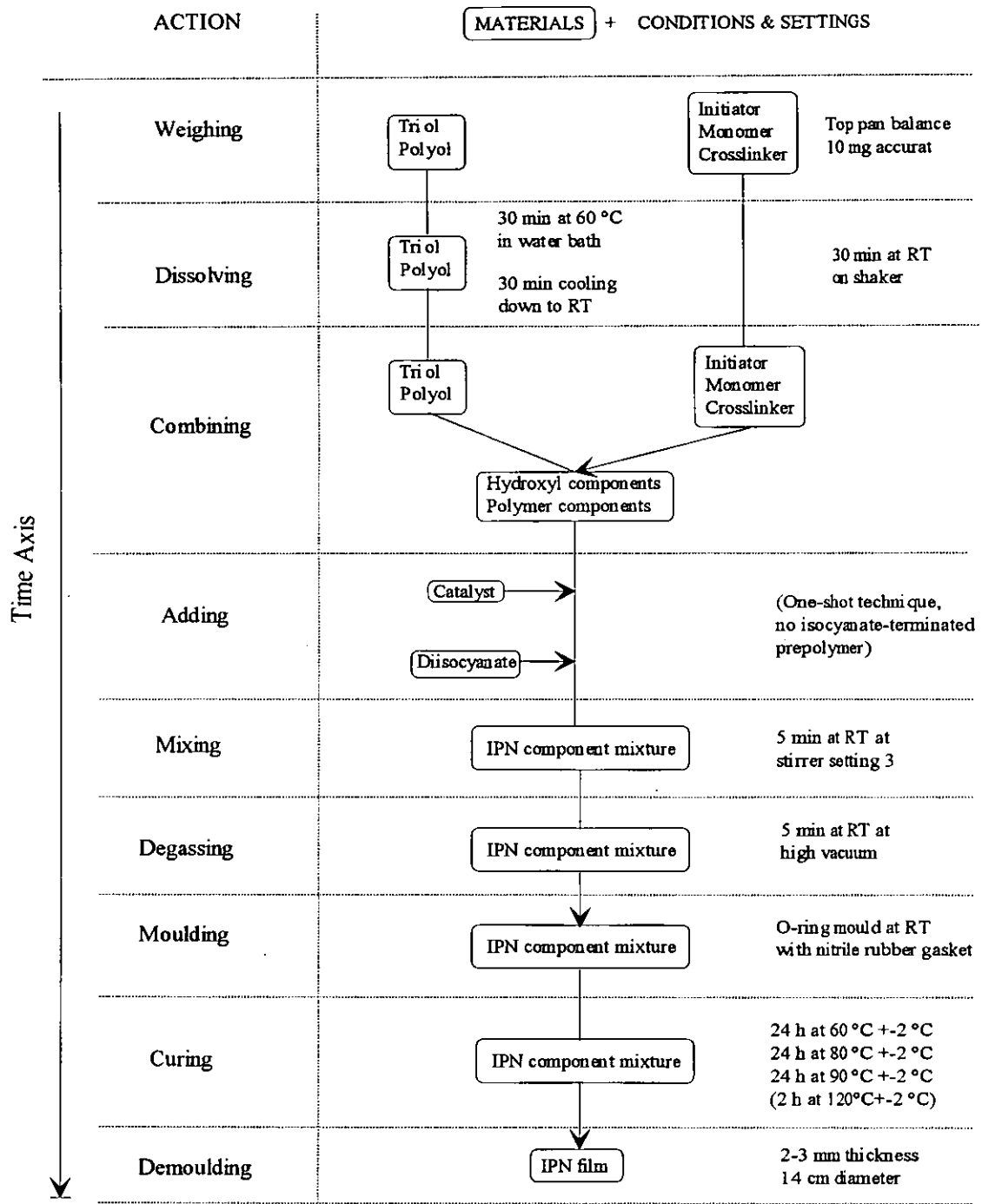

Figure 3.10 Schematic representation of the IPN film synthesis via the one-shot technique.

3.3.2.1 Preparation of the Components

Both network components were weighed into separate disposable receptacles. The triol was combined with the diol in a screw top jar. In order to bring the TMP (T_m= 58 °C) into solution, the mixture was heated up to 60°C in a waterbath. An important fact was that upon cooling down to room temperature the triol remained in solution. In the second jar, the glassy polymer component was prepared. After weighing the initiator, the monomer and the crosslinker into the receptacle, the jar was placed in a shaker for half an hour. This allowed the initiator to be completely dissolved. The polyurethane catalyst and the grafting agents or compatibilisers were added to the combined components at room temperature. Finally, the diisocyanate was weighed in (figure 3.10).

3.3.2.2 Mixing of the Materials

Immediately after addition of the diisocyanates, the mixture was put on the mixing apparatus and stirred vigorously for 5 min. The stirrer setting was fixed at 200 rpm.

3.3.2.3 Degassing of Mixture

The degassing of the mixture was conducted for 5 minutes under vacuum. After 5 minutes, no more evolution of bubbles was observed for any mixture. Weighing of the reaction mixture before and after degassing ensured that no significant amount of monomer was taken off. Any lost monomer was replaced.

3.3.2.4 Moulding of the Mixture

The mixture was carefully poured into the prepared moulds and the mould top placed onto the nitrile rubber gasket. The 5 screws were tightly fitted and the mould then placed in the 60°C preheated curing oven.

3.3.2.5 Curing Cycle in Open Air Oven

In order to assure complete curing, the curing cycle was extended over 72 h. It comprised three stages with 24 h at 60 °C ± 2 °C, 24 h at 80 °C ± 2 °C and 24 h at 90 °C ± 2 °C (figure 3.11). The curing was started at 60°C in order to prevent the monomer from evaporating prior to reacting, and, thus, creating bubbles in the film.

For contents of over 50% PS in PUR/PS IPN a fourth stage had to be included to allow a good demoulding of the IPN films. This stage comprised 1 h at 120 °C ± 2 °C.

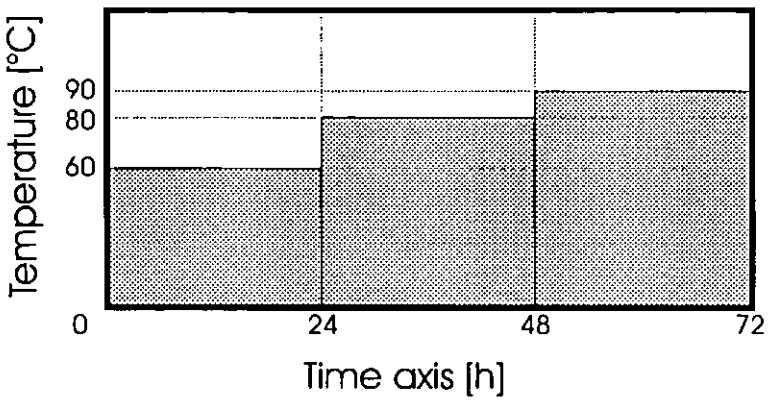

Figure 3.11 Curing cycle settings.

Because of the inertia of the steel moulds (mass: 2 kg), a heating lag in attaining the setting temperature took place. It was important to know after how long and what conversion of the polyurethane component the polymerisation of the glassy polymer started. Therefore, a recording of the actual temperatures of curing cycle in the centre of the steel mould was conducted (figure 3.12). This was done by inserting a type K thermocouple through the nitrile rubber joint into the centre of the mould.

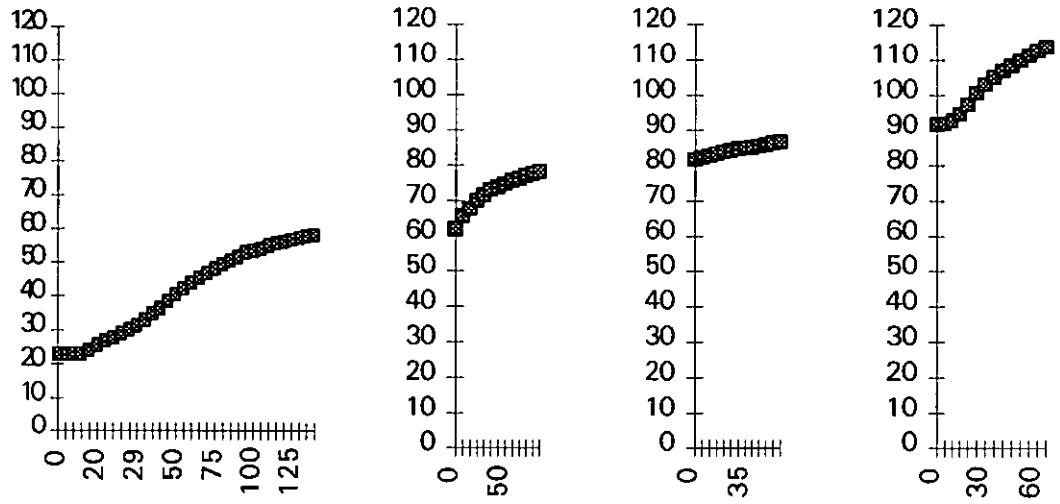

1. Curing Cycle 2. Cycle 3. Cycle (Demoulding high PS contents)

Figure 3.12 Actual curing cycle monitored via thermocouple (temperature rise in °C versus time in minutes).

This curing cycle was monitored during the production of the 60:40 PUR (TMXDI-based)/PS IPN at a PPG1025/TMP ratio of 3:1 and with 5% DVB. Slight variations of the temperatures could be the case for a more reactive diisocyanate and a higher catalyst concentration. With the knowledge of the actual curing cycle i.e. the attainment of the set temperatures, the kinetics of the IPN network formation were studied. This was done using a FTIR spectrometer fitted with a heating cell unit.

3.3.2.6 Observations During the IPN Preparation

The actual weights of the components added to the preparation mixture were recorded for all preparations. Additionally, observations concerning solubility, visual aspect of the blend before moulding, viscosity of the mixture and additional comments were noted (figure 3.8).

3.3.3 Preparation of Test Samples

The samples were cut from the 2 mm thick sheet 24 h before testing. This was important for the dynamic mechanical thermal analysis and the tensile testing where possible strain in the materials could have resulted in misleading results. The procedure for the preparation of samples for the transmission and scanning electron microscopy is outlined in sections 3.4.2 and 3.4.3.

3.4 Analysis of Products

All products were analysed by DMTA. The latter represented the most important analysis technique for this study, since information about the IPN miscibility and morphology, the engineering properties and the damping characteristics can be obtained. Interesting sheets with respect to IPN miscibility, morphology and damping properties were then further characterised by tensile testing, hardness measurements, transmission and scanning electron microscopy, modulated-temperature and conventional differential scanning calorimetry, infra-red spectroscopy with a heated cell, swelling measurements and X-ray diffraction. These techniques and the instrumentation are briefly outlined in the following sections.

3.4.1 Dynamic Mechanical Thermal Analysis (DMTA)

DMTA was the principal test method in this study, and every sheet synthesised was submitted to this test. It is recognised[151,158] that DMTA is an invaluable tool capable of providing information about molecular structure and engineering properties of polymers. Contrary to DSC, which measures the changes in heat capacity, with the DMTA technique molecular motions are examined[158]. A small sinusoidally varying stress is applied to the test specimen and the resulting strain is measured by a transducer[233]. As already outlined in section II.2.2, the strain can be divided up into an in-phase elastic-like component governed by the storage modulus E', and an out-of-phase viscous-like component governed by the loss modulus E". The third quantity determined by DMTA is the loss factor, tan δ. Additionally, isothermal studies can be conducted, and activation energies for the α and β transitions can be determined[177] using the Arrhenius relation.

Instrumentation. The DMTA instrument used in this study was the Rheometrics (formerly Polymer Laboratories) MK II dynamic mechanical thermal analyser. It consists of four main parts, namely (i) the mechanical spectrometer head with a demountable low-temperature furnace, (ii) the thermal analyser, (iii) the temperature programmer and (iv) an IBM-compatible computer with plotter. A cut away view of the mechanical spectrometer head[234] is shown in figure 3.13.

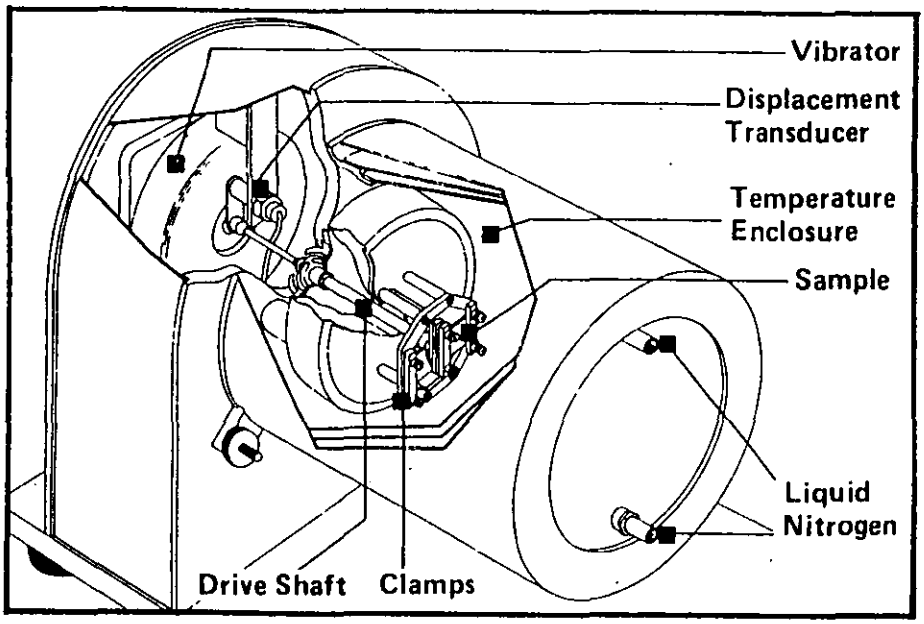

Figure 3.13 DMTA spectrometer head[234] - cut away view.

The DMTA instrument allows samples to be tested in three different modes. The shear mode is used for soft, elastomeric materials, while the tensile mode is used for fibre-forming materials. For the former, a sample in form of a disc is required, whereas a thin films are used for the latter. The bending mode is used for tough to brittle materials. Thus, the bending was mode chosen for this study (see figure 3.14).

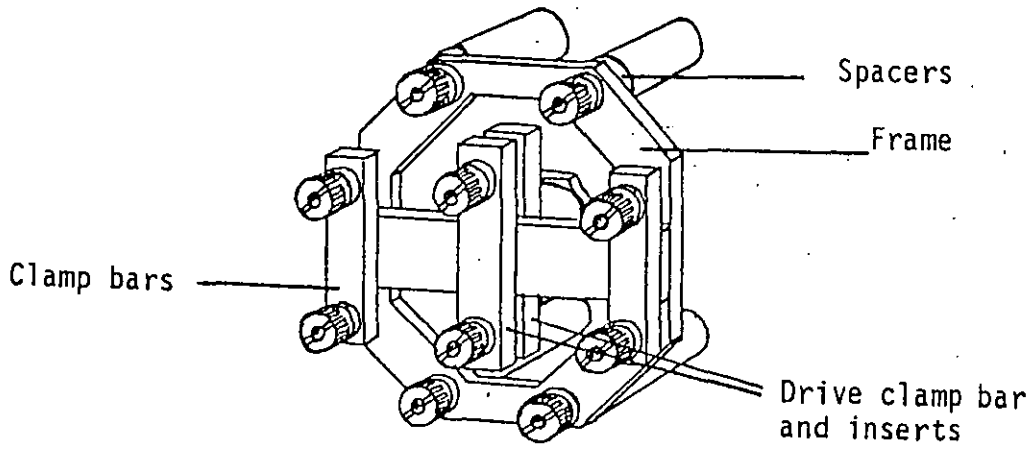

Figure 3.14 Clamping arrangement for bending mode[233].

Using the bending mode, the samples can be fixed in a single or dual cantilever clamping assembly. The single cantilever assembly is easier to use and more reliable[235], and was, therefore, used in this study. Sample specimens in form of bars are required with typical dimensions of 15 mm x 10 mm x 3 mm. The samples were analysed in a temperature range between -60 (-100) to 200 °C at a heating rate of 3 °C/min. The frequency chosen was 10 Hz. The strain amplitude was fixed at x4.

Information from DMTA data. The data obtained from the dynamic mechanical analysis give information about the transitions in polymers and the degree of miscibility in the blends. Three data curves are obtained. A profile of the loss factor (tan δ) versus temperature, the storage modulus E' and the loss modulus E" versus temperature. Any two of them define the third parameter. The loss factor and the storage modulus plot versus temperature are the most commonly used[13].

Loss factor versus temperature profile. From the loss factor versus temperature profile of a polymer blend conclusions about the composition, miscibility, phase continuity and damping ability can be drawn (figure 3.15).

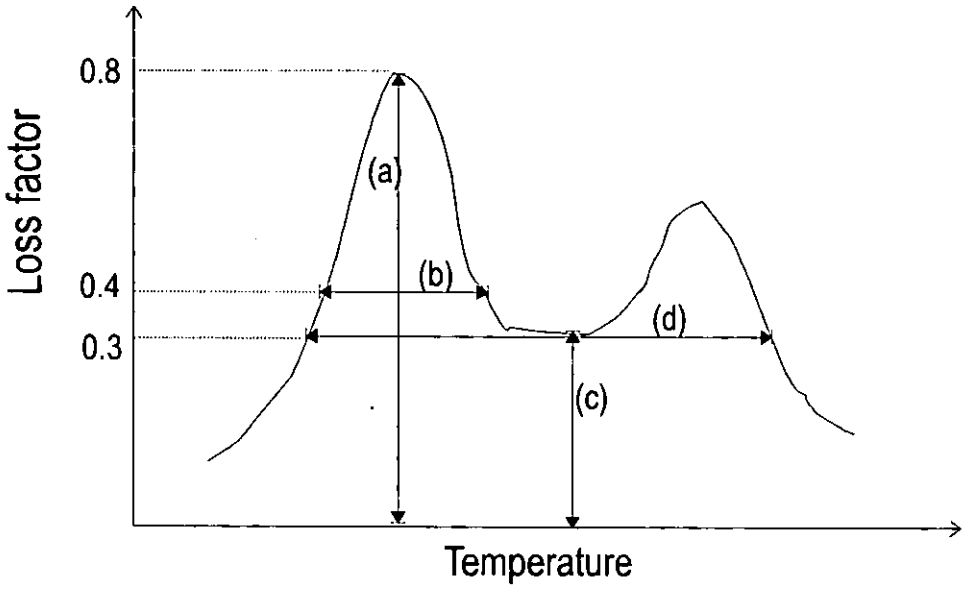

Figure 3.15 Miscibility conclusions from DMTA data.

(a) Tan δ peak heights. The heights of the tan δ peaks can give indications about the proportions of each component. Also, it has been observed[13] that the higher tan δ peak indicates the polymer that constitutes the continuous phase.

(b) Tan δ half-peak widths. The half-peak widths of the tan δ peaks are a criterion for the extent of component mixing in a polymer blend. Larger half-peak widths are an indication of better miscibility.

(c) Tan δ height at intermediate temperature. The location of the inner transition minimum and its height at this temperature reveal information about the miscibility in a polymer blend. High intermediate tan δ values are indicative for a certain degree of phase mixing being present.

(d) Tan δ range above 0.3. The temperature range over which tan δ is higher than 0.3 is an important characteristic for good damping materials.

The various degrees of miscibility that can be present in a polymer blend of polymers with well separated Tgs far apart are shown in figure 3.16.

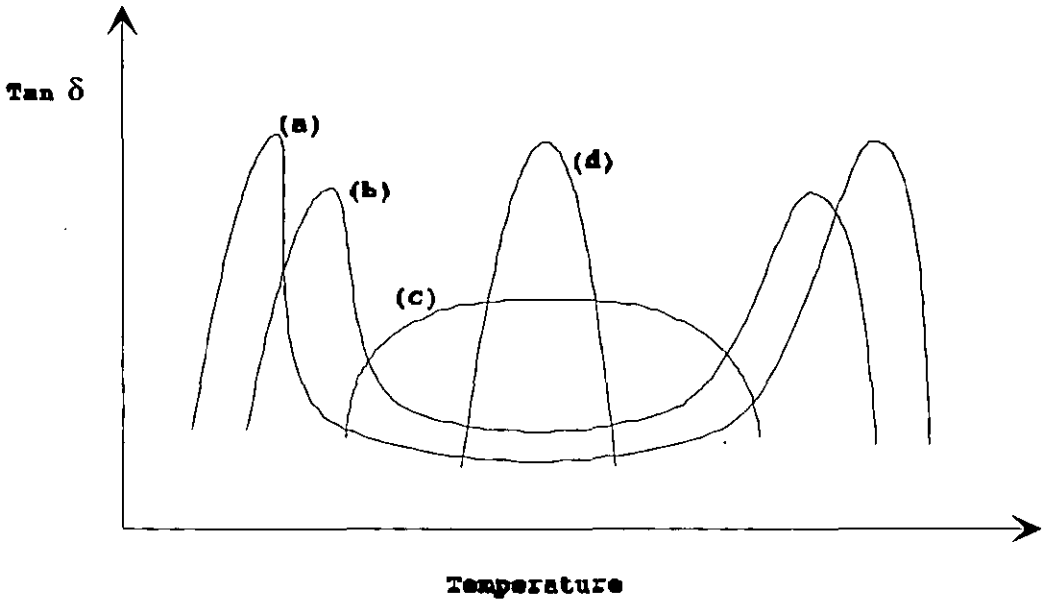

Figure 3.16 Polymer blends of various degrees of miscibility.

The location of the tan δ peaks is of paramount importance in a polymer blend study. Four possible situations are generally encountered[113].

(a) If the two polymers are immiscible, then two glass transition peaks at the location of their respective homopolymer will be seen.

(b) A blend of polymers that exhibit some degree of miscibility will have their peak locations shifted inwards. Also, the tan δ values of the inter-transition zone will be higher.

(c) A broad transition of almost rectangular shape is obtained for semi-miscible materials. Here, a microheterogeneous structure with domains in the order of 5-30 nm prevail. This structure is desired for viscoelastic damping material and is most commonly encountered in IPNs (section 2.2.5).

(d) Miscible polymers yield a single glass transition peak. Depending on the extent of miscibility it will vary in breadth.

Storage modulus versus temperature profile. From the storage modulus versus temperature profile information about the miscibility of a polymer blend can be obtained. Furthermore, a prediction of the mechanical properties at different temperatures can be made.

Figure 3.17 shows three situations with blend miscibility increasing from (a) to (c). Curve (a) depicts an immiscible polymer blend exhibiting two clearly separated glass transition peaks. (b) is characteristic for a broad transition comparable to the microheterogeneous structure (c) in figure 3.16. In (c), the polymer blend is miscible and exhibits only one Tg.

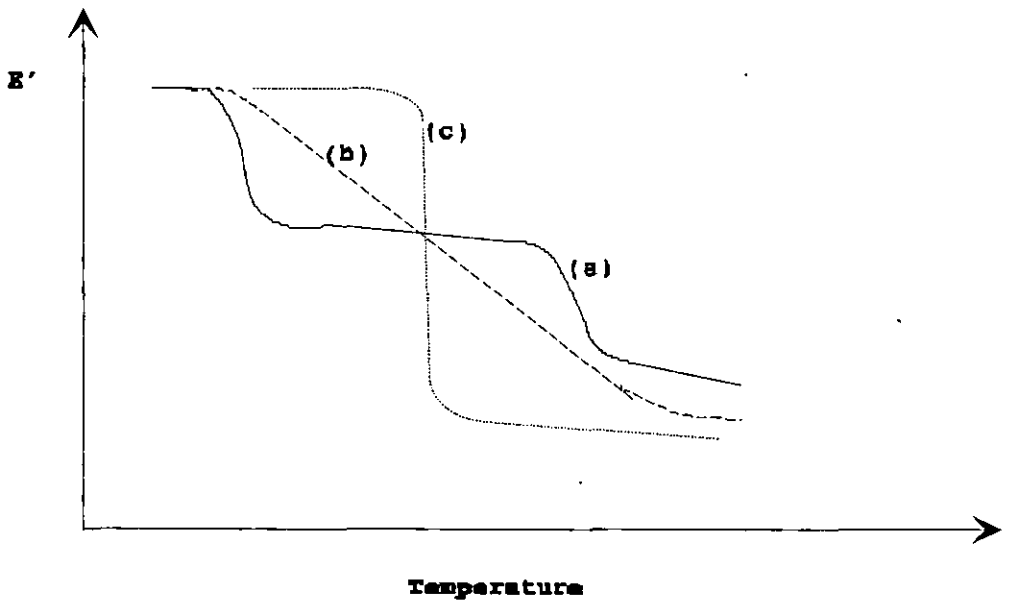

Figure 3.17 Polymer blends of various degrees of miscibility.

At Tg, E' drops by about three decades[93]. The height of the rubbery plateau modulus is influenced[185] by molar mass, crosslink density, crystallintiy, plasticisation.

Loss modulus versus temperature profile. The loss modulus E" is less frequently used for the illustration of the dynamic mechanical properties of a polymer blend. Similar to the loss factor plot, a peak is observed about the polymer Tg (section 2.2.2). With soft materials, it may be advantageous to determine Tg from the E" versus temperature profile. The height and location of the E" loss peak and the area under the

linear loss modulus versus temperature curve (LA) are important characteristics[13] for extensional layer damping applications.

3.4.2 Transmission Electron Microscopy (TEM)

Electron microscopy is a powerful tool in elucidating the morphology of multiphase polymers[236]. Consequently, TEM has been used[237,238] in many instances in order to determine the miscibility and phase segregation of polyurethanes and interpenetrating polymer networks. Furthermore, information about polymer blend morphology can be gained. This includes information about the continuous phase and the size and shape of the domains and their distribution. At high magnifications, domains in the order of 1 nm can be investigated[236]. The preparation of the samples can be difficult since ultrathin sections of the material have to be cut. The instrument[236], the specimen preparation[239,240] and the interpretation[240], and possible artefacts through electron beam damage[236] and sectioning damage[240] have been described.

Instrument. The TEM studies were conducted with a Joel 100 instrument. The instrument was run with an accelerating voltage of 60 kV and sample magnifications from 5 000 up to 300 000 times were used.

Sample Preparation. The sample preparation was difficult due to the soft character of most IPN sheets at room temperature. Thus, prior to sectioning, the sample was embedded into epoxy resin to increase the hardness. For this purpose Spurr's embedding resin[241] was used. It possesses a pot life of three days at 8-10°C and is polymerised for 9 h at 70°C. Ultrathin sections of 100 nm thickness were cut using a LKA Bromma 8800 Ultratome III ultramicrotome. In order to obtain a better contrast the Kato[239] staining technique with osmium tetroxide (OsO_4) was used. A simplified reaction scheme for how OsO_4[107] adds to unsaturated polymer chains is shown in figure 3.18.

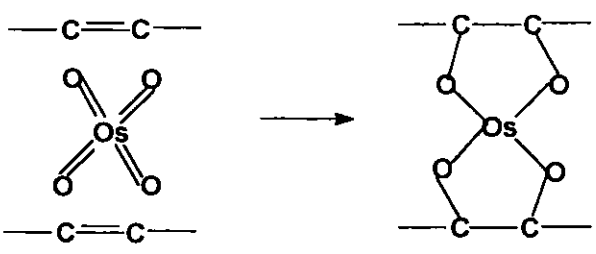

Figure 3.18 Simplified reaction scheme for OsO4 staining[107].

Osmium tetroxide is known[242] to stain preferentially the PUR component in the IPN. The ultrathin sample was cut and placed onto a copper grid. The copper grid containing the sample was then immersed into the 2% OsO_4 solution for two days. After washing off the excess OsO_4 with distilled water, the samples were dried and stored in a sample case.

3.4.3 Scanning Electron Microscopy (SEM)

Scanning electron microscopy is widely used with polymeric samples[243] and can complement[244] information gained from transmission electron microscopy. While TEM provides two-dimensional information only, SEM can give some insight into topographic features of a fracture surface[240]. Three imaging signals can be used[245], back-scattered electrons, secondary electrons and x-rays. Characteristic x-rays have well-defined energies for different atoms. Thus, analytical information can be obtained from an x-ray spectrum[244]. Back-scattered electrons are primary beam electrons which have been elastically scattered by the nuclei in the sample and escape from the surface. Thus, they can be used to obtain compositional contrast in the sample. Secondary electrons are emitted with low energy from the top few nanometers of the material. This technique yields topographic images of the sample surface.

In the present study, the SEM micrographs were taken with a Leica Cambridge Stereoscan S360 instrument. The fracture surfaces were obtained from the failed tensile test specimens. These surfaces were sputtered with gold to avoid electrostatic charge and poor image resolution.

3.4.4 Differential Scanning Calorimetry (DSC)

Differential scanning calorimetry is extensively used[158] to measure transitions in polymers and polymer blends. This technique relies upon the change[158,246] at endothermic and exothermic transitions and shows changes in the heat capacity when the polymer undergoes a secondary transition. Reference and sample pan are scanned through a pre-set time-temperature programme. The power difference that is necessary to keep these at equal temperature is plotted against the temperature. Thereby, the glass transition temperature, crystallisation, melting and degradation behaviour can be

examined. The advantages of DSC are that only a small amount of sample is required and that wide temperature ranges can be examined[158]. Recently, efforts have been made[247] to correlate DMTA and DSC results. It was attempted to predict the location of the loss factor peak of dynamic viscoelastic measurements from DSC Tg data. This would enable the damping engineer to select suitable damping materials for high frequency application from DSC data. The latter are more easily available and often tabulated[185] in literature.

A DuPont 910 Differential Scanning Calorimeter combined with the DuPont 2000 Thermal Analysis System was used for this study. The samples were run from -130 °C to +200 °C at a heating rate of 10 °C/min.

3.4.5 Modulated-temperature Differential Scanning Calorimetry (M-TDSC)

This new technique[248] was used to study the transitions in the IPNs. It differs from conventional DSC in that instead of a constant time-temperature programme, a sinusiodally varying heating rate is applied to the sample. This method makes it possible to distinguish between reversible and irreversible phenomena[248] in polymer systems. Also, the extent of mixing in polymer blends can be studied, to considerable advantage, over the glass transition region by using the M-TDSC differential of the heat capacity versus temperature signal[249].

Measurements were made using a TA Instruments M-TDSC. An oscillation amplitude of 0.8°C and an oscillation period of 60s were used throughout this investigation. A heating rate of 3°C/min was used.

3.4.6 Thermogravimetric Analysis (TGA)

Thermogravimetric analysis is part of the group of thermal analysis methods such as DSC and DMTA. TGA involves[107] the continuous measurement of the weight of a sample that is subjected to a pre-defined heating programme. TGA can be used to follow the loss of volatile components (e.g. water and plasticisers) and to determine the decomposition temperature of polymers and the inorganic filler content of composites. By combining TGA with infra-red spectroscopy and gas chromatography more detailed information about the polymer degradation process can be obtained[107].

A TG 760 Series Rheometric Scientific instrument was used in this study. Samples of 4-6 mg were analysed in air and nitrogen atmospheres in order to determine the upper survival temperatures of the IPNs and homopolymers. The heating ramp used was 10°C/min from room temperature to 700°C.

3.4.7 Tensile Testing

Stress-strain measurements are amongst the most widely used basic measurements of the mechanical properties of polymers. Information about the modulus, strength and elasticity of a material is obtained[155,156].

In the present study, the tensile tests were conducted using a Lloyd 1 2000R instrument equipped with a 500 N load cell. A crosshead speed of 50 mm/min was employed. Small size dumb-bells with a gage length of 30 mm were used throughout this study. Tests were conducted at 23°C ± 1°C and the values quoted are an average of 4-5 samples. The quantities investigated included the stress at break, the strain at break, Young's modulus and the toughness index (figure 3.19).

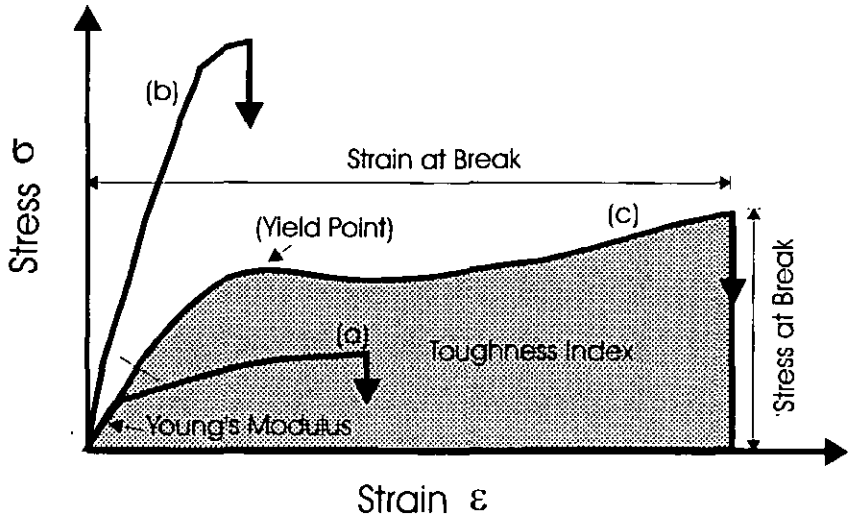

Figure 3.19 Tensile properties investigated.

In addition to the mechanical properties evaluated, there are three classes of tensile responses represented in figure 3.19. (a) is a typical stress-strain curve of a weak and

soft material, (b) of a hard and brittle and (c) of a tough and strong material. All three responses were found in IPNs of different composition.

3.4.8 Hardness Measurements

Hardness measurements determine[250] the resistance of a material to penetration into its surface layers by an indentor. The hardness of a material is directly related to its modulus, strength and elasticity[251]. The most well-known methods for determining the hardness of plastics using conical indentors are the Shore A and Shore D hardness tests.

In the present study, hardness measurements of the IPNs were conducted to investigate phase inversion. Further, hardness values are frequently quoted for commercially available PURs. Thus comparing these with the prepared IPNs should prove interesting. Shore A hardness was determined using a Zwick model 3114 gauge whilst a Jamaica Instruments gauge was used to evaluate Shore D values. The testing was conducted at room temperature (23 ± 1°C). Hardness values quoted are from an average of 8 readings taken at random over the entire specimen surface.

3.4.9 FTIR Spectrometry with Heated Cell Unit

The reaction kinetics of the individual components are known[64,252,253] to have an influence on phase separation and the concomitant properties of multiphase polymers. Therefore, the formation of a limited number of IPNs was followed via FTIR spectroscopy.

In infra-red spectroscopy, functional groups absorb[254] infra-red light of characteristic wavelengths. Following the Lambert-Beer law, the concentration of the absorbing species is proportional to the area under the peak. The depletion of the functional moieties, here, of the isocyanate and the vinyl group, were monitored during the course of the reaction. This indicated the conversion of the developing polyurethane and polymer network. An internal standard had to be chosen in order to compensate for any possible variations in sample thickness during the course of the reaction. For this study, the combined CH_2 and CH_3 area served this purpose.

The instrumentation consisted of a heated cell and controller from Specac 20100 and an FTIR spectrometer from Unicam. The temperature programme of the heating cell

was conducted according to the actual heating rate of the curing cycle. These actual temperatures were obtained by monitoring the temperature curve during a curing cycle with a thermocouple inside the mould. Spectra were taken in five minute intervals and three peak areas were integrated. The integration limits for the respective functional moieties were as follows.

NCO:	2330 - 2160 cm^{-1}
C=C:	1637 - 1622 cm^{-1}
CH_2 and CH_3:	3136 - 2810 cm^{-1}

All spectra were taken in the absorbence mode. A plot of the conversion versus time for both polymers indicated which network tended to form first under the specific reaction conditions.

3.4.10 Swelling Studies and Soxhlet Extraction

Swelling studies[93] of crosslinked polymers can be used to determine the solubility parameter δ and the average molecular weight between crosslinks (M_c). Furthermore, the sol/gel content in a crosslinked polymer system can be evaluated. For the latter, the Soxhlet extraction technique is most commonly used.

The solubility parameter can be determined by immersing a polymer sample into a series of solvents until equilibrium weight is attained. Thus, polymer samples of 0.2 g were immersed in the swelling agent until equilibrium weight was attained (72 h). Weight measurements were made by blotting the samples dry and placing them into a pre-tared capped vial. In order to account for solvent extraction of linear/low molar mass material, the dry sample weight (m_0) was obtained by re-weighing the sample after removal of the swelling agent. The swelling agent was removed by applying vacuum at 70°C for 14 days. The swelling coefficient Q was determined from the equilibrium swollen weight of the sample and the final dried weight (equation 3.5.)

$$Q = ((m-m_0)/m_0)\,(1/\rho_S), \qquad (3.5)$$

where m is the weight of the swollen polymer sample, m_0 is the dry weight and ρ_S is the density of the solvent. From the swelling data, a plot of Q versus the solubility

parameters of the swelling agents was constructed. The maximum of the plot was taken as the solubility parameter of the material.

The swelling agents series are listed in table 3.3.

Table 3.3 Solubility parameters of swelling agents.

Solvent	Solubility parameter δ[(a)] $[J/cm^3]^{1/2}$	Density @ 20°C $[g/cm^3]$	Hydrogen bonding[(b)]
Pentane	14.3	0.626	p
Diethyl ether	15.1	0.708	m
Ethyl methacrylate	17.0	0.917	m
Butyl formate	18.2	0.892	m
Methylcyclohexane	19.0	0.770	m
Cyclohexanone	20.3	0.947	m
Dimethyl acetamide	22.1	0.937	m
Dimethyl formamide	24.8	0.944	m
Methanol	29.7	0.791	s

(a) Source: Polymer Handbook, eds. J. Brandrup and E.H. Immergut[254]
(b) Hydrogen bonded: p, poorly, m, moderately, s, strongly

The average molecular weight between crosslinks (M_c) can be obtained from swelling studies using the Flory-Rehner[255,256] equation:

$$\nu_e = -1/V_S \left[(\ln(1-\nu_r)+\nu_r+\chi\nu_r^2)/(\nu_r^{1/3}-2\nu_r/F)\right] \qquad (3.6)$$

Here ν_e is the number of polymer chains per unit volume, V_S is the molar volume of swelling agent, ν_r is the volume fraction of polymer in the swollen gel, χ is the polymer-swelling agent interaction parameter and F the functionality of the system. The polymer-swelling agent interaction parameter can be determined using the semi-empirical Bristow and Watson[257] equation.

$$\chi = ß + (V_S/RT)(\delta_S-\delta_p)^2, \qquad (3.7)$$

where ß is the lattice constant (usually about 0.34), and δ the solubility parameter of the solvent and the polymer. M_c was calculated for the PUR network of different crosslink densities using cyclohexanone as swelling agent.

The sol/gel content of IPNs and homopolymer networks was characterised by soxhlet extraction studies. This technique is based on refluxing a small sample in a good solvent at elevated temperature. Linear material is extracted and, thus, information about the presence of network defects can be obtained. The gel content in percent can be calculated by the equation 3.8.

$$\% \text{ gel content} = 100\ (m_3 - m_1) / (m_2 - m_1), \qquad (3.8)$$

where m is the mass and subscript 1 is the thimble, 2 the sample and subscript 3 the gel. In the present study, 2g of the material were placed into a thimble and refluxed for 24h. As a result of the solubility parameter studies, acetone was chosen as extraction agent because of its solubility parameter of $\delta = 20.3$ and its moderate hydrogen bonding ability. It dissolved the linear forms of PUR, PEMA and PS and refluxes at moderate temperatures (bp = 56.5°C). From the weight differences after extraction the sol/gel ratio was calculated using the above equation.

3.4.11 Wide Angle X-ray Scattering (WAXS)

X-ray diffraction studies provide information about the presence of ordered arrangements of atoms and molecules in a solid substance[177]. The principle of this technique is based on the fact that the wavelength of X-rays are comparable to interatomic distances. Diffraction effects will occur[107] when X-rays are focused on a solid substance containing regularly arrayed atoms. The crystallites diffract X-ray beams from parallel planes for incident angles θ. The latter are determined by the Bragg equation.

$$n\lambda = 2d \sin\theta \qquad (3.9)$$

where n is an integer (i.e. 1, 2, etc.), λ is the wavelength of the X-rays and d is the distance between the parallel planes in the crystallites.

In the present study, WAXS was used to ascertain the presence of crystallinity in the PUR. A Shimadzu model XD-5 X-ray generator was operated at 30 kilovolts and 20 milliamperes. Nickel filtered copper kα radiation ($\lambda = 1.542$) was used throughout. Sample dimensions for the diffractometer traces were 25 x 25 x 2 mm. The scan speed was 4°/min, the chart speed 10 mm/min and the angle of scan was from 5° to 60°.

4. THE POLYURETHANE NETWORK

4.1 Choice of the Polyurethane

In all IPNs synthesised, one component was always a polyurethane. Polyurethanes are a very versatile class of polymers with quite different compositions and correspondingly different properties[204]. The latter combined with their polymerisation by the polyaddition mechanism make them an ideal choice[56,57] for combination with radically synthesised polymers in simultaneous IPN preparations. In the present study, the PUR network was formed first in most cases and, therefore, had an important bearing on the morphology and properties of the IPN. The PUR component was investigated in order to choose a suitable standard system with high damping characteristics for the IPN preparation.

It was decided that the recently developed TMXDI[258,259] would be used in the PUR hard segment. With exception to one study[194] in Hourston's research group, this diisocyanate has not been employed in IPN synthesis before. TMXDI exists[258] in the meta and para isomeric forms. The p-TMXDI is symmetrical whereas m-TMXDI possesses a highly unsymmetrical structure. In the present study, only the meta form was used. For reasons of simplicity m-TMXDI will now be referred to as TMXDI. In TMXDI, the two tertiary aliphatic isocyanate groups are shielded from the aromatic ring by methyl groups. Thus, PURs based on TMXDI exhibit[259] good hydrolytic stability and excellent weatherability. The reactivity of the isocyanate groups in TMXDI is comparatively low[259]. Aliphatic isocyanates are generally less reactive than aromatic ones (see section 2.3.2). In addition, the methyl groups exert a positive inductive effect on the tertiary NCO groups, and, furthermore, impart an added retardation due to steric hindrance[260]. A recent study[261] of viscoelastic properties of TMXDI-based PURs showed that extensive hard and soft segment phase mixing was present. This is a consequence of the unsymmetrical hard segment which is not as strongly hydrogen-bonded as those of PURs based on symmetrical diisocyanates, such as MDI. The reduced strength of the hydrogen bond manifests[259] itself in a higher elongation and lower modulus and hardness when compared to PURs based on other

diisocyanates such as MDI and IPDI. TMXDI possesses a favourable toxicity profile[259] and no allergic lung reactions have been detected.

The polyol and chain extender/crosslinker in the PUR were chosen in order to maximise the damping performance. Crosslinking was necessary in order to produce PUR networks, i.e. full IPNs. In general, chemical crosslinking in PURs can be achieved[205] in three ways, by using a triol, a triisocyanate and by working at a NCO/OH ratio higher than 1.0 which may introduce allophanate crosslinks. Working with TMXDI eliminated the latter two for this study. TMXDI is a diisocyanate and known[259] for not forming allophanates because of its low reactivity and steric hindrance. Consequently, a triol had to be used for crosslinking the PUR. TMP was chosen for this purpose. Because of its low molar mass (134 g/mol), it also had the function of a chain extender and was part of the PUR hard segment. In order to keep the PUR formulation simple, no additional difunctional chain extender such as BD was used.

The aim of the study of the PUR component was to choose a suitable polyol to be combined with TMXDI and TMP. Furthermore, the selected PUR had to be characterised and compared to other commonly used PUR systems for a better understanding of how to manipulate the IPN properties. Therefore, morphological aspects such as phase segregation and crystallinity in the PUR and the mechanical properties had to be evaluated. The investigation of the PUR also represented a basis of comparison for the study in which the PUR component was varied in a PUR/PEMA IPN (chapter 6.3).

PUR elastomer formulations are commonly described[205] by the molar ratios of polyol to diisocyanate to chain extender (or crosslinker) ratio, sometimes termed the block ratio. In the present study, all PURs were synthesised at a fixed isocyanate to hydroxyl group (NCO/OH) ratio of 1.1. The only exception to this was a study conducted in section 4.4, investigating the influence of the NCO/OH ratio. Thus, by knowing the molar ratios of any two of the three PUR elastomer building blocks the third can be determined. For reasons of simplicity, a PUR of molar ratios of, for example, PPG1025/TMXDI/TMP = 6:9.9:2 is described in the present study as TMXDI, PPG1025/TMP 3:1.

4.2 Variation in the PUR Soft Segment

The polyols that represent the soft segment of PURs are known[204] to influence strongly the material morphology and properties. Dynamic mechanical measurements were conducted in order to investigate the damping properties of the PURs based on various polyols. Thus, information concerning the location of the loss factor peak, the peak height and half-peak height and the miscibility of PUR hard and soft segment was obtained. While the soft segment was varied, the hard segment was kept constant. The hard segment consisted of TMXDI and TMP in this series.

Influence of the type of polyol. In the present study, four chemically different polyols were investigated. These included a poly(caprolactone) diol, 2 polyether-type polyols and a hydroxy-terminated poly(butadiene). The poly(caprolactone) diol (PCL) and the poly(oxy tetramethylene) glycol (PTHF) were investigated at molar masses of 1000 and 2000, whereas the polypropylene glycol (PPG) had molar masses of 1025 and 2025 and the poly(butadiene) diol (PBD) a molar mass of 2500 g/mol. Two main series were synthesised with the principal difference being the molar mass of the polyol. All materials were prepared at a molar ratio of polyol/TMP of 3:1. The loss factor and storage modulus versus temperature curves for the series with a molar mass of about 1000 g/mol are shown in figures 4.1 and 4.2. Significant differences between the three polyols were observed. The loss factor data are compiled in table 4.1. The glass transition temperature of the PTHF1000-based PUR as seen from the loss factor peak was the lowest at -11°C (figure 4.2). The loss factor peak maximum was also low at 0.81 compared to 1.08 and 1.14 for PPG1025 and PCL1000, respectively. The half-peak widths of the loss factor transition, which can be used as an indication of the damping ability of polymers (section 3.4.1), were similar for the PPG1025 and PTHF1000 at 27°C and 24°C for the PCL1000. Surprisingly, for the PCL1000 polyol loss factor values after the transition remained comparatively high with a value above 0.2. The storage modulus versus temperature curves (figure 4.2) reflected the loss factor data. The drop in E' occurred at the lowest temperature for the PTHF-based material. The storage moduli for the PPG1025 and PCL1000 were very similar. Somewhat surprising was the high rubbery plateau modulus of the PTHF1000-based material which could not be explained with certainty.

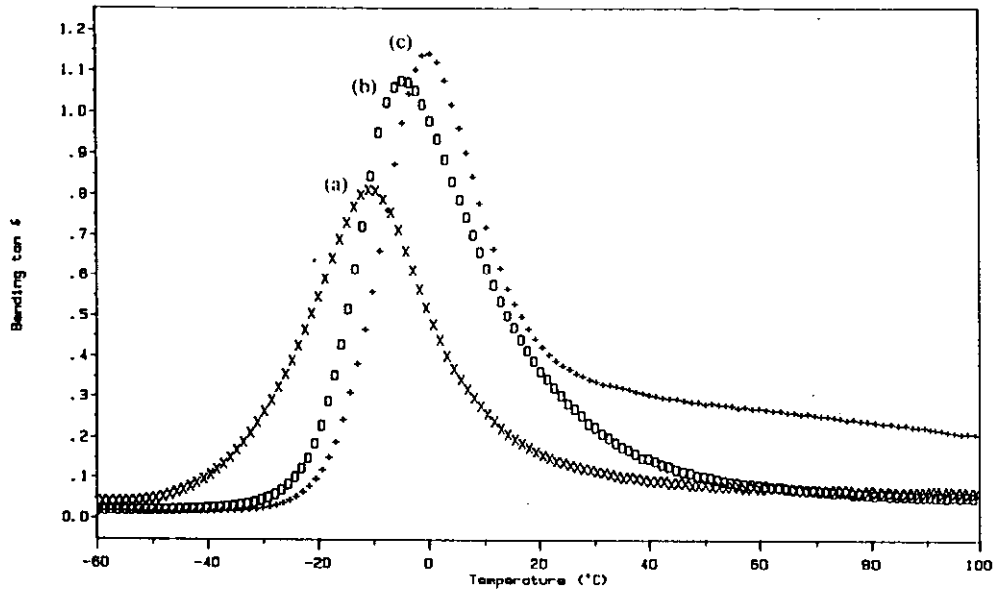

Figure 4.1 Loss factor versus temperature data for different polyol types. (a) PTHF1000, (b) PPG1025 and (c) PCL1000.

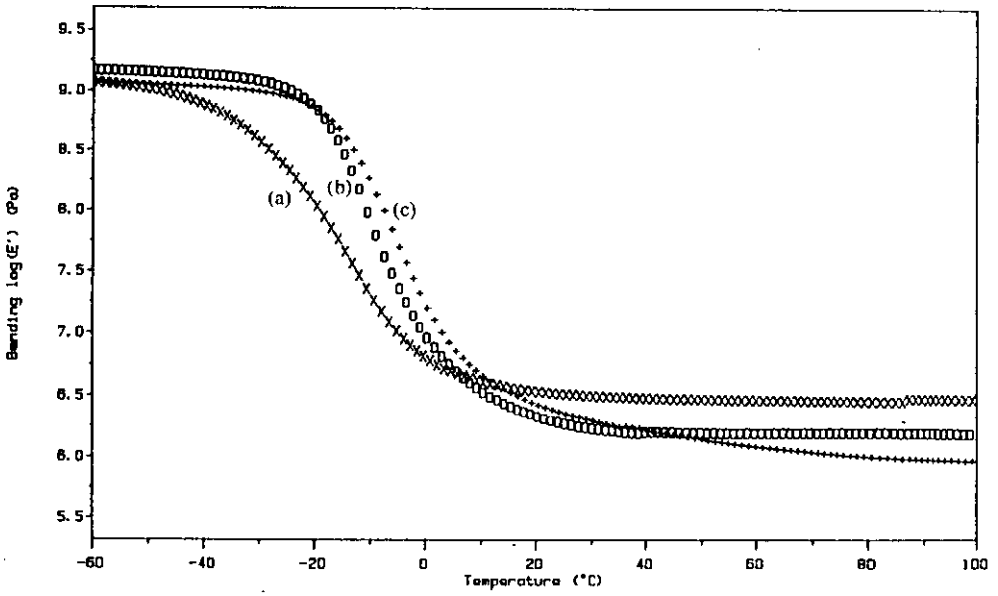

Figure 4.2 Storage moduli versus temperature for different polyol types. (a) PTHF1000, (b) PPG1025 and (c) PCL1000.

Table 4.1 Dynamic mechanical properties of the PUR networks as a function of the soft segment type.

PUR Soft segment	Tg, tan δ [10Hz, °C]	Tan δ_{max}	Half-peak width [°C]	Hard segment [weight %]
Polyol type				
PPG1025	-5	1.08	27	30
PTHF1000	-11	0.81	27	30
PCL1000	0	1.14	24	30
PPG2025	-26	1.31	20	18
PTHF2000[(a)]	-37	0.77	29	18
PCL2000[(a)]	-19	1.13	20	18
PBD2500	-45	0.89	26	15
Molar mass of PPG (for PPG1025 and PPG2025 see above)				
PPG425	40	1.53	24	50
PPG4000	-40	1.72	16	10
Crosslink density: ratio PPG1025/TMP (for 3:1 see above)				
1:1	30	0.73	46	42
2:1	4	0.92	33	33
7:1	-9	1.41	21	25
1:0	-12	1.60	16	21

(a) Measurements performed within 48 h of synthesis before crystallisation occurred (section 4.3).

The sequence of the Tg locations and of the rubbery plateau moduli for the different polyols might be explained by the extent of phase segregation in the PURs. A greater degree of phase segregation decreases[(205)] the soft segment Tg and increases the hard segment transition. Thus, the PTHF1000-based PUR seemed to exhibit the highest degree of phase segregation in the 1000 molar mass polyol series. The poorer miscibility of PTHF with the polar urethane links than of PPG could have been a result of two facts. The ether oxygen content in PTHF is lower with 22 weight % than compared to PPG with 28%. This decreased the possibility of hydrogen bond formation with the urethane link. Further, PTHF possesses a highly symmetric structure compared to the asymmetric PPG. This might have resulted in a better packing ability within and stronger interactions between the PTHF soft segments.

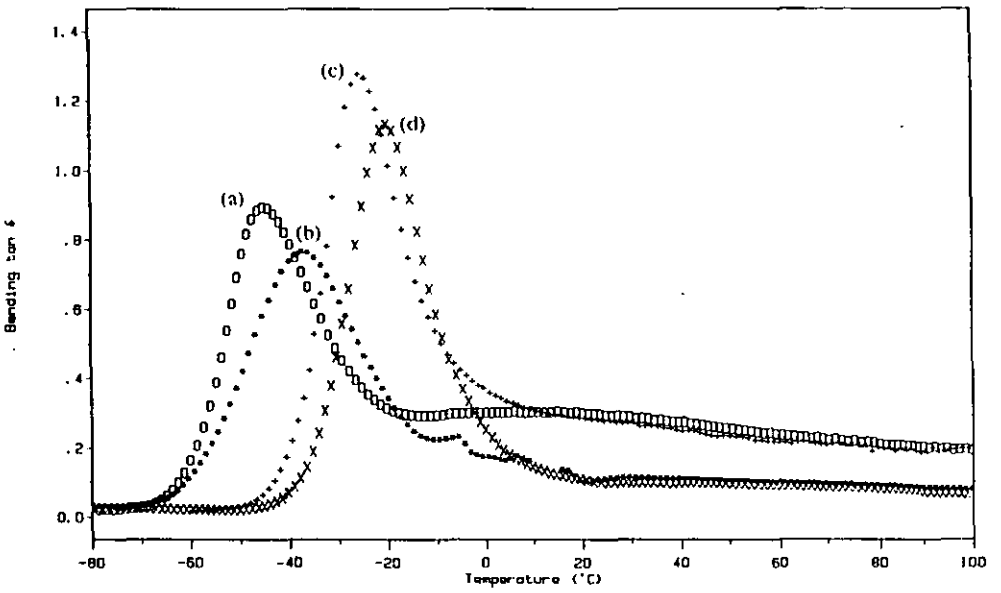

Figure 4.3 Loss factor versus temperature data for different polyol types. (a) PBD2500, (b) PTHF2000, (c) PPG2025 and (d) PCL2000.

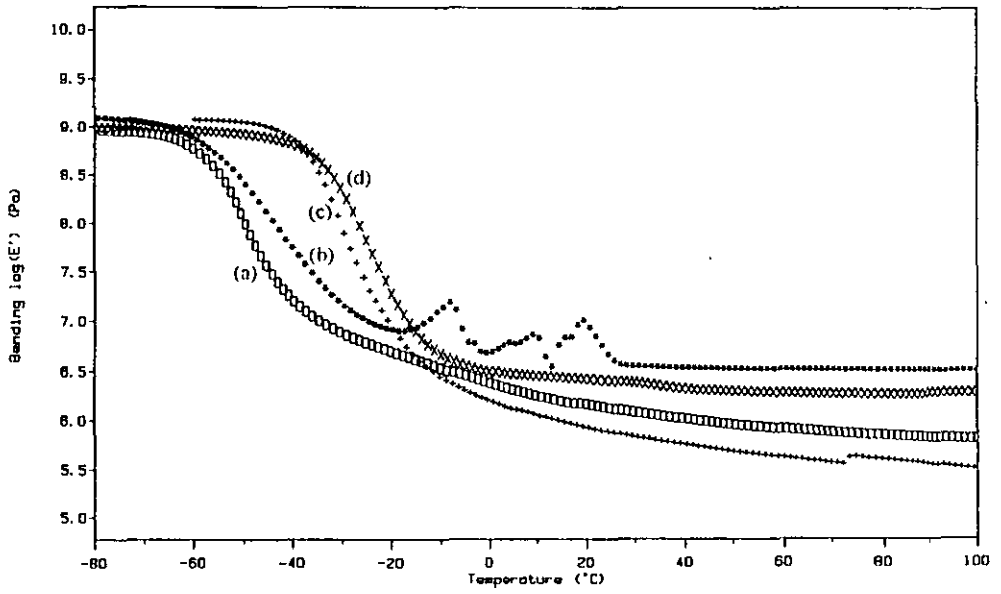

Figure 4.4 Storage modulus versus temperature data for different polyol types. (a) PBD2500, (b) PTHF2000, (c) PPG2025 and (d) PCL2000.

The highest rubbery plateau modulus for the PTHF-based PUR resulted then because of the reinforcement by the purest PUR hard segment with the highest transition. Polyester-based PURs are known[204] to possess a high degree of hard and soft segment phase mixing. This results from the ester linkage which is capable of forming stronger hydrogen bonds with the urethane link than the ether linkage. This would explain the highest Tg of the PCL1000-based PUR. The lowest rubbery plateau modulus resulted because no high transition hard segments were present that could have acted as reinforcement.

The loss factor and storage modulus versus temperature data for the 2000 molar mass series are shown in figures 4.3 and 4.4. In this series, it is important to note that the materials were quenched from 90°C to room temperature and tested within 48h of demoulding, since for PCL2000 and PTHF2000 a change in the properties over time was observed (see section 4.3). As expected, because of the highest molar mass and the greatest degree of hard-soft segment immiscibility, the PBD2500-based PUR exhibited the lowest loss factor peak at -45°C. This was followed by the PTHF2000 with -37°C, PPG2025 with -26°C and PCL2000 with -19°C. For the latter three, the sequence of the location of the Tgs was similar to the polyol1000 series. Also, the PPG (1.31) and PCL (1.13)-based PURs again exhibited clearly higher loss factor peak heights than the PTHF-based material (0.77). The PBD-based PUR exhibited a rather low loss factor value of 0.89. The storage modulus versus temperature profile of PCL2000, and in particular of the PTHF2000-based PUR, showed interesting phenomena. With PCL2000, a slight step in the E' was observed at 38°C which was not duly reflected in the loss factor curve. This is an indication that this was a primary transition, melting of polymer chains with some crystalline order. With the PTHF-based material, even more pronounced changes in the storage modulus versus temperature curve were observed. E' increased at about -15°C before falling again at 20°C. Both phenomena are related to crystallisation and melting of crystalline domains and will be further explained in section 4.3.

Influence of the molar mass of the PPG polyol. The influence of the molar mass on the dynamic mechanical properties was investigated with the PPG-type polyol. Molar masses of 425, 1025, 2025 and 4000 were investigated in a PUR based on TMXDI

and TMP. Regardless of the molar mass of the polyol, the PPG/TMP ratio was always kept constant at 3:1.

The loss factor and storage modulus versus temperature data for the PPG polyols of different molar masses are shown in figures 4.5 and 4.6. From both the loss factor and the storage modulus data, it can be noted that the molar mass of the PPG polyol exerted a strong influence on the dynamic mechanical properties of the PUR. Tg shifted from -40°C for the PPG4000-based PUR to 40°C for the PPG425-based material (table 4.1). This could be attributed to two effects. By keeping the polyol/TMP ratio at 3:1, the crosslink density of the materials was increased considerably by decreasing the molar mass of the polyol. This in turn lead to a decrease in free volume or to an increase of the activation energy of the transition and, thus, to a higher Tg. The second effect may be a copolymer effect[185]. The rigid aromatic rings of TMXDI and hydrogen bonding between the urethane links introduced stiffness into the PUR, and, thus, increased Tg. Because of the lower molar mass of PPG425, a much higher weight percentage of PUR hard segment (TMXDI and TMP) was present in the PPG425-based PUR, which resulted in a higher Tg. The hard segment (HS) content is determined[205] by relating the combined mass of the diisocyanate and the chain extender to the total mass, i.e. the hard segment and soft segment (SS) of the PUR. Mathematically, this can be expressed by equation 4.1.

$$\% \text{ HS} = \left(\frac{\text{HS}}{\text{HS} + \text{SS}} \right) 100 \qquad (4.1)$$

Here HS = 1.1 nM_D + nM_C and SS = nM_P. n is the molar ratio and M is the molar mass of the diisocyanate (D), the chain extender or crosslinker (C) and the polyol (P), respectively. The factor 1.1 results from the NCO/OH ratio of 1.1. Thus, for the PUR based on PPG425 a hard segment content of 50% resulted, whereas for the PPG4000-based PUR a mere 10% HS were present (see table 4.1). It was difficult to distinguish which of both effects was more pronounced at which crosslink densities. Even more so since phase segregation within the PUR also strongly influences the soft segment Tg. In phase-mixed PURs, the soft segment Tg shows a strong dependence[262] on the hard segment content, i.e. Tg increases as the hard segment content increases.

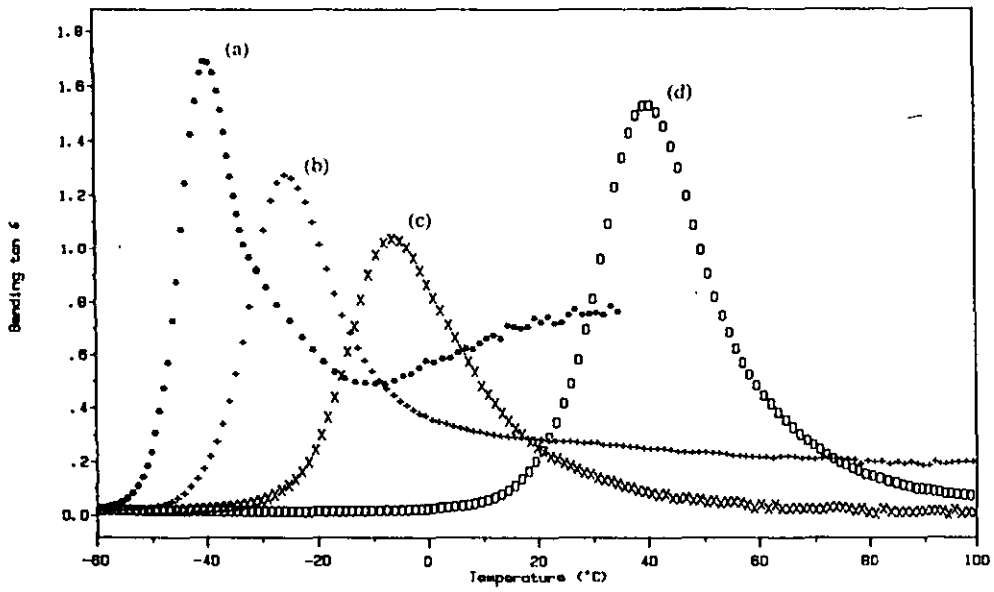

Figure 4.5 Loss factor versus temperature data for different polyol molar masses. (a) PPG4000, (b) PPG2025, (c) PPG1025 and (d) PPG425.

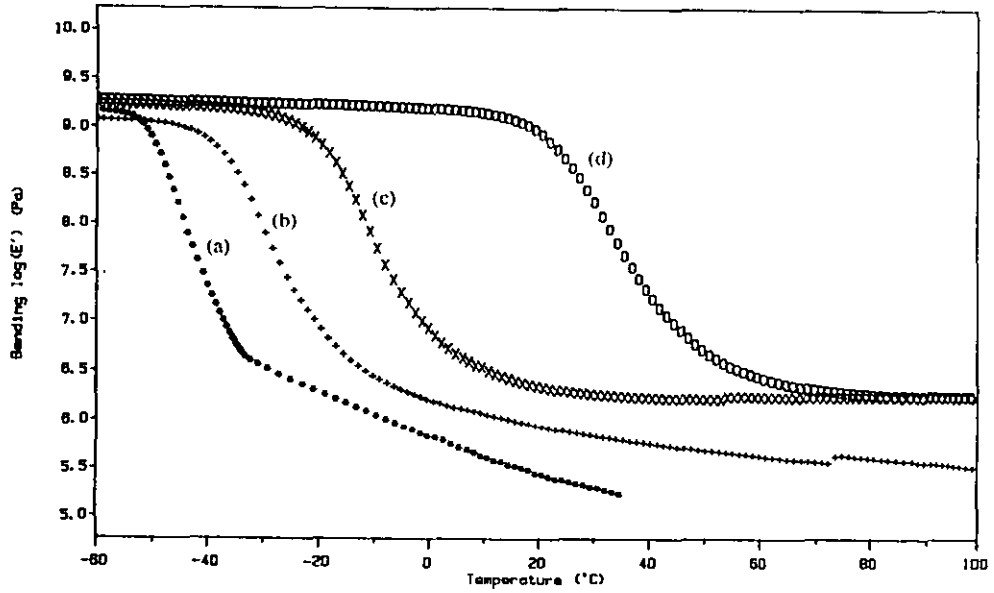

Figure 4.6 Storage moduli versus temperature for different polyol molar masses. (a) PPG4000, (b) PPG2025, (c) PPG1025 and (d) PPG425.

In contrast in highly phase segregated PURs an increase in the hard segment content hardly influences[263,264] the soft segment Tg. However, by decreasing the molar mass of the polyol in an originally phase segregated PUR a more phase mixed morphology can be brought about, resulting in an increase in Tg upon increasing the hard segment content[262-264]. In this study, the molar masses of the polyols used in the PUR decreased roughly by a factor of 2 from 4000 to 2000, 1000 and 425 g/mol. However, whereas Tg shifted by 14°C and 19°C from 4000 to 2000 and 2000 to 1000 molar mass, a 47°C shift was experienced from 1000 to 425. Preparing four series of chemically similar linear PURs by replacing TMP with BD could have lead to further elucidation of this phenomenon. However, since this was not a primary aim of the present study, it was only done with the PPG1025 (section 4.3). The PPG425-based material also exhibited an unusual behaviour with respect to the loss factor peak height. With increasing crosslink density, a decrease of the loss factor peak height is generally accompanied by a broadening of the transition peak[13]. This was observed in the series from PPG4000 over PPG2025 to PPG1025. The peak height decreased from 1.72 to 1.31 and 1.08. At the same time, the half-peak width increased from 16 to 20 and 24°C, respectively. For the PPG425-based PUR, the peak height increased to 1.53 and the half-peak width did not increase further.

Considering the storage moduli (figure 4.6) elucidated this phenomenon to some extent. Again, a clear trend was observed for PPG4000, PPG2025 and PPG1025. The storage modulus drop shifted to higher temperatures for the lower molar mass polyols and the rubbery plateau modulus increased considerably with a higher crosslink density. The latter was expected and is illustrated[118] in equation 4.2 relating the modulus of the rubbery plateau to the average molecular weight between crosslinks (M_c).

$$G = \frac{\rho RT}{M_c} \qquad (4.2)$$

Here G is the shear modulus in the rubbery plateau, ρ the density of the material, R the universal gas constant and T the absolute temperature. The above equation is strictly applicable[118] for ideal rubbers only, however, it is useful to indicate the trend with increasing crosslink density i.e. decreasing M_c. While the drop of E' shifted to higher temperatures for the PPG425-based PUR, no increase of the rubbery plateau modulus was observed compared with the PPG1025-based PUR. Thus, the crosslink

density did not seem to be significantly higher. This indicated the presence of a considerable number of network defects in the PPG425-based PUR. Network defects such as loops and loose ends cause[63] poorer mechanical properties and might also have a plasticisation effect[86]. Loose chain ends have a greater amount of chain mobility and increase the free volume. This can explain the increase in the loss factor peak height. However, the important Tg shift to 40°C is still unaccounted for. Even more so since the apparent crosslink densities of PPG1025 and PPG425, as seen by the modulus in the rubbery plateau, were very similar. The copolymer effect might, therefore, play a distinctive role. Tg involves[93] co-ordinated segmental movements of about 50 main chain atoms. As PPG425 contains roughly 21-24 main chain atoms, the hard segments have to take part in the segmental movements at Tg. For the more rigid (diisocyanates) and possibly hydrogen-bonded hard segments, a higher activation energy is necessary for segmental motions to occur. This could be an explanation for the significant difference in Tg between PPG425 and PPG1025. PPG1025 contains roughly 51-54 main chain atoms, so that segmental movements on a scale necessary for Tg can take place within the soft segment itself. Furthermore, it could be assumed that at the low molar mass of 425 g/mol, a high degree of phase mixing between soft and hard segment was present. This resulted in a shift of Tg to higher temperatures combined with an increase in the loss factor values, since the hard segment also participated in the secondary transition.

Influence of the crosslink density and determination of the average molecular weight between crosslinks (M_c). The crosslink density in PURs can be varied by altering the ratio of difunctional polyol to triol. In the study, TMXDI, PPG1025 and TMP were used as PUR components. The ratio of PPG1025/TMP was varied at 5 distinct levels. This comprised a linear PUR which was made by leaving out TMP.
The dynamic mechanical data are shown in figures 4.7 and 4.8. The pattern of the loss factor versus temperature curves (figure 4.7) is a good illustration of the influence of the crosslink density. From the linear PUR (PPG1025/TMP 1:0) to the highly crosslinked material (1:1) Tg increased by 42°C and the loss factor peak maximum decreased by more than a factor 2 (table 4.1).

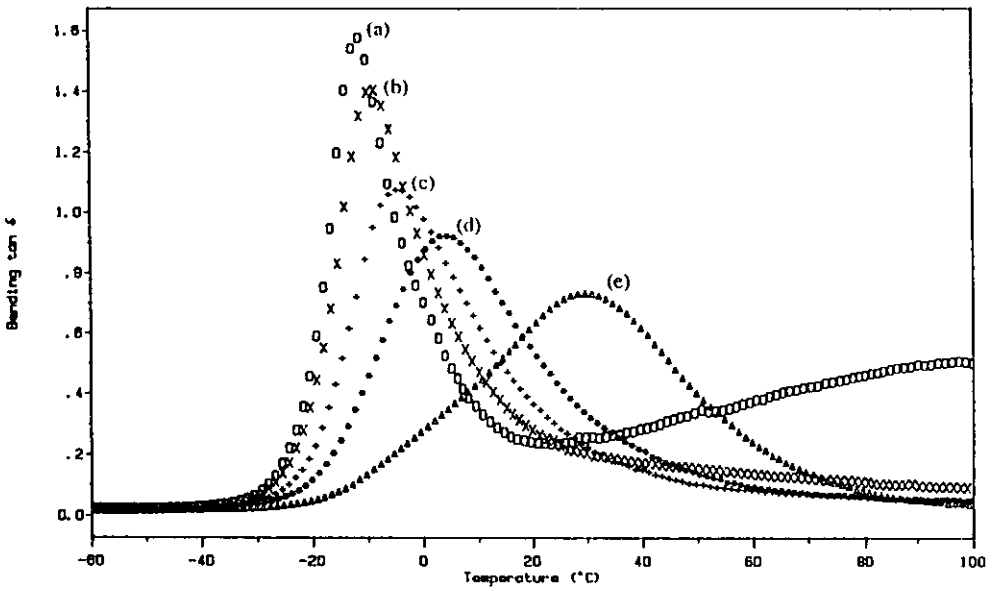

Figure 4.7 Loss factor versus temperature data for different crosslink densities. (a) PPG1025/TMP ratio 1:0, (b) 7:1, (c) 3:1, (d) 2:1 and (e) 1:1.

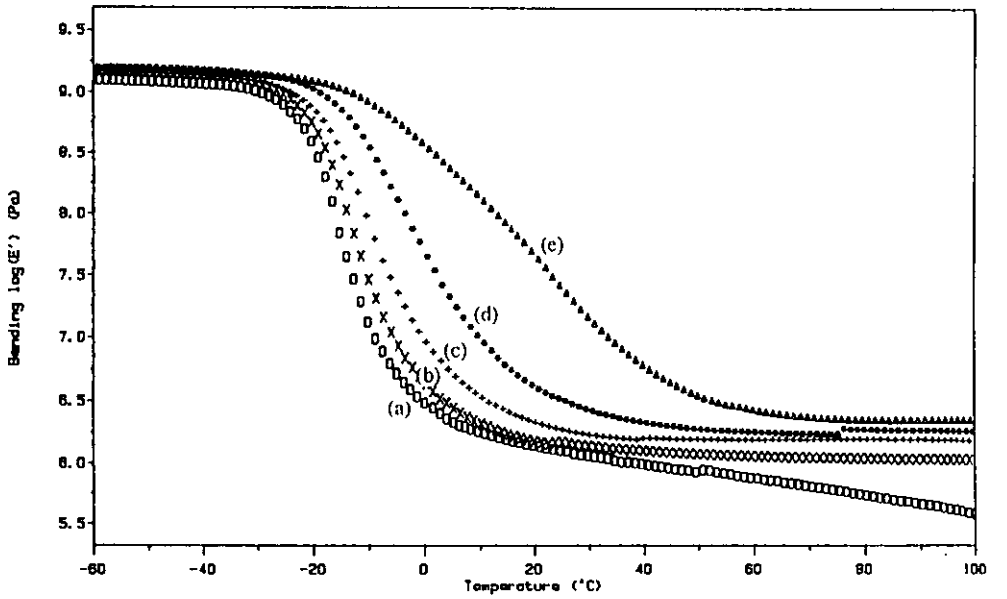

Figure 4.8 Storage moduli versus temperature for different crosslink densities. (a) PPG1025/TMP ratio 1:0, (b) 7:1, (c) 3:1, (d) 2:1 and (e) 1:1.

At the same time, the half-peak width increased by a factor of nearly 3 from 16°C to 46°C. The peak broadening upon crosslinking is believed[205] to occur because of heterogeneities in the network formation. The resulting distribution of different crosslinking densities exhibits a distribution of local transitions which cause a broad Tg. The storage modulus versus temperature curves (figure 4.8) show the same trend. The drop in storage modulus from the glassy state to the rubbery plateau shifted to higher temperatures with increasing crosslink density. While a steep drop in modulus was observed for the linear PUR, a very gradual drop resulted for the material with the highest crosslink density. The latter is typical for broad transitions. The moduli of the rubbery plateau followed the predictions. The rubbery plateau moduli increased with increasing crosslink density of the material.

Crosslinking is the dominant feature in interpenetrating polymer networks making them a special class of material[4]. Crosslinking in the PUR network had a crucial influence since this was usually the first network formed. The first network formed determines[4,24] the IPN properties to a great extent since it very often represents the continuous phase and restricts the phase domain sizes of network 2. Once the IPN is formed, it is impossible to determine the crosslink density for either network separately. It was, therefore, important to determine the crosslink density of the pure PUR networks. These crosslink densities were only an approximation though, since they were obtained from a material prepared in bulk while in the simultaneous IPNs monomer of polymer 2 acted as a solvent. The theoretical M_c was calculated and compared with experimental values obtained from swelling measurements and estimations using the Tg shift and the modulus of the rubbery plateau. The theoretical average molecular weight between crosslinks ($M_{c,t}$) was calculated using equation 4.3, derived from the assumptions that a stoichiometric equivalent ratio of NCO to OH functionalities was present, that no secondary PUR reactions, such as the formation of allophanate crosslinks, and no auto-addition of diisocyanates to form dimers and trimers occurred and that the formation of this ideal network went to completion.

$$M_{c,t} = \frac{dM_D + tM_T + \frac{(2d+3t)M_I}{2}}{\frac{3t}{2}} \qquad (4.3)$$

Here, d and t are the moles of diol and triol. M_D, M_T and M_I represent the molar mass of the diol, triol and diisocyanate, respectively. Theoretically and experimentally determined M_cs are compiled in table 4.2.

Table 4.2 Crosslink Densities of PURs with Varying PPG1025/TMP Ratio.

Crosslinking		Average molecular weight between crosslinks (M_c) Theoretical	Swelling	Nielsen eqn.	$E'_{Rub. Plat.}$
Polyurethane polyol/triol	1:1	1200	3200	900	4100
	2:1	2000	4400	2400	5200
	3:1	2900	6100	5200	6100
	7:1	6300	10000	13000	8500
	1:0	linear			

An equation relating the modulus of the rubbery plateau to M_c has been given (equation 4.2). It applies to ideal rubbers. Thus, the values determined here are only approximations of M_c. The moduli were taken at 80°C and Poisson's ratio (ν) was taken to be 0.5 to convert the tensile modulus into the shear modulus.

M_c can be obtained from swelling studies using the Flory-Rehner equation[255,256]. The equation and the procedure were described in section 3.4.11. Swelling studies generally give[93] very accurate values of M_c since, unlike in other techniques, contributions from other factors such as physical crosslinking through hydrogen bonding are not considered.

Nielsen's[265] equation relates the shift of the Tg of a crosslinked polymer to its linear counterpart to obtain M_c. The empirical equation 4.4 has been suggested[265] approximately to give M_c.

$$Tg - Tg_o = \frac{3.9 \times 10^4}{M_C} \qquad (4.4)$$

Here, Tg is the glass transition temperature of the crosslinked polymer and Tg_o that of the linear equivalent.

Comparing the M_c values (table 4.2) obtained from the different techniques, one must consider what principle the respective methods are based on. The theoretical

determination of M_c is based on the assumptions that the complete formation of an ideal network took place. In real materials, however, this situation cannot be encountered and network loops and loose ends will increase M_c. Therefore $M_{c,t}$ should be found on the lower end of the spectrum. This was the case, but for one value obtained by the Nielsen equation for the highest crosslink density. The Nielsen equation resulted in the greatest spread of M_c values for the different PPG1025/TMP ratios. This might be explained by the M_c estimation method. The calculation of M_c is based on the difference of Tg between the linear polymer and the crosslinked species. However, Tg is not only influenced by the crosslink density, but also by the introduction of TMP and TMXDI, i.e. the copolymer effect. A comparison of the weight percentage of soft segment (PPG1025) in the linear PUR to the weight percentage at a PPG1025/TMP ratio of 1:1 should prove interesting. For the linear material where one molecule (in this study, 1.1 molecule due to the NCO/OH ratio of 1.1) TMXDI (M.W. 244) is reacted with one PPG1025 segment, the soft segment weight percentage in the material is 79%. In the highly crosslinked PUR at a PPG1025/TMP (M.W. 134) ratio of 1:1, the soft segments represents only 58%. In conclusion, the low M_c obtained for high crosslink densities by the Nielsen equation might, in part, have resulted because of the introduction of copolymer which also increased Tg.

The M_c values obtained by the swelling study and by using the modulus in the rubbery plateau were relatively close. Both techniques mainly take into account chemical crosslinks, with the latter depending also on molecular entanglements and attractive forces. Both M_c series are higher than the corresponding theoretical ones. Further, the M_c values at low triol content were closer to the theoretical values (higher by factors of 1.6 and 1.4) than the ones at high triol content (higher by factors of 2.7 and 3.4). This might be explained by a higher number of network defects at a high crosslink density. Loops and loose ends occur more easily at high crosslinking densities because of the decrease in chain mobility in the forming material, resulting in unreacted functional groups. Furthermore, the probability of two triols reacting with each other increases. This has an effect[266] on the crosslink distribution, i.e. it lowers the apparent crosslink density of the PUR.

Tensile testing data and hardness measurements of the materials with the different soft segment are summarised in table 4.3. In general, mechanical properties of these crosslinked PURs were comparatively low. This resulted from several factors. First, the amount of hard segment in these PURs was low (see table 4.1). The HS content in these materials ranged from 50% to 10%. 50% hard segment was present in the PUR based on PPG425/TMP at a ratio of 3:1. It exhibited the highest tensile strength by far with 29 MPa which was directly linked to the highest Tg (40°C). Only 10% hard segment was present in the PUR based on PPG4000/TMP 3:1. Because of its soft character at room temperature (Tg = -40°C), no mechanical properties could be determined for this material.

Table 4.3 Mechanical properties as a function of PUR soft segment.

PUR Soft segment variations	Tensile properties Stress at break [MPa]	Elongation at break [%]	Young's mod. [MPa]	Toughness [J]	Hardness Shore A	D
Polyol type						
PPG1025	1.2	210	1.0	600	42	27
PTHFG1000	3.1	450	1.3	2800	54	31
PCL1000	3.2	480	1.3	2900	57	33
PPG2025	0.8	400	0.5	620	35	25
PTHF2000	9.0	1100	0.9	12000	56	31
PCL2000	13.0	1200	1.3	15000	83	44
PBD2500	1.2	190	1.4	550	48	29
Molar mass of PPG (for PPG1025 and PPG2025 see above)						
PPG425	29	540	9.0	23000	98	68
PPG4000	(a)	(a)	(a)	(a)	(a)	(a)
Crosslink density: ratio PPG1025:TMP (for 3:1 see above)						
1:1	2.8	220	1.9	1200	67	38
2:1	1.1	350	0.5	300	50	30
7:1	1.8	250	1.4	510	34	24
1:0	(a)	(a)	(a)	(a)	(a)	(a)

(a) Material too soft for tensile testing and hardness measurements.

Also, a considerable difference between the various polyol types was noticed. The PPG-type polyols exhibited the poorest mechanical properties. This is in accordance

with results from literature[211], where polyether-type polyols are known[204] to result in weaker PURs than polyester polyols. However, even though they are polyether-type polyols, the PTHF-based PURs resulted in higher mechanical properties. This can be explained by the symmetrical structure of the latter. Upon applying the strain, the tensile test specimen turned opaque. This indicated the formation of stress-induced orientation[205]. PPG-type polyols have a pendent methyl group and no stress-whitening was observed in PPG-based PURs. The PCL-based PURs were also clearly stronger than the PPG counterparts. Similar to polyester-type polyols, this is explained by the higher energy of cohesion[205] of the ester link with 12.1 kJ/mol compared to the ether link with 4.2 kJ/mol. With the latter, considerable stress-whitening was observed upon stretching.

These trends were obvious in the PURs based on the polyols of a molar mass of 1000 g/mol. However, the differences were even more pronounced for the 2000 molar mass series. With PTHF2000 and PCL2000, comparatively strong PURs resulted as indicated by a high tensile strength, elongation at break and toughness index. Again, stress-whitening was observed upon stretching. However, contrary to the 1000 series, the opacity was conserved in the failed specimens. This finding indicated that stress-induced crystallisation took place. The crystallinity in these materials is further investigated in section 4.1.3. The PURs based on PPG2025 and PBD2500 exhibited poor mechanical properties. No remaining opacity in the failed tensile test specimens was observed. Values for the elongation at break ranged from 190% for the PBD2500 based material to 1200% for the PCL2000 PUR. The Young's moduli for all PURs except the PPG425-based one (9.0 MPa), were low with values ranging from 0.5 to 1.9 MPa. The low values are not surprising since most materials had a Tg below room temperature.

The hardness values reflected the trend of the tensile results. A high Shore D hardness value of 68 resulted for the PPG425-based PUR. In contrast to the high tensile strengths, it was noted that no particularly high hardness values resulted for the unstretched PURs based on PTHF2000 (Shore D of 31) and PCL2000 (Shore D of 44). The higher value for PCL2000 resulted from the higher energy of cohesion of the carbonyl group. Upon stretching of the PCL2000- and PTMG-based PURs, a high degree of order i.e. crystallisation was induced which resulted in high values for the

tensile strength. Thus, hardness measurements corroborated the observation from tensile testing that the mechanical properties of the PUR improved upon stretching.

4.3 Variation in the PUR Hard Segment

The PUR hard segments consist of sequences of diisocyanate and short chain diols or triols. They determine the PUR properties at elevated temperatures (see section 2.3.3). In this series, the type of diisocyanate and the chain extender were varied while the PUR soft segment consisted of PPG1025.

Influence of type of diisocyanate. The diisocyanates investigated were TMXDI, IPDI, TMDI, TDI and MDI. They were chosen because of their different molecular characteristics, such as symmetry and the environment of the isocyanate group. MDI and TDI are very reactive[204] aromatic diisocyanates, whereas TMDI, IPDI and TMXDI have primary aliphatic, secondary aliphatic and tertiary aliphatic diisocyanate groups. These diisocyanates are very different with respect to both rigidity of the molecule and symmetry. MDI contains two rigid aromatic rings, yet is a symmetrical molecule. Besides TMXDI and TDI as diisocyanates containing one aromatic ring, TMDI as an entirely aliphatic and IPDI as a cycloaliphatic diisocyanate were investigated. The diisocyanates were studied in a formulation containing PPG1025/TMP at a molar ratio of 3:1. The loss factor and storage modulus versus temperature curves for the different diisocyanates are shown in figures 4.9 and 4.10. The DMTA data are compiled in table 4.4.

The loss factor maxima occurred at different temperatures for the five diisocyanates (figure 4.9). This suggested that all these PPG1025-based PURs had a phase-mixed morphology with little or no hard-soft segment segregation present. The MDI-based PUR exhibited the loss factor peak at the highest temperature (20°C), whereas the TMDI-based material had the loss factor at the lowest temperature (-17°C) (table 4.4). The different dynamic mechanical properties could be explained by the structure of the diisocyanates. The two bulky aromatic rings imparted stiffness into the PUR, and, therefore, resulted in the highest Tg.

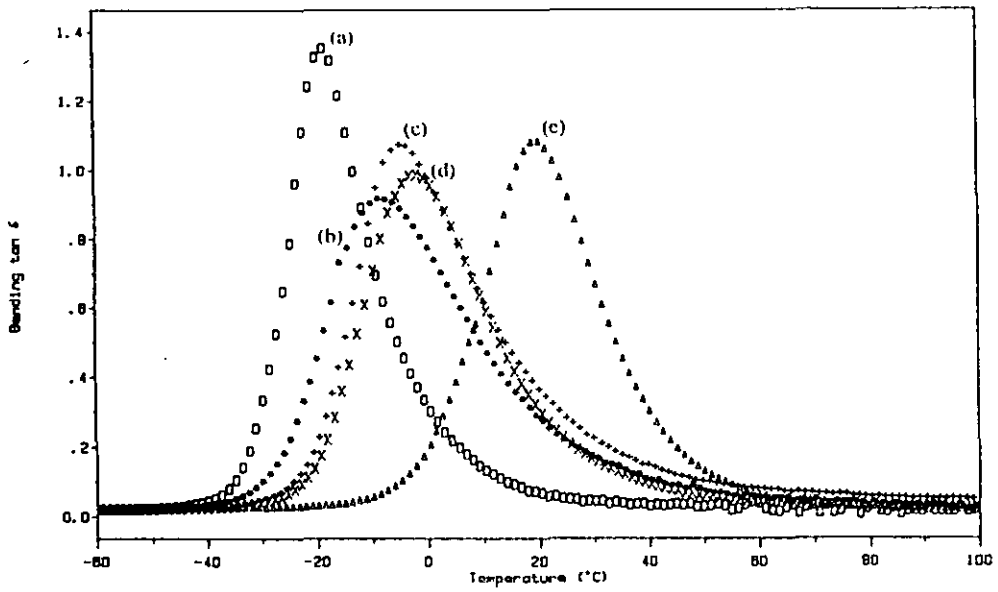

Figure 4.9 Loss factor versus temperature data for different diisocyanates. (a) TMDI, (b) TDI, (c) TMXDI, (d) IPDI and (e) MDI.

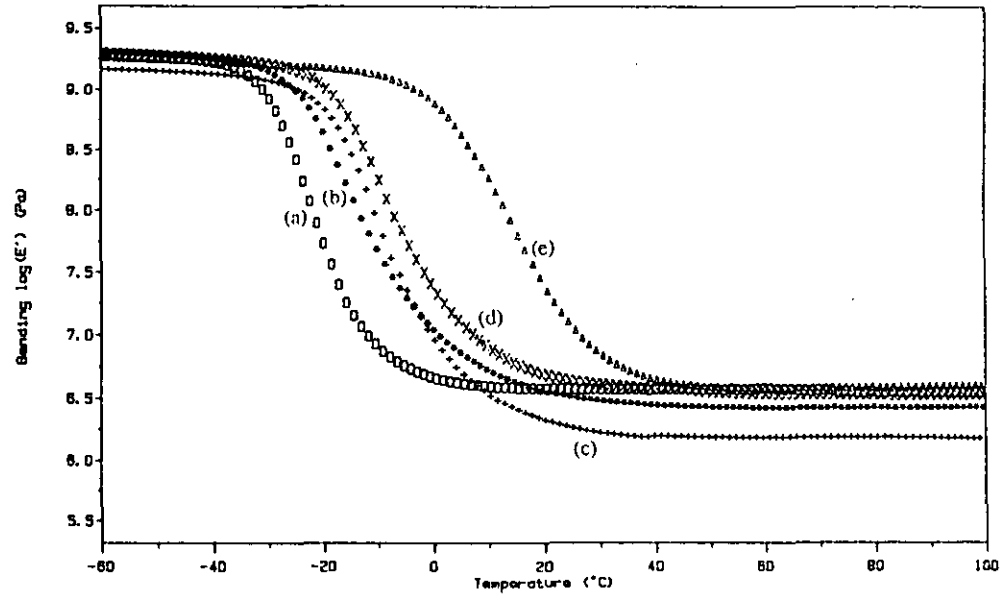

Figure 4.10 Storage modulus versus temperature data for different diisocyanates. (a) TMDI, (b) TDI, (c) TMXDI, (d) IPDI and (e) MDI.

Table 4.4 Dynamic mechanical properties of the PUR networks as a function of the hard segment.

PUR Soft segment	Tg, tan δ [10Hz, °C]	Tan δ_{max}	Half- peak width [°C]	Hard segment [wt.%]
Diisocyanate type				
TMXDI	-5	1.08	27	30
IPDI	-8	0.92	31	28
TMDI	-17	1.35	18	27
TDI	-2	0.99	26	24
MDI	20	1.09	25	30
Chain extender BD				
MDI, PPG1025/BD 3:1	14	1.33	20	28
TMXDI, PPG1025/BD 1:3	36	1.32	24	57
TMXDI, PPG1025/BD 2:3	19	1.28	30	44
TMXDI, PPG1025/BD 3:2	-3	1.30	27	33
TMXDI, PPG1025/BD 3:1	-7	1.35	21	27
TMXDI, PPG1025/BD 1:0	-12	1.60	16	21

The TDI-, TMXDI- and IPDI-based materials had their transition peaks intermediate between MDI and TMDI at -2, -5 and -8°C, respectively. Both TDI and TMXDI contain one aromatic ring, and IPDI a cycloaliphatic group. With an aliphatic chain as backbone, TMDI had the most flexible structure and, thus, the TMDI-based PUR exhibited the transition at the lowest temperature. It exhibited the highest loss factor peak height of 1.35, with the other four materials all having values of around 1.0. The storage moduli reflected the loss factor data. Surprisingly, the TMXDI-based material exhibited a significantly lower modulus in the rubbery plateau than any of the other PURs. The modulus in the rubbery plateau is influenced[185] by the molecular weight, crystallinity, plasticisation and the crosslink density. Thus, this lower rubbery plateau modulus could be an indication of the presence of a greater number of network defects in the TMXDI-based PUR. The second lowest rubbery plateau modulus resulted from the highly unsymmetrical TDI, whereas the highest modulus was obtained with the symmetrical MDI. The following section will indicate that besides M_c, physical interactions within the PUR might also have contributed to the rubbery plateau modulus.

Influence of the chain extender. The use of different chain extenders is a means of altering the PUR properties (section 2.3.3). In this study, the triol TMP was substituted by the diol BD in order to compare the damping behaviour of crosslinked and linear systems where only physical crosslinks may be present. The comparison was made with two types of materials which differed in the diisocyanate component. TMXDI as a highly unsymmetrical and MDI as a symmetrical diisocyanate were studied. The following four materials were synthesised and their dynamic mechanical properties compared (figures 4.11 and 4.12).

(i) TMXDI,	PPG1025/	TMP	3:1
(ii) TMXDI,	PPG1025/	BD	3:1
(iii) MDI,	PPG1025/	TMP	3:1
(iv) MDI,	PPG1025/	BD	3:1

The dynamic mechanical properties of both crosslinked PURs were discussed in the former section. Comparing the crosslinked to the respective linear material showed the same trend for both the MDI and the TMXDI-based PUR. The loss factor peak shifted to lower temperatures, from 20 to 14°C for MDI and from -5 to -7°C for TMXDI. However, the HS content was slightly lower for the linear materials. The crosslinked PURs had a HS content of 30 weight % whereas the linear counterparts only had 28 (MDI-based) and 27 (TMXDI-based) weight %. This slightly lower HS content could, in part, account for the lower Tg. The loss factor peak height was higher for the linear materials with 1.33 (MDI) and 1.35 (TMXDI) than for the crosslinked counterparts with 1.09 and 1.08, respectively. The loss factor peaks narrowed which was documented in a decrease of the half-peak widths (table 4.4).
The storage moduli showed similar trends (figure 4.12). The moduli in the rubbery plateau were higher for both, the crosslinked and the linear MDI-based PURs than for the TMXDI-based materials. This indicated that the rubbery plateau modulus at these temperatures is influenced by both the crosslink density of the networks and intermolecular entanglements and interactions. The more rigid structure of MDI and the presence of physical interactions such as hydrogen bonding could explain why the linear MDI-based PUR exhibited a higher rubbery plateau modulus than the crosslinked TMXDI-based PUR.

Variation of the hard segment content. A linear PUR system based on TMXDI and PPG1025 and BD in different molar ratios was used in order to investigate the influence of the hard segment content on the dynamic mechanical properties. With this system, information about the influence of the copolymer effect as opposed to the crosslink density on Tg could be gained by comparison with the crosslink study in 4.1.2. Furthermore, phase segregation in the PUR was studied. No hard segment transition was observed with the crosslinked PUR series. This could be because of a lack of phase segregation as a result of a miscible hard and soft segment, or because of a restriction of the ability to phase separate hindered by chemical crosslinks. The chemical crosslinks could also have prevented the formation of some ordered structure in the hard segments i.e. the presence of a primary transition and suppressed a possible secondary transition.

The dynamic mechanical data of the PURs with different hard segment content are shown in figures 4.13 and 4.14. Tg shifted to higher temperatures with increasing hard segment content. With the exception of the material with the lowest hard segment content of 21 wt.%, which exhibited a loss factor maximum of 1.60, the other four PURs exhibited very similar loss factor heights of about 1.30. This was in contrast to the findings from the series where the crosslink density was varied (section 4.2) where a steady decrease of the loss factor peak maximum with increasing Tg was observed. In order to investigate the influence of the hard segment content on a plot of Tg versus the latter was constructed (figure 4.15). The increase in Tg with increasing hard segment content indicated that extensive phase mixing was present, since in phase segregated PURs the soft segment Tg is not affected[263,264] by the hard segment content. This was not surprising since both PPG (see section 4.2) and TMXDI[259] have been found to yield a high degree of hard and soft segment phase mixing. In addition to the series of the linear PURs, the PUR series based on different PPG1025/TMP molar ratios and the one with different molar masses of the PPG polyol were plotted in figure 4.15. Direct comparison of both series that were based on PPG1025 resulted in the following findings. At very low crosslink densities (PPG1025/TMP 7:1, $M_{c,t}$ = 6300 g/mol) the crosslinked and the linear PUR followed the same trend at similar hard segment contents. With increasing crosslink density, however, a pronounced difference became obvious.

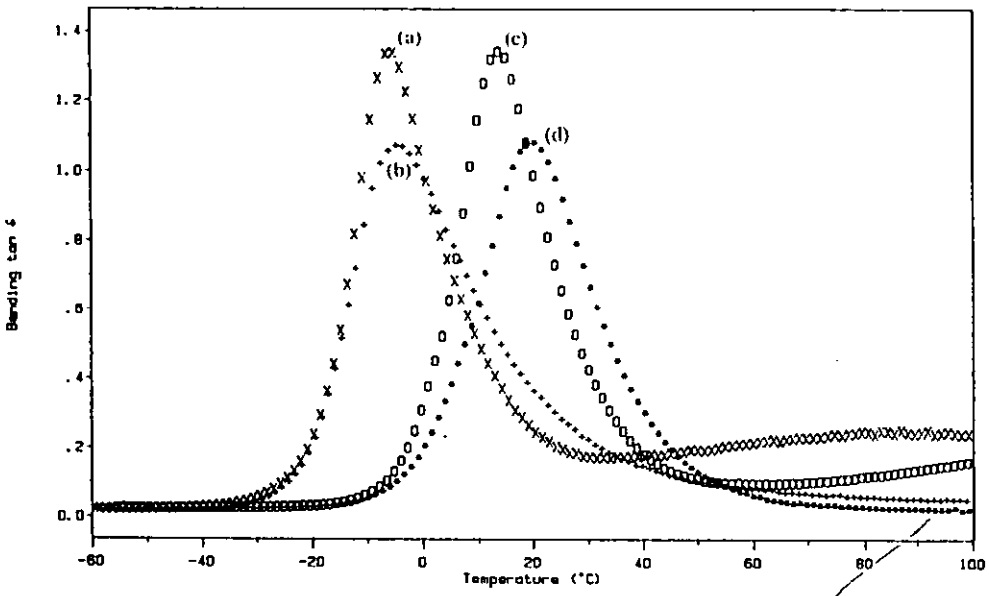

Figure 4.11 Loss factor versus temperature data for different chain extenders. (a) TMXDI, PPG1025/BD 3:1, (b) TMXDI, PPG1025/TMP 3:1, (c) MDI, PPG1025/ BD 3:1 and (d) MDI, PPG1025/ TMP 3:1.

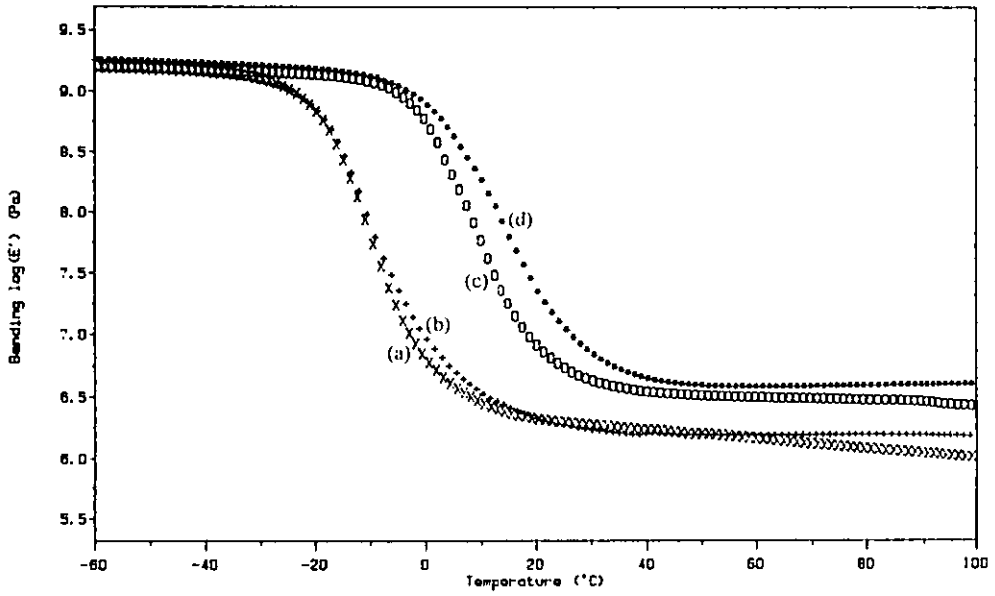

Figure 4.12 Storage modulus versus temperature data for different chain extenders. (a) TMXDI, PPG1025/BD 3:1, (b) TMXDI, PPG1025/TMP 3:1, (c) MDI, PPG1025/ BD 3:1 and (d) MDI, PPG1025/ TMP 3:1.

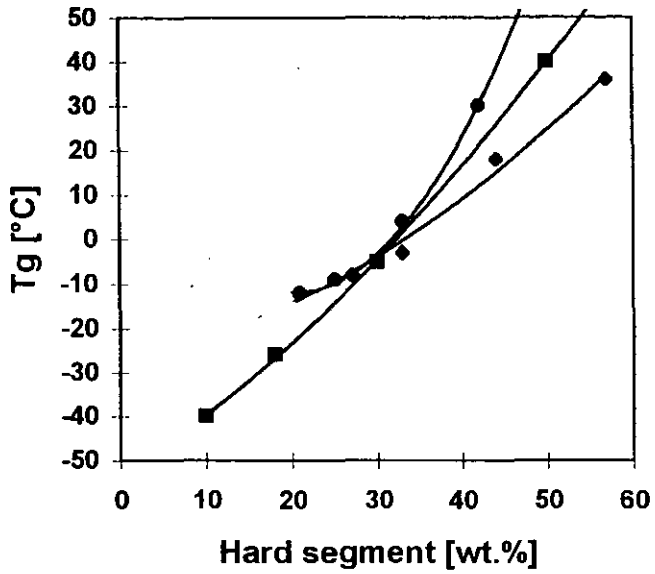

Figure 4.15 Glass transition temperature versus hard segment content. (■) TMXDI, PPG/TMP 3:1: 4000, 2025, 1025, 425, (●) TMXDI, PPG1025/TMP: 1:0, 7:1, 3:1, 2:1, 1:1, (◆) TMXDI, PPG1025/BD: 1:0, 3:1, 3:2, 2:3 and 1:3. (all from left to right).

The increase in Tg was much steeper for the crosslinked than for the linear PUR. This indicated that for the crosslinked PUR both the copolymer effect and crosslinking contributed to the increase in Tg. All linear PURs exhibited higher loss factor maxima than the crosslinked counterparts. Also, their half-peak widths were narrower than those of the crosslinked counterparts. This showed that the effect of crosslinking increased at higher crosslink densities. Without chain extender or crosslinker, the PPG1025-based (TMXDI) PURs had a lower temperature limit of the soft segment Tg at -12°C. By choosing lower molar mass polyols, the Tg range was extended to lower temperatures. This resulted from the lower hard segment content. With PPG1025 and TMXDI the minimum hard segment content was 18 weight %, whereas with higher molar mass polyols such as PPG4000 lower hard segment contents (10%), and, thus, lower soft segment Tgs (-40°C) were obtained. The values of the plot of Tg versus hard segment content for the polyols of different molar masses were situated in-between the crosslinked and linear PPG1025-PUR series.

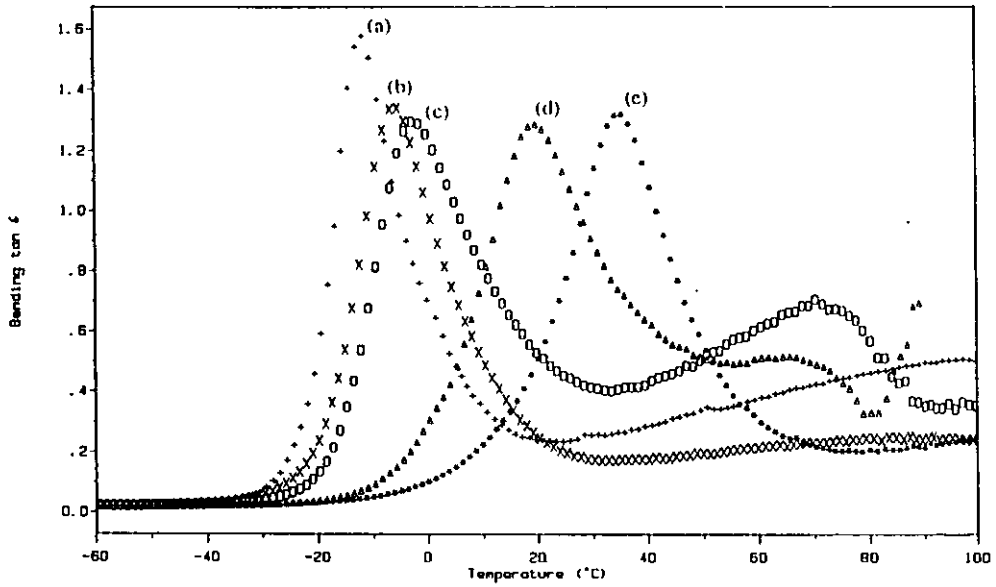

Figure 4.13 Loss factor versus temperature data for linear PURs of different hard segment content. (a) m-TMXDI, PPG1025/BD 1:0; hard segment content by weight: 21%, (b) 3:1; 27%, (c) 2:1; 33%, (d) 2:3; 44% and (e) 1:3; 57%.

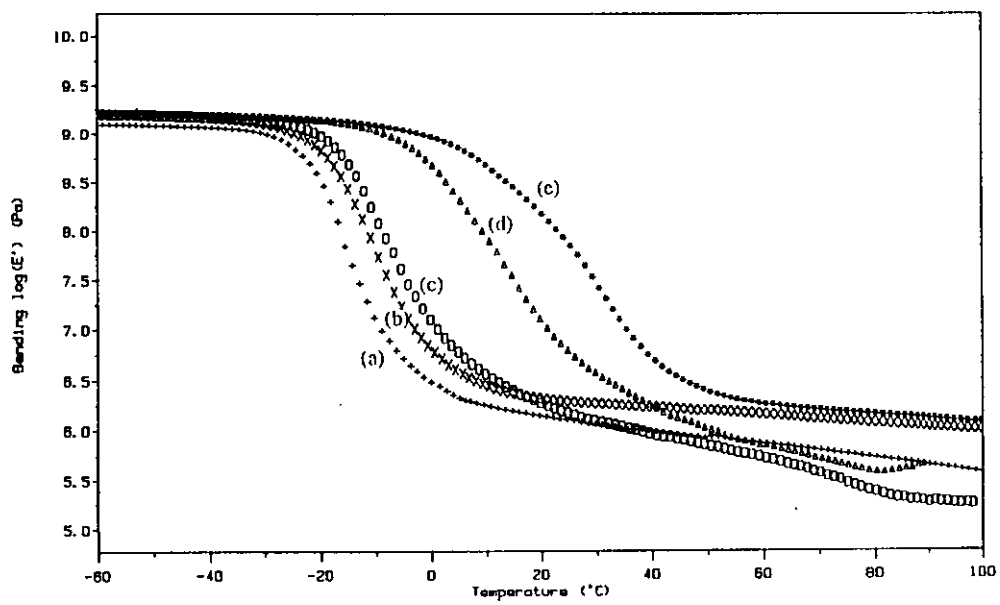

Figure 4.14 Storage moduli versus temperature for linear PURs of different hard segment content. (a) TMXDI, PPG1025/BD 1:0; hard segment content by weight: 21%, (b) 3:1; 27%, (c) 2:1; 33%, (d) 2:3; 44% and (e) 1:3; 57%.

The storage moduli versus temperature (figure 4.14) reflected the trends of loss factor profile in terms of the location of the storage modulus drop. For the rubbery plateau modulus, a general trend of higher values for PURs with higher HS contents was observed. The mechanical properties of the PURs with varying hard segments are shown in table 4.5.

Table 4.5 Mechanical properties as a function of the PUR hard segment.

PUR	Tensile properties				Hardness	
Hard segment variations	Stress at break [MPa]	Elongation at break [%]	Young's mod. [MPa]	Toughness [J]	Shore A	Shore D
Diisocyanate type (PPG1025/TMP 3:1)						
TMXDI	1.2	210	1.0	0.60	42	27
IPDI	1.8	140	2.1	0.49	57	32
TMDI	1.1	120	1.0	0.28	54	31
TDI	1.6	110	1.9	0.39	61	35
MDI	3.1	170	3.0	0.91	66	38
Chain extender BD (PPG1025/BD 3:1)						
MDI, BD	[a]5.4	1200	2.5	11.8	61	34
TMXDI, BD	[a]0.2	1300	0.3	-	-	-

(a) Maximum tensile strength.

As seen from the values for the stress at break, Young's modulus and Shore hardness, the weakest and softest PURs were obtained with TMXDI and TMDI. Slightly better mechanical properties resulted from the IPDI- and TDI-based materials. The symmetrical MDI yielded the highest values in this series. The TMXDI-based PUR had the highest elongation at break with 210%. However, with exception of the MDI-based PUR, differences between the other materials were comparatively little. This can be explained on the grounds of the hard segment contents (table 4.4). They were fairly low with values ranging from 24 to 30 wt.%. Consequently, it was principally the soft segment that determined the material properties.

A comparison of the mechanical properties of the linear MDI-based PUR with the crosslinked counterpart revealed a distinctively different property profile. Both PURs were prepared at a ratio of 3:1 PPG1025 to BD or TMP, respectively. The

crosslinked PUR exhibited a higher Young's modulus (3.0 compared to 2.5 MPa) and higher Shore hardness values (table 4.5). The latter might be explained by the crosslinking imparting a higher hardness. Also, the slightly higher hard segment content (table 4.4) of 30 wt.% compared to 28 wt.% might have contributed to this effect. However, a higher tensile strength and elongation at break were obtained for the linear MDI-based PUR. The difference in the latter was considerable with 170% compared to 1200% for the linear material. This would be expected since the linear chains can slide past each other without breaking unlike in the crosslinked material. The higher tensile strength (5.4 MPa compared to 3.1) of the linear PUR was somewhat surprising. It can be explained by a mechanism similar to the PTHF2000 and PCL2000-based PURs in section 4.1. Upon stretching, a certain degree of order is introduced in the PUR. In this case, it was the hard segments which were aligned and not the soft segments. However, no opacity, indicating crystallisation, in the test specimens was observed. As a result of the higher tensile strength and the higher elongation, also a significantly higher value (11.8 J compared to 0.91 J) for the toughness index resulted for the linear MDI-based PUR.

The linear TMXDI-based PURs were generally too soft for tensile testing and hardness measurements. However, for comparison with the MDI-based counterpart, the values for the TMXDI, PPG1025/BD 3:1 PUR are given (table 4.5). Again, the linear PUR (1300%) exhibited a much higher value for the elongation at break than the crosslinked counterpart (210%). However, while the linear MDI-based PUR had a higher maximum tensile strength than the crosslinked counterpart, a very low value of 0.2 MPa resulted for the linear TMXDI-based material. The maximum tensile strength for the linear TMXDI-based PUR was obtained at an elongation of about 200%. At the elongation at break (1300%), the tensile strength tended towards extremely low values. For the linear MDI-based PUR, the maximum tensile strength was obtained at an elongation of about 900%.

The better mechanical properties of the MDI-based compared to the TMXDI-based linear PUR can be explained by the fundamental structural difference in both diisocyanate molecules. The symmetrical structure of MDI allowed strong hydrogen bonding to occur, which, together some with π-electron interaction[204] between the aromatic rings, was responsible for the comparatively good mechanical properties. Thus, it was found that crosslinking in PURs based on TMXDI and PPG1025 greatly

improved the mechanical properties. In PURs based on MDI and PPG1025, crosslinking resulted in a pronounced decrease in the elongation at break and even decreased the maximum the tensile strength.

4.4 Investigation of NCO/OH Ratio and PUR Morphology

In altering the isocyanate to hydroxyl ratio in a PUR, network defects such as loose ends can be intentionally introduced. These network defects can act as plasticisers[63,86], and, thus, change the engineering properties and improve the damping performance[13,152]. Crystallinity in the PURs for damping applications is generally unwanted[152], since this imparts a stiffening of the PUR and decreases the volume fraction of material that is available for secondary transitions.

Influence of NCO/OH ratio. By working at lower or higher NCO/OH ratios than 1, network defects such as loose chain ends may be introduced. A PUR network consisting of TMXDI and PPG1025/TMP 3:1 was investigated at NCO/OH ratios of 0.9, 1.0, 1.1 and 1.2.

The dynamic mechanical data for the NCO/OH ratios studied are shown in figures 4.16 and 4.17. The PUR with a NCO/OH ratio of 0.9 exhibited the lowest transition (-9°C) combined with the highest loss factor peak maximum with 1.31. Since plasticisation is known[13] to shift the Tg to lower temperatures and increase damping, it was concluded that a significant number of dangling polyol chains were present in this material. The going off scale of the loss factor curve at temperatures higher than 20°C, furthermore, indicated poor network formation. The materials made at NCO/OH ratios of 1.0 and 1.1 had very similar loss factor versus temperature profiles. While the location of the loss factor peak was virtually at the same temperature (-5°C), the former material exhibited a slightly higher peak maximum of 1.18 compared to 1.08. At a NCO/OH ratio of 1.2, the transition shifted to a slightly higher temperature (-2°) and had a maximum peak height of 1.11. The higher transition might be explained by the increased amount of hard segment in the PUR. A particularity of this material was that the loss factor values did not decrease to a value below 0.1 after the Tg transition, but remained fairly high (figure 4.16).

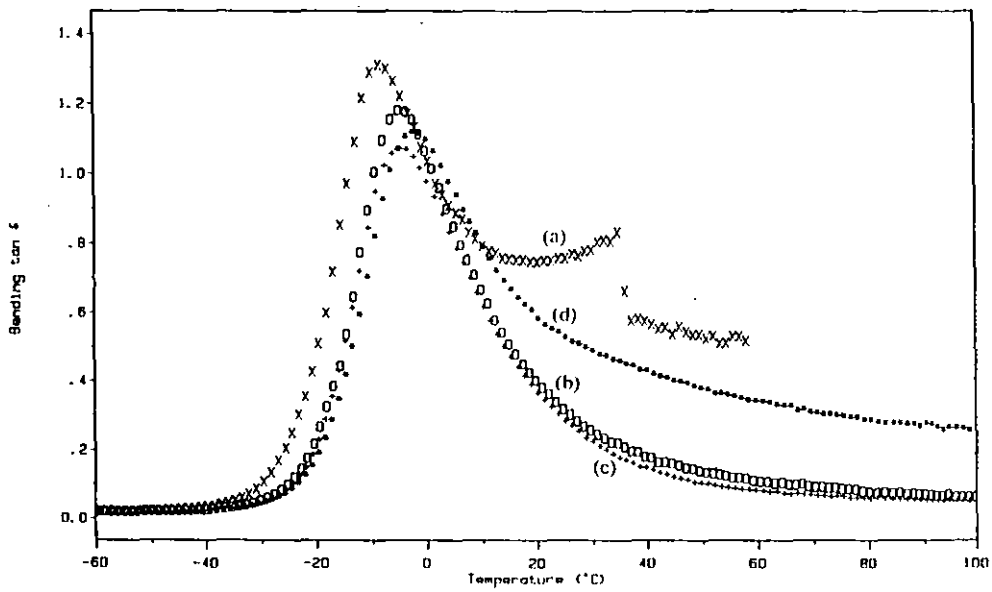

Figure 4.16 Loss factor versus temperature data for different NCO/OH ratios. (a) 0.9, (b) 1.0, (c) 1.1 and (d) 1.2.

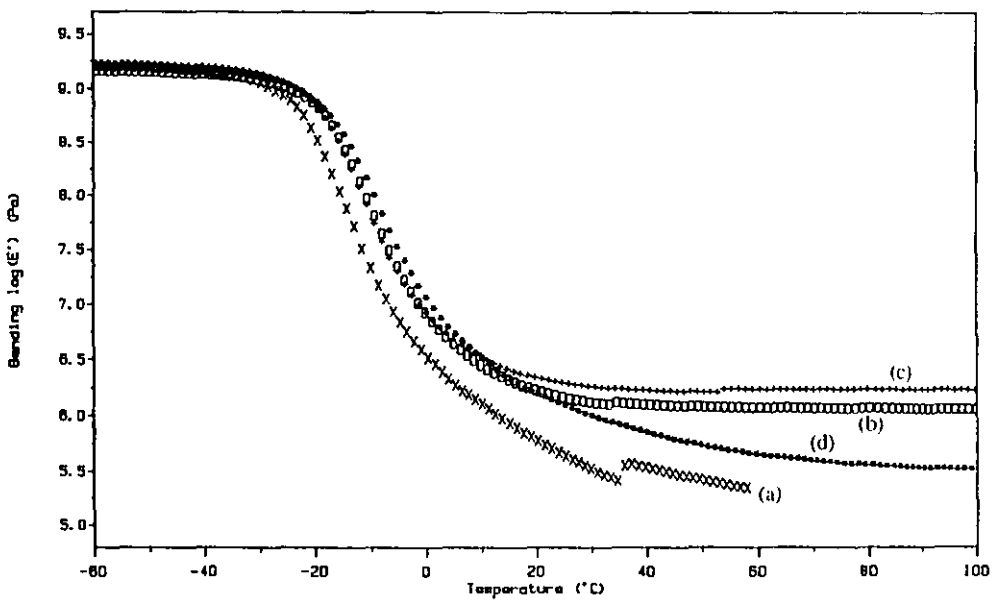

Figure 4.17 Storage modulus versus temperature data for different NCO/OH ratios. (a) 0.9, (b) 1.0, (c) 1.1 and (d) 1.2.

The storage moduli confirmed that the PUR prepared at a NCO/OH ratio of 0.9 had the poorest mechanical properties as seen from the rubbery plateau modulus. The second weakest material was obtained at the ratio of 1.2. The NCO/OH ratios of 1.0 and 1.1 had similar storage moduli, with the 1.1 still exhibiting a higher rubbery plateau. The fact that a NCO/OH ratio of 1.1 resulted in the best network formation and not a ratio of 1.0, as might have been expected, might have been due to the formation of additional crosslinks through allophanate links. However, generally, temperatures higher than 100°C are needed[203] for this reaction to take place, particularly for diisocyanates of a low reactivity such as TMXDI. Also, at ratio of NCO/OH of 1.2 an even greater number of allophanate links could have been formed. However, this PUR exhibited significantly poorer mechanical properties than the material prepared at a NCO/OH ratio of 1.0. Another explanation might be that despite of greatest care humidity was not fully excluded and, thus, a slightly higher NCO/OH ratio was advantageous for the stoichiometry. A similar phenomenon of a NCO/OH ratio of 1.1 resulting in the lowest average molecular weight between crosslinks had been observed[267] in a system based on Adiprene L-100, 1,4-butanediol and trimethylol propane.

Crystallinity in PURs. Important requirements for crystallinity[93] are a regularity of the molecule/polymer structure and the presence of forces of cohesion such as van der Waals-type attractive forces and hydrogen bonding. Factors that control the melting temperature include polarity and hydrogen bonding as well as packing capability. In PURs, crystallinity can be encountered both in the hard and in the soft segment (see section 2.3.3).

In general, crystallinity for PURs based on symmetrical polyols is only observed[204] at polyol molar masses of 2000 g/mol and higher. In this study, 4 polyol types of a molar mass of 2000 and higher were investigated in a PUR based on TMXDI and TMP. The ratio of polyol/TMP was 3:1. 24 hours after demoulding, the PURs prepared with all four polyols were still transparent. However, differences in the PUR properties with time were observed. Repeating the DMTA analysis after a shelf life of 6 months at room temperature resulted in similar data for the PBD2500- and PPG2025-based PURs. However, with PCL2000 and PTHF2000 the DMTA profile changed considerably (figures 4.18 and 4.19). Also, the PCL2000-based PUR was

completely opaque and that based on PTHF2000 was translucent. The phenomenon of soft segment crystallisation at ambient temperatures with time is termed cold hardening[205]. It can have detrimental consequences because it can impart brittleness, as for example[205] in PUR coatings. Cold hardening can be avoided[205] by using polyols of a molar mass of less than 2000 g/mol and by the use of copolyols to provide structural irregularity. In the loss factor versus temperature profile of the material containing PCL2000 (figure 4.18), a drop of the loss factor height by a factor of 4 from 1.13 to 0.25 was observed. Also the transition maximum shifted to higher temperatures from -19°C to -6°C and a further transition was observed between 50 and 60°C. Characteristic for semi-crystalline polymers is that the drop in storage modulus at Tg is much less pronounced (figure 4.18). At the temperature of the melting point, Tm, however, a dramatic modulus drop was observed. The modulus drop for the PCL2000 took place between 40 and 50°C. This value corresponds well with the temperature found by DSC for the melting point of the pure PCL2000 polyol of 53°C (section 3.1.4.3). Very similar DMTA data were obtained for the PTHF2000-based PUR. The location of the loss factor peak shifted from -37°C to -32°C for the aged material and the peak maximum decreased from 0.77 to 0.42. A transition shoulder from -10 to 20°C was observed in both materials. This shoulder was also reflected in the storage moduli. However, with PTHF2000, a further phenomenon was observed. From around -15°C onwards, an increase in the modulus took place. A significant increase in the storage modulus[185] can be caused by the occurrence of a chemical reaction i.e. crosslinking or by the formation of crystalline domains. In this case the storage modulus increase was ascribed to formation of crystalline order in the PUR soft segment. Clear melting phenomena were observed for both the unaged and aged PUR between 20 and 30°C. This was in good agreement with the melting point of the pure PTHF2000 polyol (33°C).

The occurrence of crystallinity in the PUR soft segment was corroborated by DSC studies (figures 4.20 and 4.21). The measurements were conducted on the materials with a shelf live of 6 months at room temperature. Besides PCL2000- and PTHF2000-based PURs also the 1000 molar mass equivalents were investigated. However, for both the PCL1000 and the PTHF1000-based PURs no melting endotherm was obtained (figures 4.20 and 4.21).

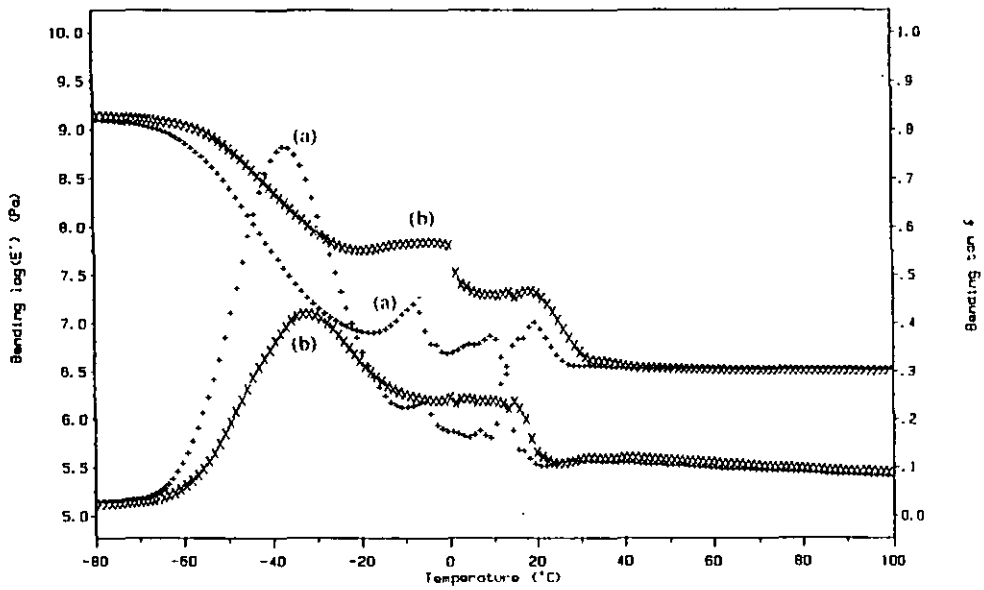

Figure 4.18 Comparison of storage modulus and loss factor versus temperature profile of the PUR (TMXDI, PCL2000/TMP 3:1). (a) quenched from 90°C to room temperature, (b) after a shelf-life of 6 months at room temperature.

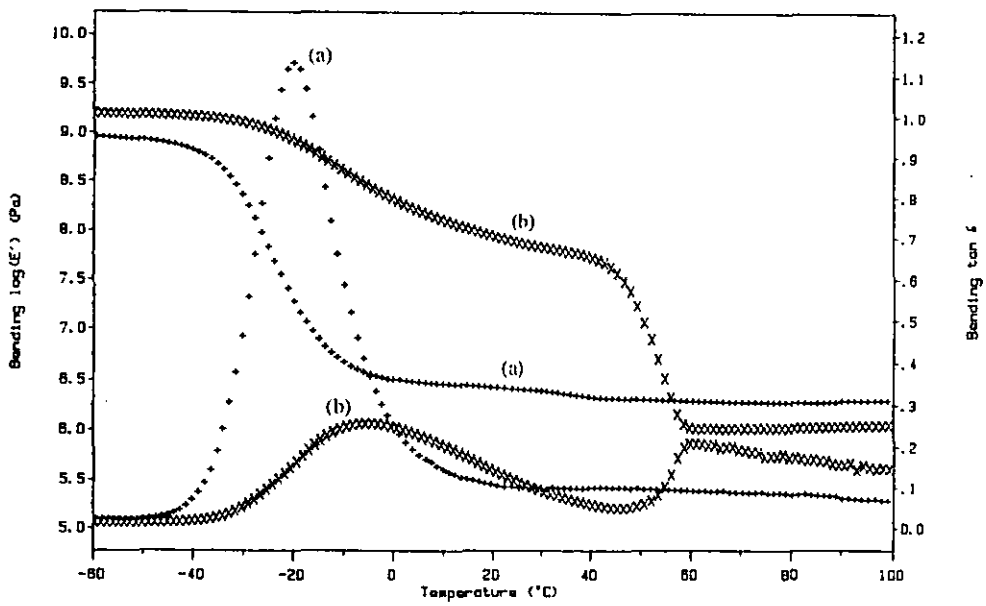

Figure 4.19 Comparison of storage modulus and loss factor versus temperature profile of a the PUR (TMXDI, PTHF2000/TMP 3:1). (a) quenched from 90°C to room temperature, (b) after a shelf-life of 6 months at room temperature.

The onset of Tg for PCL1000 was at -30°C. For PTHF1000 Tg onset was about -53°C. However, it has to be noted that many PUR Tgs were difficult to detect with DSC measurements. For the PCL2000-based PUR, a small melting endotherm was found at 21°C followed by a bigger and sharper one at 41°C. For the PTHF2000-based material, again two phenomena were observed. An exothermic crystallisation peak was found at -13°C which changed into a melting peak at 17°C. The presence of the crystallisation exotherm resulted from quenching the PUR from room temperature to -120°C.

By comparing the melting endotherm area of the PCL- and PTHF-based PURs to those of the respective polyols, an estimation of the degree of crystallinity can be made. The heats of fusion for the PCL2000 and PTHF2000 polyols were 72 and 107 J/g, respectively (section 3.1.4.3). Both PURs based on these polyols contained 82 % SS (table 4.1). Thus, relating the heats of fusion obtained for the PURs based on PCL2000 (22 J/g) and PTHF2000 (41 J/g) to the heats of fusion for the polyols should give a rough estimation of the degree crystallinity in the PUR soft segments. To do so, both polyols had to be taken as 100% crystalline. From this calculation it resulted that 37 wt.% of the PCL2000-PUR soft segment and 47% of the PTHF2000-PUR were crystalline. This correlates well with the observed lower melting points for the polyols in the PURs. These melting points of 41°C and 17°C were closer to those of the respective PCL1000 (36°C) and PTHF1000 (24°C) polyols. This indicated that only segments of the 2000 polyol chains were able to crystallise. Their mobility was restricted by attachment through urethane linkages and crosslinks.

Hard segment crystallinity for highly symmetrical diisocyanates combined with symmetrical chain extenders has been reported[268]. Crystallinity of the PUR prepared from MDI and PPG1025/BD 3:1 was investigated by DSC measurements. Even though MDI and BD are known[204] to be able to produce PURs with hard segment crystallinity, no melting endotherm was observed for this material.

Wide angle x-ray diffraction (WAXD) is commonly used[107,269-272] to investigate crystallinity in polymers (section 3.12). Three PURs were investigated in order to confirm the findings from DSC. Diffractometer traces for the three materials are shown in figure 4.22. The WAXD data confirmed the DSC results.

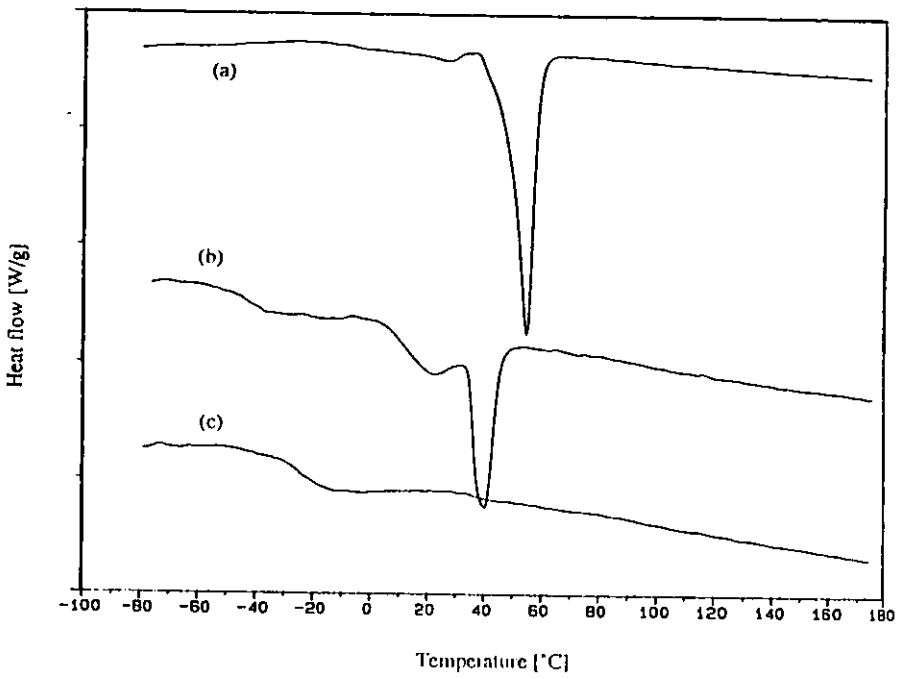

Figure 4.20 DSC traces. (a) PCL2000, (b) TMXDI, PCL2000/TMP 3:1 (c) TMXDI, PCL1000/TMP 3:1. (One scale mark [W/g] corresponds to 0.2 for (b) and (c) and 0.6 for (a)).

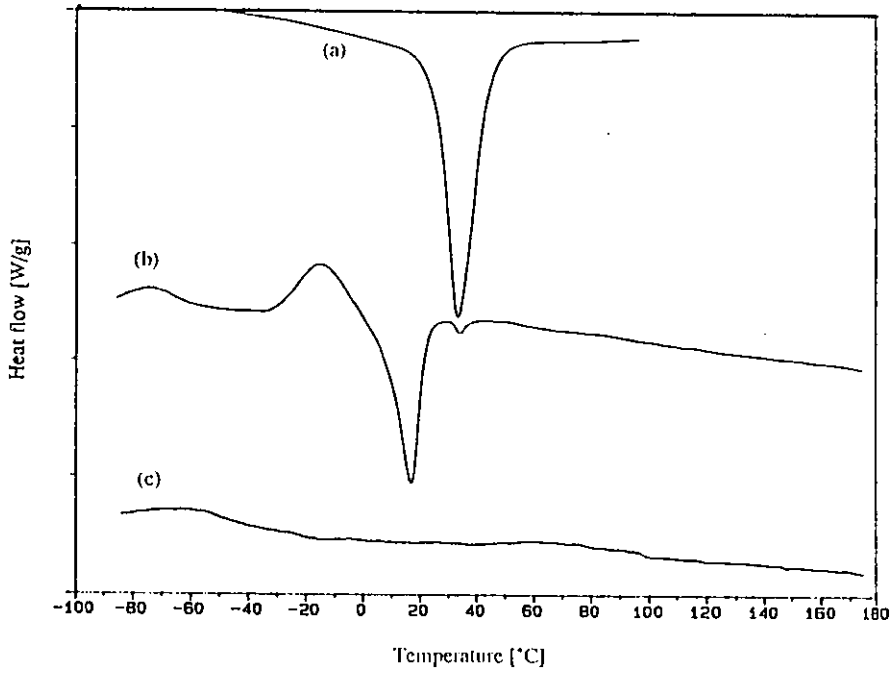

Figure 4.21 DSC traces. (a) PTHF2000, (b) TMXDI, PTHF2000/TMP 3:1 (c) TMXDI, PTHF1000/TMP 3:1. (One scale mark [W/g] corresponds to 0.3 for (b) and (c) and 0.9 for (a)).

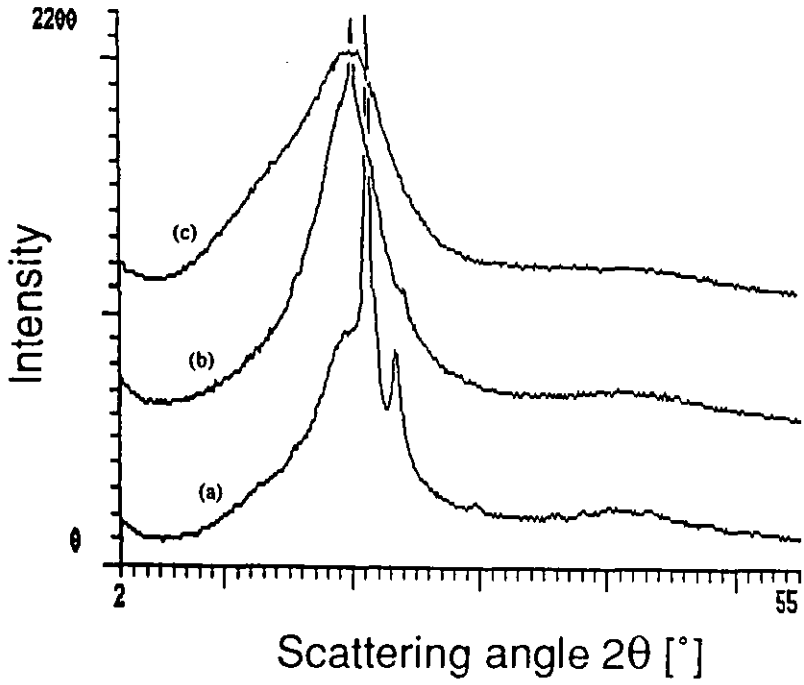

Figure 4.22 Wide-angle X-ray diffraction spectra. (a) TMXDI, PCL2000/TMP 3:1, (b) TMXDI, PTHF2000/TMP 3:1 and (c) MDI, PPG1025/BD 3:1.

No crystallinity in the hard segment of the PUR based on MDI, PPG1025/BD 3:1 was observed. The X-ray pattern of this material (figure 4.22) resulted in broad peak. This broad halo is typical[107] of amorphous polymers where no ordered regions exist. On the other hand, sharp diffraction peaks were found for PURs based on PCL2000 and PTHF2000. Using Bragg's equation[107,177], the distance between the atomic layers, the d spacing, can be calculated (section 3.4.11). Correlating Bragg's d spacings with known values for PCL and PTHF, respectively, confirmed the presence of crystallinity in the PUR soft segment. For the PUR based on PCL2000 two distinctive peaks were observed on top of a diffuse peak at $2\theta = 21.2°$ and 23.5°. A much smaller third peak was observed at $2\theta = 19.5°$. These peaks resulted in Bragg's d spacing values of 0.379, 0.419 and 0.455 nm which were in good agreement with those found for the polycaprolactone[269] homopolymer of 0.375, 0.414 and 0.457 nm. The small deviations may be because of the occurrence of some phase mixing of a hard and soft segment blocks. Investigations of pure PTHF[270-272] showed prominent crystalline diffraction peaks at d spacings of 0.445 and 0.366 nm. The presence of a major crystalline diffraction peak (figure 4.22) at $2\theta = 19.9$ and a minor one at $2\theta = 24.1$

corresponding to d spacings of 0.446 nm and 0.369, respectively, therefore could be assigned to the crystallites present in the PTHF soft segment domains.

Not only ageing provoked an increase in crystallinity. The tensile test specimen of both PURs changed their optical appearance upon stretching. For the PCL2000- and the PTHF2000-based PURs, the whitening was still present after the applied force was released. Opacity is characteristic for semi-crystalline polymers[93] since the refractive indices of the amorphous and the crystalline region are different. Thus, crystallinity was induced by stretching the PURs.

Phase segregation in PURs. Most of the favourable properties such as the high strength and wear resistance of PURs result[204-207] from their phase segregated structure. The soft segment transition occurs[204] at sub-ambient temperatures. For the hard segment, up to three endothermic transitions[268] can be seen, at 70-80, 140-170 and 190°C. These are melting of shortest average hard segment at 70-80°C, at 140-170°C melting of long hard segment with long range order and crystalline melting at 190°C and above. The appearance of DSC endotherms[268] is a function of hard segment length. Thus, a PUR with short hard segment length only exhibits the lowest temperature transition.

In the present study, only the low temperature transition which was ascribed to the PUR soft segment and in some cases melting of the soft segment were observed by dynamic mechanical analysis. Neither a second Tg, nor a melting point for ordered hard segments was observed. Thus, no phase segregated structure could be observed by DMTA. DSC and modulated-temperature DSC measurements did not show a transition for the hard segment either. The finding that no, or only very limited, phase segregation was present in the investigated PURs based on TMXDI and PPG1025 was further corroborated by the study on varying the PUR hard segment (section 4.3). Tg increased with increasing hard segment content. This is an indication[205] of considerable hard and soft segment phase mixing. The absence of a noticeable phase segregation might be a result of several factors. The principal diisocyanate (TMXDI) and polyol (PPG1025) had both asymmetrical structures which limit or prevent phase segregation. Further, the weight percentage of hard segment was generally low[272] in the PURs synthesised. In the PUR that consisted of TMXDI (244 MW) and PPG1025

and TMP (135 MW) at a ratio of 3:1, the hard segment represented only 30 weight % of the material. 17 weight % percent of this hard segment was TMXDI between two PPG1025 units, thus dissolved in the soft segment. Effectively, there was only 13 weight % hard segment present. Crosslinking is a further factor that might have prevented phase segregation. Crosslinking took place exclusively in the hard segment, thus, suppressing both a possible Tg and the occurrence of crystalline order. Also, the formation of a segregated structure is strongly hindered by chemical crosslinks.

5. Polyurethane / Polystyrene IPNs

Polymer blends have been the subject of numerous investigations[1], academic and industrial. By carefully choosing the polymer pair, new materials with synergistic properties can be developed[3,4]. In the present study, elastomeric PURs were combined with immiscible and semi-miscible high Tg plastics using the IPN technology. The PUR consisted in most cases of TMXDI and PPG1025/TMP at a molar ratio of 3:1 (chapter 4). PUR and polystyrene (PS) are highly immiscible polymers because of the polar nature of the PUR compared to the essentially non-polar PS and the pronounced difference in their solubility parameters[254] of 20.5 $(J/cm^3)^{1/2}$ and 18.5 $(J/cm^3)^{1/2}$, respectively. Blends of these two linear polymers result[273,274], consequently, in highly immiscible materials with poor mechanical properties. In the composition study, the extent of PUR/PS IPN miscibility and phase mixing was determined to correlate the findings with the dynamic mechanical and mechanical properties. In order to obtain a microheterogeneous morphology methods of improving the IPN miscibility were applied. These included varying the crosslink density in both networks, the introduction of inter-network grafting, the incorporation of compatibilisers and the introduction of oppositely charged ionic groups.

5.1 PUR/PS IPNs Investigated and Transitions in Polystyrene

Several full PUR/PS IPNs[112,127,149,275], semi-IPNs[64-66] and linear blends[273,274] have been investigated for various applications, such as gas separation membranes[46,66,276]. Due to the immiscibility of their constituent polymers, fundamental studies of means to restrict phase separation have been conducted. The influence of the synthesis temperature[66,273,277,278], the synthesis pressure[60,148,275], the synthesis using a common solvent[149] and the reaction kinetics[64,65] on phase separation have been studied. Also, the effect of composition[127,275], crosslink density[66,112,127,278] and of inter-network grafting on transparency[112] of PUR/PS IPNs were investigated. No study into the use of PUR/PS IPNs as energy absorbing materials has been conducted. Thus, no attempt has been made to obtain a broad and high transition region through the use of inter-network grafting and the incorporation of compatibilisers.

In order to understand the dynamic mechanical data of PUR/PS IPNs, it is essential to know the transitions of both constituent homopolymers. The transitions of the polyurethane are dependent[204,205] upon the soft segment, its chemical composition and molar mass and, furthermore, upon the miscibility of the soft segment with the hard segment. The PUR transition behaviour has been fully discussed in chapter 4. In PS, five principal types of molecular motions can be encountered[279,280]. With decreasing temperature, these are the liquid-liquid transition T_{ll} (160°C), the glass transition Tg (100°C), the β transition (50°C), and the γ (-143°C) and the δ (-233°C) transition. Due to the temperature range where they occur and their magnitude, only the first three transitions are of importance for this study. The T_{ll} transition is explained[281] as a $liquid_1$ - $liquid_2$ transition involving the entire chain. Tg involves[93] long-range chain motions of 10-50 main chain atoms. The β transition in PS is believed[279] to be caused by torsional vibrations of the phenyl groups. It is particularly pronounced[282] in quenched and crosslinked PS and increases with higher crosslinking. It was, therefore, concluded[279] that under some conditions crosslinking might increase free volume. In this study, all three transitions were found in several IPNs.

5.2 PUR/PS IPN Composition Study

Aim of this study was to investigate the influence of composition on IPN miscibility and the dynamic mechanical and mechanical properties of the materials. While composition studies[127,275] have been conducted with PUR/PS IPNs, these did not comprise the full composition range. In this study, the full composition range was studied using 10 weight % increments. The PUR/PS IPNs were prepared at a diol/triol ratio of 3:1 in the PUR component and at 5 mol % divinylbenzene (DVB) in the PS. Both the pure PUR and the pure PS networks were also moulded using the same experimental technique (section 3.3). From the DMTA data, one specific composition was selected for the subsequent study of means to enhance miscibility in the IPN.

DMTA studies. The miscibility of two polymer components greatly influences[283] the mechanical properties of a polymer blend and can be assessed[190] from DMTA

data. Two separate loss factor peaks indicate[113] an immiscible system, whereas one peak indicates a high degree of miscibility (section 3.4.1). The latter is only strictly true for polymers with Tgs that are more than 10-20°C apart. An intermediate degree of miscibility might result in a broad almost rectangular loss factor transition, with both homopolymer transitions significantly shifted inward. These materials exhibit frequently a microheterogeneous morphology[13]. The materials with a microheterogeneous morphology are often used to construct high damping systems[24,284]. Thus, the parameters of interest for the present study were the respective loss factor peak heights, the values for the loss factor at the inter-transition region and the loss factor peak location. The extent to which they allow the drawing of conclusions about IPN miscibility and phase continuity has been outlined in greater detail in section 3.4.1. The loss factor versus temperature data for the PUR/PS composition series with a PPG1025/TMP ratio of 3:1 and 5 mol % DVB are shown in figures 5.1 and 5.2. The dynamic mechanical properties are given in table 5.1.

Table 5.1 Dynamic mechanical properties (10 Hz) of the PUR/PS IPN and the homonetworks as a function of composition.

Composition IPN	Tg [tan δ, °C]		Tan δ maximum		Inter-transition
% PS	PUR	PS	PUR	PS	height at 67°C
0	-5	-	1.10	-	-
10	-4	150	1.00	0.28	0.24
20	-2	148	0.94	0.31	0.32
30	-1	146	0.77	0.35	0.22
40	-3	140	0.62	0.42	0.17
50	1	139	0.49	0.52	0.18
60	2	136	0.37	0.67	0.16
70	-4	131	0.21	1.11	0.13
80	-20	131	0.10	1.82	0.03
90	-22	127	0.02	1.91	0.03
100	-	128	-	2.30	0.02

As expected for an immiscible polymer pair, two well-separated tan δ transitions were observed, with low values for the loss factor in the inter-transition region. A plot of the PUR and PS loss factor peak heights versus the PS content is shown in figure 5.3.

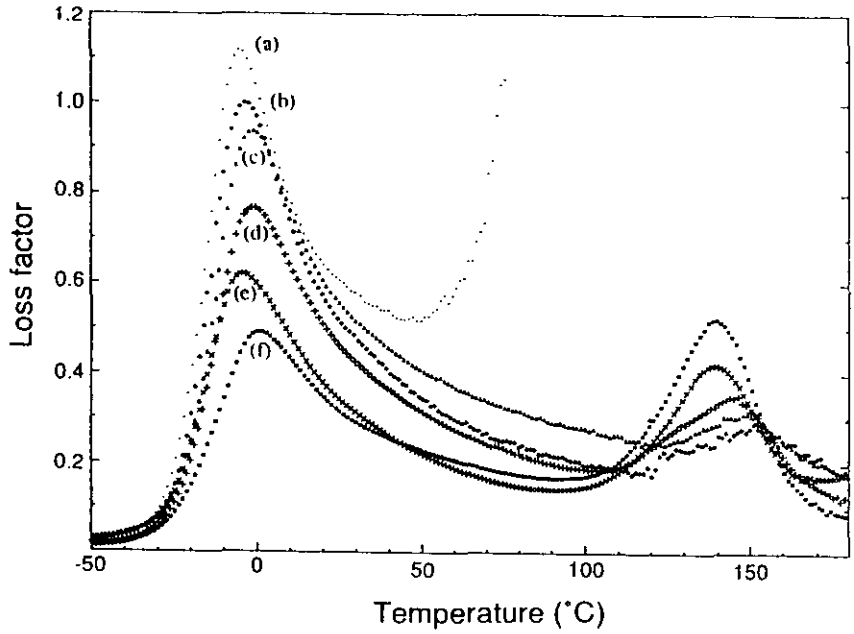

Figure 5.1 Loss factor (tan δ) versus temperature data for PUR/PS IPN compositions. (a) 100 PUR, (b) 90:10 PUR/PS, (c) 80:20, (d) 70:30, (e) 60:40 and (f) 50:50.

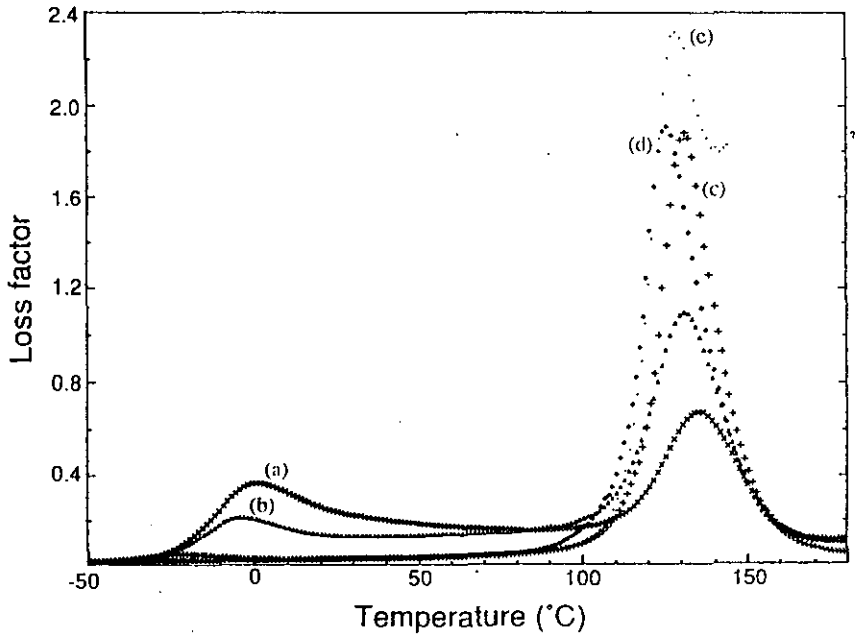

Figure 5.2 Loss factor (tan δ) versus temperature data for PUR/PS IPN compositions. (a) 40:60 PUR/PS, (b) 30:70, (c) 20:80, (d) 10:90 and (e) 100 PS.

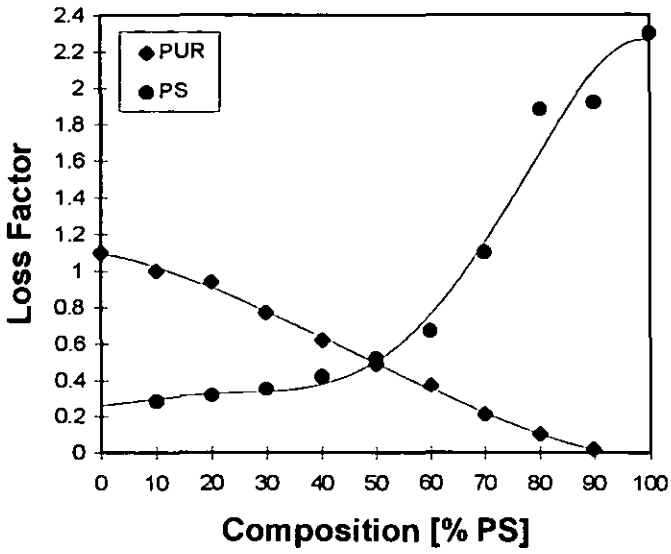

Figure 5.3 Loss factor peak height against PUR/PS IPN composition.

The trend of the loss factor peak height of the components clearly followed the composition (figure 5.3). At these crosslinking levels, the PS loss factor values were generally higher than those of the PUR of equal content in the IPN. The PUR loss factor decreased almost linearly with decreasing PUR content from 1.10 for the pure PUR to 0.02 for the 10:90 PUR/PS IPN. For the PS loss factor values a different trend was observed. A slow increase up to the 40:60 PUR/PS composition (tan δ = 0.67) was followed by a higher loss factor (1.10) for the 30:70 and very high values of 1.80 and 1.90 for the 20:80 and 10:90 IPNs, respectively. The loss factor peak height can give an indication about phase continuity[4] of a polymer blend, the material exhibiting the higher peak representing the more continuous phase. Two transition peaks of the same height may be an indication for dual phase continuity[4]. From the data in figure 5.3, phase inversion took place between the 60:40 and the 50:50 PUR/PS IPN composition. However, one has to consider that the PS homonetwork (2.30) exhibited a higher loss factor value than the PUR (1.10) by a factor of more than two. Therefore, equal peak height might not have been the right criterion for phase inversion in this PUR/PS system. On the other hand, the sharp increase in loss factor at the 30:70 composition might be an indication for phase inversion taking place at these higher PS contents. The loss factor values of the inter-transition region are given in table 5.1. The values were taken at the intermediate temperature (67°C)

between the PUR and PS homonetwork glass transitions. Generally, the inter-transition loss factor values were very low and decreased with decreasing PUR content in the IPN. The overall loss factor peak height of the PUR decreased and so did the inter-transition values. The low values were an indication of very limited phase mixing and little interface area in the IPNs. A further and possibly more sensitive indication of phase mixing in IPNs is the loss factor peak location (section 3.4.1). Figure 5.4 shows the location of the Tgs as obtained from the loss factor peak versus IPN composition.

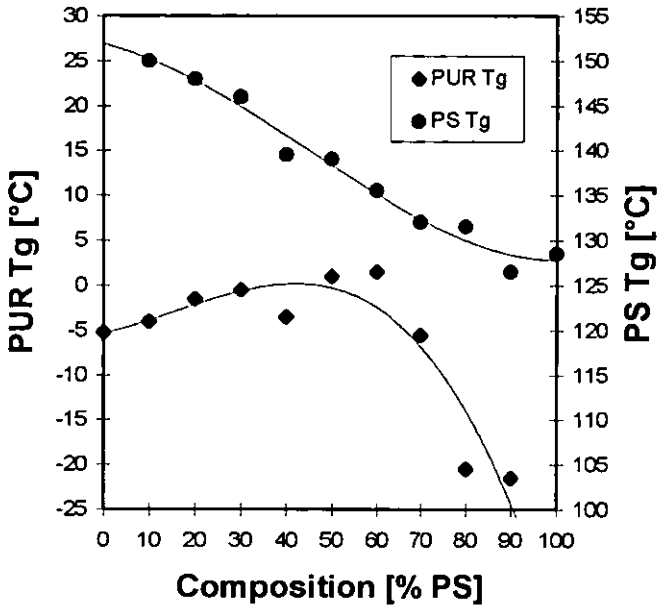

Figure 5.4 Loss factor peak location against PUR/PS IPN composition.

Comparing the IPNs to the homopolymer networks, a Tg shift was observed for both polymers with changing composition. For the polyurethane transition, Tg maxima existed at the 50:50 and 40:60 compositions. For both lower and higher PUR contents, Tg values were found to decrease continually, though more dramatically for the lower PUR compositions. The PUR transition increased slightly, from -5 to 2°C, as the PUR weight fraction decreased from 100:0 to 40:60 PUR/PS (table 5.1). From the 30:70 PUR/PS composition onwards, it fell considerably by more than 20°C to a Tg of -22°C for the PUR in the 10:90 PUR/PS composition. The PS transition constantly shifted to lower temperatures with increasing PS weight fraction. The decrease was significant, with a difference of more than 20°C between the PS transition in the 90:10 PUR/PS IPN (150°C) and the PS homonetwork (128°C). This

trend was very surprising and could not be explained with certainty. Similar findings of higher Tgs for the PS transition in blends with PUR than for the corresponding pure PS were made with a PUR/PS IPN composition series with lower crosslink densities[285], with an isophorone diisocyanate (IPDI)-based PUR/PS IPN[194] and with a diphenylmethane diisocyanate-based PUR/PS mechanical linear blend[286]. The increase in the PS transition at higher PUR contents indicated that PS segments were less free to move in the IPNs than in the pure PS network. Reasons for the latter could be an increase in crosslink density through grafting or some other specific intermolecular interactions[287] between the polystyrene and polyurethane polymer chains. A PS Tg shift to higher temperatures has also been observed[288] in high impact polystyrene. It was believed[288] that area of contact between the PS and the polybutadiene and the extent of grafting influenced the PS Tg. An increase in crosslink density of the matrix because of grafting shifted[288] the PS Tg to higher temperatures. In the study on mechanical blends of linear PUR and PS, Theocaris and Kefalas[286] believed that the interactions of the π-electrons of the aromatic ring-containing PUR hard segments with the PS phenyl side groups were responsible for the increase in PS Tg in the polymer blends. The rigid hard segments were believed[286] to have had a Tg in the order of 160°C. Chugthai[194] believed that some kind of anti-plasticisation effect and essentially pure PS phases were the grounds of the PS Tg shift in IPDI-based PUR/PS IPNs. All these explanations were not entirely satisfactory for the present PUR/PS IPNs. In the latter, no unsaturation was present and the reaction was conducted under comparatively mild conditions so that no significant extent of grafting was believed to have occurred. Interactions of phenyl π-electrons were not possible in the PUR/PS IPN based on the cycloaliphatic IPDI. Cowie[287] pointed out that not only interactions between π-electrons of phenyl rings have been observed, but that the π-electrons of a phenyl ring can interact with electron lone pairs, as was observed[289] in PS/polyvinylmethylether blends. Thus, in the present study, interaction of the PS π-electrons with the electron lone pairs of the ether oxygen in the PUR soft segment or the electron lone pair of the nitrogen atoms in the hard segments would have been possible. However, because of the much higher content of ether oxygen compared to nitrogen as a result of the high soft segment content of this PUR with 69 weight % (section 4.3) a PS Tg shift to lower

temperatures and increased phase mixing with the PUR soft segment would have been expected. However, the opposite effect was observed in the present study. A recent FTIR study[290] on hydrogen bonding of linear PURs in a styrene solvent has shed new light on this phenomenon. Feve, Lam and co-workers[290] found that when increasing the amount of styrene solvent from 0 to 90% in the solution, an additional N-H stretching vibration appeared. This absorption peak was found intermediate to be between the free (3447 cm^{-1}) and the - to the carbonyl group - hydrogen-bonded (3347 cm^{-1}) N-H stretching. In their opinion, the additional vibrational band that appeared at 3400 cm^{-1} was due to the hydrogen-bonded N-H stretching between the N-H and the π orbitals of the aromatic rings of the PS. The fact that this band was located between the free and the hydrogen-bonded N-H stretching gave an indication of its average strength. Thus, interaction of the N-H hydrogen of the rigid PUR hard segment with π orbitals of the PS phenyl rings could have led to an increase in PS Tg. This effect was more pronounced at higher PUR compositions in the PUR/PS IPN since more urethane links were present. Also, the PS domain sizes decreased considerably which will be seen later by TEM. This PS domain size decrease resulted in a greater surface area and, thus, higher contact area with the PUR. This explained why the PS Tg of the 90:10 PUR/PS IPN was the highest at 150°C as seen from DMTA compared to 128°C for the PS homonetwork. However, the less significant increase of Tg for the PUR component from 100 PUR to the 40:60 PUR/PS composition might be explained by increased phase mixing with the PS. Also, the increase of the PS weight fraction might result in a tighter PS network and, thus, decrease the free volume for the PUR component. From the 30:70 to the 10:90 composition, a decrease of the PUR transition was observed. A similar phenomenon has been attributed to plasticisation effects[63,86] in polymer blends. Dissolved PS chains in PUR domains might have disrupted the interactions between urethane links. More likely in this study, however, is that the PUR network was incompletely formed[63,110]. Consequences of an incomplete reaction are more dramatic[291] in step-growth polymerisations than in radically polymerised materials because of a much steeper fall in molecular weight at lower conversions. Thus, a lower molecular weight PUR polymer/oligomer lead to a Tg shift towards lower temperatures. The storage and the loss moduli versus temperature plots for the PUR/PS IPN composition series are shown in figures 5.5 and 5.6.

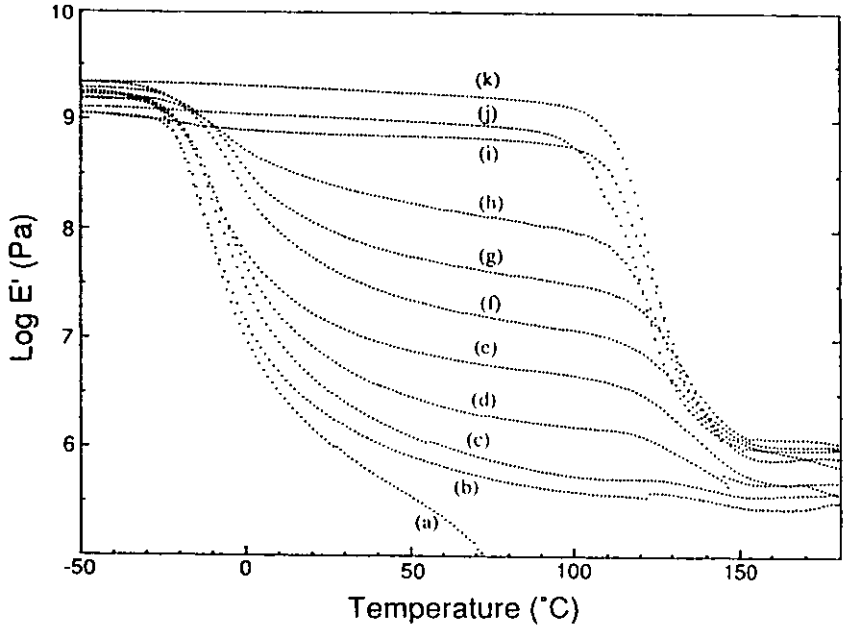

Figure 5.5 Storage moduli versus temperature for the PUR/PS IPN compositions. (a) 100 PUR, (b) 90:10 PUR/PS, (c) 80:20, (d) 70:30, (e) 60:40, (f) 50:50, (g) 40:60, (h) 30:70, (i) 20:80, (j) 10:90 and (k) 100 PS.

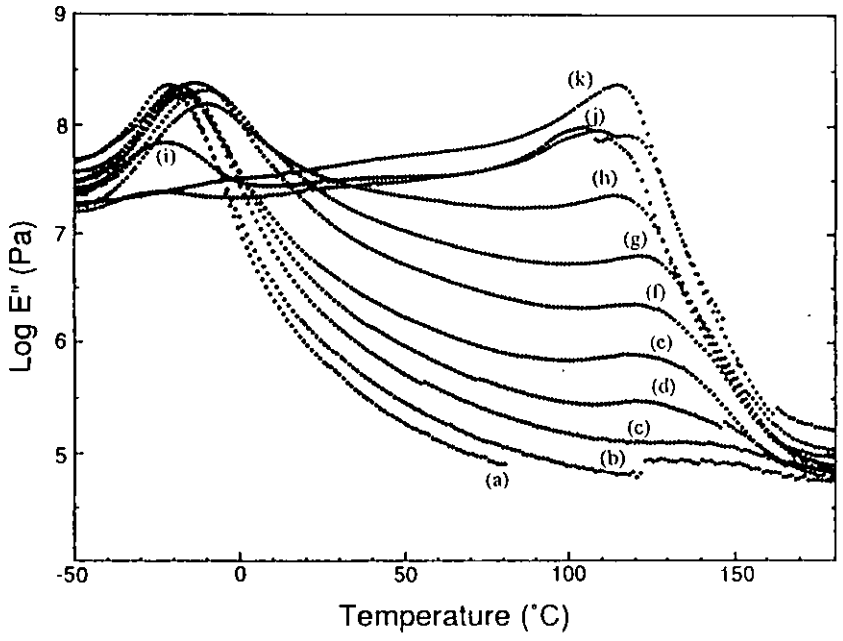

Figure 5.6 Loss moduli versus temperature for the PUR/PS compositions. (a) 100 PUR, (b) 90:10 PUR/PS, (c) 80:20, (d) 70:30, (e) 60:40, (f) 50:50, (g) 40:60, (h) 30:70, (i) 20:80, (j) 10:90 and (k) 100 PS.

The storage moduli reflected the trend of the loss factor values. A pronounced drop in modulus occurred at the PUR and PS transitions. The two-step drop mechanism of the storage moduli indicated[4,185] gross phase separation in the IPNs. With increasing volume fraction of the PS component, the rubbery plateau between the PUR Tg and the PS Tg increased to higher moduli reflecting the change in composition. The 20:80 PUR/PS IPN exhibited a high modulus plateau between the PUR and the PS transition. A similar finding had been made with the comparatively high loss factor peak height (figure 5.3). This phenomenon was likely to be caused by compositional variations across the IPN sheet. However, this could, perhaps, also have indicated a change in the IPN morphology, i.e. continuous phase. The loss modulus versus temperature showed two distinct transitions (figure 5.6). Similar to the results from the loss factor data, the PUR exhibited its Tg at the highest temperature for the 40:60 PUR/PS composition. The PS transition decreased with decreasing PS content. The PUR loss modulus peak was predominant from the 90:10 to the 30:70 compositions inclusive. The change in the dominant peak occurred between the 30:70 and 20:80 PUR/PS composition, again possibly indicating a change of IPN morphology.

From the dynamic mechanical data, the PUR/PS IPNs clearly exhibited gross phase separation over the full composition range. The highest degree of phase mixing seemed to occur at intermediate compositions. This was evidenced by the inward shift of the PUR peak (figure 5.4). The visual appearance of the films also indicated a phase-separated system with only the pure PUR and PS networks being transparent. Some degree of transparency was still present at PUR levels of 80 and 90%. This indicated that the PS domains were close to the wavelength of visible light. Similar results of smaller PS phase domains with increasing PUR content were found[149] studying different PUR/PS compositions by TEM. This was explained[149] by the combined effect of an increased rate of PUR network formation and an increased viscosity of the medium, which are both counteracting phase separation. The opacity observed at the other compositions is characteristic[64] of phase-separated materials and PUR/PS IPNs are known[65] for their immiscibility. This criterion has been used[112] to study the phase separation in PUR/PS IPNs by monitoring their transparency.

Modulated-temperature DSC studies. Conventional DSC did not prove sensitive enough to detect Tgs in the IPNs. However, with this relatively new technique[248,249] both transitions could be detected over most of the IPN composition range. Exceptions were the 90:10 and the 10:90 compositions where no transition could be assigned to the minor component. The M-TDSC traces for the 60:40 and 20:80 PUR/PS IPN compositions are shown in figure 5.7. The Tg values versus IPN composition are shown in figure 5.8.

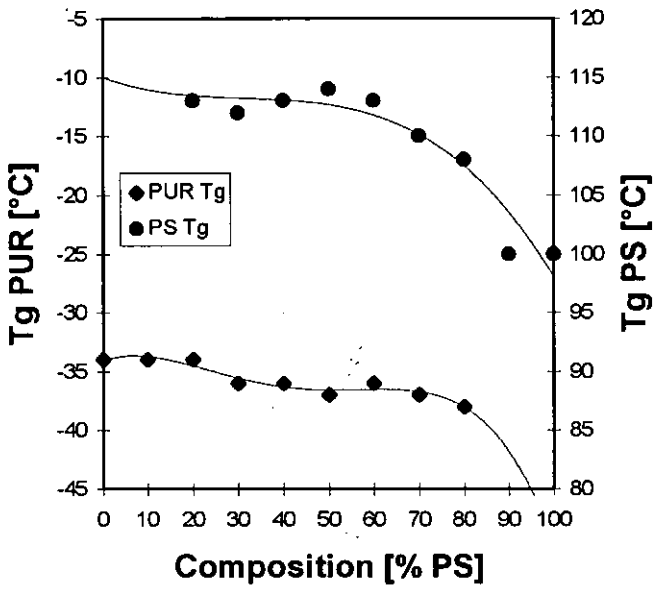

Figure 5.8 M-TDSC Tg data versus PUR/PS IPN composition.

Two transition peaks in the derivative heat capacity versus temperature data were observed. IPN composition was to some extent reflected in the peak height. The Tgs for the homonetworks were -34°C for the PUR and 100°C for the PS. This compared to transition values of -5°C and 128°C obtained from the DMTA measurements (loss factor, 10 Hz). Because of the dynamic nature of the experiment, the latter were higher by 29°C and 28°C, respectively. Tg values from M-TDSC also varied with changing composition. The PUR Tg decreased slightly from -34°C for the PUR homonetwork to -38°C for the transition in the 20:80 PUR/PS. The PS transition obtained from M-TDSC showed trends similar to the Tg values obtained from DMTA. With increasing weight percent of the PS, Tg shifted to lower temperatures. While the PS transition in the 80:20 PUR/PS was at 114°C, Tg for the PS homonetwork was 100°C.

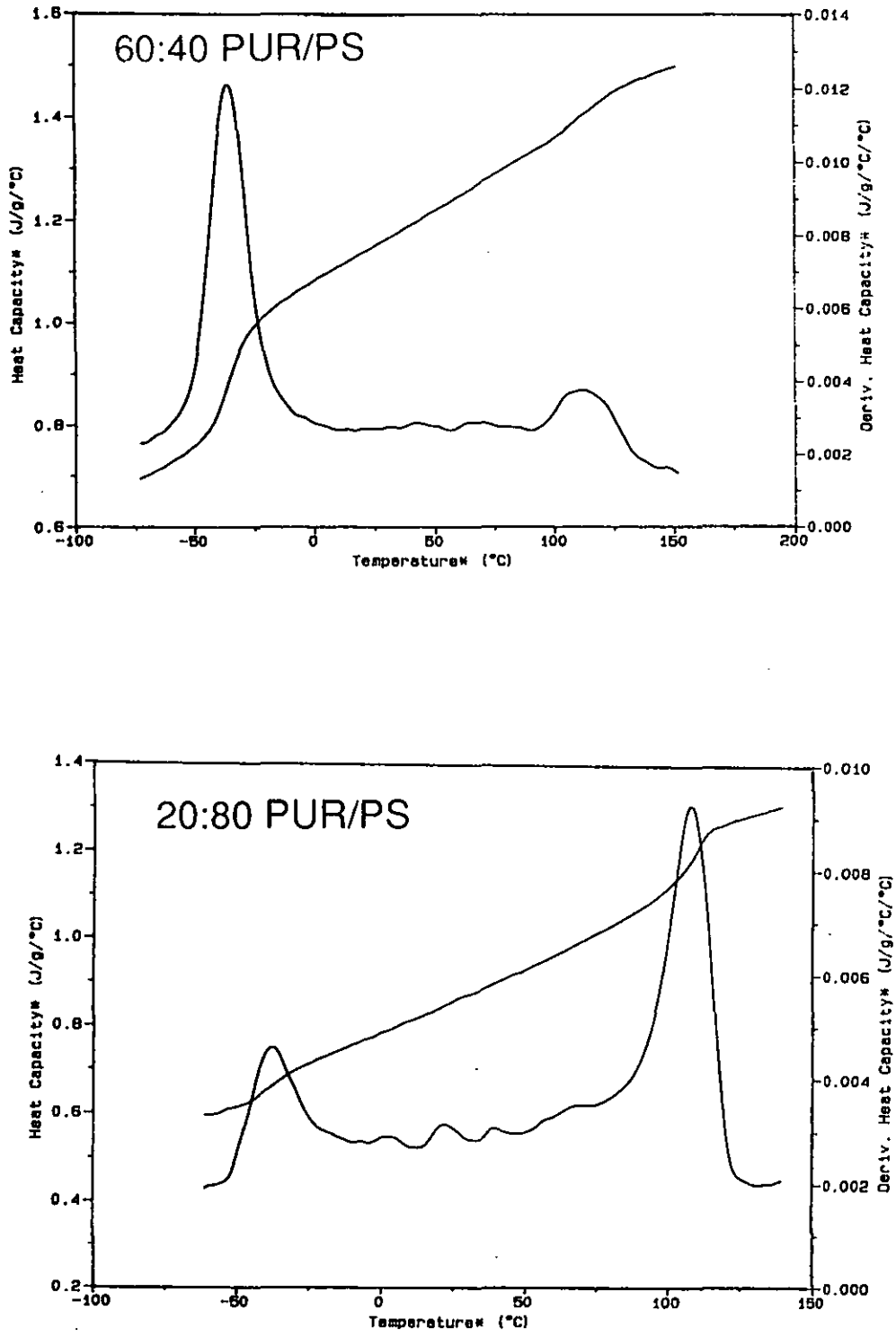

Figure 5.7 M-TDSC traces for the 60:40 and 20:80 PUR/PS IPN compositions.

Stress-strain and hardness measurements. The mechanical properties of the composition series were investigated by tensile testing and Shore A and D hardness measurements. The stress and elongation at break, Young's modulus, the toughness index and values for Shore A and D hardness are given in table 5.2

Table 5.2 Mechanical properties of the PUR/PS IPN as a function of composition.

PUR/PS IPN Composition	Tensile properties				Hardness Shore	
	Stress at break	Strain at break	Young's modulus	Toughness		
[% PS]	[MPa]	[%]	[MPa]	[J]	A	D
0	1.2	210	1.0	0.6	40	25
10	2.4	430	1.1	2.0	43	25
20	4.2	530	1.7	4.0	49	27
30	12	770	4.3	14	59	35
40	13	310	7.2	4.2	75	41
50	10	230	10	2.3	83	52
60	7	83	33	0.6	94	59
70	14	20	83	0.3	96	68
80	36	8	830	0.4	98	95
90	45	7	1000	0.5	99	96
100	47	7	1300	0.4	99	97

As expected, by combining an elastomer with a plastic, an important change in mechanical properties was observed. A plot of the stress and strain at break versus IPN composition is show in figure 5.9. The stress at break showed some scatter, but generally increased with increasing PS weight percent. However, a certain pattern was observed. Stress at break values were very low (below 5 MPa) for the 90:10 and 80:20 PUR/PS IPNs. They rose with increasing PS content up to 13 MPa for the 60:40 PUR/PS IPN. Surprisingly, they fell again to a value of 7 MPa at the 40:60 composition. From the 30:70 composition on stress at break values increased dramatically with a further increase of PS weight percent. This trend can, perhaps, be explained by looking at the phase continuity of the IPNs. The continuous phase is known[4] to influence greatly the mechanical properties of IPNs. From the DMTA data it was believed that phase inversion took place between the 60:40 and 20:80 PUR/PS composition. The increasing stress at break up to the 60:40 IPN could be

explained by the reinforcing effect of the PUR by the PS. Increasing further the PS content might have lead to bigger PS domains, and, as a consequence, a decreased phase continuity of the PUR network. This weaker PUR network caused by a decrease in PUR content and phase continuity lead to lower stress at break values. It was, perhaps, only at the 30:70 PUR/PS that the PS phases exhibited some degree of phase continuity, which could account for the again increasing stress at break values. At the 20:80 PUR/PS IPN, PS was likely to have exhibited the continuous phase. This manifested itself in a steep increase in stress at break from 14 MPa for the 30:70 to 36 MPa for the 20:80 PUR/PS IPN composition. Further evidence for above assumptions were obtained from TEM and SEM studies which are reported in a subsequent section.

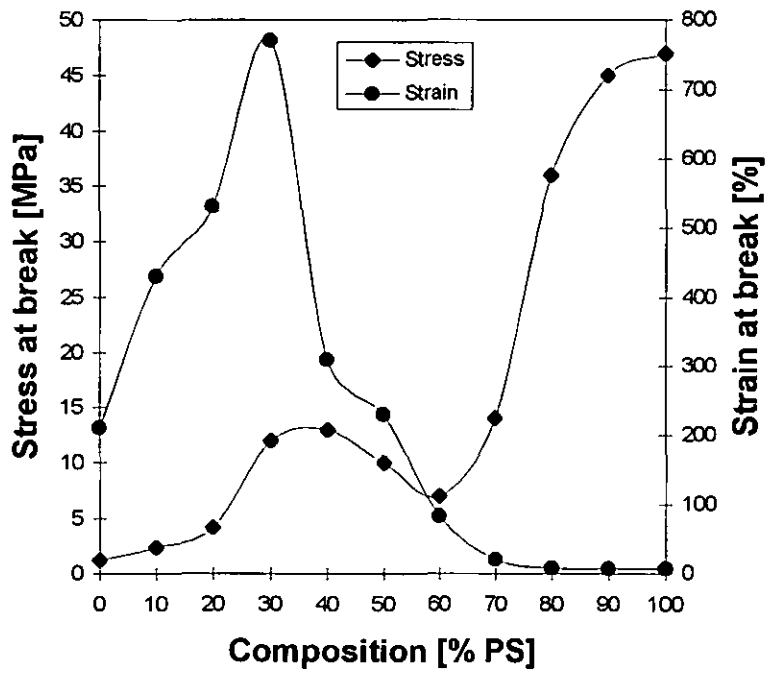

Figure 5.9 Stress and strain at break versus PUR/PS IPN compositions.

The strain at break versus IPN composition exhibited a different trend (figure 5.9). The strain at break values went through a maximum of 770% at the 70:30 PUR/PS IPN composition. Clearly inferior values were obtained for IPNs with both higher PUR contents and even more pronounced with lower PUR contents. The increase in strain at break from 100 PUR to the 70:30 PUR/PS IPN compositions could be explained by a decrease in the tightness of the PUR network because of the PS

domains. The PUR chains were able to align and the more loose network only broke at higher elongations. The decrease in strain at break from the 60:40 PUR/PS IPN compared to the 100 PS was a combination of two factors. From the 60:40 to the 30:70 PUR/PS compositions, the PUR content decreased and, very probably, so did the phase continuity of the PUR. Fewer PUR chains were able to slide along each other causing an early failure. The extremely low values for the strain at break for compositions where PS represented the continuous phase (from 20:80 to 10:90 PUR/PS) were explained by the glassy, and, thus, brittle nature of PS at room temperature.

The toughness index is a function of the stress and the strain at break. Because of the high strain at break value, the toughness index also exhibited a maximum at the 70:30 composition. Young's modulus values followed a trend similar to the stress at break. The modulus increased with increasing PS weight percent (table 5.2). A sharp increase from 83 MPa to 830 MPa took place between the 30:70 and 20:80 PUR/PS IPN compositions. A detailed description of the modulus-composition behaviour is given in a subsequent section.

A plot of Shore A and D values against IPN composition is shown in figure 5.10.

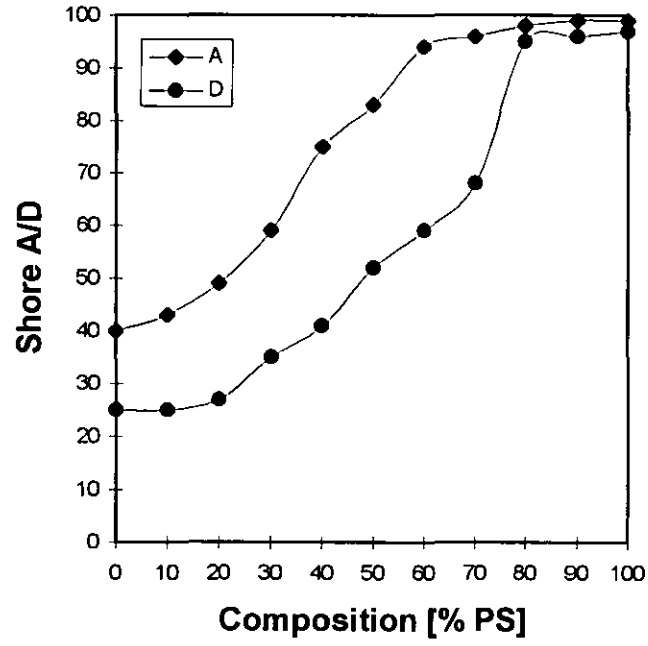

Figure 5.10 Shore A and D hardness versus PUR/PS IPN composition.

Shore A hardness values exhibited a sigmoidal curve shape. A slightly higher than expected increase in Shore A hardness occurred about the 70:30 to 60:40 PUR/PS compositions. This might have indicated a change in the continuous phase. However, it has to be considered that the useful working ranges for the Shore hardness measurements are[292] between 10 and 90 for Shore A (between 30 and 90 for Shore D). Thus, reliable results for Shore A were only obtained for compositions up to a PS content of 50% and compositions with higher PS contents could not be evaluated by Shore A. For Shore D hardness values, a linear pattern was found for an increase in PS content from the 70:30 to the 30:70 PUR/PS composition. Again, the data obtained outside the optimum operating range are not very reliable. However, a very significant increase in hardness was observed between the 30:70 (Shore D 68) and the 20:80 (Shore D 95) PUR/PS compositions. A behaviour similar to the Young's modulus was not surprising since hardness is directly related[250] to modulus and strength. Thus, from Shore A measurements a slight increase in hardness about the 70:30 PUR/PS composition was in evidence whereas from Shore D a very important increase was observed between the 30:70 and 20:80 PUR/PS IPN compositions.

Modulus-composition Studies. Modulus-composition studies[58,73,80,83,110,127,293,294] have been conducted to investigate phase continuity and phase inversion[98] in polymer blends. This is done by relating[295] the shear or tensile moduli to theoretical modulus-composition models. Several theories have been developed[124-126,296] to predict the elastic properties of a multiphase system to its composition and morphology. These have been reviewed by Nielsen[297,298,299], Dickie[300,301] and Hourston[267]. Most theories assume perfect adhesion between the phases and the sample being macroscopically homogeneous and isotropic. Kerner[296] derived a theory for a matrix with spherical inclusions. The upper and lower bounds of the modulus of this two-phase polymer material are given by the equation 5.1.

$$\frac{G}{G_1} = \frac{(1-\phi_2)G_1 + (\alpha+\phi_2)G_2}{(1+\alpha\phi_2)G_1 + \alpha(1-\phi_2)G_2} \qquad (5.1)$$

Here, subscripts 1 and 2 refer to the matrix and the inclusions, respectively. G is the shear modulus, ϕ is the volume fraction and α is a function of the matrix Poisson

ratio, ν_1, $\alpha = 2(4-5\nu_1)/(7-5\nu_1)$. A model which predicts phase inversion at mid-range compositions in two-phase polymer systems was developed by Budiansky[126].

$$\frac{\phi_1}{1+\varepsilon(\frac{G_1}{G}-1)} + \frac{\phi_2}{1+\varepsilon(\frac{G_2}{G}-1)} = 1 \qquad (5.2)$$

Again, ϕ is the volume fraction, $\varepsilon = 2(4-5\nu)/15(1-\nu)$, ν is the Poisson's ratio of the composite, G is the shear modulus and subscripts 1 and 2 represent the component polymers. A general mixing equation which often successfully predicts certain properties of composites with two continuous phases has been presented by Nielsen[299].

$$P^n = \phi_1 P_1^n + \phi_2 P_2^n, \qquad -1 < n < 1 \qquad (5.3)$$

P is a property such as elastic modulus or thermal conductivity. n is some function of the morphology of the system. For n = 1, the ordinary rule of mixtures results, whereas n = -1 describes the inverse rule of mixtures. The logarithmic rule of mixtures[185] results for n = 0. The Davies[124,125] equation, which Hourston and Zia[267] class as a special solution to the Nielsen equation[299], is designed for systems in which both components are present as continuous phases. It is given by equation 5.4, where G and ϕ have been previously defined.

$$G^{1/5} = \phi_1 G_1^{1/5} + \phi_2 G_2^{1/5} \qquad (5.4)$$

In general, conversion from the shear to the tensile modulus, E, can be done using the equation $E = 2G(1+\nu)$. However, this was not done since the error that is introduced by using E in the expressions for G is small[294] when compared to the predictions of the three models and in the order of the error in the measurement of E. Poisson's ratio for the homopolymers were assumed to be 0.5 for the polyurethane and 0.35 for the PS[80], and the Poisson's ratios for the compositions were calculated using the weighted average[80,294] of the Poisson's ratio of the two components.

So far, the fit of experimental data to modulus-composition theories has been contradictory. Hourston and Zia[128] found the Davies equation to fit their data well for simultaneous semi-2 polyurethane/polymethyl acrylate IPNs. For semi-2

PUR/PMA IPNs[267], a close fit by the Davies equation was obtained by changing the exponent to 1/10. A PUR/polyvinylacetate (PVAc) semi-1 IPN series[267] fitted the Davies equation well, when the exponent was altered to 1/6. They reasoned that this was an indication for better miscibility in the semi-1 PUR/PVAc system than in the semi-2 PUR/PMA IPN. Good fits with the Davies equation were also obtained by Allen et al.[293] for PUR/PMMA and PUR/polyacrylonitrile IPNs. Akay and Rollins[58] compared the modulus versus composition plots of simultaneous and sequential PUR/PMMA IPNs. They found the elastic modulus-composition plots to comply with Budiansky's phase inversion model for simultaneous IPNs and with a dual-phase continuity model (Davies equation) for sequential IPNs. The dynamic storage moduli, however, behaved according to the Davies equation. For other simultaneous full and semi PUR/PMMA IPNs, Klempner et al.[80] found a fairly good fit with the Budiansky equation. The fit was better for the Young's modulus versus composition data than for the respective shear modulus versus composition data, a fact that was attributed to experimental errors. In most of these studies, however, the conclusions drawn were based on three and four composition points[100], which makes it difficult to make predictions over the whole composition range. Therefore, in the present study, the entire composition range was prepared in 10 weight percent increments.

Figure 5.11 shows the Young's moduli versus IPN composition together with four modulus-composition predictions. The experimental data showed some scatter and did not fit any of the predictions. However, some similarity with the Budiansky model which predicts phase inversion at mid-range compositions existed. The experimental data suggested that phase inversion took place between the 30:70 and the 20:80 PUR/PS IPN compositions. In addition to log E, a linear plot of E versus composition is shown to illustrate the pronounced increase in E between the 30:70 and the 20:80 composition. In addition to Young's modulus, the dynamic storage moduli E' (10 Hz) of the IPNs and homonetworks were also plotted against the composition (figure 5.12). A slightly different pattern was observed at different temperatures. Again, the experimental data points for the storage modulus did not fit exactly any of the theoretical models investigated. However, clearly the shape of the Budiansky equation, involving phase inversion at the intermediate composition, gives the best approximation. The storage modulus taken at 0°C seemed to have the phase inversion between the 70:30 and the 60:40 PUR/PS IPN compositions.

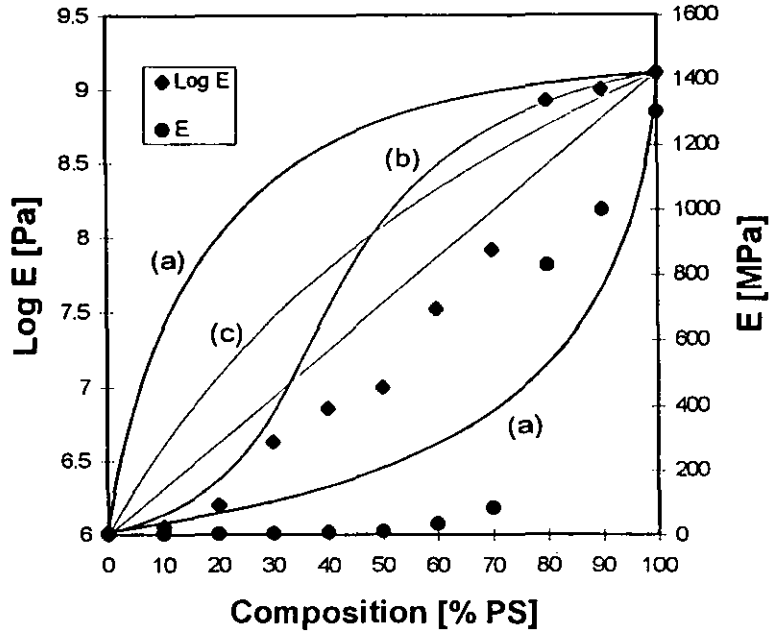

Figure 5.11 Log Young's modulus E and linear E versus composition and modulus-composition curves. (a) Kerner model, (b) Budiansky and (c) Davies.

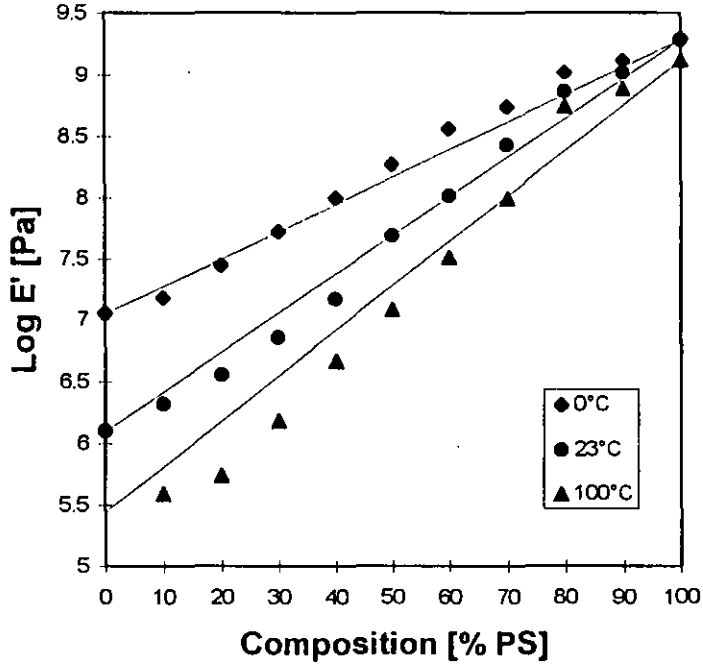

Figure 5.12 Dynamic storage moduli versus IPN composition taken at 0°C, 23°C and 100°C.

From the moduli taken at 23°C, it appeared that phase inversion occurred at the 40:60 PUR/PS composition. However, taking the moduli taken at 100°C resulted in the phase inversion occurring at higher PS contents, namely, between the 30:70 and 20:80 compositions. Thus, it was noted that the temperature at which the moduli were taken had an important bearing on the shape of the modulus-composition plot. With the moduli taken at increasingly higher temperatures, the location where the logarithmic rule of mixing was crossed moved to higher PS contents. The intermediate temperature between the PUR and the PS transition (67°C) might be most appropriate to conduct modulus-composition studies. 67°C is roughly intermediate between 23°C (phase inversion at 40:60 PUR/PS) and 100°C (phase inversion at 20:80 PUR/PS). Consequently, phase inversion at 67°C might have taken place at the 30:70 PUR/PS IPN composition. The influence of the temperature where the modulus values are taken will be further discussed in section 6.1.

Morphology via TEM and SEM. The IPN morphology of the composition study was further investigated via TEM and SEM in order to corroborate the findings from DMTA and mechanical testing. At this point it should be emphasised that TEM only offers a two-dimensional picture of the IPN morphology. Thus, domains that appear spherical in shape might also be cylindrical or even worm-like inter-connected structures[94]. The latter is even more likely if many domains exhibit an ellipsoidal shape. Thus, conclusions about phase continuity cannot be made with certainty from TEM results alone. Better indications about phase continuity can be obtained[94] via DMTA and SEM. The fracture surfaces of the failed tensile test specimens were investigated by SEM. Tensile testing was conducted at room temperature, thus, above the glass transition of the PUR network (-34°C) and below that of the PS network (100°C). Because of the different failure behaviour of the two materials, separate phases or inhomogeneities in the IPN were expected to become readily visible. The micrograph of the pure PUR network exhibited a surprisingly clean fracture pattern (figure 5.13(a)). The surface structure that appeared on this micrograph was believed to be an artefact resulting from the sample preparation rather than an indication of hard and soft segment segregation within the PUR. The artefact resulted from melting of the low Tg PUR because of overheating during the gold sputtering process.

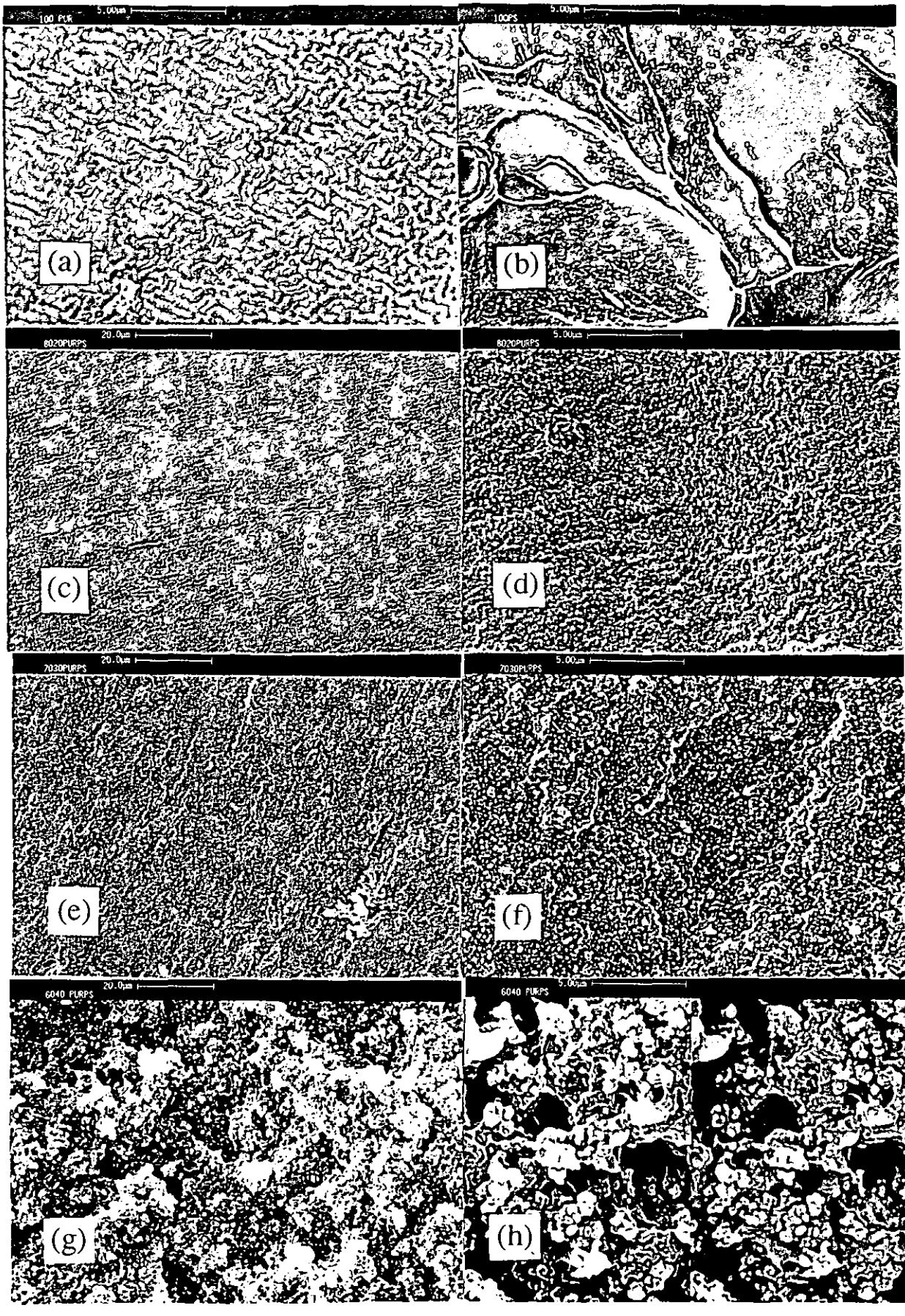

Figure 5.13 SEM micrographs for different PUR/PS compositions. (a) 100 PUR, (b) 100 PS, (c) & (d) 80:20 PUR/PS, (e)&(f) 70:30 and (g)&(h) 60:40.

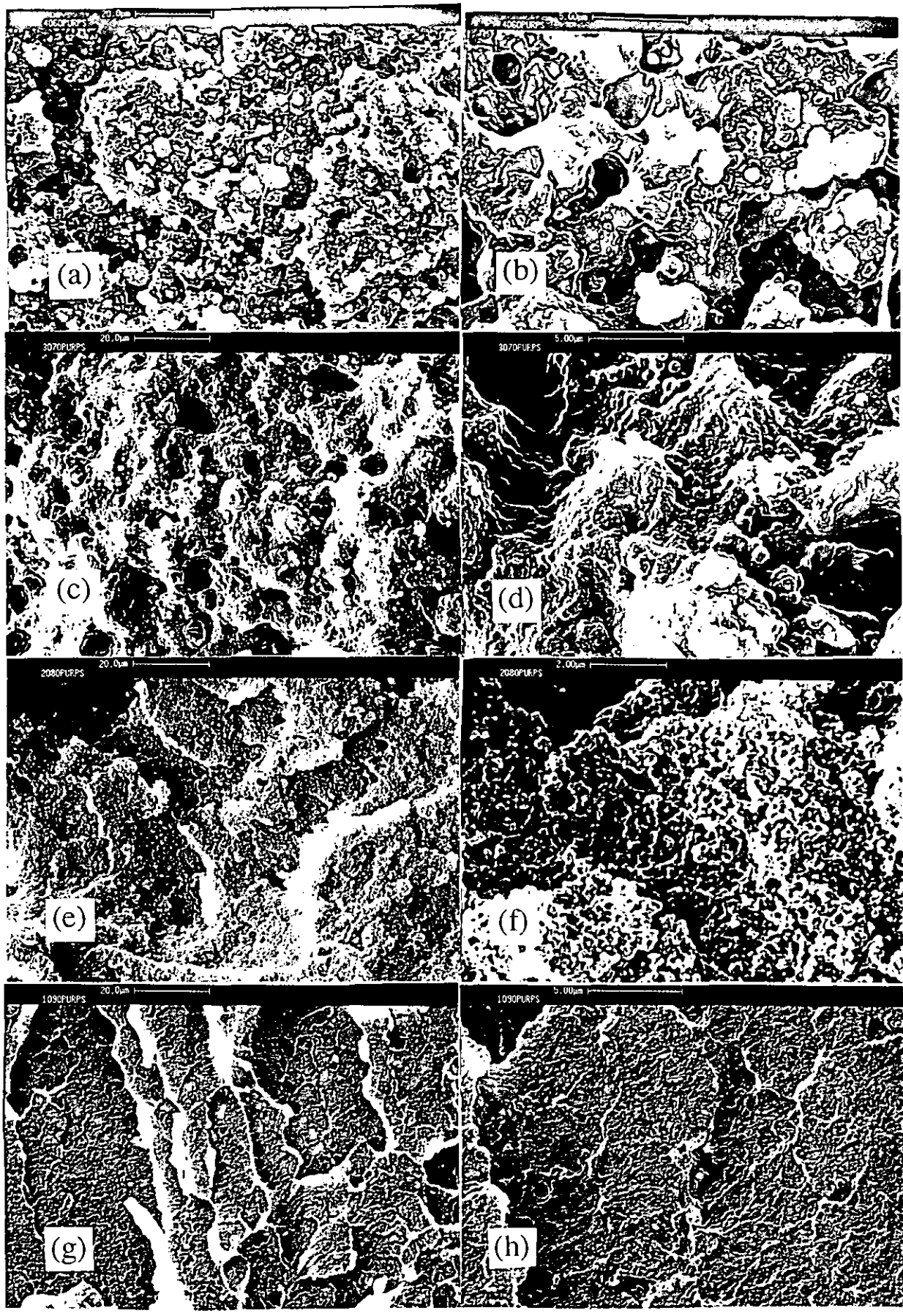

Figure 5.14 SEM micrographs for different PUR/PS compositions. (a)&(b) 40:60 PUR/PS, (c)&(d) 30:70, (e)&(f) 20:80 and (g)&(h) 10:90.

The scanning electron micrograph of the pure PS is shown in figure 5.13(b). A brittle failure was observed with little surface structure being present. With increasing PS weight fraction, a number of interesting findings with respect to phase continuity were made. The SEM micrograph of the 80:20 PUR/PS IPN showed a fairly homogeneously fractured PUR at a low magnification of 5 k (figure 5.13(c)). At a magnification of 20 k, a presumably PUR matrix with small PS domains of 50-200 nm was observed (figure 5.13(d)). A slight hint of the melting artefact was still noted at that IPN composition. However, it disappeared at higher PS contents because of the higher PS softening temperature. At the 70:30 composition (figure 5.13(e)), a rougher surface structure was noted at a magnification of 5 k. At 20 k (figure 5.13(f)), it could be observed that the PS domains also increased in size to 100 - 300 nm. The SEM micrographs (figure 5.13(g) and (h)) of the 60:40 PUR/PS IPN composition showed the same trend, yet much more pronounced. The fracture surface exhibited a highly irregular structure at a magnification of 5 k and the domain size increased even further to 200 - 800 nm. In addition to these domains, cylinder-shaped cavities in the matrix were observed (figure 13(h)). The presence of important cavities and comparatively large domain sizes indicated that phase mixing and cohesion between the PUR and PS phases were poor. This corroborated the findings obtained from DMTA of a grossly phase separated IPN morphology. At this 60:40 composition, the PS network might have exhibited a limited degree of phase continuity. However, it was believed that the PUR network still constituted the matrix, with the dispersed PS domains considerably increasing in size. The cavities observed throughout the 60:40 to the 40:60 PUR/PS IPN compositions were, most likely, PS-rich cylindrical domains. Up to the 40:60 PUR/PS IPN, the PUR network was still believed to have constituted the more continuous phase. So far in this SEM study secondary electrons emitted form the material surface were used as the imaging signal. This technique yields[245] topographic images of the sample surface. It was attempted to obtain some compositional information of the sample by using the back-scattered electron mode. Back-scattered electrons are primary beam electrons that have been elastically scattered by the nuclei in the sample and escape from the surface. In order to enhance the contrast of mass of the nuclei, staining with osmium tetroxide was conducted. With this information, it was hoped to elucidate further the question of which component represented the matrix and which component was present in discrete

domains or cylinders. Figure 5.13(h) directly compares the secondary electron (left side) to the back-scattered mode (right side). It was hoped that the osmium tetroxide-stained PUR phase would appear lighter because of a higher percentage of back-scattered electrons. However, it was observed that the surface characteristics had a much stronger effect than the difference in nuclear mass. Since no additional information was gained using the back-scattering mode, it was solely continued with the secondary electron imaging technique.

A maximum of structure irregularities and cylindrical cavities were observed for the 40:60 composition (figure 5.14(a)). Also, the domain size was the largest with diameters of 600 nm to 2μ (figure 5.14(b)). At the 30:70 PUR/PS composition (figure 5.14(c)), an important change in IPN morphology was observed from the fracture surface. Clearly fewer and shallower cavities were observed. The fracture surface though still appeared very rough (figure 5.14(d)). This might have been the beginning of phase inversion to a predominantly PS-matrix. At the 20:80 PUR/PS IPN composition (figure 5.14(e)), the cylindrical cavities had completely disappeared. At a magnification of 5 k, the surface structure showed similarities to the 100 PS fracture surface. At 50 k though, a fine morphology of small interconnected cylinders of 100-150 nm in diameter was noted (figure 5.14(f)). The 10:90 composition exhibited an even finer morphology (figure 5.14(g)). The inter-connected cylinders disappeared and numerous very small domains of about 50-100 nm diameter appeared. Thus, from the SEM micrographs, a two-phase morphology with gross phase separation was observed. Particularly when considering the lower magnifications, three different structures were noted. Up to the 70:30 PUR/PS IPN composition, a fairly regular fracture surface was obtained, with domain size increasing with higher PS content. The 60:40 to 30:70 compositions had a highly irregular fracture surface which showed the presence of large cylindrical cavities. The latter might have indicated some degree of phase continuity of both phases. The 20:80 and 10:90 compositions exhibited again a smoother fracture surface having some resemblance with that of 100 PS. Thus, the mechanical data were corroborated to a high degree by the SEM evidence.

In order to complement the SEM studies, TEM micrographs were taken to elucidate further phase domain size and shape (figures 5.15 and 5.16). Even though an indication of phase domain sizes could be obtained by the SEM studies, these

estimations were limited because of the difficulty in determining the exact borders of phase domains and because of not high enough magnifications. The TEM sample preparation, including the staining technique and the instrumentation, were reported in section 3.4.2. Osmium tetroxide stains preferentially[4] the PUR. Thus, the darker regions in the TEM micrographs consist of PUR or have[65] a high PUR content. A micrograph of the osmium tetroxide-stained pure PUR was taken. However, no microstructure as a result of possible hard and soft segment segregation was observed. TEM studies[204] of phase segregated MDI-based PURs revealed microphase separation with hard segment domain sizes in the order of 10 - 20 nm. The TEM micrograph of the 80:20 PUR/PS is shown in figure 5.15(a). Many very small PS phase domains of 10 - 100 nm in diameter were noted. The fact that they appeared darker than the matrix is a consequence of a surrounding PUR shell of high purity.

In a recent study, He and co-workers[65] investigated a 30:70 PUR/PS IPN by SEM. Selective degradation of the PUR by treatment with an ethanolic sodium hydroxide solution revealed the existence of a shell surrounding the PS domains. The shell contained[65] rather more PUR than the matrix since no obvious degradation could be observed for the latter. A model explaining the development of the PUR/PS morphology was given and a concentration curve going from the noduli towards the matrix was also presented[65]. If the same phenomenon of a high purity PUR shell surrounding PS domains were to have occurred in the present study, it might have been detectable by TEM. A PUR shell of high purity surrounding PS domains should have been stained to a greater extent by osmium tetroxide than the matrix, and, therefore, appear darker. That was precisely what was observed in most TEM micrographs in figures 5.15 and 5.16. The latter confirmed the theory of He and co-workers[65] and explained the phenomenon of dark PS domains in micrographs of the present study. It might also have indicated that the IPN matrix did, perhaps, not consist of pure PUR, but that it probably had some PS dissolved in it. Figures 5.15(b) and (c) show micrographs of the 70:30 PUR/PS IPN. The phase domain sizes clearly increased to values between 20 - 200 nm. While the phase domain sizes in the 80:20 IPN were fairly uniform (figure 5.15 (a)), also some larger phase domains of up to 500 nm were found in the 70:30 PUR/PS IPN (figure 5.15 (b)).

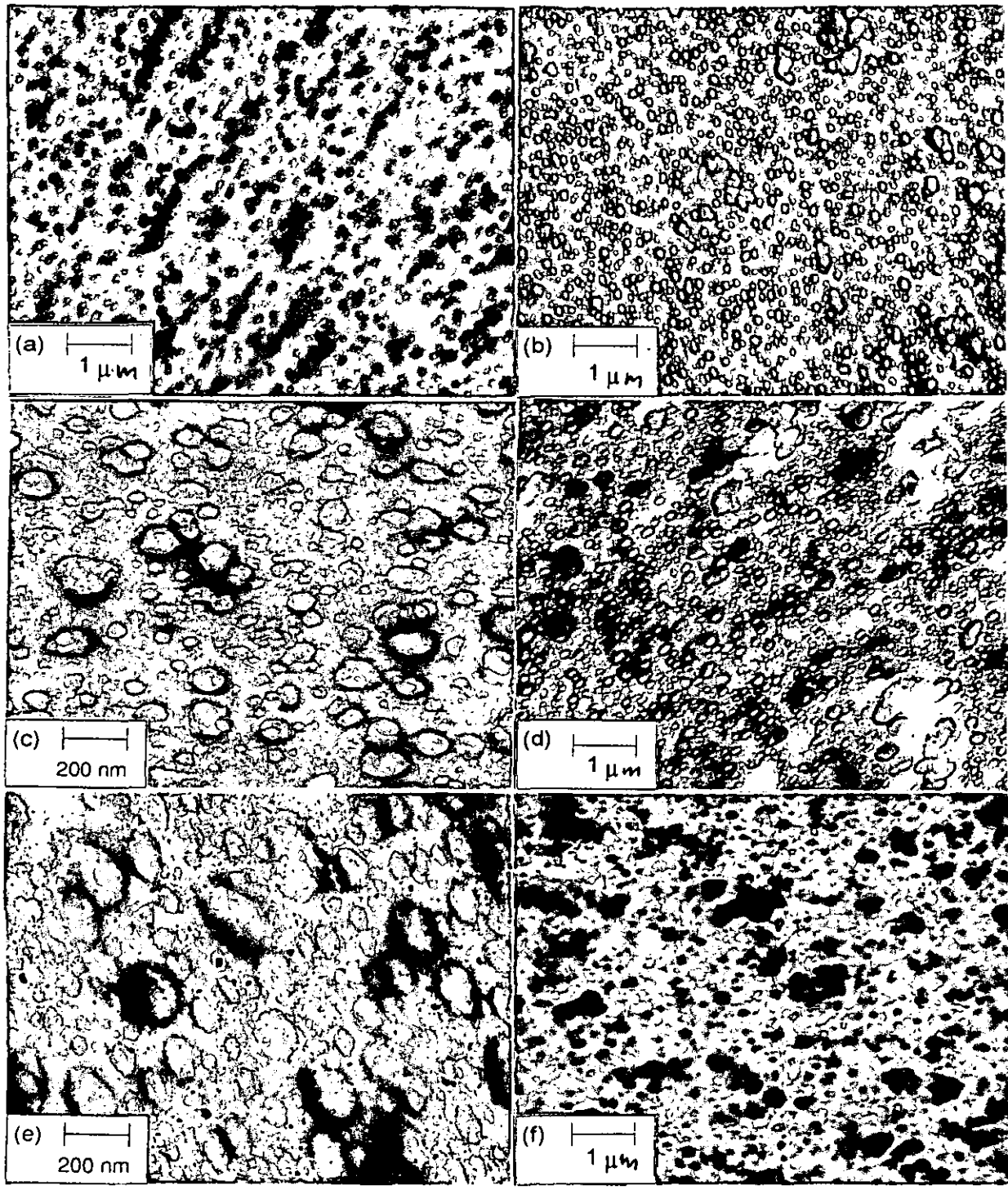

Figure 5.15 TEM micrographs for different PUR/PS IPN compositions. (a) 80:20 PUR/PS, (b) & (c) 70:30, (d) & (e) 60:40 and (f) 60:40, unstained.

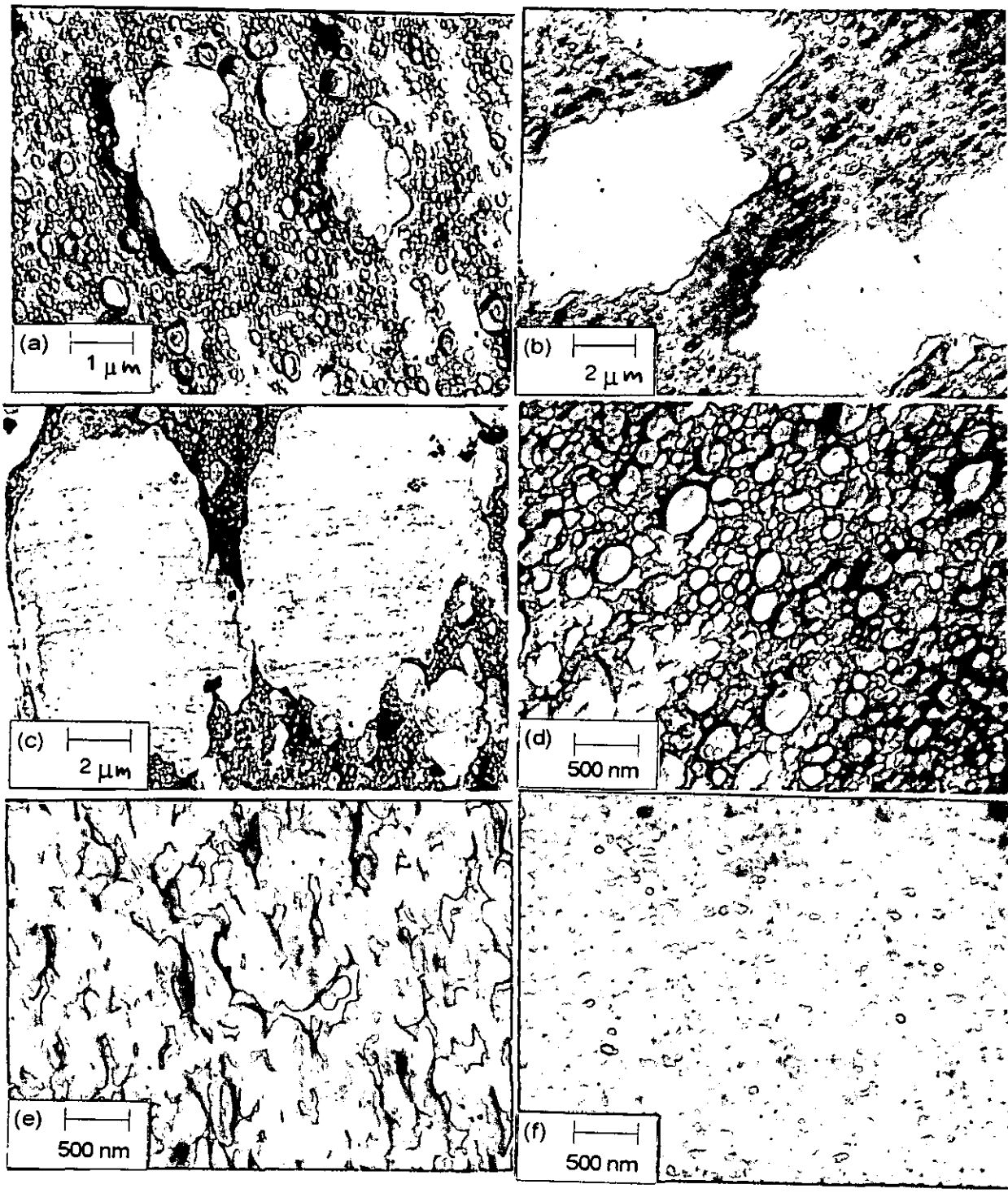

Figure 5.16 TEM micrographs of different PUR/PS compositions. (a) 50:50 PUR/PS, (b) 40:60, (c) & (d) 30:70 PUR/PS, (e) 20:80 and (f) 10:90.

A further PS phase domain size increase was observed for the 60:40 PUR/PS IPN. Figures 5.15(d) and (e) show that a distribution of PS phase domain sizes was obtained. Numerous smaller domains of about 50 - 200 nm and few bigger domains in the order 400 - 700 nm were observed. Many domains had an ellipsoidal shape which could have been an indication of cylindrical domains. The dark-stained PUR was believed to have constituted the continuous phase at this composition since no pronounced change in morphology was observed. Thus, the white PS domains were dispersed in the PUR matrix. Again, dark-stained shells surrounding PS phase domains were evident (figure 5.15(e)). In addition, numerous small black particles were observed in this micrograph. These were staining artefacts, resulting from osmium tetroxide or osmium dioxide crystals that had not been completely washed away after the staining process. Figure 5.15(f) depicts the same 60:40 PUR/PS IPN composition, however, unstained. A reasonably good electron contrast was present in the unstained IPN. In the unstained IPN, the PS domains appeared darker than the PUR matrix, indicating that the electron density of the PS was higher than that of the PUR. With increasing PS content, larger PS phase domains appeared. Also, within the lighter PUR matrix variations were noted similar to those in some stained electron mircographs. These might have indicated variations of the PS content that was dissolved in the predominantly PUR matrix. These darker matrix regions were more frequently observed around agglomerates of PS domains and appeared to be to some extent interconnected. This might be an indication that as the PS polymerised, first spheres and then cylindrical PS-rich domains formed. This could have indicated a change from a nucleation and growth to a spinodal decomposition phase separation mechanism. A similar phenomenon was noted[57] for a polybutadiene/PS IPN. However, it has to be emphasised that the variations in matrix darkness could have also been caused by slight variations in sample film thickness. At the 50:50 PUR/PS IPN composition a distribution of small (100 - 200 nm) and larger (500 - 700 nm) PS domains was observed (figure 5.16(a)). In addition to these, numerous PS domains of 1 - 3 μ also appeared. This trend was continued with the 40:60 composition (figure 5.15(b)). While a distribution of small PS domains was still observed, the big domains were in the order of 2 - 6 μ. At the 30:70 composition, even larger PS domains were noted (figure 5.16(c)). It was not clear any more which phase represented the continuous phase. Even though the volume fraction of the PS domains appeared to be

greater than the area of the PUR enriched phases, the latter still appeared more continuous. Also, phases with high PUR content and dispersed PS domains were observed. Figure 5.15(d) shows that also very small PS phase domains of 50 - 400 nm were still present. A dramatic change in IPN morphology was observed at the 20:80 PUR/PS IPN composition. This composition showed predominant interconnected PS phases (figure 5.16(e)). In addition, inbetween the light PS phase, dark worm-like domains were observed. These were believed to consist of a PUR/PS blend. Thus, at the 20:80 composition phase inversion had occurred. The morphology of the 20:80 composition observed by TEM had a very strong resemblance to the SEM micrographs in figure 5.14(f). The 10:90 composition showed a hardly resolvable morphology with very small dark PUR domains of 30-80 nm in diameter.

In conclusion, TEM micrographs showed that in addition to large PS phase domains, also small domain sizes of about 10 - 20 nm were obtained because of the enforced mixing through crosslinking. However, the two well-separated loss factor peaks in the dynamic mechanical spectrum and the opacity of the IPN sheet indicated gross phase separation. Thus, in addition to phase domain size, emphasis has to be placed on phase domain shape and purity of the phase domains in order be able to make predictions about IPN miscibility from transmission electron micrographs. Well-defined phase boundaries were a better indication for an immiscible IPN than was phase domain size. Phase inversion occurred between the 30:70 and 20:80 PUR/PS IPN compositions.

Thermogravimetric analysis (TGA). TGA can be employed[291] to assess the thermal stability and decomposition temperature and to study the decomposition mechanism and products of polymers. For the latter, combination with other analytical techniques such as infra-red spectroscopy and gas chromatography is needed[302].

In a previous TGA study on IPNs, Kim, Klempner and Frisch[81] found improved thermal properties for a PUR/PMMA IPN. They concluded that the depolymerising MMA acted as a radical scavenger and, thus, improved the thermal stability of the PUR. The same authors[127] reported a higher weight retention of the PUR/PS IPNs above 400°C compared to the respective homopolymers. Kim and Kim[149] also found an enhancement of thermal stability in PUR/PS IPNs. This enhancement was more pronounced in IPNs that had been synthesised in the presence of a common solvent, a

fact that they attributed to a higher degree of interpenetration in these IPNs. TGA studies of selected PUR/PS IPN compositions were conducted. The percent weight loss versus temperature is shown in figure 5.17.

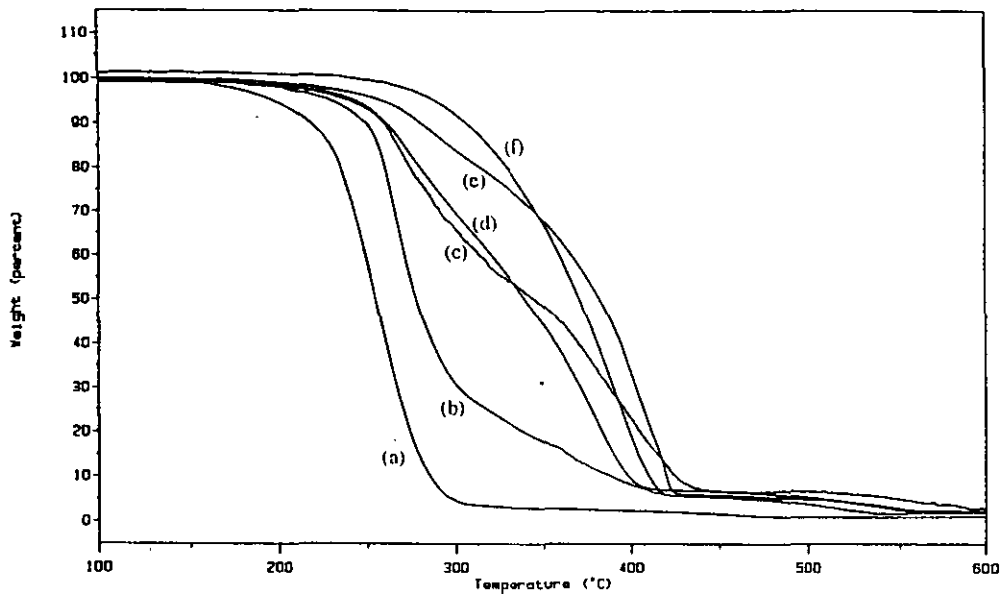

Figure 5.17 Percent weight loss versus temperature for PUR/PS IPN compositions. (a) 100 PUR, (b) 80:20 PUR/PS, (c) 60:40, (d) 40:60 (e) 20:80 and (f) 100 PS.

While the previous studies were conducted in a nitrogen atmosphere, in the present study an air atmosphere was used in order to simulate better environmental conditions. The PUR was found to have the poorest thermal stability (figure 5.17(a)). Considerable weight loss started to occur at 230°C and at 300°C less than 5% of the initial weight remained. The three main decomposition reactions for polyurethanes are[206] the dissociation into the isocyanate and the alcohol, the formation of a primary amine, CO_2 and an olefin or the formation of a secondary amine and carbon dioxide (section 2.3.2). While the dissociation into the isocyanate and alcohol can occur[203] at temperatures as low as 140°C, it did not affect the TGA trace since no volatile components escaped. The latter two reactions are known[206] to occur above 200°C which was confirmed in this study by the major weight loss at 230°C. The 80:20 PUR/PS IPN composition exhibited a better thermal stability (figure 5.17(b)). Major weight loss started to occur only at 260°C. Also a two-stage drop in weight was

observed. A very steep weight loss down to 30% over 30°C was followed by a more gradual degradation down to 5% over 110°C. This corresponded to some extent to the weight percentages of PUR and PS present in the IPN. The PS network had a much better thermal stability and significant weight loss started to occur only at temperatures above 300°C (figure 5.17(f)). The weight loss proceeded in an essentially one-step drop down to 3% weight retention. Both the 60:40 and 40:60 compositions had a similar thermal properties profile (figures 5.17(c) and (d)). The two-step weight loss started at 270°C. The 20:80 composition showed a surprising phenomenon (figure 5.17(e)). While a weight loss of the first 25% occurred at temperatures lower than the PS decomposition, the remaining 75% were lost at temperatures higher than for the 100 PS network. This was similar to the findings made by Kim, Klempner and Frisch[127] who observed a higher weight retention above 400°C for PUR/PS IPNs. Thus, the TGA analyses in an air atmosphere showed that compared to pure PUR the IPNs showed some improvement in the thermal properties. However, no or only a very limited synergism of the thermal properties of the IPNs was observed. Over most of the composition, the curves exhibited mere averages of the constituent PUR and PS homonetworks.

Selection of the 60:40 PUR/PS IPN composition for further study. The 60:40 PUR/PS IPN composition was the obvious choice for the continuation of this study. Most importantly, a material with a pronounced low Tg transition had to be chosen since it was one of the aims of this study to develop damping materials covering a wide temperature range, including room temperature. Also, at this composition, both the PUR and the PS loss factor peaks were clearly discernible and well developed (figures 5.18 and 5.19). This is one prerequisite for miscibility studies. Since for such a study the shift of the loss factor peak location of the components and the loss factor peak height of the inter-transition zone serve as miscibility indicators. Furthermore, a very good reproducibility of this composition was observed. Even though reproducible results were obtained over the whole composition range, a slight variation of the composition within the sheets was observed at higher polystyrene contents. A more practical aspect of this choice was that due to the predominant polyurethane component and its elastomeric nature good demoulding was possible without putting too much strain on the film.

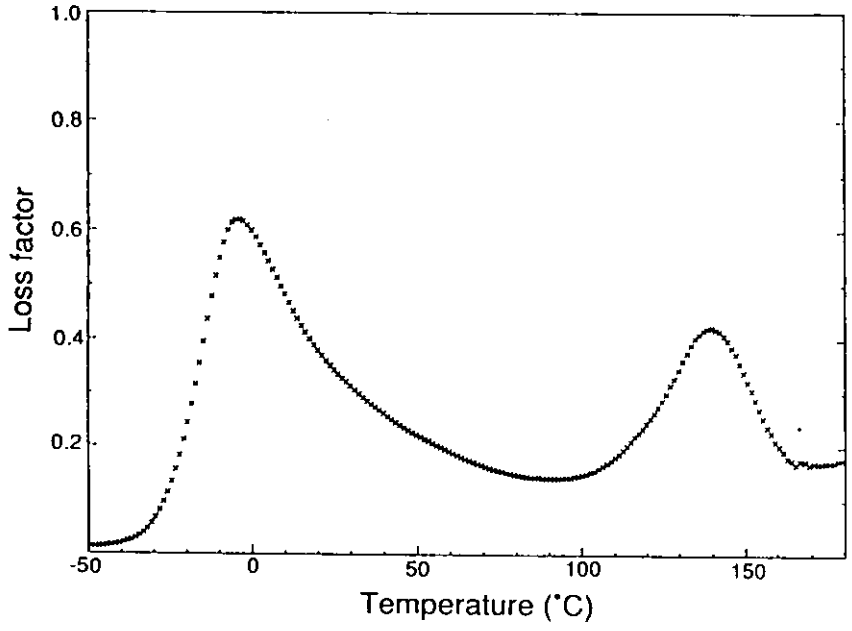

Figure 5.18 Loss factor versus temperature data for the 60:40 PUR/PS IPN.

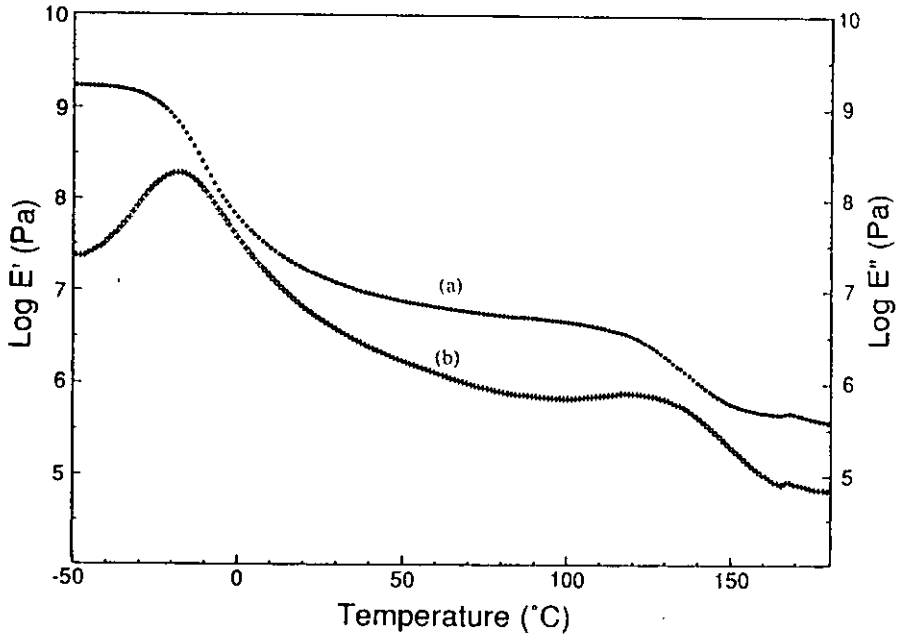

Figure 5.19 Storage (a) and loss moduli (b) versus temperature for the 60:40 PUR/PS IPN.

60:40 PUR/PS IPN - stirred synthesis. The synthesis procedure and conditions were shown to have an influence on the extent of phase separation in IPNs (section 5.1). The miscibility of PUR/PS IPNs has been reported to be improved and the inter-transition values raised on conducting the synthesis at low temperature[66], under high pressure[274] and in a common solvent[149]. In this study, a stirred polymerisation was conducted in order to increase the amount of phase mixing and to obtain a high inter-transition zone. The synthesis procedure deviated from that outlined in section 3.3.2 in that after combining and mixing all components for 5 mins, the mixture was allowed to prepolymerise under moderate stirring for 30 min at 60°C, still in the reaction vessel. The stirring had to be conducted at moderate speed (approximately 120 rpm) in order not to introduce air bubbles into the increasingly viscous reaction mixture. At gelation, the cloudy and highly viscous mixture was moulded and cured according to the previous curing cycle.

DMTA studies. Figures 5.20 and 5.21 show the DMTA data for the stirred 60:40 PUR/PS IPN and the conventionally produced equivalent. Both IPNs were crosslinked at a PPG1025/TMP ratio of 7:1 and 1% DVB. From the DMTA data, it was noted that the two glass transition peaks of both IPNs were located at similar temperatures. These were -5°C and -3°C for the PUR transition and 127°C and 123°C for the PS transition for the conventional and stirred polymerisation, respectively. The slight inward shift of the transitions for the stirred IPN could have indicated less pure component phases. Further, an inversion of the peak heights was observed. In the conventionally synthesised IPN, the loss factor value of the PUR peak (0.63) was slightly higher than the PS peak (0.59). Whereas in the stirred IPN, the PS (1.08) was clearly higher than PUR transition (0.48), indicating, perhaps, a change in the continuous phase. Similar to the preparation of high impact PS (HIPS)[303], this was caused by the lower viscosity of styrene monomers/oligomers. The PUR reaction proceeded first, yet, the formation of a macroscopic PUR network was to a certain degree impeded by the stirring. Even though the PUR component was present in the higher volume fraction with 60 weight % and was the first formed network, it was PS that seemed to form the more continuous phase. The most remarkable difference with respect to the damping characteristics of this material, however, was the high loss factor values (0.45) of the stirred IPN for the inter-transition values compared to those of the conventionally moulded IPN (0.18).

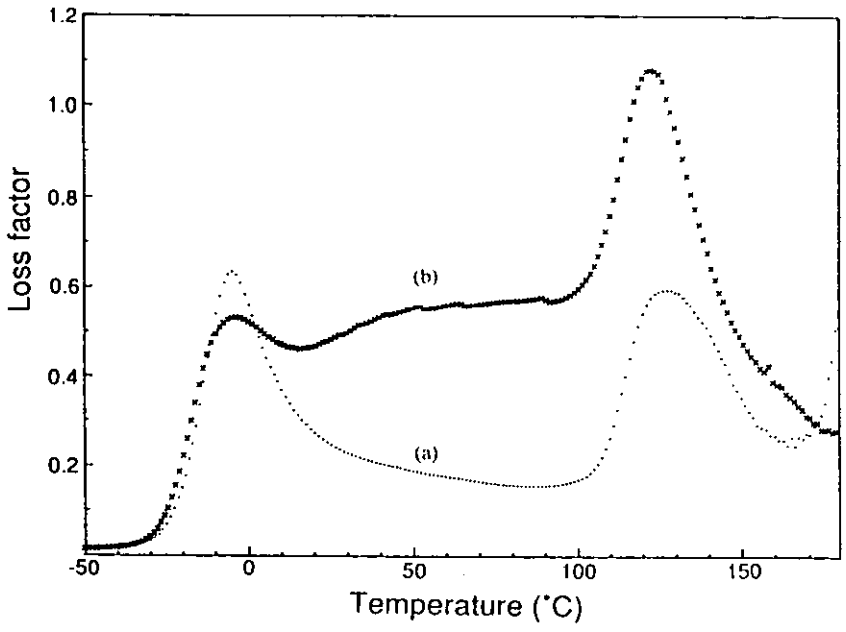

Figure 5.20 Loss factor versus temperature data for the conventional (a) and stirred (b) 60:40 PUR(PPG1025/TMP 7:1) / PS(1%DVB) IPN.

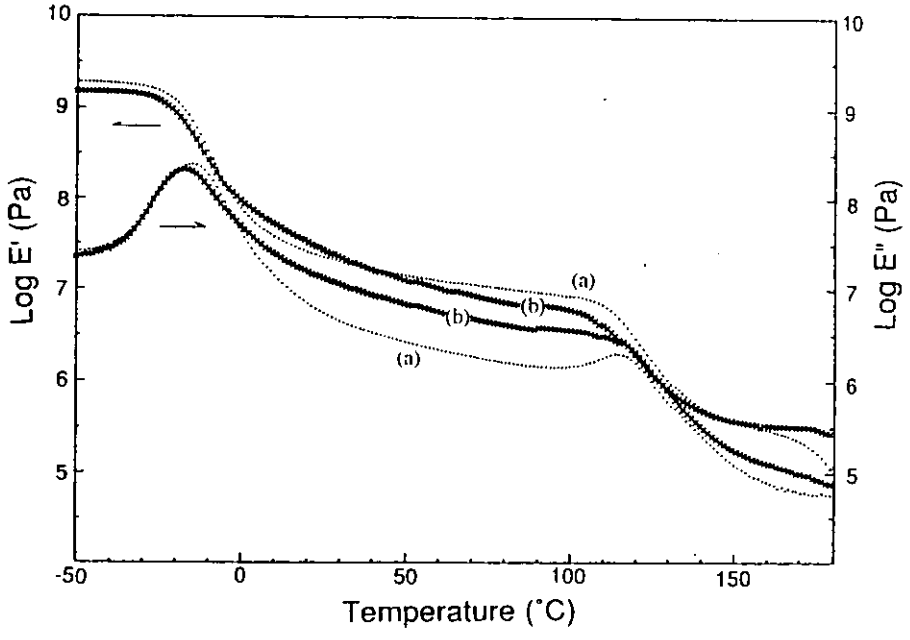

Figure 5.21 Storage and loss moduli versus temperature for the conventional (a) and stirred (b) 60:40 PUR(PPG1025/TMP 7:1) / PS(1%DVB) IPN.

Consequently, the area under the loss factor curve, TA, of the stirred IPN was very high compared to the conventionally synthesised counterpart. The former indicated that a region with a substantially mixed interface existed. This could be explained on the grounds that mixing was conducted up to a high viscosity. Both networks were forming simultaneously. Growing PS chains were trapped in the developing PUR network and vice versa, leading to increased component mixing. Because of the high viscosity and entanglement, PS chain movement leading to phase separation was impeded and proceeded only at a much slower rate than in the conventional synthesis. At moulding, the entire system was interlocked by completion of the network formation.

TEM studies. The conclusions drawn from the DMTA data were confirmed by TEM micrographs. The conventional synthesis resulted in light PS domains dispersed in dark OsO_4-stained PUR matrix. The morphology of the stirred system was clearly more complex (figure 5.22). Besides PS domains in a PUR matrix (figure 5.22(a)), also finely dispersed PUR domains in a PS matrix (figure 5.22(b)) and PUR domains in PS domains in a PUR matrix could be observed (figure 5.22(c)). A great distribution of phase domain sizes was obtained. PUR domains in PS phases varied from 20 nm in the ellipsoidal PS phases in figure 5.22(a) to 1 μ in figure 5.22(b). In addition to obvious changes in phase domain sizes, the composition of the matrices might also have changed. The latter had already been indicated by the inward-shift of the PUR and the PS transitions form the DMTA data. In conclusion, this stirred 60:40 PUR/PS IPN resulted in a high damping material with a loss factor range > 0.3 from -19°C to 145°C and a very high TA area. This preparation process might be worth further study. However, reproducibility of the materials was a major problem since exact timing of the transfer into the mould was essential. Also, because of the high viscosity, the reaction mixture could not be degassed after stirring so that the presence of small air bubbles could not be excluded. To what extent air bubbles could have been responsible for the very high damping characteristics was not entirely clear. However, PUR foam when compared to the respective PUR elastomer using the same Polymer Laboratories MKII DMTA analyser did not show any significant increase in loss factor values.

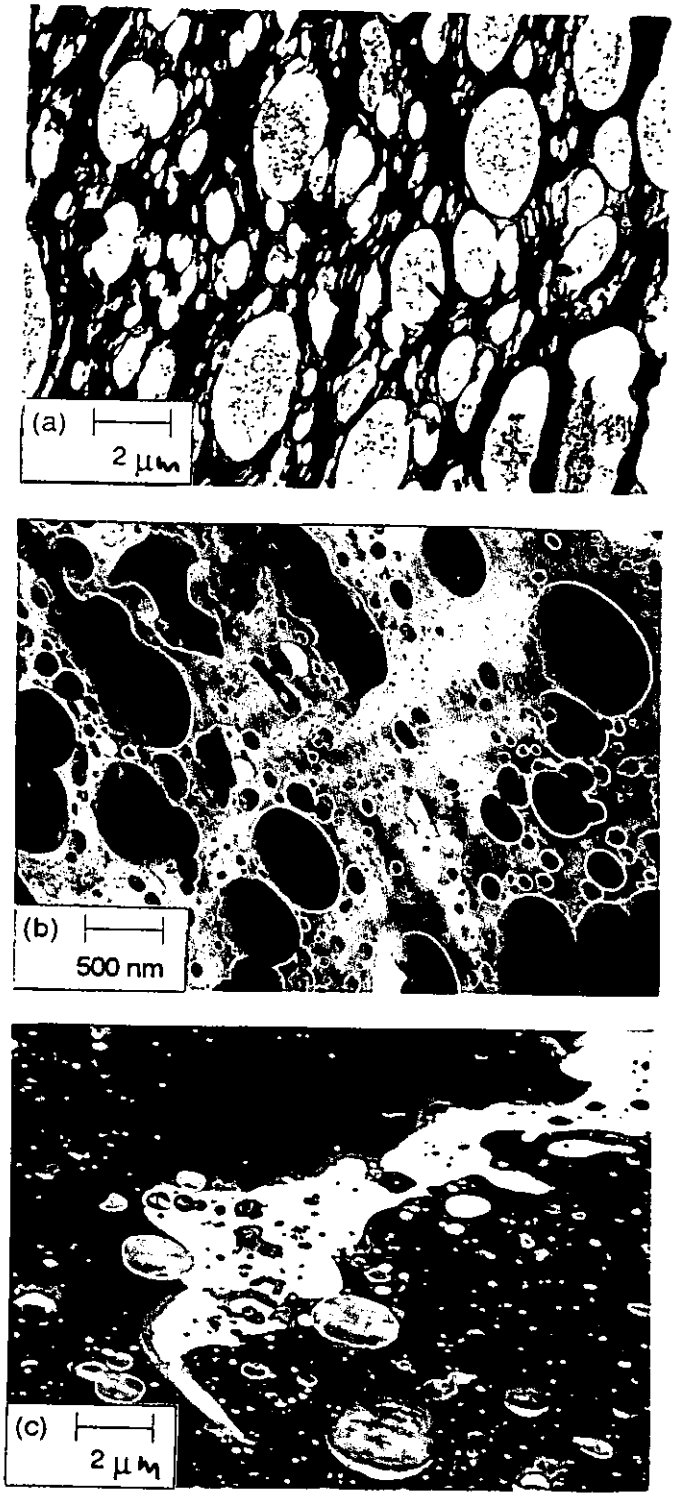

Figure 5.22 TEM studies for the stirred 60:40 PUR/PS IPN.

Influence of the reaction kinetics and the curing cycle. The reaction kinetics of the 60:40 PUR/PS IPN were studied since they have an important bearing[4] on the IPN morphology and properties (section 2.1.2). It is known[100] that the first-formed network greatly influences the IPN properties. The reaction rates of the PUR and the PS components were monitored by FTIR spectroscopy. A plot of the percent conversion versus time is shown in figure 5.23.

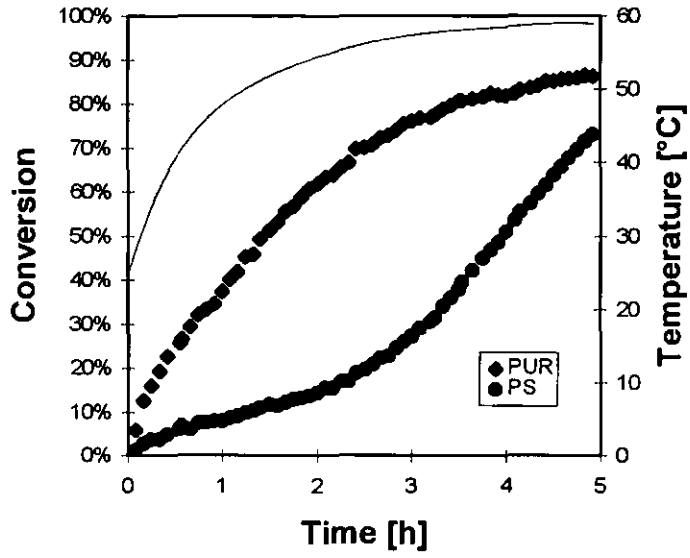

Figure 5.23 PUR and PS conversions versus reaction time in the 60:40 PUR/PS.

The actual temperature profile measured in the mould by insertion of a thermocouple during the curing cycle was remodelled with the heated cell unit. This temperature profile is represented by the solid line in figure 5.23. The conversion curves of both networks were monitored by following integrated peak areas versus time. The integration limits of the respective functional groups were 2330-2160 cm^{-1} for the isocyanate and 1637-1622 cm^{-1} for the vinyl group. Under the present reaction conditions, the PUR reaction proceeded faster than the PS formation. Up to a PUR conversion of 80%, the two conversion curves did not cross each other. However, during the later stages of the PUR formation, a considerable amount of PS polymer was already present. For example, at a PUR conversion of 75% already 30% of the PS monomer had reacted. Due to the different reaction mechanisms, linear PUR at 75% conversion would have been of oligomeric character. However, since the PUR component was crosslinked by TMP, a network had already formed at that stage. The 30% reacted PS monomer had formed polymer. The presence of PS during the

formation of the PUR is known[64,65] to result in grossly phase separated materials because of the high immiscibility of both polymers. Because of the tertiary nature of the NCO group, the rate of the PUR formation was comparatively slow. A more reactive NCO group such as in an aromatic diisocyanate might, thus, have resulted in less phase separated IPNs. Thus, selecting a more reactive diisocyanate could be a means of decreasing phase separation under the given reaction conditions.

The influence of the curing cycle on the DMTA data of the IPNs was briefly investigated. A series of 4 IPN sheets of similar chemical composition were prepared and cured simultaneously. Again, the 60:40 PUR/PS IPN composition crosslinked at a PPG1025/TMP ratio of 3:1 and 5% DVB was chosen for this series. The general curing cycle was conducted and interrupted at several stages. One mould was taken out after 24 h at 60°C and 80°C. The second IPN represented the general curing cycle and was demoulded after further 24 h at 90°C. The third sheet was taken out after 2 more h at 120°C. This last curing cycle was applied to PUR/PS IPNs with a PS content of 60% or greater. Instead of 2h, the last IPN was left in the oven for 24 h at 120°C. The DMTA data in figures 5.24 and 5.25 indicated that there existed only slight differences in the first three sheets. The loss factor peak locations and peak heights were very similar for the IPNs cured at 24 h at 60°C and 80°C and 24 h at 60°C, 80°C and 90°C (figure 5.24(a) and (b)). The IPN that was cured for a further 2 h at 120°C exhibited a slightly lower PUR loss factor peak while the PS loss factor was somewhat higher. The IPN cured for a further 24 h at 120°C (figure 5.24(d)) showed clear signs of degradation of the PUR network. Compared to the IPN that was cured according to general curing cycle (figure 5.24(b)), the PUR transition peak diminished to half the original size from 0.64 to 0.32 and shifted to a lower temperature of -13°C compared to -2°C. The PS transition on the other hand almost tripled in size from 0.42 to 1.04, and also shifted to a lower temperature of 127°C compared to 139°C. The PUR transition shift to lower temperatures occurred because of a decrease in molar mass and partial break up of the PUR network. A second factor, perhaps, was a plasticisation effect which was caused by loose soft segment ends and fragments. A further indication for this theory was that the polystyrene peak was almost three times its original height and also shifted towards lower temperatures.

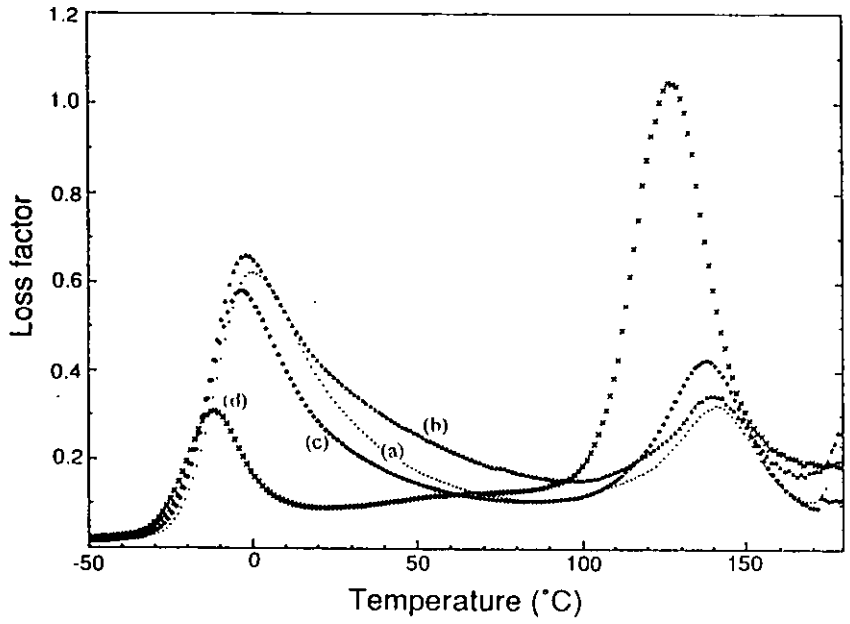

Figure 5.24 Loss factor versus temperature data for the 60:40 PUR/PS IPNs cured according to different curing cycles. 24 h @ (a) 60°C and 80°C, (b) 60°C, 80°C and 90°C, (c) 60°C, 80°C and 2 h @ 90°C, (d) 60°C, 80°C and 90°C.

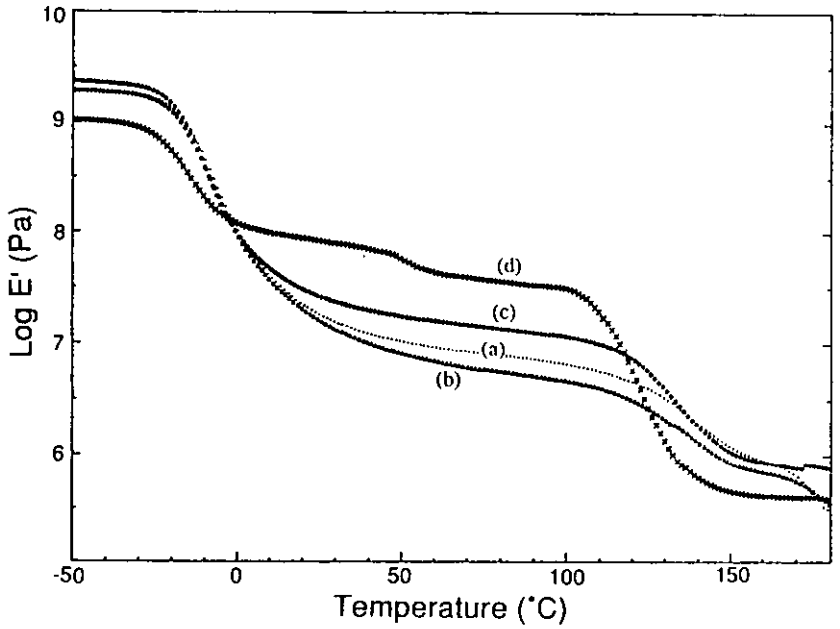

Figure 5.25 Storage modulus versus temperature data for the 60:40 PUR/PS IPNs cured according to different curing cycles. 24 h @ (a) 60°C and 80°C, (b) 60°C, 80°C and 90°C, (c) 60°C, 80°C and 2 h @ 90°C, (d) 60°C, 80°C and 90°C.

Thus, the restrictions of the PUR network ceased to exist and the PS became more continuous which was reflected in the increase in transition peak height. The decrease of the PS Tg could, perhaps, be explained by a decrease of urethane links which resulted in a decrease of hydrogen-bond interactions between the N-H and the π orbitals of the PS phenyl rings. Equally important was that the contact area of the PUR with the PS was believed to have decreased. A relatively tight PUR network restricted the domain size of the PS. Upon the break-up of the network, PS domains could form larger and more continuous domains, and, thus, decrease the possible hydrogen-bond interactions between the N-H and the PS phenyl rings.

From the storage moduli versus temperature a similar trend was observed (figure 5.25). A two-step drop corroborating the immiscible nature of the IPN was observed for all moduli. For curves (a), (b) and (c), the storage modulus drop in the PUR transition was very pronounced. This was further demonstrated by the comparatively low plateau moduli between the two transitions. The IPN cured for a further 24h at 120°C additional to the general curing cycle exhibited a different profile. The storage modulus drop at the PUR transition was less pronounced and the inter-transition plateau consequently higher than for the other three materials. A further very small modulus drop in the plateau modulus was observed at about 50°C. This transition was not reflected in the loss factor versus temperature profile and might thus have been a primary transition. In this IPN it could have been the melting of some associated hard segments. Association of hard segments was facilitated by the dissociation of the PUR network because of an increase in chain mobility. The degradation or better dissociation of the PUR network into the isocyanate and the diol at that low a temperature was surprising. Generally, a urethane group between two alkyl groups is said[204] to be thermostable up to 250°C, whereas one between two aryls dissociates at about 120°C. The degradation in this case, however, is surprising since the urethane group was situated between two alkyl groups. The fact that PUR IPNs with PS or PMMA exhibit a somewhat higher thermal stability[127,275] due to the radical scavenger effect of the depolymerising polymer was not of importance at these low temperatures. One explanation for this early degradation could be the relatively high amount, 1 weight %, of stannous octoate present in the IPN sheet, which is also known[204] to promote PUR dissociation and degradation.

5.3 Variation of the Crosslink Density of the 60:40 PUR/PS IPN

The crosslink density is generally believed[100,112,128] to have an important effect on IPN morphology. Studies[100,112] have revealed that especially the crosslink density of the first-formed network exerts a strong influence on the phase domain sizes in IPNs. The aim of this study was to investigate the influence of the crosslink density in both networks on the IPN morphology. Thus, the effect of crosslinking on the loss factor versus temperature profile, phase mixing, the continuous phase and the phase domain sizes were studied using DMTA, M-TDSC and TEM. Two crosslinking series were conducted at the 60:40 PUR/PS IPN composition, including two semi-IPNs. Six different diol/triol ratios in the PUR were investigated at a fixed DVB level of 5 mol % in the PS component. The ratios were varied from no TMP in the semi-2 IPN to a high TMP content at a PPG1025/TMP ratio of 1:3. The other series was conducted at a fixed PPG1025/TMP ratio of 3:1. Six different crosslinking levels in the PS network were investigated. These ranged from 0 mol % DVB in the semi-1 IPN to 20 mol % DVB.

DMTA studies. Figure 5.26 shows the loss factor and storage modulus versus temperature data of the 60:40 PUR/PS IPNs at a fixed DVB level of 5 mol % and varying diol/triol ratios. The DMTA data are given in table 5.3, together with values for the theoretical average molar mass between crosslinks, $M_{c,t}$, for the PUR. $M_{c,t}$ was calculated by using equation (4.3).

Table 5.3 DMTA data for the 60:40 PUR/PS IPNs at 5 mol % DVB level and varying PPG1025/TMP ratios.

Ratio PPG1025/TMP	$M_{c,t}$ [g/mol]	(PUR) Tg [°C]	IPN PUR Tg [°C]	IPN PUR tan δ	IPN PS Tg [°C]	IPN PS tan δ
1:3	620		88	0.51	134	0.45
1:1	1180	(30)	37	0.51	138	0.32
3:1	2870	(-5)	-1	0.62	139	0.36
9:2	4110		-9	0.63	139	0.50
7:1	6260	(-9)	-12	0.65	139	0.78
1:0	linear	(-12)	-19	0.52	132	1.09

( ) Tg values for PUR homonetworks from section 4.2.

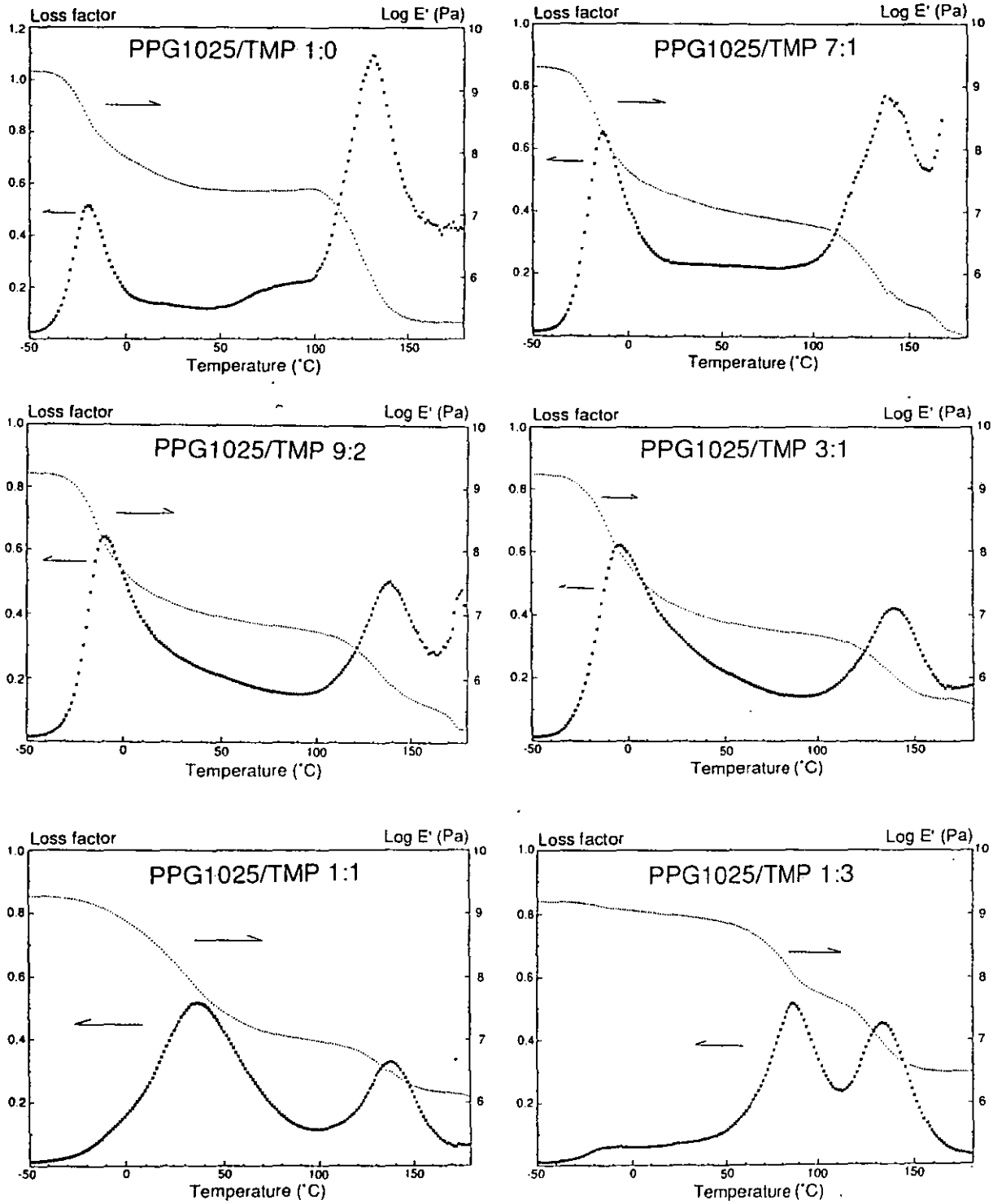

Figure 5.26 DMTA data for 60:40 PUR/PS IPNs at a 5 mol % DVB level and varying PPG1025/TMP levels.

The loss factor peak height of the PUR decreased slightly with higher crosslinking and became broader (figures 5.26 and 5.27).

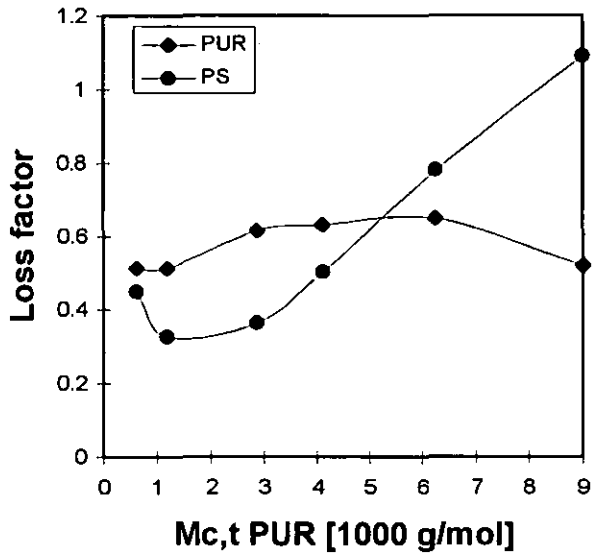

Figure 5.27 Loss factor height versus PUR $M_{c,t}$ in the 60:40 PUR/PS IPNs.

An exception to this was the uncrosslinked semi-2 60:40 PUR/PS IPN, where the loss factor value of the PUR was lower than in any of the other IPNs. A decrease in loss factor peak height was expected since higher crosslinking limits[185] the segmental movements which are the basis of Tg. A similar tendency of decreasing loss factor heights with higher crosslinking was observed for the PUR homonetworks in chapter 4.2. However, the linear PUR homopolymer exhibited, as expected, the highest loss factor peak. Thus, the different behaviour of the PUR transition in the IPN must have been caused by the PS network. The loss factor versus temperature data for this semi-2 IPN (figure 5.26) showed considerably higher loss factor values for the PS transition (1.09) than for the PUR (0.52). The small transition spanning from 60°C to 90°C did not stem from a region of increased PUR-PS phase mixing, but was the β transition[279] of the PS network. It appeared that the PS was the dominant component and exhibited a higher degree of phase continuity. The latter, combined with fact that PS is glassy at the PUR transition and was crosslinked, might have accounted for the lower PUR transition peak height for the semi-2 IPN. The location of the PUR loss factor peak in the IPNs shifted strongly to higher temperatures with increasing crosslinking density from -19°C for the linear PUR to 88°C for the highly crosslinked PUR (figure 5.28).

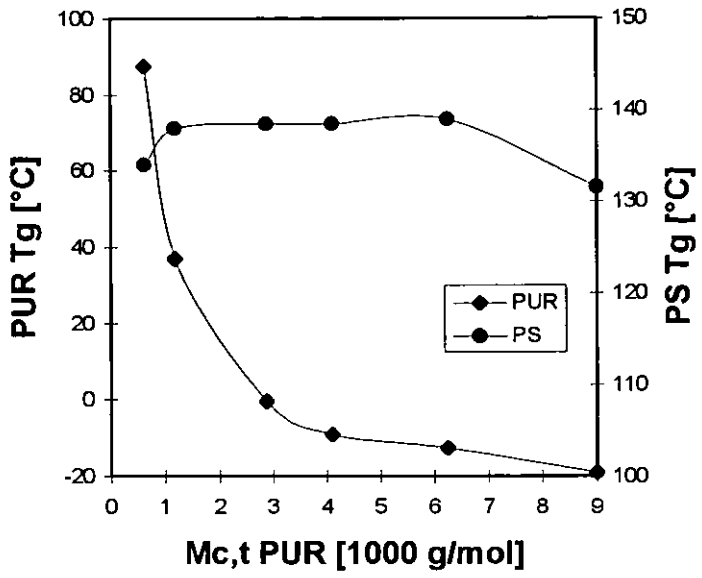

Figure 5.28 Loss factor peak locations versus PUR $M_{c,t}$ in the 60:40 PUR/PS IPNs.

Comparing these Tg values to those of the PUR homonetworks of similar crosslinking density illustrated the influence of the PS network. The Tg values of the linear (-19°C) and the PPG1025/TMP 7:1 (-12°C) crosslinked PUR transitions in the IPNs were lower than those of the corresponding PUR homonetworks (-12°C and -9°C, respectively). This could have been a result of a plasticisation effect[63,86] of PS chains dispersed in the PUR matrix hindering hydrogen bonding between PUR hard segments. More likely, perhaps, was a dilution effect of the PUR precursors by polystyrene. The PUR was essentially formed in solution with 40% styrene as solvent. Because of the dilution on the reactive groups, the reaction only proceeded to a lower conversion, which resulted in a lower Tg. This effect was very pronounced for the linear material and at a low crosslinking density of a PPG1025/TMP ratio of 7:1. With increasing crosslinking density, however, the molar mass increased towards infinity because of the increased presence of multifunctional precursors. Thus, because of the network formation, the molar mass build up proceeded at a much faster pace to high molar masses even without complete reaction of the functional groups. The PUR network caused forming PS chains to be trapped, and this increased the PUR Tg. The latter was observed for the IPNs crosslinked at PPG1025/TMP ratios of 3:1 and 1:1. Here, the Tg values for the PUR transition were higher with -1°C and 37°C than those of the corresponding PUR homonetworks with -5°C and 30°C, respectively.

The variation of the crosslink density in the PUR also influenced the PS transition. The PS transition decreased constantly in height, with exception of the highly crosslinked IPN at a PPG1025/TMP ratio of 1:3. At no or low crosslinking in the PUR (PPG1025/TMP ratios of 1:0 and 7:1), the PS transition peak was higher than the PUR peak (table 5.3). This changed with higher crosslink densities. Since the higher transition is usually taken[4] as an indication for the continuous phase, this could have meant that crosslinking influenced phase continuity. It has been found[100,112] that the first-formed network represents the continuous phase, and, thus, controls the properties of the IPN. However, this study indicated that if the first-formed network is too lightly crosslinked, the second network can still alter the property profile. Further evidence for this observation was found in the study varying the DVB concentration. While a pronounced difference was observed in the PS loss factor peak heights, the PS peak location remained very stable and most Tg values were between 138°C and 139°C (figure 5.27). Exceptions were the two extreme situations, the linear and the highly crosslinked PUR, where lower Tg values were obtained. In the semi-2 IPN, the PS transition was found to have been 7°C lower at 132°C. This could have been because of the fact that the segmental movements of the PS were less restricted by the linear PUR than by the PUR network. This could also have indicated a decrease of hydrogen-bond interactions between the N-H of the urethane link and the PS phenyl π orbital[290]. The decrease of these interactions could have been a result of fewer urethane links due to the linear character of the PUR. Another reason for a decreasing contact area might have been a decrease of PS surface area due to bigger phase domain sizes (see TEM micrographs). At the high crosslinking density (PPG1025/TMP ratio of 1:3), the inward-shift of the transition might well have indicated a higher degree of forced component mixing. A further indication for a higher degree of forced component mixing was the high inter-transition value of 0.24 (figure 5.25). It might have been expected that with increasing PUR crosslinking, the PS transition would be shifted to higher temperatures because of a decrease in free volume. However, this effect was probably not very pronounced because of the high immiscibility of the phase domains. Also, it might have been compensated through the increased degree of forced mixing at higher crosslinking, which in turn, would have caused an inward shift of the PS transition.

Varying the crosslinking density of the PS network showed less pronounced effects by far and was less conclusive. The loss factor and storage modulus versus temperature data of the 60:40 IPNs at a fixed PPG1025/TMP ratio of 3:1 and varying DVB levels are shown in figure 5.28. The DMTA data are given in table 5.4. The loss factor peak heights are plotted versus $M_{c,t}$ of the PS network in figure 5.29. $M_{c,t}$ was calculated using a modification of a previously reported equation[304].

$$M_{c,t} = \frac{X_M M_M + X_X M_X}{2X_X} \qquad (5.5)$$

X_M and X_X are the mol fractions and M_M and M_X are the molar masses of the styrene monomer and DVB crosslinker, respectively. The higher DVB molar mass of 130 g/mol was taken into account by the second component in the sum. The PUR transition heights generally decreased with increasing DVB content (figure 5.30). The same general trend was noted for PS transition heights up to crosslinking levels of 10% DVB. At 20% DVB, however, the PS transition increased from a loss factor value of 0.31 to a value of 0.44.

Table 5.4 DMTA data for the 60:40 PUR/PS IPNs at a fixed PPG1025/TMP ratio of 3:1 and at varying DVB levels.

Crosslinker	$M_{c,t}$	PUR		PS	
[% DVB]	[g/mol]	Tg [°C]	tan δ	Tg [°C]	tan δ
20	500	-5	0.39	130	0.44
10	1100	-2	0.53	125	0.31
7.5	1400	-4	0.52	121	0.34
5	2100	-1	0.62	139	0.36
2.5	4200	-9	0.57	128	0.49
0	linear	-2	0.76	134	0.47

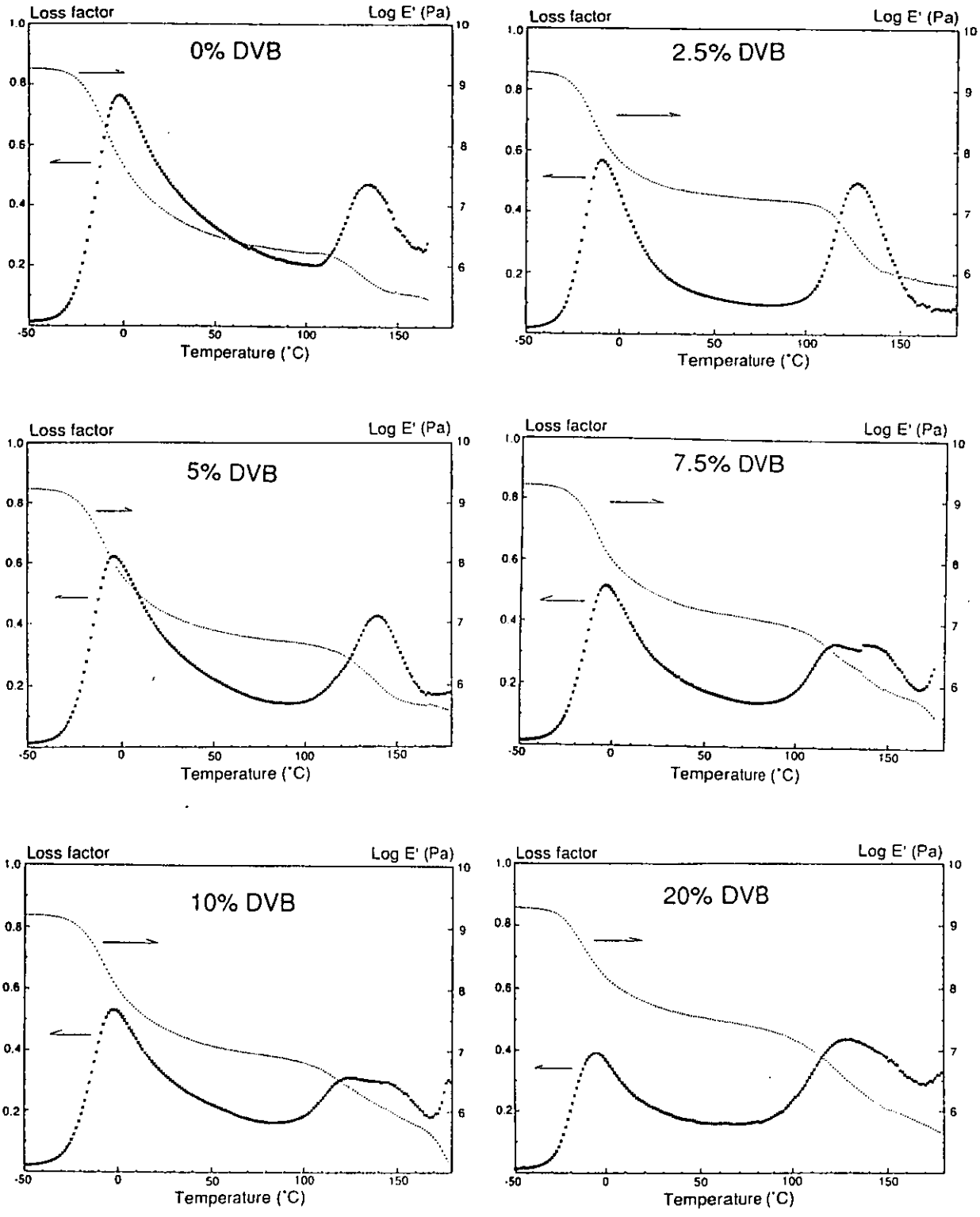

Figure 5.29 DMTA data for 60:40 PUR/PS IPNs at a fixed PPG1025/TMP ratio of 3:1 and at varying DVB levels.

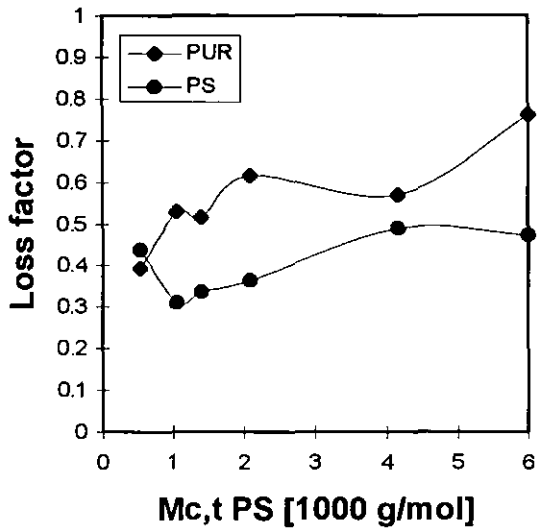

Figure 5.30 Loss factor height versus PS $M_{c,t}$ for the 60:40 PUR/PS IPNs.

The PS transition was for the first time in this series higher than the PUR transition, possibly indicating a change of the continuous phase or dual phase continuity. Again, this might have indicated that the crosslinking level in both networks and not exclusively that of the first-formed network determined the IPN morphology. The influence of the crosslinking level on phase continuity might have been a combination of two factors. A more lightly crosslinked PUR network was more susceptible to segmental movements when swollen with styrene monomer, allowing the latter to develop a more continuous polymer network. Also increasing the amount of crosslinker could have brought about a change in the reactivity rates of the system. This is particularly true for the crosslinking of styrene, since it is known[305] that DVB possesses a far higher reactivity than the latter. Another side effect of the difference in reactivity of DVB and styrene is that important variations in the crosslinking density of PS networks can result[305]. This, combined with the fact that some DVB is too sterically hindered[305,306] to act as a crosslinker, sometimes causes the PS network not to be completely homogeneous, especially at high DVB levels. With increasing crosslinking densities, the PS transition increased in breadth, particularly at DVB levels of 7.5% and higher (figure 5.29). Thus, because of the relatively broad PS transitions, it was at times difficult to assign a value for Tg. It was, perhaps, for these reasons that no clear trend could be observed for the PUR and PS peak locations (figure 5.31).

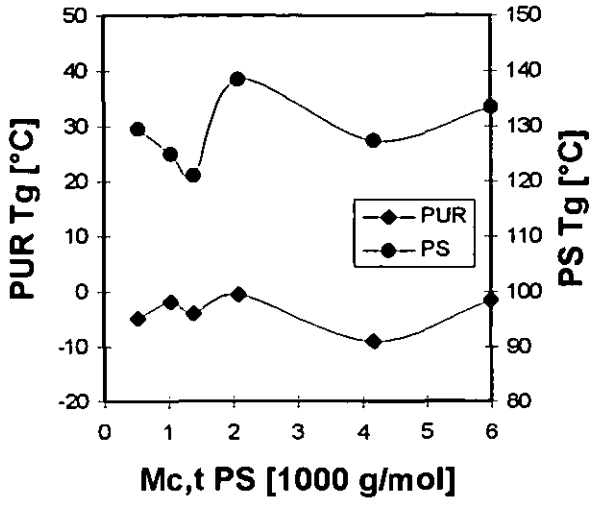

Figure 5.31 Loss factor peak location versus PS $M_{c,t}$ for the 60:40 PUR/PS IPNs.

A number of phenomena are influencing the location of the PS transition. Higher crosslinking generally causes a shift of Tg to higher temperatures, while it also might have resulted in an increase in forced mixing with the PUR. It has been experienced[112] before that incorporation of DVB levels greater than 3% did not further increase transparency in PUR/PS IPNs. The ineffectiveness of high DVB contents was explained in two ways. Either not all of the available vinyl groups of DVB could react due to the high viscosity of the reaction medium or the presence of the polyurethane network opposed the polystyrene network formation. In conclusion, it could be seen that the area under the loss factor curve, TA, generally decreased with higher crosslinking. Increasing the crosslinking in the first-formed network had a much more pronounced effect than in the second network formed. At a higher PUR crosslink density, the PUR transition shifted to higher temperatures, yet hardly changed in size. The PS transition on the other hand remained at the same temperature, however, strongly decreased in height. Apart from a general decrease of the loss factor values, no clear trends for the loss factor peak locations were observed for an increase in crosslink density of the PS network.

Modulated-temperature DSC studies. The variation of the crosslink level in the PUR proved to influence more dramatically the loss factor data than a variation of the crosslink level in the PS. Therefore, the M-TDSC data were obtained for PUR

crosslinking series. Plots of the derivative of the heat capacity versus temperature for 60:40 PUR/PS IPNs of three different crosslinking densities are shown in figure 5.32. The PUR soft segment transition shifts to higher temperatures, as determined by the M-TDSC data, were much less pronounced (lower by a factor of 3) than those observed from the DMTA data. The PUR Tgs (M-TDSC) were located at -38, -33 and -26°C for PUR crosslinking ratios of PPG1025/TMP of 7:1, 3:1 and 1:1, respectively. With increasing crosslinking of the PUR, the PS transition shifted to slightly higher temperatures. The PS Tg was found at 108, 110 and 115°C for PUR crosslinking ratios of PPG1025/TMP of 7:1, 3:1 and 1:1, respectively. This is in contrast to the findings from the DMTA data, where it remained at the same location. However, again it has to be emphasised that while the determination of the PUR Tg was straightforward, a broad PS transition made the exact determination of the PS Tg difficult. In addition to the shift to higher temperatures of the PUR Tg, its breadth increased for higher crosslinking levels. Also, the change in heat capacity occurred more gradually as was substantiated by the decrease in peak height of the derivative of the heat capacity.

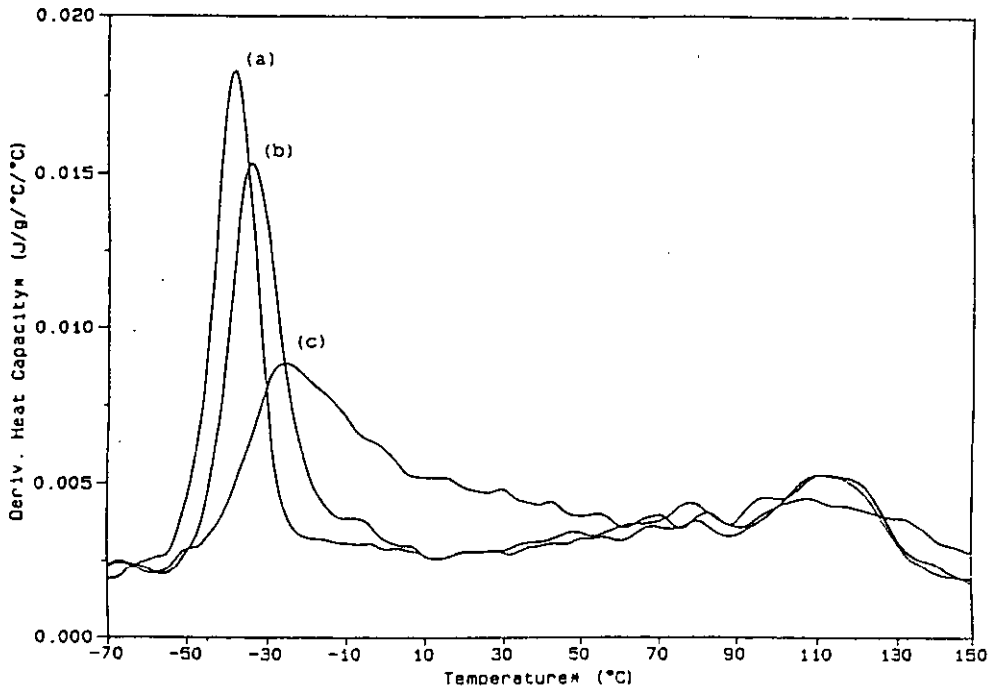

Figure 5.32 Derivative heat capacity versus temperature for 60:40 PUR/PS IPNs at a 5 mol % DVB level and at varying PPG1025/TMP ratios. (a) PPG1025/TMP 7:1, (b) 3:1 and (c) 1:1.

Morphology by TEM. TEM studies were conducted in order to confirm the findings from DMTA and M-TDSC and to elucidate further the IPN morphology. Four IPNs with highly different crosslinking densities in the PUR network were investigated. These were 60:40 PUR/PS IPNs with PPG1025/TMP ratios of 1:0, 7:1, 1:1 and 1:3. The TEM micrographs of these IPNs showed a distinctly different morphology (figure 5.33). Generally, with increasing crosslinking density of the PUR component, the phase domain sizes of the PS decreased. The semi-2 60:40 PUR/PS IPN (PPG1025/TMP ratio of 1:0) had very large PS phase domain sizes of 500 nm to several microns and the PS phases appeared to be interconnected (figure 5.33(a)). Thus, both the dark PUR and the white PS phases were believed to have exhibited some degree of continuity. It had been observed by DMTA that when the PUR was linear the loss factor peak of the PS was twice the size of the PUR. The latter indicated that the PS phases were interconnected. Thus, the TEM micrographs confirmed the findings from DMTA (figure 5.26). At a low crosslinking level of the 60:40 PUR/PS IPN of a PPG1025/TMP ratio of 7:1, the PS phase domains remained fairly large (figure 5.33(c)). However, the PS phases appeared to be less interconnected. The micrograph of the IPN crosslinked at a PPG1025/TMP ratio of 1:1 showed generally smaller phase domains in the order of 50 - 200 nm (figure 5.33(d)). The matrix seemed to be of a lighter shade than that of the 7:1 crosslinked IPN. At the highest crosslinking density of a PPG1025/TMP ratio of 1:3 in addition to sporadic larger domains (figure 5.33(e)), even smaller PS phase domains were observed (figure 5.33(d)). Osmium tetroxide-stained and unstained micrographs showed very similar patterns. In both micrographs, the PS domains were darker than the PUR-rich matrix. This indicated that the osmium tetroxide staining of the PUR was less effective at higher crosslinking densities. While the exact mechanism of the staining with osmium tetroxide is not known, it is believed[205] that some interaction with the ether oxygens of the PUR soft segments occurs. With increasing crosslink densities of the PUR network, the amount of soft segment decreased. The IPN crosslinked at a 7:1 PPG1025/TMP ratio had a soft segment content of 75% while that of a 1:3 ratio had a soft segment content of only 35%. Thus, fewer interactions between osmium tetroxide and the matrix explained the lighter shade of the latter.

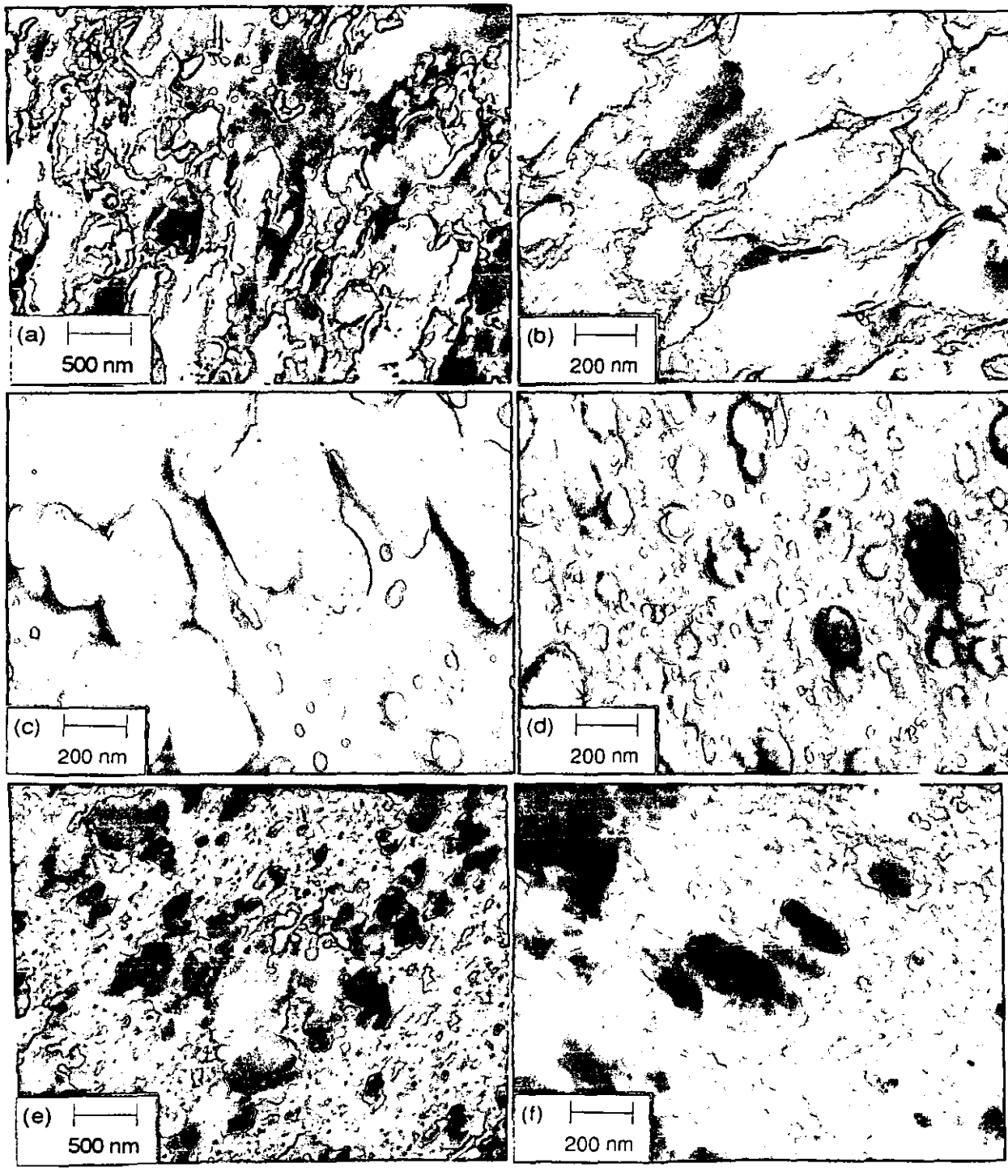

Figure 5.33 TEM micrographs for 60:40 PUR/PS IPNs at a 5 mol % DVB level and at varying PPG1025/TMP ratios. (a)&(b) PPG1025/TMP ratio 1:0, (c) 7:1, (d) 1:1 and (d)&(e) 1:3.

A higher PS content in the PUR-rich matrix - which could have impeded staining to some extent - was not too likely to have caused the lighter shade of the matrix. Since PS had a higher electron density than the unstained PUR, a PUR matrix with high contents of dissolved PS would have resulted in a darkening of the matrix of the unstained IPN. However, this was not observed. In conclusion, the TEM micrographs supported the findings from the DMTA data of a more interconnected PS phase morphology at low PUR crosslinking levels and smaller PS phase domain sizes at high PUR crosslinking densities.

5.4 Inter-network Grafting

The introduction of inter-network grafting has been found[112,134-139] to be very effective in reducing phase separation in IPNs (section 2.1.4). Consequently, it could represent an important means of obtaining a broad transition region from two polymers with Tgs far apart. The objective of this study was to investigate the efficiency of various grafting agents in provoking an inward-shift of the two transition peaks to result in a high and broad transition zone. The height and shape of the transition zone is very important with respect to the damping ability of IPNs. The grafting sites in the PUR network were created by the use of unsaturated compounds containing either hydroxyl or isocyanate entities. The 5 grafting agents evaluated were 2-butene-1,4-diol (BED), 7-octene-1,2-diol (OED), α,ω-poly(butadiene) diol (PBD), 2-hydroxylethyl methacrylate (HEMA) and benzene-1(1-isocyanato-1-methylethyl)-3-(1-methylethenyl) (TMI). All grafting agents were incorporated into the 60:40 PUR/PS IPN composition. The latter was crosslinked at a PPG1025/TMP ratio of 3:1 and with 5 mol % DVB. The grafting agents were incorporated at four distinct levels of 1, 2.5, 5, and 10 weight %. The NCO/OH ratio was constantly kept at 1.1 by adjusting the amount of TMXDI used. The choice of the grafting agents was made in order to investigate the efficiency of unsaturation in different chemical environments under the present reaction conditions. Those were dialkenes, ω-alkenes, methacrylates and α-methylstyrene-type environments.

DMTA studies. DMTA studies were conducted with all 60:40 PUR/PS IPNs grafted with different levels of the 5 grafting agents. The efficiency of the grafting agents was

evaluated according to the criteria described in chapter 3.4.1. In brief, these were the location and height of the loss factor peaks and the height of the inter-transition region. Figures 5.34 to 5.37 show the loss factor versus temperature data for the BED-, PBD-, HEMA- and TMI-grafted 60:40 PUR/PS IPNs. The DMTA data of the OED-grafted IPNs were very similar to those of the BED-grafted IPNs and, thus, are not shown. For the TMI-grafted IPNs the storage and loss moduli are shown in figures 5.38 and 5.39. The incorporation of BED resulted in a shift to higher temperatures of the PUR loss factor peak (figure 5.34). This shift was significant with a temperature difference of 65°C from -3°C for 0% BED to 62°C for 10% BED incorporation. The PUR transition heights on the other hand remained fairly constant. The PS transition first shifted to slightly higher temperatures for 1, 2.5 and 5% BED incorporations before it shifted inwards for the incorporation level of 10% grafting agent. The PS transition height increased substantially with increasing BED incorporation from 0.36 for 0% BED to 0.83 for 10% BED. This increase could not be explained since when increasing the crosslinking density in the PUR in a previous study (figure 5.26) no such trend was observed. Grafting could not account for this transition increase since the occurrence of the latter would have rather depressed the transition height as a consequence of a decrease in segmental mobility. Furthermore, it was not thought that the shift of the PUR transition to higher temperatures was the result of a significant extent of inter-network grafting. BED has a low molar mass of 88 g/mol and was, therefore, part of the PUR hard segment, together with the extra TMXDI that had to be used to keep the NCO/OH ratio at 1.1. Thus, the higher percentage of hard segment combined with the increased crosslinking density in the PUR both provoked an increase in PUR Tg (sections 4.2 and 4.3). The inter-transition region increased to a certain extent with a higher amount of BED. This, however, could be explained on the grounds of the PUR transition peak moving closer to the PS transition. Because of the PUR transition breadth, the inter-transition values did not fall to values as low as for the 60:40 PUR/PS without BED. Also, a tighter PUR network is known[100,112] to result in a higher degree of forced segmental mixing. A similar increase of the inter-transition values was observed in the crosslinking study at the highest PPG1025/TMP ratio of 1:3 (figure 5.26). Thus, a higher degree of phase mixing might have caused the inward-shift of the PS transition at the 10% BED.

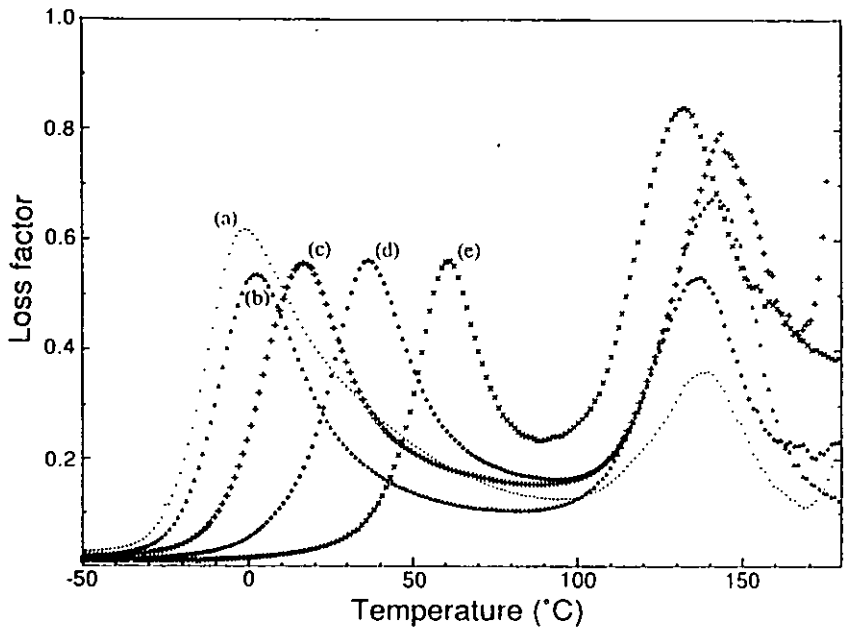

Figure 5.34 Loss factor versus temperature data for the 60:40 PUR/PS IPNs grafted with different weight percentages of BED. (a) 0 weight % BED, (b) 1%, (c) 2.5%, (d) 5% and (e) 10%.

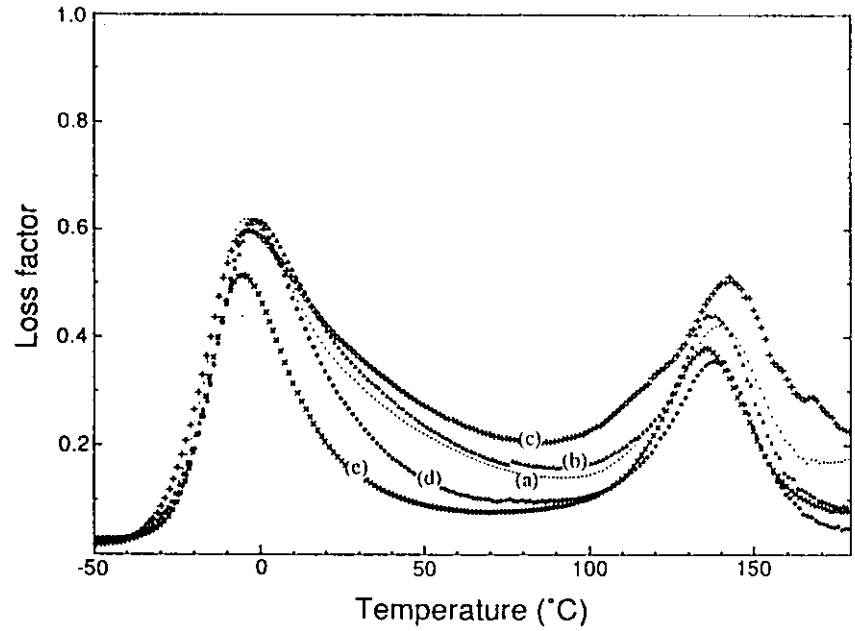

Figure 5.35 Loss factor versus temperature data for the 60:40 PUR/PS IPNs grafted with different weight percentages of PBD. (a) 0 weight % PBD, (b) 1%, (c) 2.5%, (d) 5% and (e) 10%.

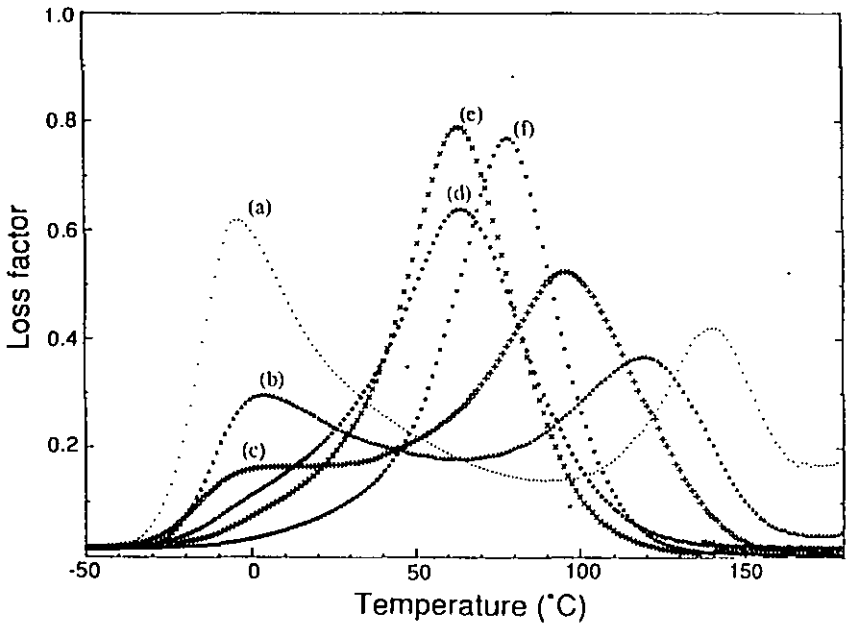

Figure 5.36 Loss factor versus temperature data for the 60:40 PUR/PS IPNs grafted with different weight percentages of HEMA. (a) 0 weight % HEMA, (b) 0.5%, (c) 1%, (d) 2.5%, (e) 5% and (f) 10%.

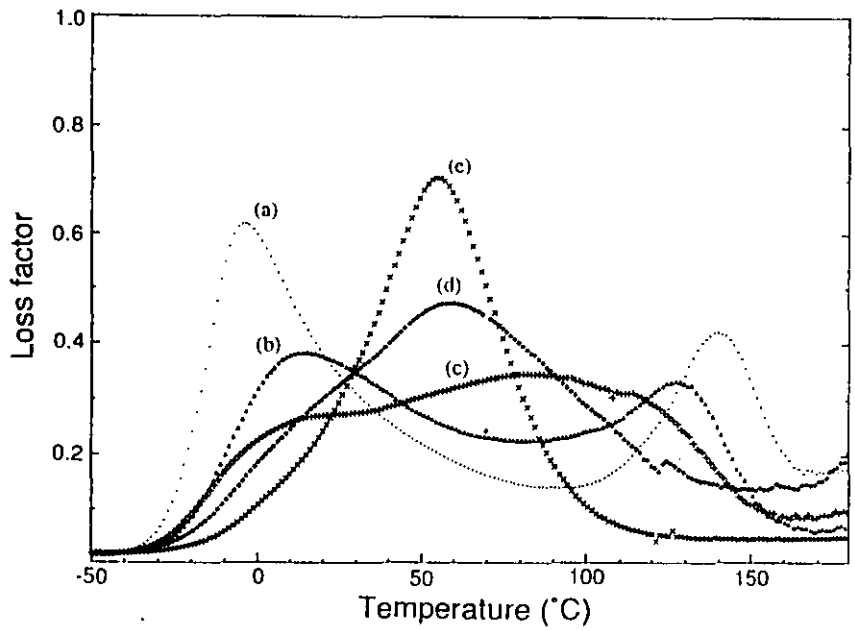

Figure 5.37 Loss factor versus temperature data for the 60:40 PUR/PS IPNs grafted with different weight percentages of TMI. (a) 0 weight % TMI, (b) 1%, (c) 2.5%, (d) 5% and (e) 10%.

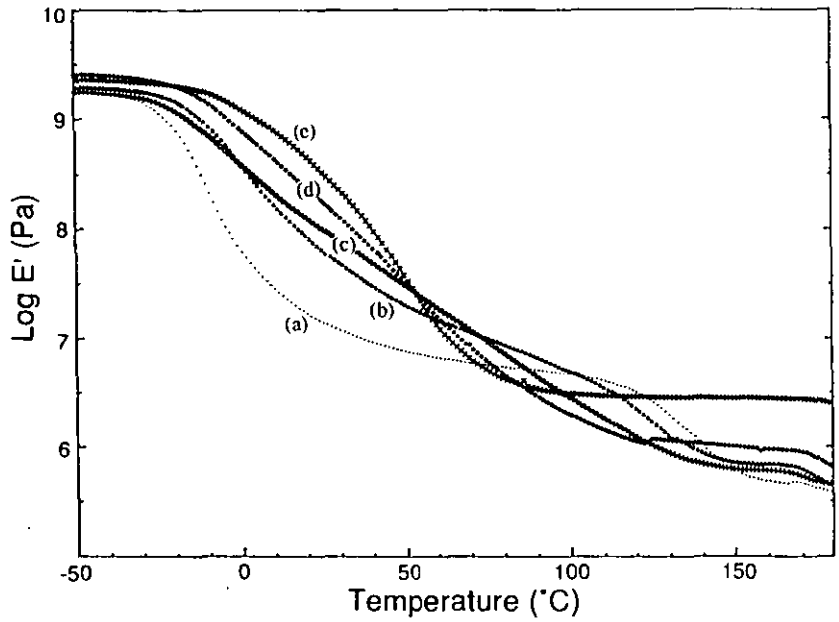

Figure 5.38 Storage moduli versus temperature for the 60:40 PUR/PS IPNs grafted with different weight percentages of TMI. (a) 0 weight % TMI, (b) 1%, (c) 2.5%, (d) 5% and (e) 10%.

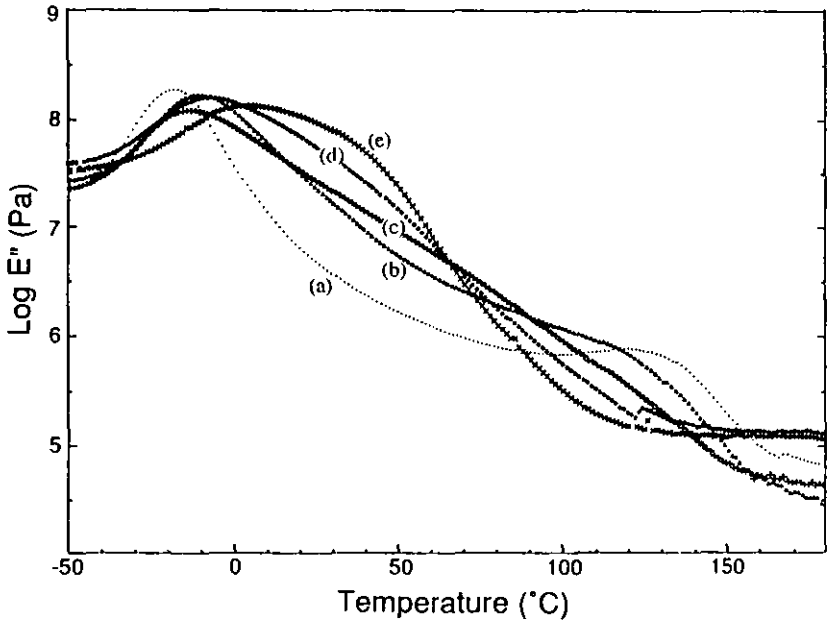

Figure 5.39 Loss moduli versus temperature for the 60:40 PUR/PS IPNs grafted with different weight percentages of TMI. (a) 0 weight % TMI, (b) 1%, (c) 2.5%, (d) 5% and (e) 10%.

Consequently, it was concluded that the unsaturation in the BED did not encourage significant inter-network grafting to occur. Very similar DMTA data were obtained with the OED study (data not shown). The PUR transition shifted continually to higher temperatures. The shifts were, however, less significant than for BED. This was because of the higher molar mass of OED, which at 144 g/mol is almost twice that of BED. As a consequence, at similar weight percentage incorporation levels, fewer urethane links were formed. Thus, the DMTA data for the PUR peak locations with 5% BED and 10% OED were found to be very similar. The 5% BED transition peak was slightly lower by 6°C at 36°C than that of 10% OED, which was at 42°C. With the incorporation of OED, no significant shift of the PS transition was noted. Only the IPN with a 10% OED incorporation showed a slightly lower value by 3°C. Again, this could be explained with the higher degree of forced segmental mixing due to higher crosslinking in the PUR component.

Instead of being incorporated into the PUR hard segment as were both, BED and OED, PBD was part of the soft segment. With the PBD-incorporation no significant changes in the loss factor versus temperature profile were observed (figure 5.35). Both transition peaks remained roughly at the temperatures of the ungrafted 60:40 PUR/PS IPN. Thus, again, it was thought that, if at all, only a very limited amount of inter-network grafting occurred. Since the molar mass of the PBD with 2580 g/mol was higher than that of the PUR soft segment PPG1025, a decrease in the PUR Tg might have been expected. However, it was observed in another study[307] that when using polyols of mixed molar masses the location of the PUR soft segment Tg mainly followed that of the lower molar mass polyol. The fact that a small transition peak of the PBD was found at -70°C might have indicated limited miscibility of the two polyols. The half-peak width of the PUR and the height of the inter-transition region decreased with increasing amount of incorporated PBD. An exception to this was the 2.5% PBD incorporation which exhibited the highest inter-transition values. However, it was believed that the latter was not a representative sample. The general decrease in the inter-transition heights could have indicated a decrease in forced phase mixing due to decreasing crosslinking density in the PUR network. More likely, however, was another explanation. PBD-based PURs are highly phase segregated[205], since no interactions are possible between the soft and the hard segment. In polyether-based PURs, hydrogen bonding between the ether and the urethane link allowed for some

phase mixing to occur. The latter results in a broadening of the PUR transition (section 2.3.2). Thus, with increasing PBD-incorporation, the affinity to the PUR hard segment was weakened resulting in a sharper soft segment transition peak. The findings that no significant inter-network grafting occurred with PBD were in contrast to a study of PBD-grafted PUR/PMMA IPNs[138]. Hourston and co-workers[138] found that the average molecular weight between crosslinks decreased with the incorporation of the grafting agent. On the grounds of this observation, it was concluded that a significant amount of inter-network grafting took place.

The incorporation of HEMA was conducted at 5 different levels, starting at 0.5% (figure 5.36). This was done since already an incorporation level of 1% produced a strong compatibilising effect. HEMA is known[308] to form a random statistical copolymer with styrene when it is polymerised by free radical initiation. The primary hydroxyl group was expected to react with TMXDI. Thus, it was not surprising that HEMA was readily incorporated into both networks. At 2.5% HEMA incorporation, only one transition peak was observed (figure 5.36(d)). The transition peak was located at 63°C, roughly intermediate between the PUR (-3°C) and PS (139°C) transitions of the 60:40 PUR/PS IPN. At 5% the transition peak became narrower and increased in size from a loss factor of 0.63 for the 2.5% to 0.78. At 10% HEMA-incorporation the transition peak decreased slightly in height and shifted to a higher temperature (78°C). The latter was believed to have been the effect of a higher crosslinking density in the 10%-grafted IPN.

TMI was also found to be very effective in increasing the phase mixing in the 60:40 PUR/PS IPN (figure 5.37). Already a 1 % TMI-incorporation produced a pronounced inward-shift of both transition peaks. The PUR transition shifted from -3°C to 13°C and the PS from 139°C to 128°C. Also, the inter-transition values increased considerably from a loss factor value of 0.16 to 0.23. At an incorporation level of 2.5% TMI, the transitions of the respective homonetworks could not be resolved any more. A very broad transition region was obtained at this TMI level. The almost rectangular shape of the DMTA data indicated the presence of a microheterogeneous system. This morphology and further TMI-grafted IPNs will be further investigated by TEM and SEM in a subsequent section. The loss factor values were equal or greater than 0.3 for a temperature range of 80°C, from 45°C to 125°C. Thus, this grafted IPN exhibited good damping properties. At higher TMI incorporation levels

of 5 and 10%, still higher degrees of phase mixing resulted. However, these materials were less interesting for damping purposes since the temperature range over which they exhibited high damping characteristics was much narrower. The storage moduli versus temperature reflected the loss factor data (figure 5.38). While a two-step drop in modulus was observed for the ungrafted 60:40 PUR/PS IPN, the profile changed considerably with increasing TMI-incorporation. At 1% TMI, still a two-step drop in modulus was noted. However, the decrease in modulus at the PUR and the PS transitions was less pronounced and extended over a wider temperature range. At 2.5% TMI, an almost linear (on a logarithmic scale) decrease in storage modulus was observed. IPNs with higher TMI levels of 5% and 10% exhibited only a one-step drop in the storage modulus. The latter was steeper and occurred over a narrower temperature range for the 10%-grafted IPN than for the 5%-grafted counterpart. Furthermore, a general increase in the storage modulus plateau after the PS transition was observed. While no significant differences were observed for TMI incorporations of 0, 1 and 2.5%, the storage moduli after the PS transition were significantly higher for the 5 and 10%-grafted IPNs. A similar phenomenon of increasing storage moduli in the rubbery plateau was observed with increasing crosslinking density in the PUR homonetworks (section 4.2). This indicated that inter-network grafting increased the apparent crosslinking density in the 60:40 PUR/PS IPN. The loss moduli versus temperature plots exhibited trends similar to the storage moduli (figure 5.39). For extensional layer damping the loss modulus is of major importance[7,22,150], since both stiffness (a high storage modulus) and high energy dissipation (high loss factor values) are needed. While the 2.5% TMI-grafted IPN exhibited high loss factor values over a broad temperature range, no broad temperature range with high loss moduli was obtained. The 10% TMI-grafted IPN exhibited the best property profile for extensional layer damping applications with high values for the loss modulus spanning a temperature range of about 50°C, from -5°C to 45°C. In this temperature range, the product of the loss factor and the storage modulus (which amounts to the loss modulus) was higher than the loss moduli below the Tg of the IPN. Thus, it was believed that the 10% TMI-grafted 60:40 PUR/PS IPN might be a high damping material in this temperature region for extensional layer damping applications.

Efficiency of grafting agents. It was found that only some of the grafting agents caused an inward shift of both the PUR and the PS Tg values. This indicated that not all grafting agents were actually incorporated into both polymer networks. Both HEMA and TMI were very efficient grafting agents and resulted in the grafted IPNs exhibiting a single loss factor peak in the DMTA data. A single loss factor peak was obtained even with small quantities such as, for example, with a 2.5% HEMA incorporation. The efficiency of such small quantities was further proof of the observation that no significant inter-network grafting was introduced by the use of BED, OED and PBD.

Comparing TMI (MW 201 g/mol) to HEMA (MW 130 g/mol) revealed that the latter was a considerably more efficient grafting agent, even when considering the difference in molar masses. At a HEMA level of 2.5%, a much narrower single transition peak was observed than with 5% TMI. HEMA incorporations above 1% also resulted in transparent films, while the 2.5% TMI-grafted IPN sheet was translucent. The fact that TMI was less effective than HEMA was a result of lower percentage of TMI being incorporated into both networks. The latter could be because of the NCO functionality or the vinyl group or both did not react as readily with the respective polymer networks than did the functional groups of HEMA. Since an NCO/OH ratio of 1.1 was used throughout the study, some excess NCO remained unreacted in the IPNs. The reactivities of the NCO groups of TMXDI and TMI are known[259] to be very similar. Thus, in the absence of secondary PUR reactions with the urethane link, roughly 9% of the TMI NCO groups might not have reacted with the PUR network. However, the difference in efficiency between HEMA and TMI was clearly greater than 9%. Thus, the vinyl group in TMI must have also been a contributing factor to the poorer grafting efficiency. When TMI is polymerised[260] with acrylate or methacrylate monomers, it enters the polymer at a faster rate than the acrylic compound does. However, if styrene is the comonomer, styrene enters the polymer faster than does TMI[260]. This might have resulted in some TMI vinyl groups remaining unreacted at the end of the polymerisation. A combination of both factors could explain the reduced grafting efficiency of TMI compared to HEMA. However, while HEMA was the most efficient grafting agent, no such broad loss factor transition range was obtained as with TMI. At 1% HEMA incorporation a major part of the transition curve shifted towards the higher temperature PS transition. This

might have been attributed to the way in which it was incorporated into the PUR network. TMI with the pendent NCO functionality was very likely to have been linked directly to a polyol soft segment. HEMA, with the OH moiety, on the other hand, was in any case linked to a rigid diisocyanate i.e. the PUR hard segment. While no interactions are known to exist between the PPG polyol and PS, some interactions between the PUR hard segment and the PS are[290] possible. Amongst these interactions in the present study might have been π - π electron interactions[287] between the TMXDI and the PS phenyl rings and hydrogen bonding between the urethane N-H and the π - orbitals of the PS phenyl rings[290]. Thus, additional interactions between the PUR hard segment and the PS might have contributed to a decrease in breadth and shift to higher temperatures of the transition region.

BED, OED and PBD were not incorporated into the PS network to a significant extent. This was due to the fact that only double bonds in a certain environment are prone to react with PS under the given reaction conditions. An indication of whether a particular unsaturated monomer is capable of performing well as a grafting agent is given by its method of polymerisation[285]. A monomer which itself can be polymerised via the free radical mechanism should perform well as a grafting agent. A number of monomers with unsaturation cannot be polymerised via the free radical mechanism. This is the case of monomers[309] with symmetrically distributed unsaturations, monomers carrying two bulky substituents and of allylic monomers due to resonance stabilisation. Also, monomers do not polymerise for thermodynamic reasons such as, for example, α-methylstyrene. Some of these monomers that cannot react with their own radicals still can react with another monomer yielding a copolymer, and, therefore, still could be useful as grafting agents. One example for the latter was TMI. For unreactive unsaturated compounds grafting can be brought about by changing the reaction conditions. By conducting the polymerisation under more severe reaction conditions such a synthesis under high pressure and at high temperatures combined with a suitable catalyst such as, for example, dicumyl peroxide could have resulted in grafting with the less reactive grafting agents. The fact that styrene was the co-monomer could also have played some role. In free radical polymerisations, the reactivity of the monomer is influenced by resonance stability, polarity and steric effects[177]. Styrene forms a very stable radical due to the strong electron withdrawing effect of the phenyl ring. Thus, the electron is delocalised over the entire ring,

resulting in a high resonance stabilisation. However, if the monomer is highly reactive to form a radical, the radical is relatively stable and unreactive. Consequently, the formed styrene radical is unreactive and further chain propagation is comparatively slow. This applies especially to compounds whose monomer is not reactive, i.e. where the radical is not stabilised. Consequently, with a less stabilised, and, thus, more reactive radical and/or different reaction conditions some more of the investigated grafting agents could have proved efficient.

Modulated-temperature DSC studies. The TMI-grafted 60:40 PUR/PS IPNs were investigated by M-TDSC. Figure 5.40 shows the heat capacity and the differential heat capacity versus temperature plots. The data of the ungrafted 60:40 PUR/PS IPN are shown in figure 5.40(a). For the latter well-defined PUR and PS transitions were observed at -36°C and 112°C, respectively. At 1% TMI incorporation, the PUR transition shifted to a slightly higher temperature (-32°C), while no clear transition temperature could be assigned to the PS. The same trend continued at the 2.5% TMI-grafting. The PUR transition temperature shifted to -27°C and a shoulder for the PS at 73°C was observed. The change in heat capacity of the PUR transition was less steep, but was found to occur over a broader temperature range of about 50°C. This indicated a greater compositional variation in the PUR-rich phase, but could also have resulted from variations of crosslinking densities. At 5% TMI incorporation, the main transition shifted to -23°C, while for the PS transition only a small shoulder was observed. At 10% TMI-incorporation, one broad transition was obtained at -17°C. The shoulder for the PS transition was still noticeable even though it had further decreased in size.

Thus, the M-TDSC data indicated a two-phase morphology of the TMI-grafted IPNs at all grafting levels. However, at 10% TMI-grafting a high degree of miscibility was achieved. M-TDSC seemed to be somewhat more sensitive in detecting a two-phase morphology in IPNs, since from DMTA one fairly narrow loss factor peak was observed for the 10% TMI-grafted IPN. Further comparisons of the two techniques will have to be made.

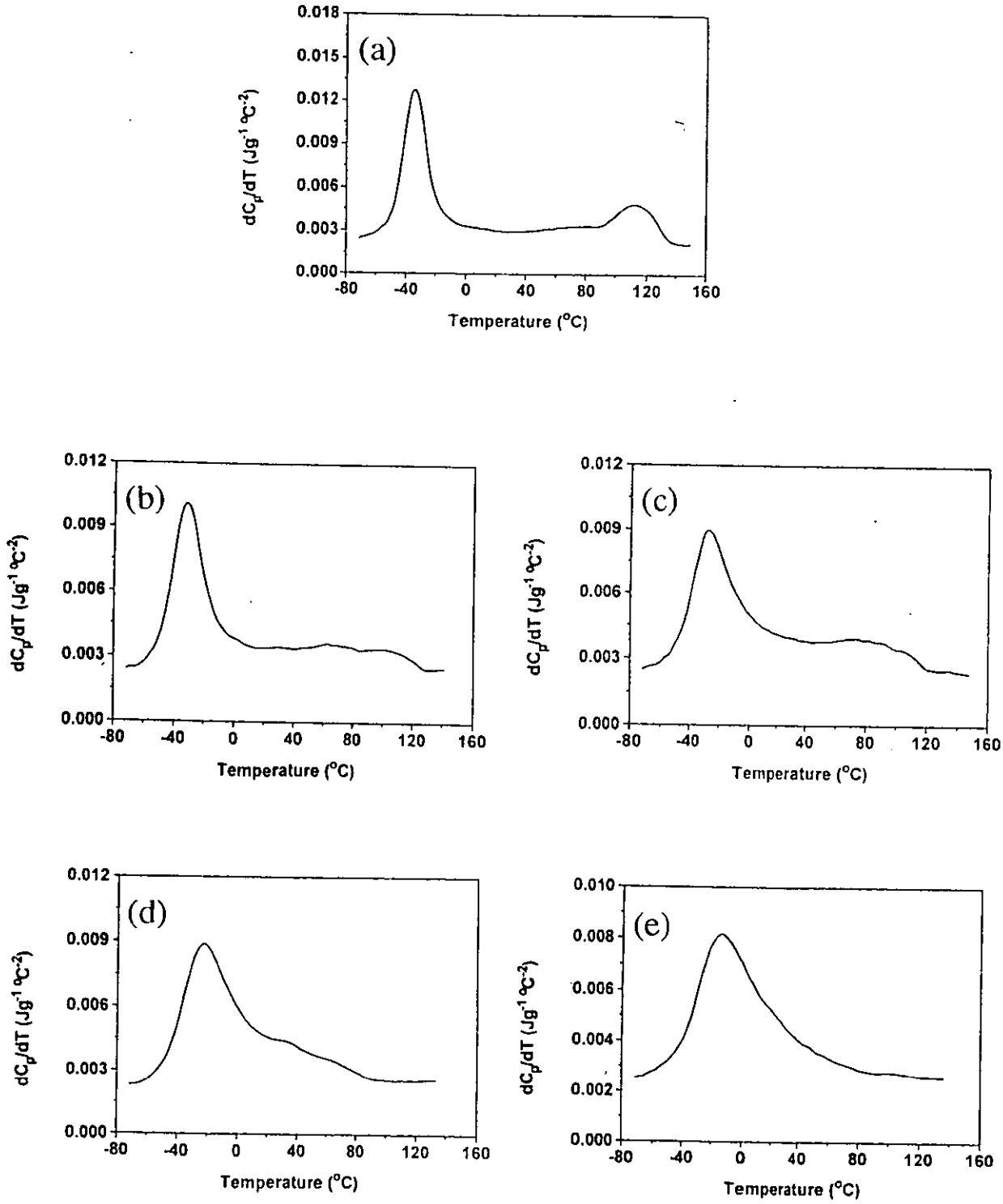

Figure 5.40 M-TDSC traces for the TMI-grafted 60:40 PUR/PS IPNs. (a) 0% TMI, (b) 1%, (c) 2.5%, (d) 5% and (e) 10%.

Stress-strain and hardness measurements. The mechanical properties of the TMI-grafted 60:40 PUR/PS IPNs were investigated by tensile testing and Shore A and D hardness measurements. The stress and strain at break, Young's modulus, the toughness index and values for Shore A and D hardness are given in table 5.5.

Table 5.5 Mechanical properties of grafted 60:40 PUR/PS IPN as a function of TMI-level.

PUR/PS IPN	Tensile properties				Hardness	
Grafting level [% TMI]	Stress at break [MPa]	Strain at break [%]	Young's modulus [MPa]	Toughness [J]	Shore A	Shore D
0	13.0	310	7	4.2	75	41
1	13.6	240	24	4.5	86	52
2.5	12.2	160	61	3.4	93	61
5	11.2	120	83	2.2	95	64
10	10.1	90	100	1.7	97	67

The stress at break decreased slightly from 13 MPa for the ungrafted to 10.1 MPa for the 10% TMI-grafted 60:40 PUR/PS IPN (table 5.5). The strain at break strongly decreased from 310% for the ungrafted to 90% for the 10% TMI-grafted 60:40 PUR/PS IPN. As a consequence, values for the toughness index also decreased considerably from 4.2 J to 1.7 J. Young's moduli on the other hand increased dramatically with increased TMI-incorporation. The ungrafted 60:40 PUR/PS IPN had a Young's modulus of 7 MPa. With an incorporation of 10% TMI, the Young's modulus increased by more than ten-fold to 100 MPa. Since hardness is related to Young's modulus the hardness values also increased strongly (table 5.5). The increase in Young's moduli and hardness values were expected because of a combination of two factors. First, as a result of inter-network grafting the crosslinking density increased which in turn led to a higher stiffness of the IPN. However, the increase in crosslink density alone could not have accounted for the high Young's moduli. The PUR network based on a PPG soft segment with the highest crosslink density had a Young's modulus of 9 MPa (section 4.2). Thus, a second very probably much more important factor must have been a change in IPN morphology. It was believed that PS

phase domains were to some extent interconnected and exhibited some phase continuity. Since PS was in the glassy state at room temperature, a pronounced increase in modulus would be expected. On the same grounds, the decrease in strain at break was expected. The slight decrease in stress at break, however, came as a surprise. One possible explanation could be that the PUR network was less well formed and less continuous. TMI has one NCO group and as a consequence terminated the PUR network. If the pendent vinyl group of the TMI did not react with the PS network, a loose end which weakened the PUR network resulted.

Morphology by TEM and SEM. From the DMTA data it was found that inter-network grafting had a profound influence on the IPN morphology. This could be confirmed with the help of the TEM and SEM studies. Again, the TMI-grafted 60:40 PUR/PS IPN series was investigated. Figures 5.41 and 5.42 show TEM and SEM micrographs of this series. The ungrafted 60:40 PUR/PS IPNs showed phase domain sizes between 30 and 300 nm (figure 5.15(d)). At 1% TMI-incorporation, the phase domain sizes decreased considerably to values of 20 - 100 nm, while some bigger domains were still present (figure 5.41(a)). The change in IPN morphology was important. Not only did the phase domain size decrease, but also a change in the PS domain shape was observed. The phase domains of the ungrafted IPNs were spherical and the phase boundaries between the PS domains and the PUR matrix were well-defined (figure 5.15(e)). For the 1% TMI-grafted IPN, the PS domains were much more irregularly shaped and the phase boundaries were no longer as well-defined. At 2.5% TMI-incorporation, an even greater change in morphology occurred. For this IPN, an almost rectangular loss factor transition profile was observed from the DMTA data (figure 5.35(c)). Clear PS phase domains were not present any more and a very fine morphology with structures in the order of 10 to 50 nm was seen (figure 5.41(c)). Both phases seemed to exhibit some degree of continuity. The unstained micrograph taken at a lower magnification of 20 k (figure 5.41(d)) indicated that some bigger PS domains (dark) were still present. However, the extremely fine morphology was also evident in this micrograph. At 5% TMI-incorporation, the morphology was even finer and no PS phase domains could be resolved any more (figure 5.41(e)).

Figure 5.41 TEM micrographs for the TMI-grafted 60:40 PUR/PS IPNs. (a)&(b) 1% TMI, (c) 2.5%, (d) 2.5%, unstained (e) 5% and (f) 10%.

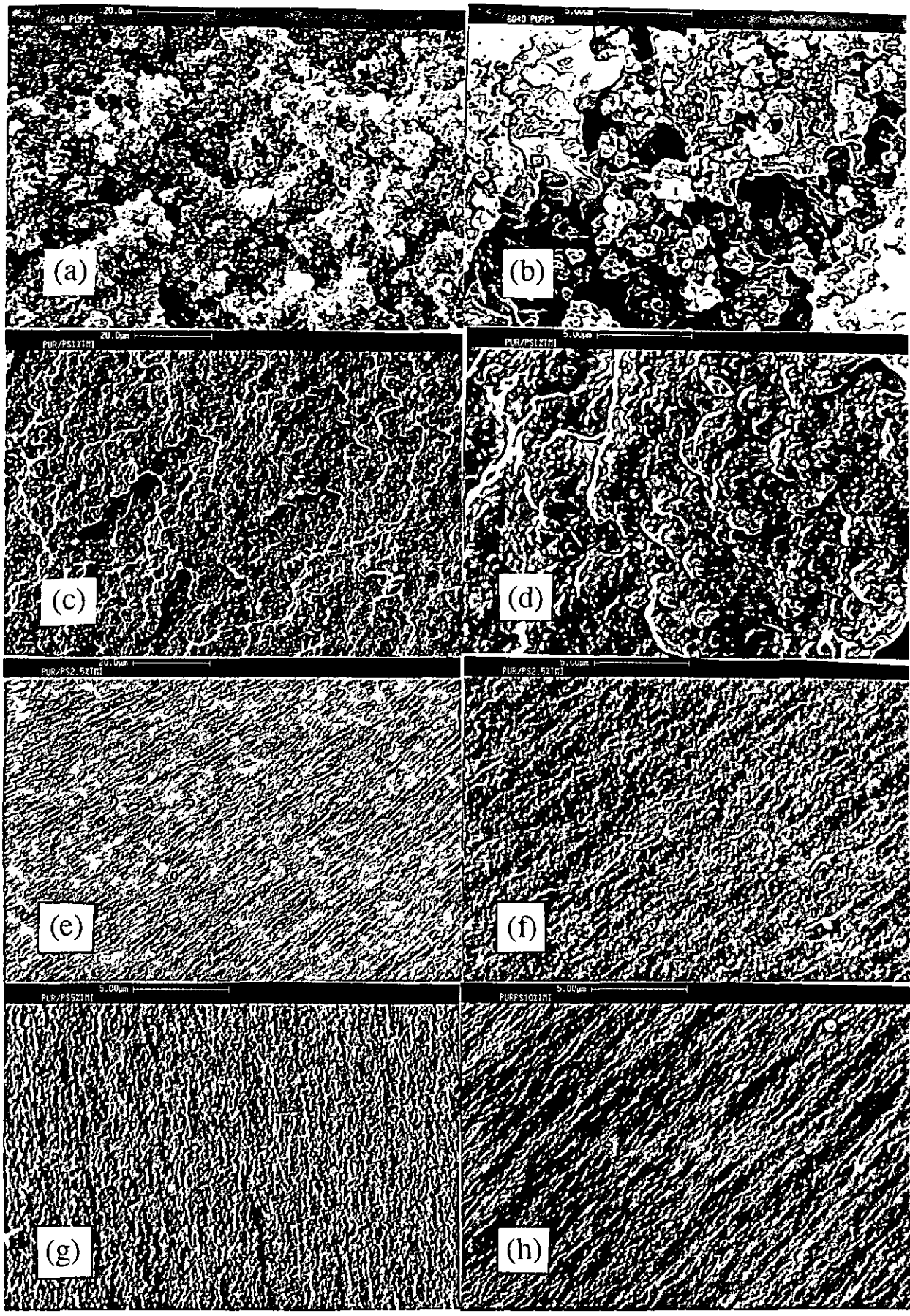

Figure 5.42 SEM micrographs for the TMI-grafted 60:40 PUR/PS IPNs. (a)&(b) 0% TMI, (c)&(d) 1%, (e)&(f) 2.5%, (g) 5% and (f) 10%.

At 10% TMI-grafting, no more phase structures could be resolved (figure 5.41(f). This was in good agreement with the DMTA data. While for the 5% grafted IPN one fairly broad loss factor peak was obtained, a narrow peak similar in breadth to a homopolymer was obtained for the 10% TMI-grafted IPN (figure 5.37). The SEM micrographs also corroborated the findings of a decrease in phase domain size and an increase in component mixing with higher levels of TMI. The ungrafted 60:40 PUR/PS IPN had a rough fracture surface (figure 5.42(a)). A higher magnification showed numerous voids of 1- 3 μ diameter (figure 5.42(b)). An important change in morphology was observed upon the incorporation of TMI. At 1% TMI, the fracture surface of the IPN became less irregular (figure 5.42(c)) and the cavities disappeared (figure 5.42(d)). At 2.5% TMI, the fracture surface further increased in smoothness (figure 5.42(e) and (f)). TMI levels of 5% and 10% produced a further increase in smoothness. From the SEM micrographs, it appeared that important changes in IPN morphology took place at TMI incorporation levels of 1% and 2.5% while at higher levels only small gains in phase mixing were observed. While both TEM and DMTA also indicated that the most important morphology changes occurred at TMI incorporation levels of 1% and 2.5%, a difference in morphology was also noted at 5% and 10% TMI incorporation.

5.5 Incorporation of Compatibilisers

Even though compatibilisers are commonly used[1,3,93] in polymer blends, no such work has been reported in the literature for IPNs. In the present study, reactive triblock-type compatibilisers with both ends incorporated into the PS network were investigated. Three compatibiliser-types were synthesised from the PUR raw materials (section 3.1.2). A urethane acrylate (UA2) was prepared from PUR precursors in a TMXDI/PPG1025/HEMA ratio of 1:2:2. The HEMA-TMXDI compatibiliser consisted of a HEMA-terminated TMXDI diisocyanate. The TMI-PPG1025 compatibiliser was a PPG1025 molecule end-tipped with TMI. These compatibilisers were investigated at the same incorporation levels as the grafting agents, at 1, 2.5, 5, and 10 weight %. They were incorporated into a 60:40 PUR/PS IPN which was crosslinked at a PPG1025/TMP ratio of 3:1 and 5 mol % DVB.

DMTA studies. The loss factor versus temperature data of 60:40 PUR/PS IPNs with the three different compatibilisers are shown in figures 5.43-45. The storage moduli versus temperature for the 60:40 PUR/PS IPN with different TMI-PPG1025 levels are given in figure 5.46. The loss factor versus temperature data of the IPNs with incorporated UA2 compatibiliser showed important changes at high compatibiliser incorporation levels. The location of the PUR transition remained at temperatures of about -3°C. The only exception was the 5% compatibilised IPN which had a somewhat higher PUR Tg of 3°C. However, a clear trend of decreasing PUR loss factor peak heights was observed with higher levels of compatibilisers. The 60:40 PUR/PS IPN without compatibiliser had a loss factor value of 0.62, whereas the IPN containing 10% compatibiliser had a much lower value of 0.27. The PS transition shifted continually to lower temperatures. The PS Tg values were at temperatures of 140, 137, 131, 121 and 103°C for UA2 compatibiliser incorporation levels of 0, 1, 2.5, 5 and 10 weight %, respectively. The PS transition heights were at loss factor values about 0.4, with only the IPN containing 10% UA2 exhibiting a higher value of 0.50. This shift of the PS transition to lower temperatures was the more pronounced the more compatibiliser was incorporated into the IPN. However, even at an incorporation level of 10%, two clearly separate transitions for the PUR and the PS were observed. Also, the inter-transition region loss factor values did not increase significantly.

With the incorporation of HEMA-TMXDI compatibiliser, no significant change in Tg location was observed for either of the two transitions (figure 5.43). The PUR loss factor peak height decreased continually with increasing compatibiliser incorporation. The PS transition had a tendency to increase with higher compatibiliser levels. The latter indicated that the HEMA-TMXDI compatibiliser was mainly incorporated into the PS network. Besides slight inconsistencies at 5% HEMA-TMXDI incorporation, no change in the inter-transition height could be noticed. The PUR transition is principally caused by the soft segment. It was, thus, not too surprising that no transition shift was observed since this compatibiliser did not contain any polyol moiety.

Figure 5.44 shows the loss factor versus temperature data for the 60:40 PUR/PS IPN with various levels of TMI-PPG1025 compatibilisers.

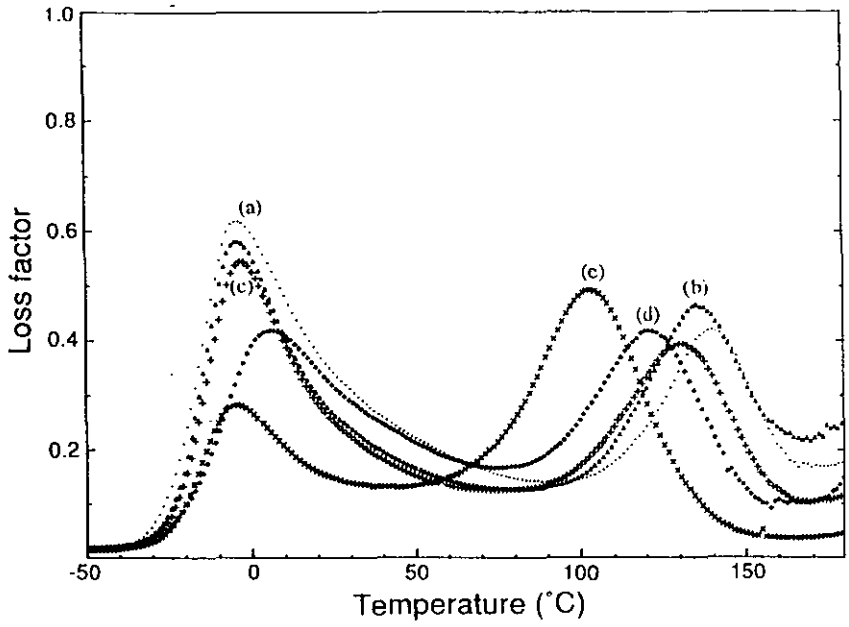

Figure 5.43 Loss factor versus temperature data for the 60:40 PUR/PS IPNs with different levels of UA2 compatibilisers. (a) 0% UA2, (b) 1%, (c) 2.5%, (d) 5% and (e) 10%.

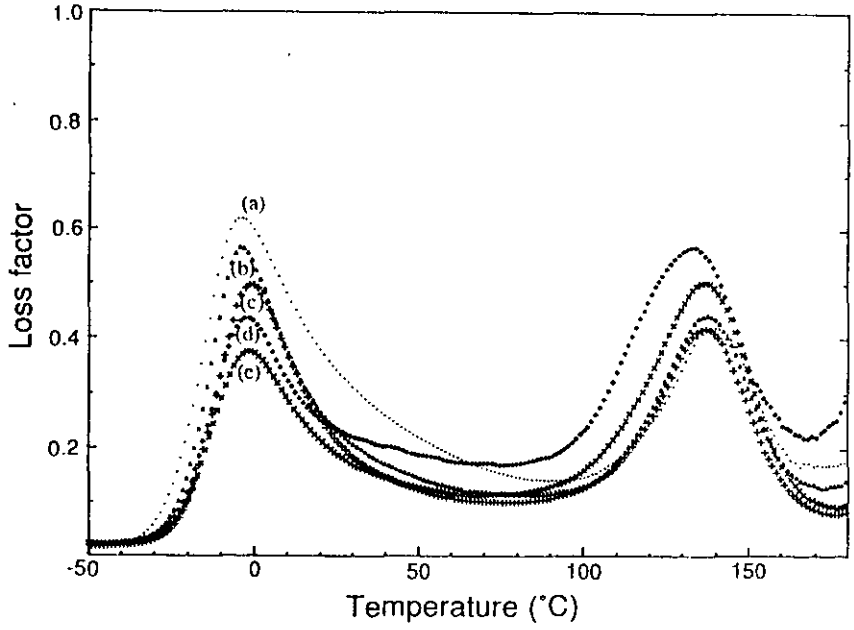

Figure 5.44 Loss factor versus temperature data for the 60:40 PUR/PS IPNs with different levels of TMXDI-HEMA compatibilisers. (a) 0% TMXDI-HEMA, (b) 1%, (c) 2.5%, (d) 5% and (e) 10%.

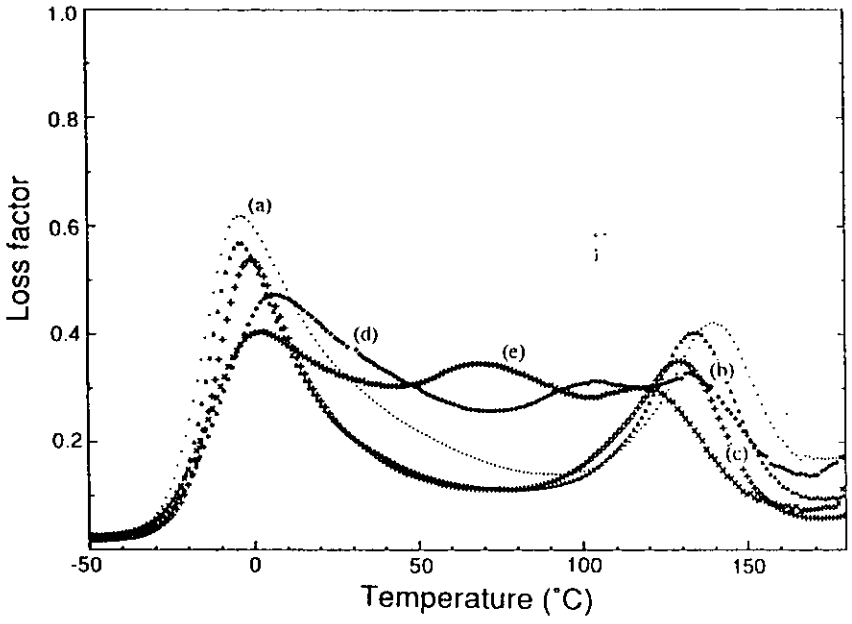

Figure 5.45 Loss factor versus temperature data for the 60:40 PUR/PS IPNs with different levels of TMI-PPG1025 compatibilisers. (a) 0% TMI-PPG1025, (b) 1%, (c) 2.5%, (d) 5% and (e) 10%.

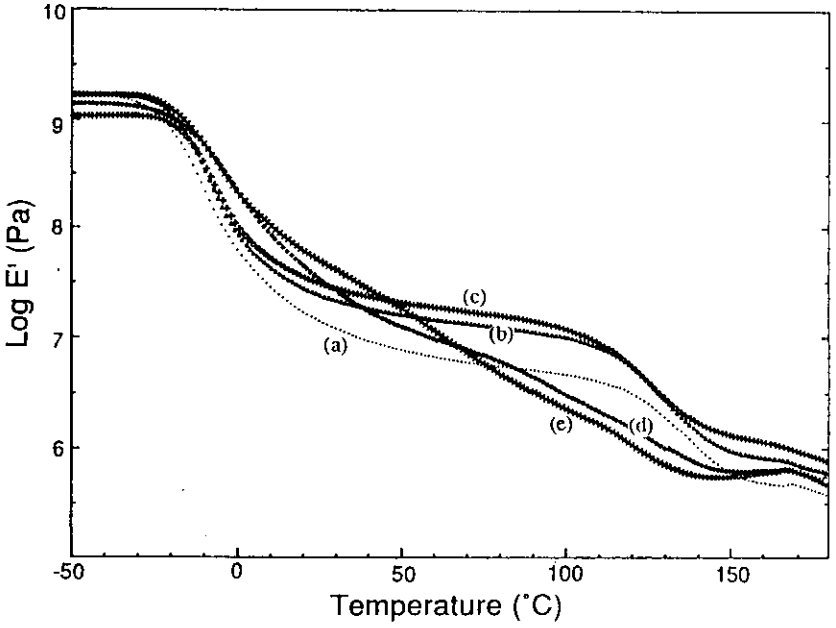

Figure 5.46 Storage moduli versus temperature for the 60:40 PUR/PS IPNs with different levels of TMI-PPG1025 compatibilisers. (a) 0% TMI-PPG1025, (b) 1%, (c) 2.5%, (d) 5% and (e) 10%.

At low incorporation levels of 1 and 2.5%, only a moderate inward-shift of both the PUR and the PS transitions was noted. At 2.5% TMI-PPG1025-incorporation, the Tg values of PUR and PS were at 0°C and 129°C, respectively, which compared to -3°C and 140°C for the uncompatibilised IPN. The inter-transition loss factor values remained low at 0.15. However, at a 5% TMI-PPG1025 incorporation, the loss factor profile differed greatly from the previous two compatibiliser-types. The PUR transition shifted inwards to 6°C. The PS transition split into two parts, with one part exhibiting a transition at 100°C and the other part at 130°C. However, more importantly, the inter-transition values increased considerably from a loss factor value of 0.15 to a value of 0.26. At a 10% TMI-PPG1025 incorporation level, three transition peaks were observed. One of a predominantly PUR-rich phase at 2°C, one transition at 67°C and the third transition stemming from a predominantly PS-rich phase at 118°C. As a result of the appearance of the third transition intermediate between those of the PUR and PS, very high inter-transition loss factor values of greater than 0.3 were observed. The transition at 67°C must have been a result of the incorporation of the 10% TMI-PPG1025 compatibiliser. However, its origin was not clear. It could have been that the formation of a significant amount of interface between the PS domains and the predominantly PUR matrix was encouraged by the compatibiliser. In theory, the third transition might also have mainly consisted of compatibiliser reacted with itself. The latter was highly unlikely though since it is known[260] that the vinyl group of TMI is not able to form a homopolymer by free radical initiation. Most recently a different explanation[310-312] for an intermediate damping peak in polymer composites was given. Hiltner and co-workers[310] believe that the intermediate peak is purely of mechanical origin and is a general feature of co-continuous polymer blends. After the lower Tg of polymer 1 the storage modulus (E'_1) and the loss modulus (E''_1) change rapidly with temperature. The loss factor values increase since E'_1 falls more rapidly than E''_1. In contrast, the storage (E'_2) and loss (E''_2) moduli of polymer 2 change very little with temperature in this region. However, the storage modulus of the composite can not drop below the modulus of the glassy layer, E'_2, although the ability to absorb energy is still determined[310] to a great extent by E''_1. The latter continues to decrease. Thus, the loss factor ceases to increase, passes through a maximum and starts to decrease. In the present study, the mechanism proposed by Hiltner and co-workers[310] was not very likely to have

occurred because of the crosslinked nature of the PUR network. The loss factor versus temperature data for the PUR homonetwork did not exhibit an increase in loss factor values after the soft segment transition at -5°C (section 4.1). This was a result of its crosslinked nature. The PUR E' did not drop as dramatically to very low values as generally happens in uncrosslinked polymers. Thus, as a consequence of the prolonged rubbery plateau due to crosslinking, the loss factor values remained very low up to temperatures higher than 120°C. If the crosslinking of the PUR had been impeded to some extent because of the incorporation of 10% TMI-PPG1025 compatibiliser, such an intermediate mechanical damping peak would have been possible. However, incomplete crosslinking would have resulted in a different loss factor profile as was seen in the crosslinking study in section 5.3 for the semi-2 60:40 PUR/PS IPN. Thus, the most likely explanation of the third intermediate damping peak remained that it resulted from an interface layer of increased thickness between the PS-rich domains and the PUR-rich matrix. The pronounced difference in the loss factor profile between the 1, 2.5% and 5 and 10% compatibiliser incorporation was difficult to explain. The constant decrease in the PUR transition peak height indicated that the TMI-PPG1025 compatibiliser was predominantly incorporated into the PS network. At low incorporation percentages, most compatibiliser molecules might have been located within the PS-rich domains. It was, perhaps, only at 5% and higher levels that a sufficient amount of compatibiliser moieties were located at the PS phase domain boundaries. These could then act as compatibilisers and increase the interface area. Also, in a radical copolymerisation of styrene and TMI, TMI is known[260] to enter the forming copolymer at a significantly lower rate than does styrene. Thus, any unreacted traces of vinyl monomer at the end of the polymerisation will be foremost the vinyl functionality of TMI. As a consequence, not all of the compatibiliser molecules might have actually incorporated into the PS network. If the latter were true, a way of improving the efficiency of the compatibiliser would be to use isocyanatoethyl methacryate (IEM)[313] as the end-capping agent for PPG1025. IEM is known[313] to be more reactive in radical polymerisations, and, thus, will enter the copolymer at a faster rate than styrene in a copolymerisation of these two monomers. The storage moduli versus temperature of the TMI-PPG1025-compatibilised 60:40 PUR/PS IPN are shown in figure 5.45. The IPNs with 0, 1 and 2.5% TMI-PPG1025 showed a two-step drop in storage modulus. Reflecting the loss factor profile, an

almost linear (on a logarithmic scale) drop in storage modulus was observed for 5 and 10% incorporation. With the incorporation of 10% TMI-PPG1025 compatibiliser into the 60:40 PUR/PS IPN, the loss factor values were greater than 0.3 over a temperature range of 130°C. Thus, a material with high damping characteristics was obtained. This material was investigated further by M-TDSC and TEM in order to study the nature of the intermediate damping peak and to elucidate the morphology of this high damping IPN.

Modulated-temperature DSC studies. The M-TDSC data of the 60:40 PUR/PS IPNs without compatibiliser are shown in figure 5.40(a). The M-TDSC data for 0, 5 and 10% TMI-PPG1025 compatibilised 60:40 PUR/PS IPNs are shown in figure 5.47. The PUR transition in form of the peak of the derivative heat capacity versus temperature shifted to slightly higher temperatures for higher TMI-PPG1025 compatibilisation levels.

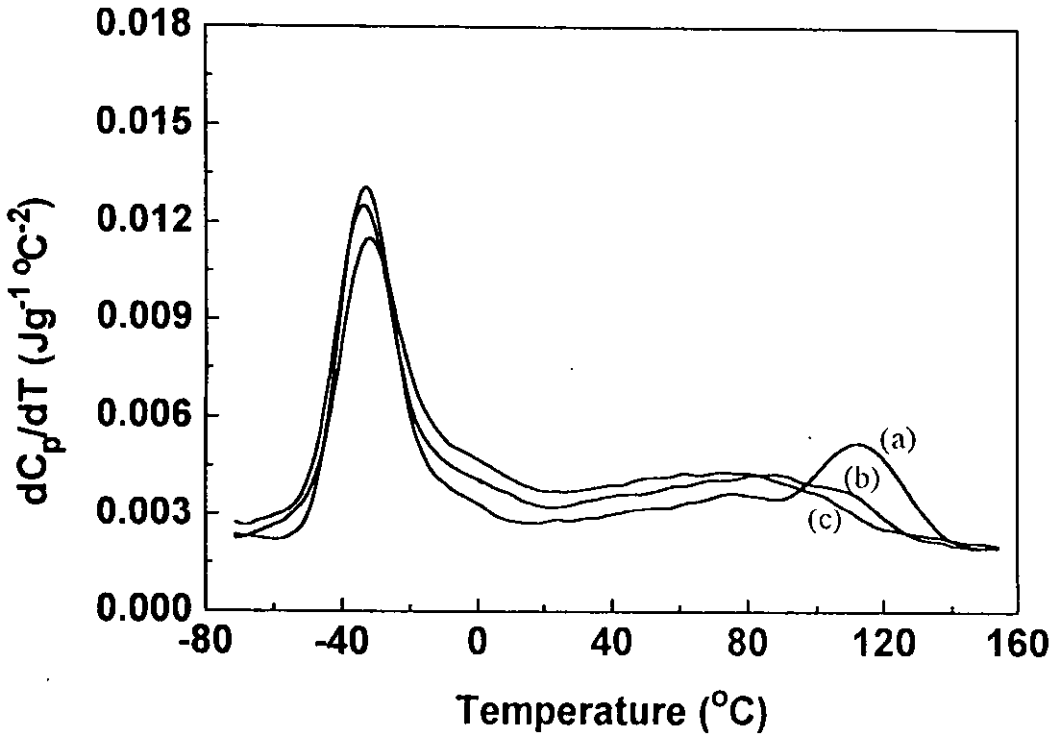

Figure 5.47 M-TDSC data for the 60:40 PUR/PS IPN with various levels of compatibilisers. (a) 0% TMI-PPG1025, (b) 5% and (d) 10%.

The peak height slightly decreased which indicated that the transition extended over a broader temperature range. The PS transition shifted to lower temperatures. The shifts were more pronounced than those of the PUR. However, it was difficult to assign a clear PS Tg because of the breadth of the PS transitions. No clear transition peak for the third intermediate damping peak which had been observed from the DMTA data could be seen.

Morphology by TEM. The morphology of the IPNs with 5 and 10% TMI-PPG1025 compatibiliser were compared to the uncompatibilised 60:40 PUR/PS IPN (figure 5.48). The PS phase domains of the uncompatibilised 60:40 PUR/PS IPN were in the order of 30 - 300 nm (figure 5.48(a)). The phase domains decreased significantly for the IPN with 5% TMI-PPG1025 compatibiliser (figure 5.48(b) and (c)). Most domains were in the order of 30 - 100 nm, yet some larger PS domains of 200 - 300 nm still remained. The unstained micrograph of the same IPN confirmed the phase domain sizes and distribution. However, it did not provide any further information about the IPN morphology (figure 5.48(d)). At 10% TMI-PPG1025, the phase domain sizes decreased further to 20 - 80 nm (figure 5.48(e)). The shape of the phase domains was more irregular and the phase boundaries were less clear than for the uncompatibilised IPN. Also, it appeared that the PS phases were more interconnected in the 10% compatibilised than in the uncompatibilised IPN. In addition to a dark PUR-rich matrix and white PS-rich domains, no third phase was observed which could have been responsible for the intermediate damping peak. It was, therefore, believed that the interface between the less-well defined PS-rich domains and the PUR-rich matrix had increased in thickness. The morphology of the 10% TMI-PPG1025-compatibilised 60:40 PUR/PS IPN had some resemblance to the 1% TMI-grafted IPN (figure 5.41(b)). The latter had slightly smaller phase domains, but the PS domains in both materials had a fairly irregular shape and ill-defined interface area. The PS phase domains were not surrounded by a dark osmium tetroxide stained shell of high purity PUR either in the 1% TMI-grafted or in the 10% TMI-PPG1025-compatibilised IPN. This might have indicated the presence of an interface area consisting of a compositional mixture of PUR and PS.

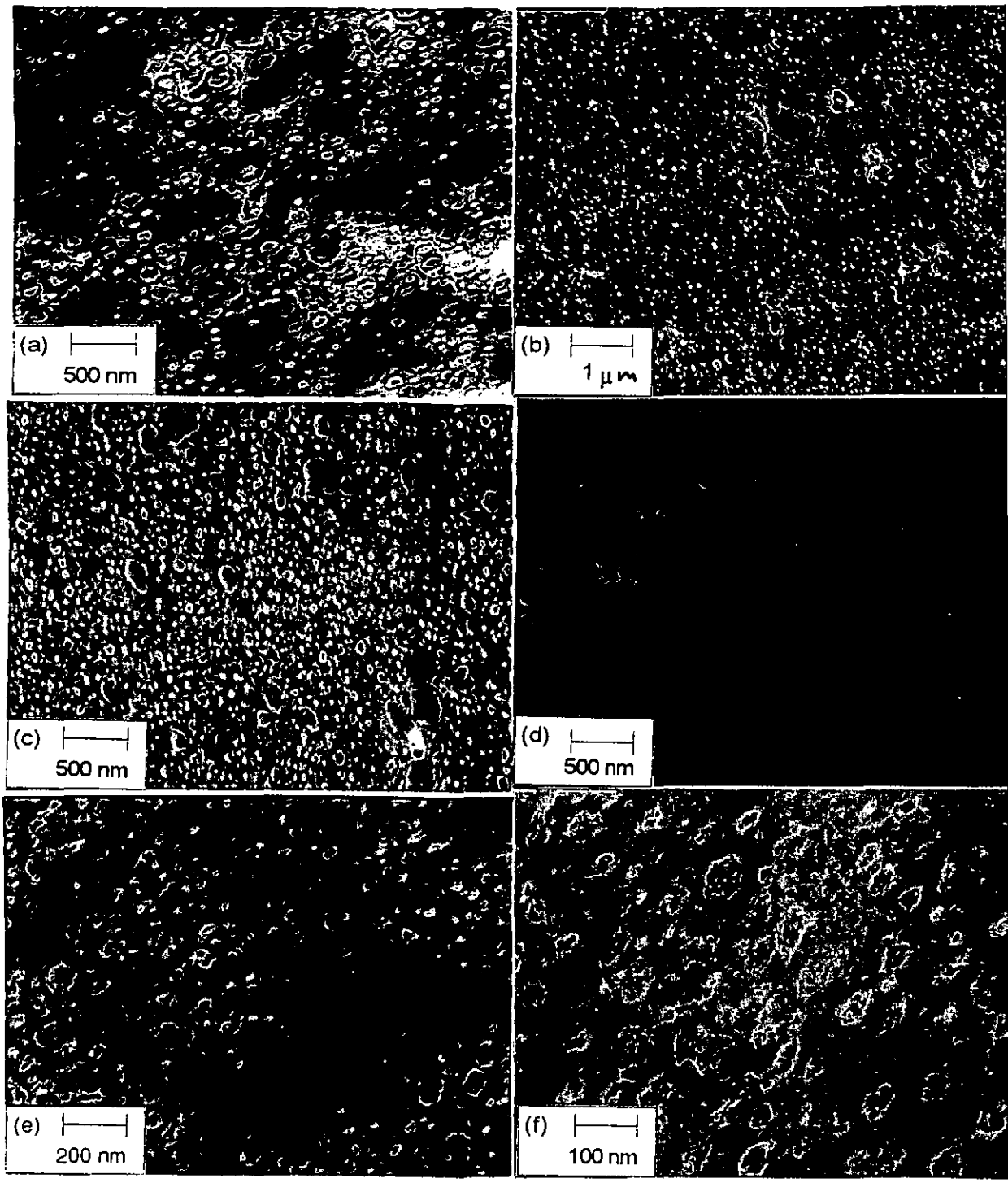

Figure 5.48 TEM micrograph for the 60:40 PUR/PS IPNs with different levels of TMI-PPG1025 compatibilisers. (a) 0% TMI-PPG1025, (b)&(c) 5%, (d) 5%, unstained and (e)&(f) 10%.

However, the 1% TMI-grafted IPN exhibited only two transition peaks in the DMTA spectrum. This might have indicated that if an interface area existed, it was not of a significant thickness and to small to exhibit its own Tg (smaller than 10 nm). The transition shape of the 10% TMI-PPG1025-compatibilised IPN as seen from the DMTA data had more similarity with the 2.5% TMI-grafted IPN. Even though with both an almost rectangular transition profile was obtained, there existed considerable differences in the respective IPN morphologies. The 2.5% TMI-grafted IPN showed a much finer structure whereas in the compatibilised IPN at least two separate phases were noted.

5.6 Introduction of Ionic Interactions

A great number of studies[314,315,316] have been devoted to ionomers based on sulfonated polystyrene, poly(phenylene) oxide and segmented polyurethanes. Fewer studies have been reported[143] in the literature with regard to the improvement in miscibility in polymer blends[145] and IPNs[143,144,146] by introducing opposite charged groups into the polymer backbone. The most commonly used[317] anionic species contain either carboxylate or sulphonate groups. The former are typically prepared by co-polymerisation of acrylic or methacrylic acid (MAA) with some co-monomer by free radical polymerisation[143] while the latter are more commonly prepared by functionalisation of a preformed polymer[318]. Because of the simultaneous one-shot polymerisation route for the IPNs, only the incorporation of potentially charged groups (MAA) was practicable in the present study. The ionomer properties are influenced[316] by various factors notably ion content, type and position of ionic group, type of polymer backbone and type of counter ion. Most commonly inorganic cations such as alkali and transition metals are used as counter ions. In the present study, an organic molecule, a tertiary amine, that was incorporated into the PUR network was selected for neutralisation of the MAA. Two types of structures of ionomers have been reported[319]. Ionic aggregates termed multiplets consist of small numbers of associated ion-pairs that are dispersed in a low-polarity matrix. If the multiplets are close enough together for these regions of restricted mobility to overlap, larger regions of restricted mobility are formed. When such a region is large enough to exhibit its own Tg and behaves as a separate phase, it is termed a cluster[315]. Aim of the present study was to use ionic interactions to control IPN miscibility in order to

obtain a semi-miscible morphology with high damping characteristics. Because of the constraints of time no detailed study into the structure of the ionic aggregates could be undertaken. Also, studying the ionic aggregates in PUR ionomers is difficult[315] because the ionic groups are not placed at random intervals along the polymer backbone. Further complications are the PUR phase segregation into hard and soft segments and possible crystallinity.

Thus, the tertiary amine, N-methyldiethanolamine (MDEA), was incorporated into the PUR network while MAA was copolymerised with the styrene monomer. Incorporation of the agents was conducted at 0.5, 1, 2, 2.5 and 3 MAA weight % levels. The MAA weight percentages were taken with respect to the total component weight and the equivalent moles of MDEA (MW 119) added to result in a ratio of potentially opposite charged groups of 1:1. Two compositions were studied, the 60:40 and the 70:30 PUR/PS IPN. At 3 weight % in the 70:30 composition, the highest MAA (MW 86) incorporation corresponded to 12 mol % MAA in the PS. The success of this method depended on the transfer of the carboxylic acid proton to the tertiary amine base to result in the formation of an ion pair. The schematic interaction between MDEA and MAA is shown in figure 5.49.

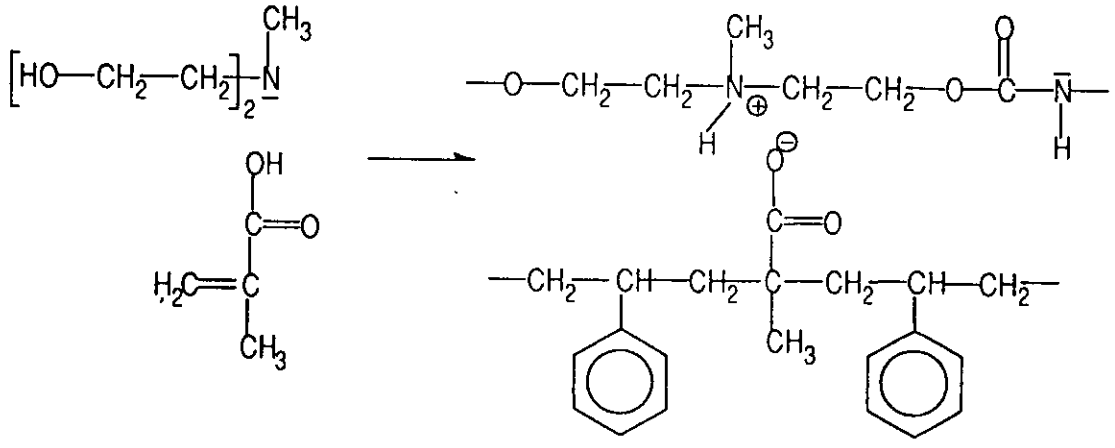

Figure 5.49 Interaction of tertiary amine (MDEA) and pendent carboxylic acid groups (MAA).

Values for the acidity constant (K_a) or the negative power of 10 of the acidity constant (pK_a) were not readily available for MDEA and MAA. Also, these pK_a values are determined[320] in water. It is known[316] that aqueous pK_a values could have been at best indicative, since acidities determined in aqueous media cannot be

extrapolated with certainty to organic media. Thus, a preliminary experimental study was undertaken in order to ascertain that this neutralisation reaction occurred. Equimolar amounts of MDEA and MAA were weighed into a glass bottle and mixed at room temperature under high stirring. An immediate strong exothermic reaction indicated that proton transfer was achieved. Five minutes after the initial mixing the glass bottle had cooled down to room temperature indicating that the neutralisation reaction was completed. Thus, it was decided that no change to the standard preparation procedure was necessary. All components were combined, mixed at high speed for five minutes, degassed and subsequently moulded (section 3.3.2).

DMTA studies. DMTA studies of ionomers can be used to characterise indirectly their microstructure, to establish structure property relationships and to determine their damping characteristics. The formation of an ionomer results[317] in three important changes in the dynamic mechanical properties of a polymeric material. First, the Tg generally increases with increasing ionisation. This is a result of the reduced polymer backbone mobility because of the formation of ionic crosslinks. Second, an extended rubbery plateau modulus above Tg is observed, again because of the ionic network. Third, a high temperature mechanical loss peak is observed above Tg which is due to motion in the ion-rich phase. Thus, miscibility and damping characteristics of the ionic IPNs were investigated by DMTA. Figure 5.50 shows the loss factor versus temperature data for the 60:40 PUR/PS IPN composition at various ionic charge group levels. The loss factor and the storage and loss moduli for the 60:40 PUR/PS IPN with 3% ionic groups are shown in figure 5.51. For the 70:30 PUR/PS of different levels of ionic groups the loss factor and storage modulus versus temperature data are shown in figures 5.52 and 5.53.

The 60:40 PUR/PS IPN with different levels of MAA and equivalent MDEA ionic groups showed significant changes in the loss factor versus temperature profile (figure 5.50). The loss factor data for 0 and 1% ionic groups were very similar (figure 5.50(a) and (b)).

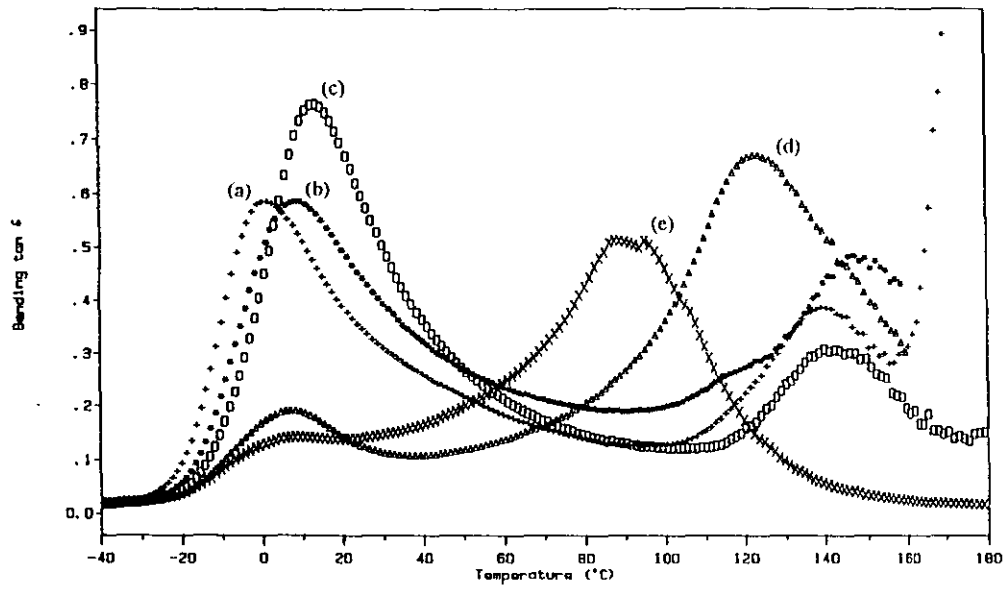

Figure 5.50 Loss factor versus temperature data for the 60:40 PUR/PS IPN at various levels of MAA weight percentages and MDEA equivalents. (a) 0%, (b) 0.5%, (c) 1%, (d) 2% and (e) 3%.

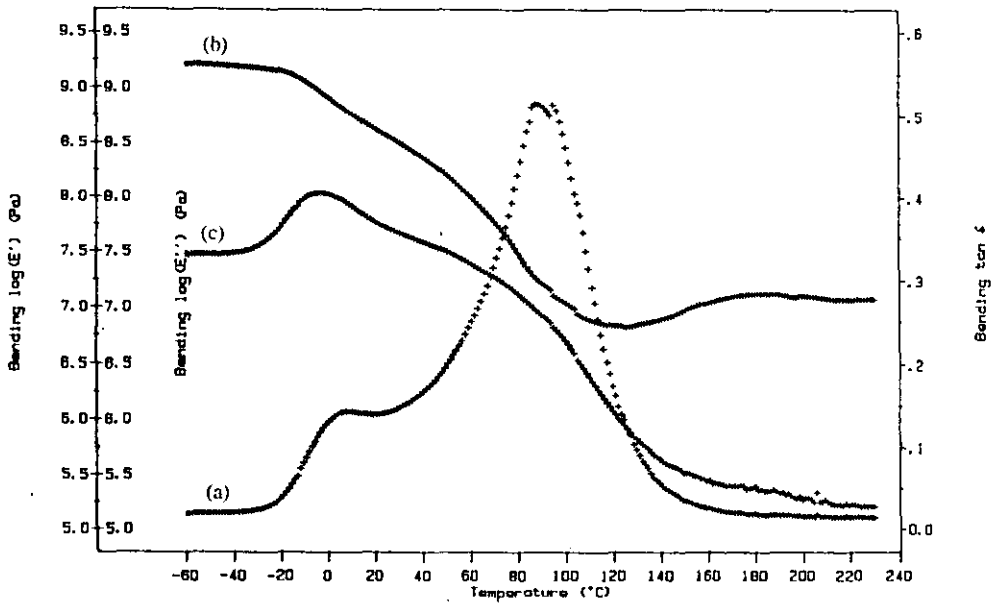

Figure 5.51 Loss factor (a), storage modulus (b) and loss modulus data (c) versus temperature data for the 60:40 PUR/PS IPN at 3% MAA weight percentages and MDEA equivalents.

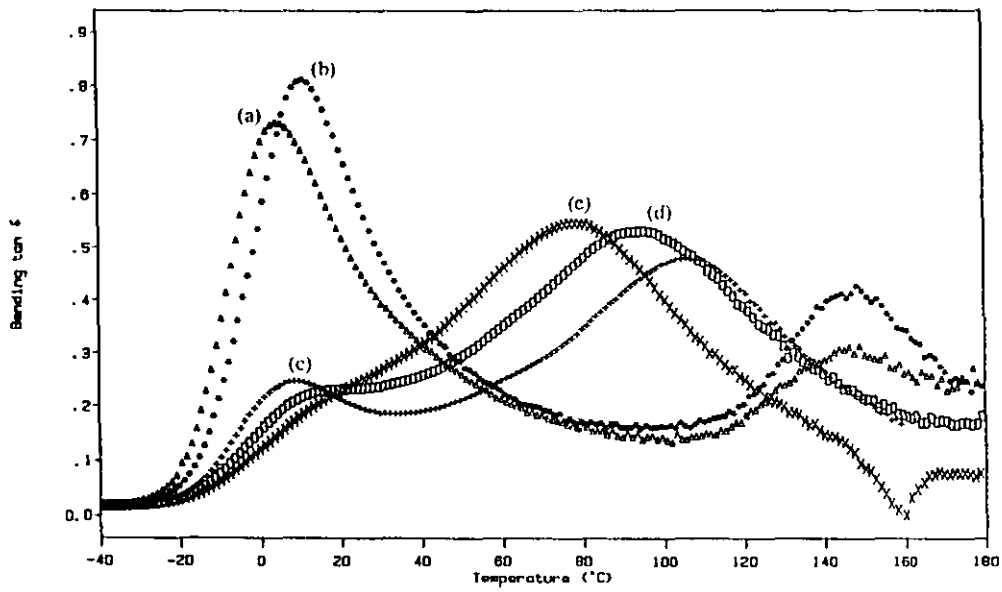

Figure 5.52 Loss factor versus temperature data for the 70:30 PUR/PS IPN at various levels of MAA weight percentages and MDEA equivalents. (a) 0%, (b) 1%, (c) 2%, (d) 2.5% and (e) 3%.

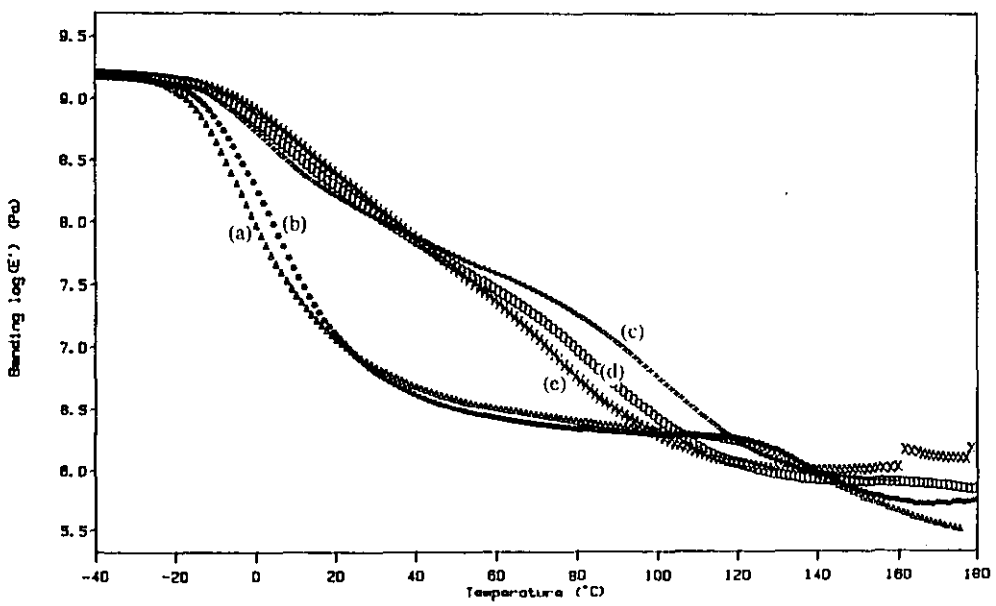

Figure 5.53 Storage moduli versus temperature data for the 70:30 PUR/PS IPN at various levels of MAA weight percentages and MDEA equivalents. (a) 0%, (b) 1%, (c) 2%, (d) 2.5% and (e) 3%.

At 1% incorporation, the PUR transition shifted to a slightly higher temperature (11°C) and increased in height while the PS transition slightly decreased in height. At 2% incorporation of ionic groups, a dramatic change in the peak shape took place. The PUR transition, while still being roughly at the same location (6°C), decreased by a factor of 4 to a loss factor of 0.19 compared to 0.80 for the IPN with 1% ionic groups. The PS transition on the other hand shifted to a lower temperature (120°C) and increased considerably in size (0.68). At a level of 3% ionic groups, the PUR transition remained at the same temperature (6°C) and slightly decreased in size to 0.13. No more two transition peaks were observed, but the PUR transition figured as a shoulder to the PS transition. The latter further decreased in size to 0.50 and shifted strongly inwards to 89°C. The fact that a pronounced PUR shoulder was still present at 3% ionic incorporation could be explained by the site of the ionic interactions in the PUR. The tertiary amine group was incorporated into the PUR hard segment. Thus, the interactions that were introduced by the MAA increased mainly the miscibility of the P(S-MAA) with the PUR hard segment. This might explain why the PUR soft segment transition still remained at a low temperature while a strong shift of the entire PS transition to lower temperatures was observed. Figure 5.51 shows the loss factor, storage modulus and loss modulus data versus temperature for the 60:40 PUR/PS IPN at 3% incorporation of ionic groups. The storage moduli decreased in a slight two-step drop up to a temperature of 120°C. At temperatures higher than 120°C an increase in the storage moduli was observed. For 60:40 PUR/PS IPNs without ionic groups the storage moduli decreased considerably at 180°C because of a softening of the dual network system. However, for the 60:40 PUR/PS IPN with 3% ionic groups values for E' were still very high at 180°C with 13 MPa and continued to rise up to a temperature of 185°C. The extended rubbery plateau modulus is generally believed[314] to have resulted from the oppositlely charged ionic groups acting as additional crosslinks. The fact that the storage modulus not only exhibited an extended plateau, but even increased could be explained as follows. In general, a significant increase in storage modulus can be caused[185] by the occurrence of a chemical reaction i.e. crosslinking or by the formation of crystalline domains. In the present study, the increase in E' must have been caused by the formation of additional ionic crosslinks. At higher temperatures, a higher degree of chain segment mobility was obtained in the

IPN. Carboxylic acid groups of the PS network that had not been neutralised or linked to quaternised amine structures came into contact with tertiary amine groups in the PUR network. As a result of the formation of additional crosslinks by the neutralisation reaction, the storage modulus increased. At 185°C, a slight decrease in E' was observed which might have been associated to the breakdown of some ionic crosslinks. Viscoelastic measurements on ionomers have shown[314] the existence of a high temperature loss peak between 200 and 240°C, which has been termed the ionic cluster transition. This glass transition of the clustered material has been interpreted by most researchers as ion hopping[315]. Ion hopping is[315] as a process by which the ion pairs migrate from one multiplet to another. The loss moduli versus temperature showed that in the present study, this high temperature loss peak was not present up to a temperature of 230°C (figure 5.51(c)). The present PUR/PS IPNs could not be studied at higher temperatures because of the onset of PUR degradation which started to take place at 220°C (section 5.2).

A considerable broadening and compatibilising effect was achieved by the incorporation of 3% ionic groups into the 60:40 PUR/PS IPN. However, the transition height at the low temperature end had severely decreased. In order to increase the height of the PUR soft segment transition, the 70:30 PUR/PS IPN composition was chosen for the incorporation of ionic groups. Again, a very similar transition profile resulted from the 0 and 1% incorporation of ionic groups (figure 5.52(a) and (b)). At 2% incorporation, the transition shape changed considerably in that the PS transition became predominant. Similar to the 60:40 PUR/PS IPNs the PUR transition decreased from a loss factor value of 0.81 (1% ionic groups) to 0.24 while remaining roughly at the same temperature (8°C). The PS transition on the other hand shifted to a lower temperature (106°C) and increased from 0.41 (1% ionic groups) to 0.48. A further increase in ionic groups (2.5 and 3%) provoked a further increase in PS loss factor height (0.53 and 0.55, respectively) and a shift to lower temperatures (94 and 78°C) of the PS Tg. With increasing incorporation of ionic groups the PUR low temperature transition decreased further. At 3% ionic groups, it was only present as a shoulder. The latter indicated a pronounced increase in miscibility between the IPN components. The storage moduli of these 70:30 PUR/PS IPNs reflected the trends of the loss factor data (figure 5.53). The storage moduli of

the IPNs with 2, 2.5 and 3% incorporation of ionic groups almost decreased in a linear pattern which indicated a high degree of phase mixing in these IPNs.

The increase in phase mixing in these IPNs with ionic groups must have been brought about by specific intermolecular interactions between the PUR and the PS networks. Through the copolymerisation of MAA with styrene and the incorporation of MDEA into the polyurethane there were three kinds of interactions possible between the two polymer networks. The carboxylic acid groups of MAA could form hydrogen bonds with the urethane link. If neutralisation occurred, ionic interactions were possible between carboxylate anions and quaternised amine moieties in the PUR. The introduction of inter-network grafting might have been a third mechanism of the MAA to improve PUR-PS phase mixing. Under certain conditions, isocyanates react with carboxylic acid groups to result in the formation of CO_2 and an amide (section 2.3.2). However, the carboxyl group of the MAA was unlikely to react with the forming PUR because its reaction rate with the NCO is much slower than that of the primary hydroxyl groups. Also, because of the low curing temperatures (maximum 90°C) and the low reactivity of the tertiary NCO groups of the TMXDI no amide formation was believed to have taken place. An IR spectrum further confirmed the absence of new peaks due to the carboxyl-NCO reaction.

It was of interest to ascertain whether the increase in miscibility was brought about by the formation of ion pairs or whether hydrogen bonding introduced by the MAA moieties in the PS alone was sufficient to achieve compatibilisation. Therefore, a 60:40 PUR/PS IPN with 3 weight % MAA and no MDEA was prepared. To complement the present study, the corresponding 60:40 PUR/PS IPN without MAA, but with the stoichiometric amount corresponding to 3 weight % MAA of MDEA was also prepared. These latter two were compared to the 60:40 PUR/PS IPN with 3% ionic groups and to that without ionic groups, respectively. The loss factor and storage modulus versus temperature data for these 4 IPNs are shown in figures 5.54 and 5.55. Surprisingly, very similar DMTA data were observed for the 60:40 PUR/PS IPNs with 3% ionic groups and for that with the 3% MAA alone (figures 5.54 and 5.55). The loss factor transition heights in both IPNs were virtually the same with 0.13 and 0.52 for the PUR and the PS, respectively.

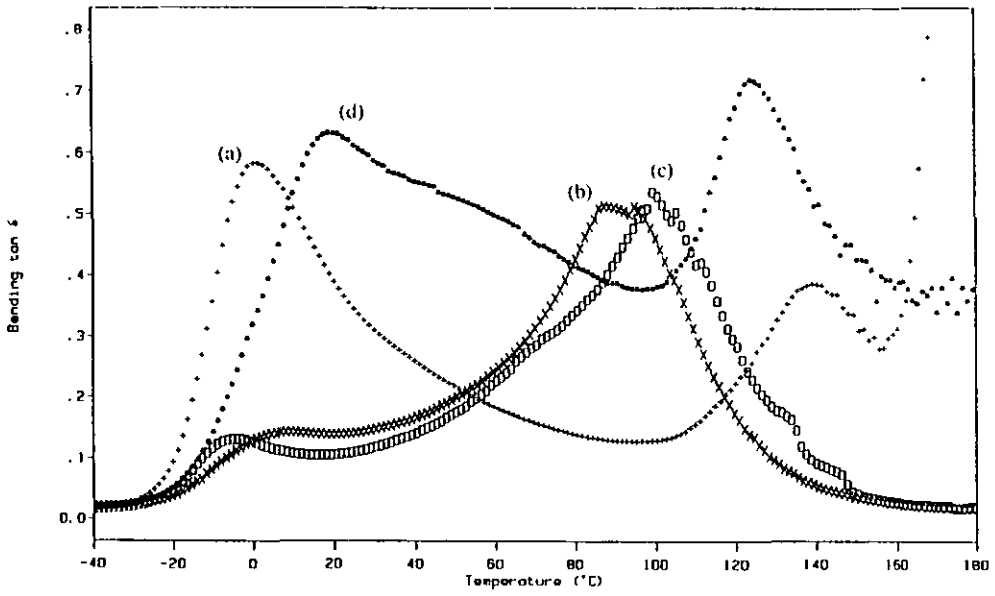

Figure 5.54 Loss factor versus temperature data for the 60:40 PUR/PS IPN at various levels of MAA weight percentages and MDEA equivalents. (a) 3% MAA & equivalent MDEA, (b) 3% MAA and (c) MDEA equivalent to 3% MAA.

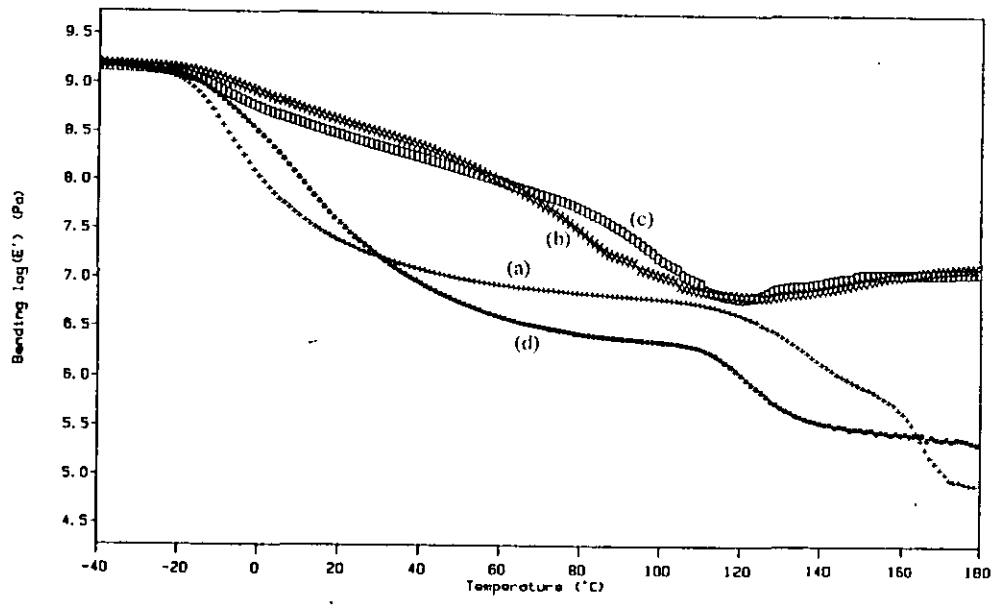

Figure 5.55 Storage moduli versus temperature for the 60:40 PUR/PS IPN at various levels of MAA weight percentages and MDEA equivalents. (a) 3% MAA & equivalent MDEA, (b) 3% MAA and (c) MDEA equivalent to 3% MAA.

The Tg locations of the IPN with 3% MAA were at -4°C and 100°C for the PUR and the PS, respectively. The 3% ionic groups exhibited a slightly more phase-mixed morphology with transitions at 6°C and 90°C for the PUR and the PS, respectively. The storage moduli versus temperature of both IPNs were also very similar (figure 5.55). Both IPNs had increasing moduli at temperatures higher than 120°C. The similar DMTA data indicated that no tertiary amine was necessary to neutralise the carboxylic acid group of the MAA in order to bring about an increase in miscibility in the PUR/PS IPN. These results can be explained in two possible ways. First, no neutralisation of the carboxylic acid occurred and the increase in miscibility was brought about by hydrogen bonding with the urethane link alone. This was the explanation given by Frisch and co-workers[146] when investigating PUR/P(MMA-MAA) IPNs. They suggested[146] that a decrease in phase separation in PUR/P(MMA-MAA) IPNs was brought about by additional hydrogen bonding between the carboxyl groups and the urethane links in the PUR. A second possibility could be that neutralisation of the carboxylic acid group took place involving the nitrogen in the urethane link. From the results in the present study, the latter was much more likely. The extension of the rubbery plateau modulus to higher temperatures and the increase of the latter at temperatures higher than 120°C can only be explained by strong ionic interactions. Hydrogen bonding generally becomes[93] very weak at temperatures higher than 80°C. In the literature, some studies[321-323] have suggested that urethane nitrogens in PUR chains are capable of undergoing quarternisation. In a recent study[321] investigating PUR/PS ionomer blends, Natansohn and co-workers[321] found that the labile protons of sulfonic acid groups were transferred preferentially to allophanates, followed by urethane nitrogens and finally by tertiary amine nitrogens. Thus, the latter explained the efficiency of 3% MAA incorporation in bringing about an increase in IPN miscibility. A neutralisation reaction between the MAA and the nitrogen in the urethane link must have taken place. However, when both MAA and MDEA were present in the initial mixture, as in the preparation procedure in the present study, the proton transfer was believed to have occurred mainly with the MDEA since during the initial mixing only very few urethane links had formed. The efficiency of MAA in increasing IPN miscibility might be a function of the incorporation level and, furthermore, of the degree of MAA neutralisation. The extent of proton transfer from the MAA to the MEDA or urethane nitrogens could be a

function of its acid strength and the basicity of the nitrogens. In the present study, the extent of proton transfer was difficult to quantify. Fan and Bazuin[316] recently attempted to make a quantitative calculation of the extent of proton transfer. Investigating tertiary amines of different basicity, they related the area under the absorption band at 900 - 906 cm^{-1} to the degree of neutralisation of the ionic groups. In the present study, however, this was not undertaken. Because of the dual crosslinked nature of the IPNs, it was difficult to obtain IR spectra of a high enough quality.

Another surprising result was obtained when comparing the DMTA data of the unmodified 60:40 PUR/PS IPN to the respective counterpart containing 3% MAA equivalent of MDEA. The loss factor versus temperature data showed an inward shift of the PUR and the PS transition for the IPN containing the MDEA moieties. The PUR transition shifted from 1°C to 19°C while the PS Tg shifted from 140°C to 122°C. More importantly, the PUR transition was extremely broad and exhibited high loss factor values up to a temperature of 100°C. As a consequence, the inter-transition values were extremely high with a lowest value of 0.38 compared to a value of 0.13 for the unmodified 60:40 PUR/PS IPN. The storage moduli exhibited both a two-step drop mechanism indicating a phase separated morphology for both IPNs (figure 5.55). The storage moduli at the PUR transition decreased more gradually and over a broader temperature range for the MDEA-containing IPN. This reflected the broader PUR loss factor transition. The pronounced difference between both IPNs could not be explained with certainty and further study is needed. The fact that MDEA as a tertiary amine is also a strong catalyst for the PUR reaction might have played some role. Tin-based catalysts such as stannous octoate used in combination with tertiary amines are known[260] to exhibit a synergistic effect. Thus, the resulting increase in reaction rate of the PUR network might have had some repercussions of the IPN morphology. The fact that tertiary amines are known[203] to favour the reaction of isocyanates with water was not believed to have had any influence since great care was taken to exclude humidity. The IPN with MDEA had very high damping characteristics with loss factor values of higher than 0.3 starting at 0°C up to the high end of the DMTA experiment (180°C). At 180°C, however, the mechanical properties were poor which manifested itself in a low storage moduli of 0.3 MPa.

Stress-strain and hardness measurements. Miscible and semi-miscible polymer blends often present advantages over immiscible blends[1,3]. Thus, the mechanical properties of the 70:30 PUR/PS IPNs with improved miscibility through the incorporation of opposite charged groups were investigated by tensile testing and Shore A and D hardness measurements. The stress and elongation at break, Young's modulus, the toughness index and values for Shore A and D hardness are given in table 5.6.

Table 5.6 Mechanical properties for 70:30 PUR/PS IPNs with different levels of oppositely charged groups.

PUR/PS IPN	Tensile properties				Hardness	
MAA level	Stress at break	Strain at break	Young's modulus	Toughness	Shore	
[weight %]	[MPa]	[%]	[MPa]	[J]	A	D
0	12	770	4	14	59	35
1	13	330	4	7	67	44
2	14	370	85	12	92	61
2.5	14	360	82	13	93	61
3	14	330	89	10	94	61

The values for the stress at break increased with increasing content of ionic groups. However, the increase was not very significant. The unmodified 70:30 PUR/PS had a value for the stress at break of 12 MPa, whereas the corresponding IPN with 3% ionic groups exhibited a value (14 MPa) which was higher by 17%. The values for the strain at break showed a significant decrease with higher ionic group contents. They fell by more than half from the unmodified (770%) to the IPN containing 3% ionic groups (330%). Since the values for the toughness index are a function of the stress and the strain at break, the former were also lower for the IPNs containing ionic groups (table 5.6). The fact that the toughness index values were not as low as expected for the IPNs with 2, 2.5 and 3% ionic groups was because the shape of the stress-strain curve had changed. For the 70:30 PUR/PS IPNs with 0 and 1% ionic groups high tensile stress values were only obtained at high elongations. The IPNs with 2, 2.5 and 3% ionic groups had high tensile stress values right form the start. As

a consequence, relatively high areas under the stress-strain curve were obtained for the latter despite their low values for the strain at break. The important change in IPN properties that was observed from the DMTA data between the 1 and 2% incorporation of ionic groups was even more pronounced in the Young's moduli. The latter increased from low values of 4 MPa for 0 and 1% ionic incorporation by a factor of more than 20 to 85, 83 and 89 MPa for the IPNs with 2, 2.5 and 3% ionic groups, respectively. The hardness values also reflected the dramatic change in the properties of the IPNs (table 5.6). This dramatic increase in modulus was believed to have resulted from a change in IPN morphology. The only explanation possible was that the glassy PS network must have assumed some degree of continuity at 2% ionic group incorporation. In order to confirm this assumption, the morphology of these 70:30 PUR/PS IPNs with different ionic group contents were investigated by TEM and SEM.

Morphology by TEM and SEM. The findings made from DMTA and tensile testing for the 70:30 PUR/PS IPN composition with various levels of opposite charged groups were confirmed by electron microscopy. The TEM micrographs showed significant changes in the IPN morphology (figure 5.54). At 1% ionic group incorporation, the PS phase domain sizes were between 100 and 300 nm (figure 5.54(a)). Surprisingly, they were clearly greater than in the 70:30 PUR/PS IPN without ionic groups where PS domains in the order of 50 - 200 nm were observed (figure 5.15(b)). Also, significantly fewer PS domains were noted and their shape was more irregular. At a higher magnification, it was observed that PS domains had joined together to from these bigger aggregates (figure 5.54(b)). At 2% ionic group incorporation, a substantial change in IPN morphology occurred. The PS phase domains became smaller and surprisingly formed an interconnected network (figures 5.54(c) and (d)). The fact that the PS network assumed some degree of continuity at this incorporation level explained very well the findings from the DMTA data and tensile testing. At a 2% incorporation of ionic groups, the PS loss factor transition was higher than that of the PUR indicating some degree of phase continuity of PS.

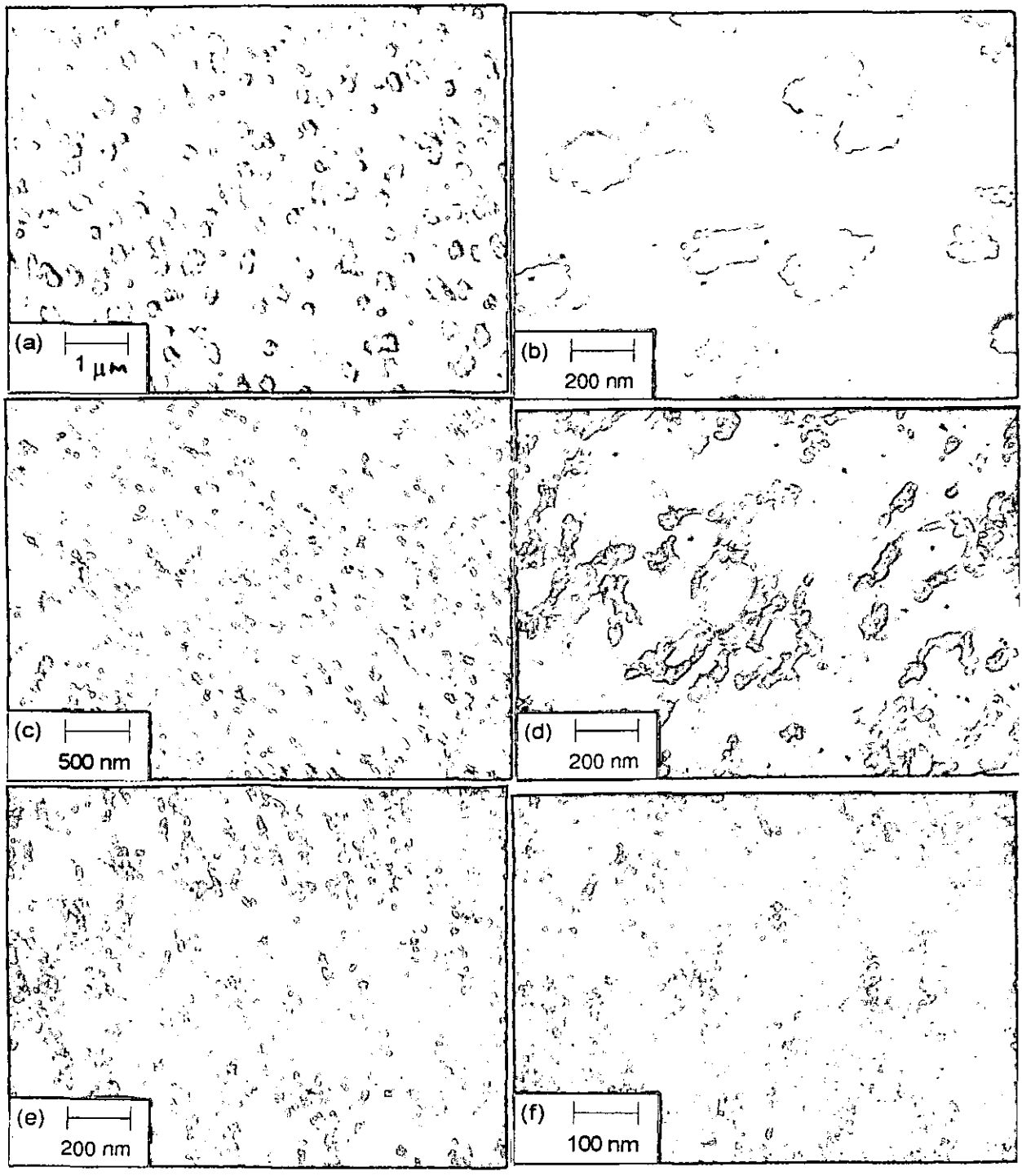

Figure 5.56 TEM micrographs for the 70:30 PUR/PS IPNs with different levels of oppositely charged groups. (a)&(b) 1%, (c)&(d) 2% and (e)&(f) 3%.

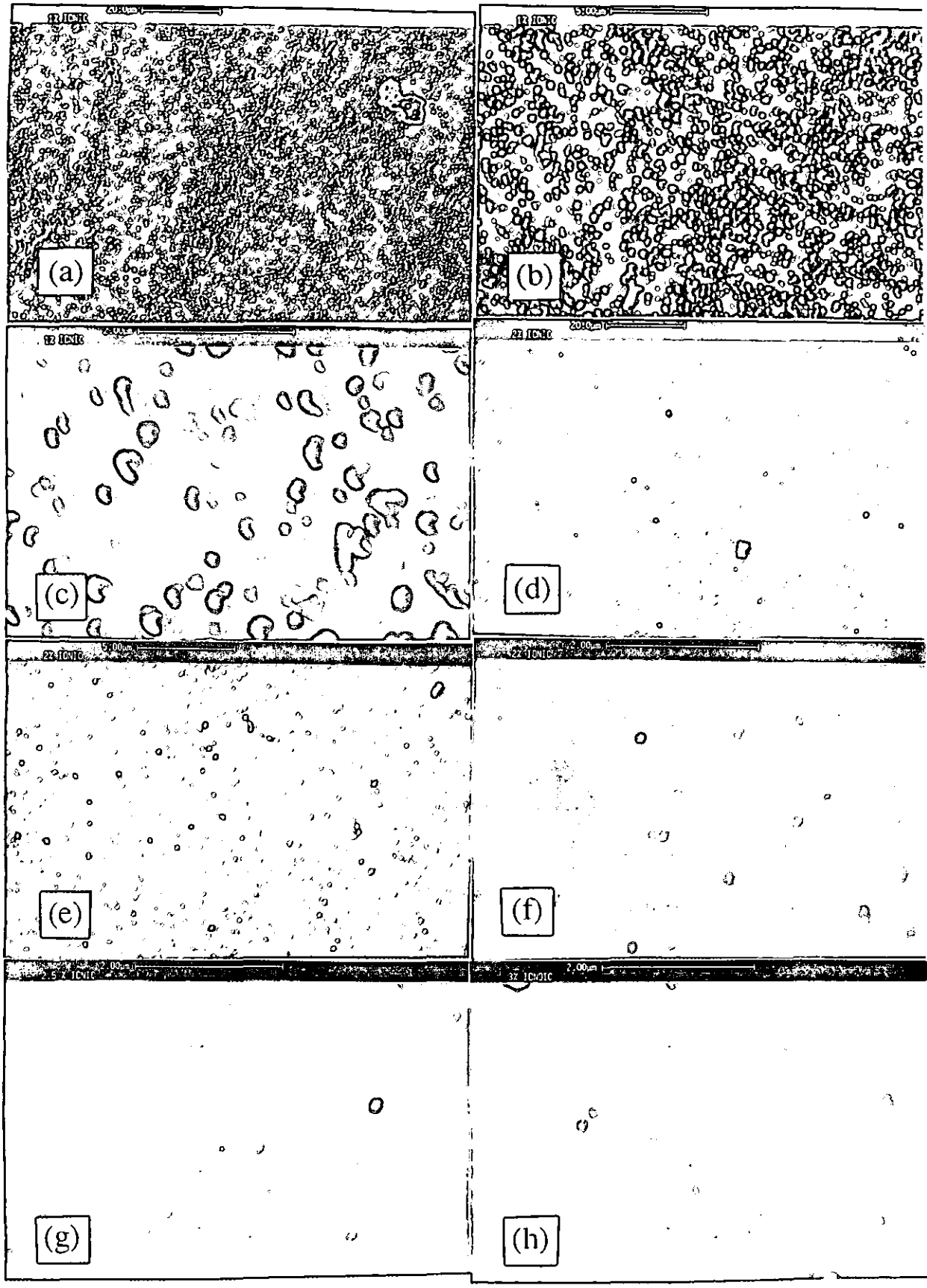

Figure 5.57 SEM micrographs for the 70:30 PUR/PS IPNs with different levels of oppositely charged groups. (a)&(b)&(c) 1% ionic groups, (d)&(e)&(f) 2%, (g) 2.5% and (h) 3%.

At 3% ionic groups, the PS phase structure was even finer and the network exhibited a higher degree of continuity (figure 5.54(e) and (f)). The SEM micrographs confirmed to some extent the findings from TEM. However, limitations of SEM were poor contrast between the phases and the fact that not sufficiently high magnifications could be achieved with good resolution. It was observed that the phase structure decreased with increasing ionic group content (figure 5.55). From figure 5.55(a) the PS phase domain size of the 70:30 PUR/PS IPN with 1% ionic groups was found to have ranged from 100 to 400 nm, corroborating the TEM results (100 - 300 nm). Also, the PS phase domains at 1% incorporation of ionic groups (figure 5.55(b) were larger than for the corresponding unmodified 70:30 PUR/PS IPN (figure 5.13(f)). A similar phenomenon had been observed with TEM. However, the formation of a network structure at ionic incorporations of 2% and higher could not be observed because of aforementioned limitations of SEM.

In conclusion, TEM confirmed the DMTA data of higher degrees of phase mixing with increasing incorporation levels of ionic groups. A broad transition was obtained for the 70:30 PUR/PS IPN with an incorporation level 3% ionic groups. The broad transition was believed to have been a result of a co-continuous morphology with a high degree of phase mixing. In addition to information about the morphology of these IPNs with ionic groups, more general information regarding IPN morphologies might be deducted. The micrographs of the 70:30 PUR/PS IPNs with different levels of ionic groups might have revealed some information about the extent of phase separation of IPNs from polymer pairs with different levels of miscibility. The IPN morphology changed with decreasing incorporation of ionic groups from 3, to 2 to 1 to 0% from a very fine morphology of co-continuous networks (3%), to more phase separated co-continuous networks (2%), to irregularly shaped PS domains in a PUR matrix and finally to spherical well-defined PS domains surrounded by a PUR shell of high purity (0%). These changes in morphology might be a general feature of changes in IPN morphology from polymer pairs of decreasing miscibility. Further studies investigating both incorporation levels between 1 and 2% ionic groups and with higher incorporation levels than 3% might prove interesting.

6. Polyurethane / Poly(ethyl methacrylate) IPNs

In the previous study in chapter 5, the morphology, phase continuity and concomitant mechanical and thermal properties of PUR/PS IPNs as a highly immiscible polymer pair were investigated. The gross phase separation was reduced by crosslinking, inter-network grafting, and the incorporation of compatibilisers and oppositely charged ionic groups. In this chapter, PUR/poly(ethyl methacrylate) (PEMA) IPNs were investigated as a semi-miscible polymer pair. The difference in solubility parameters[254] between PUR (δ = 20.5 $(J/cm^3)^{1/2}$) and PEMA (δ = 18.3 $(J/cm^3)^{1/2}$) was similar to that between PUR and PS (δ = 18.5 $(J/cm^3)^{1/2}$). However, contrary to PUR/PS blends, the presence in both polymers of groups of some polarity was believed to have increased the PUR-PEMA miscibility. Thus, again, elastomeric PUR was combined with a high-Tg plastic, PEMA. The same PUR was employed in the PUR/PEMA IPNs as was used in the PUR/PS IPN study. The PUR consisted in most cases of TMXDI and PPG1025/TMP at a molar ratio of 3:1 (chapter 4). Also, the same experimental procedure for the preparation of the IPNs was used (chapter 3). Since both the same preparation procedure and PUR were employed direct comparison between immiscible and semi-miscible IPNs was possible.

In the literature, only two studies[324,325] on PUR/PEMA IPNs have been reported. In a series of investigations on castor oil-based IPNs, Suthar and co-workers[324] studied the resistance to chemical reagents, optical properties, thermal behaviour and mechanical and dynamic mechanical properties of PUR/PEMA IPNs. The PUR was based on castor oil and MDI. Investigating three (15:85, 25:75 and 35:65) simultaneous PUR/PEMA IPN compositions they found improved resistance to chemical reagents compared to the respective homopolymers. From the DMTA data, they concluded that considerable phase mixing existed, whereas in SEM micrographs two distinct phases were observed. The PUR was believed to have represented the continuous phase in all IPN compositions. In the second study[325] on PUR/PEMA IPNs, the damping ability of 70:30 compositions of PUR/polyethylacrylate and PUR/PEMA IPNs were compared to 70:30 compositions of PUR/polymethylacrylate and PUR/PMMA IPNs, respectively. The PURs were based on a polyepichlorohydrin polyol (MW 1000 g/mol), TMP and TDI. A microphase-separated morphology and a

broadening of the Tg region was shown by TEM micrographs and DMTA data. Chen and co-workers[325] found that the IPNs with the pendent ethyl groups exhibited considerably higher loss factor values than those with the methyl groups. Thus, so far no detailed study on the morphology and phase continuity of PUR/PEMA IPNs has been conducted. Consequently, the aim of the present study on PUR/PEMA IPNs was to elucidate further the morphology and concomitant mechanical and thermal properties of PUR/PEMA IPNs as potentially high damping materials. The main focus was placed on studying the IPN miscibility and phase continuity and how the latter influenced the damping characteristics. Therefore, the full IPN composition range was investigated using DMTA, M-TDSC, stress-strain and hardness measurements and swelling studies. The storage and the elastic moduli were compared to modulus-composition theories to predict phase continuity and phase inversion. TEM and SEM were used to corroborate the findings from the mechanical and thermal tests. Furthermore, factors to alter the PUR/PEMA morphology were investigated. These included varying the crosslinking density in both networks and variations in the PUR network.

6.1 PUR/PEMA IPN Composition Study

The full composition range of PUR/PEMA IPNs was investigated in 10 weight % increments. Special focus was placed on phase continuity since the latter strongly influences the mechanical properties of the polymer blend. Similar to the PUR/PS IPN compositions, the PUR/PEMA IPNs were prepared at a PPG1025/TMP ratio of 3:1 in the PUR component and at 5 mol % tetraethyleneglycol dimethacrylate (TEGDM) in the PEMA.

DMTA studies. DMTA data can be used to study the morphology i.e. the miscibility and phase continuity of a polymer blend as was explained in section 3.4.1. The loss factor versus temperature data for both homonetworks and PUR/PEMA IPN compositions are shown in figures 6.1 and 6.2. The storage and loss moduli versus temperature of these IPNs are presented in figures 6.3 and 6.4. The DMTA data (10 Hz), including the Tg values, the loss factor peak heights, the inter-transition values at 50°C and the half-peak widths are listed in table 6.1.

Table 6.1 Dynamic mechanical properties (10 Hz) for the PUR/PEMA IPNs and homonetworks as a function of composition.

IPN Composition [% PEMA]	Tg [tan δ, °C] PUR	PEMA	Tan δ maximum PUR	PEMA	Inter-transition height at 50°C	Half-peak width[d] [°C] PUR	PEMA
0	-5	-	1.08	-	(0.10)[c]	27	-
10	3	-	0.84	-	0.24	43	-
20	10	-	0.63	-	0.28	57	-
30[a]	18	87	0.40	0.42	0.40	-	153
40[a]	10	87	0.30	0.48	0.35	-	131
50[a]	✓-10	27[b] 88	0.14	0.26[b] 0.75	0.32	-	64
60[a]	✓-12	88	0.08	0.78	0.32	-	55
70	-	79	-	0.81	0.39	-	50
80	-	85	-	0.95	0.32	-	46
90	-	95	-	1.06	0.27	-	42
100	-	105	-	1.04	(0.12)[c]	-	41

(a) Glass transition temperatures at these compositions were difficult to determine because of the presence of a significant shoulder for the second component.

(b) A small intermediate third transition was observed for the 50:50 PUR/PEMA IPN.

(c) No second transition was present at these IPN compositions.

(d) Half-peak widths were given for the component with the highest loss factor transition peak.

While for the PUR/PS IPNs two Tg values were obtained for all IPN compositions, only one transition with a more or less developed shoulder was observed in the PUR/PEMA IPNs. A single transition peak in the loss factor versus temperature data was observed for the 90:10, 80:20, 30:70, 20:80 and 10:90 PUR/PEMA IPN compositions. The intermediate compositions between 70:30 and 40:60 appeared phase-separated to some extent and exhibited a loss factor shoulder for the second transition. The fact that the Tg for the PUR shoulder at the 50:50 and 40:60 PUR/PEMA compositions was even at a lower temperature than that of the PUR homonetwork can be explained by a plasticisation effect[86] and, probably more importantly, by an incompletely formed PUR network[63] containing defects such as loose chain ends.

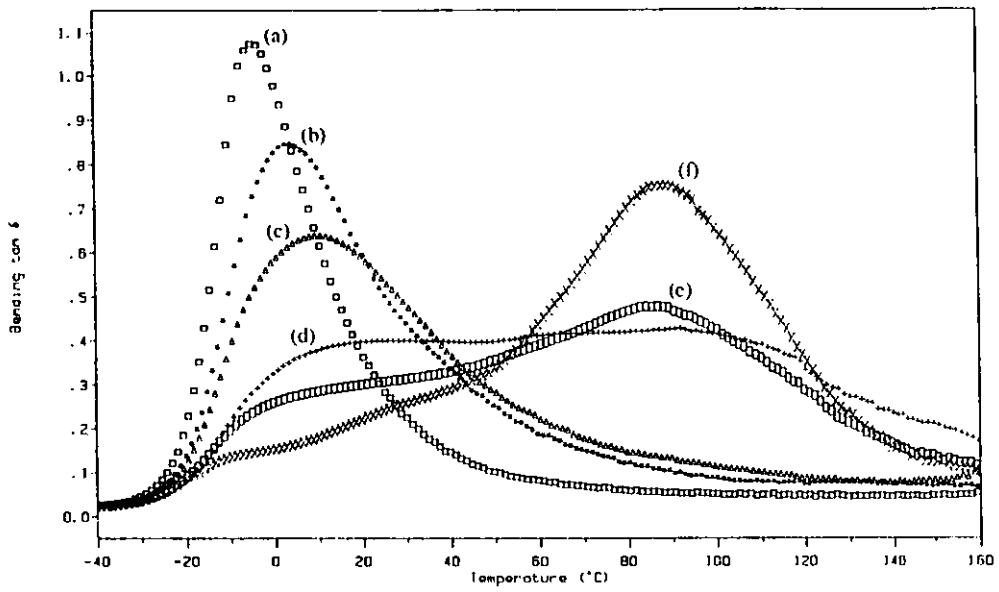

Figure 6.1 Loss factor versus temperature data for the PUR/PEMA IPN compositions. (a) 100 PUR, (b) 90:10 PUR/PEMA, (c) 80:20, (d) 70:30, (e) 60:40 and (f) 50:50.

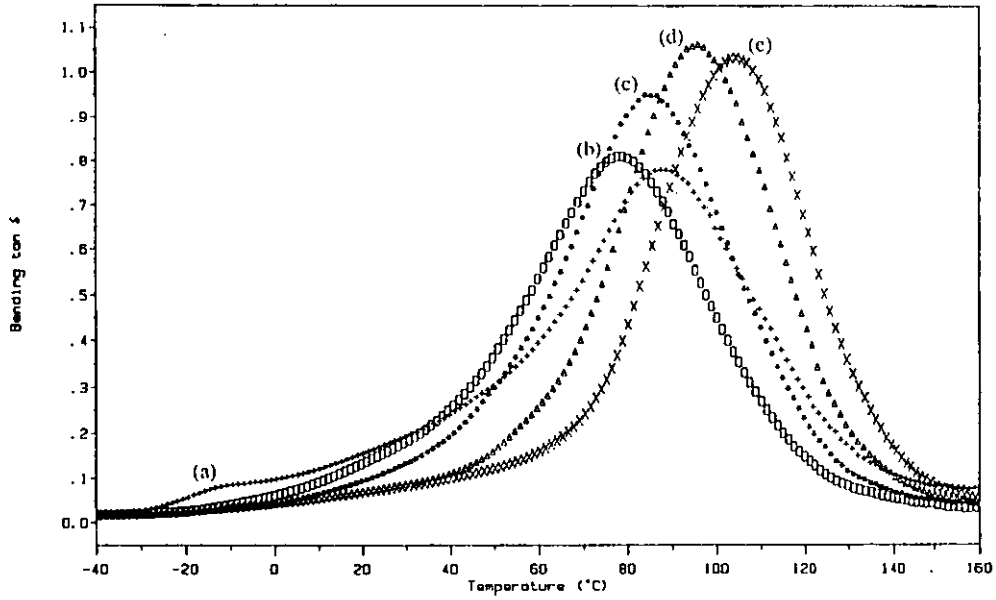

Figure 6.2 Loss factor versus temperature data for the PUR/PEMA IPN compositions. (a) 40:60 PUR/PEMA, (b) 30:70, (c) 20:80, (d) 10:90 and (e) 100 PEMA.

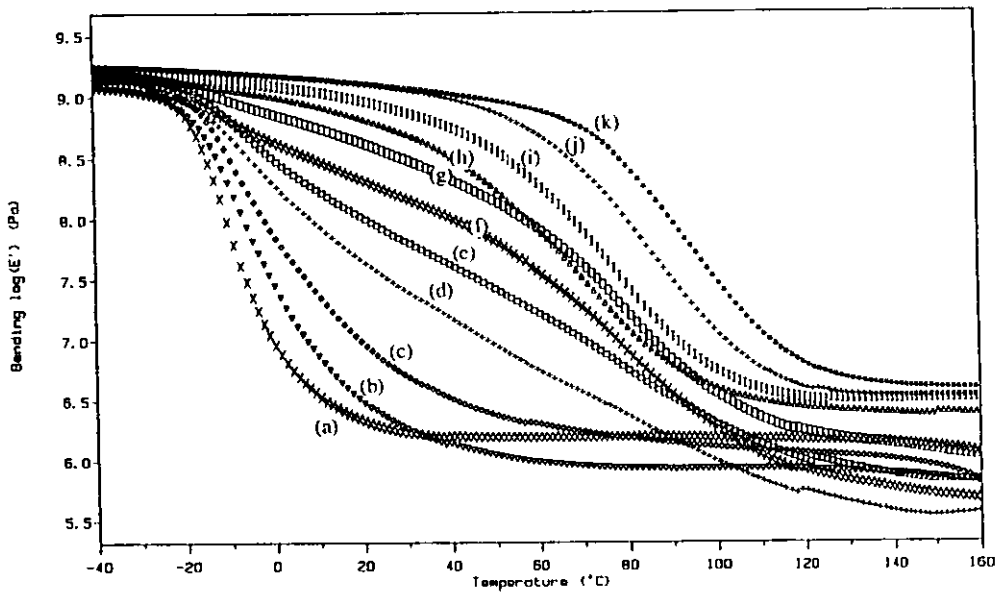

Figure 6.3 Storage moduli versus temperature for the PUR/PEMA IPN compositions. (a) 100 PUR, (b) 90:10 PUR/PEMA, (c) 80:20, (d) 70:30, (e) 60:40, (f) 50:50, (g) 40:60, (h) 30:70, (i) 20:80, (j) 10:90 and (k) 100 PEMA.

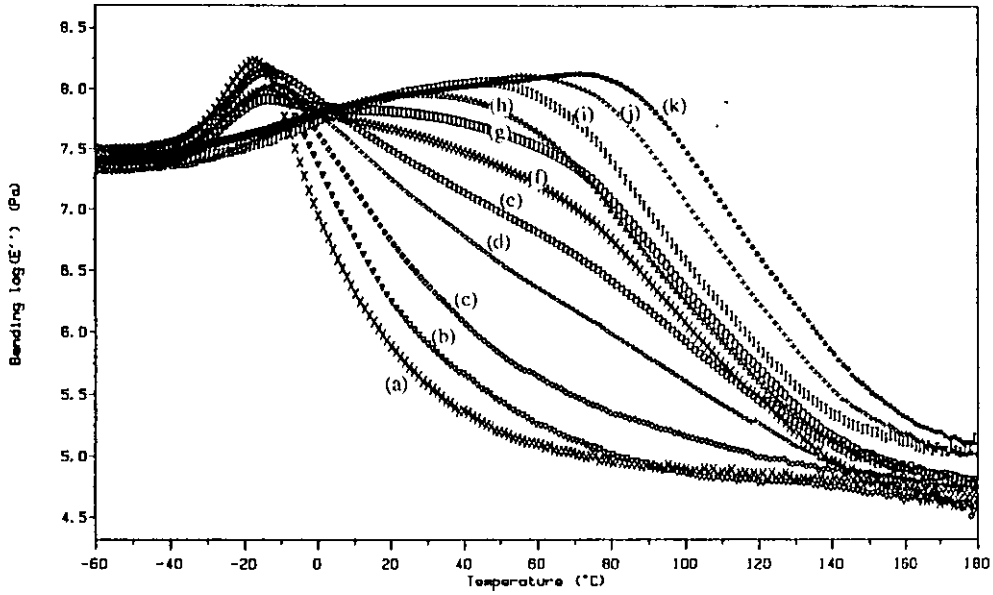

Figure 6.4 Loss moduli versus temperature for the PUR/PEMA IPN compositions. (a) 100 PUR, (b) 90:10 PUR/PEMA, (c) 80:20, (d) 70:30, (e) 60:40, (f) 50:50, (g) 40:60, (h) 30:70, (i) 20:80, (j) 10:90 and (k) 100 PEMA.

A similar trend of very low PUR Tg values was observed at high PS contents in the PUR/PS IPNs (section 5.2). The 50:50 PUR/PEMA IPN composition showed three transitions, one main peak at 88°C with two shoulders at 27°C and -10°C. A similar phenomenon has been reported[63,86,147] previously for PUR/PMMA IPNs and was explained by the presence of a substantial interface region. Another possible, however, very different explanation could be that the intermediate damping peak[310-312] was of mechanical origin as was explained in section 5.4. The latter phenomenon will be further investigated by M-TDSC and TEM.

Figure 6.5 shows a plot of the IPN Tg values versus PEMA content. Tg values obtained from both the loss factor and the loss modulus peaks were reported. These were compared to the Fox[184] equation (equation 2.17) which predicts a concave curve for Tg versus composition.

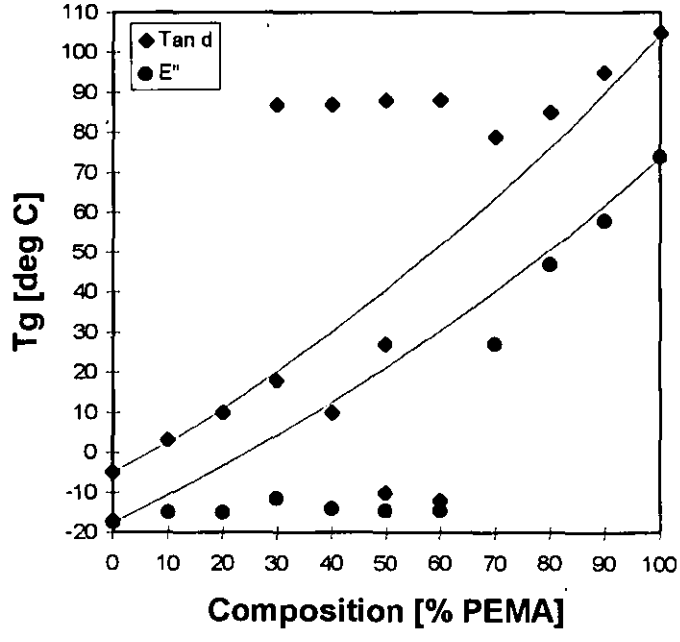

Figure 6.5 IPN Tg values from the loss factor (tan δ) and the loss modulus (E") peaks versus PEMA content. The solid lines represent the respective Tg predictions by the Fox equation.

Looking at the loss factor Tg data, only the data points for the 90:10, 80:20 and 70:30 PUR/PEMA IPNs were in line with the prediction. Even though essentially only a single Tg was obtained for the IPNs containing 70, 80 and 90% PEMA, a good fit with the Fox[184] equation did not result. The mid-range compositions were not

expected to fit the prediction, since unsymmetrical transitions with important shoulders were obtained. Yet, no gross phase separation took place, which was corroborated by the in-ward shift of the transition peaks, high inter-transition loss factor values and a large temperature range for the half-peak widths (table 6.1). Surprisingly, the pattern of the loss modulus Tg peaks versus PEMA content differed quite significantly from the correspondingly loss factor values. The fact that the E" Tg values were lower was expected since as a polymer goes through its Tg the E" peak always occurs[4] before that of the loss factor. However, the E" Tg values gave a more phase-separated picture of the IPNs. The E" peaks changed only marginally up to the 30:70 PUR/PEMA IPN composition (figure 6.5). At this composition a major Tg shift to higher temperatures occurred. The prediction by the Fox[184] equation only fitted well the 20:80 and 10:90 PUR/PEMA IPNs. While most loss factor Tg values were higher than the prediction, those of the loss modulus were all below the predicted curve.

Unlike the PUR/PS IPNs, the loss factor peak heights versus composition that of the PUR/PEMA IPNs could not be shown for both the PUR and the PEMA networks. Over most of the composition range only one loss factor peak resulted from this semi-miscible IPN. Figure 6.6 shows the highest loss factor values and values for the half-peak width for the IPN compositions versus PEMA content. The loss factor peak maxima had their lowest values at the 70:30 PUR/PEMA IPN composition with 0.42. IPNs with both lower and higher PEMA contents exhibited significantly higher loss factor values (table 6.1). The PUR homopolymer network (1.08), the 10:90 PUR/PEMA IPN (1.06) and the PEMA homonetwork (1.04) had the highest loss factor values. The half-peak widths exhibited the opposite trend. Similar to the loss factor values in the inter-transition region the half-peak widths can be used as a measure[326] of the level of mixing of the components in a phase-separated polymer system. The PUR (27°C) and PEMA (41°C) homonetworks had the lowest half-peak widths. At the 70:30 PUR/PEMA IPN composition the half-peak width was the highest with 153°C. The inter-transition loss factor values at 50°C showed a similar trend to the half-peak widths (table 6.1). The highest inter-transition value of 0.40 was obtained with the 70:30 PUR/PEMA IPN composition. The trends of the loss factor peak heights and the half-peak widths corroborated earlier findings[327] that

limits to the area under the loss factor area exist and that the loss factor peak heights and the transition breadth cannot be chosen independently.

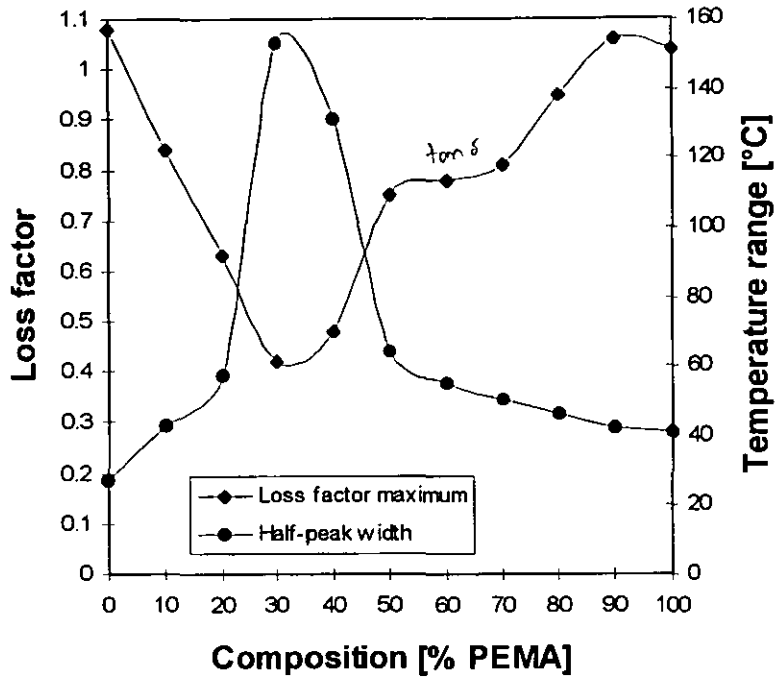

Figure 6.6 Loss factor maxima and half-peak widths for the PUR/PEMA IPN compositions versus PEMA content.

The storage moduli versus temperature for the PUR/PEMA IPN compositions are shown in figure 6.3. From these data, it appeared that the PUR/PEMA IPNs had a semi-miscible morphology. The storage moduli did not decrease in a clear-cut two-step manner, which would be indicative of two-phase polymer blends. For the 70:30 composition, for example, E' steadily decreased in an almost linear mode until it reached the rubbery plateau (figure 6.3(d)). The storage modulus in the rubbery plateau was highest for the pure PEMA network (figure 6.3(k)). The latter was crosslinked with 5 mol % TEGDM which amounted to a theoretical average molar mass between crosslinks ($M_{c,t}$) of 1300 g/mol. The lower E' of the rubbery plateau for the pure PUR network could be explained because of a higher $M_{c,t}$. A PPG1025/TMP ratio of 3:1 resulted in an $M_{c,t}$ of 2900 g/mol. Surprisingly, intermediate compositions such as the 70:30 and the 50:50 IPN exhibited even lower storage moduli in the rubbery plateau region than either of the two homonetworks. This was indicative of a lower apparent crosslinking density in these IPNs. This might be explained on the grounds that when both networks were continuous they impeded the complete

formation of the other. Incomplete network formation of the PUR was already suspected from the low Tg data for PUR contents of 50% and lower.

The loss moduli versus temperature confirmed that no gross phase separation existed (figure 6.4). Only one transition peak was observed for all IPN compositions. This was unlike the loss moduli of the PUR/PS IPNs that all exhibited two clear transition peaks (figure 5.6). However, some IPNs such as for example the 40:60 PUR/PEMA composition (figure 6.4(g)) showed a broad peak shape with an important shoulder indicating some degree of phase separation.

Modulated-temperature DSC studies. M-TDSC studies were conducted in order to investigate further IPN miscibility and Tg behaviour (figures 6.8 to 6.11). Figure 6.7 shows the PUR/PEMA IPN Tg values versus the PEMA content as observed from the peak of the derivative of the heat capacity. The latter were again compared with the prediction by the Fox[184] equation (equation 2.17).

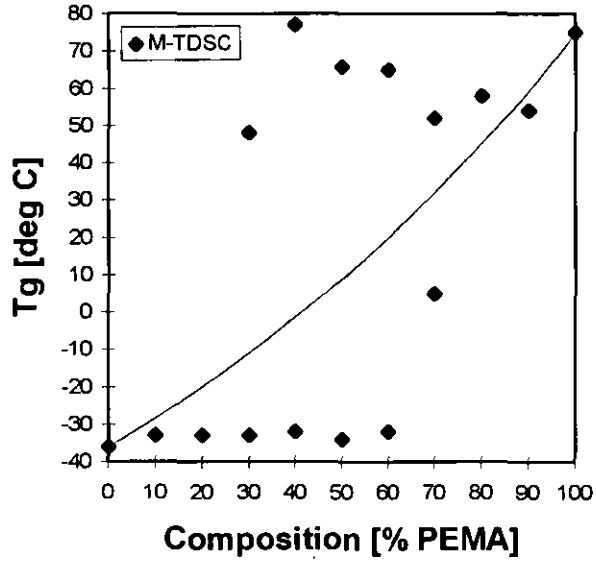

Figure 6.7 IPN Tg values from M-TDSC versus PEMA content. The solid line represents the Tg prediction by the Fox equation.

Generally, the M-TDSC data for the PEMA/PUR IPNs showed a less phase-separated morphology than that for the PUR/PS IPNs (section 5.2). However, the differences as seen by M-TDSC data were less pronounced than those observed by DMTA.

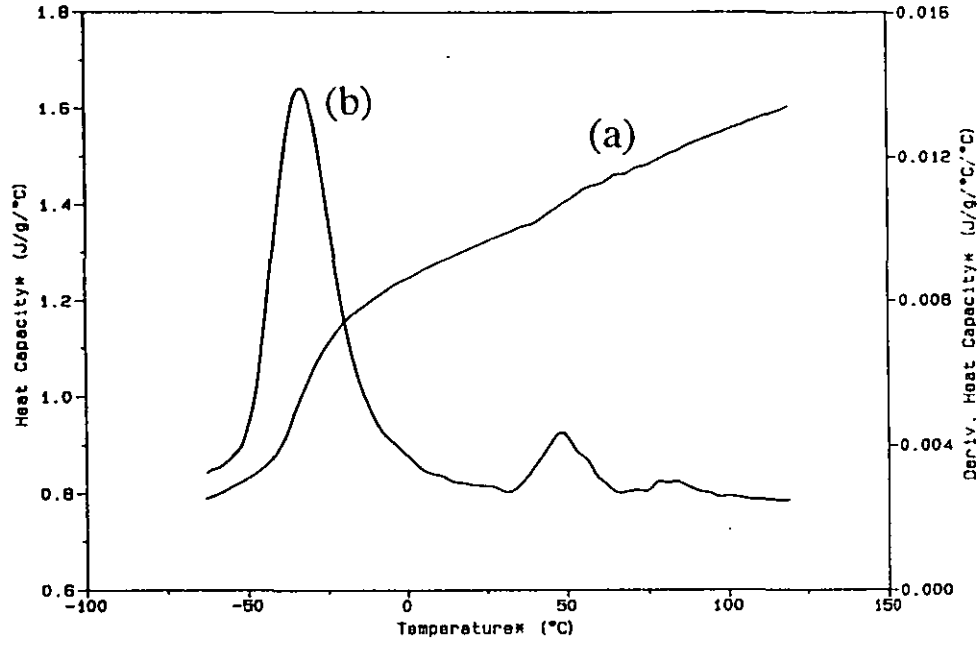

Figure 6.8 Heat capacity (a) and derivative heat capacity (b) for the 70:30 PUR/PEMA IPN.

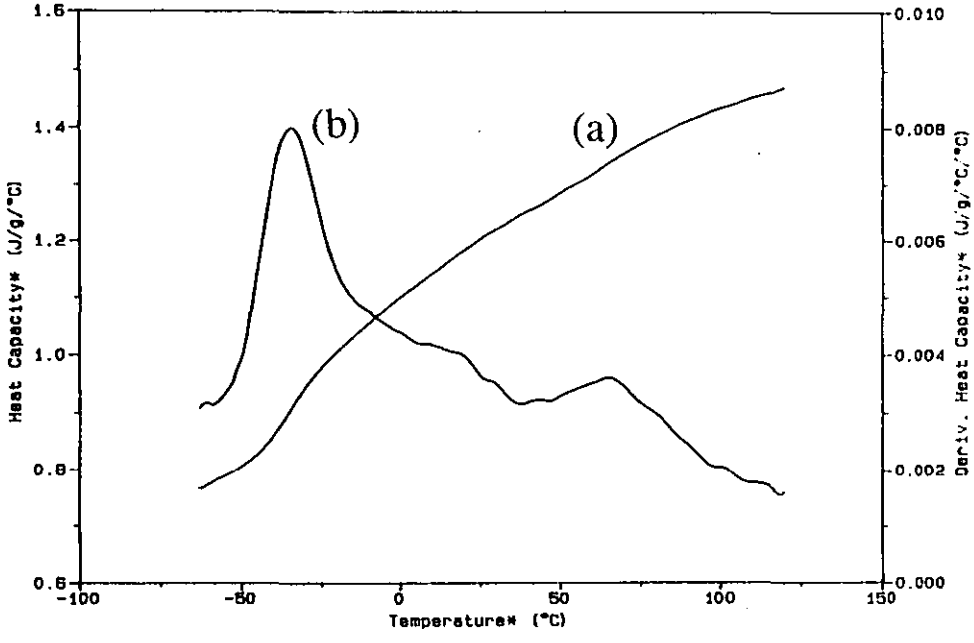

Figure 6.9 Heat capacity (a) and derivative heat capacity (b) for the 50:50 PUR/PEMA IPN.

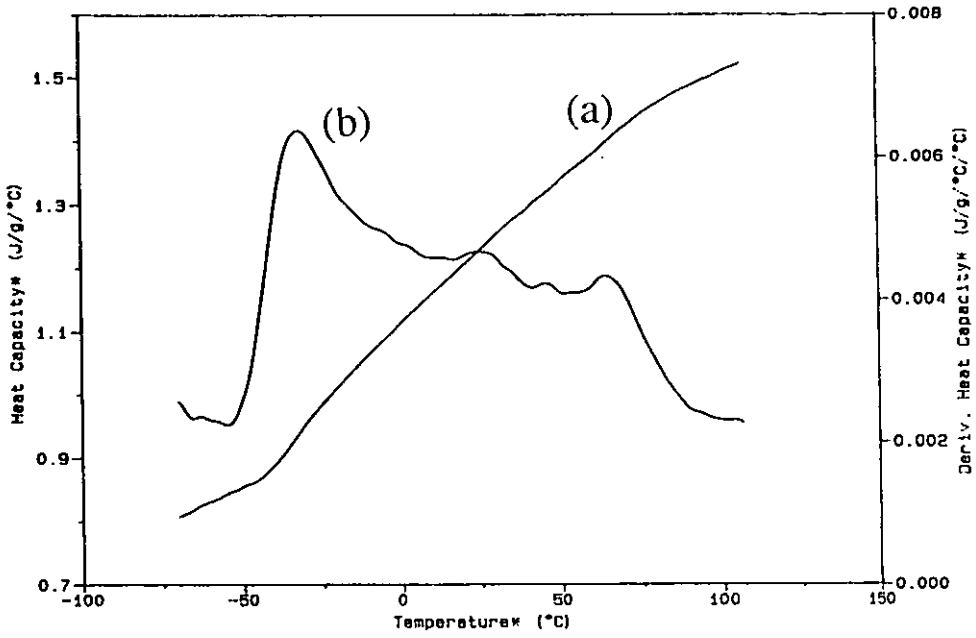

Figure 6.10 Heat capacity (a) and derivative heat capacity (b) for the 40:60 PUR/PEMA IPN.

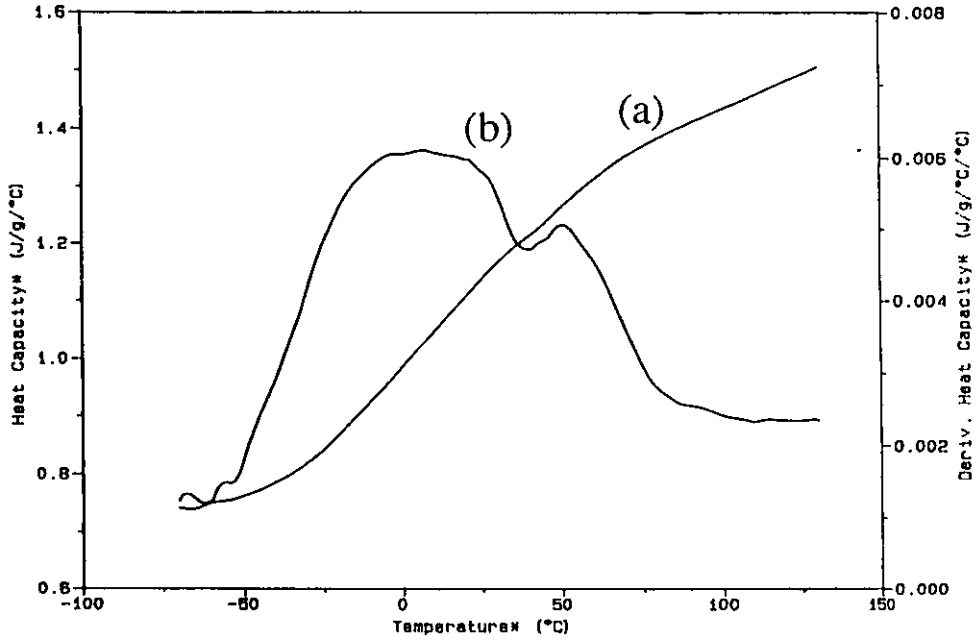

Figure 6.11 Heat capacity (a) and derivative heat capacity (b) for the 30:70 PUR/PEMA IPN.

The PUR transitions remained at about the same location for compositions of 100% to 40% PUR. At PUR contents of 30% and less, the PUR transitions were difficult to distinguish. The PEMA transitions showed some scatter in part because it was difficult to assign clearly the PEMA Tg (figures 6.8 to 6.11). Intermediate transition peaks appeared at some compositions, such as, for example, for the 50:50 and 40:60 PUR/PEMA IPNs (figures 6.9 and 6.10). At other compositions, the transition spectrum was very broad and it was difficult to assign a clear PEMA Tg (figure 6.11). Both phenomena might have accounted for the scatter of the PEMA Tg data. The slight intermediate DMTA damping peak for the 50:50 PUR/PEMA IPN was reflected by a third M-TDSC transition peak between the PUR (-33°C) and the PEMA (67°C) at 18°C. Thus, M-TDSC corroborated that the intermediate transition must have stemmed from a phase-mixed interface region and was not a purely mechanical phenomenon.

With the M-TDSC Tg data the poorest fit with the Fox equation resulted. From the Tg values determined by M-TDSC, the PUR/PEMA IPNs appeared to be more phase separated than from the DMTA Tg data. The latter might have been a result from a higher resolution potential of M-TDSC with the latter being more sensitive to phase separation. A high resolution potential of M-TDSC was already found in a study[328] on the Tg behaviour of PMMA/poly(styrene-co-acrylonitrile) blends. Studying physical polymer mixtures using M-TDSC Hourston and co-workers[328] showed that differences in transition temperatures of the constituent polymers as small as 10°C could be readily resolved.

Stress-strain and hardness measurements. The mechanical properties of the composition series were investigated by tensile testing and Shore A and D hardness measurements. The stress and elongation at break, Young's modulus, the toughness index and values for Shore A and D hardness are given in table 6.2. As was expected by combining an elastomeric with a glassy polymer, an important change in mechanical properties was observed. A plot of the stress and strain at break versus IPN composition is show in figure 6.11. The stress at break showed some scatter, but generally increased with increasing PEMA content. However, a certain pattern was observed which was somewhat similar to that of the PUR/PS IPNs (section 5.2). The values for the stress at break showed three distinctive regions.

Table 6.2 Mechanical properties of the PUR/PEMA IPNs as a function of composition.

IPN Composition [% PEMA]	Tensile properties Stress at break [MPa]	Strain at break [%]	Young's modulus [MPa]	Toughness [J]	Hardness Shore A	Hardness Shore D
0	1.2	210	1.0	0.6	40	25
10	1.4	280	1.3	1.1	41	27
20	4.2	410	3.3	2.7	46	28
30	9.3	360	8.0	7.5	74	41
40	9.6	230	39	4.6	85	49
50	10	110	70	3.7	94	62
60	13	75	210	3.7	98	70
70	12	44	300	2.5	99	79
80	18	22	500	1.8	99	88
90	32	12	770	1.1	99	95
100	45	10	870	0.9	99	97

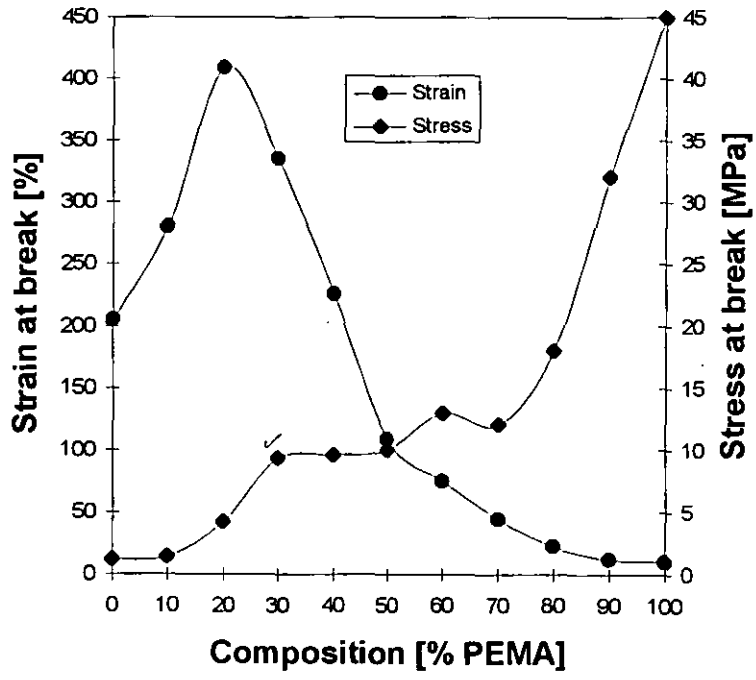

Figure 6.12 Stress and strain at break versus PUR/PEMA IPN composition.

The first region had the stress at break values increasing continually from the 100 PUR (1.2 MPa) to the 70:30 PUR/PEMA IPN (9.3 MPa). The values for the 100:0, 90:10 and 80:20 PUR/PEMA IPNs were below 4.2 MPa. From DMTA data, it was noted that at these 3 compositions it was the PUR network that constituted predominantly the matrix. The increase to 9.3 MPa for the 70:30 PUR/PEMA IPN represented a more than two-fold increase in stress at break. At this composition, the DMTA data had PUR and PEMA loss factor values of roughly equal heights, perhaps, indicating some phase continuity of the PEMA network. In the second region from the 70:30 to the 30:70 PUR/PEMA IPN compositions the stress at break values generally increased slowly from 9.3 to 12 MPa. These fairly constant stress at break values might have indicated that at these mid-range compositions a co-continuous morphology was present. From the 20:80 PUR/PEMA IPN to the 100 PEMA a rapid increase in the stress at break values from 18 MPa to 45 MPa was observed. This was an indication of a further change in IPN morphology to an increasingly predominant PEMA matrix, with very little or no continuity of the PUR network. The finding of an important change in morphology about the 30:70 PUR/PEMA composition was corroborated by the loss modulus peak locations (figure 6.5). The loss modulus is the product of the storage modulus and the loss factor. The transition location and magnitude for the latter two depend strongly upon the miscibility and connectivity of the polymer components. For a completely miscible polymer blend, the location of the linear E" peak would move to increasingly higher temperatures with increasing fractions of the higher Tg polymer. In this semi-miscible PUR/PEMA IPN, a different pattern was observed. The loss modulus peak location remained very much unchanged up to around 70 weight % PEMA. At this composition, a major E" peak shift towards higher temperatures occurred. This is a strong indication that the properties of the 30:70 PUR/PEMA IPN were to a great extent determined by a continuous PEMA phase with discontinuous PUR domains dispersed in it. At lower PEMA compositions, the PUR component influenced the IPN properties significantly, and was, thus, thought to be continuous to some degree.

For both the strain at break and the toughness index, true synergistic effects were observed, with the IPN surpassing, by far, either of the two homonetworks. These special properties were both obtained around the 70:30 PUR/PEMA composition. This might be explained by the fact that both networks were continuous to some

extent and that network interpenetration was achieved on a high level. The strain at break values exhibited a maximum between the 80:20 and 70:30 PUR/PEMA IPN composition (table 6.2). The largest strain at break (410%) was almost twice as high as that of the pure PUR network (210%). The location of the highest strain at break between the 80:20 and 70:30 PUR/PEMA IPN compositions coincided with the lowest storage modulus for the 70:30 PUR/PEMA IPN in the rubbery region at 140°C (figure 6.3). This might have been an indication of a lower apparent crosslinking density in the IPN and indicated that both networks did prevent each other from developing fully.

The toughness index for the 70:30 PUR/PEMA IPN with 7.5 J was more than 7 times as high as either of the homonetwork values (table 6.2). This coincided with the broad loss factor transition that was found from the DMTA data (6.1(d)). Thus, this 70:30 PUR/PEMA composition possessed very good energy absorbing characteristics.

The Shore A and D indentation hardness values versus IPN composition are shown in figure 6.13.

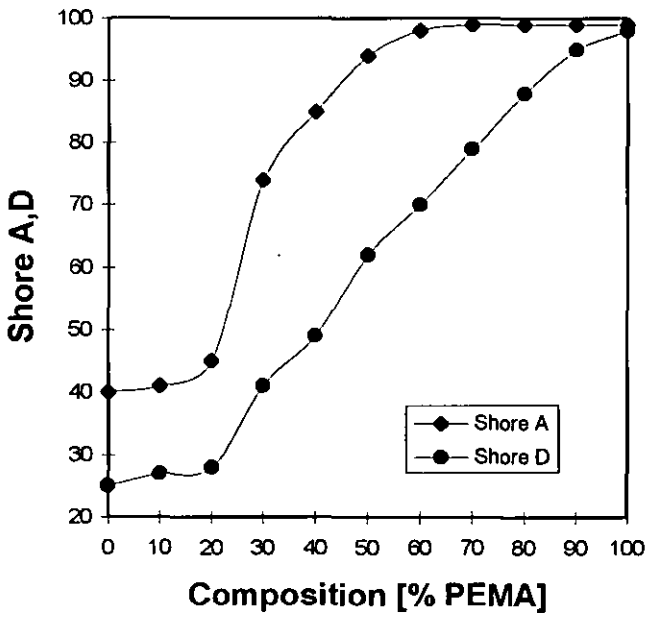

Figure 6.13 Shore A and D versus PUR/PEMA IPN composition.

The Shore A values exhibited a sigmoidal curve shape. A considerable increase in Shore A hardness was found for the 70:30 PUR/PEMA composition which might have indicated a change in the continuous phase. For Shore D hardness values, a

linear pattern was found for an increase in PEMA content. However, it must be emphasised that the data obtained at the outer ranges are not very reliable. The useful working ranges were indicated[286] to be between 10 and 90 for Shore A and between 30 and 90 for Shore D. Thus, the possible change in IPN morphology at the 70:30 composition was below the useful operating range of Shore D.

Modulus-composition studies. The plot of the Young's or storage moduli versus composition at a given temperature can be related to models which allow predictions about phase continuity and phase inversion in a polymer blend to be made. The equations for the Kerner, Davies and Budiansky models were described in section 5.2. Also, a brief review of modulus-composition studies on IPNs was given. Some IPNs followed the Budiansky model while most researchers found their data to fit best the Davies equation indicating dual-phase continuity. The fact that no clear conclusions could be drawn might have been because of the fact that in most cases only three to four data points were employed to make predictions over the full composition range. The PUR/PS IPN composition series in chapter 5 resembled best the Budiansky model and phase inversion was believed to have occurred between the 30:70 and the 20:80 PUR/PS IPN composition. The dynamic storage moduli (10 Hz) at 23°C of the PUR/PEMA IPNs and the PUR and PEMA homonetworks are plotted against the composition in figure 6.14. The experimental data points for the storage moduli did not fit exactly any of the theoretical models investigated. However, clearly the shape of the Budiansky equation, involving phase inversion at the intermediate composition, gave the best approximation. From the storage moduli for this simultaneous PUR/PEMA IPN phase inversion seemed to have taken place at the 80:20 PUR/PEMA IPN composition. The Young's moduli obtained from tensile testing at room temperature are shown versus composition in figure 6.15. Akay and Rollins[58] observed different trends for Young's moduli and dynamic storage moduli, with the former following the Budiansky and the latter the Davies equation. In contrast to that, in the present study, the curve shapes of Young's moduli versus composition were very similar to those of the dynamic storage moduli. The values for the latter were higher than the Young's moduli which was explained by the frequency effect.

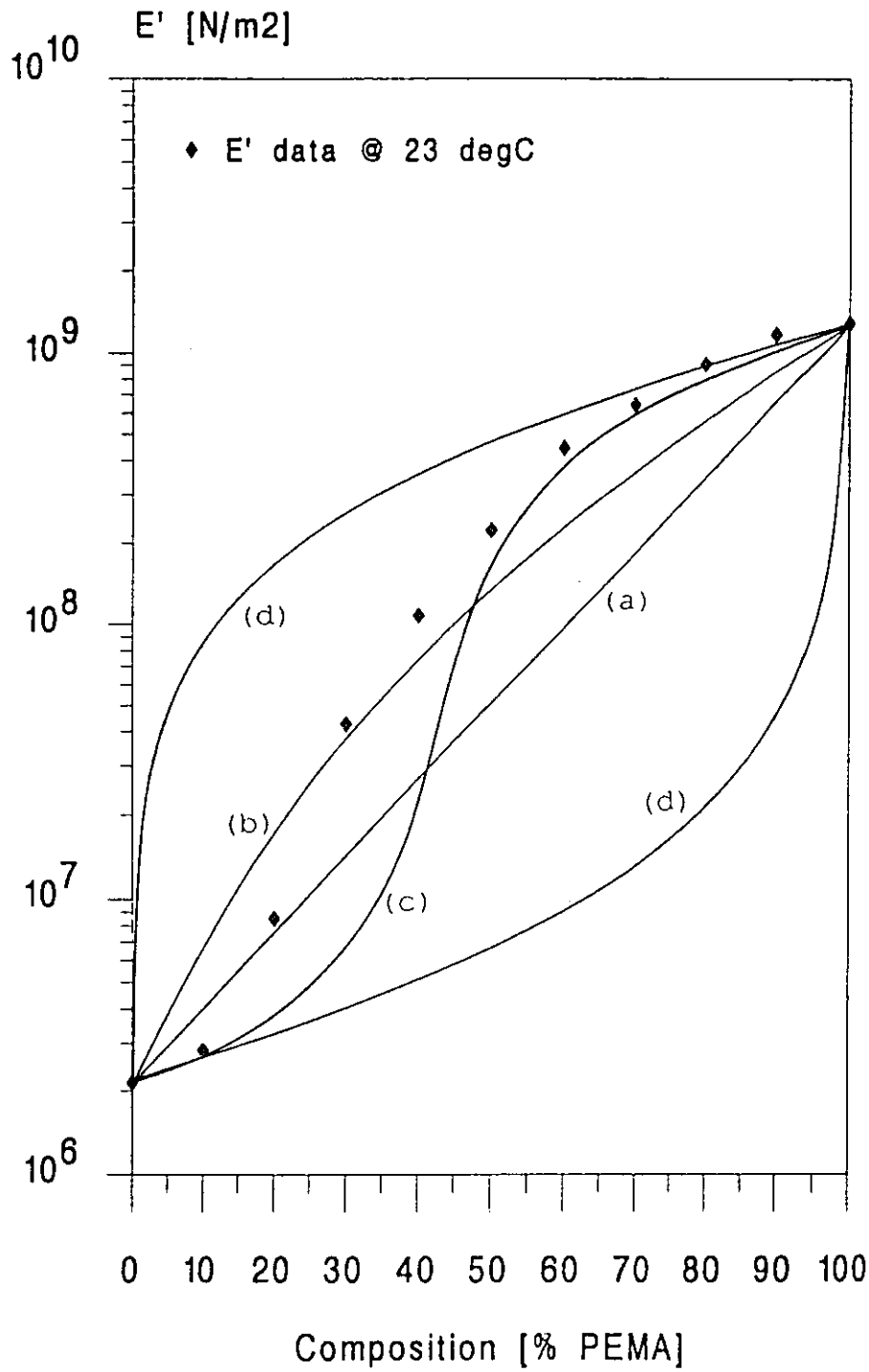

Figure 6.14 Storage moduli (23°C, 10 Hz) versus IPN composition compared with modulus composition models. (a) the logarithmic rule of mixing, (b) the Davies equation, (c) the Budiansky equation and (d) the upper and lower bounds of the Kerner equation.

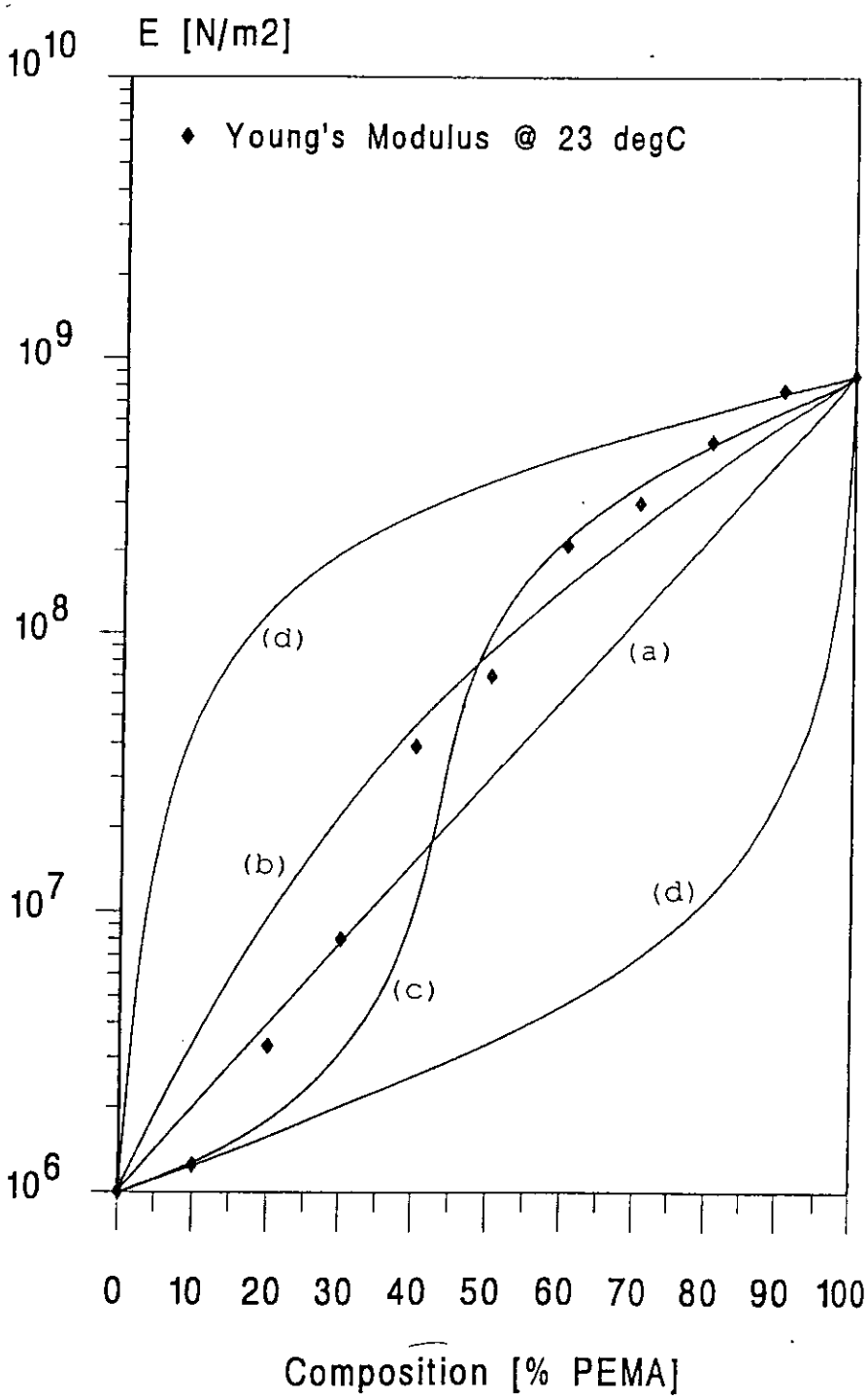

Figure 6.15 Young's moduli (23°C) versus IPN composition compared with modulus composition models. (a) the logarithmic rule of mixing, (b) the Davies equation, (c) the Budiansky equation and (d) the upper and lower bounds of the Kerner equation.

Phase inversion seemed to have taken place at a slightly higher PEMA content, namely at the 70:30 PUR/PEMA IPN composition. An important factor that has been neglected so far in modulus-composition studies is the temperature at which the investigation is conducted. Because of its practical importance and convenience for tensile testing, most modulus-composition studies have been conducted using room temperature data, irrespective of the glass transition temperatures of the constituent polymers. The fact that temperature might have an influence on the shape of the modulus-composition curve was experienced in figures 6.14 and 6.15. From the dynamic storage modulus data phase inversion seemed to have occurred at a lower PEMA content (20%) than from Young's modulus (30%). Since in dynamic experiments frequency is equivalent[93] to temperature, it seemed that by conducting modulus-composition studies closer to the Tg of the lower Tg component, phase inversion was apparently shifted to lower weight fractions of the higher Tg polymer. In order to confirm this assumption, plots of storage moduli versus composition were made at 0°C, 10°C, 23°, 43°C and 80°C (figure 6.16). These temperatures were chosen because one (0°C) was near the glass transition of the PUR network (-5°C from the loss factor peak) and 80°C was relatively near the PEMA network Tg (105°C). The temperatures of the half-step drop of the pure PUR network (-9°C) and of the pure PEMA network (95°C) storage moduli were determined in figure 6.3. The temperature (43°C) intermediate between these two points was chosen for this modulus-composition study. The five curves in figure 6.16 clearly confirmed the above idea. Conducting the modulus-composition studies at temperatures nearer to the lower Tg polymer resulted in an apparent phase inversion at lower weight fractions of the higher Tg polymer (figure 6.16(d) to (b)). An extreme case is shown in figure 6.16(a), where no phase inversion appeared to be occurring with the curve resembling the Davies equation for dual-phase continuity. At the other extreme of 80°C, the curve was concave in shape. Thus, altering the exponent (1/5) from the Davies equation to a value for the exponent n of $0 > n > -1$ and introducing it into Nielsen's general mixing equation[185] (section 5.2) would have yielded a similar concave curve shape. Between these two extremes, intermediate curve shapes were obtained at different temperatures.

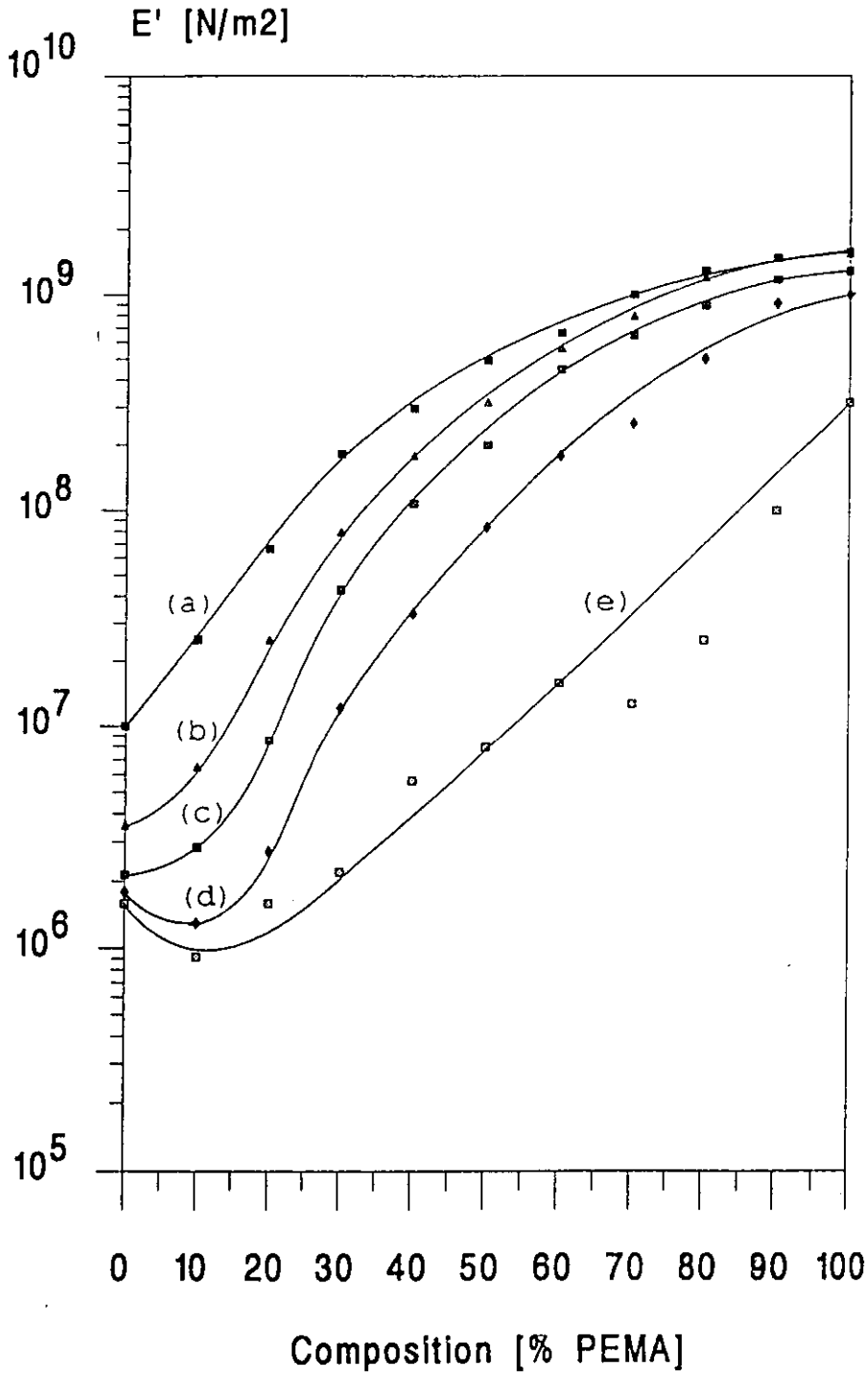

Figure 6.16 Storage moduli versus IPN composition taken at different temperatures. (a) E' data at 0°C, (b) at 10°C, (c) at 23°C, (d) at 43°C and (e) at 80°C. The solid lines are the best fit through the data points.

The irregularities, particularly in the curve at 80°C, changing from the 40:60 to the 30:70 composition were due to a difference in miscibility/morphology of the IPN which was already in evidence in figures 6.2 and 6.3 and table 6.1. The same irregularities were seen, to a lesser extent, in the modulus-composition study at 43°C. At this intermediate temperature between the half-step drop of the homonetwork storage moduli, phase inversion seemed to have taken place at the 70:30 PUR/PEMA IPN composition. This further corroborated the finding of co-continuous phases which had already been indicated by the equal loss factor peak heights in the DMTA data (figure 6.1). The fact that the Young's modulus versus composition plot predicted, correctly, the phase inversion to have taken place at the 70:30 composition was because the latter was determined by a static test. Tgs obtained from DSC measurements for the PUR (-38°C) and the PEMA (75°C) homonetworks happened to be approximately 30°C lower, so that room temperature (23°C) was very close to the intermediate temperature (19°C). Thus, it can be concluded that contradictory results in the literature might have arisen because of an insufficient number of composition data points and disregard of the effect of the temperature on the test results.

In conclusion, a new insight regarding modulus-composition studies has been gained. The temperature, at which the modulus values were taken, was seen to influence greatly the shape of the modulus-composition plot. An important change from Davies-like data to Budiansky-like data, indicating phase inversion at the mid-range composition, was observed. It was, therefore, suggested that in order to make such modulus-composition studies, modulus data should be taken at the intermediate temperature of the half-drop of the storage modulus curves of the PUR and PEMA homonetworks. Following this suggestion in the present study indicated that phase inversion to took place at the 70:30 composition, which was in accordance with the findings from complimentary experimental techniques.

Morphology by TEM and SEM. TEM and SEM studies were undertaken in order to further characterise the IPN morphology, i.e. the phase continuity, phase domain size and shape. Figures 6.17 and 18 show the TEM micrographs and figure 6.19 the SEM micrographs. The former were stained with OsO_4. SEM studies were conducted on the fractured surfaces of the tensile testing specimens.

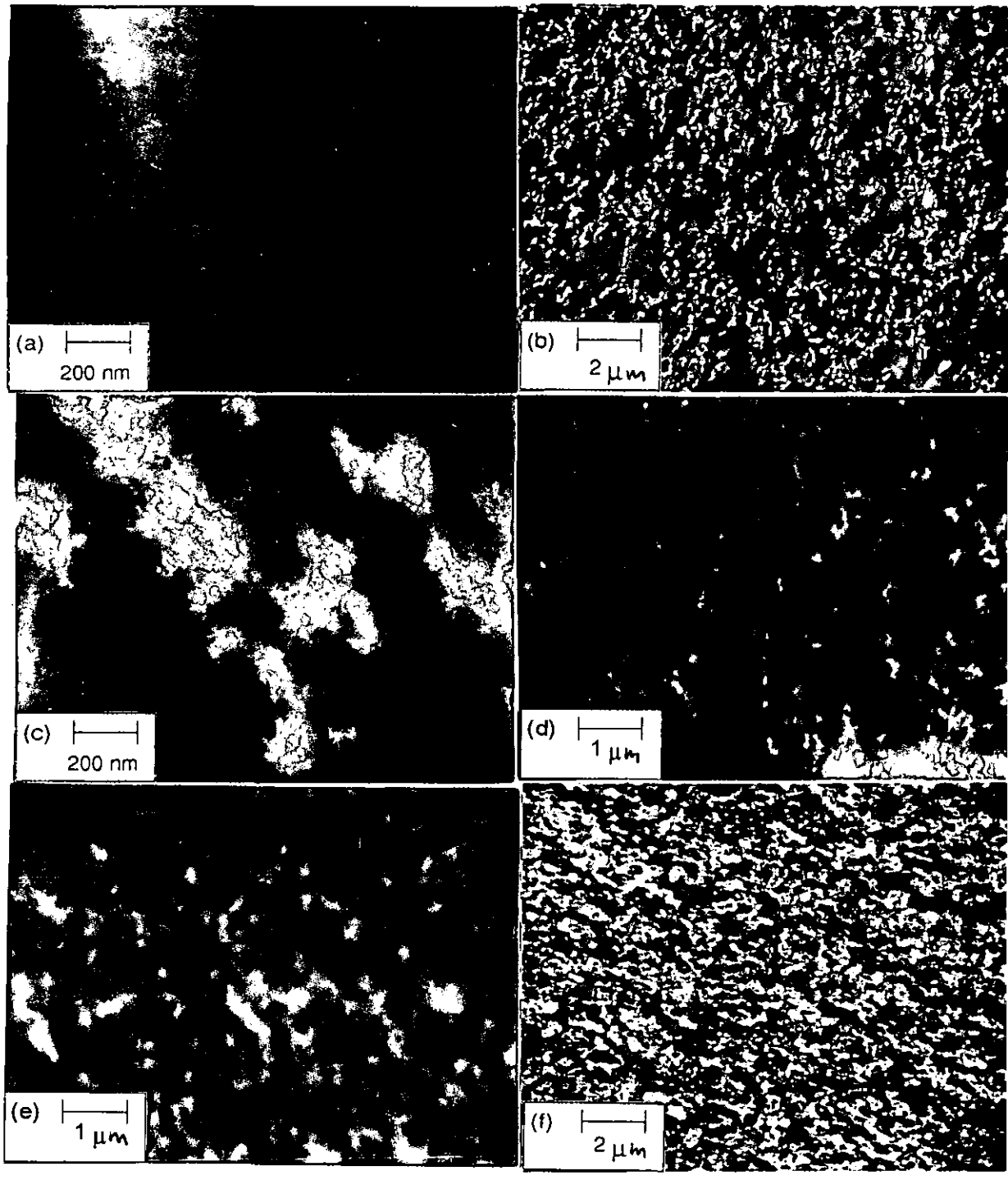

Figure 6.17 TEM micrographs for PUR/PEMA IPN compositions. (a) 80:20 PUR/PEMA, (b)&(c) 70:30, (d) 60:40, (e) 60:40, unstained and (f) 50:50.

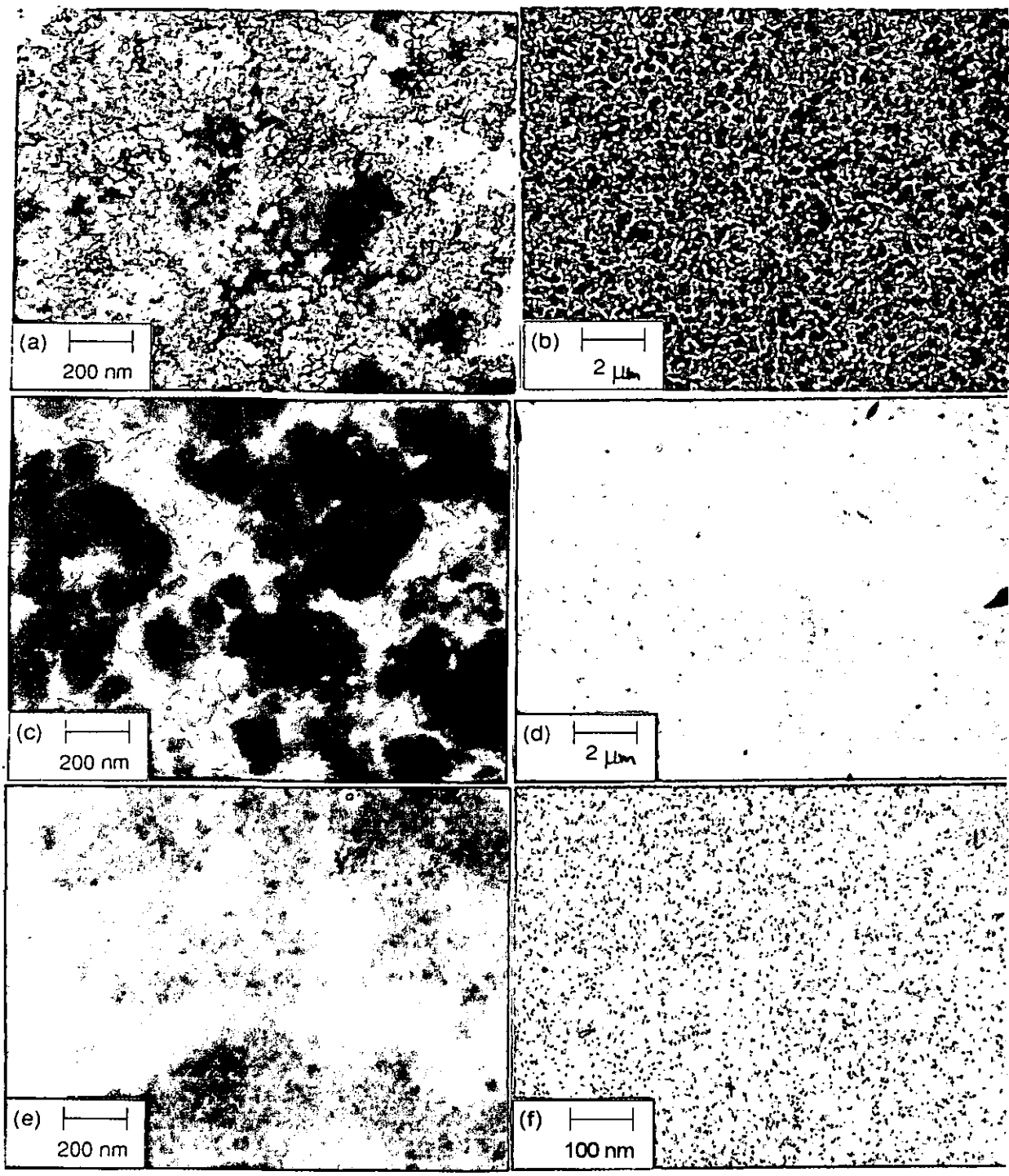

Figure 6.18 TEM micrographs for PUR/PEMA IPN compositions. (a) 50:50 PUR/PEMA, (b)&(c) 40:60, (d)&(e) 30:70 and (f) 20:80.

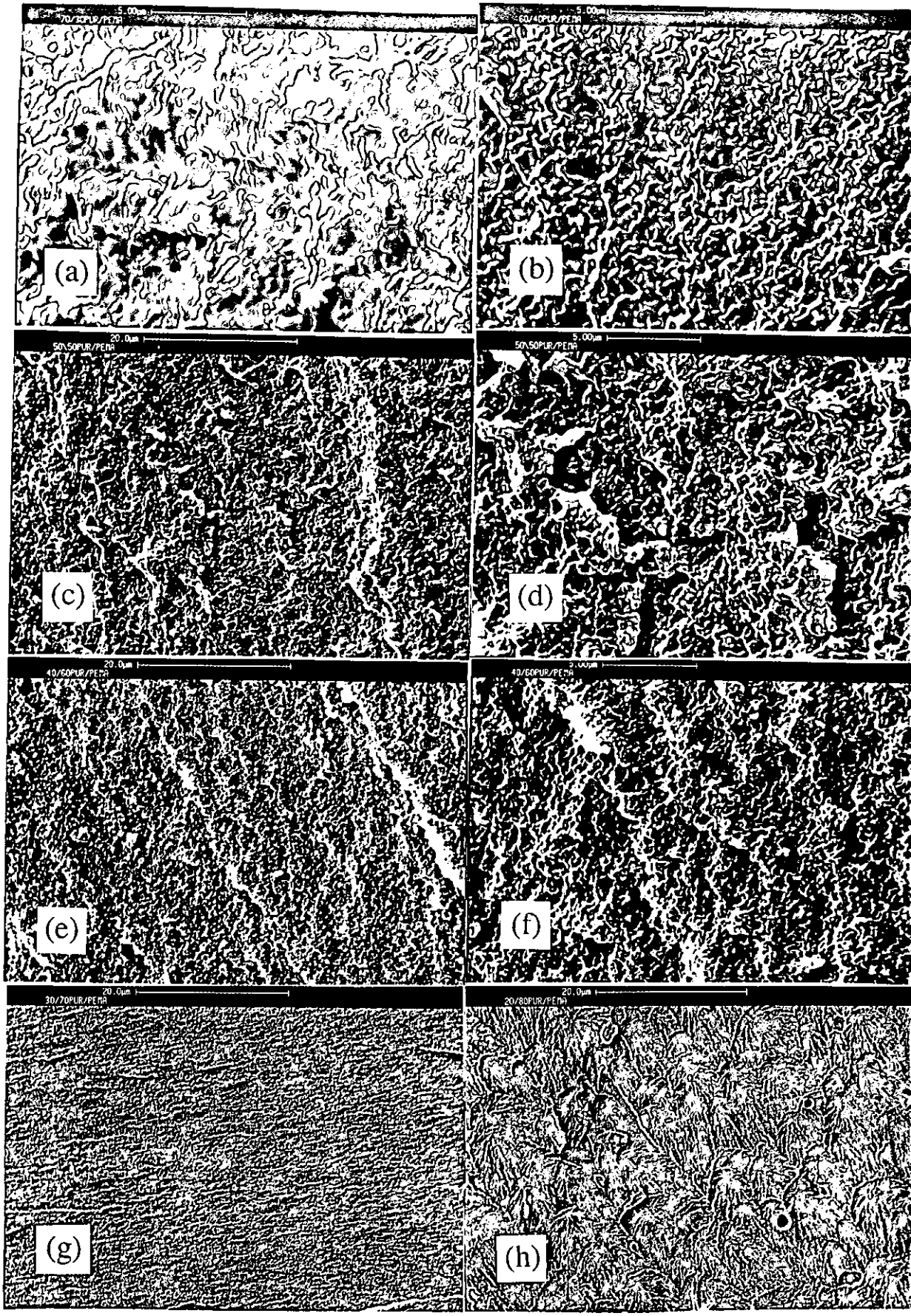

Figure 6.19 SEM micrographs for PUR/PEMA IPN compositions. (a) 70:30 PUR/PEMA, (b) 60:40, (c)&(d) 50:50, (e)&(f) 40:60, (g) 30:70 and (h) 20:80.

For all PUR/PEMA IPN compositions, no gross phase separation was observed by TEM. Contrary to the PUR/PS IPNs where the phase domains were spherical in shape the phase domains in the PUR/PEMA IPNs were not that well-defined which indicated better phase mixing. The IPN morphology changed considerably with composition. The 90:10 and the 80:20 PUR/PEMA IPNs were difficult to ultramicrotome because of their soft nature at room temperature. The micrograph of the 80:20 PUR/PEMA IPN showed a very fine morphology with white PEMA domains in the order of 5-40 nm in a dark OsO_4-stained PUR matrix (figure 6.17(a)). For the 70:30 PUR/PEMA IPN composition white interconnected domains of PEMA in a dominant PUR matrix were observed (figure 6.17(b)). Thus, the TEM micrograph corroborated the DMTA findings of some degree of continuity of both phases. At a higher magnification of 50 k, in addition to a dark PUR matrix and white PEMA domains, an important interface with different shades of grey was in evidence (figure 6.17(c)). This interface of varying composition might have been on the ground of the very broad loss factor transition with high inter-transition values. The 60:40 PUR/PEMA IPN had bigger and more interconnected PEMA phase domains (figure 6.17(d)). The unstained IPN had a much weaker phase contrast (figure 6.17(e)). However, the same pattern was observed indicating that the PUR had a higher electron density than the PEMA. Since no additional information was gained from the unstained 60:40 PUR/PEMA IPN, no further studies were undertaken on the unstained specimens. With an increasing amount of PEMA, the white phase became more dominant. At the 50:50 PUR/PEMA composition, interconnected PUR and PEMA phases were present to an equal extent (figure 6.17(f)). A superstructure which exhibited phase domains in the range of 100-500 nm was observed. Also, a finer structure which in most cases could be described as PUR domains within PEMA domains within a PUR matrix was observed (figure 6.18(a)). Here, very small phase domains of 5-50 nm were noted. The latter structure might be responsible for the third transition that was observed in the loss factor versus temperature curve at the 50:50 composition. At the 40:60 PUR/PEMA composition, both phases still appeared to be co-continuous (figure 6.18(b)). However, a general trend towards a PEMA matrix with dispersed PUR domains of 50-300 nm was observed (figure 6.18(c)). At the 30:70 composition, a change in the properties to a predominantly PEMA-dominated profile was found in the mechanical tests. The micrograph of this composition showed

fairly small (5 - 50 nm) PUR domains in a PEMA matrix (figures 6.18(d) and (e)), which was in good agreement with the observations made from the mechanical tests. At the 20:80 composition, the PUR phase domains were only just resolvable by TEM (figure 6.18(f)). The PUR domains were in the order of 1-10 nm. Consequently, TEM micrographs confirmed that the mid-compositions had a dual-phase morphology with phase separation occurring on a 30 - 300 nm scale being present. The IPNs at the outer composition ranges had a clearly finer morphology with one dominant matrix containing the other polymer dispersed in it.

The SEM micrographs of the PUR/PEMA IPNs (figure 6.19) confirmed a finer morphology for the latter than was observed for the PUR/PS IPN composition in section 5.2. The SEM micrograph of the 70:30 PUR/PEMA IPN composition showed a relatively smooth fracture surface (figure 6.19(a)). No small phase domains as were seen in the 70:30 PUR/PS IPNs could be detected with confidence. At the 60:40 PUR/PEMA IPN composition, a rougher surface was observed (figure 6.19(b)). However, still no clear phase domains were noted. It was thought that the surface roughness could stem from interconnected PEMA cylinders. However, no such large cavities as were observed for the 60:40 PUR/PS IPNs (figure 5.(h)) were noted. A somewhat rougher fracture surface was found for the 50:50 PUR/PEMA IPN composition (figure 6.19(c) and (d)). A limited number of small interconnected cavities were in evidence (figure 6.19(d)). The latter might have been evidence for a certain degree of connectivity of both phases. At the 40:60 PUR/PEMA IPN composition, clearly fewer and shallower cavities were noted on the fracture surface (figures 6.19(e) and (f)). The fracture surface for the 30:70 PUR/PEMA IPN was considerably smoother, perhaps, indicating that PEMA predominantly constituted the matrix at this IPN composition (figure 6.19(g)). The 20:80 PUR/PEMA IPN composition (figure 6.19(h)) had a fracture surface that was similar to the 100 PEMA. In conclusion, it was evident that SEM was not as useful to investigate the PUR/PEMA IPN morphology as it was studying the PUR/PS IPNs. This was a result of the much smaller phase domains of the PUR/PEMA IPN compositions and a morphology that was to a lesser extent phase-separated than that of the PUR/PS IPNs.

Swelling studies. Swelling studies[93] can be used to determine the average molecular weight between crosslinks, $M_{c,t}$, the solubility parameter, δ, and the sol/gel content of a crosslinked polymeric material. The $M_{c,t}$ values of the PUR networks were calculated and compared with the experimentally determined values in section 4.2. In the present study, the solubility parameters were determined for the PUR network, the 50:50 PUR/PEMA IPN and the PEMA network (figure 6.20).

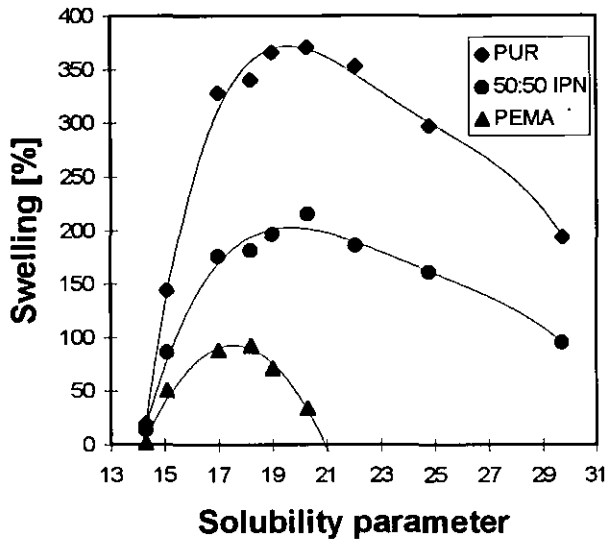

Figure 6.20 Swelling data of the 100 PUR, 50:50 PUR/PEMA IPN and 100 PEMA. The swelling solvent series comprised pentane (δ = 14.3), diethyl ether (δ = 15.1), ethyl methacrylate (δ = 17.0), butylformate (δ = 18.2), methyl cyclohexane (δ = 19.0), cyclohexanone (δ = 20.3), dimethyl acetamide (δ = 22.1) and methanol (δ = 29.7). The solubility parameters in $(J/cm^3)^{1/2}$ were taken from reference 254.

The procedure and a table with the different swelling agents were reported in section 3.4.10. With the exception of pentane (weak) and methane (strong), all solvents used were moderately hydrogen bonding. This was done in order to eliminate additional interactions that might have been caused by different degrees of swelling agent polarity. By swelling the material in a series of swelling agents of different solubility parameters, a curve was constructed. The swelling agent that resulted in the highest degree of swelling of the material was taken as the closest to the material solubility parameter. In the present study, the peaks of the swelling curves were fairly broad which made the determination of an exact solubility parameter difficult. Nevertheless,

the values of 20.3 $(J/cm^3)^{1/2}$ for the PUR and 18.0 $(J/cm^3)^{1/2}$ for the PEMA were in very good agreement with the literature values[254] of 20.5 $(J/cm^3)^{1/2}$ and 18.3 $(J/cm^3)^{1/2}$, respectively. The swelling percentages of the 50:50 PUR IPN were intermediate between the PUR and PEMA networks. The location of the highest swelling behaviour was very similar to the PUR network. Thus, the solubility parameter of the 50:50 PUR/PEMA IPN was similar to that of the PUR network (20.3 $(J/cm^3)^{1/2}$). Using cyclohexanone as swelling agent, the swelling behaviour of the full PUR/PEMA IPN composition series was studied. The percent swelling against composition is shown in figure 6.21.

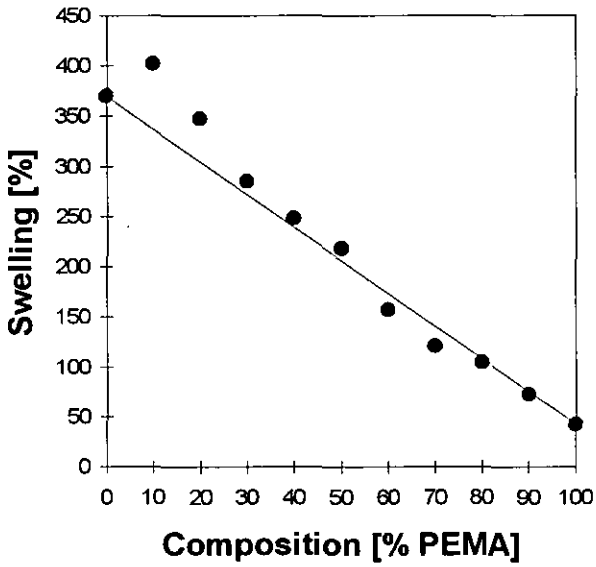

Figure 6.21 Swelling studies of the PUR/PEMA IPN compositions. The swelling agent was cyclohexanone.

The trend of the swelling percentages were generally in line with expectations. At high PUR contents of 90 and 80% slightly higher values were obtained. This could have indicated that the PUR network did not form completely. A slightly looser PUR network was swollen to a greater extent by the swelling agent. The slightly lower than expected swelling percentages at 40 and 30% PUR might have indicated that some PUR domains enclosed in a PEMA matrix could not be swollen to the same extent as the PUR network. However, the deviations from the expected swelling values at lower PUR contents were only very small (> 10%).

Soxhlet extraction studies were conducted in order to confirm a complete network formation. The full composition series was investigated. Refluxing acetone was used as the extraction solvent according to the procedure outlined in section 3.4.10. All IPNs and both homonetworks had a gel content of greater than 96%. This confirmed that complete network formation took place at a PPG1025/TMP ratio of 3:1 in the PUR and a crosslinker level of 5% TEGDM in the PEMA network.

Selection of the 70:30 PUR/PEMA IPN composition. The 70:30 PUR/PEMA IPN composition was chosen for further study because of the very broad loss factor transition region that was obtained by DMTA. A microheterogeneous morphology with phase domains in the order of 10 - 200 nm was confirmed by TEM. Furthermore, stress-strain measurements revealed synergistic effects which manifested itself in maxima for the strain at break and the toughness index. The loss factor and storage and loss moduli are shown in figures 6.22 and 6.23. The loss factor values were greater than 0.3 over a temperature region of 130°C (figure 6.22). The storage and loss moduli versus temperature reflected the loss factor profile. Both moduli fell continually in a linear manner which is characteristic[152] for a broad loss factor transition caused by a microheterogeneous morphology.

The reaction kinetics of the 70:30 PUR/PEMA IPN were studied by FT-IR with a heated cell unit. The same procedure (section 3.4.9) as in section 5.2 for the PUR/PS IPNs was applied. Since a very similar conversion versus time pattern to that of the PUR/PS IPN was obtained the data are not shown here. The study confirmed that the PUR was formed to a great extent (70% conversion) before the onset of the EMA polymerisation. This indicated that the EMA polymerisation proceeded at a slightly higher rate than the PS formation.

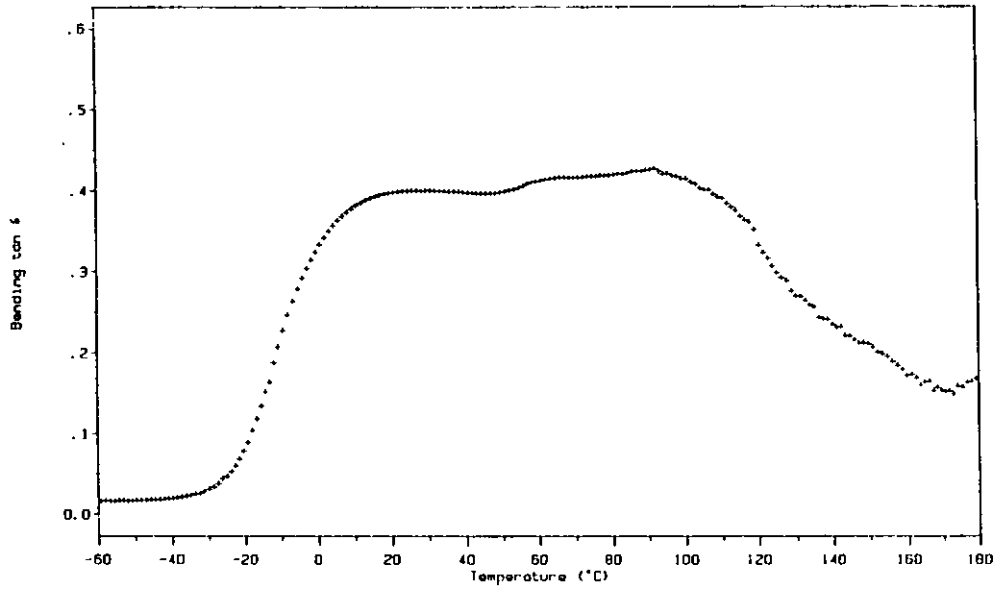

Figure 6.22 Loss factor versus temperature data for the 70:30 PUR/PEMA IPN.

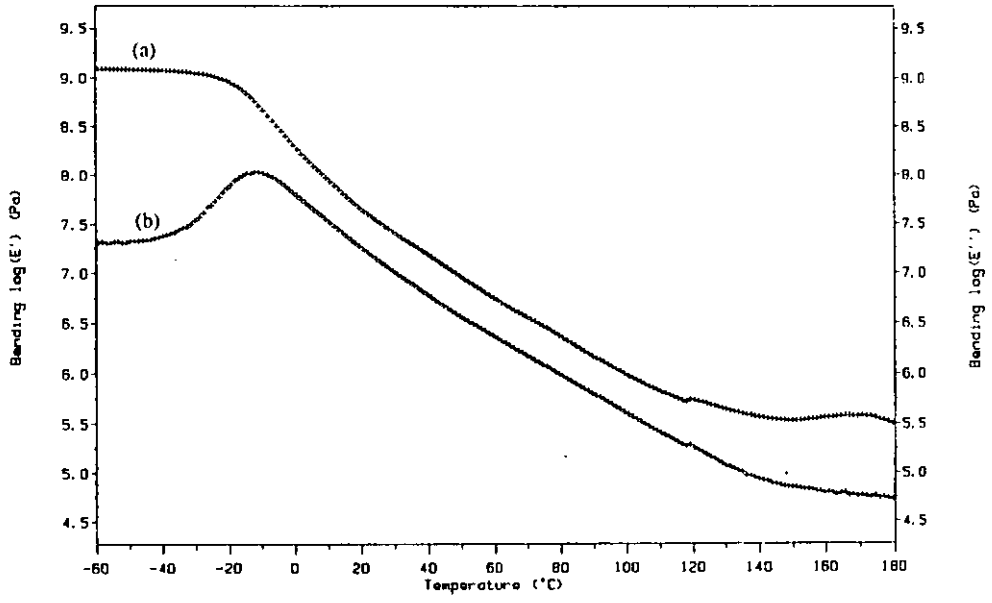

Figure 6.23 Storage modulus (a) and loss modulus (b) versus temperature for the 70:30 PUR/PEMA IPN.

6.2 Variation of the Crosslink Density in the 70:30 PUR/PEMA IPN

The special properties of IPNs are brought about by permanent interlocking of polymer chains through chemical crosslinks[4]. TEM studies[100] revealed that high crosslinking of the first-formed network restricts the phase domain size for the second polymer. Thus, the crosslinking density in the polymer networks greatly influences the mechanical properties and the damping characteristics. In the PUR/PS IPN crosslinking study, it was found that crosslinking decreased the phase domain sizes and influenced the phase continuity and reaction kinetics (section 5.3). In the present study, the influence of the crosslink density in both networks in a PUR/PEMA IPN was investigated. The 70:30 PUR/PEMA IPN composition was selected for this crosslinking study because of its broad loss factor transition (section 6.1). DMTA studies were conducted in order to determine the inherent damping of the IPNs. The influence of crosslinking on the morphology, the thermal and the mechanical properties was determined using TEM, M-TDSC, TGA and stress-strain and hardness measurements.

DMTA studies. The thermoset character makes IPNs very difficult to characterise[329]. Therefore, the values for the theoretical average molar mass between crosslinks, $M_{c,t}$, were calculated for the constituent homopolymers in order to correlate these with the DMTA data. The calculation of the PUR $M_{c,t}$ and the experimental determination by equilibrium swelling, the rubbery plateau modulus and the use of the Nielsen equation[265] were fully discussed in section 4.3. The crosslinking density of the PEMA network was calculated using equation 5.5. Because of the high TEGDM molar mass of 330 g/mol, this was taken into account by the second component in the sum. Figures 6.24 and 6.25 show the loss factor and the storage modulus versus temperature data for the 70:30 PUR/PEMA IPN at a fixed crosslinked level of 5 mol % TEGDM and various PPG1025/TMP ratios. The DMTA data are given in table 6.3 together with $M_{c,t}$ values. The DMTA data for the PUR homonetworks from section 4.2 are also given for comparison. The loss factor data showed, as expected, that with increasing triol content, the PUR transition moved to increasingly higher temperatures. The semi-2 PUR/PEMA IPN which was synthesised by leaving out the triol in the PUR had the lowest Tg with -16°C (figure 6.24(a)).

Table 6.3 Dynamic mechanical properties (10 Hz) of the 70:30 PUR/PEMA IPN as a function of crosslink density.

IPN PUR/PEMA	$M_{c,t}$ [g/mol] PUR/PEMA	Tg [tan δ, °C] [PUR]	PUR	PEMA	Tan δ maximum [PUR]	PUR	PEMA	Half-peak width [°C]
1:1 / 5%	1200 / 1300	[30]	54	(a)	[0.73]	0.60	-	72
2:1 / 5%	2000 / 1300	[4]	29	(a)	[0.92]	0.55	-	82
3:1 / 10%	2900 / 700		18	95		0.47	0.26	118
3:1 / 5%	2900 / 1300	[-5]	18	87	[1.08]	0.40	0.42	156
3:1 / 2.5%	2900 / 2400		20	75		0.43	0.42	131
3:1 / 1%	2900 / 5800		45	(a)		0.50	-	111
3:1 / 0%	2900 / linear		29	(a)		0.60	-	84
7:1 / 5%	6300 / 1300	[-9]	-9	75	[1.41]	0.39	0.43	149
1:0 / 5%	linear / 1300	[-12]	-16	(b)	[1.60]	0.40	(b)	(b)

(a) No glass transition temperature for the second component could be determined.

(b) Material became too soft for measurement.

[ ] Values in square brackets are for the PUR homonetworks (section 4.2).

The loss factor peak height of the PUR in the IPN (0.40) was four times lower than that in the PUR homonetwork (1.60). This might have indicated that the linear PUR in the IPN exhibited only limited phase continuity. No loss factor transition peak was obtained for the PEMA network because of an important softening of the IPN at temperatures above 50°C. With increasing triol content in the PUR, the Tg shifted to higher temperatures. At a PPG1025/TMP ratio of 7:1, the PUR transition shifted to -9°C. A very broad transition plateau was obtained which made the determination of the PEMA transition (~75°C) difficult (figure 6.24(b)). The loss factor values were greater than 0.3 from -23°C to 108°C, thus, making this IPN an excellent damping material. The IPN crosslinked at a PPG/TMP ratio of 3:1 was discussed in section 6.1. It had an equally broad high damping transition at a slightly higher temperature range. The loss factor values were greater than 0.3 for a temperature range of 130°C, from -4°C to 126°C. The latter two IPNs had PUR and PEMA loss factor peaks of roughly equal heights which suggested dual-phase continuity in these materials.

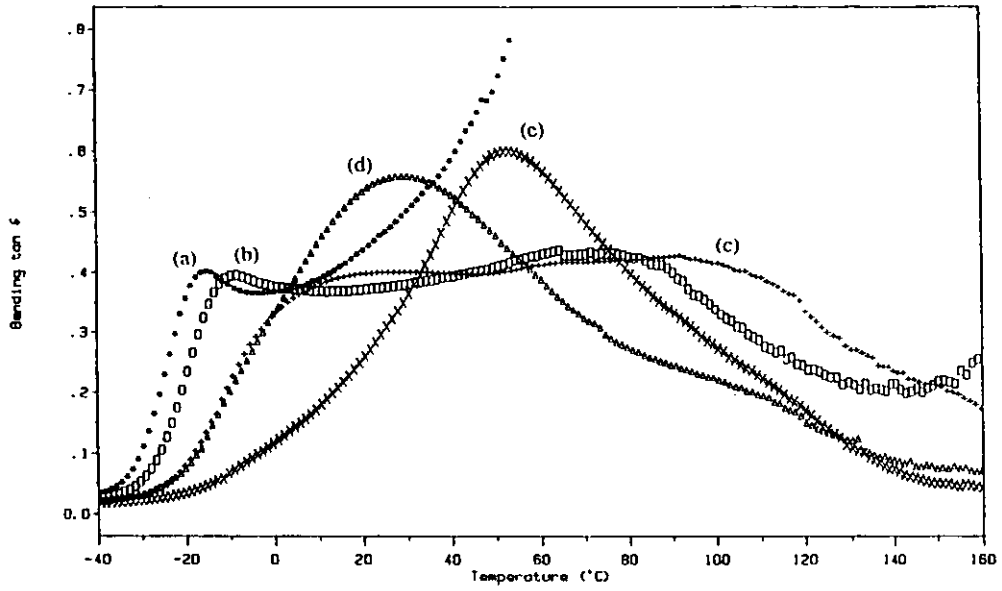

Figure 6.24 Loss factor versus temperature data for the 70:30 PUR/PEMA IPNs crosslinked with 5 mol % TEGDM and different PUR network crosslinking levels. (a) PPG1025/TMP 1:0, (b) 7:1, (c) 3:1, (d) 2:1 and (e) 1:1.

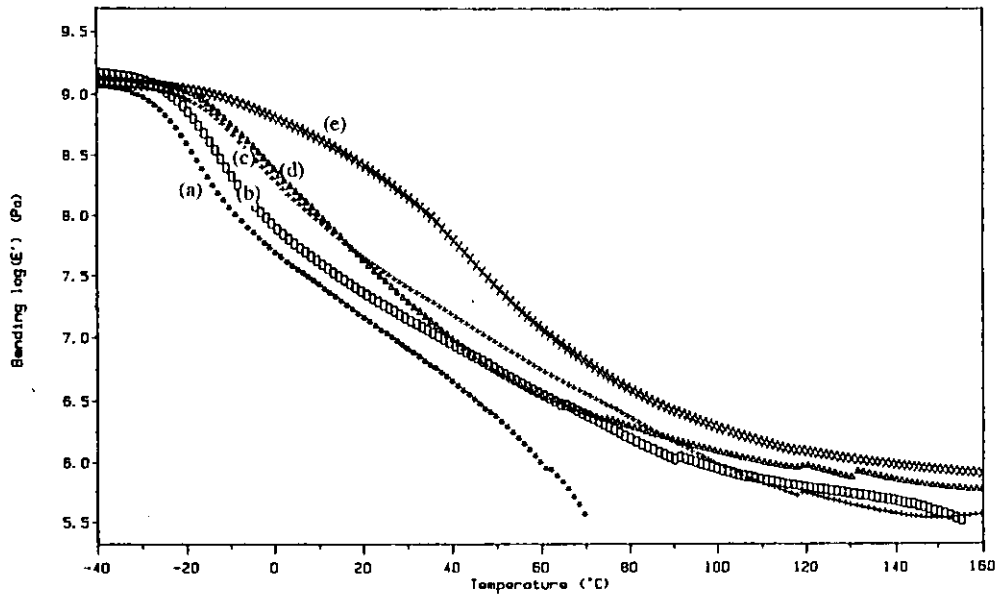

Figure 6.25 Storage moduli versus temperature for the 70:30 PUR/PEMA IPNs crosslinked with 5 mol % TEGDM and different PUR network crosslinking levels. (a) PPG1025/TMP 1:0, (b) 7:1, (c) 3:1, (d) 2:1 and (e) 1:1.

the PUR networks. At a PPG1025/TMP ratio of 1:1, for example, the PUR Tg of the IPN was 54°C, whereas the Tg of the respective PUR network (30°C) was lower by 24°C. For the IPN only one Tg was observed. The latter confirmed that the PUR transition in the IPN did not stem from pure PUR, but from a highly phase mixed PUR-PEMA region. The storage moduli versus temperature profile confirmed the trend of higher Tg values for higher crosslinking densities in the PUR (figure 6.25). Also, the softening of the semi-2 IPN at temperatures of higher than 50°C was mirrored by the abrupt decrease in the storage modulus values. The storage moduli versus temperature profile of the full PUR/PEMA IPNs decreased gradually with increasing temperatures. The latter was evidence of a semi-miscible morphology. The highest crosslinking density in the IPN crosslinked at a PPG1025/TMP ratio of 1:1 was reflected by the highest rubbery plateau modulus.

In addition to the crosslinking density in the PUR network, also that in the PEMA component of the IPN was varied. While varying the PEMA crosslinking levels, the PPG1025/TMP ratio was fixed at 3:1. The loss factor and storage modulus versus temperature data for the 70:30 PUR/PEMA IPNs with the different PEMA crosslinking densities are shown in figures 6.26 and 6.27. Increasing the crosslinker level moved part of the IPN transition to higher temperatures. The transition split into two parts, with the PUR part shifting to slightly lower temperatures, whereas the PEMA strongly shifted to higher temperatures (table 6.3). Thus, as opposed to higher crosslinking in the PUR, higher crosslinking in the PEMA generally resulted in a broadening of the IPN transition peak. The latter indicated the presence of a less phase-mixed IPN system. The semi-1 IPN with 0% TEGDM crosslinker exhibited the highest loss factor peak (0.60) and the narrowest loss factor half-peak width with 84°C (table 6.3). No significant high-temperature shoulder for the PEMA transition was present. This suggested that the best mixing occurred with this IPN. With increasing amount of crosslinker, the transition breadth increased and the PEMA transition moved to higher temperatures. At a 1% TEGDM incorporation level, a single, clearly broader transition peak was, however, still obtained. The less phase-mixed structure manifested itself in a lower loss factor peak height (0.50) and a higher half-peak width value (111°C). Furthermore, as a consequence of the increased crosslinking density, the IPN Tg shifted from 29°C to 45°C.

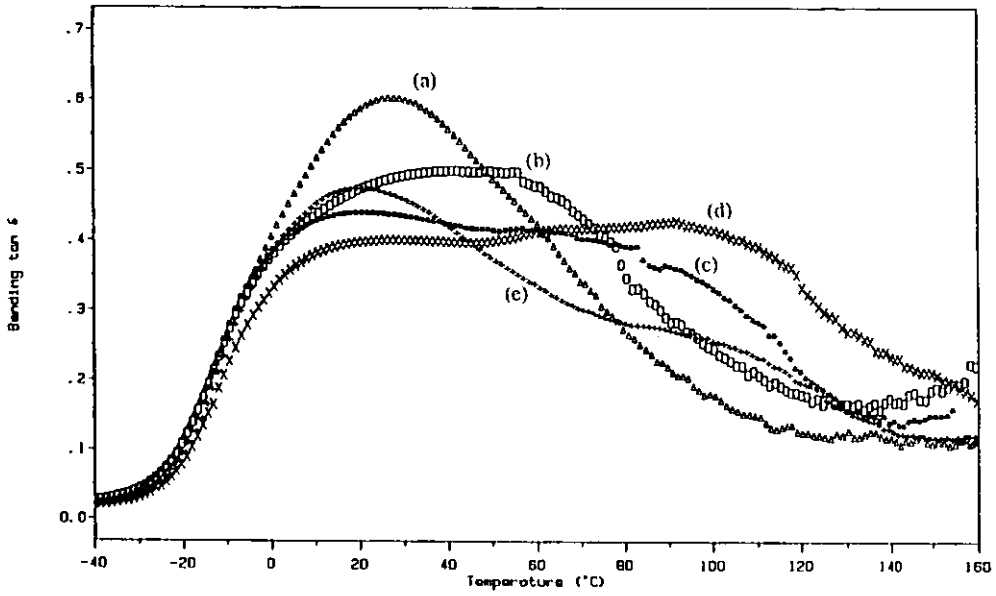

Figure 6.26 Loss factor versus temperature data for 70:30 PUR/PEMA IPNs with a PPG1025/TMP ratio of 3:1 and different PEMA network crosslinking levels. (a) 0% TEGDM, (b) 1%, (c) 2.5%, (d) 5% and (e) 10%.

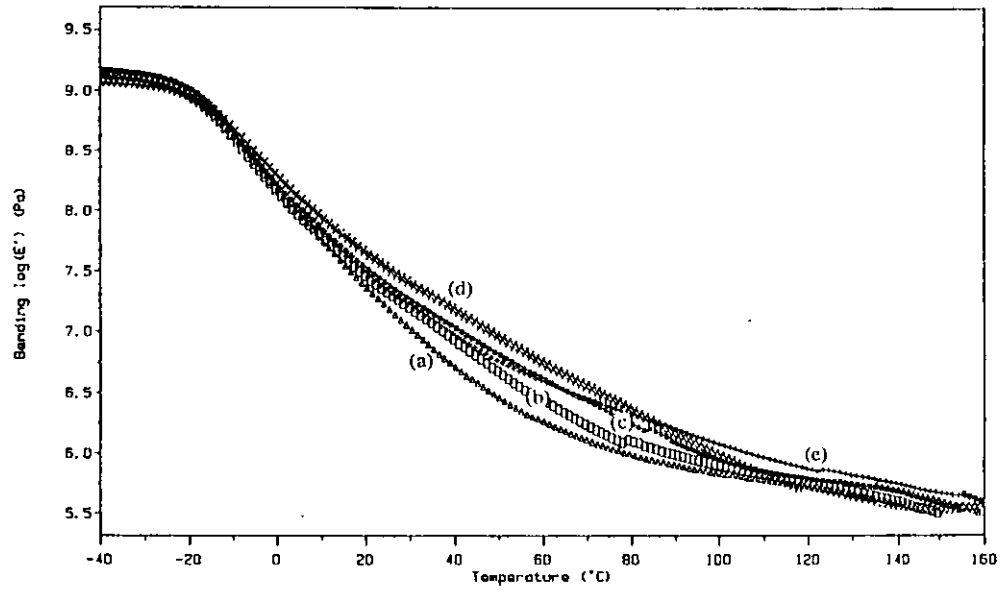

Figure 6.27 Storage moduli versus temperature for 70:30 PUR/PEMA IPNs with a PPG1025/TMP ratio of 3:1 and different PEMA network crosslinking levels. (a) 0% TEGDM, (b) 1%, (c) 2.5%, (d) 5% and (e) 10%.

With 2.5% TEGDM, a split of the IPN transition peak occurred. Part of the transition moved to lower temperatures (the PUR transition) while a very significant shoulder appeared at the high-temperature end. Also, the half-peak width further increased to a value of 131°C. The material with the broadest transition with a half-peak width of 156°C was obtained with 5% TEGDM crosslinking. Further, increasing the crosslinking to 10% TEGDM, led to a significant decrease in the loss factor height for the PEMA transition because of reduced chain segment mobility. The storage moduli versus temperature showed that altering the crosslinking density in the first-formed network had a more pronounced effect on the dynamic mechanical properties of the IPN (figure 6.27) than had changing the crosslinking density in the PEMA. From the storage moduli very little difference between the 5 IPNs with different PEMA crosslinking levels were observed. Comparing the loss factor and the storage modulus data of the PEMA crosslinking study, it appeared that the loss factor data were more sensitive to changes in crosslinking density in the higher Tg IPN component than the storage moduli. The differences observed between increasing the crosslink density in the PUR and in the PEMA component might be explained by the following points. Increasing the PEMA crosslinking shifted the transition to higher temperatures, thus, away from the PUR transition. Whereas higher crosslinking in the PUR shifted the transition towards the PEMA transition. Higher crosslinking in the first-formed PUR network increased phase mixing by restricting the domain size of the PEMA network. Higher crosslinking of the PEMA network had little influence on the already formed PUR network and rather decompatibilised the IPN by decreasing the PEMA chain segment mobility and increasing the PEMA Tg.

Modulated-temperature DSC studies. The Tg behaviour of the 70:30 PUR/PEMA IPNs of varying crosslinking density in both networks was investigated by M-TDSC. Because of the high degree of enforced phase mixing and the resulting breadth of the transitions the determination of Tg was difficult at times. This was particularly true for the PEMA transition. The general trend of the Tg behaviour was similar for both the DMTA and M-TDSC studies, however, some substantial differences existed. M-TDSC seemed to have been more sensitive to phase separation than was DMTA. With the exception of the IPN crosslinked at a PPG1025/TMP ratio of 1:1, two M-TDSC Tg transitions were resolved for all compositions (table 6.4).

Table 6.4 M-TDSC Tg values for 70:30 PUR/PEMA IPNs of varying crosslinking densities in both networks.

Crosslinking PUR / PEMA	Tg [°C] PUR / PEMA	Crosslinking PUR / PEMA	Tg [°C] PUR / PEMA
1:1 / 5%	-19 / (a)	3:1 / 10%	-32 / 60
2:1 / 5%	-29 / 62	3:1 / 5%	-33 / 48
3:1 / 5%	-33 / 48	3:1 / 2.5%	-32 / 53
7:1 / 5%	-38 / 62	3:1 / 1%	-33 / 50
1:0 / 5%	-41 / 62	3:1 / 0%	(b)

(a) No second transition could be determined with certainty.
(b) Material not investigated.

One example for the higher sensitivity of M-TDSC was the 70:30 PUR/PEMA IPN crosslinked at a PPG1025/TMP ratio of 3:1 and 1% TEGDM. The DMTA loss factor data exhibited one fairly broad IPN transition at 45°C (table 6.3 and figure 6.26(b)), whereas the M-TDSC data showed a PUR transition at -33°C and a PEMA transition at 50°C (figure 6.28).

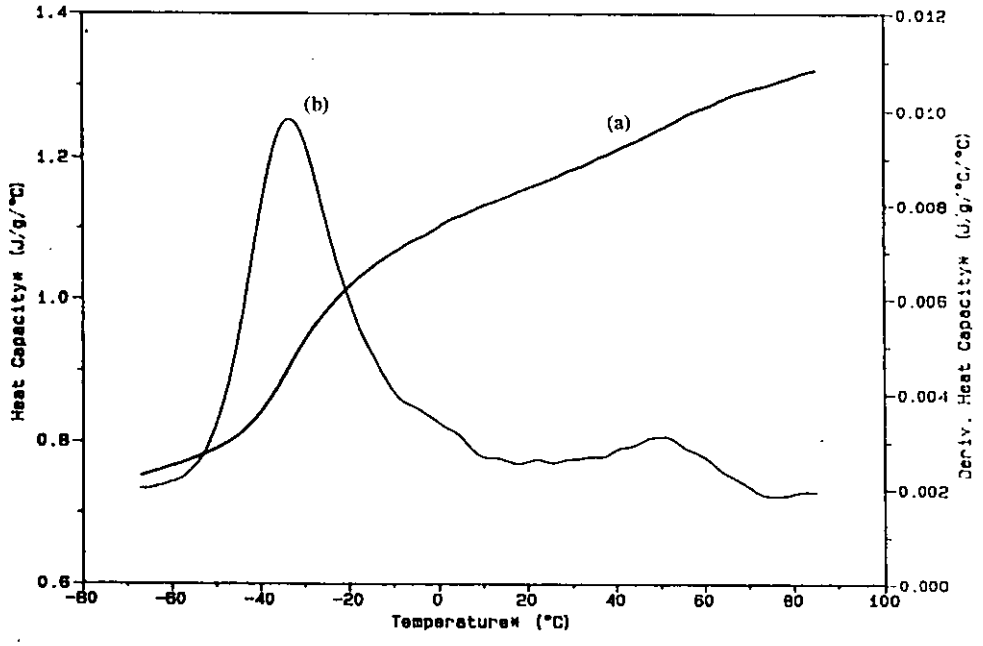

Figure 6.28 Heat capacity (a) and derivative heat capacity (b) of the 70:30 PUR/PEMA crosslinked at a PPG1025/TMP ratio 3:1 and 1% TEGDM.

Similar to the DMTA data, increasing the crosslinking density in the PUR network resulted in a steadily increasing PUR M-TDSC Tg. The magnitude of the Tg increase, however, was very different. The PUR Tg of the semi-2 70:30 PUR/PEMA IPN was -16°C and -41°C for the DMTA and M-TDSC studies, respectively. When changing the crosslinking density in the IPN PUR from a PPG1025/TMP ratio of 1:0 to 1:1, the Tg shifted to 54°C (DMTA) and -19°C (M-TDSC). From DMTA data, a Tg increase of 70°C was obtained, while a mere 22°C were noticed with M-TDSC. The more than three-fold lower Tg shift in the M-TDSC data showed that the different measurement principles of both techniques strongly influenced the Tg results. In this study, when varying the PUR crosslinking density and keeping the PEMA crosslinking density fixed, no clear trend could be noticed for the PEMA transition. At the highest PUR crosslinking density of a PPG1025/TMP ratio of 1:1, the PEMA transition could not be determined with certainty. With the exception of one scattered value (48°C) the PEMA Tg remained at 62°C for all other PUR crosslinking densities.

Increasing the PEMA crosslinking density resulted in less pronounced Tg changes. The PEMA transition had a tendency to increase with higher crosslinking level (table 6.4). The PUR Tgs on the other hand remained unchanged. Thus, again it was noted that the crosslinking density in the first-formed PUR network influenced the IPN behaviour to a much greater extent. Some differences between the M-TDSC and the DMTA data were in evidence. In addition to a difference in sensitivity to phase-separated structures, also the observed transition magnitudes and the Tg shifts with increasing crosslinking were different. While from the DMTA data similar loss factor peak heights were observed for most 70:30 PUR/PEMA IPNs, the PUR transition was clearly dominant in the M-TDSC traces. Consequently, M-TDSC measurements might be more sensitive to a difference in heat capacity and polymer weight fraction whereas DMTA might be to a greater degree influenced by phase continuity.

Stress-strain and hardness measurements. The mechanical properties were investigated by tensile testing and hardness measurements. A compilation of the results is shown in table 6.5. In order to quantify the effect of the crosslinking on the mechanical properties, the stress at break and the strain at break were plotted against $M_{c,t}$ for both crosslink series (figures 6.29 and 6.30). With increasing PUR crosslinking density, an increase in the stress at break values was in evidence (table

6.5). A more than ten-fold increase in stress at break was noted from the semi-2 70:30 PUR/PEMA(5% TEGDM) IPN (0.8 MPa) compared to the corresponding IPN crosslinked at a PPG1025/TMP ratio of 1:1 (13.3 MPa). Thus, when plotting the stress at break against $M_{c,t}$ a steep rise of the values was noted (figure 6.29). The second series in this figure exhibited a much less pronounced increase in stress at break. This was the data series for varying PEMA crosslinking levels with the PUR crosslinking fixed at a ratio of PPG1025/TMP of 3:1. The stress at break increase was only in the order of 40% from 6.7 MPa for the semi-1 70:30 PUR(PPG1025/TMP 3:1)/PEMA IPN to 9.6 MPa for the corresponding IPN crosslinked at 10% TEGDM.

Table 6.5 Mechanical properties of the 70:30 PUR/PEMA IPN as a function of the crosslink density.

Crosslinking 70:30 IPN PUR/PEMA	Tensile properties: Stress at break [MPa]	Strain at break [%]	Young's modulus [MPa]	Toughness [J]	Hardness[(a)] Shore A
1:1 / 5%	13.3	280	33.5	7.9	92
2:1 / 5%	9.4	380	8.3	7.0	71
3:1 / 10%	9.6	380	8.0	7.5	77
3:1 / 5%	9.4	360	8.0	7.6	74
3:1 / 2.5%	8.5	450	7.6	7.0	71
3:1 / 1%	6.9	550	7.3	5.7	67
3:1 / 0%	6.7	640	6.2	6.8	61
7:1 / 5%	4.3	490	6.7	4.1	60
1:0 / 5%	0.8	200	2.5	0.3	45
1:0 / 0%	0.8	590	0.8	0.9	30

(a) Shore D values were not evaluated since most were below the useful working range.

The important difference in the steepness of the two lines connecting the data points confirmed once more that the crosslinking density in the PUR network had a much stronger effect on the IPN properties than that in the PEMA network (figure 6.29). The strain at break values showed a similar general trend for both the PUR and PEMA crosslinking series (table 6.5 and figure 6.30). An increase in the strain at break values was obtained with decreasing crosslinking density.

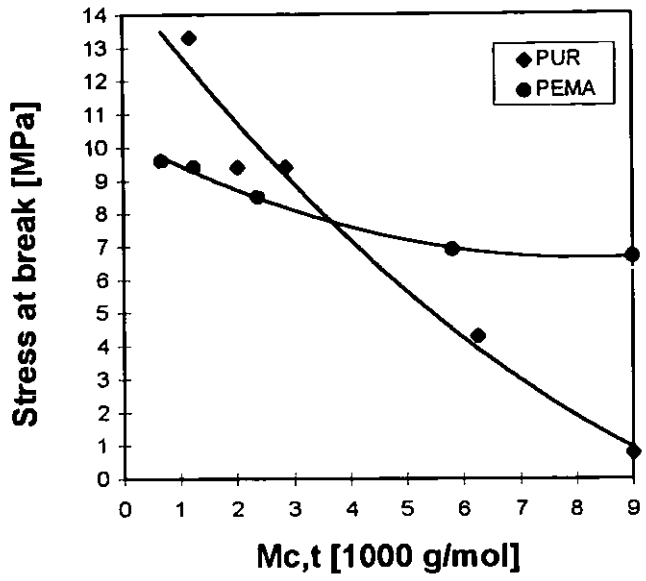

Figure 6.29 Stress at break versus $M_{c,t}$ data. The solid lines are the best fit through the 70:30 PUR/PEMA(5% TEGDM) IPNs with different PPG1025/TMP ratios (PUR) and the 70:30 PUR(PPG1025/TMP 3:1)/PEMA IPNs with different TEGDM levels (PEMA).

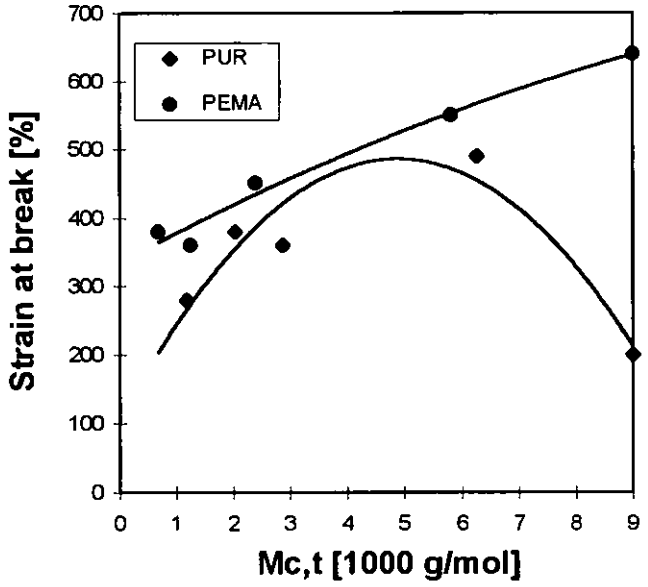

Figure 6.30 Strain at break versus $M_{c,t}$ data. The solid lines are the best fit through the 70:30 PUR/PEMA(5% TEGDM) IPNs with different PPG1025/TMP ratios (PUR) and the 70:30 PUR(PPG1025/TMP 3:1)/PEMA IPNs with different TEGDM levels (PEMA).

The only exception was the semi-2 IPN where the PUR was present in the linear form. This IPN resulted in the lowest strain at break (200%) of all materials. From the DMTA data, it was observed that this material was more phase-separated (figure 6.24(a)), a fact that could have accounted for the poorer mechanical properties. The change in the strain at break values with decreasing $M_{c,t}$ was not as pronounced as for the PUR stress at break data. As a consequence of the latter, higher values for the toughness index were obtained with the higher crosslinked IPNs which exhibited higher values for the stress at break. Thus, the 70:30 PUR(PPG1025/TMP 1:1)/PEMA(5% TEGDM) IPN that exhibited the highest stress at break (13.3 MPa) had also the highest toughness index (7.9 J). Higher crosslinking generally resulted in increased values for the Young's modulus. The increase was much more pronounced for changing the crosslinking density in the PUR network than in the PEMA. For the former, the Young's moduli increased from a value of 2.5 MPa for the semi-2 70:30 PUR/PEMA IPN to 33.5 MPa for the corresponding IPN crosslinked at a PPG1025/TMP ratio of 1:1. On the other hand, when varying the crosslinking density of the PEMA network the Young's moduli merely increased from 6.2 MPa to 8.0 MPa. The Shore A hardness values showed the same trend as the Young's moduli. Varying the crosslinking density in the PUR network resulted in changes of the Shore A values from 45 to 92, while with variations of the PEMA network crosslinking density only a change from 61 to 77 was obtained. The latter re-emphasised the importance of the first-formed network, but, furthermore, indicated that the PUR network was continuous to a greater extent in the present 70:30 PUR/PEMA IPNs.

TGA studies. TGA studies were conducted with the two homopolymer networks, the 70:30 PUR/PEMA linear blend and IPNs of different crosslink density. Similar to the TGA study on the PUR/PS IPNs (section 5.2), the present investigation revealed a different degradation pattern for the homopolymers and the respective IPNs (figure 6.31). Both homopolymers degraded essentially in a one-step mechanism, whereas a two-step mechanism was observed for the IPNs. PEMA was thermally stable up to 270°C, whereas the PUR network started to decompose significantly at 200°C (all measurements were conducted in air atmosphere). Comparing four 70:30 PUR/PEMA compositions with different crosslinking densities, considerable differences in the thermal stability were noted.

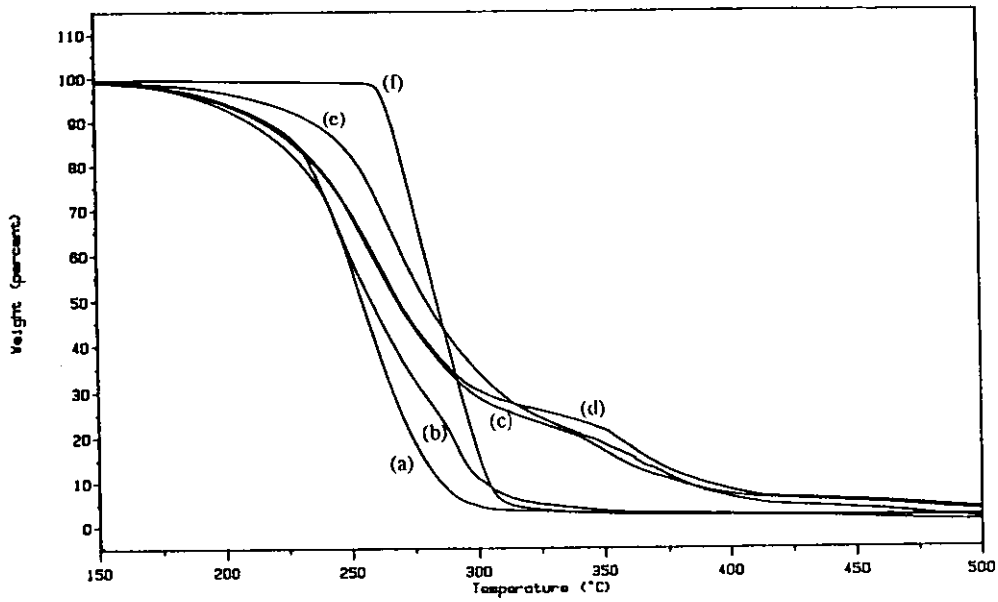

Figure 6.31 Percent weight loss versus temperature. (a) PUR(PPG1025/TMP 3:1) homonetwork, (b) 70:30 PUR/PEMA linear blend, (c) 70:30 PUR (3:1)/PEMA(5% TEGDM) IPN, (d) 70:30 PUR(3:1)/PEMA(10%), (e) 70:30 PUR (1:1)/PEMA(5%) and (f) PEMA(5%) homonetwork.

The linear blend was clearly inferior to the IPNs (figure 6.13(b)). Looking at the three full 70:30 PUR/PEMA IPNs of different crosslinking densities, it was noted that the crosslinking density in the PUR network determined the thermal properties of the IPNs. The IPN with the highest PUR crosslinking level (PPG1025/TMP ratio of 1:1) was thermostable up to the highest temperature. On the other hand, only a slight improvement in weight retention between 300°C and 400°C was noticed for the IPN crosslinked with 10% TEGDM compared to that crosslinked at 5% TEGDM (figures 6.31(d) and (c)). It was interesting to note that all IPNs exhibited a clearly higher weight retention than either homonetworks and the linear 70:30 PUR-PEMA blend at temperatures higher than 300°C. However, the latter was of little practical importance since at 300°C only roughly 30 weight percent of the material were present.

Morphology by TEM. TEM micrographs were prepared in order to investigate the influence of the crosslinking density on the IPN morphology. The dark regions consist predominantly of PUR which is preferentially stained[239] by OsO_4. The three IPNs investigated are shown in figure 6.32.

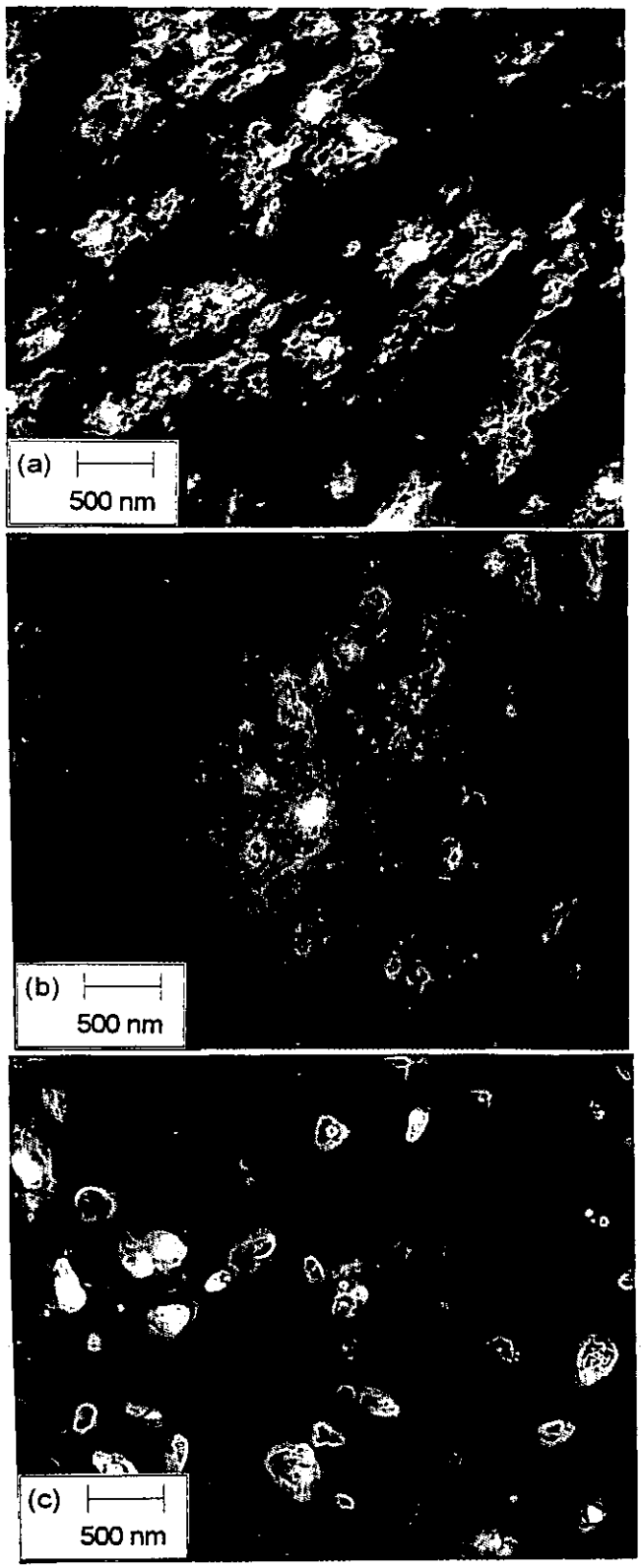

Figure 6.32 TEM micrographs for the 70:30 PUR/PEMA IPNs at a 5 mol % DVB level and at varying PPG1025/TMP ratios. (a) PPG1025/TMP ratio 7:1, 5% TEGDM, (b) 1:1, 5% and (c) 3:1, 10%.

The broadest half-peak width, 156°C (table 6.3), was obtained with the IPN crosslinked at a PPG1025/TMP ratio of 3:1 and 5% TEGDM. The TEM micrograph of this 70:30 PUR/PEMA IPN was shown in figure 6.17(b) and (c). It had PEMA domains in the order of 50 - 300 nm. The TEM micrograph of the corresponding IPN crosslinked at a PPG1025/TMP ratio of 7:1 and 5% TEGDM is shown in figure 6.23(a). It had an almost equally broad (149°C) half-peak width. The PEMA phase domains appeared somewhat bigger (50 - 400 nm), which was almost certainly due to the lower PUR crosslink density. The latter IPN was compared with the IPN with the narrowest half-peak width (72°C), which was crosslinked at a PPG1025/TMP ratio of 1:1 and 5% TEGDM. The TEM micrograph of this material showed a clearly finer phase structure (figure 6.23(b)). In addition to some larger domain structures (100 - 300 nm), many very small domains of 10 - 100 nm were present. This confirmed earlier findings[100] that a tighter network of the material that forms first restricts the domain size of the second-formed network. Increasing the crosslinking density of the second network was also investigated. Figure 6.32(c) shows the IPN crosslinked at a PPG1025/TMP ratio of 3:1 and with 10% TEGDM. It could be seen that crosslinking in the second formed PEMA network led to rather larger and much better-defined phase domains. This confirmed the findings from the DMTA data of poorer phase mixing and poorer phase continuity of the PEMA phase in the 10% TEGDM-crosslinked IPN. Compared to the IPN that was crosslinked at a PPG1025/TMP ratio of 3:1 and 5% TEGDM, the PEMA loss factor transition shifted to a higher temperature (from 87°C to 95°C) and decreased in height (from 0.42 to 0.26). Thus, with increasing crosslink density in the PEMA network, a coarser IPN morphology with purer and less continuous PEMA domains was obtained. The latter was not expected.

6.3 Variation in the PUR Network

PURs are[205] a very versatile class of materials (section 2.3) and, thus, open up further avenues for changing the IPN properties. In the present study, (i) a variation in the molar mass of the PPG polyol, (ii) the use of different types of polyols and (iii) a variation in the PUR hard segment were investigated. The variation of the PUR network was conducted in a 70:30 PUR/PEMA IPN which was crosslinked at 5

mol% TEGDM. The IPNs were investigated by DMTA and stress-strain and hardness measurements.

DMTA studies. The loss factor and storage modulus versus temperature data for the three studies are shown in figures 6.33 to 6.38. The DMTA data for the IPNs are shown in table 6.6. In varying the molar mass of the PUR soft segment, it was attempted to tailor the IPN maximum damping ability. By using higher molar mass PPG polyols the damping range was extended to lower temperatures. The loss factor versus temperature data for the 70:30 PUR(PPG4000/TMP 3:1)/PEMA(5% TEGDM) IPN containing a polyol of a molar mass of 4000 showed a phase-separated morphology (figure 6.33(a)).

Table 6.6 Dynamic mechanical properties (10 Hz) of the 70:30 PUR/PEMA IPNs as a function of the PUR network.

70:30 IPN PUR / PEMA	Tg [tan δ, °C] [PUR]	PUR / PEMA	Tan δ maximum [PUR]	PUR / PEMA	Inter-transition minimum	Half-peak width[°C]
Soft segment variation (TMXDI, polyol/TMP 3:1)						
PPG425	[40]	53 / (a)	[1.53]	0.80 / (a)	(a)	52
PPG1025	[-5]	18 / 87	[1.08]	0.40 / 0.42	0.40	156
PPG2025	[-26]	-25 / 96	[1.31]	0.41 / 0.39	0.32	198
PPG4000	[-40]	-41 / 72	[1.72]	0.57 / 0.55	0.26	(b)
PTHF2000	[-37]	-40 / 117	[0.77]	0.33 / 0.43	0.12	(b)
PCL2000	[-19]	-21 / 117	[1.13]	0.27 / 0.48	0.10	(b)
PBD2500	[-45]	-44 / 103	[0.89]	0.35 / 0.22	0.12	(b)
Hard segment variation (PPG1025/chain extender 3:1)						
TMXDI, TMP	[-5]	18 / 87	[1.08]	0.40 / 0.42	0.40	156
TMXDI, BD[(d)]	[-7]	5/85/126	[1.35]	0.36/0.55/0.48	0.36	186
MDI, TMP	[20]	37 / (a)	[1.09]	0.67 / (a)	(a)	59
MDI, BD	[14]	10 / (c)	[1.33]	0.38 / (c)	(c)	(c)

[ ] Values in square brackets are for the PUR homonetworks (section 4.2).

(a) No glass transition temperature for the second component could be determined.

(b) Not applicable because of low inter-transition values.

(c) Material became too soft for measurement.

(d) One main transition peak with two main shoulders were observed.

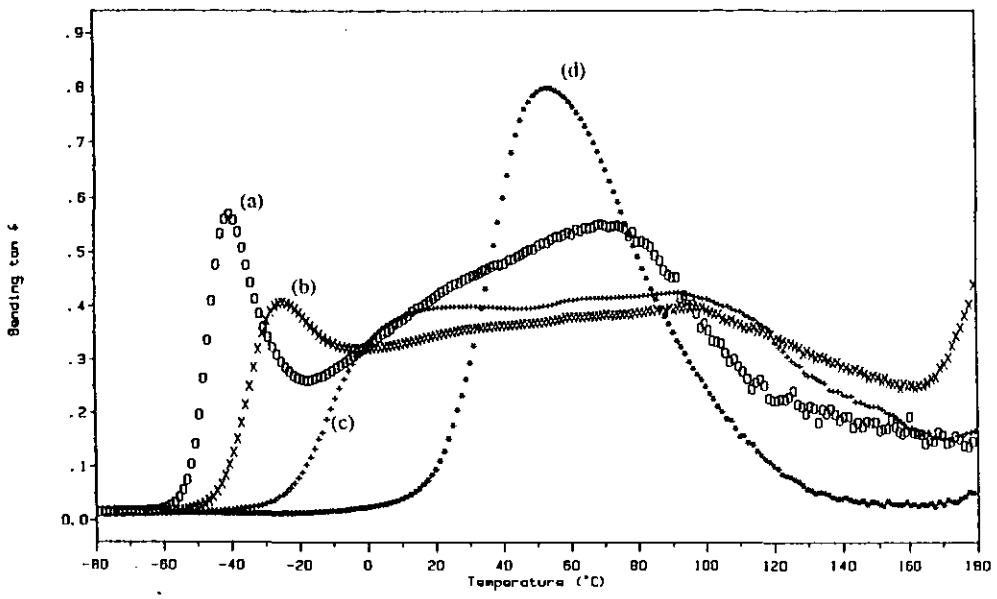

Figure 6.33 Loss factor versus temperature data for the 70:30 PUR/PEMA IPNs as a function of molar mass of the PPG polyol at a constant polyol/TMP ratio of 3:1. (a) PPG4000, (b) PPG2025, (c) PPG1025 and (d) PPG425.

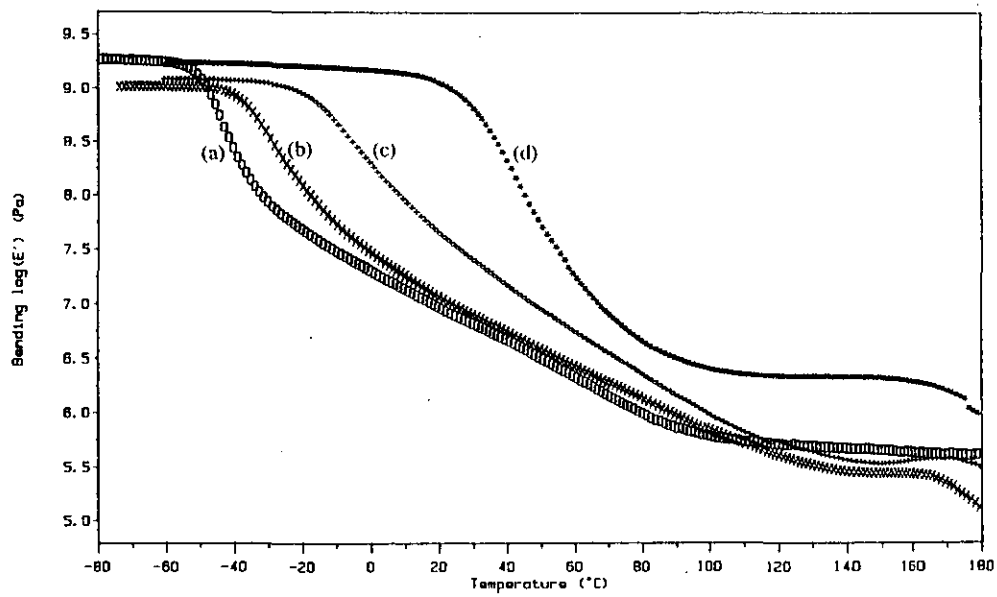

Figure 6.34 Storage moduli versus temperature for the 70:30 PUR/PEMA IPNs as a function of molar mass of the PPG polyol at a constant polyol/TMP ratio of 3:1. (a) PPG4000, (b) PPG2025, (c) PPG1025 and (d) PPG425.

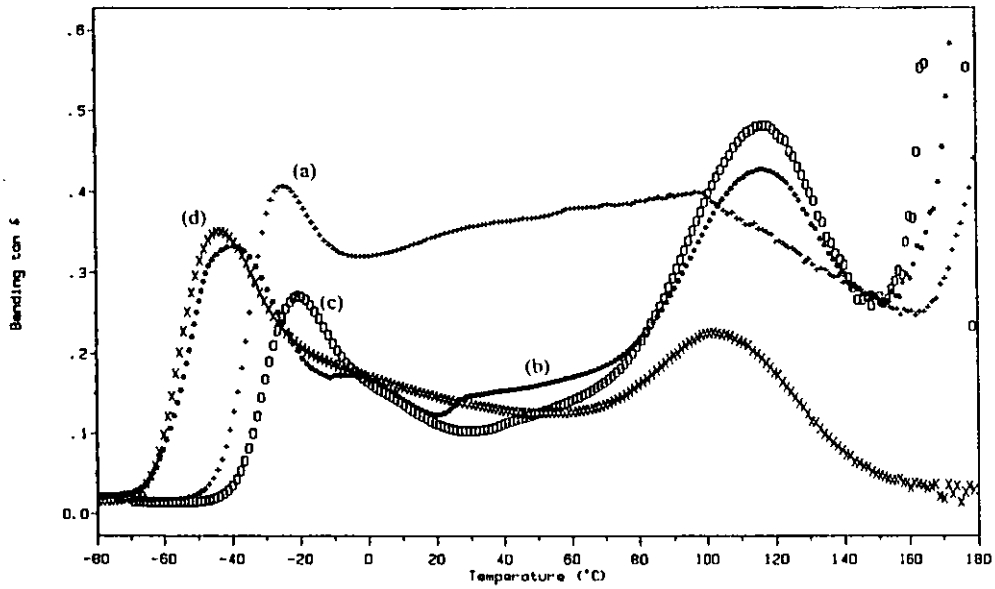

Figure 6.35 Loss factor versus temperature data for the 70:30 PUR/PEMA IPNs as a function of type of the polyol at a constant polyol/TMP ratio of 3:1. (a) PPG2025, (b) PTHF2000, (c) PCL2000 and (d) PBD2500.

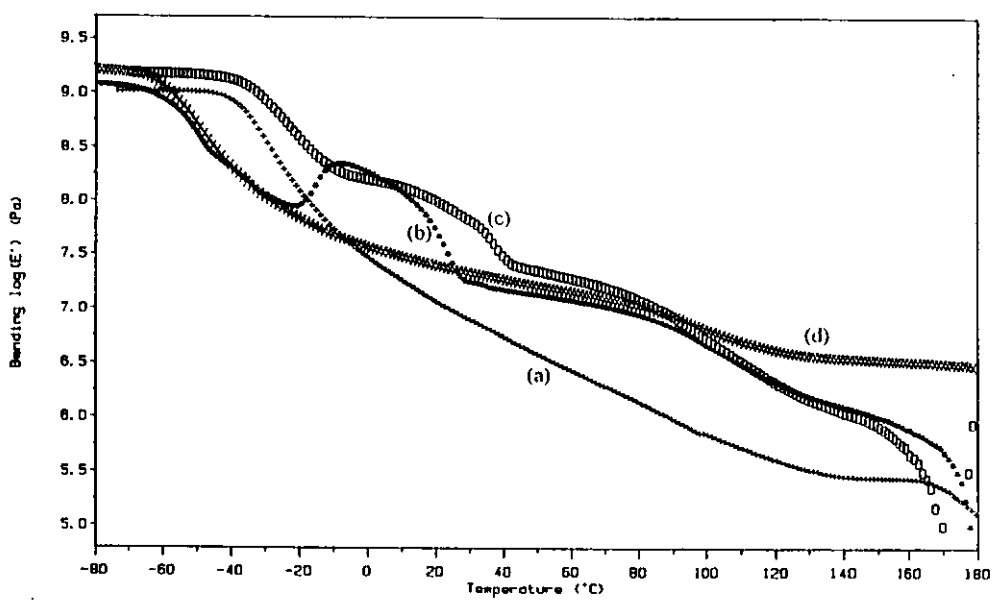

Figure 6.36 Storage moduli versus temperature for the 70:30 PUR/PEMA IPNs as a function of type of the polyol at a constant polyol/TMP ratio of 3:1. (a) PPG2025, (b) PTHF2000, (c) PCL2000 and (d) PBD2500.

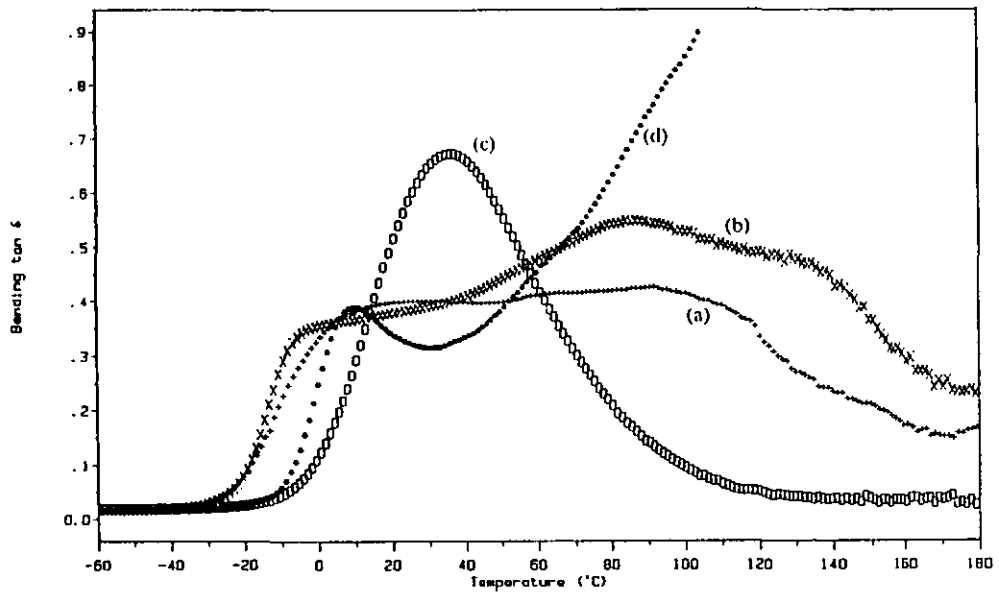

Figure 6.37 Loss factor versus temperature data for the 70:30 PUR/PEMA IPNs as a function of PUR hard segment. (a) TMXDI, PPG1025/TMP 3:1, (b) TMXDI, PPG1025/BD 3:1, (c) MDI, PPG1025/TMP 3:1 and (d) MDI, PPG1025/BD 3:1.

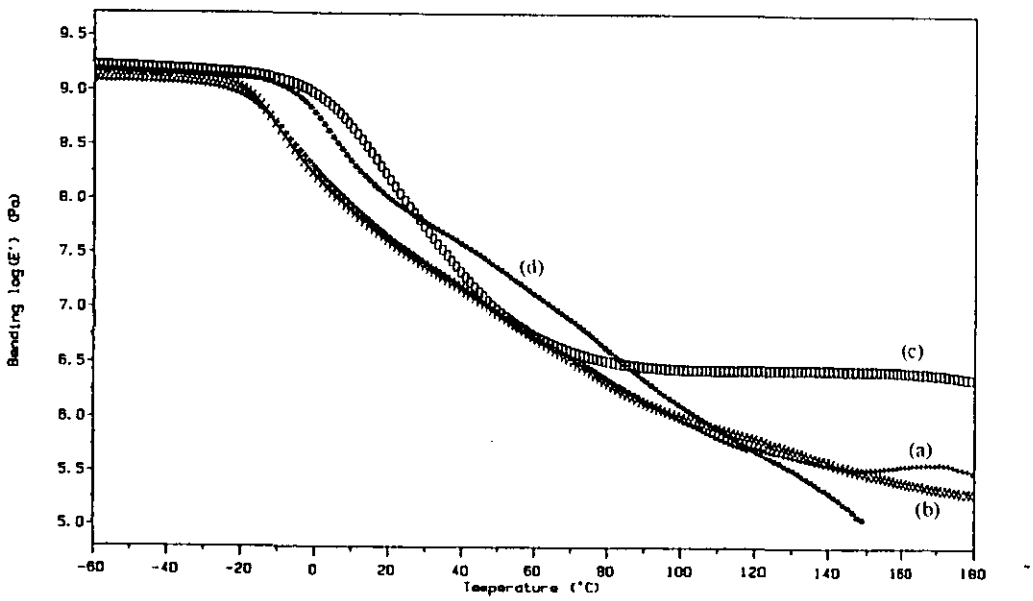

Figure 6.38 Storage moduli versus temperature for the 70:30 PUR/PEMA IPNs as a function of PUR hard segment. (a) TMXDI, PPG1025/TMP 3:1, (b) TMXDI, PPG1025/BD 3:1, (c) MDI, PPG1025/TMP 3:1 and (d) MDI, PPG1025/BD 3:1.

Two loss factor peaks were observed, at -41°C and 72°C (table 6.6). The loss factor value for the inter-transition minimum was relatively high at 0.26, indicating some degree of phase-mixing. In this study, the inter-transition minima were given instead of the inter-transition value. This was done since a great number of these IPNs had highly unsymmetrical transition profiles. Thus, taking the loss factor height at a fixed temperature between the Tg temperatures of the constituent homopolymer networks might have resulted in an unrepresentatively high value. The IPN containing the PPG2025 polyol showed a much more phase-mixed loss factor profile (figure 6.33(b)). The PUR transition peak was at -25°C and the PEMA transition was very broad (96°C). With the exception of the slightly higher PUR transition peak (0.41), the transition had an almost rectangular shape. The inter-transition loss factor minimum was very high with 0.32 confirming a high degree of component mixing. The transition half-peak width of 198°C was exceptionally high. Also, the temperature range where the loss factor were greater than 0.3 was broad (160°C) spanning from -33° to 127°C. This IPN was a potentially excellent damping material. The 70:30 PUR/PEMA IPN containing the PPG1025 had been discussed in sections 6.1 and 6.2. A highly phase mixed structure manifested itself in a very broad, almost regular loss factor transition profile (figure 6.33(c)). It was an almost equally good damping material with loss factor values greater than 0.3 spanning a temperature range of 130°C. Further decreasing the molar mass of the PPG polyol to 425 resulted in one high (0.80) loss factor peak. The highly phase mixed morphology manifested itself in a comparatively narrow half-peak width (52°C). The IPN PUR Tg values were compared to those of the respective PUR homonetworks (table 6.6). For PPG molar masses of 4000 and 2025, the PUR Tgs were very similar for the IPNs and the PUR homonetworks. However, the loss factor heights decreased considerably from the PUR to the IPNs from 1.72 to 0.57 for PPG4000 and from 1.31 to 0.41 for PPG2025. The PEMA transition on the other hand shifted to lower temperatures. The Tg of the PEMA homonetwork crosslinked at 5% TEGDM was at 105°C (table 6.1). Thus, the fact that the PEMA Tg was at 72°C and 96°C for the IPNs based on PPG4000 and PPG2025 indicated that these transitions did not result from pure PEMA. The morphology of these two IPNs could, therefore, best be described by two different phases. An essentially pure PUR phase existed together with a phase-mixed region of varying compositions which was responsible for the broad transition range

at the high-temperature transition end. A different trend was observed for the IPNs based on PPG1025 and PPG425. For these IPNs, in addition to PEMA shift to lower temperatures, also a significant in-ward shift of the PUR transitions was observed. It shifted from -5°C for the PUR homonetwork to 18°C for the IPN PUR Tg for PPG1025 and from 40°C to 53°C for PPG425. This indicated that a high degree of enforced component mixing was present. The broad transition profile stemmed from a distribution of regions of different PUR and PEMA compositions. It was believed that neither pure PUR nor pure PEMA phases existed in these IPNs. Clearly, the latter could be only concluded on the basis of the resolution of the DMTA experiment which is[107] in the order of 10 nm. The different loss factor behaviour of the PPG4000- and PPG2025- on the one hand and PPG1025- and PPG425-based IPNs on the other hand was likely to have been caused by two factors. One of which was that the crosslink density of the PUR network in the four IPNs was very different. Using equation 4.3, the calculated $M_{c,t}$ values for the respective PUR networks were 1700, 2900, 4900 and 8800 g/mol for the PPG425, PPG1025, PPG2025 and PPG4000, respectively. Because of the clearly lower $M_{c,t}$ values, PPG425 and PPG1025 were more effective in causing a degree of enforced phase mixing. A second factor was the increased miscibility of the PUR networks containing more polar urethane links. Since intermolecular interactions were possible between the PEMA carbonyl and the N-H bond of the urethane link, a higher hard segment content was believed to have been favourable for increased phase mixing. The hard segment contents of the respective PUR networks were given in table 4.1. With increasing molar mass of the PPG polyol the hard segment contents were 50, 30, 18 and 10 weight %. Thus, the IPN PUR networks based on the lower molar mass PPG425 and PPG1025 had stronger interactions with the PEMA resulting in a better IPN miscibility. Both the better miscibility combined with a higher degree of enforced mixing resulted in the better phase-mixing of the IPNs based on the low molar mass PPGs. The storage moduli confirmed above findings (figure 6.34).

In addition to molar mass of the PPG polyol, the influence of the type of polyol was also investigated. The loss factor and storage modulus versus temperature data revealed very different profiles even though all polyols had roughly the same molar mass of 2000 g/mol (figures 6.35 and 6.36). The IPN based on PPG2025 has been discussed in the previous paragraph. A high degree of enforced component mixing

resulted in an extremely broad loss factor transition (figure 6.35(a)). On the other hand, the 70:30 PUR/PEMA IPNs based on PTHF2000, PCL2000 and PBD2500 all exhibited a pronounced two-phase morphology. The latter was corroborated by the very low values (0.10 to 0.12) for the inter-transition minimum. For the PPG2025-based IPN this value was three times as high (0.32). For the IPNs based on PTHF2000, and PCL2000 some kind of transition was observed around 0°C - 10°C in the loss factor profile. These transitions were even more pronounced in the storage modulus versus temperature data (figure 6.36). Similar phenomena, however at slightly higher temperatures, were observed for the PUR homonetworks based on these two polyols (figures 4.18 and 4.19). Using DSC and WAXD techniques confirmed that these were primary transitions due to crystallisation and melting of PTHF2000 and PCL2000 chain segments (section 4.4). The fact that these phenomena occurred at lower temperatures indicated that not the entire chain participated in the crystallisation or melting process. The presence of some degree of crystallinity in the soft segments of these two IPNs corroborated that the PUR and the PEMA were grossly phase-separated. The fact that the polyols were able to crystallise might well have been a driving force for phase separation, since the chemical nature of both polyols was not that different from PPG2025, which resulted in a phase mixed PUR/PEMA IPN morphology. The storage modulus versus temperature profile of the PBD2500-based IPN had a two-step drop mechanism indicating gross phase separation. The poor phase mixing was not surprising. Polybutadiene has[254] a low solubility parameter (δ = 17.2 $(J/cm^3)^{1/2}$) and does not contain any heteroatoms. As a consequence no interactions between the polybutadiene and PEMA were possible. The high rubbery plateau modulus at 180°C indicated that, perhaps, because of the high degree of phase separation a high degree of network formation was obtained. A further possibility might have been that some grafting between the PBD and the PEMA network occurred. In the latter case, an in-ward shift of both transitions would have been expected. However, the transitions for the PUR (-44°C) and the PEMA (103°C) in the IPN were virtually the same as those for the respective PUR (-45°C) and PEMA (105°C) homonetworks. The latter made it rather unlikely that a significant amount of inter-network grafting had occurred.

The PUR hard segment was varied in two ways. The TMP triol was replaced by 1,4-butanediol (BD). The use of BD as chain extender is known[204] to result in highly ordered hard segments with strong hydrogen bonding. Thus, the chemically crosslinked PUR networks were compared to the physically crosslinked equivalents. The latter was done for MDI- and TMXDI-based 70:30 PUR(PPG1025/BD 3:1)/PEMA(5% PEMA). Also, the respective chemically crosslinked IPNs based on MDI and TMXDI were compared. The chemically crosslinked TMXDI- and MDI-based 70:30 PUR(PPG1025/TMP)/PEMA(5% TEGDM) IPNs showed very different loss factor versus temperature data (figure 6.37(a) and (c)). As already discussed in sections 6.1 and 6.2, the loss factor transition of the TMXDI-based IPN was very broad, which was mirrored by a half-peak width of 156°C. That of the MDI-based IPN on the other hand exhibited only one transition with a fairly narrow half-peak width of 59°C. Compared to the respective MDI-based PUR homonetwork, the loss factor peak height had decreased from 1.09 to 0.67 and shifted from 20°C to 37°C. A faster PUR reaction rate of the MDI-based IPN might have caused this very different transition profile. The PUR was believed to have been formed completely before the onset of the EMA polymerisation. As a consequence, the formed PUR network restricted the PEMA phase domain sizes which resulted in a higher degree of enforced phase mixing. However, as a result the temperature range of the transition was clearly inferior to that of the TMXDI-based IPN. Comparing the chemically (TMP) to the physically (BD) crosslinked 70:30 PUR(TMXDI, PPG1025/TMP or BD 3:1)/PEMA(5% TEGDM) IPN resulted in an interesting finding. The BD-based IPN had an even broader transition range than the TMP-based IPN. The loss factor values were greater than 0.3 over a temperature range of 170°C. The transition shape was slightly different. One major transition peak at 85°C with a low- (5°C) and a high-temperature (125°C) shoulder were observed. The broader transition range indicated that the physically crosslinked IPN was slightly less phase-separated than the chemically crosslinked IPN. The physically crosslinked MDI-based had a very different loss factor profile. A PUR transition peak was observed at 10°C. No second transition could be determined because the IPN became very soft and the loss factor values did not cease to rise at temperatures higher than 100°C. The difference between the TMXDI- and the MDI-based physically crosslinked IPNs might be explained as follows. In the MDI-based IPN, the PUR network was formed before the

onset of the EMA polymerisation. This restricted the phase domain size for the PEMA. In addition, it also prevented the PEMA from forming a complete and continuous second polymer network. As the test temperature increased to values of higher than 80°C, the physical PUR network formed through hydrogen bonding became increasingly weaker and, thus, the IPN increasingly softer. While in the slower reacting TMXDI-based IPN some phase continuity of the PEMA existed that prevented the IPN from an important softening that was not the case for the MDI-based IPN. The storage modulus versus temperature profiles confirmed that the physically crosslinked MDI-based IPN had the lowest storage modulus above a temperature of 120°C. It was, furthermore, observed that the chemically crosslinked IPN based on MDI had an exceptionally high rubbery modulus at 180°C. The latter also corroborated the belief that the faster reaction rate of the MDI-based IPN was crucial in determining the IPN morphology. It allowed a more complete formation of the PUR network while hindering the formation of phase continuity of the PEMA network. On the other hand, the storage moduli of both TMXDI-based IPNs were fairly similar (figure 6.38(a) and (b)).

Stress-strain and hardness measurement. The mechanical properties of these IPNs with variations in the PUR network were determined by tensile testing and hardness measurements (table 6.7). The mechanical properties showed equally pronounced differences when varying the PPG molar mass as did the DMTA data. The stress at break, Young's modulus, the toughness index and the Shore hardness values greatly increased with decreasing PPG molar mass. The latter was a result of an increase in PUR hard segment content and increased crosslinking densities which increased the PUR-PEMA miscibility and phase mixing. With exception of the PPG4000-based IPN, the strain at break values showed the opposite trend. The latter was expected since a decrease in crosslinking density generally results in higher strain at break values. The very low strain value for the PPG4000-based IPN might have been a result of the considerably phase-separated IPN morphology which was observed by the loss factor profile. The variation of the type of polyol also resulted in marked differences in the IPN properties. The PPG2025- and PBD2500-based IPNs exhibited generally poorer mechanical properties than the PTHF2000- and PCL2000-based

IPNs. The pronounced differences between these two groups were already evident in the mechanical properties of the PUR homonetworks (table 4.3).

Table 6.7 Mechanical properties of the 70:30 PUR/PEMA IPNs as a function of the PUR component.

70:30 IPN PUR/PEMA	Tensile properties				Hardness Shore	
	Stress at break [MPa]	Strain at break [%]	Young's modulus [MPa]	Toughness [J]	A	D
Soft segment variation (TMXDI, polyol/TMP 3:1)						
PPG425	24	310	83	14.7	97	84
PPG1025	9.4	360	8.0	7.6	74	41
PPG2025	5.1	580	1.0	5.9	59	32
PPG4000	0.3	70	0.9	0.1	28	22
PTHF2000	18	480	10	18.2	86	55
PCL2000	25	530	30	27.1	96	65
PBD2500	6.1	150	6.7	1.9	81	51
Hard segment variation (PPG1025/chain extender 3:1)						
TMXDI/TMP	9.4	360	8.0	7.6	74	41
TMXDI/BD	2.2[a]	350	7.0	2.1	71	37
MDI/TMP	11.2	330	9.3	6.8	83	50
MDI/BD	4.5[a]	290	12.1	2.9	84	49

(a) Maximum stress.

These differences were clearly due to the crystallinity that was encountered in the PTHF2000- and PCL2000-based materials. The stress-strain measurements further accentuated these differences since it is known[156] that high strain can induce or further increase crystallinity in polymers. Thus, the very high stress at break values for the PTHF2000 and PCL2000-based IPNs with 10 MPa and 18MPa were not surprising. The variation of the PUR hard segment also resulted in IPNs with a different property profile. The stress at break values of the chemically crosslinked TMXDI- (9.4 MPa) and MDI-based (11.2 MPa) IPNs were clearly higher than those of the physically crosslinked equivalents (2.2 MPa and 4.5 MPa, respectively). Surprisingly, the strain at break values for the IPNs where the PUR was chemically crosslinked were fairly similar to those where the PUR had physical crosslinks only.

As a result, the values for the toughness index of the IPNs with chemically crosslinked PUR were higher than those of the physically crosslinked counterparts.

In conclusion, it was found that varying the PUR network had an important bearing on the mechanical properties of the IPN. In the present study, a variation of the type and the molar mass of the soft segment polyol had a more pronounced influence than a variation in the diisocyanate and chain extender.

6.4 High Damping Materials

The damping characteristics of IPNs can be assessed from DMTA experiments, namely from the loss factor and loss modulus data. These are two important quantities since in constrained layer damping applications, the loss factor of the viscoelastic layer greatly influences[7,22,150] the damping ability of the system. On the other hand, in extensional layer damping, maximisation of E" is desired[22]. Only at a very high system loss factor, i.e. for a high thickness ratio of the polymer layer compared to the substrate, does[22] the loss factor make a higher contribution to the damping ability than E'. Thus, the PUR/PEMA IPNs of the crosslinking and the composition studies were further investigated in terms of their damping characteristics. Also, selected PUR/PS IPNs were discussed again in this section. The temperature range where the loss factor values were greater than 0.3 was already given, together with the loss factor half-peak widths. Further characteristics that have been used as an indication of the energy absorbing ability[164-166] of polymeric materials will be employed in this section to quantify the IPN damping characteristics. These were the areas under both the linear loss modulus curve, LA, and the linear loss factor curve, TA (section 2.2.3).

TA and LA areas. The calculation principles for the temperature range where the loss factor ≥ 0.3, the TA area, the temperature range where $E'' > E''$ below Tg and two LA areas are shown in figure 6.40 for the linear 70:30 PUR/PEMA polymer blend. TA was obtained by extrapolation of the loss factor curve at the lower and upper temperature limit and subsequent integration of the area under the curve (figure 6.40(b)). In order to integrate the LA area base-line corrections[167] similar to in infra-

red spectroscopy were made. In the present study, LA is given with two different straight line type base-line corrections[167].

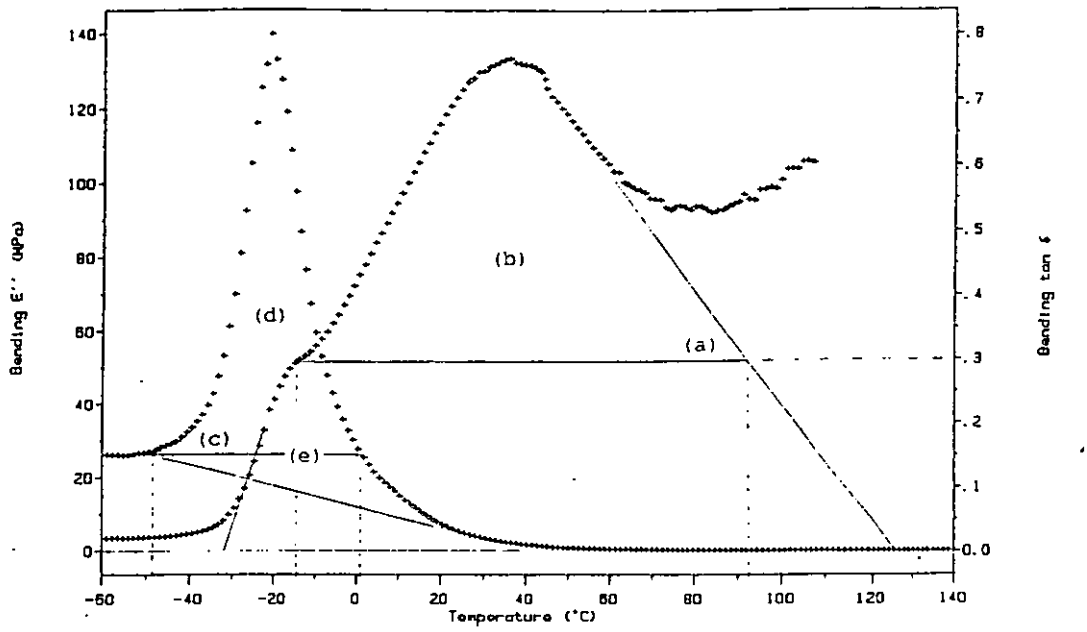

Figure 6.40 DMTA data for the 70:30 linear PUR/PEMA blend. Illustration of (a) the loss factor temperature range where the tan δ values are greater than 0.3 (tan δ > 0.3 [K]), (b) the extrapolation and area under the linear loss factor curve (TA [K]), (c) the loss modulus temperature range where the E" values are higher than at the constant value below Tg (E" > $E"_c$), (d) the area under the linear loss modulus curve above the constant E" (LA_c [GPaK]) and (e) for the straight base-line type (LA [GPaK]).

Also, the temperature range where the loss modulus was greater than the constant loss modulus value below Tg (E" > $E"_c$) was given. This was done because assessing the damping ability of a polymer for extensional layer damping in terms of the area under the E" curve might not be appropriate. Part of the loss modulus versus temperature curve exhibited lower E" values than did the polymer below its Tg. Below Tg, loss factor values for polymers[172] are in the range of 0.01 - 0.02, which combined with the high modulus of 2-3 GPa results in constant E" values of 20-60 MPa. A better way might be to indicate the temperature range where E" of the blend is higher than below Tg (E">$E"_c$), and give the area of this curve (LA_c). Thus, the second base-line type was applied in a manner to calculate LA_c.

The results for the damping characteristics of the PUR/PEMA IPNs and selected PUR/PS IPNs are shown in table 6.8. The loss factor versus temperature data for the PUR/PEMA IPNs of different compositions are shown in figures 6.1 and 6.2. Figure 6.41 shows a plot of the temperatures where the loss factors were greater or equal to 0.3 versus IPN composition.

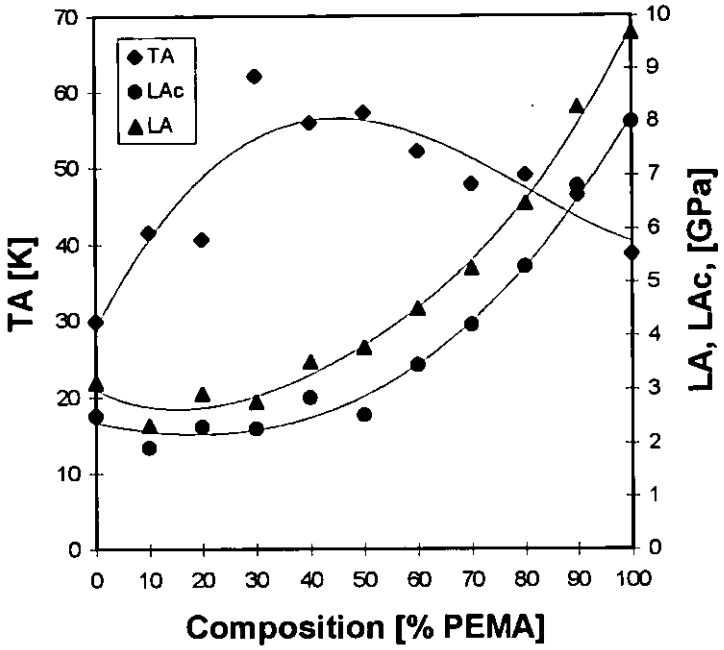

Figure 6.41 Values for the area under the linear loss factor curve, TA, and loss modulus curve, LA, versus PUR/PEMA IPN composition.

As already discussed in section 6.1 the 70:30 PUR/PEMA IPN exhibited a very broad and almost rectangular transition which is characteristic[152] for semi-miscible, microheterogeneous polymer blends. This composition exhibited the widest temperature range of loss factor values of greater than or equal to 0.3 over 130°C (table 6.8). It also had the highest value for the TA area with 62 K. Significantly lower TA values were found both below and above the 70:30 PUR/PEMA composition. From the data in table 6.8, it was, furthermore, observed that the TA area and the range where the loss factor was ≥ 0.3 had a similar trend.

Table 6.8 Damping characteristics of 70:30 PUR/PEMA IPNs as a function of composition and crosslinking density and selected 60:40 PUR/PS IPNs.

IPN	Loss factor, tan $\delta^{(a)}$		Loss modulus, $E''^{(a)}$		
	>0.3 [K]	TA [K]	>E"c	LA_C [GPaK]	LA [GPaK]
PUR/PEMA IPNs of different composition [% PEMA]					
0	37	30	43	2.5	3.1
10	60	42	45	1.9	2.3
20	62	41	48	2.3	2.9
30	130	62	58	2.3	2.8
40	100	56	70	2.9	3.5
50	82	57	86	2.5	3.8
60	71	52	110	3.5	4.5
70	65	48	113	4.2	5.3
80	65	49	116	5.3	6.5
90	62	46	128	6.8	8.3
100	59	38	142	8.0	9.7
70:30 PUR/PEMA IPNs of various crosslinking densities [PPG1025/TMP/%TEGDM]					
1:1 / 5%	72	48	87	2.7	3.4
2:1 / 5%	79	51	58	2.4	3.1
3:1 / 10%	79	49	57	2.2	2.6
3:1 / 5%	130	62	58	2.2	2.7
3:1 / 2.5%	115	55	53	2.5	3.0
3:1 / 1%	96	54	49	2.1	2.6
3:1 / 0%	84	50	50	2.4	3.1
7:1 / 5%	125	59	45	2.6	3.0
1:0 / 5%	(b)	(b)	39	2.1	2.4
1:0 / 0%	(108)	68	49	1.9	2.4
60:40 PUR/PS IPNs					
2.5% Grafting TMI	80	47	74	3.5	4.0
5% Grafting TMI	70	47	78	4.5	5.6
10% Grafting TMI	51	35	86	3.7	4.4
10% Compatibiliser	135	52	55	3.8	4.6
Stirred polym.	164	85	63	3.5	3.8

(a) The abbreviations are explained in figure 6.40.

(b) Not available due to softening of the material.

( ) For values in brackets substantial curve extrapolation had to be conducted.

The log loss modulus versus temperature data for the PUR/PEMA IPN composition series are shown in figure 6.4. However, for the calculation of LA the linear loss modulus versus temperature data was needed. In order to illustrate the LA area findings, the linear loss modulus versus temperature data are shown in figure 6.42 for selected PUR/PEMA IPN compositions.

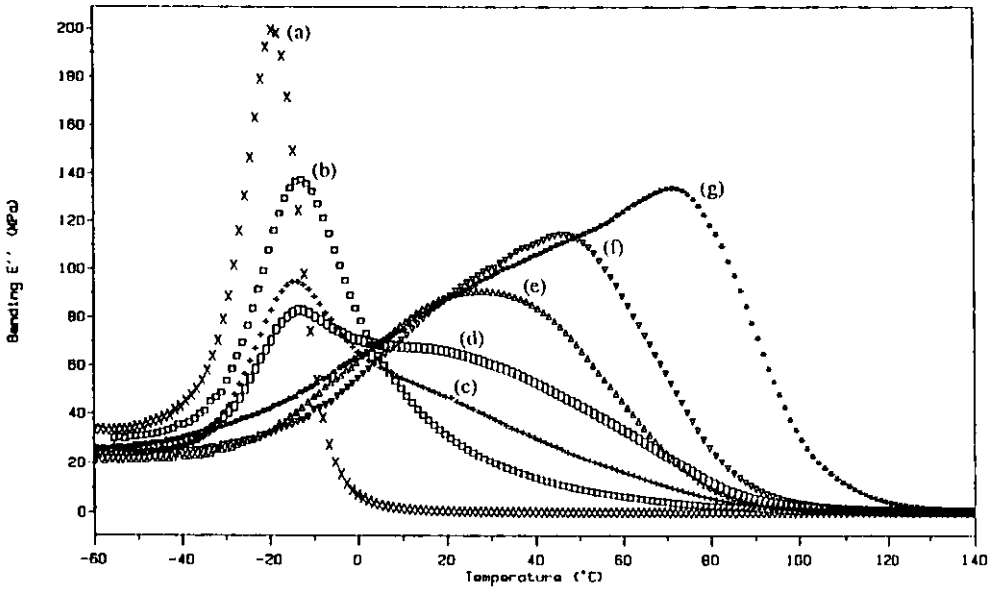

Figure 6.42 Linear loss moduli versus temperature for PUR/PEMA IPN compositions. (a) 100 PUR, (b) 60:40 PUR/PEMA IPN, (c) 50:50, (d) 40:60, (e) 30:70, (f) 20:80 and (g) 100 PEMA.

The peak location and peak shape varied greatly with the IPN composition. These variations were already discussed in section 6.1. In brief, from the 40:60 to the 30:70 composition a major change in E" peak location and shape took place. The peak maximum shifted from -13°C to 30°C and the 30:70 composition was dominated by the PEMA. The breadth of the temperature range where $E'' > E''_c$ steadily increased with increasing PEMA content from a value of 43°C for the 100 PUR to 142°C to the PEMA homonetwork (table 6.8). However, the maximum damping peak shifted to a higher temperatures with increasing PEMA (figure 6.42). The area under the linear loss modulus curve, LA, followed a similar trend, with the highest LA values being

obtained for the PEMA homonetwork. The trends for the LA values were different from that of the TA, yet similar for both types of base-lines. The LA and LA_c values continually increased with increasing PEMA content. Further, it was observed that values for LA were clearly below those expected from the linear rule of mixing of the two homonetwork LA values (figure 6.41). This is in contrast to the earlier thought[168] that semi-miscible IPNs exhibit larger LA values, whereas only very miscible and highly immiscible blends result in low values for LA. In this composition study, the network first-formed was rubbery and network 2 was glassy. Also, the LA value for network 1 was much lower than the LA value for network 2, both factors, that might have had an influence on the LA values. Equally important could have been the relatively good miscibility of both polymers, which was noted from the DMTA data of the linear blend in figure 1. Introducing crosslinks into the PEMA resulted in a considerable broadening of the polymer blend transition. The PEMA transition shifted clearly to higher temperatures and a decompatibilising effect was believed to have occurred (section 6.2). In conclusion, it was found that in the PUR/PEMA IPN composition series the TA area had an optimum at the 70:30 composition, whereas LA increased with increasing PEMA component. LA values were yet lower than the linear rule of mixing suggested.

Crosslinking also proved to have an influence on the TA area and the temperature range where the loss factor was ≥ 0.3. From the values in table 6.8 it was noted that generally low crosslinking in the PUR network resulted in greater values for both TA and the temperature range where the loss factor was ≥ 0.3. An exception to this was the IPN crosslinked at a diol/triol ratio of 3:1 and 5% TEGDM which exhibited maxima for both TA (62 K) and the temperature range where the loss factor was ≥ 0.3 (130°C). 5% TEGDM crosslinking also proved to be the optimum level for the crosslinking of the PEMA network. Higher and lower crosslinking in the PEMA network resulted in lower loss factor damping characteristics. Generally, the same tendency was observed for TA, the temperature range where the loss factor was ≥ 0.3 and also for the half-peak widths (table 6.3).

The loss modulus versus temperature data revealed a different pattern, yet again similar tendencies for both LA baseline-types were observed. Both LAs seemed to increase slightly with higher crosslinking in the PUR, as did the temperature range where $E'' > E''_c$. On the other hand, both LAs and $E'' > E''_c$ were not influenced to a

significant extent by the crosslinking of the glassy network. This can be explained by the nature of E". The latter is the product of the storage modulus and the loss factor. When an amorphous polymer undergoes its Tg, E' decreases by 3-4 decades, while loss factor values can, at best, increase by 2 decades from 0.02 to 2. Thus, E' determines E" to a large extent. In a broad IPN transition, the component at the higher temperature transition end does not make any contribution to E" because of the low E' value that overrides the loss factor increase.

The five 60:40 PUR/PS IPNs that are listed in table 6.8 exhibited a broad loss factor transition range. The DMTA data and the TEM micrographs had been shown and discussed in depth in chapter 5. The 60:40 PUR/PS IPN grafted with 2.5% TMI exhibited one broad transition with loss factor values ≥ 0.3 from 45°C to 125°C. At higher incorporation levels of 5% and 10% TMI a clearly more narrow transition resulted. In table 6.8, it can be seen that the values for the TA area were steadily falling with increasing grafting agent content. On the other hand, the temperature range where E" was greater than the constant E" below Tg increased with increasing grafting agent content. The LA area seemed rather to increase at first and than decrease again at high grafting levels of 10%. This seemed to be true for both base-line types.

The 60:40 PUR/PS IPN with 10% TMI-PPG1025 compatibiliser had a broad and high transition of 135°C, spanning from -12°C to 123°C. Despite the microheterogeneous morphology, the LA and LA_c values were fairly low. This was further corroborated by the low temperature range (55°C) where $E'' > E''_c$.

The 60:40 PUR/PS IPN that was synthesised by a stirred polymerisation showed very high inter-transition values which resulted in a very broad loss factor peak region. The loss factor values were ≥ 0.3 from -19°C to 145°C. Consequently, the TA area of the stirred system was very high with a value of 85 K compared to the conventionally synthesised counterpart which had a value of 58 K. This stirred IPN had the highest TA area of all IPNs investigated. On the other hand, both LA areas (3.5 and 3.8 GPaK) and the temperature range (63°C) where $E'' > E''_c$ were amongst the lowest of all 60:40 PUR/PS IPNs investigated.

In conclusion, it was found that no relation between the TA and the LA areas was found. Values for the TA area seemed to be higher for IPNs with a predominantly elastomeric continuous phase. Also, a low crosslinking level in the elastomeric

network generally increased TA. LA increased with higher contents of the glassy IPN component. A high level of crosslinking in the elastomeric network increased LA. Generally, it had to be said that loss factor data showed excellent reproducibility, whereas the magnitude of the loss modulus data was much more susceptible to variations. The latter were a result of variations in clamping the test specimens. This was acknowledged in earlier studies[59,330] where a variation of E" of up to 30% was observed[59]. Also, the loss modulus data determined by different instruments are known[164-166] to vary considerably. Chang and co-workers[164-166] tried to compensate for the latter by introducing a correction factor. However, the clamping variations still remain a considerable problem when comparing loss modulus data.

7. IPNS CONTAINING LATEX PARTICLES

One major potential application for IPNs is in the field of sound and vibration damping[4,13,153]. In real damping applications, wide variations of temperature and frequency are experienced, thus requiring damping systems with a high and broad loss factor range. One method to broaden further the temperature range of IPNs are three-component IPNs. By choosing three polymer components with Tgs far apart a broad transition range might be achieved. A very limited number of studies have been conducted on three-component IPNs by Klempner and Frisch[331,332] and by Wang and co-workers[333]. The simultaneous syntheses of these three-component IPNs relied on three independent polymerisation reactions, isocyanate and epoxy curing and a free radical reaction. In the present study, a different approach was investigated. PS latex particles were prepared first, and, then. mixed and reacted with PUR precursors, methacrylic monomer and crosslinker. Structured latex particles have been used for the toughening of homopolymers such as thermoplastic PMMA[334] and thermosets such as epoxy resins[335]. For this purpose, latex particles with a diameter[335] between 0.2 - 2 μm with a low Tg core polymer are most commonly used. In the present study, glassy functionalised and unfunctionalised PS particles were incorporated into an elastomeric IPN. The objective of this study was to develop materials that exhibit better mechanical properties at high temperatures than the PUR/poly(n-butyl methacrylate) (PBMA) two-component IPN. The latter is a good damping material with high intrinsic damping characteristics over a limited temperature/frequency range. The principal objective was to broaden further the damping temperature range by the incorporation of functionalised latex particles into the PUR/PBMA IPN. In addition to extending the transition region to higher temperatures, the PS latex particles should act as a polymeric filler in the IPN, since at the Tg transitions of the PUR and the PBMA, the PS latex particles are still in the glassy state. Fillers are known to be able to broaden[185,197] the damping range and increase[13,185,333] the damping ability by introducing additional damping mechanisms. They can resonate[336] and/or reflect impinging sound waves back through the polymer. Also, energy can be converted[185,197] into heat through an increase in friction and shear in the system. This is achieved through particle - particle friction[185] in filler agglomerates, particle -

polymer friction or through filler particles acting as mini-constrained layer[197] systems. The composition range of the filler which will yield improved damping is likely to be limited by two factors. Too little filler will be ineffective, while too much will decrease the volume percentage of the IPN, so that the height of the Tg transition will be reduced and shifted out of the desired damping range. Increasing the damping ability through the creation of additional shear in the system and broadening the damping range might require different weight fractions of filler addition. While 7% has been found as an optimum[333] for the former, around 20% of a polymer is needed to observe an effect on the dynamic mechanical property profile. Thus, the PS composite latex particles were incorporated at 17 weight %. A 70:30 PUR/PBMA IPN composition was chosen because of the special properties found at this composition for many PUR/methacrylic IPNs[110].

7.1 Synthesis of IPNs Containing Functional Latex Particles

The preparation of the three-component IPNs differed considerably from that of the two-component IPNs. Since the three-component IPNs represented only a small part of this study and in order not to complicate further the experimental chapter, the synthesis was not covered there. Therefore, a brief outline of the preparation procedure is given in the following.

Materials. The PUR network was made from TMXDI and PPG1025/TMP at a ratio of 3:1. The acrylic component consisted of n-butyl methacrylate monomer (BMA) which was crosslinked with TEGDM. The DVB crosslinked PS latex particles were initiated with 4,4-azobis(4-cyanovaleric acid) (AVA). 2-Hydroxyethyl methacrylate (HEMA) was incorporated into the PS latex particles to provide surface functionality. Dodecyl sulphate sodium salt (DSS) was used as the emulsifier.

Synthesis of PS and PS-HEMA latex particles. Crosslinked (1 mol% DVB) PS latex particles and functionalised particles containing HEMA were synthesised by emulsion polymerisation (figure 7.1). A S/DVB mixture was used to form a seed. Thus, 10% of the charge was added with the initiator after conditioning the water - emulsifier system for 1h under nitrogen at 75°C.

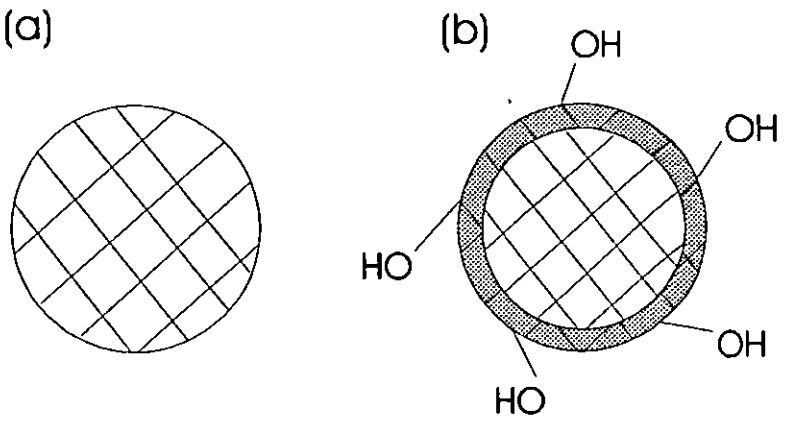

Figure 7.1 Schematic representation of the crosslinked (a) and the HEMA-functionalised (b) PS latex particles.

The remaining 90% S/DVB was fed in two stages over 4h. 80% was added over 3h. After a further 30 minutes, the remaining 10%, with the HEMA, was added. Finally, the latex was cryo-crashed, filtered and washed with hot water. The copolymerisation ratios[254] for S and HEMA are $r_1 = 0.57$ and $r_2 = 0.65$, which indicated a tendency towards an alternating copolymerisation. This, together with the low levels of HEMA, meant that no substantial poly(hydroxyethyl methacrylate) (PHEMA) segments were formed. The latter was important since both HEMA and PHEMA are strongly hydrophilic. The latices were synthesised at overall HEMA levels of 0, 0.5 and 3 weight percent.

Characterisation of the latex particles. Photon correlation spectroscopy yielded particle sizes between 90 to 100 nm for the PS latex and the PS-HEMA composite latex particles. Particle sizing via TEM resulted in lower values of 60 to 80 nm (figure 7.2).

Diffuse reflectance infra red spectroscopy studies were conducted in order to confirm the incorporation of the HEMA into the PS latex particles (figure 7.3). Comparing the spectra obtained from the PS latex and the functional latex, the incorporation of HEMA was obvious from the presence of two additional absorption peaks. The hydroxyl peak appeared at 3458 cm^{-1} and the carbonyl stretching at 1745 cm^{-1}.

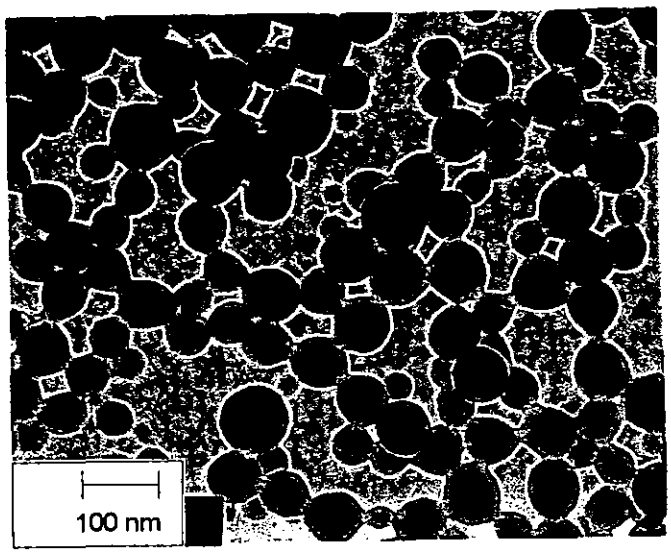

Figure 7.2 TEM micrograph of structural PS-HEMA latex particles on a carbon film.

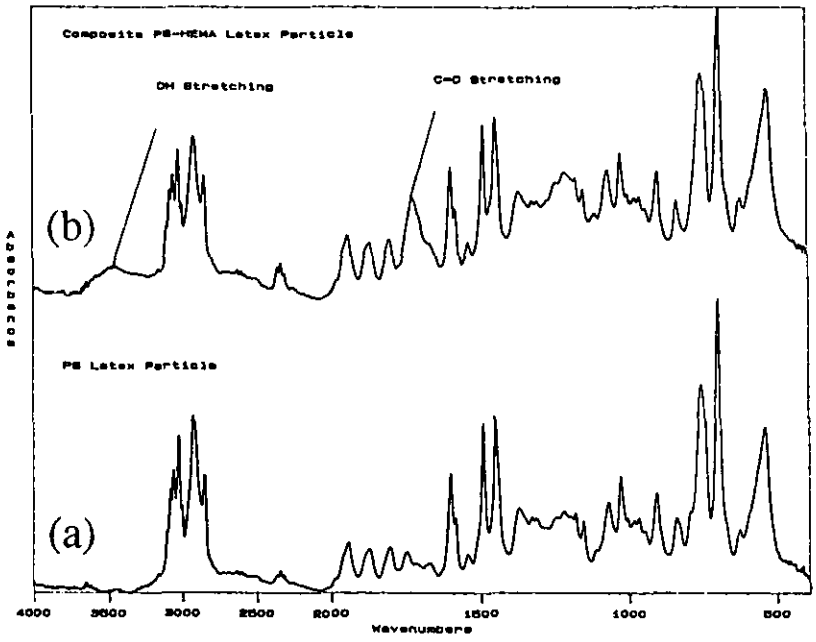

Figure 7.3 Diffusion reflectance infra red spectra of (a) the PS and (b) the HEMA-functionalised PS latex particles.

M-TDSC studies revealed a lower Tg for the functionalised particle than for the pure crosslinked PS latex (figure 7.4). The glass transition temperature of PHEMA[254] is 65°C.

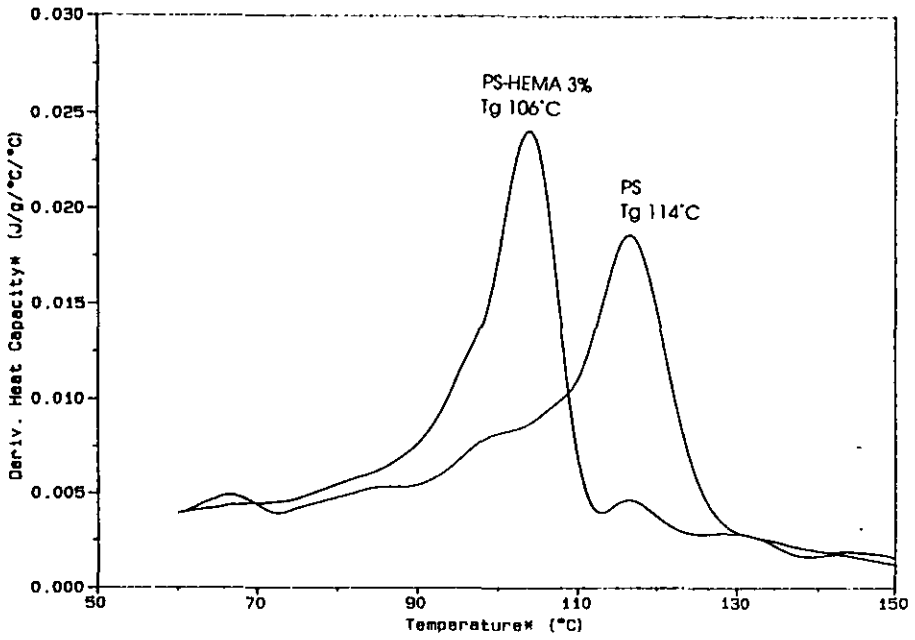

Figure 7.4 Comparison of the differential of heat capacity versus temperature for the polystyrene and the HEMA-functionalised latex particles.

IPN Preparation. The AIBN was dissolved in the BMA/TEGDM mixture. In a separate receptacle, the TMP was melted and dissolved in the PPG1025 at 60°C. At room temperature, the latex particles were dispersed in the polyol mixture using a high speed mixer and the mixture was subsequently degassed. Both components were combined and the PUR catalyst and the TMXDI added. For the preparation of the IPNs with the hydroxyl-functionalised latex particles, an additional stoichiometric amount of diisocyanate (TMXDI) was added to the original formulation in order to ascertain good network formation. The mixture was stirred at high speed for 5 minutes and then degassed for 1 minute. Then, the mixture was cast into a stainless steel spring-loaded O-ring mould, which had been pre-treated with release agent. The moulds were placed into an open air oven for curing. The curing cycle consisted of three stages of 24h at 60°C, 24h at 80°C and 24h at 90°C. Four IPNs were synthesised at a 70:30 PUR/PBMA composition. One of which was the two-

component PUR/PBMA IPN, whereas the remaining three contained 20 parts (17 weight %) of unfunctionalised and HEMA-functionalised (0.5 and 3 weight % of HEMA) PS latex particles.

7.2 Properties and Morphology of IPNs Containing Latex Particles

The properties and morphology of the IPNs containing latex particles were characterised using DMTA, stress-strain and hardness measurements and by SEM and TEM micrographs.

DMTA studies. PUR and PBMA are a partially miscible polymer pair. Both contain groups that exhibit some polarity and their solubility parameters, determined by equilibrium swelling, are 20.3 $(J/cm^3)^{1/2}$ for the PUR[284] and 17.9 $(J/cm^3)^{1/2}$ for the PBMA[254]. The 70:30 PUR/PBMA IPN exhibited a broad transition peak with high loss factor values spanning both Tg transitions (figure 7.5 (a)). However, its usefulness at temperatures higher than 80°C was very limited because of the significant softening of the material. At 80°C, the mechanical properties were poor which was manifested in the storage modulus curve approaching 0.1 MPa (figure 7.6). Incorporation of the latex particles was conducted in order to increase the working temperature range of the damping material. The PS latex particles were swollen to some extent by the monomer/crosslinker/initiator mixture and, thus, upon polymerisation, physically entangled with the methacrylic network. The incorporation of 20 parts of 1 mol% DVB crosslinked PS latex particles into the IPN sheet resulted in an additional peak at 148°C in the loss factor curve (table 7.1 and figure 7.5). The storage modulus curve now remained greater than 0.1 MPa until above 160°C (figure 7.6). Yet, the inter-transition loss factor values were low (0.11) because of the poor miscibility between PBMA and PS. A better result was obtained with the hydroxyl functionalised latex particles which were also incorporated at 20 parts by weight. In addition to the forced physical entanglement with the PBMA network, the hydroxyl functionality of the latex particles could also react with the TMXDI to become chemically linked to the PUR network, thus, improving the dispersion of the latex particles. The latter could be observed by the inward shift of the PS transition from 148°C to 131°C for the 0.5% and to 118°C for the 3% HEMA functionalised latex particles.

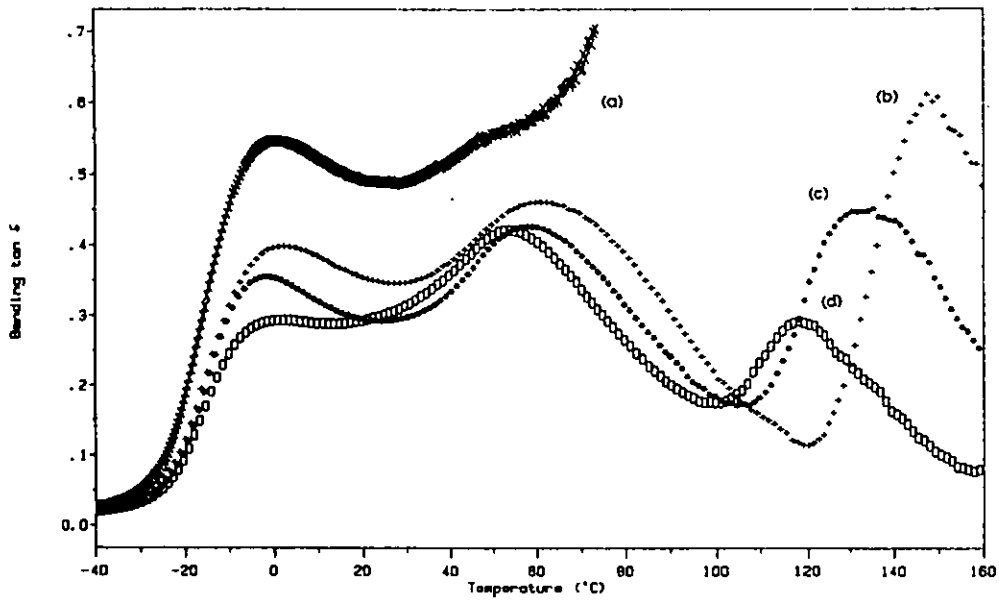

Figure 7.5 Loss factor versus temperature for the 70:30 PUR/PBMA IPNs containing latex particles. (a) 70:30 PUR/PBMA IPN without latex particles, (b) + 17% PS, (c) + 17% PS-(0.5%HEMA) and (d) + 17% PS-(3%HEMA).

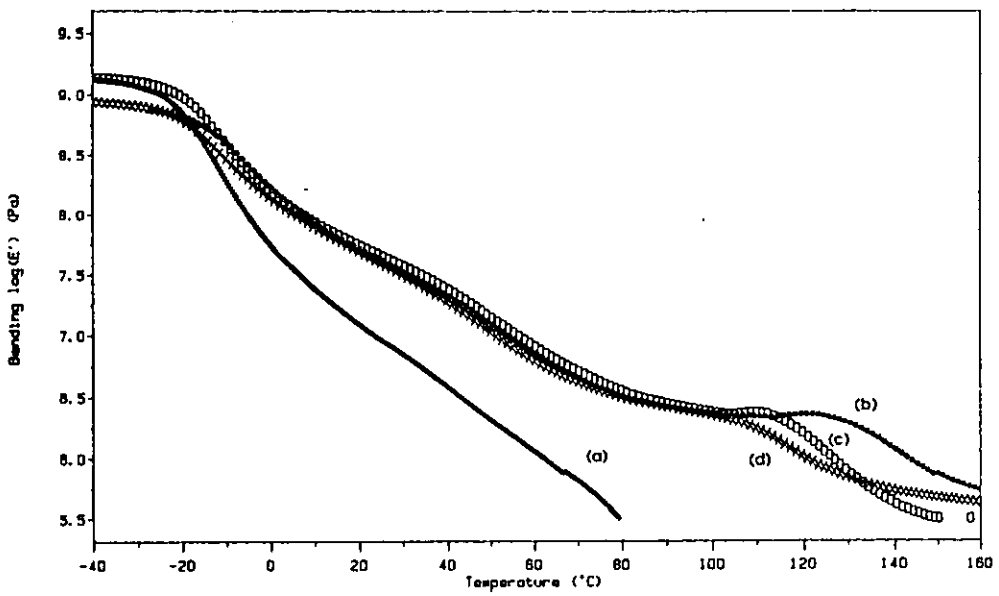

Figure 7.6 Storage moduli versus temperature for the 70:30 PUR/PBMA IPNs containing latex particles. (a) 70:30 PUR/PBMA IPN without latex particles, (b) + 17% PS, (c) + 17% PS-(0.5%HEMA) and (d) + 17% PS-(3%HEMA).

Further, a clear increase of the loss factor value for the inter-transition was observed from 0.11 for the system with the PS latex to 0.18 for both PS-HEMA functionalised latex particles. However, for a good damping material, a loss factor value of 0.3[172] over the entire transition should be achieved. Therefore, further increase of miscibility of the latex particles with the IPN is needed in order to obtain a good damping material. This may be achieved either by allowing more time for the PS latex particles to be swollen to a greater extend or by selecting a latex polymer with a solubility parameter closer to that of the methacrylic component. Work with PMMA latex particles might prove interesting.

The area under the linear loss factor curve, TA, is an indication of the damping ability of a material (section 6.4). In this study, it was difficult to compare the respective TA areas since the PUR/PBMA IPN became too soft at higher temperatures. Therefore, it was difficult to establish whether the PS latex particles acted as a filler and so imparted additional damping mechanisms into the material. Yet, from assessing the areas of the three-component IPNs, it could be noted that the incorporation of HEMA decreased the TA area. This could be attributed to the increase in crosslink density that was brought about by the functionalised latex particles. The pendent hydroxyl functionality of the HEMA-PS latex particles grafted onto the forming PUR network to form trifunctional crosslinks. These additional crosslinks decreased further the segmental mobility within the PUR network, resulting in a weakening of the glass transition phenomenon which in turn showed itself in lower values for the loss factor.

Stress-strain and hardness measurements. The tensile testing results are listed in table 7.1. Behaviour typical of a filled polymer[156,185] was observed. An increase in Young's modulus was combined with a decrease in elongation and stress at break. The Young's modulus increased from 1.9 MPa for the PUR/PBMA IPN to 14, 15 and 21 MPa for the materials with the incorporated latex particles. The values for the elongation at break decreased considerably from 450% for the two-component IPN to less than 200% for all of the three-component IPNs. As a result, the toughness index also decreased by half from 3.6 J to around 2 J for the three PS-filled IPNs. For the stress at break, a more differentiated pattern was observed. The 70:30 PUR/PBMA IPN exhibited a greater value (4.3 MPa) than the IPN filled with 17 weight % PS latex particles (3.7 MPa).

Table 7.1 Dynamic mechanical and mechanical properties of the IPNs.

Samples 70:30 IPN PUR/PBMA	DMTA [10 Hz] Tg [tan δ /°C] PUR/PBMA/PS	Tensile properties Stress at break [MPa]	Elongation at break [%]	Young's modulus [MPa]	Toughness [J]	Hardness Shore A
70:30 IPN	-2/ (a)	4.3	450	1.9	3.6	48
+PS	-2/62/148	3.7	170	14	1.8	76
+PS-HEMA0.5%	-2/59/131	4.6	160	15	1.8	80
+PS-HEMA 3%	-2/55/118	7.4	180	21	2.5	86

(a) Material became too soft for measurement.

This indicated that the latex particles were not entangled to a great extent with the PBMA component. Upon introduction of HEMA into the PS latex particles, the stress at break values increased. With 0.5% HEMA incorporated in the PS latex, a slightly higher value of 4.6 MPa than for the two-component IPN was obtained. At 3% HEMA incorporation, the highest value by far with 7.4 MPa resulted for the stress at break. This indicated a better adhesion between the composite latex particles and the matrix which was caused by the formation of covalent bonds from the reaction of the hydroxyl groups with the isocyanate groups.

The Shore A hardness values increased strongly (table 7.1) with the incorporation of the functional latex particles from a value of 48 for the PUR/PBMA to 76 for the material with 17% PS latex particles. The functionalised particles resulted in even higher values with 80 for the particles with 0.5% HEMA and 86 for the material with 3% HEMA.

Morphology by TEM and SEM. TEM studies were conducted to investigate the IPN morphology (figure 7.7). Again, for a better contrast, the samples were stained with osmium tetroxide which is known[242] to stain the PUR preferentially. For the PUR/PBMA IPN, a fine morphology with very small phase domains was observed (figure 7.7(a)). Both larger PEMA-rich (white) domains of 200 - 300 nm and smaller domains of 40 - 70 nm in size were present.

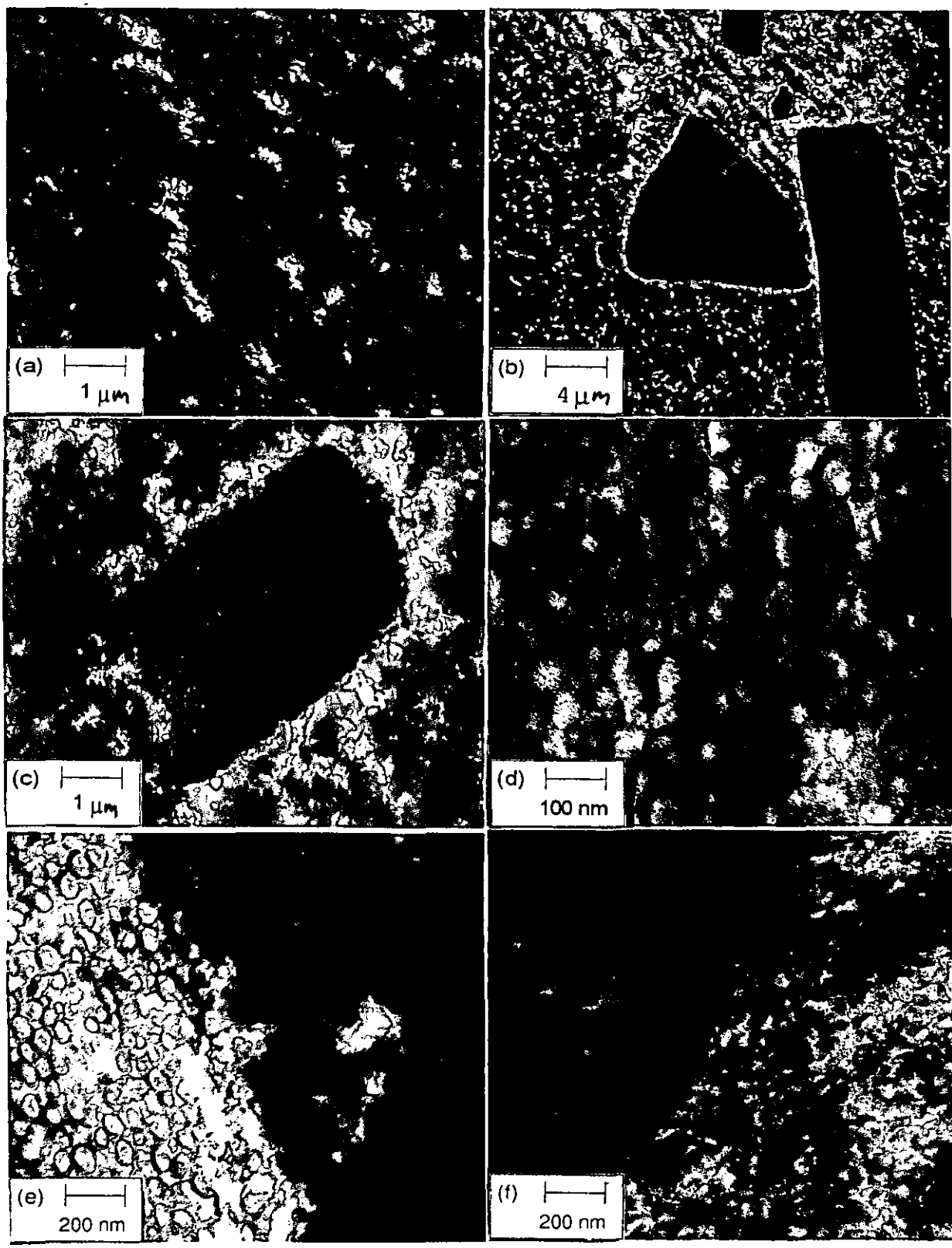

Figure 7.7 TEM micrographs for the 70:30 PUR/PBMA IPNs containing latex particles. (a) 70:30 PUR/PBMA IPNs without latex particles, (b)&(c)&(d)&(e) + 17% PS and (f) + 17% PS-(3%HEMA).

An even stronger indication of some degree of miscibility of the PUR/PBMA IPN than the small phase domain sizes was the blurred interface area. Various shades of grey indicated that the composition was changing only gradually, whereas in immiscible IPNs, such as, for example, in PUR/PS IPNs[4] (chapter 5) clear-cut interfaces were observed. The TEM micrographs of the three-component IPNs with the incorporated latex particles were all macroscopically similar in morphology and showed that the majority of the latex particles were not dispersed on an individual level. Agglomerates of the latex particles in the IPN matrix could be seen (figure 7.7(b) to (f)). The size of these agglomerates was in the order of 2 - 30 μm with a trend towards a smaller agglomerate size for the materials with the higher degree of functionalisation in the latex particles. This trend towards smaller agglomerate sizes might be explained by the reaction of the forming PUR network during the 5 minutes mixing period with the hydroxyl-functionalised latex particles. Functionalised latex particles that were chemically linked with the forming PUR network were believed to have been more prone to being torn out of the agglomerates, thus, leading to the partial break-up of the latter. A micrograph of one PS latex particle agglomerate of 3 - 4 μ which is surrounded by a PUR/PBMA matrix is shown in figure 7.7(c). The individual PS latex particles (white) can be seen in a dark agglomerate matrix. It was difficult to determine whether the agglomerate matrix was predominately composed of PUR or PBMA. Figure 7.7(c) would indicate that the dark agglomerate matrix consisted mainly of osmium tetroxide-stained PUR. However, besides osmium tetroxide staining, the electron density (darkness) of the phases is also strongly influenced by the thickness of the ultrathin sample section. In this study, ultramicrotoming was conducted at room temperature. As a result, there was a pronounced difference in hardness of the PS-rich agglomerates and the surrounding matrix because of the high glass transition temperature of the PS. This might have led to a variation in section thickness which in turn could explain that in other micrographs (figures 7.7(e) and (f)), the agglomerate matrix appeared lighter than the surrounding PUR/PBMA matrix. Further, the TEM micrographs confirmed that the PS latex particles were not swollen to a great extent by the BMA monomer and the crosslinker. A comparison at the same magnification between the latex particles measured on a carbon film (figure 7.2) and the particles in an ultramicrotomed section of the three-component IPN with 17% PS latex particles (figure 7.7(d)) showed them

to be very similar in size. At a high magnification of 50 k times, an additional difference between the incorporation of unfunctionalised and functionalised latex particles was noted. At a functionalisation level of 3% HEMA in the PS latex particles, numerous single functionalised PS particles were also observed outside the agglomerates in the PUR/PBMA matrix. Still, the interface between the PS latex particles agglomerates and the PUR/PBMA matrix was clearly visible, but much less well-defined for the material with the 3% HEMA functionalised PS latex particle agglomerates. Figures 7.7(e) and (f) showed similar interface regions of a material with unfunctionalised PS latex particles and with 3% HEMA functionalised particles. While in figure 7.7(e) the single latex particles can be easily distinguished, much less well-defined interfaces within the agglomerate matrix were seen in figure 7.7(f). This was believed to have stemmed from the reaction of the functionalised latex particles with the PUR network. The dark regions represent PUR-rich zones. Reaction between the forming PUR network and the functionalised latex particles lead to the greater degree of forced mixing seen in this micrograph.

SEM micrographs were prepared from the fractured tensile test specimens (figure 7.8). The micrograph of the two-component 70:30 PUR/PBMA IPN is shown in figure 7.8(a). A fairly fine phase morphology was observed. Upon the incorporation of 17% PS latex particles, a comparatively irregular surface structure resulted (figure 7.8(b)). Agglomerates of latex particles of 5 - 50 μ in size were observed. Incorporating HEMA-functionalised latex particles seemed to have resulted in considerably smaller agglomerate sizes of 2 - 20 μ (figure 7.8(c)). At a magnification of 5 K it could be seen how the agglomerates were embedded into the PUR/PBMA IPN matrix (figure 7.8(d)). At even higher magnifications (~ 10ᵏ) the single latex particles in the agglomerates were observed (figures 7.8(e) and (f)). The size of 60 - 90 nm was in good accordance with the findings from the TEM micrographs (60 - 80 nm). Comparing the IPNs containing PS and PS-HEMA-functionalised latex particles it could be observed that the functionalised latex particles seemed to have been better joined/mixed with the IPN PUR/PBMA matrix. This was believed to have resulted from the OH surface functionality of the latex particles that reacted with the forming PUR network.

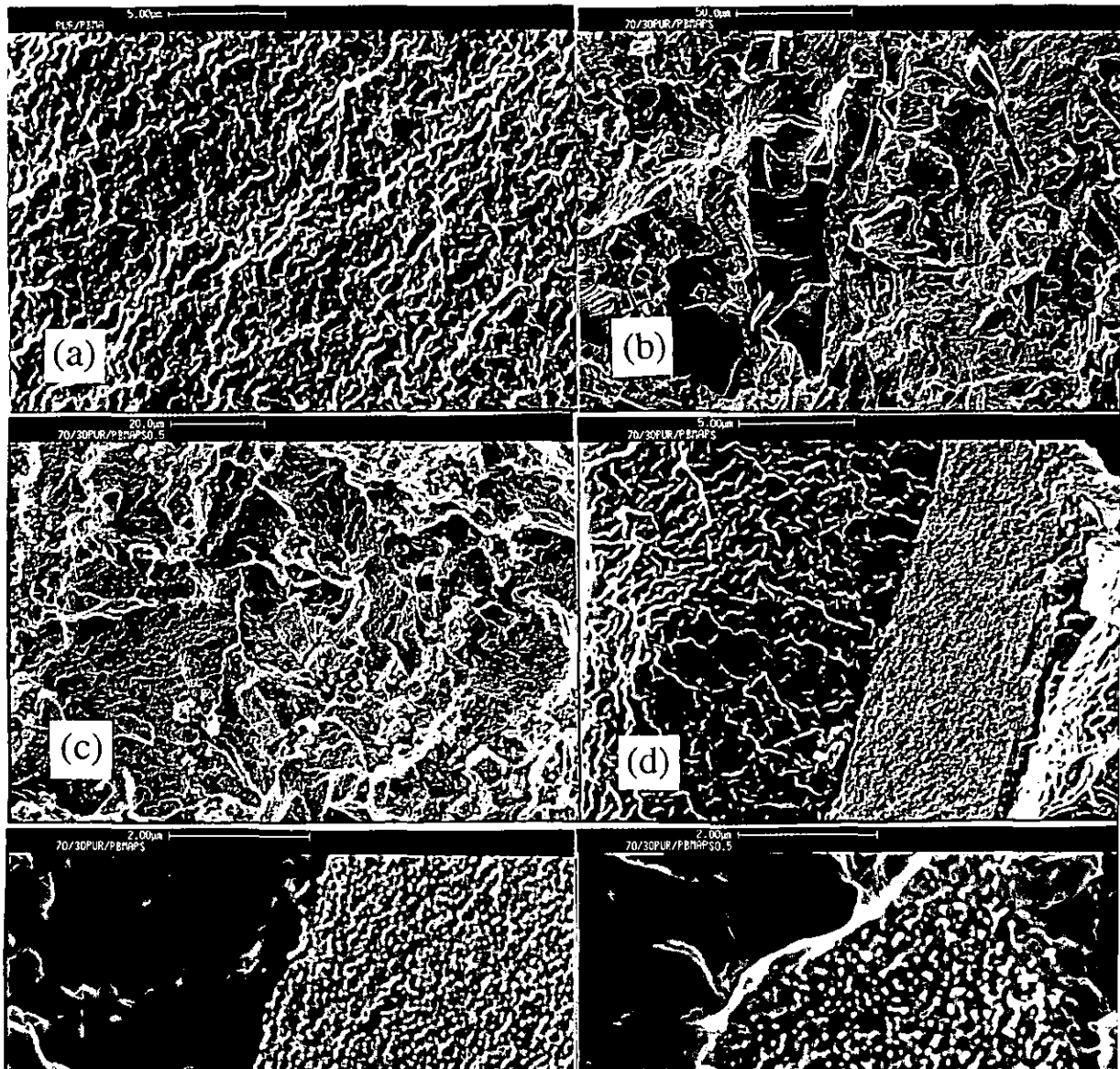

Figure 7.8 SEM micrographs for the 70:30 PUR/PBMA IPNs containing latex particles. (a) 70:30 PUR/PBMA IPN without latex particles, (b) + 17% PS, (c) + 17% PS-(0.5%HEMA), (d)&(e) + 17% PS and (f) + 17% PS-(0.5%HEMA).

The SEM micrographs clearly confirmed that the latex particles were not dispersed on an individual level, but that they formed agglomerates of varying sizes. The fact that they were not dispersed individually might have accounted for their marked influence in the DMTA data. On the other hand, a better dispersion might have resulted in stronger materials with better mechanical properties. Also, an increase of the PS - PUR/PBMA interface might have resulted, leading to a higher degree of interpenetration between the different polymer networks. The latter might have increased the friction in the system leading to higher damping characteristics. Thus, future work in this area should concentrate on obtaining a better dispersion of the latex particles. This might be achieved by either an improvement of the dispersion process of the latex particles or by modifying the surface of the latter making them more stable in the PUR precursor/monomer reaction medium.

8. Conclusions and Further Work

8.1 Achievement of Controlled IPN Morphology

IPN morphology, i.e. the phase miscibility, phase continuity and phase domain sizes and shapes were investigated for the highly immiscible PUR/PS polymer pair and the semi-miscible PUR/PEMA polymer pair. Methods used to control the IPN morphology were the variation of the crosslink density in both networks, the introduction of inter-network grafting, compatibilisers and ionic interactions and the variation of the PUR components.

PUR/PS IPNs. In the PUR/PS IPN composition series, all compositions were found to have a grossly phase-separated morphology. All compositions had two well-separated loss factor transitions and exhibited a two-step drop in the storage modulus versus temperature data. The DMTA Tg data were confirmed by M-TDSC. With decreasing PUR content, the PUR Tg values increased first and then strongly decreased from the 40:60 PUR/PS IPN composition onwards. The latter was explained by first, an increase in phase mixing as a result of interpenetration of the two networks. At lower PUR contents, complete network formation was impeded, which resulted in even lower Tg values than were observed for the pure PUR network. The PS transition shifted to higher temperatures with lower PS contents. The origin of this phenomenon could not be resolved with certainty. However, it was believed that it resulted from interactions between the hydrogen atoms of the urethane links and the π-electron orbitals of the PS phenyl rings. The phase domain sizes of the PS domains decreased with decreasing PS content. The latter caused an increase of the PUR hard segment - PS contact area and, thus, resulted in an increase of the PS Tg. Modulus-composition studies were conducted to investigate the IPN phase continuity. The curve of log modulus versus IPN composition had the best fit with the Budiansky model. From the Young's and the storage moduli, it appeared that phase inversion took place at the 30:70 PUR/PS IPN composition. However, it was noted that the temperature at which the moduli were taken had an important bearing on the composition where phase inversion occurred. Generally, taking the moduli at lower temperatures shifted the phase inversion to lower contents of the polymer with the

higher Tg. SEM and TEM micrographs corroborated the two-phase morphology and the occurrence of phase inversion about the 30:70 PUR/PS IPN composition. SEM studies showed a very irregular fracture surface and deep cavities over the mid-range compositions, from the 60:40 to the 30:70 PUR/PS IPNs. TEM showed that the PS phase domains continually increased with increasing PS content up to the 30:70 PUR/PS IPN composition. The PS domains were spherical. The PUR-PS phase boundary was well-defined and in most cases a dark shell of high PUR content surrounded the PS domains.

Crosslinking in either network did not significantly improve miscibility of the two networks as observed by DMTA data. However, it was observed that crosslinking seemed to influence the IPN phase continuity. Generally, the component with the higher crosslink density represented the more continuous phase. TEM micrographs showed that the phase domain sizes decreased considerably with increasing crosslink density. However, even at high crosslink levels and very small domain sizes of 20 - 200 nm a two-phase morphology was observed by both DMTA and M-TDSC.

The 60:40 PUR/PS IPN had two loss factor peaks of roughly equal height and was thus selected for the subsequent studies. Inter-network grafting was successful in increasing phase mixing. At levels of 5 weight % TMI (or HEMA), only one loss factor transition peak was observed in the DMTA data. The M-TDSC data for these IPNs showed one main transition and a considerable shoulder indicating that M-TDSC had a higher sensitivity to phase separated structures. The introduction of additional crosslinks by inter-network grafting was mirrored in the decrease of the strain at break with increasing grafting level. Surprisingly, the stress at break values decreased slightly from 13 MPa for the ungrafted to 10 MPa for the 10% TMI grafted IPN. Young's modulus and the hardness values strongly increased with higher grafting levels. TEM and SEM studies corroborated the decrease in phase domain sizes and the increase in phase mixing. At 10% TMI grafting, no phase structure could be resolved even at a 100 k magnification.

From the four different reactive compatibilisers, only the one that resembled most closely the PUR soft segment was successful in increasing the inter-transition height. At 10% TMI-PPG1025, one broad transition range was obtained. In addition to small PUR and PS transitions, a third intermediate transition was observed. Even though it was difficult to find conclusive evidence from the M-TDSC and the TEM studies it

was not believed that the intermediate damping peak was not purely a mechanical phenomenon. Instead, it was thought that a highly phase-mixed interface region was on the grounds of the intermediate damping peak.

The introduction of ionic interactions also proved effective in reducing phase separation and achieving a fine phase morphology. An incorporation level of 1% MAA in combination with a tertiary amine (MDEA) still exhibited gross phase separation as seen by the loss factor data. At 2% and 3%, the PUR and the PS loss factor peaks shifted inwards. The higher degree of phase mixing in the latter was also mirrored in higher inter-transition loss factor values. Surprisingly, the incorporation of 3% MAA without tertiary amine resulted in very similar DMTA data to the former IPN. This could be explained by the fact that the urethane nitrogen atom was also capable of neutralising the carboxylic acid groups in the PS network. The introduction of 3% MDEA without MAA resulted in a material with a high inter-transition region and a broad and high loss factor transition range. The latter could not be explained with certainty and will need further investigation. TEM micrographs explained the change in transition shape that was observed between 1% and 2% MAA and MDEA levels. At 1%, separate agglomerates of PS were observed. At 2%, the PS domains started to form a macroscopic network structure. Thus, the PS was continuous to a great extent and strongly influenced the IPN properties. The latter was mirrored in the PS transition that was higher than that of the PUR. SEM micrographs confirmed that with increasing ionic group content, a finer phase morphology resulted.

PUR/PEMA IPNs. The DMTA data of the PUR/PEMA IPN composition series confirmed the semi-miscible nature of this polymer pair. The latter manifested itself in a significant inward shift of the loss factor peaks and an essentially single-step drop mechanism of the storage moduli. A matrix of predominantly PUR with dispersed PEMA was believed to exist at the 90:10 and 80:20 PUR/PEMA compositions. The 70:30 PUR/PEMA IPN composition exhibited a very broad and almost rectangular loss factor transition. The equal loss factor peak height was an indication of dual-phase continuity. The mid-range IPN compositions from 70:30 to 40:60 PUR/PEMA all were slightly less miscible than the outer ranges. For these compositions, a significant shoulder in the loss factor data was apparent for the second component. From the 30:70 to 10:90 IPN compositions, a predominantly PEMA matrix with

dissolved, discontinuous PUR was observed from the DMTA data. The Tg data from the M-TDSC experiment indicated a higher degree of phase separation in the PUR/PEMA IPNs. This indicated again that M-TDSC might be more sensitive to phase-separated structures. Further study comparing DMTA and M-TDSC Tg results will be needed. Strong synergistic effects were observed for the mechanical properties about the 70:30 PUR/PEMA IPN composition. This composition exhibited the highest values by far for the strain at break and toughness index. Shore A hardness values also strongly increased at the 70:30 PUR/PEMA IPN composition. The stress at break, on the other hand, showed an increase in three different regimes with increasing PEMA content. The new insight gained from the PUR/PS IPN composition series regarding modulus-composition studies was corroborated in these PUR/PEMA IPNs. The temperature at which the modulus values were taken influenced greatly the shape of the modulus-composition plot. When taking the moduli at higher temperatures, the latter changed from Davies-like behaviour to Budiansky-like behaviour, indicating phase inversion at the mid-range composition. It was, therefore, suggested that in order to make such modulus-composition studies, modulus data should be taken at the intermediate temperature of the half-drop of the storage modulus curves of the PUR and PEMA homonetworks. Following this suggestion in the present study indicated that phase inversion to took place at the 70:30 composition, which was in accordance with the findings from complimentary experimental techniques. TEM micrographs fully confirmed the findings from DMTA and the modulus-composition study. For the 70:30 PUR/PEMA IPN a predominately PUR matrix with interconnected PEMA domains was noted. Generally, a fine phase morphology was observed in the TEM micrographs. Contrary to the PS phase domains, the PEMA domains did not exhibit a sharp contrast with the PUR matrix. The presence of a highly mixed, relatively large interface area was mirrored in the various shades of grey in the TEM micrographs. The outer compositions had very small phase domains of 3 - 30 nm of the lesser polymer, whereas the mid-range compositions had phase domain sizes between 10 - 500 nm. SEM micrographs showed a clearly smoother fracture surface for the PUR/PEMA IPNs than for their PUR/PS counterparts which confirmed the better phase mixing of the former. In conclusion, it was believed that the fact that phase inversion in the PUR/PEMA IPN (70:30) and the PUR/PS IPN (30:70) occurred at very different compositions despite

the same preparation procedure was a result of the differences in miscibility of the two polymer pairs. The high interfacial tension between the PUR and the PS domains prevented the latter from achieving a degree of continuity at low PS contents. In PUR/PS IPNs, phase separation occurred before the mechanical ramification of a phase-mixed morphology.

The influence of the crosslink density of both networks was investigated in the 70:30 PUR/PEMA IPN. Control of crosslinking was successful in adjusting the Tg location and the transition shape and, thus, tailoring the damping profile. Crosslinking of the PUR network seemed to increase phase mixing, resulting in a narrower and higher transition shifted to higher temperatures. Crosslinking in the second-formed PEMA network decompatibilised the IPNs which resulted in a broadening of the transition and some very broad transitions resulted. Crosslinking of the PUR (first-formed network with higher weight percentage) exerted a stronger influence on the mechanical properties such as stress at break and Young's modulus. TGA results revealed a two-step degradation pattern for the IPNs, as opposed to the one-step pattern of both homopolymer networks. TEM micrographs confirmed a finer morphology for the materials with a higher crosslink density in the PUR, whereas increasing the crosslink density in the PEMA network resulted in a decrease of phase mixing.

The variation of the PUR network in the 70:30 PUR/PEMA IPN strongly altered the IPN morphology and properties. Using PPG polyols of increasing molar masses (which amounted to a decreasing crosslink density) resulted in less phase mixed IPNs. For a PPG polyol of a molar mass of 425 $g \cdot mol^{-1}$ one loss factor peak was obtained whereas for a molar mass of 4000 two well-separated transitions resulted. The mechanical properties for the PPG425-based IPN were much higher. IPNs based on PPG1025 and PPG2025 resulted in very broad loss factor transition regions. The latter indicated that a considerable degree of phase mixing was present. Comparing the PPG2025 with different polyol-types of similar molar mass resulted in IPNs with very different properties. IPNs based on PCL2000 and PTHF2000 polyols exhibited some degree of crystallinity and were - maybe as a result of the latter - phase-separated. The PBD2500-based IPN also showed two clearly separated transitions in the DMTA data. A variation of the diisocyanate and the chain extender also considerably changed the dynamic mechanical properties of the IPNs. The highest mechanical properties

were obtained from the PCL2000- and PTHF2000-based IPNs because of their partly crystalline structure.

8.2 Development of High Damping Materials

A number of IPNs with high damping characteristics over a broad temperature range were developed. This was achieved both with the highly immiscible polymer pair, PUR/PS, and with the semi-miscible PUR/PEMA IPN. For the former, the use of grafting agents, compatibilisers, charged groups or a change in the polymerisation conditions was needed in order to bring about the desired properties.

IPNs with a broad loss factor range ≥ 0.3. A number of IPNs with excellent damping properties were developed. The damping ability of some of these were characterised by the area under the linear loss factor (TA) and loss modulus (LA) data. The TA area was generally seen to follow the same trend as the temperature region where the loss factor values were ≥ 0.3. Generally, with an increase in crosslink density values for both quantities decreased. However, there were exceptions. For example, as a consequence of low crosslink levels in the PPG4000-based 70:30 PUR/PEMA IPN, the material had a phase-separated loss factor profile. The inter-transition loss factor values dropped below 0.3 and, thus, strongly restricted the useful damping region. Another example was the study of the variation of the crosslinking density of the PEMA network in the 70:30 PUR/PEMA IPN. For the latter a higher temperature where the loss factor ≥ 0.3 and higher values for the TA area resulted when increasing the PEMA crosslinking from 0% to 5% TEGDM. The eight best damping materials as seen from the temperature range where the loss factor was ≥ 0.3 are given in table 8.1.

High damping IPNs were developed from both PUR/PEMA and PUR/PS IPNs. However, it was believed that the PUR/PEMA IPNs generally exhibited better damping characteristics. Tailoring the latter was easier, simply by varying the PUR network. The stirred 60:40 PUR/PS IPN that performed best amongst the PUR/PS IPNs was very difficult to synthesise reproducibly. The 60:40 IPN with 3% MDEA had a high transition range. However, the mechanical properties at the upper transition end were extremely poor.

Table 8.1 High damping IPNs as judged by the temperature range where the loss factor was ≥ 0.3.

IPN identification	Temperature range loss factor ≥ 0.3 [°C]	From [°C]	To [°C]
70:30 PUR(PPG2025/TMP 3:1)/PEMA(5%)	171	-33	138
70:30 PUR(PPG1025/BD 3:1)/PEMA(5%)	168	-10	158
60:40 PUR/PS IPN, stirred polym.	164	-19	145
60:40 PUR/PS IPN, + 3% MDEA	162[(a)]	-2	160[(a)]
60:40 PUR/PS, + 10% TMI-PPG1025	135	-12	123
70:30 PUR(PPG1025/TMP 3:1)/PEMA(5%)	130	-5	125
70:30 PUR(PPG1025/TMP 7:1)/PEMA(5%)	127	-19	108
60:40 PUR/PS, + 2.5% TMI	80	45	125

(a) Curve extrapolation had to be conducted for the high temperature end of the PS loss factor peak.

This manifested itself in the very low storage moduli. Also, the loss factor values at the higher PS transition end did not decrease below a value of 0.3; because of significant softening. The 70:30 PUR/PEMA based on a PPG2025 polyol had the greatest temperature range with 171°C of loss factor values ≥ 0.3 (table 8.1). The damping range was centred about room temperature. It was a potentially excellent damping material. Even if substantial variations of temperature (± 50°C) or frequency (7 decades) towards higher or lower temperatures occurred there would still be an important high damping safety margin.

Characterisation of the damping ability of the IPNs by using the loss modulus and related quantities was more difficult by far than using the loss factor. The loss modulus and related quantities such as the LA area were subject to variations due to differences in sample clamping. Consequently, no emphasis was placed on the latter in this study. In brief, in the PUR/PEMA IPN composition study, it was observed that the LA area increased with increasing PEMA content. Thus, the highest LA area was obtained with the PEMA homonetwork. However, the E" maximum and, thus, the maximum extensional layer damping ability varied with IPN composition. When varying the crosslink density in the 70:30 PUR/PEMA IPN, it was observed that

higher crosslinking in the first-formed PUR network seemed to increase slightly the LA. On the other hand, no obvious change in the LA area was noticed when altering the crosslink density in the PEMA network.

IPNs containing functional latex particles. The incorporation of 17 weight % of composite PS latex particles significantly altered the property profile of a 70:30 PUR/ PBMA IPN. The mechanical properties of the IPN were significantly improved by the incorporation of latex particles. This was evident in the higher values for the Young's modulus and the Shore A hardness. Also, increased values for the storage modulus in the higher temperature range from 80°C to 140°C were found. Functional latex particles with hydroxyl functionality exhibited a better mixing with the microheterogeneous PUR/PBMA IPN than unfunctionalised PS latex particles, and, therefore, resulted in materials with better damping properties in the temperature range between 80°C and 140°C. TEM micrographs confirmed the improved mixing of the functionalised latex particles with the IPN matrix. Further, it was observed that the latex particles were not dispersed on an individual level, but that agglomerates of a size between 2 - 40 μ were formed.

8.3 Recommendations for Future Work

Research often raises more questions ... it answers. In the course of this study it was observed that the following points will need further study.

1) More work is needed to investigate the IPN morphology and phase continuity and factors influencing the latter. The use of SAXS and solid-state NMR for characterisation of highly miscible IPN systems might yield further valuable information. A wider comparison of the advantages and limitations of DMTA and M-TDSC as a means of studying polymer Tg behaviour, morphology and properties should prove interesting.

2) A continuation of the development of high damping IPNs with latex particles might result in an even broader transition range. Functionalised latex particles of a polymer that is inherently more miscible with the monomer mixture and, thus, swollen to a

greater extent might prove interesting. Ways of improving the dispersion of the latex particles should be investigated. The latter might be achieved by changing the preparation procedure. Changing the order of addition, allowing more time for the latex particles to be swollen in the monomer mixture and/or working at a higher reaction mixture viscosity might be some avenues that might be worth following up. Also, improving the stability of the dispersion by chemically modifying the latex particle shell might prove interesting. For example, copolymerising a methacrylate-terminated PPG polyol into the latex particle shell should dramatically improve the latex particle stability in the PUR precursors.

In the present study, it was attempted to increase the high temperature properties of the PUR/PBMA IPN. The incorporation of latex particles with core Tg values intermediate or below the two IPN polymers might result in interesting materials. Also, instead of working with high Tg core latex particles as organic fillers, the use of composite particles of inorganic filler overcoated with polymer might result in materials with a high inherent damping ability.

3) A number of potentially high damping materials were developed in the present study. However, testing these damping materials under controlled conditions in simple extensional and constrained layer damping systems is needed. The latter will hopefully determine whether, for example, the high temperature end of the loss factor transition makes a high contribution to the system damping even though the material mechanical properties are already very weak.

4) It should be attempted to make IPNs more relevant for industrial applications. To overcome their thermoset character, which results in disadvantages in processing and recycling two directions can be chosen. Thermoplastic IPNs based on versatile PURs and methacrylic polymers might be developed using intramolecular interactions such as hydrogen bonding or ionic interactions. Also, latex IPNs made, for example, by combining PUR dispersions with (meth)acrylics could result in products with interesting properties. Finally, extending the use of the RIM technology to polymer pairs other than PUR and epoxy to prepare IPNs might result in interesting materials.

9. REFERENCES

(1) S. Rostami, in 'Multicomponent Polymer Systems', eds. I.S. Miles and S. Rostami, Longman Scientific & Technical, Harlow (1992).

(2) K.B. Sinclair and R.B. Wilson, *Chemistry & Industry*, **21**, 857 (1994).

(3) D.R. Paul, and S. Newman, 'Polymer Blends', Vol. 1&2, Academic Press, New York (1978).

(4) L.H. Sperling, 'Interpenetrating Polymer Networks and Related Materials', Plenum Press, New York (1981).

(5) P.A. Nelson and S.J. Elliot, 'Active Control of Sound', Academic Press, London (1993).

(6) C. Stahle, 'Pioneering Damping in Space in Proceedings of Damping', Workshop Damping '89, West Palm Beach, FL (1989).

(7) E.E. Ungar, in 'Noise and Vibration Control', L.L.Beranek, Chap. 14, McGraw-Hill, New York (1979).

(8) L. Kinsler, A.R. Frey, A.B. Coppens and J.V. Sanders, 'Fundamentals of Acoustics', 3rd edition, John Wiley & Sons, New York (1982).

(9) R.D. Bruce, Noise Pollution in 'Encyclopedia of Chemical Technology', Vol. 16, John Wiley & Sons (1982).

(10) K.D. Kryter, 'The Effects of Noise on Man', Academic Press, New York (1970).

(11) T.R. Ferguson, Damping - A Key To More, Faster, Farther, Higher in 'Proceedings of Damping', Workshop Damping '89, West Palm Beach, FL (1989).

(12) L. Rogers, Introduction in 'Sound and Vibration Damping with Polymers', R.D. Corsaro and L.H. Sperling,.ACS Symp., Ser. 424, Washington, DC (1990).

(13) L.H. Sperling, in 'Sound and Vibration Damping with Polymers', R.D. Corsaro and L.H. Sperling, ACS Symp., Ser. 424, Washington, DC (1990).

(14) J.B. Hunt, 'Dynamic Vibration Absorbers', Mechanical Engineering Publications Ltd., London (1968).

(15) M. Drake, in 'Sound and Vibration Damping with Polymers', R.D. Corsaro and L.H. Sperling, ACS Symp., Ser. 424, Washington, DC (1990).

(16) J. Jarzynski, in 'Sound and Vibration Damping with Polymers', R.D. Corsaro and L.H. Sperling, ACS Symp., Ser. 424, Washington, DC (1990).

(17) N.W. Hagood and A. von Flotow, Damping of Structural Vibrations with Piezoelectric Materials in 'Proceedings of Damping', Workshop Damping '89, West Palm Beach, FL (1989).

(18) B.W. Maxfield, A. Kuramoto, J.K. Hulbert and P. Smiley, Electromagnetic Vibration Dampers in 'Proceedings of Damping', Workshop Damping '89, West Palm Beach, FL (1989).

(19) D.T.H. Wong and H.L. Williams, *J. Appl. Polym. Sci.*, **28**, 2187 (1983).

(20) G.L. Ball and I.O. Salyer, *J. Acoust. Soc. Am.*, **39**, 663 (1966).

(21) D.J. Ferry, 'Viscoelastic Properties of Polymers', John Wiley & Sons, 3rd edition, New York (1983).

(22) E.M. Kerwin and E.E. Ungar, in 'Sound and Vibration Damping with Polymers', R.D. Corsaro and L.H. Spering, ACS Symp., Ser. 424, Washington, DC (1990).

(23) D.J. Hourston and I.D. Hughes, *J. Appl. Polym. Sci.*, **21**, 3093 (1977).

(24) D. Klempner and L. Berkowski, in 'Encyclopedia of Polymer Science and Engineering', eds. H.F. Mark, N.M. Bikales, G.C. Overberger and G. Menges, Vol. 8, John Wiley & Sons, New York (1987).

(25) L.H. Sperling, in 'Comprehensive Polymer Science', eds. G. Allen and J.C. Bevington, Vol. 6, Pergamon Press, New York (1989).

(26) S.A.M. Ali and D.J. Hourston, in 'Advances in Interpenetrating Polymer Networks', Vol. IV, eds. D. Klempner and K.C. Frisch, Technomic, Lancaster, PA (1994).

(27) J.R. Aylsworth, U.S. Pat. 1, 111, 284 (1914).

(28) J.R. Millar, *J. Chem. Soc.*, 1311 (1960).

(29) L.H. Sperling and D.W. Friedman, *J. Polym. Sci. Polym. Phys.*, **7**, 425 (1969).

(30) H.L. Frisch, D. Klempner and K.C. Frisch, *Polym. Lett.*, **7**, 775 (1969).

(31) H.L. Frisch, L. Wang, W. Huang, Y.H. Hua, H.X. Xiao and K.C. Frisch, *J. Appl. Polym. Sci.*, **43**, 475 (1991).

(32) W. Ring, I. Mita, A.D. Jenkins and N.M. Bikales, *Pure Appl. Chem.*, **40**, 476, (1967).

(33) L.G. Donarum, H.G. Elias, D.J. Meier and L.H. Sperling, Polym. Chem. Nomencl. Committee, ACS (1984).

(34) R.B. Fox, J.J. Fay, U. Sorathia and L.H. Sperling, in 'Sound and Vibration Damping with Polymers', eds. R.D. Corsaro and L.H. Sperling, ACS Symp., Ser. 424, Washington, DC (1990).

(35) J.A. Manson and L.H. Sperling, in 'Polymer Blends and Composites', Plenum Press, New York (1976).

(36) V. Huelck, D.A. Thomas and L.H. Sperling, *Macromolecules*, **5**, 340 (1972).

(37) R.H. Sheu, M.S. El-Aasser and J.W. Vanderhoff, *J. Polym. Sci. Polym. Chem.*, **28**, 629 (1990).

(38) D.A. Greenhill, D.J. Hourston and J.A. Waters, in 'Sound and Vibration Damping with Polymers', eds. R.D. Corsaro and L.H. Sperling, ACS Symp., Ser. 424, Washington, DC (1990).

(39) V.I. Eliseeva, *Prog. Org. Coat.*, **13**, 195 (1985).

(40) J.C. Daniel, *Makromol. Chem. Suppl.*, **10**, 359 (1985).

(41) K.C. Frisch, D. Klempner, H.X. Xiao, E. Cassidy and H.L. Frisch, *Polym. Eng. Sci.*, **25**, 12 (1985).

(42) J. Ferrarini, D.M. Longnecker, N.N. Shah, J. Feltzin and G.G. Greth, 33rd Annual Conference, Reinforced Plastics Conference Institute, 9-D, 1 (1978).

(43) R. Pernice, K.C. Frisch and R. Navare, *J. Cell. Plast.*, **3/4**, 121 (1982).

(44) B.M. Kolarz, *Angew. Makromol. Chem.*, **90**, 167, 183 (1980).

(45) J.A. Cox, R. Gajek, G.R. Litwinski, J. Carnaham and W. Trochimczuk, *Anal. Chem.*, **54**, 1153 (1982).

(46) D.S. Lee, W.K. Kang, J.H. An and S.C. Kim, *J. Membrane Sci.*, **75**, 15 (1992).

(47) R.P. Kusy, B.J. Lytwyn and D.T. Turner, *J. Dent. Res.*, **55**, 452 (1976).

(48) E.H. Harris and S.H. Feairhekker, *Polym. Eng. Sci.*, **17**, 287 (1977).

(49) L.H. Sperling, T.W. Chiu, R.G. Gramlich and D.A. Thomas, *J. Paint. Technol.*, **46**, 47 (1974).

(50) D.J. Hourston and J.A. McCluskey, *J. Appl. Polym. Sci.*, **31**, 645 (1986).

(51) K.F. Mueller and S.J. Heiber, *J. Appl. Polym. Sci.*, **27**, 4043 (1982).

(52) W. Eck, *Advanced Materials*, **7**, 800 (1995).

(53) D.J. Hourston and F.-U. Schäfer, *Polym. Adv. Technol.*, **7**, 1 (1996).

(54) D.J. Hourston and Y. Zia, *Polymer*, **20**, 1497 (1979).

(55) D. Klempner, C.L. Wang, M. Ashtiani and K.C. Frisch, *J. Appl. Polym. Sci.*, **32**, 4197 (1986).

(56) L.H. Sperling, in 'Multicomponent Polymer Materials', eds. D.R. Paul and L.H. Sperling, ACS 211, American Chemical Society, Washington, DC (1986).

(57) L.H. Sperling, in 'Interpenetrating Polymer Networks', eds. D. Klempner, L.H. Sperling and L.A. Utracki, Advances in Chemistry Series 239, American Chemical Society, Washington, DC (1994).

(58) M. Akay and S.N. Rollins, *Polymer*, **34**, 1865 (1993).

(59) R.B. Fox, J.L. Bittner, J.A. Hinkley and W. Carter, *Polym. Eng. Sci.*, **25**, 157 (1985).

(60) J.H. Lee and S.C. Kim, *Macromolecules*, **19**, 644 (1986).

(61) N. Devia, J.A. Mason, L.H. Sperling and A. Conde, *Macromolecules*, **12**, 360 (1979).

(62) S.R. Jin, J.-M. Widmaier and G.C. Meyer, *Polymer*, **29**, 346 (1988).

(63) M.T. Tabka, J.-M. Widmaier and G.C. Meyer, *Plastics Rubber Comp. Process. Appl.*, **16**, 11 (1991).

(64) X. He, J.-M. Widmaier and G.C. Meyer, *Polym. Inter.*, **32**, 289 (1993).

(65) X. He, J.-M. Widmaier and G.C. Meyer, *Polym. Inter.*, **32**, 295 (1993).

(66) D.S. Lee, D.S. Jung, T.H Kim and S.C. Kim, *J. Membrane Sci.*, **60**, 233 (1991).

(67) D.S. Lee, W.K. Kang, J.H. An and S.C. Kim, *J. Membrane Sci.*, **75**, 15 (1992).

(68) Y. Suzuki, T. Frijimoto, S. Tsunoda and K.J. Shibayama, *Macromol. Sci. Phys.*, **17**, 787 (1980).

(69) M. Song, Ph.D thesis, Jilin University, People's Republic of China, in L.H. Sperling, Advances in Interpenetrating Polymer Networks, eds. D. Klempner and K.C. Frisch, Vol. IV, Technomic, Lancaster, PA (1994).

(70) N. Parizel, G.C. Meyer and G. Weill, *Polymer*, **34**, 2495 (1993).

(71) C.-J. Tung and T.-C. Hsu, *J. Appl. Polym. Sci.*, **46**, 1759 (1992).

(72) R.E. Touhsaent, D.A. Thomas and L.H. Sperling, *J. Polym. Sci.*, **46C**, 175 (1974).

(73) P.G. Klein, J.R. Ebdon and D.J. Hourston, *Polymer*, **29**, 1079 (1988).

(74) S.N. Derrough, C. Rouf, J.-M. Widmaier and G.C. Meier, *Polym. Prepr*, **72**, 1 (1992).

(75) L.H. Sperling, in 'Advances in Interpenetrating Polymer Networks', Vol. IV, eds. D. Klempner and K.C. Frisch, Technomic, Lancaster, PA (1994).

(76) T. Hur, J.A. Manson, R.W. Hertzberg and L.H. Sperling, *J. Appl. Polym. Sci.*, **39**, 1933 (1990).

(77) S.C. Kim, D. Klempner, K.C. Frisch, W.Radigan and H.L. Frisch, *Macromolecules*, **9**, 258 (1976).

(78) S.C. Kim, D. Klempner, K.C. Frisch and H.L. Frisch, *Macromolecules*, **9**, 263 (1976).

(79) S.C. Kim, D. Klempner, K.C. Frisch, W.Radigan and H.L. Frisch, *Macromolecules*, **10**, 1191 (1977).

(80) S.C. Kim, D. Klempner, K.C. Frisch, W.Radigan and H.L. Frisch, *Macromolecules*, **10**, 1187 (1977).

(81) S.C. Kim, D. Klempner, K.C. Frisch, *J. Appl. Polym. Sci.*, **21**, 1289 (1977).

(82) Ph. Heim, C. Wrotecki, M. Avenel and P. Gaillard, *Polymer*, **34**, 8 (1993).

(83) M. Akay and S.N. Rollins, *Polymer*, **34**, 967 (1993).

(84) N. Parizel, G.C. Meyer and G. Weill, *Polymer*, **36**, 2323 (1995).

(85) V. Mishra and L.H. Sperling, *Polymer*, **36**, 18 (1995).

(86) V. Mishra, F. Du Prez and L.H. Sperling, *Polym. Mater. Sci. Eng.*, **72**, 124 (1995).

(87) A.M. Fernandez, J.A. Manson and L.H. Sperling, in 'Renewable Resource Materials: New Polymer Sources', eds. C.E. Carraher and L.H. Sperling, Plenum Press, New York (1986).

(88) P. Patel, T. Shah and B. Suthar, *J. Appl. Polym. Sci.*, **40**, 1037 (1990).

(89) L.H. Sperling, J.A. Manson and M.A. Linne, *J. Polym. Mater.*, **1**, 54 (1984).

(90) S.S. Kelley, T.C. Ward and W.G. Glasser, *J. Appl. Polym. Sci.*, **41**, 2813 (1990).

(91) H.L. Frisch, D. Klempner, H.K. Yoon and K.C. Frisch, *Macromolecules*, **13**, 1016 (1980).

(92) B.J. Bauer and R.M. Briber, in 'Advances in IPNs', eds. D. Klempner and K.C. Frisch, Technomic Publishing, Lancaster PA (1994).

(93) L.H. Sperling, 'Introduction to Physical Polymer Science', 2nd ed., John Wiley & Sons Inc., New York (1992).

(94) J.H. An and L.H. Sperling, in 'Cross-linked Polymers', ACS Series 367, eds. R.A. Dickie, S.S. Labana and R.S. Bauer, American Chemical Society, Washington, DC (1988).

(95) M. Vollmer and A. Weber, *Z. Phys. Chem.*, **119**, 277 (1925).

(96) J.W. Cahn, *J. Chem. Phys.*, **42**, 93 (1965).

(97) W.P. Gergen, *Kautsch. Gummi*, **37**, 4 (1984).

(98) G. M. Jordhamo, J.A. Manson and L.H. Sperling, *Polym. Eng. Sci.*, **26**, 517 (1986).

(99) A.A. Donatelli, L.H. Sperling, and D.A. Thomas, *J. Appl. Polym. Sci.*, **21**, 1189 (1977).

(100) A.A. Donatelli, L.H. Sperling, D.A. Thomas, *Macromolecules*, 9, 671, 676 (1976).

(101) D.A. Thomas, *J. Polym. Sci. Polym. Symp.*, **60**, 189 (1977).

(102) K. Kato, *Polym. Eng. Sci.*, **7**, 38 (1967).

(103) D.J. Walsh and S. Rostani, *Advances in Polymer Science*, **70**, 121 (1985).

(104) Y. Lipatov, S.V.V. Shilov, V.A. Bogdanovic, L.V. Karabanova and L.M. Sergeeva, *J. Polym. Sci. Polym. Phys. Ed.*, **25**, 43 (1987).

(105) B.J. Bauer, R.M. Briber and B. Dickens, in 'Interpenetrating Polymer Networks', ACS 239, eds. D. Klempner, L.H. Sperling and L.A. Utracki, ACS, Washington, DC (1994).

(106) J.H. An, A.M. Fernandez and L.H. Sperling, *Macromolecules*, 20, 191 (1987).

(107) U.W. Gedde, 'Polymer Physics', Chapman & Hall, London (1995).

(108) K.C. Frisch, D. Klempner, S. Migdal, H.L. Frisch, and H. Ghiradella, *Polym. Eng. Sci.*, **14**, 76 (1974).

(109) I. Alig, M. Junker, W. Jenninger, H.L. Frisch and M. Schulz, Conference Lecture, Morphology of Polymers, Prague, July (1995).

(110) D.J. Hourston and F.-U. Schäfer, *Polymer*, in press, (1996).

(111) K.J. Yeo, L.H. Sperling and D.A. Thomas, *Polym. Eng. Sci.*, **21** (11), 696 (1981).

(112) V. Nevissas, J.-M. Widmaier and G.C. Meyer, *J. Appl. Polym. Sci.*, **36**, 1467 (1988).

(113) S. Yao, in 'Advances in IPNs', Vol. IV, eds. D. Klempner and K.C. Frisch, Technomic Publishing Company Inc., Lancaster, PA (1994).

(114) L.H. Sperling, in 'Polymers for Advanced Technologies', 635, VCH, New York (1988).

(115) P. Penczek, 'Polymer Blends', Plenum Press, New York (1980).

(116) C.H.M. Jaques, H.B. Hopfenberg and V. Stannett, *Polym. Eng. Sci.*, **13**, 81 (1973).

(117) W.J. MacKnight, F.E. Karasz and J.R. Fried, in 'Polymer Blends', Vol. 1, eds. D.R. Paul and S. Newman, Academic Press, New York (1978).

(118) D.W. Clegg and A.A. Collyer, 'Polymeric Materials', The Institute of Materials, London (1993).

(119) T. Tabka, J.-M. Widmaier and G.C. Meyer, *Polym. Mater. Sci. Eng.*, **60**, 659 (1989).

(120) X. He, J.-M. Widmaier and G.C. Meyer, *Polym. Mater. Sci. Eng.*, **65**, 44 (1991).

(121) M.T. Tabka, J.-M. Widmaier and G.C. Meyer, in 'Sound and Vibration Damping', eds. R.D. Corsaro and L.H. Sperling, ACS Symp., Ser. 424, Washington, DC (1990).

(122) G.C. Meyer and P.Y. Mehrenberger, *Eur. Polym. J.*, **13**, 383 (1977).

(123) A.A. Donatelli, L.H. Sperling and D.A. Thomas, in 'Recent Advances in Polymer Blends', Grafts and Blocks, Plenum Press, New York (1974).

(124) W.E.A. Davies, *J. Phys. D*, **4**, 1176 (1971).

(125) W.E.A. Davies, *J. Phys. D*, **4**, 1325 (1971).

(126) B. Budiansky, *J. Mech. Phys. Solids*, **13**, 223 (1965).

(127) S.C. Kim, D. Klempner, K.C. Frisch, H.L. Frisch and H. Ghiradella, *Polym. Eng. Sci.*, **15**, 339 (1975).

(128) D.J. Hourston and Y. Zia, *J. Appl. Polym. Sci.*, **28**, 3849 (1983).

(129) D.J. Hourston and J.A. McCluskey, *J. Appl. Polym. Sci.*, **30**, 2157 (1985).

(130) V. Nevissas, J.-M. Widmaier and G.C. Meyer, *J. Appl. Polym. Sci.*, **36**, 1467 (1989).

(131) L.H. Sperling and J.-M. Widmaier, *Polym. Eng. Sci.*, **23**, 693 (1983).

(132) B.J. Bauer, R.M. Briber and C.C. Han, *Macromolecules*, **22**, 940 (1989).

(133) J.J. Fay, C.J. Murphy, D.A. Thomas and L.H. Sperling, in 'Sound and Vibration Damping with Polymers', eds. R.D. Corsaro and L.H. Sperling, ACS Symposium Series 424, American Chemical Society, Washington, DC (1990).

(134) K.C. Frisch, D. Klempner, S. Migdall and H.L. Frisch, *J. Polym. Sci., Polym. Chem. Ed.*, **12**, 885 (1974).

(135) Y.C. Chou and L.J. Lee, *Polym. Mater. Sci. Eng.*, **65**, 57 (1991).

(136) B.J. Bauer, R.M. Briber and B. Dickens, *Polym. Mater. Sci. Eng.*, **65**, 5 (1991).

(137) B.J. Bauer and R.M. Briber, *Polym. Prepr.*, **31**, 578 (1990).

(138) D.J. Hourston and Y. Zia, *J. Appl. Polym. Sci.*, **29**, 629 (1984).

(139) P.R. Scarito and L.H. Sperling, *J. Polym. Sci.*, **46 C**, 175 (1974).

(140) E.F. Cassidy, H.X. Xiao, K.C. Frisch and L.H. Frisch, *J. Polym. Sci. Polym. Chem.*, **22**, 1851 (1984).

(141) J.-M. Widmaier and L.H. Sperling, *Macromolecules*, **15**, 625 (1982).

(142) J.-M. Widmaier and L.H. Sperling, *J. Appl. Polym. Sci.*, **27**, 3513 (1982).

(143) H.X. Xiao, K.C. Frisch and H.L. Frisch, *J. Polym. Sci. Polym. Chem. Ed.*, **22**, 1035 (1984).

(144) K.H. Hsieh, L.M. Chou and S.S. Wong, *Die Angew. Makromol. Chem.*, **168**, 145 (1989).

(145) A. Eisenberg, P. Smith and S.-L. Zhou, *Polym. Eng. Sci.*, **22**, 1117 (1982).

(146) H.X. Xiao, K.C. Frisch and H.L. Frisch, *J. Polym. Sci. Polym. Chem. Ed.*, **21**, 2547 (1983).

(147) D.S. Lee and S.C. Kim, *Macromolecules*, **17**, 268 (1984).

(148) D.S. Lee and S.C. Kim, *Macromolecules*, **17**, 2193 (1984).

(149) S.K. Kim and S.C. Kim, *Polym. Bulletin*, **23**, 141 (1990).

(150) A.D. Nashif, D.I. Jones and J.P. Henderson, 'Vibration Damping', John Wiley & Sons, New York (1985).

(151) M.J. Guest and J.H. Daly, in 'Polymer Yearbook', Harwood Academic Publishers, Chur (1993).

(152) S. Yao, in 'Advances in IPNs', Vol. IV, eds. D. Klempner and K.C. Frisch, Technomic Publishing Company Inc., Lancaster, PA (1994).

(153) D. Sophia, D. Klempner, V. Sendijarevic, B. Suthar and K.C. Frisch, in 'Interpenetrating Polymer Networks', Advances in Chemistry Series 239, eds. D. Klempner, L.H. Sperling and L.A. Utracki, ACS, Washington DC (1994).

(154) J.J. Aklonis and W.J. MacKnight, 'Introduction to Polymer Viscoelasticity', 2nd edition, John Wiley & Sons, New York (1983).

(155) I.M. Ward, 'An Introduction To Mechanical Properties Of Solid Polymers', John Wiley & Sons Ltd., Chichester (1993).

(156) A.W. Birley, B. Haworth and J. Batchelor, 'Physics of Plastics', Hanser Publishers, Munich (1991).

(157) A. Takemura and H. Mizumachi, in 'Advances in Interpentrating Polymer Networks,' Vol. III, eds. D. Klempner and K.C. Frisch, Technomic Publishing AG, Lancaster, PA (1991).

(158) B.J. Hunt and M.F. James, in 'Polymer Characterisation', Blackie Academic & Professional, London (1993).

(159) A.F. Yee and M.T. Takemori, *J. Polym. Sci. Polym. Phys. Ed.*, **20**, 205 (1982).

(160) J. Dulbac, in 'Sound and Vibration Damping with Polymers', eds. R.D Corsaro and L.H. Sperling, ACS 424, American Chemical Society, Washington, DC (1990).

(161) H. Oberst, *Phil. Trans. Roy. Soc.*, A, **2**, 444 (1969).

(162) D.J. Hourston and J.A. McCluskey, *J. Appl. Polym. Sci.*, **31**, 645 (1986).

(163) H. Oberst, *Koll.-Z., Z. Polymers*, **64**, 216 (1967).

(164) M.C.O. Chang, D.A. Thomas and L.H. Sperling, *J. Polym. Mat.*, **6**, 61 (1989).

(165) M.C.O. Chang, D.A. Thomas and L.H. Sperling, *J. Appl. Polym. Sci.*, **34**, 409 (1987).

(166) M.C.O. Chang, D.A. Thomas and L.H. Sperling, *J. Polym. Mat.*, **6**, 348 (1989).

(167) J.J. Fay, D.A. Thomas and L.H. Sperling, *J. Appl. Polym. Sci.*, **43**, 1617 (1991).

(168) J.J. Fay, C.J. Murphy, D.A. Thomas and L.H. Sperling, *Polym. Eng. Sci.*, **31**, 1731 (1991).

(169) H. Keskkula, S.G. Turley and R.F. Boyer, *J. Appl. Polym. Sci.*, **15**, 351 (1971).

(170) J.N. Foster, L.H. Sperling and D.A. Thomas, *J. Appl. Polym. Sci.*, **33**, 2637 (1987).

(171) Y.S. Lipatov, in 'Advances in Interpenetrating Polymer Networks', eds. D. Klempner and K.C. Frisch, Technomic, Lancaster, PA (1989).

(172) S. Yao, M. Jia, X. Yan and Y. Wang, in 'Polymers and Biomaterials', eds. H. Feng, Y. Han and L. Huang, Elsevier B.V. (1991).

(173) B. Hartmann, in 'Sound and Vibration Damping with Polymers', eds. R.D Corsaro and L.H. Sperling, ACS 424, American Chemical Society, Washington, DC (1990).

(174) B. Hartmann, G.F. Lee and J.D. Lee, *J. Acoust. Soc. Am.*, **95**, 226 (1994).

(175) J.B. Hunt, 'Dynamic Vibration Absorbers', Mechanical Engineering Publications Ltd., London (1979).

(176) J.H. Harker, 'Generalized Methods of Vibration Analysis', John Wiley & Sons, New York (1983).

(177) J.M.G. Cowie, 'Polymers: Chemistry and Physics of Modern Materials', 2nd ed., Blackie Academic & Professional, London (1991).

(178) P. Gradin, P.G. Howgate, R. Selden and R. Brown, in "Comprehensive Polymer Science," eds. Allen and Bevington (1989).

(179) D.G. Fradkin, F.N. Foster, L.H. Sperling and D.A. Thomas, *Rubber Chem. Technol.*, **59**, 225 (1986).

(180) B. Hartmann, *Polym. Mat. Sci. Eng.*, **60**, 227 (1989).

(181) T. Murayama, in 'Dynamic Mechanical Analysis of Polymeric Materials', Elsevier, Amsterdam (1978).

(182) J.M. Pochan, C.L. Beatty and D.F. Hinman, *Macromolecles*, **11**, 1156 (1977).

(183) M.Gordon and J.S. Taylor, *J. Appl. Chem.*, **2**, 493 (1952).

(184) T.G. Fox, *Bull. Am. Phys. Soc.*, **1**, 123 (1956).

(185) L.E. Nielsen, 'Mechanical Properties of Polymers and Composites', Vol. 1+2, Marcel Dekker, New York (1974).

(186) R.N. Capps, *J. Acoust. Soc. Amer.*, **73**, 2000 (1983).

(187) M.L. Williams, *J. Phys. Chem.*, **59**, 95 (1955).

(188) M.L. Williams, R.F. Landel and J.D. Ferry, *J. Am. Chem. Soc.*, **77**, 3701 (1955).

(189) K. Wolf, *Kunststoffe*, **41**, 89 (1951).

(190) D.S. Kaplan, *J. Appl. Polym. Sci.*, **20**, 2615 (1976).

(191) M. Takayanagi, H. Harima and Y. Iwata, Mem. Fac. Eng., Kyushu University, Japan, 23, 1 (1963).

(192) M. Akay, S.N. Rollins and E. Riordan, *Polymer*, **29**, 37 (1988).

(193) L.H. Sperling, T.W. Chiu and D.A. Thomas, *J. Appl. Polym. Sci.*, **17**, 2443 (1973).

(194) N. Chughtai, Ph.D. Thesis, Polymer Centre, Lancaster University (1993).

(195) D.J. Hourston, R. Satgurunathan and H. Varma, *J. Appl. Polym. Sci.*, **31**, 1955 (1986).

(196) D. Klempner, L. Berkowski and K.C. Frisch, *Rubber World*, **192**, 16 (1985).

(197) D.T.H. Wong and H.L. Williams, *J. Appl. Polym. Sci.*, **28**, 2187 (1983).

(198) R.Y. Ting and R.N. Capps, in 'Sound and Vibration Damping with Polymers', eds. R.D Corsaro and L.H. Sperling, ACS 424, American Chemical Society, Washington, DC (1990).

(199) J.N. Forster and L.H. Sperling, *J. Appl. Polym. Sci.*, **33**, 2637 (1987).

(200) D.J. Hourston and J.A. McCluskey, *Polymer*, **20**, 1573 (1979).

(201) D. Klempner, B. Muni, M. Okorafor and K.C. Frisch, in "Advances in IPNs," eds. D. Klempner and K.C. Frisch, Vol. II, Technomic, Lancaster, PA (1990).

(202) D. Klempner, L.C. Wang, M. Ashtiani and K.C. Frisch, *J. Appl. Polym. Sci.*, **32**, 4197 (1986).

(203) J.H. Saunders and K.C. Frisch, 'Polyurethanes Chemistry and Technology', Part 1, Interscience Publishers, New York (1962).

(204) G. Oertel, 'Polyurethane Handbook', 2nd ed., Carl Hanser Verlag, Munich (1994).

(205) C. Hepburn, 'Polyurethane Elastomers', 2nd Edition, Elsevier Applied Science Publishers, London (1992).

(206) G.G. Odian, 'Principles of Polymerization', 3rd edition, Wiley Interscience (1991).

(207) G. Woods, 'The ICI Polyurethane Book', 2nd edition, John Wiley & Sons, Chichester (1990).

(208) K.C. Frisch, in 'Polyurethane Technology', ed. P.F. Bruins, Intersience Publishers, New York (1969).

(209) Bayer AG PUR Application Research Department, 'Bayer-Polyurethanes' (1979).

(210) P. Rempp and E.W. Merrill, 'Polymer Synthesis', 2nd edition, Hüting u. Wepf, Basel (1991).

(211) H. Kipphardt, Polyurethanes World Congress 1987, Aachen, Germany (1987).

(212) M. Xu, J. MacKnight, C.H.Y. Chen and E.L. Thomas, *Polymer*, **24**, 1327 (1983).

(213) D.A. Heyman and O.M. Grace, *J. Cellular Plastics*, **21**, 2, 101 (1985).

(214) L.B. Weisfeld, J.R. Little and W.E. Wolstenholme, *J. Polym. Sci.*, **56**, 455 (1962).

(215) K.A. Pigott, B.F. Frye, K.R. Allen, S. Steingiser, W.C. Darr, J.H. Saunders and E.E. Hardy, *J. Chem. Eng. Data*, **5**, 391 (1960).

(216) W. Berger and H.W. Kammer, *Makromol. Chem. Macromol. Symp.*, **12**, 145 (1987).

(217) T.R. Heskteh, S.L Cooper and J.W.C. van Bogart, *Polym. Eng. Sci.*, **20**, 3, 190 (1980).

(218) D. Dietrich and K. Uhlig, in 'Ullmann's Encyclopedia of Industrial Chemistry', Vol. A 21, VCH Publishers Inc., Weinheim (1992).

(219) I. Blackwell and K.H. Gardner, *Polymer*, **20**, 13 (1979).

(220) J.T. Koberstein and R.S. Stein, *J. Polym. Sci. Polym. Phys.*, **21**, 1439 (1983).

(221) W. Goyert and H. Hespe, *Kunststoffe*, **68**, 819 (1978).

(222) M. Tanaka and T. Nakaya, *J. Macromol. Sci. Chem. A*, **24**, 777 (1987).

(223) K. Hoffmann and R. Bonart, *Makromol. Chem.*, **184**, 1529 (1983).

(224) D.C. Allport and A.A. Mohajer, in 'Block Copolymers', D.C. Allport and W.H. Janes, Applied Science Publishers LTD (1973).

(225) C.W. Brunn, *J. Polym. Sci.*, **16**, 323 (1955).

(226) H.Y. Chen, R.M. Briber, E.L. Thomas, M. Xu and W.J. MacKnight, *Polymer*, **24**, 1333 (1983).

(227) I. Goodman, in "Developments in Block-Copolymers," ed. I. Goodman, Applied Science (1985).

(228) Y. Camberlin and J.P. Pascault, *J. Polym. Sci. Polym. Phys.*, **22**, 1835 (1984).

(229) J.G. Dillon, 'Infrared Spectroscopy Atlas of Polyurethanes', Technomic Publishing Company Inc., Lancaster, PA (1989).

(230) D.J. David and H.B. Stanley, 'Analytical Chemistry of Polyurethanes', Interscience, New York (1969).

(231) D.A. Skoog and D.M. West, 'Fundamentals of Analytical Chemistry', Holt, Rinehart and Winston, 3rd ed., New York (1976).

(232) E. Schröder, G. Müller and K.-F. Arndt, "Polymer Characterization," Hanser Publishers, München (1989).

(233) DMTA Mk III User manuel, Rheometric Scientific (1995).

(234) J.W.M. Furson and R.E. Wetton, in 'DMTA Users Meeting', Polymer Laboratories, Loughborough (1981).

(235) J. Duncan, private communication (1994).

(236) D. Vesely , in 'Polymer Blends and Alloys', eds. M.J. Folkes and P.S. Hope, Blackie Academic & Professional, London (1993).

(237) D.S. Lee and S.C. Kim, *Macromolecules*, **17**, 268 (1984).

(238) K.J. Yeo, L.H. Sperling and D.A. Thomas, *Polym. Eng. Sci.*, **22**, 190 (1982).

(239) K. Kato, *Polym. Eng. Sci.*, **1**, 38 (1967).

(240) D.A. Thomas, in 'Advances in Preparation and Characterisation of Multiphase Polymer Systems', eds. R.J. Ambros and S.L. Aggarwal, John Wiley & Sons, New York (1978).

(241) A.R. Spurr, *J. Ultrastructure Research*, **26**, 31 (1961).

(242) M. Matsuo, T.K. Kwei, D. Klempner and H.L. Frisch, *Polym. Eng. Sci.*, **10**, 327 (1970).

(243) J.R. White and E.L. Thomas, *Rubber Chem. Technol.*, **57**, 457 (1984).

(244) L.C. Sawyer and D.T. Grupp, 'Polymer Microscopy', Chapman and Hall, London (1987).

(245) S. Wischnitzer, 'Introduction to Electron Microscopy', 3rd edition, Pergamon Press, New York (1981).

(246) G. Kampf, 'Characterisation of Plastics by Physical Methods', Hanser, Berlin (1986).

(247) A.K. Sircar and M.L. Drake, in 'Sound and Vibration Damping with Polymers', eds. R.D. Corsaro and L.H. Sperling, ACS 424, American Chemical Society, Washington, DC (1990).

(248) M. Reading, *Trends Polym. Sci.*, **8**, 248 (1993).

(249) M. Song, A. Hammiche, H.M. Pollock, D.J. Hourston and M. Reading, *Polymer*, **36**, 3313 (1995).

(250) A.Ya. Malkin, A.A. Askadsky, V.V. Kovriga and A.E. Chalykh, 'Experimental methods of Polymer Physics', Prentice-Hall Inc., New Jersey (1983).

(251) P.I. Donnelly, *'Mechanical Properties of Polymers'*, Wiley - Interscience, New York (1971).

(252) H. Djomo, A. Morin, M. Damyanidu and G.C. Meyer, *Polymer*, **24**, 65 (1983).

(253) Y.S Lipatov, G.M. Semenovitch, S.I. Skiba, L.V. Karabanova and L.M. Sergeeva, *Polymer*, **33**, 361 (1992).

(254) J. Brandrup and E.H. Immergut, 'Polymer Handbook', Wiley-Interscience, 3rd edition, New York (1989).

(255) P.J. Flory and J. Rehner, *J. Chem. Phys.*, **11**, 521 (1943).

(256) J.P. Bell, *J. Polym. Sci.*, A2, **8**, 417 (1970).

(257) G.M. Bristow and W.F. Watson, *Trans. Faraday Soc.*, **54**, 1731 (1958).

(258) V.D. Arendt, R.E. Logan, and R. Saxon, *J. Cell. Plast.*, **11**, 376 (1982).

(259) Technical Information, TMXDI® (META) aliphatic isocyanate, Cytec Industries (1992).

(260) R.W. Dexter, R. Saxon and D.E. Fiori, *J. Coat. Technol.*, **58**, 43 (1986).

(261) R.N. Capps, G.M. Stack, M.Q. Samuels and L.L. Beumel, *J. Appl. Polym. Sci.*, **45**, 1175 (1992).

(262) J.W.C. Van Bogart, A. Lilaonitkul, L.E. Lerner and S.L. Cooper, *J. Macromol. Sci.*, **B17**(2), 267 (1980).

(263) C.G. Seefried, J.V. Koleske and F.E. Critchfield, *J. Appl. Polym. Sci.*, **19**, 2493 (1975).

(264) C.G. Seefried, J.V. Koleske and F.E. Critchfield, *J. Appl. Polym. Sci.*, **19**, 2503 (1975).

(265) L.E. Nielsen, 'Mechanical Properties of Polymers', Reinhold, New York (1967).

(266) B. Nabeth, I. Corniglion and J.P. Pascault, *J. Polym. Sci., Polym. Phys.*, **34**, 401 (1996).

(267) D.J. Hourston and Y. Zia, *J. Appl. Polym. Sci.*, **28**, 3745 (1983).

(268) R.W. Seymour and S.L. Cooper, *Macromolecules*, **6**, 48 (1973).

(269) R.F. Wolf and C.C. Stueber, *Rubber Age*, **86**, 1009 (1960).

(270) K. Imada, T. Miyakawa, Y. Chatani, H. Tadokoro and S. Murahashi, *Makromol. Chem.*, **83**, 113 (1965).

(271) K. Sreenivasan, *Eur. Polym. J.*, **27**, 811 (1991).

(272) Y.Q. Zhu, Y.J. Huang, Z.G. Chi and H.J. Shen, *Eur. Polym. J.*, **30**, 12, 1493 (1994).

(273) D.S. Lee and S.C. Kim, *Macromolecules*, **17**, 2222 (1984).

(274) D.S. Lee and S.C. Kim, *Macromolecules*, **18**, 2173 (1985).

(275) B.S. Kim, D.S. Lee and S.C. Kim, *Macromolecules*, **19**, 2589 (1986).

(276) D.S. Lee, T.M. Tak, G.S. Kim and S.C. Kim, *Polym. Adv. Tech.*, **1**, 231 (1991).

(277) D.S. Lee and T.S. Park, *Polym. J.*, **23**, 241 (1991).

(278) D.S. Lee and T.S. Park, *J. Appl. Polym. Sci.*, **43**, 481 (1991).

(279) R.F. Boyer and S.G. Truley, *Midl. Macromol. Monogr.*, **4**, 333 (1978).

(280) M.C. Shen and A. Eisenberg, *Rubber Chem. Technol.*, **43**, 95 (1970).

(281) J.S. Stadnicki, J.K. Gillham and R.F. Boyer, *Midl. Macromol. Monogr.*, **4**, 333 (1978).

(282) K.-H. Illers and E. Jenckel, *Rheol. Acta*, **1**, 322 (1958).

(283) D.R. Paul, in 'Multicomponent Materials', eds. D.R. Paul and L.H. Sperling, ACS Ser. 211, American Chemical Society, Washington (1986).

(284) D.J. Hourston and F.-U. Schäfer, *High Perform. Polym.*, **8**, 1 (1996).

(285) D.J. Hourston and F.-U. Schäfer, unpublished results.

(286) P.S. Theocaris and V. Kefalas, *J. Appl. Polym. Sci.*, **42**, 3059 (1991).

(287) J.M.G. Cowie, in 'Integration of Fundamental Polymer Science and Technology', eds. L.A. Kleintjens and P.I. Lemstra, Elsevier Applied Science Publishers, London (1986).

(288) V. Kefalas, P.S. Theocaris and E. Kontou, *Polym. Composites*, 9(3), 229 (1988).

(289) D. Garcia, *J. Polym. Sci. Polym. Phys. Ed.*, **22**, 1773 (1984).

(290) F.C. Wang, M. Feve, T.M. Lam and J.-P. Pascault, *J. Polym. Sci. Polym. Phys. Ed.*, **32**, 1315 (1994).

(291) F.W. Billmeyer, 'Textbook of Polymer Science', 3rd edition, John Wiley & Sons, New York (1984).

(292) Technical literature, Operation instructions Zwick 3102, Zwick, Ulm (1975).

(293) G. Allen, M.J. Bowden, S.M. Todd, D.J. Blundell, G.M. Jeffs and W.E.A. Davies, *Polymer*, **15**, 28 (1974).

(294) A.J. Ryan, J.L. Stanford and R.H. Still, *Polymer*, **32**, 1426 (1991).

(295) O. Olabisi, L.M. Robeson and M.T. Shaw, 'Polymer-Polymer Miscibility', Academic Press, New York (1979).

(296) E.H. Kerner, *Proc. Phys. Soc.*, **B69**, 808 (1956).

(297) L.E. Nielsen, 'Predicting Properties of Mixtures', Dekker, New York (1978).

(298) L.E. Nielsen, *Rheo. Acta*, **13**, 594 (1974).

(299) L.E. Nielsen, *J. Appl. Polym. Sci.*, **21**, 1579 (1977).

(300) R.A. Dickie, in 'Polymer Blends', ed. D.R. Paul, Ch. 8, Academic Press, New York (1978).

(301) R.A. Dickie, *J. Appl. Polym. Sci.*, **17**, 45 (1973).

(302) F. Rodriguez, 'Principles of Polymer Systems', 3rd edition, Hemisphere Publishing Corporation, New York (1989).

(303) H. Oliva, *Rev. Tec. Univ. Zulia*, **16**, 67 (1993).

(304) V.E. Shashoua and R.G. Beaman, *J. Polym. Sci.*, **33**, 101 (1958).

(305) R. Okasha, G. Hild and P. Rempp, *Eur. Polym. J.*, **15**, 975 (1979).

(306) S. Xue, Z. Zhang and S. Ying, *Polymer*, **30**, 1268 (1989).

(307) D.J. Hourston and F.-U. Schäfer, unpublished results.

(308) D.G. Castner, *J. Biomater. Sci. Polymer Ed.*, **3**, 6, 463 (1992).

(309) P. Rempp and E.W. Merrill, 'Polymer Synthesis', 2nd edition, Hüting & Wepf Verlag, Basel (1991).

(310) S. Nazarenko, D. Haderski, A. Hiltner and E. Baer, *J. Appl. Polym. Sci.*, **35**(21), 1682 (1995).

(311) B. Gregory, A. Hiltner and E. Baer, *Polym. Eng. Sci.*, **27**, 568 (1987).

(312) L.E. Nielsen, *Polym. Eng. Sci.*, **17**, 713 (1977).

(313) M.R. Thomas, *J. Coat. Technol.*, **55** (703), 55 (1983).

(314) E.P. Douglas, A.J. Waddon and W.J. MacKnight, *Macromolecules*, **27**, 4344 (1994).

(315) B. Hird and A. Eisenberg, *Macromolecules*, **25**, 6466 (1992).

(316) X.-D. Fan and C.G. Bazuin, *Macromolecules*, **28**, 8209 (1995).

(317) L.A. Utracki, D.J. Walsh and R.A. Weiss, in 'Multiphase Polymers: Blends and Ionomers', eds. L.A. Utracki and R.A. Weiss, ACS Symposium Series 395, American Chemical Society, Washington , DC (1989).

(318) M. Rutkowska, M. Jastrzebska, J.-S. Kim and A. Eisenberg, *J. Appl. Polym. Sci.*, **48**, 521 (1993).

(319) A. Eisenberg, *Macromolecules*, **3**, 147 (1970).

(320) P.W. Atkins, 'Physical Chemistry', 4th edition, Oxford University Press, Oxford (1990).

(321) A. Natansohn, M. Rutkowska and A. Eisenberg, *Polymer*, **28**, 885 (1987).

(322) M. Rutkowska and A. Eisenberg, *J. Appl. Polym. Sci.*, **29**, 755 (1984).

(323) D. Acierno, F.P. La Mantia and G. Polizzotti, *J. Polym. Sci. Polym. Phys. Ed.*, **17**, 1903 (1979).

(324) P. Patel, T. Shah and B. Suthar, *J. Appl. Polym. Sci.*, **40**, 1037 (1990).

(325) Q. Chen, H. Ge, D. Chen, X. He and X. Yu, *J. Appl. Polym. Sci.*, **54**, 1191 (1994).

(326) D. J. Hourston and M.G. Huson, *J. Appl. Polym. Sci.*, **45**, 1753 (1992).

(327) B. Hartmann, G.F. Lee and J.D. Lee, J. Acoust. Soc., **95**, 226 (1994).

(328) M. Song, A. Hammiche, H.M. Pollock, D.J. Hourston and M. Reading, *Polymer*, **36**, 3313 (1995).

(329) G. Tieghi, M. Levi, A. Fallini and F. Danusso, *Polymer*, **32**, 39 (1991).

(330) D.J. Massa, *J. Appl. Phys.*, **44**, 2595 (1973).

(331) D. Klempner, K.C. Frisch, H.X. Xiao and H.L. Frisch, *Polym. Eng. Sci.*, **25**, 488 (1985).

(332) D. Klempner, K.C. Frisch, H.X. Xio, E. Cassidy and H.L. Frisch, Multicomponent Polymer Materials, ACS 210, 1986.

(333) J. Wang, Y. Li and X. Tang, in *Advances in IPNs*, Vol. IV, eds. D. Klempner and K.C. Frisch, Technomic Publishing, Lancaster PA, 1994.

(334) P.A. Lovell, J. McDonald, D.E.J. Saunders, M.N. Sherratt and R.J. Young, in *Toughend Plastics*, ACS 233, eds. C.K. Riew and A.J. Kinloch, American Chemical Society, Washington, DC, 1993.

(335) H.-J. Sue, E.I. Garcia-Meitin, D.M. Pickelman and P.C. Yang, in *Toughened Plastics*, ACS 233, eds. C.K. Riew and A.J. Kinloch, American Chemical Society, Washington, DC, 1993.

(336) A.F. Chen and H.L. Williams, *J. Appl. Polym. Sci.*, **20**, 3387 (1976).

10. LIST OF PUBLICATIONS

(1) D.J. Hourston and F.-U. Schäfer, "Damping characteristics of polyurethane-based simultaneous interpenetrating polymer networks", *High Perform. Polym.*, **8**, 19-34 (1996).

(2) D.J. Hourston and F.-U. Schäfer, "Polyurethane/polystyrene one-shot interpenetrating polymer networks with good damping ability: Transition broadening through crosslinking, inter-network grafting and compatibilisation", *Polym. Adv. Technol.*, **7**, 1-8 (1996).

(3) D.J. Hourston and F.-U. Schäfer, "Poly(ether urethane)/poly(ethyl methacrylate) interpenetrating polymer networks: Morphology, phase continuity and mechanical properties as a function of composition", *Polymer*, in press.

(4) D.J. Hourston, F.-U. Schäfer and J.S. Bates, "Synthesis, characterisation and properties of interpenetrating polymer networks containing functionalised latex particles", *J. Appl. Polym. Sci.*, in press.

(5) D.J. Hourston and F.-U. Schäfer, "Poly(ether urethane)/poly(ethyl methacrylate) interpenetrating polymer networks with good energy absorbing ability: The influence of the crosslink density in both networks", *J. Appl. Polym. Sci.*, submitted.

(6) D.J. Hourston and F.-U. Schäfer, "Morphology and properties of m-TMXDI-based poly(ether urethane)/polystyrene interpenetrating polymer networks as a function of composition", *Polymer*, in preparation.